

**REVIEW OF LITERATURE AND ASSESSMENT  
OF FACTORS RELEVANT TO PERFORMANCE OF  
GROUTED SYSTEMS FOR RADIOACTIVE  
WASTE DISPOSAL**

*Prepared for*

**U.S. Nuclear Regulatory Commission  
Contract NRC NRC-02-07-006**

*Prepared by*

**R.T. Pabalan<sup>1</sup>  
F.P. Glasser<sup>2</sup>  
D.A. Pickett<sup>1</sup>  
G.R. Walter<sup>1</sup>  
S. Biswas<sup>1</sup>  
M.R. Juckett<sup>1</sup>  
L.M. Sabido<sup>1</sup>  
J.L. Myers<sup>1</sup>**

<sup>1</sup>Center for Nuclear Waste Regulatory Analyses  
6220 Culebra Road  
San Antonio, Texas 78228-0510

<sup>2</sup>University of Aberdeen  
Aberdeen, Scotland, United Kingdom

**Center for Nuclear Waste Regulatory Analyses  
San Antonio, Texas**

**April 2009**

## ABSTRACT

For many decades, radioactive wastes related to the reprocessing of nuclear fuel have been stored in underground storage tanks at former nuclear materials production sites at Aiken, South Carolina (Savannah River Site); Hanford, Washington; and Idaho Falls, Idaho (Idaho National Laboratory). The U.S. Department of Energy (DOE) plans to remove highly radioactive or key radionuclides from the tanks to the maximum extent practical and close the emptied tanks by filling the tanks, pipework, and concrete vaults with grout. This cement-based material is expected to provide structural support, encapsulate and stabilize the residual tank waste and tank heel, act as a physical barrier to inhibit the flow of groundwater through the waste, and serve as a barrier to plant roots or to inadvertent intrusion by burrowing animals or humans drilling or excavating at the site. DOE performance assessments demonstrating that disposal actions at the sites will meet performance objectives have included quantitatively evaluating the influence of cement-based barriers in mitigating radionuclide release to the environment. In these performance assessments, assumptions are made regarding the physical integrity (e.g., hydraulic conductivity) and chemical condition (e.g., pH and Eh affecting radionuclide solubility and sorption) of the cement-based engineered barrier and the changes to these properties that occur with time. Although much research has been done on the use of cement-based materials for immobilizing and stabilizing toxic metals and radioactive wastes, the ability of these materials to maintain the low permeability and other properties necessary to retain radionuclides for the long time periods—up to 10,000 years—required for nuclear waste disposal is uncertain.

This report was prepared for the U.S. Nuclear Regulatory Commission (NRC) to provide information NRC staff can use in their consultations with DOE. This information will support independent evaluation of the DOE performance assessments related to tank closures and disposal of radioactive wastes in near-surface disposal facilities. This report briefly reviews the nature of Portland cement and the hydration and setting of cement-based materials. Degradation mechanisms, broadly classified into chemical and physical processes, and the role of the service environment in the degradation of cement-based materials are discussed. The report reviews published modeling approaches, ranging from simple diffusion or empirical equations to more complex coupled reactive–transport models, for predicting the chemical degradation of cement-based materials. Conceptual and mathematical models that can be used to evaluate the potential influence of fast pathways and bypassing pathways on radionuclide releases from grouted tanks are discussed. Further, the report summarizes and evaluates models and data available for estimating radionuclide release from cement-based waste forms. Finally, factors, as well as features, events, and processes, that are potentially important to evaluating the performance of grouted tanks and concrete vaults at DOE sites are assessed.

Additional information is provided in two appendices. Data derived from published literature related to the permeability and diffusion properties of cement-based materials are presented in Appendix A. In Appendix B, available data are reviewed and new models for solubility limits are developed for selected radioelements in environments expected in cement-based disposal facilities at the Savannah River Site and Idaho National Laboratory.

# CONTENTS

Section	Page
ABSTRACT .....	iii
FIGURES .....	ix
TABLES .....	xiii
EXECUTIVE SUMMARY .....	xv
ACKNOWLEDGMENTS .....	xvii
1 INTRODUCTION .....	1-1
1.1 Background Information .....	1-1
1.2 Objective of Report .....	1-3
2 NATURE OF PORTLAND CEMENT .....	2-1
2.1 Production .....	2-1
2.2 Product Variability .....	2-1
2.3 Cement Products .....	2-1
2.4 Supplementary Cement Materials .....	2-1
2.5 Organic Matter in Cement .....	2-2
3 HYDRATION OF CEMENT .....	3-1
3.1 General Considerations .....	3-1
3.2 Cement Hydration Products .....	3-3
4 DEGRADATION OF CEMENT-BASED ENGINEERED BARRIERS .....	4-1
4.1 Chemical Degradation Mechanisms .....	4-1
4.1.1 Carbonation .....	4-1
4.1.2 Sulfate Attack .....	4-5
4.1.3 Leaching .....	4-7
4.1.4 Corrosion .....	4-11
4.1.5 Alkali–Silica Reaction .....	4-16
4.2 Physical Degradation Mechanisms .....	4-16
4.2.1 Shrinkage .....	4-16
4.2.2 Thermal Cracking .....	4-20
4.2.3 Freezing and Thawing .....	4-21
4.3 Durability and the Composite Nature of Concrete .....	4-21
4.4 Role of the Service Environment .....	4-22
4.5 Standards and Standard Methods for Testing Performance in Service Environments .....	4-25
4.6 Limitations of Tests on Performance of Cement-Based Materials .....	4-26
4.7 Framework for Predicting the Long-Term Behavior of Cement-Based Engineered Barriers .....	4-27
5 APPROACHES TO MODELING THE DEGRADATION OF CEMENT-BASED MATERIALS .....	5-1
5.1 Carbonation .....	5-2
5.2 Sulfate Attack .....	5-9
5.2.1 Empirical Correlation .....	5-9
5.2.2 Reactive–Transport Models .....	5-10

## CONTENTS (continued)

Section	Page
5.3	Leaching..... 5-22
5.3.1	Chemical Models of Leaching..... 5-22
5.3.2	Reactive–Transport Leaching Models ..... 5-30
5.4	Summary ..... 5-45
6	CONCEPTUAL AND MATHEMATICAL MODELS OF POTENTIAL FAST AND BYPASSING PATHWAYS ASSOCIATED WITH <i>IN-SITU</i> TANK CLOSURES..... 6-1
6.1	Identification and Classification of Potential Fast and Bypassing Pathways .... 6-1
6.1.1	Cracks in Grout and Concrete Structures ..... 6-6
6.1.2	Conduits..... 6-9
6.2	Movement of Fluids Through Potential Fast and Bypassing Pathways..... 6-11
6.2.1	Fluid Flow in Cracks ..... 6-13
6.2.2	Flow Through Conduits..... 6-20
6.3	Mass Transport Processes Related to Fast and Bypassing Pathways ..... 6-22
6.3.1	Mass Transport in Microcracks..... 6-23
6.3.2	Mass Transport in Macrocracks..... 6-25
6.3.3	Mass Transport in Conduits..... 6-26
6.3.4	Representation of Microcrack/Mortar Interactions ..... 6-27
6.4	Summary and Recommendations ..... 6-31
7	EVALUATION OF RADIONUCLIDE RELEASE MECHANISMS FOR CEMENT-BASED WASTE FORMS ..... 7-1
7.1	Introduction..... 7-1
7.2	Radionuclide Release Models for Cementitious Systems ..... 7-2
7.2.1	Key Chemical and Physical Characteristics of the System ..... 7-2
7.2.1.1	Brief Descriptions of Grouted Tank and Saltstone Systems ..... 7-2
7.2.1.2	Literature Information on Chemical Conditions ..... 7-3
7.2.1.3	Chemical Evolution as Represented in Grouted Tank and Saltstone Performance Assessments ..... 7-4
7.2.2	Overview of Conceptual Models ..... 7-6
7.2.2.1	Waste Form Dissolution With Congruent Release..... 7-6
7.2.2.2	Diffusion ..... 7-6
7.2.2.3	Surface Rinse ..... 7-7
7.2.2.4	Solubility Control ..... 7-7
7.2.2.5	Combined Models ..... 7-7
7.3	Review of Relevant Literature Data..... 7-8
7.3.1	Leaching Data..... 7-8
7.3.1.1	Site-Specific Data..... 7-9
7.3.1.2	Literature Data ..... 7-11
7.3.2	Solubility Data..... 7-12
7.3.3	Other Data on Radionuclide/Waste Form Partitioning..... 7-12
7.3.3.1	Site-Specific Partitioning Data..... 7-12
7.3.3.2	Literature Partitioning Data ..... 7-14

## CONTENTS (continued)

Section	Page
7.3.4	Evaluation of Models in Light of Data ..... 7-15
7.3.5	Relative Importance of Diffusive and Advective Release ..... 7-19
7.4	Summary and Recommendations ..... 7-21
8	ASSESSMENT OF FACTORS IMPORTANT TO PERFORMANCE OF GROUTED TANKS AND CONCRETE VAULTS AT U.S. DEPARTMENT OF ENERGY SITES..... 8-1
8.1	General Considerations..... 8-5
8.2	Key Features, Events, and Processes in Closed Systems..... 8-8
8.2.1	Evolution of Grout pH ..... 8-8
8.2.2	Evolution of Grout Redox Potential..... 8-10
8.2.3	Shrinkage..... 8-13
8.2.4	Cracking Due to Thermal Effects..... 8-14
8.2.5	Cracking Due to Moisture Changes..... 8-16
8.2.6	Grout Curing Conditions ..... 8-17
8.2.7	Waste–Grout Interaction..... 8-19
8.2.8	Effect of Chemical Admixtures..... 8-20
8.2.9	Effect of Fly Ash Selection..... 8-22
8.3	Key Features, Events, and Processes in Open Systems ..... 8-23
8.3.1	Fast Pathways and Bypassing Pathways ..... 8-23
8.3.2	Carbonation of Tank Grouts ..... 8-26
8.3.3	Environmental Effects on Redox Potential ..... 8-27
8.3.4	Leaching and Wet–Dry Cycling ..... 8-27
8.3.5	Sulfate Attack..... 8-28
8.4	Immobilization of Technetium in Tank Grouts ..... 8-28
8.5	Scoping Assessments of Tank Grout Degradation..... 8-30
8.5.1	Scenario 1: No Interaction With the External Environment..... 8-31
8.5.2	Scenario 2: Limited Infiltration of Water; Carbonation as Dominant Degradation Mechanism ..... 8-33
8.5.3	Scenario 3: Infiltration Scenario..... 8-41
8.6	Summary and Recommendations ..... 8-43
9	REFERENCES ..... 9-1
APPENDIX A	— PERMEABILITY AND DIFFUSION PROPERTIES OF CEMENTITIOUS MATERIALS
APPENDIX B	— RADIONUCLIDE SOLUBILITY LIMITS IN CEMENT-BASED MATERIAL PORE FLUIDS

## FIGURES

Figure	Page
4-1 Leaching Zones in Hydrated Portland Cement Leached by Pure Water (Kamali, et al., 2004) .....	4-8
4-2 Empirical Correlations Showing the Impact of Natural Waters Containing Dissolved Carbon Dioxide on Portland Cement .....	4-9
4-3 Aggressivity of Groundwater to Cement as a Function of Dissolved Carbon Dioxide ( $H_2CO_3^*$ ) Concentration .....	4-10
4-4 Example of Corrosion-Induced Damage of Concrete Structure .....	4-12
4-5 Initiation and Propagation Periods for Corrosion in a Reinforced Cement-Based Structure .....	4-13
4-6 Relationship of Critical Chloride Content to Environmental Conditions and Quality of Concrete Cover .....	4-14
4-7 Typical Ranges of Corrosion Rate of Carbon Steel in Concrete Exposed to Different Environmental Conditions .....	4-15
4-8 Illustration Showing No Crack Development in Cement-Based Material That Is Free to Shrink (Slab on Rollers) .....	4-18
4-9 Relationship Between Total Water Content and Drying Shrinkage .....	4-18
4-10 Effect of Water/Cement Ratio and Aggregate Content on Shrinkage .....	4-19
4-11 Drying Shrinkage and Carbonation Shrinkage of Mortar at Different Relative Humidities .....	4-19
4-12 Principal Logic Steps Involved in Predicting the Long-Term Behavior of Materials Based on ASTM Standard C1174–04 .....	4-28
5-1 Initiation and Propagation Periods for Corrosion of a Reinforced Concrete Structure .....	5-3
5-2 Minimum and Maximum Values of Corrosion Rate of Steel Reinforcement in Carbonated Concrete as a Function of Relative Humidity .....	5-4
5-3 Comparison of Carbonation Depth as a Function of Time Calculated Using the Model of Papadakis, et al. (1991a, 1989) and Experimental Data .....	5-8
5-4 Carbonation Depth Calculated as a Function of Relative Humidity Versus Experimental Data .....	5-8
5-5 Schematic of the Sulfate Attack Model Tixier and Mobasher (2003a,b) Developed ..	5-14
5-6 Schematic Representation of Sulfate Penetration and Reaction Showing Profiles of Sulfate Concentration (U) at Times $t = 0$ and $t > 0$ .....	5-14
5-7 Schematic Representation of (a) Diffusivity Profile and (b) Sulfate Concentration Profile for a Cracked ( $D_A$ ) and Uncracked ( $D_B$ ) Specimen .....	5-15
5-8 Effect of Diffusivity on the Expansion of a Cement-Based Material With Different Levels of Damage Due to Sulfate-Induced Cracking .....	5-15
5-9 Effect of Initial Gypsum Content (...) on the Sulfate Reaction-Induced Expansion of a Specimen Containing 6 Percent Tricalcium Aluminate .....	5-16
5-10 Schematic Representation of a Concrete Slab Marchand, et al. (1999) Considered in Numerical Simulations of Sulfate Attack .....	5-19
5-11 Results of Simulations of Sulfate Attack Showing the Penetration of Degradation Front in a Concrete Slab as a Function of Time .....	5-20
5-12 Comparison of Measured Sulfur Profile in Cement Sample Exposed to a 0.05 mol/L $Na_2SO_4$ Solution ... With Sulfur Profile Calculated Using STADIUM .....	5-20
5-13 Calcium Concentration of Solutions in Equilibrium With C-S-H Berner (1992a) Calculated .....	5-23

## FIGURES (continued)

Figure	Page
5-14 pH of Solutions in Equilibrium With C-S-H Berner (1992a) Calculated, Compared With Experimental Data.....	5-24
5-15 Calculated Evolution of Pore Water Composition of a Sulfate-Resistant Cement Degrading in a Marl-Type Groundwater.....	5-25
5-16 Calculated Evolution of the Solid Phase Inventory of a Pozzolanic Cement Degrading in a Marl-Type Groundwater.....	5-25
5-17 Evolution of Pore Water pH in a Sulfate-Resistant Portland Cement Degrading in Pure Water and in a Marl-Type Groundwater .....	5-26
5-18 Distribution of Solid Phases in Blends of Ordinary Portland Cement and Blast Furnace Slag Calculated Using CEMCHEM .....	5-27
5-19 Results of PHREEQE Calculations of Mixing Cement Pore Water and Groundwater .....	5-29
5-20 Representation of the Leaching Model of Adenot and Richet (1997), Which Is Made up of Zones of Constant Mineralogy .....	5-31
5-21 Profiles Adenot, et al. (1997) Calculated of Ettringite, Monosulfate, Portlandite, and C-S-H After 8.5 Months of Degradation by a pH 11.5 Solution.....	5-33
5-22 Study Domain Moranville, et al. (2004) Used in Modeling Cement Leaching .....	5-35
5-23 Calculated pH and Calcium Concentration Profiles Within Degrading Portland Cement Paste at Different Timesteps .....	5-35
5-24 Evolution With Time of Porosity and Volume Proportion of Solids in Degrading Portland Cement Paste Moranville, et al. (2004) Calculated.....	5-36
5-25 Relative Quantities of Solid Phases and of Calcium and Sulfur in Those Solids Versus Depth of Portland Cement Paste After 1,286 Hours of Simulated Leaching..	5-36
5-26 Comparison of Total Calcium Profile Determined Using an Electron Microprobe (in CPS, Counts per Second) With the Total Calcium Profile.....	5-38
5-27 Calculated Degradation Depth of Concrete in Contact With (a) Water and (b) Bentonite.....	5-39
5-28 Cross Section Through the Near Field of a Cementitious Repository and Its Simplified Representation in the MCOTAC Model .....	5-40
5-29 Concentration of Model Solids and Porosity Changes Calculated for (a) 1 Year and (b) 2,000 Years of Interaction of Cement Vault With Groundwater .....	5-41
5-30 Schematic Illustration of CHEQMATE Cells Used in the CHEQFRAC Model.....	5-43
5-31 pH of Groundwater Versus Distance in the Crack of a Cement-Based Backfill of a Nuclear Waste Repository .....	5-43
6-1 Cross Section of a Typical Tank With Cooling Coils at the Idaho National Laboratory.....	6-2
6-2 Tank Configurations at the Savannah River Site .....	6-2
6-3 Photograph Showing the Internal Structure and Cooling Coils of Tank WM-185 During Construction at the Idaho National Laboratory Tank Farm Facility.....	6-3
6-4 Conceptual Illustration of Grouted Tank at the Savannah River Site .....	6-4
6-5 Illustration of (a) Grouted Tank and Vault and (b) Placement of Reducing Grout ... at the Idaho Nuclear Technology and Engineering Center.....	6-5
6-6 Illustration of Types of Microcracks in a Concrete Matrix.....	6-7
6-7 Features That May Act as Conduits in a Typical Tank at the Idaho National Laboratory.....	6-9
6-8 Illustration of Fast and Bypassing Conduit Pathways .....	6-10

## FIGURES (continued)

Figure	Page
6-9	Liquid Flow Regimes in an Annular Space Around a Grouted Pipe..... 6-10
6-10	Fluid and Mass Transport Processes in Annular Spaces..... 6-12
6-11	Illustration of (i) Percolation Diverted Away From Waste Form Through Cracks and Conduits in Vault Wall and (ii) Flow Into the Waste Form Through a Conduit ..... 6-12
6-12	Conduit Flow Along a Grout Pour Interface Due to Perching on a Grout Layer..... 6-13
6-13	Illustration of Capillary Flow Through a Microcrack in a Porous Matrix..... 6-14
6-14	Illustration of Discrete Fracture and Transport Model ..... 6-17
6-15	Conceptual Illustration of Flow and Transport Coupling in a Dual Porosity Continuum Model ..... 6-17
6-16	Conceptual Illustration of Chemical Disequilibrium Between Fluid in a Microcrack and a Reducing Aggregate ..... 6-23
6-17	Conceptual Illustration of the Multiple Interacting Continua (MINC) Modeling Approach ..... 6-25
6-18	Illustration of Difference in Flow and Transport Geometry Between a Fracture and a Small Conduit ..... 6-27
6-19	Conceptual Model of Advective Flow Through Microcracks With Diffusion in Mortar ..... 6-28
6-20	Ratio of Time for Mass in a Crack to Exchange 90 Percent of Mass With Mortar by Diffusion to Advective Travel Time Through a Crack..... 6-30
6-21	Illustration of Concept of Penetration Depth in Mortar With Fast-Moving Fluid in Crack ..... 6-31
6-22	Diffusion Penetration Depth as a Function of Crack Aperture Based on Advective Travel Time Through a 1-cm [0.4-in]-Long Crack..... 6-32
7-1	Four Modeled Conditions for Radionuclide Release From Grouted Tanks in the Closure Concept for F-Area Tank Farm at Savannah River Site ..... 7-5
7-2	Two Different Fits to Leaching Data on Sodium From a Portland Cement (From Fuhrmann, et al., 1990, Figure A1). “CFL” Means Cumulative Fraction Leached..... 7-17
7-3	Fits of Various Release Models to Data on Sr-90 From Field Lysimeters at Oak Ridge and Argonne National Laboratories ..... 7-18
8-1	Typical Tank and Vault Layout and Dimensions at the Idaho National Laboratory Tank Farm Facility (From DOE–Idaho, 2003) ..... 8-1
8-2	Tank Configurations at the Savannah River Site: (a) Cooled Waste Storage Tank, Type 1; (b) Cooled Waste Storage Tank, Type II..... 8-2
8-3	Schematic of a Grout-Filled Tank and Vault at the Idaho National Laboratory Tank Farm Facility Showing the Vault Volume and the Grout Mass ..... 8-3
8-4	Schematic of an Engineered Barrier System to Close Tanks at the Harford Site ..... 8-4
8-5	Photographs Taken After a Test Grout Pour at the Idaho National Laboratory Tank Farm Facility Showing Visible Cracks at Approximately 1-m [3.3-ft] Spacing ... 8-18
8-6	Illustration of Water Flow in the Hydrologically Unsaturated Zone Around a Vault or Tank Due to Increased Saturation Above the Vault or Tank..... 8-25
8-7	Nomograph Showing the Decrease of Portlandite in Portland Cement–Fly Ash Blends After Reaction Is Completed ..... 8-32

## FIGURES (continued)

Figure		Page
8-8	Impact of Carbonation on Mass-Balance of Hydrated Model Cement Paste at 25 °C [77 °F] at Saturated Relative Humidity (From Glasser and Matschei, 2007) ...	8-37
8-9	Impact of Carbonation on Mass Balance of Hydrated Model Cement Paste (Enlarged Detail From Figure 8-8) .....	8-37
8-10	Evolution of the (a) Ca/Si Molar Ratio of C-S-H (b) Pore Water pH in a Model Cement Undergoing Carbonation .....	8-39

## TABLES

Table	Page
3-1 Mineralogy of Hydrated Portland Cement .....	3-4
4-1 Carbonation Mechanisms of Portland Cement Grouts in Humid Atmospheres .....	4-3
4-2 Representation of the Zonal Pattern in Leached Concretes .....	4-8
4-3 Environmentally Abundant Substances Aggressive to Portland Cement.....	4-23
4-4 Relative Susceptibility of Cement-Based Materials to Attack by Aggressive Chemical Species Present in Service Environments .....	4-24
4-5 Severity of Exposure of Cement-Based Material Subjected to Sulfate Attack .....	4-24
5-1 List of Parameters Used in Sulfate Attack Model.....	5-12
5-2 Comparison of Scanning Electron Microscopy Observations and STADIUM Simulation Results .....	5-21
5-3 Selected Model Solids Berner Used To Describe the Solubility Behavior of C-S-H at Varying Ca/Si Ratio .....	5-23
5-4 Comparison of Predicted Pore Fluid Compositions With Measured Data on 5-Year-Old Cements .....	5-28
5-5 Calculated Pore Solution Composition (Columns 3–5) of Cements at Equilibrium With Groundwater (Composition Given in Column 2).....	5-29
5-6 Comparison of Calculated and Measured Degraded Thickness .....	5-34
5-7 Degraded Thickness After 300 and 1,000 Years Calculated .....	5-34
5-8 Reviewed Chemical Degradation Models .....	5-46
6-1 Categories and Features That May Act as Fast or Bypassing Pathways Associated With In-Place Tank Closures .....	6-5
7-1 Selected Preliminary Measured and Previously Recommended $K_d$ Values (mL/g) for the Reducing Grout Formulation for Savannah River Site F-Area Tank Farm.....	7-13
8-1 Grout Mix Formulations for Closing of Tanks and Vaults at the Idaho National Laboratory Tank Farm Facility .....	8-4
8-2 General Bases for the Design and Development of the U.S. Department of Energy Grout Formulations .....	8-5
8-3 Desired Short- and Long-Term Grout Properties .....	8-7
8-4 Poisoning Capacity and Eh in Cement Blends.....	8-10
8-5 Inorganic Constituents That Affect Solidification of Cement-Based Materials .....	8-19
8-6 Environmental Factors Affecting the Interaction Between Soil Gases and Cement–Steel Composites .....	8-26
8-7 Key Features and Processes Affecting Tank Grout Performance.....	8-34
8-8 Probable Causes of Grout Degradation for Scenarios With Limited Percolation of Meteoric Water.....	8-36
8-9 Calculated Phase Assemblages in the Course of Carbonation at 25 °C [77 °F].....	8-38

## EXECUTIVE SUMMARY

For many decades, radioactive wastes related to the reprocessing of nuclear fuel have been stored in underground storage tanks at former nuclear materials production sites at Aiken, South Carolina (Savannah River Site); Hanford, Washington; and Idaho Falls, Idaho (Idaho National Laboratory). Management of these tanks has been a long-standing challenge. The U.S. Department of Energy (DOE) plans to remove highly radioactive or key radionuclides from the tanks to the maximum extent practical. DOE plans to close the emptied tanks by filling the tanks, pipework, and concrete vaults with grout. This cement-based material is expected to provide structural support, encapsulate and stabilize the residual tank waste and tank heel, act as a physical barrier to inhibit the flow of groundwater through the waste, and serve as a barrier to plant roots or to inadvertent intrusion by burrowing animals or humans drilling or excavating at the site. By immobilizing the waste and acting as a barrier around it, the cement-based material is expected to reduce the likelihood of radiological constituents being released from the waste and transported into the environment.

DOE performance assessment calculations rely on the ability of cement-based materials to serve as a barrier to (i) groundwater influx and (ii) release and transport of radionuclides from the grouted tanks and concrete vaults. As a result, performance assessments demonstrating that disposal actions at the sites will meet performance objectives have included quantitatively evaluating the influence of cement-based barriers in mitigating radionuclide release to the environment. In these performance assessments, assumptions are made regarding the physical integrity (e.g., hydraulic conductivity) and chemical condition (e.g., pH and Eh affecting radionuclide solubility and sorption) of the cement-based engineered barrier and the changes to these properties that occur with time. Although much research has been done on the use of cement-based materials for immobilizing and stabilizing toxic metals and radioactive wastes, understanding of the performance of these materials is largely based on short-term tests. The use of cement-based materials for the long periods involved in radioactive waste disposal is outside the general operating envelope for industrial applications, and the ability of these materials to maintain the low permeability and other properties necessary to retain radionuclides for the long time periods—up to 10,000 years—required for nuclear waste disposal is uncertain.

This report was prepared for the U.S. Nuclear Regulatory Commission (NRC) to provide information NRC staff can use in their consultations with DOE. This information will support independent evaluation of the DOE performance assessments related to tank closures and disposal of radioactive wastes in near-surface disposal facilities. Because of the risk significance of engineered barrier performance to demonstrating compliance of DOE disposal actions with regulatory performance objectives, the NRC staff must understand and evaluate the important factors pertaining to the performance of cement-based engineered barriers at DOE sites. This report briefly reviews the nature of Portland cement and the hydration and setting of cement-based materials. Degradation mechanisms, broadly classified into chemical and physical processes, and the role of the service environment in the degradation of cement-based materials are discussed. The report reviews published modeling approaches, ranging from simple diffusion or empirical equations to more complex coupled reactive–transport models, for predicting the chemical degradation of cement-based materials. Conceptual and mathematical models that can be used to evaluate the potential influence of fast pathways and bypassing pathways on radionuclide releases from grouted tanks are discussed. Further, the report summarizes and evaluates models and data available for estimating radionuclide release from cement-based wasteforms. Finally, factors, as well as features, events, and processes, that are potentially important to evaluating the performance of grouted tanks and concrete vaults at DOE sites are assessed.

Additional information is provided in two appendices. Data derived from published literature related to the permeability and diffusion properties of cement-based materials are presented in Appendix A. In Appendix B, available data are reviewed and new models for solubility limits are developed for selected radioelements in environments expected in cement-based disposal facilities at the Savannah River Site and Idaho National Laboratory.

The literature survey indicated that much of the research on cement-based materials commenced in the 1970s. Although the science of modeling the future performance of cement-based materials has advanced considerably since then, more effort must be expended on modeling and linking modeling to experiments and real-world observations of large systems over extended timeframes. Although it is still far from an exact science, modeling the degradation of cement-based materials, even in its present form, allows a new and critical examination of the nature of the problem and of data needs for quantification. It also provides a systematic framework for kinetic and equilibrium studies and for linking deterministic and probabilistic approaches. This report describes the present state of knowledge and develops these themes. As appropriate, additional data needs are also identified.<sup>1</sup>

---

<sup>1</sup>This report should not be interpreted as endorsing any particular model approach or data source for DOE use, nor does this report constitute a consultative review of any specific DOE model, performance assessment, or waste determination.

## ACKNOWLEDGMENTS

This report describes work performed by the Center for Nuclear Waste Regulatory Analyses (CNWRA) and its contractors for the U.S. Nuclear Regulatory Commission (NRC) under Contract No. NRC-02-07-006. The activities reported here were performed on behalf of the NRC Office of Federal and State Materials and Environmental Management Programs, Division of Waste Management and Environmental Protection. This report is an independent product of the CNWRA and does not necessarily reflect the view or regulatory position of NRC.

The authors wish to thank L. Caseres, E. Percy, J. Myers, S. Stothoff, D. Turner, G. Wittmeyer, and NRC staff for their helpful reviews. Thanks also are expressed to L. Mulverhill for her editorial review and to L. Selvey and B. Street for secretarial support.

## QUALITY OF DATA, ANALYSES, AND CODE DEVELOPMENT

**DATA:** The CNWRA-generated data referenced in this report meet the quality assurance requirements described in the Geosciences and Engineering Division Quality Assurance Manual. Data from other sources are included with references to their source. Sources of these non-CNWRA data should be consulted for determining levels of quality assurance.

**ANALYSES AND CODES:** This report includes results of calculations performed using Geochemist's Workbench<sup>®</sup> (RockWare, Inc., 2005). Data reduction and plotting were accomplished using Microsoft<sup>®</sup> Excel<sup>®</sup> (Microsoft Corporation, 2002). Calculations were documented in Scientific Notebooks 877E (Sabido, 2007), 925E (Pickett, 2008), and 927E (Myers, 2009).

### References

Microsoft Corporation. "Excel." Redland, Washington: Microsoft Corporation. 2002.

Myers, J. "Radionuclide Solubility Limits for Cement-Based Systems." Scientific Notebook 927E. San Antonio, Texas: CNWRA. 2009.

Pickett, D.A. "Radionuclide Solubility Limit Calculations for Cement-Based Systems." San Antonio, Texas: CNWRA. 2008.

RockWare, Inc. "Geochemist's Workbench Professional Version 6.0." Golden, Colorado: RockWare, Inc. 2005.

Sabido, L. "Actinide Mobility." Scientific Notebook 877E. San Antonio, Texas: CNWRA. 2007

# 1 INTRODUCTION

## 1.1 Background Information<sup>1</sup>

For many decades, radioactive wastes related to the reprocessing of nuclear fuel have been stored in underground storage tanks at former nuclear materials production sites at Aiken, South Carolina (Savannah River Site); Hanford, Washington; and Idaho Falls, Idaho (Idaho National Laboratory). The underground tanks are made of either stainless steel or carbon steel; the liquid wastes transferred into the carbon steel tanks were made alkaline to be compatible with the tank material. Management of these tanks has been a long-standing challenge, and the tank wastes have been the subject of much research, partly to define the present inventory and partly to develop remediation methods. The U.S. Department of Energy (DOE) overall approach for managing the tank wastes at Hanford and Savannah River is to remove the waste from and clean the tanks to the maximum extent practical; separate the recovered waste into high- and low-activity fractions; and dispose of the residual tank wastes and heels and recovered low-activity waste onsite in a manner that protects human health and the environment (National Research Council, 2006). At the Savannah River Site, the low-activity waste stream will be immobilized in the Saltstone Production Facility, where liquid waste will be mixed with grout—a cement-based material—to create a waste form referred to as saltstone for disposal onsite as monoliths in the concrete vaults of the Saltstone Disposal Facility. Most of the tank waste at the Idaho National Laboratory had been converted into a solid form using calcination, a process during which the aqueous waste is rapidly evaporated and anions such as nitrate and carbonate are decomposed to yield a granular solid. The granular calcine waste is presently stored at the Idaho National Laboratory in bin sets located below (or partially below) the ground surface, but eventually will be put in a form suitable for disposal in a monitored geologic repository (National Research Council, 2006). DOE plans to convert the remaining liquid radioactive waste, called sodium-bearing waste produced mostly from the second and third cycles of spent nuclear fuel reprocessing and waste calcination, using steam reforming for disposal at the Waste Isolation Pilot Plant near Carlsbad, New Mexico (the DOE-preferred disposal path) or at a geologic repository for spent nuclear fuel and high-level waste (DOE, 2005). DOE intends to operationally “close” the tanks at Savannah River Site and Idaho National Laboratory by filling the tanks and associated ancillary equipment with grout and sealing external penetrations. Groups of tanks eventually will be formally closed, and engineered covers will be emplaced to minimize water infiltration to the tanks. Hanford has not yet finalized its tank closure plan but, for planning purposes, is assuming a closure configuration that uses grout as the tank fill material based on research and field experience gained at the Savannah River Site (National Research Council, 2006).

There are 243 underground waste storage tanks at the 3 DOE sites—177 at the Hanford site, 51 at the Savannah River Site, and 15 at the Idaho National Laboratory.<sup>2</sup> The three sites are at different points in their removal and stabilization of tank wastes. At the Idaho National

---

<sup>1</sup>The information presented here regarding radioactive waste tanks at DOE sites is based on references available at the time this report was prepared. The status of these tanks may have changed since publication of the references.

<sup>2</sup>High-level wastes also were stored in two underground tanks at a former commercial spent fuel reprocessing facility at West Valley, New York. Acidic waste generated by PUREX processing was neutralized with sodium hydroxide and stored in a carbon steel tank (Tank 8–D2), whereas acidic waste generated by THOREX processing was stored without neutralization in a stainless steel tank (Tank 8–D4). More than 98 percent of these wastes have been removed from the tanks and solidified into glass inside 275 stainless steel canisters, which are stored in a shielded cell at the facility awaiting future disposal in a geologic repository. Final closure of the underground tanks at West Valley is awaiting a final decision regarding the decommissioning of the facilities at the site.

Laboratory tank farm facility, tank cleaning was initiated in 2002 and, to date, seven of the eleven 1,136-m<sup>3</sup> [300,000-gal] tanks and all four of the 113-m<sup>3</sup> [30,000-gal] tanks have been cleaned (DOE–Idaho, 2005). After cleaning activities are completed for all of the tanks and ancillary equipment in the tank farm facility, DOE plans to stabilize the tank farm facility by filling the tank system with grout for final closure, which is planned for 2012. In late 2006, grouting three of the four smaller tanks at Idaho National Laboratory was completed. At the Savannah River Site, 2 of the 51 tanks (Tanks 17 and 20) were filled with grout and closed in 1997, and 3 other tanks (Tanks 16, 18, and 19) were cleaned and taken out of service. Plans are being finalized to grout and close Tanks 18 and 19. At Hanford, waste retrieval has been completed on only 4 of the 177 tanks, and options for tank closure at the site are still being evaluated (National Research Council, 2006).

As indicated in the preceding paragraph, DOE plans to close emptied tanks by filling the tanks with grout. One or more layers of engineered grout will be emplaced to (i) provide structural support (i.e., prevent potential collapse of the roof and wall due to the weight of the overburden and the lateral pressure from the surrounding soil), (ii) encapsulate and stabilize the residual tank waste and tank heel, and (iii) act as a physical barrier that would inhibit the flow of groundwater through the waste. Some tanks also would have a high-strength layer of grout that would serve as a barrier to penetration by plant roots or to inadvertent intrusion by burrowing animals or humans drilling or excavating at the site.

The DOE decision to use a cement-based material such as grout for tank closure and near-surface disposal (e.g., Saltstone Disposal Facility at the Savannah River Site) is partially based on the worldwide use of these materials to solidify and stabilize low- and intermediate-level radioactive wastes (International Atomic Energy Agency, 2004, 2000, 1999) and on the mature stage of development of this technology. The use of grout is standard technology that has stabilized Resource Conservation and Recovery Act heavy metals, such as chromium, lead, and mercury, and produced solid waste forms that meet the U.S. Environmental Protection Agency requirements (National Research Council, 1999). By immobilizing the waste and acting as a barrier around it, the cement-based material is expected to reduce the likelihood of radiological constituents being released from the waste and transported into the environment.

DOE performance assessment calculations rely on the ability of cement-based materials to serve as a barrier to (i) groundwater influx and (ii) release and transport of radionuclides from the grouted tanks and concrete vaults. As a result, quantitatively evaluating the influence of these materials in mitigating radionuclide release to the environment is an important component of performance assessments DOE conducted to demonstrate that tank closure and low-activity waste disposal in near-surface disposal facilities will meet the appropriate performance objectives (e.g., 10 CFR Part 61, Subpart C). In these performance assessments, assumptions are made regarding the physical integrity (e.g., hydraulic conductivity) and chemical condition (e.g., pH and Eh affecting radionuclide solubility and sorption) of the cement-based material. Because these performance assessment calculations typically are carried out to peak dose within 10,000 years, assumptions also are made regarding changes to the physical and chemical properties of the cement-based material to account for degradation that is expected to occur with time. For example, the performance assessment DOE conducted to support its plan to grout and close Tanks 18 and 19 at the Savannah River Site assumed that the grout maintains its ability to serve as an intact hydraulic barrier for 500 years and maintains its alkalinity and reducing capability for 10,000 years (DOE–Savannah River Site, 2005). In the Idaho National Laboratory tank farm facility closure performance assessment, the main assumptions include failure of the outer vault grout at 100 years, failure of the tank and tank

grout at 500 years, and persistence of the alkalinity and reducing capability of the grout for 10,000 years (DOE–Idaho, 2005). In the performance assessment DOE conducted to support its plan to dispose of waste onsite in the Saltstone Disposal Facility at the Savannah River Site, assumptions were made regarding the hydraulic conductivity of the concrete vault and saltstone and the changes in this property during the 10,000-year time period of interest (Cook, et al., 2005).

Although much research has been done on the use of cement-based materials for immobilizing and stabilizing toxic metals and radioactive wastes and some studies have been performed on the grout formulations DOE has used or plans to use for tank closure and near-surface vault disposal, understanding of the performance of the cement-based materials is largely based on laboratory experiments simulating simplified exposure conditions. These experiments are generally not more than a few years in duration and given the expectation of performance for 10,000 years, they are of limited value for quantitative extrapolation over this timeframe. Also, scaling effects are an issue: laboratory scale studies do not necessarily achieve the same short-term (1 to 2 years) properties as are achieved in larger scale trials.

A committee of the National Research Council of the National Academy of Sciences that evaluated the management of radioactive waste streams stored at Hanford, Savannah River Site, and Idaho National Laboratory reported that despite the considerable amount of work that DOE contractors had done, the committee had received little quantitative information to support the assumptions regarding grout performance in the DOE performance assessments (National Research Council, 2006). The committee stated that “the use of grout for the long periods involved in the disposal of radioactive waste (more than 100 years) is outside the general operating envelope for cement-based materials in industrial applications” and that “there are no good precedents for cement-based materials to maintain very low permeability to water and other properties necessary to retain radionuclides for the very long times required by DOE.” The U.S. Nuclear Regulatory Commission (NRC) staff, in its review of DOE performance assessments pertaining to the Saltstone Disposal Facility at the Savannah River Site and the tank farm facility at Idaho National Laboratory, also acknowledged the significant uncertainties in the DOE assumptions regarding the performance of the cement-based engineered barriers (NRC, 2006, 2005).

## **1.2 Objective of Report**

This report was prepared for NRC to provide information that can be used to support its independent evaluation of the DOE performance assessments related to tank closures and disposal of radioactive waste in near-surface disposal facilities. Because of the risk significance of engineered barrier performance to demonstrating the compliance of the DOE disposal actions with appropriate performance objectives, the NRC staff determined there is a need to understand the important mechanisms and parameters related to modeling cement-based material degradation for abstraction into radionuclide release models (Barr, et al., 2007).

Section 1 of the report provides background information on the use of cement-based materials in tank closures and disposal of radioactive wastes in near-surface disposal facilities at DOE sites. Section 2 reviews the nature of Portland cement, and Section 3 briefly discusses the hydration and setting of cement-based materials. Section 4 gives a general discussion of degradation mechanisms, broadly classified into chemical and physical processes, and the role of the service environment in the degradation of cement-based materials. Section 5 reviews several published models for predicting the chemical degradation of cement-based

materials—from simple diffusion or empirical equations to more complex coupled reactive-transport models. Section 6 discusses conceptual and mathematical models that can be used to evaluate the potential influence of fast pathways and bypassing pathways on radionuclide releases from grouted tanks. Section 7 summarizes and evaluates models and data available for estimating radionuclide release from cement-based waste forms. Section 8 assesses factors, as well as features, events, and processes, that are potentially important to evaluating the performance of grouted tanks and concrete vaults at DOE sites.

Additional information is provided in two appendices. Data derived from published literature related to the permeability and diffusion properties of cement-based materials are presented in Appendix A. In Appendix B, available data are reviewed and new models for solubility limits are developed for selected radioelements in environments expected in cement-based disposal facilities at the Savannah River Site and Idaho National Laboratory.

## 2 NATURE OF PORTLAND CEMENT

### 2.1 Production

Portland cement is a manufactured product made by carefully batching and grinding raw materials to achieve a constant target composition. The raw materials comprise primarily a calcareous material, such as limestone or chalk, and alumina and silica found as clay or shale. The physical mixture of reactants is heated in a large rotary kiln at high temperatures, typically 1,450 °C [2,642 °F], to achieve a series of mineralogical changes, and the resulting partially fused product, termed clinker, is cooled and again ground. The surface area of the ground product is typically on the order of 2,500–4,000 cm<sup>2</sup>/g [1,220–1,950 ft<sup>2</sup>/lb]. To put this surface area into perspective, the median particle size of the finished cement is on the order of 10–20 μm [ $3.9 \times 10^{-4}$  in]. During final grinding, several percent of calcium sulfate is introduced, typically as gypsum (CaSO<sub>4</sub>·2H<sub>2</sub>O), to delay the stiffening reactions that occur when cement is subsequently mixed with water.

The cement manufacturing process is continuous and on a large scale. Only few commercial kilns produce less than 2,000 metric tons/day [2,200 ton/day] of clinker. The process is rather inflexible, and in recent decades, it has become common practice to produce only a few types of cement except where a mixed market exists for special types (e.g., oil well cement). Property changes required in civil engineering applications are instead achieved by adding supplementary cement materials, such as fly ash, slag, or silica fume, to Portland cement and by using chemical admixtures.

### 2.2 Product Variability

Cements, even if nominally of the same composition, may vary in setting characteristics, and the manufacturer therefore will adjust the calcium sulfate type and content to achieve consistent times for initial setting and, thereafter, consistent final set times and strength gain. For example, the same cement may require variable sulfate addition between winter and summer, with more gypsum being added on hot days or in hot climates than in cold weathers. Civil engineers find benefit in rapid strength gain, and most manufacturers will also optimize compressive strengths, typically at 1, 3, 7, and 28 days.

### 2.3 Cement Products

Cement normally is mixed with sand and water to form mortar, or with sand and coarser mineral aggregate to form concrete. Free-flowing formulations, termed grout, are usually cement-rich mixes that may contain fine-grained aggregates. The mineral aggregates chosen for mortars, grouts, and concretes are not normally reactive with cement, although as will be shown in a later section, this may not be true particularly when millennial time scales are considered.

### 2.4 Supplementary Cement Materials

Many standards and specifications also permit adding supplementary cement materials as a partial replacement for cement. The supplementary materials must react with cement, eventually becoming an integral part of the binder, and this requirement, coupled with restrictions on availability and cost, limits the choice of supplementary cement materials. These supplementary materials are used to reduce heat evolution in the course of setting, to decrease the energy required to manufacture the batch, and to improve the physical structure of the

cement paste. The composition and physical characteristics of supplementary materials are generally governed by performance-related standards with secondary chemical and physical limits, but because many supplementary cement materials are themselves industrial wastes, performance-based specifications may permit large variations in composition, particle-size distribution, mineralogy, and other characteristics. The relevant standards are heavily biased toward short-term performance. While the permitted variations may not be important to civil engineering, in the context of nuclear waste immobilization they may significantly affect the properties of the resulting composite or blended cement. Thus, while Portland cements are relatively highly specified both by performance and prescription, the performance-based (for the most part) specifications of supplementary cement materials permit greater variability and, consequently, a broader envelope of compositions and physical characteristics. Examples will be given in a subsequent section.

Supplementary materials permitted by standards or specifications also may include powdered limestone. In the past, cements made with supplementary materials activated by Portland cement were referred to as “blended cements.” However, some codes now permit adding up to 5 percent of these supplementary materials to “Portland cement” without special labeling. This change is being debated in the United States and has the approval of ASTM International, American Concrete Institute, the manufacturing sector, and all states except California. Thus, national specification is subject to review and change. Therefore, “Portland cement” cannot be assumed to have constant composition or mineralogy. Moreover, permitted but undeclared supplementary materials can themselves exhibit substantial variability. In conventional cementing, rather low percentages of supplementary cement materials are often specified. However, cement in nuclear waste grouts may comprise much less than 50 percent of the total cementitious matrix such that more characterization data are needed for supplementary cement materials to assess realistic performance scenarios. For example, the engineered grout placements and encapsulation grout pours for closure of the tank farm facility at the Idaho National Laboratory have a mix design that includes 230 lb [104 kg] of cement, 118 lb [54 kg] of Class F fly ash, and 352 lb [160 kg] of ground blast furnace slag per cubic yard of product (Thorne, 2007).

## **2.5 Organic Matter in Cement**

Cements also may contain significant organic content. Organic matter arises from several sources. For example, many mills use so-called “grinding aids” to assist in reducing the particle size of finished clinkers. These grinding aids are surfactants of various kinds, of which amines (e.g., triethanolamine) and polyhydric alcohols are possibly the most effective (Taylor, 1997). Because the organic component has to be water dispersible, the organic molecule will usually contain a functional polar group or groups. However, as low-purity technical grades of the organic chemical are used as grinding aids, the precise molecular composition of the grinding aid is not defined, and a wide range of molecular units may be present. Additionally, the ball mills and ancillary machinery may leak traces of lubricant that becomes mixed with the product. Furthermore, gypsum added at the grinding stage is often of natural origin and may contain significant organic content. Thus, commercial Portland cement typically contains organic matter at the tens to hundreds of parts per million concentration. This content does not cause problems with civil engineering applications. However, suggestions to use organics in formulations intended for nuclear waste barriers often have been questioned because organics could act as potential complexants that could enhance the release and transport of radionuclides. In that context, note that commercial cements, as supplied, have a significant and varied organic content.

## 3 HYDRATION OF CEMENT

### 3.1 General Considerations

Owing to its commercial importance, thousands of papers and numerous books have been written on the hydration and setting of Portland cement. This report does not review these studies in detail, but certain conclusions relevant to the present applications should be noted.

Hydration and setting of cement are initiated by mixing a dry powder (clinker) with water. The fresh, wet mix has to be used normally within a few hours after mixing. Upon mixing with water, the clinker reacts to form hydrated cement paste, an interlocking network of solid phases that give the cement-based material its strength and stability. Several features of the setting and hardening process strongly influence the properties of the hardened product.

- The reaction between cement and water is chemical in nature. In the course of reaction, liquid water (sometimes termed mix water) is converted to chemically bound water. Thus, the cement hydration products contain a spectrum of bound water: some loosely bound, but much of which is more strongly bonded. Indeed, more water than required for hydration may be added; the excess water is referred to as pore water.
- The physical consequences of the hydration reactions are referred to as “setting” and “hardening.” Setting is stiffening without significant development of compressive strength and typically occurs within a few hours after mixing (Taylor, 1997). Hardening involves significant development of compressive strength and normally is a slower process than setting. The setting and hardening reactions are thermodynamically favored and occur spontaneously, although equilibrium may not be attained. Reactions leading to setting and hardening are irreversible.
- The nonequilibrium products of hydration are reproducible and are well characterized in the literature. Foremost among these phases and comprising >50 percent of the cement mass is an amorphous to poorly crystalline calcium silicate hydrate (C-S-H), variously referred to as “cement gel” or “tobermorite gel.” This phase is largely responsible for the strength and cementing properties of the hardened cement paste.
- The setting process involves the formation of colloidlike solids and, like most colloidal reactions, can be affected by chemical interferences. For example, some soluble components such as calcium chloride accelerate the setting process, whereas others such as lead or zinc salts, phosphates, or borates retard it. Various mechanisms have been proposed to explain the interference on the setting process, including effects on the precipitation or dissolution of cement phases, flocculation of the colloidlike solids, changes in the pH of the cement pore solution, precipitation of new solids, and sorption onto cement phases (van Eijk, 2001). The potential of soluble species present in the waste liquids and storage tank heels to interfere with the setting process may need to be considered.
- Hardening and strength gains of cementitious matrices continue after setting with further hydration reactions. Cement does not set by evaporation of water, as is sometimes supposed. Indeed, water may need to be conserved (e.g., by protecting fresh cement to reduce water evaporation) to ensure its proper hardening.

- The cement clinker is polymineralic. Initially, each mineral reacts separately with water. However, within minutes of the start of hydration, the constituent minerals begin reacting with each other via the aqueous phase as well as with water (the pH of which increases).
- Much of the early stage reaction between cement and water occurs by dissolution of anhydrous (or nearly so) clinker minerals, with subsequent precipitation of hydrated solids. However, as reaction proceeds, a thickening film of hydration product partially protects the residual anhydrous grains. The supply of water necessary to sustain this process must diffuse through the ever-thickening product layer. Thus, the initially rapid rate of reaction slows with time. Because the cement grains are small, the product layer likely is never more than a few tens of microns thick.
- The reaction of clinker with water is strongly exothermic (liberates heat). Because the thermal conductivity of cement-based material is relatively low, the material can act as an insulator and a large increase in temperature can result in the interior of a large mass of cement-based material due to hydration reactions. Therefore, excessive temperature rise in large masses of hydrating cement must be prevented to avoid thermal cracking.
- The hydrate mineralogy is also sensitive to temperature. Problems with formation of unstable (at lower temperatures) hydrate assemblages and concomitant dimensional changes in the posthardening period are best avoided by limiting the maximum temperature achieved during cement hydration.
- Cement hydration always results in a net shrinkage even if hydration occurs isothermally. Shrinkage occurring within an already hardened matrix will somewhat increase porosity but, if not controlled, also will lead to cracking.
- Hardened cement is an intrinsically brittle material, and for that reason, cracking is a commonly encountered response to thermal cycling due to hydration reactions as well as to internal changes in the specific volume of its constituent solids.
- The water content, often expressed as the water/cement weight ratio, is an important design parameter. On one hand, too little water will not give a flowable or pumpable mix. On the other hand, too much water will give an excessively porous structure with relatively low strength.
- As with other porous materials, pores present in hardened cement can be disconnected and have little influence on the overall permeability of the material. But as the connectivity of pores increases, the permeability increases.
- The measurement of either porosity or permeability is complex. Different techniques applied to the same material can give substantial divergence in measured values, although similar trends in porosity or permeability are generally obtained when comparing different materials. A review of literature data on the permeability and diffusion properties of cement-based materials is presented in Appendix A of this report.
- The quality of cement matrices depends in part on formulation, mixing, and emplacement, as well as execution. The long-term performance depends to a significant extent on the quality of the emplaced cement-based material that, in turn, relates to the previously noted considerations. Low cement quality due to poor mix design cannot be rectified subsequently. Poor site practices will impair the best mix design.

- Many factors affect scaling up from laboratory-sized formulations to full-scale emplacement, but robust mix design, coupled with experience of grouting and actual trials, should anticipate these problems and reduce the impact of scaling effects to within acceptable limits. Nonuniform mixing and segregation in the course of placement are associated with full-scale emplacement and are less common in the laboratory.
- The ultimate strength of cement matrices is controlled by hydrogen bonding. These hydrogen bond forces are high in Portland cement and manifest at an early stage. Thus, the solids are coherent and flocculate even in the presence of excess water. This strong tendency to flocculate enables cement and cement-based products (mortars, concretes) to be emplaced under water. This property is referred to as “hydraulic.” Thus, Portland cements comprise a class of hydraulic cements, distinct from other nonhydraulic types, which do not harden under water.
- While hardened cement may attain high compressive strengths, perhaps up to 200 MPa, it remains weak in tension. Like glass and ceramic, it is inherently brittle. If tensile and impact forces in the service environment are anticipated, the use of reinforcements need to be considered.
- The permeability of hardened cement paste free from flaws is comparable within an order of magnitude with that of granite and other dense rocks {i.e., on the order of  $10^{-13}$  m/s [ $3 \times 10^{-13}$  ft/s]}. In practice, however, higher values are frequently encountered. Permeability is enhanced by the use of high water/cement ratios as well as the presence of poor packing at interfaces, for example, between cement and aggregate or between cement and steel. Cracks, of course, also increase permeability.
- Portland cements have been in use since the 1820s and, consequently, there is much information about their durability and performance. Although this information often relates to aboveground exposures and fluctuating service conditions, considerable generic experience shows the durability of cements and concretes over nearly two centuries.
- The above considerations also apply to cement containing supplementary cement materials but over shorter time scales, perhaps 100 years. But because supplementary cement materials differ in physical and chemical characteristics from Portland cement, range widely in composition and granulometry, and also react at different rates, each class of supplementary cement material must be considered separately to assess its impact on future properties of cement-based materials.

### 3.2 Cement Hydration Products

Cements comprise six principal oxides: CaO, Al<sub>2</sub>O<sub>3</sub>, Fe<sub>2</sub>O<sub>3</sub>, SiO<sub>2</sub>, SO<sub>3</sub>, and H<sub>2</sub>O. If the cement has been blended with calcium carbonate, a seventh component, CO<sub>2</sub>, has to be added to the list. Together these oxides comprise approximately 98 percent by weight of the total mass. In the course of hydration, four solid phases or families of phases develop as shown in Table 3-1. The most abundant phase is designated as C-S-H (CaO–SiO<sub>2</sub>–H<sub>2</sub>O). The C-S-H phase is a rigid but relatively noncrystalline gellike substance. It does not have an exact water content, because it contains nanoscale pores that hold weakly bound water as well as a spectrum of more strongly bonded water necessary to form the C-S-H structure. Some of this water varies reversibly in amount with changing temperature and relative humidity. C-S-H generally has an atomic Ca/Si ratio in the range 1.7–2.0—again the exact ratio is in dispute—and is possibly

variable depending on the possibility of intercalating  $\text{Ca(OH)}_2$ . The crystalline phases have definite compositions or compositions variable over definite limits. Table 3-1 gives representative compositions for these phases. A standard compilation (National Research Council, 1972, entry XII-D, p. 19) notes the variable composition of C-S-H and associates the reported x-ray pattern with the formula  $1.5\text{-}2.0\text{CaO} \cdot \text{SiO}_2(\text{H}_2\text{O})^n$ , where n is indefinite.

Table 3-1 is an approximate guide to the mineralogy of a normally hydrated cement paste. Minor replacement of aluminum by iron is not shown. Cements cured at higher temperature and cement undergoing alteration in its service environment may lead to the development of other phases, as described in a subsequent section.

In addition to the solid phases, most cementitious formulations contain excess water not consumed by hydration (i.e., water exceeding the amount required to satisfy the chemical hydration of the solids). Calculation of the amount of water required, and hence the boundary between just enough water and excess water, is complicated by a number of factors: slow hydration of certain clinker phases that may persist for decades, even slower hydration of supplementary cement materials, and the difficulty of distinguishing between the “free” and “bound” water contents. Brouwers (2004) reviewed these problems in a historical context. However, for plain Portland cements, the boundary lies at a water/cement weight ratio of about 0.30–0.35 (i.e., formulations made to higher water/cement ratios and not subjected to evaporation will contain a permanent excess of water). This water will typically dissolve some cement substances.

Calculation supported by expression of pore fluid at high pressure from commercial cements (Taylor, 1987) shows that at 20 °C [68 °F], the composition of Portland cement pore fluid becomes nearly constant after a few weeks of hydration. The pore fluid has a high pH—in the range 12.5–14. The higher end of that pH range, above the value (pH ~12.5) conditioned by the solubility of portlandite [ $\text{Ca(OH)}_2$ ], arises from the slight sodium and potassium contents of commercial cement, much of which is readily soluble. The solubility of sodium and potassium, effectively present as hydroxides, suppresses calcium solubility. Hydration at higher temperatures above 40 °C [104 °F] tends to enhance the solubility of sulfate in the pore fluid.

Less is known about the long-term evolution of the pore fluid of cement formulated with supplementary cement materials such as fly ash. In the medium term—up to a few years—reaction of fly ash incorporates alumina into C-S-H, and the Ca/Si ratio of C-S-H

<b>Table 3-1. Mineralogy of Hydrated Portland Cement</b>			
<b>Crystallinity</b>	<b>Mineral Name</b>	<b>Shorthand</b>	<b>Representative Formula</b>
Low	(none)	C-S-H	$1.7\text{CaO} \cdot \text{SiO}_2 \cdot 2\text{H}_2\text{O}$
High	Portlandite	CH	$\text{Ca(OH)}_2$
High	Ettringite	C6A\$3H32*	$3\text{CaO} \cdot \text{Al}_2\text{O}_3 \cdot 3\text{CaSO}_4 \cdot 32\text{H}_2\text{O}$
High/medium	Hydrocalumite†	C4A\$H12-19	$4\text{CaO} \cdot \text{Al}_2\text{O}_3 \cdot \text{SO}_3 \cdot 12\text{-}19\text{H}_2\text{O}$
*\$ is cement literature shorthand for sulfur. †Hydrocalumite has 2OH in place of SO <sub>4</sub> .			

decreases. As a consequence, the sorption potential of the chemically modified C-S-H for alkali increases (Glasser, 1992), and alkalis have less impact on pore fluid chemistry. The same effect occurs for slag but is less marked.

If cement and concrete are exposed to drying conditions, pore fluid will be lost by evaporation from the surface of the material. The amount of water lost is influenced by temperature, ambient relative humidity, and wind velocity (Taylor, 1997). This loss of water can lead to shrinkage and to surface cracking. Also, the water-filled pores simply can become empty pores (i.e., gas filled) after evaporation. This porosity is important because it affects degradation processes such as carbonation.

## 4 DEGRADATION OF CEMENT-BASED ENGINEERED BARRIERS

An important factor that is considered in evaluating the safety case for cement-based nuclear waste repositories is the performance lifetime of cement-based engineered barriers. For example, for tank closures and waste disposal in near-surface facilities at the U.S. Department of Energy (DOE) sites in Aiken, South Carolina, and Idaho Falls, Idaho, DOE expects concrete vault and grouted waste forms to provide significant barriers that would mitigate the release and transport of radionuclides to the environment. Performance assessments conducted to determine whether disposal actions at these sites will meet performance objectives typically make assumptions regarding the physical and chemical integrity of the cement-based engineered barriers. Assumptions also are made regarding changes in the properties of these barriers due to degradation that is expected to occur during the long time period of interest—typically 10,000 years. These assumptions generally are based on current knowledge of degradation mechanisms of cement-based materials. Much of this knowledge is derived from a mixture of civil engineering experience and focused laboratory testing. The abundance of these experiences is not surprising: Portland cement has been in use since its invention and marketing by Joseph Aspdin in 1824 and has been used in a wide range of environmental exposures. Compositions and specifications have changed somewhat with time, but the original Aspdin product still bears a close generic relationship to commercial products supplied today. So the accumulated literature on cement degradation is relevant to the present issue of cement-based engineered barrier performance.

A variety of degradation mechanisms can compromise the performance lifetime of cement-based materials. The more important mechanisms identified in the literature are discussed in this section, but only in a general sense; degradation mechanisms potentially important to grouted tanks and concrete vaults are assessed in Section 8. The various mechanisms can be classified broadly into chemical and physical processes. However, note that chemical and physical mechanisms act in a synergistic manner and degradation of cement-based materials seldom can be ascribed to an isolated process. The primary chemical degradation mechanisms for cement-based materials discussed in this report are (i) carbonation, (ii) sulfate attack, (iii) leaching, (iv) corrosion, and (v) alkali–silica reaction. The main physical degradation mechanisms discussed are (i) shrinkage, (ii) thermal cracking, and (iii) freeze–thaw.

### 4.1 Chemical Degradation Mechanisms

#### 4.1.1 Carbonation

Carbonation is considered the most common chemical reaction affecting the performance of cement-based materials in natural environments (Macias, et al., 1997). Carbonation involves the reaction of dissolved carbonate species, originating mainly from atmospheric  $\text{CO}_2(\text{g})$ , with the cement. Much has been written about the interaction of  $\text{CO}_2$  and cement. This literature and the implication of  $\text{CO}_2$ –cement interaction to degradation of cement-based materials become clearer if carbonation is classified into two types according to mechanism: (i) carbonation through the gas phase and (ii) carbonation through the aqueous phase. Both types could be relevant to grouted tank performance, but require different treatments. Although both types of carbonation involve the interaction of the cement-based material with an aqueous phase, dissolution reactions are relatively unimportant in the former type compared to the latter. Carbonation through the gas phase, detailed in this section, involves the reaction of  $\text{CO}_2$  with the calcium component of the cement, resulting in the precipitation of calcium carbonate.

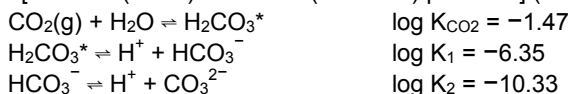
Carbonation through the aqueous phase is characterized by rapid dissolution of the cement matrix, often with comparatively little accumulation of solid calcium carbonate; this process is detailed in the section on leaching (Section 4.1.3).

Carbonation through the gas phase is important to consider as a degradation mechanism because CO<sub>2</sub> is an essential gaseous component of the atmosphere and is present in the pores of unconsolidated materials, such as soils, and in aqueous solutions (e.g., rain, fresh and saline waters). Thus, it is a mobile and abundant geochemical component, in addition to being strongly reactive with Portland cement. The concentration of CO<sub>2</sub> in the standard atmosphere is about 380 ppm (equivalent to about  $3.5 \times 10^{-3.5}$  atm) and is rising, with predictions it may reach 500 ppm before the end of this century. The level of CO<sub>2</sub> in soil and unconsolidated earth media is much influenced by biological activity (including decay of organic matter) and also by dissolution of minerals and emanations from deeper levels of the Earth's crust. Additionally, a number of CO<sub>2</sub> removal mechanisms exist in seawater (e.g., exoskeleton formation by corals and shellfish). Thus, CO<sub>2</sub> concentration may fluctuate from place to place and, at shallow terrestrial depths, may vary seasonally with biological activity, temperature, precipitation, and recharge. In seawater, near-surface layers approach saturation with respect to the standard atmosphere concentration of CO<sub>2</sub>. However, the concentration does not increase with depth as predicted from ideal gas theory, mainly because of slow mixing and active removal by biological activity and mineral formation as well as by sequestration in the course of alteration of subsea basalts.

Cement products exposed to the atmosphere undergo carbonation by sorption of gaseous CO<sub>2</sub>. The equilibrium and kinetic aspects of CO<sub>2</sub> sorption by cement are well understood. Dow and Glasser (2003) and Glasser and Matschei (2007) presented models for different aspects of reaction involving formation of a thin film of water on cement solids; Table 4-1 shows the principal stages. The reaction requires a little moisture to proceed because the first step is dissolution of CO<sub>2</sub> gas in a film of moisture at the surface of cement grains. The fine pore structure of cement enables a film of water to condense spontaneously across a broad range of humidity due to capillary effects, so conditions for carbonation to occur are not unlikely. CO<sub>2</sub> gas is rapidly hydrated upon dissolution, and the aqueous species is described formally as CO<sub>2(aq)</sub> (i.e., dissolved molecular CO<sub>2</sub>). Dissolved CO<sub>2</sub> gradually ionizes to form bicarbonate and carbonate species (HCO<sub>3</sub><sup>-</sup> and CO<sub>3</sub><sup>2-</sup>, respectively) as well as protons, H<sup>+</sup>.<sup>1</sup> Because protons are produced, the solution becomes acidic. These reactions are observed in everyday life; for example, rain is normally slightly acidic owing to dissolution and ionization of CO<sub>2</sub>, with bicarbonate as the main ionized species.

However, when condensation occurs onto Portland cement, the cement buffers the pH of the water film to high values. Under these conditions of high pH, the main dissolved CO<sub>2</sub> species is carbonate (CO<sub>3</sub><sup>2-</sup>). Across the range of CO<sub>2</sub> pressures and temperatures likely to be encountered in atmospheric or shallow subsurface exposure, which may include near-surface low-level waste disposal sites, all cement substances will react with CO<sub>2</sub>. The most significant

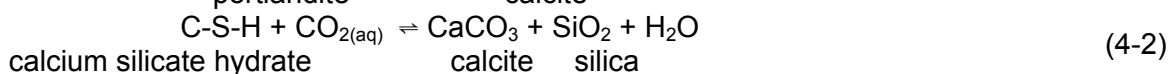
<sup>1</sup>Chemical equilibria involving CO<sub>2(g)</sub>, HCO<sub>3</sub><sup>-</sup>, and CO<sub>3</sub><sup>2-</sup> are described by the following reactions and equilibrium constants [at 25 °C (77 °F) and 1 bar (0.99 atm) pressure] (Langmuir, 1997):



where H<sub>2</sub>CO<sub>3</sub>\* = CO<sub>2(aq)</sub> + H<sub>2</sub>CO<sub>3</sub>. The concentration of H<sub>2</sub>CO<sub>3</sub> in solution is less than 0.3 percent the concentration of CO<sub>2(aq)</sub> {at 25 °C [77 °F]}. Because it is difficult to distinguish between H<sub>2</sub>CO<sub>3</sub> and CO<sub>2(aq)</sub> analytically, the quantity H<sub>2</sub>CO<sub>3</sub>\* is generally reported in water analyses. In some references, H<sub>2</sub>CO<sub>3</sub>\* is called carbonic acid and H<sub>2</sub>CO<sub>3</sub> is referred to as *true* carbonic acid.

<b>Table 4-1. Carbonation Mechanisms of Portland Cement Grouts in Humid Atmospheres</b>	
<b>Mechanistic Description of Step</b>	<b>Comment</b>
(1) Gaseous CO <sub>2</sub> dissolves in water	Transport of CO <sub>2</sub> occurs across an air–water interface
(2a) Equilibration of CO <sub>2</sub> with water (2b) Dissolution of calcium, silica, hydroxyl, and other species from cement	Formation of CO <sub>2</sub> (aq), HCO <sub>3</sub> <sup>-</sup> , and CO <sub>3</sub> <sup>2-</sup> ; kinetics accelerated by hydroxyl ions
(3a) Diffusion of carbon species through the aqueous phase toward cement solids (3b) Dissolution of calcium from cement solids	As solids dissolve/react, additional water is liberated
(4) Precipitation of calcium carbonate	Thickening product layer slows reaction; calcium carbonate precipitates as calcite, aragonite, and vaterite, or mixtures thereof
(5) Formation of other solid phases	Hydrous alumina, silica, and iron oxide necessary to balance reaction
(6) Development of zoned attack layer	Changes in pH and mineralogy do not meet conditions for application of Fick's laws

carbonation reaction occurs with portlandite, but reaction also occurs with C-S-H. The products of reaction are invariably calcium carbonate, as in the following reactions



Carbonation initially decalcifies the C-S-H gel (i.e., reduces the Ca/Si ratio of the C-S-H); further reaction destroys the C-S-H, with formation of hydrous silica and calcium carbonate (Taylor, 1997). Thus, for Portland cement, the stoichiometry of carbonation can be calculated from the mass of calcium per unit volume. The stable phase of calcium carbonate typically is calcite, but two other polymorphs, aragonite and vaterite, are frequently observed.

The mass balances of this process are completed by noting that water is liberated: all calcium carbonate polymorphs are essentially anhydrous, resulting in a net release of water. This liberated water can contribute to the film of water required to sustain the reaction. Under constant conditions, the rate of reaction tends to be self-regulating: excess water fills the pore network, decreases the geometric area available for diffusion of gaseous CO<sub>2</sub>, and slows the carbonation reaction. That is why the reaction slows at high humidity; to facilitate carbonation, the optimum relative humidity is 50–70 percent. However, note that although liquid water is essential to facilitate the reaction, the mass of water relative to the mass of cement is never sufficient to dissolve a significant fraction of the total mass of cement solid. Thus, the overall mass balances are comparatively simple: CO<sub>2</sub> is gained as carbonate, and water is lost. Dissolution and leaching are not significant factors during carbonation through the gas phase,

except insofar as local recrystallization of the matrix occurs as the carbonation “front” penetrates to greater depths within the cement.

The physical and chemical consequences of carbonation have important impacts. One of these is carbonation shrinkage. However, the resulting surface microcracking is unlikely to be continuous, and carbonation shrinkage does not normally disrupt the cement-based material. Carbonation has an indirect effect important specifically to cement-based materials with embedded steel (e.g., concrete vaults with steel reinforcements): it reduces the pH of the cement pore water. For example, a saturated solution of portlandite has a pH about 12.5, whereas after carbonation, the pH is controlled mainly by the solubility of calcite. At equilibrium with the standard atmosphere CO<sub>2</sub> concentration and a temperature of 18 °C [64 °F], the solubility of calcite is  $5.5 \times 10^{-4}$  molal and the pH of the saturated solution is 8.28. At the lower pH, the passive oxide layer on the steel surface that protects it from corrosion is destabilized, thus allowing corrosion to occur if oxygen and moisture necessary for corrosion reactions are present (see Section 4.1.4).

Carbonation can have a positive effect on performance. Because calcite has a greater molar volume than the portlandite it replaces, the permeability of the cement-based material can be reduced by calcite precipitation in the pore spaces. The overall effect could be an increased resistance to other chemical degradation mechanisms that are controlled by the permeability of the material. Carbonation also could immobilize radionuclides such as Cs-137 and Sr-90 from nuclear waste mixed with cementitious material, as Komarneni and Roy (1981) experimentally demonstrated. In this case, the action of CO<sub>2</sub> helped form a chemical barrier to cesium and strontium migration by forming insoluble carbonate solids. Bin-Shafique, et al. (1998) also observed that carbonation reduced the leaching rate of strontium from cementitious waste forms. However, the leaching rates of cadmium, cobalt, calcium, lead, and nitrate were observed in that study to increase upon carbonation, which the authors ascribed to “microcracking and/or the rearrangement of pores to remove or decrease occluded areas” in the carbonated samples (Bin-Shafique, et al., 1998). Strontium was interpreted to be more tightly bound in the carbonated waste form through solid solution in calcium carbonate.

The rate of carbonation depends on the rate at which the reactive species can diffuse through the pore system of the cement-based material. This diffusion is orders of magnitude faster in air (as CO<sub>2</sub> gas) than in water (as dissolved CO<sub>2(aq)</sub>, HCO<sub>3</sub><sup>-</sup>, or CO<sub>3</sub><sup>2-</sup> species); thus the rate of carbonation depends on the moisture content of the cement-based material, and wetting–drying cycles enhance the carbonation reaction by imbining CO<sub>2</sub>-containing water into the pore network. The wetting time, as well as the frequency and duration of wetting–drying cycles, are important factors. Because wetting of cement-based materials is faster than drying, more frequent, shorter periods of wetting are more effective in reducing carbonation progression than less frequent, longer periods of wetting (Bertolini, et al., 2004).

The permeability of the cement-based material through which the carbonate species must diffuse also strongly influences the carbonation rate. Thus, factors that affect permeability, such as cement mixture composition, water/cement ratio, and degree of hydration, also influence the carbonation rate (Neville, 1996). The lower the cement content and the higher the water/cement ratio, the greater the carbonation progression; the influence of cement content appears to be less significant compared to the water/cement ratio (Thiéry, 2006).

At constant temperature and humidity, carbonation generally progresses proportional to the square root of time (t) as in the following equation

$$D = xt^{1/2} \quad (4-3)$$

where  $D$  is the depth from the surface and  $x$  is a material parameter that depends on the resistance of the matrix to permeation. To quantify the carbonation reaction, the rate at which  $\text{CO}_2$  replenishment will occur and the effective activity of  $\text{CO}_2$  in the near-field environment are needed.

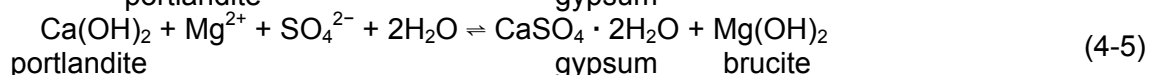
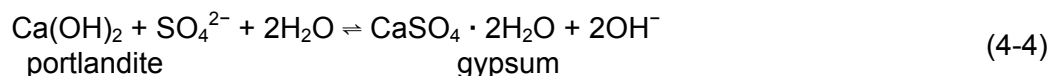
The use of supplementary cement materials, such as blast furnace slag, fly ash, or silica fume, may enhance carbonation. The mineral additions decrease the amount of portlandite in the hardened cement paste so that a lower amount of  $\text{CO}_2$  is needed to remove all the portlandite and decrease the pH of the cement-based material. On the other hand, pozzolanic reactions between Portland cement and supplementary cement materials, which involve an attack by  $\text{OH}^-$  ions from the former on the  $\text{SiO}_2$  or  $\text{Al}_2\text{O}_3\text{-SiO}_2$  framework of the latter (Taylor, 1997), result in a denser structure of the hardened cement paste, which decreases the  $\text{CO}_2$  diffusion coefficient and slows carbonation. Thus, the lower alkalinity of cements due to the addition of supplementary cement materials can be compensated by the lower permeability of the hardened cement pastes (Bertolini, et al., 2004). Which factor prevails depends on the circumstances of each situation.

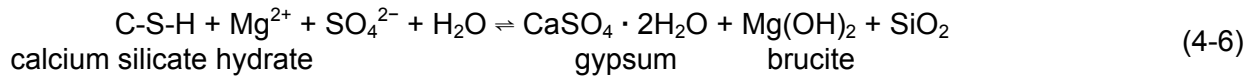
The products of carbonation of cement-based materials rich in fly ash and blast furnace slag, such as those proposed for grouting tanks at DOE sites, are not well established, but a reduction of pH almost certainly will accompany carbonation. The pH reduction implies (i) loss of ability, associated with high pH, to immobilize certain radionuclides, such as uranium, thorium, and actinides, through sorption and precipitation; (ii) disruption of the passivation of embedded steel (if relevant) and tank walls and onset of more rapid corrosion; and (iii) possible release of radionuclides formerly precipitated in the high pH regime. Normal Portland cements do not tend to lose strength or coherence in the course of carbonation, but it remains to be established whether this behavior extends to DOE grout formulations.

#### 4.1.2 Sulfate Attack

Sulfate attack is a process whereby sulfate ions in solution chemically react with compounds present in hydrated cement. This process can lead to disruptive expansion, strength loss, and/or disintegration, depending on the circumstances. For cement-based materials buried in soils, sulfate attack can be a common form of degradation because sulfates of sodium, potassium, calcium, and magnesium occur in groundwater and soil pore waters naturally or from anthropogenic sources. In cement-based waste forms, the waste itself could be a source of sulfate.

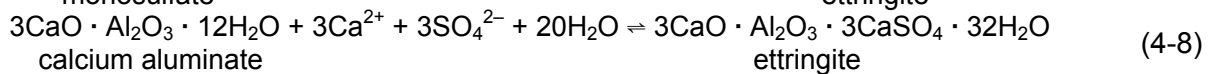
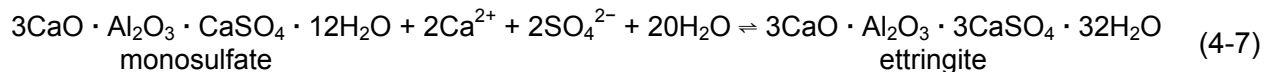
Although all the soluble sulfates adversely affect cement, the mechanism and severity of attack depend on the cation present in solution. The usual chemical reactions with aqueous sulfate can be represented as follows





For solutions containing dissolved sodium sulfate, sulfate attack is caused by reaction with sulfate ions (Reaction 4-4), whereas for solutions containing dissolved magnesium sulfate, both sulfate and magnesium ions participate in the degradation reaction (Reactions 4-5 and 4-6). Studies have shown that, other factors being equal, magnesium sulfate solutions are more aggressive than sodium sulfate solutions of the same concentration. Reactions of cement phases with magnesium sulfate solutions (Reactions 4-5 and 4-6) are enhanced by the very low solubility of brucite.

For solutions with dissolved calcium sulfate, additional reactions can be represented by



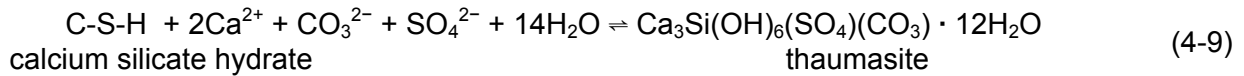
The resulting products, gypsum and ettringite, have a greater volume than the solids they replace and thus lead to expansion. Deleterious expansive sulfate reactions commonly are ascribed to the formation of ettringite because of its much larger molar volume compared to gypsum {710 cm<sup>3</sup>/mol [43 in<sup>3</sup>/mol] for ettringite versus 75 cm<sup>3</sup>/mol [4.6 in<sup>3</sup>/mol] for gypsum}, although damage due to gypsum formation also has been proposed (Tian and Cohen, 2000). In addition, decalcification and destruction of C-S-H, which is the major binding component of hydrated Portland cement, lead to a loss of strength and disintegration of the hardened cement paste; this process is particularly serious for magnesium sulfate solutions because these solutions attack both C-S-H and portlandite.

Sulfate attack is controlled by diffusion of sulfate ions into the saturated pores of the cement-based material. Therefore, susceptibility to sulfate attack is lower for materials with lower permeability. Also, the resistance of plain Portland cement to sulfate attack decreases with increasing content of tricalcium aluminate in the clinker; indeed, a sulfate-resisting Portland cement, referred to in the United States as Type V cement, was developed with a reduced tricalcium aluminate content. The resistance to sulfate attack also can be increased by adding supplementary cement materials, such as fly ash, blast furnace slag, and silica fume, in the mixture. The silica in such materials reacts with portlandite, thus diminishing the portlandite that could react with sulfate ions to produce gypsum. More importantly, the pozzolanic reaction significantly reduces the permeability of the hydrated cement, thus preventing the ingress of sulfate into the cement-based material.

The rate at which sulfate attack of cement-based materials occurs depends also on the rate at which the sulfate removed by the reaction with cement is replenished. Thus, in evaluating the potential for sulfate attack on buried cement-based materials, groundwater movement must be considered. Sulfate attack will be less severe in stagnant groundwater than in flowing groundwater.

Under conditions of high humidity and temperatures of around 5–10 °C [41–50 °F], sulfate solutions can attack cement-based materials to produce thaumasite

[Ca<sub>3</sub>Si(OH)<sub>6</sub>(SO<sub>4</sub>)(CO<sub>3</sub>) · 12H<sub>2</sub>O] if reactive silicate is present and there is an adequate supply of carbonate ions as represented by the following reaction



Thaumasite formation has more serious consequences than ettringite formation; it decomposes C-S-H and thus destroys the binding capacity of the cement paste. Because degradation involves the silicate and not the aluminate component of the hardened cement paste, sulfate-resisting Portland cement does not appear to offer any special protection against thaumasite formation. However, there are only a few cases in which thaumasite formation has been identified as the principal cause of deterioration (Taylor, 1997).

### 4.1.3 Leaching

Leaching is a process by which a liquid dissolves and removes the soluble components of a material. Leaching by percolating or flowing water can sometimes severely damage cement-based materials (e.g., in dams, pipes, or conduits) and can potentially degrade cement-based engineered barriers used in long-term storage of nuclear wastes (Taylor, 1997). Water can dissolve soluble phases in the hydrated cement paste, preferentially portlandite, but also the silicate and aluminate phases. These phases are stable under the alkaline pH condition of the cement pore waters, but are susceptible to dissolution when exposed to waters with much lower pH. For example, pure water in equilibrium with atmospheric CO<sub>2</sub> gas (10<sup>-3.5</sup> atm) has a pH of 5.6, but in soil environments, the pH could be even lower due to higher CO<sub>2</sub> concentrations resulting from biogenic activity, which would lead to higher leaching rates. The attack is severe at pH values below 5.5 and very severe at pHs lower than 4.5 (Neville, 1996). Soil organic acids, if present, may enhance the lowering of pH and leaching.

Experimental studies on leaching have shown that when cement contacts a reservoir of water having an ionic composition different from (typically lower in concentration than) that of the cement pore solution, various ions diffuse, driven by the concentration gradient between the pore solution and external water. For example, calcium and hydroxide ions in cement pore water diffuse outward toward the external water. Because the system is in chemical disequilibrium, dissolution also occurs. Typically, portlandite is the first cement phase to dissolve because of its high solubility, followed by the less soluble monosulfate, and then ettringite. Lastly, C-S-H is progressively decalcified and transformed into a silica gel. Thus, the leached zone is characterized by a succession of dissolution fronts, as represented in Figure 4-1 (Kamali, et al., 2004) and Table 4-2 (Lagerblad, 2001). If the groundwater contacting the cement contains carbonate and magnesium ions, these ions diffuse inward, resulting in precipitation of calcite at or near the surface and magnesium enrichment in the silica gel layer, as indicated in Table 4-2. Table 4-2 also shows there is a progressive increase in porosity from Zone 6 through Zone 3 as dissolution of the cement phases occurs, but this trend is reversed in Zones 1 and 2 due to precipitation of calcite.

Leaching of cement-based materials is enhanced by the presence of dissolved CO<sub>2</sub>, a mechanism referred to in Section 4.1.1 as carbonation through the aqueous phase. This process is characterized by rapid dissolution of the cement matrix with comparatively little solid calcium carbonate accumulation. This process is more complex than carbonation through the gas phase (discussed in Section 4.1.1) because of three additional factors: (i) an excess of water, which can dissolve cement substances; (ii) the speciation and concentration of CO<sub>2</sub> in

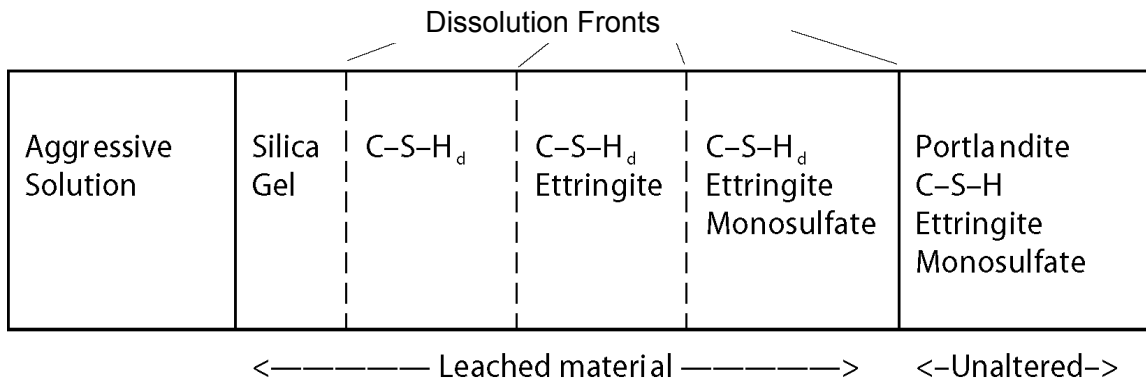


**Figure 4-1. Leaching Zones in Hydrated Portland Cement Leached by Pure Water (Kamali, et al., 2004) [C-S-H<sub>d</sub>—Decalcified C-S-H]**

**Table 4-2. Representation of the Zonal Pattern in Leached Concretes\***

	Zone 1	Zone 2	Zone 3	Zone 4	Zone 5	Zone 6
<b>Phases†</b>	Calcite Silica Gel Hydroxides	Silica Gel Calcite Hydroxides	Silica Gel C-S-H† Hydroxides	C-S-H(2) Ettringite	C-S-H(1) Ettringite	C-S-H Portlandite Ettringite
Al <sub>2</sub> O <sub>3</sub> content	High	Medium	Low	Low	Low	Low
MgO content	High	Medium	Low	None	None	None
CaO/SiO <sub>2</sub>	<0.1	<0.5	0.5–1.0	~1.0	1.0–1.6	1.6–1.7
Ca concentration (mmol/kg)	Low	<2	< 4	<10	10–20	>20
Si concentration (mmol/kg)	1.5	4.2	1.5	1.5	< 1	< 1
pH	7	~10	10.0–10.5	>10.5	10.5–12.4	>12.4
Porosity	Low	Medium	High	Medium	Low	Very Low

\*Lagerblad, B. "Leaching Performance of Concrete Based on Studies of Samples From Old Concrete Constructions." TR-01-27. Stockholm, Sweden: Swedish Nuclear Fuel and Waste Management Co. 2001.  
†C-S-H(2) has less volume than C-S-H(1). The silica gel also contains Al<sub>2</sub>O<sub>3</sub> and MgO. The MgO content and CaO/SiO<sub>2</sub> ratio are approximate and relate to the content in silica gel.

water vary significantly with wide-ranging consequences to performance of cement-based materials in natural environments; and (iii) water may contain ions other than carbon species that are deleterious to cement [the effect of other ions (e.g., Mg<sup>2+</sup> and SO<sub>4</sub><sup>2-</sup>) are discussed in other sections]. Biehl (1928) was the first to quantify the importance of dissolved CO<sub>2</sub> and apply the concept of "aggressive CO<sub>2</sub>". This concept arises from the fact that dissolved CO<sub>2</sub> undergoes a series of complex reactions in the presence of calcium carbonate and forms aqueous carbonate species, resulting in reduced solution acidity and only a portion of the total dissolved CO<sub>2</sub> available to react with cement phases (Cowie and Glasser, 1992). Biehl (1928)

graphically derived values of aggressive  $\text{CO}_2$  content based on conventional water analysis and correlated the observed deterioration of water culverts that had been in service for 20 years with the aggressive  $\text{CO}_2$  content. He concluded that deterioration had taken place only in concrete that had been exposed to water containing more than 17 ppm aggressive  $\text{CO}_2$ . This limit is arbitrary and depends on the definition of acceptable damage. Other authors, notably Pistors (1963) and Roger (1973), have avoided the necessity of determining aggressive  $\text{CO}_2$  content by constructing graphs or tables that classify groundwater compositions deleterious to cement-based structures. Figure 4-2 illustrates the relative aggressivity of natural waters toward Portland cement depending on the dissolved concentration of bicarbonate ion and excess  $\text{CO}_2$ . Alternatively, a modeling approach can be used to understand aggressivity of  $\text{CO}_2$ -containing water, for example, as Cowie and Glasser (1992) presented. Using data Plummer and Busenberg (1982) calculated and measured, Cowie and Glasser (1992) demonstrated that the relevant equilibria can be solved readily using MINEQL, a computer program for calculating chemical equilibria in aqueous systems. For example, Figure 4-3, taken from Cowie and Glasser (1992), illustrates the aggressivity to cements of groundwater relative to pure water as a function of dissolved  $\text{CO}_2$  concentration. These various studies show that a wide range of acidic,  $\text{CO}_2$ -containing waters exist, which are orders of magnitude more deleterious to cement than plain water, mainly as a consequence of their enhanced ability to dissolve cement phases. The occurrence of waters potentially aggressive to cement-based materials is site specific, but disturbance caused by construction or waste decomposition affecting  $\text{CO}_2$  balances also needs to be taken into account in assessing aggressivity.

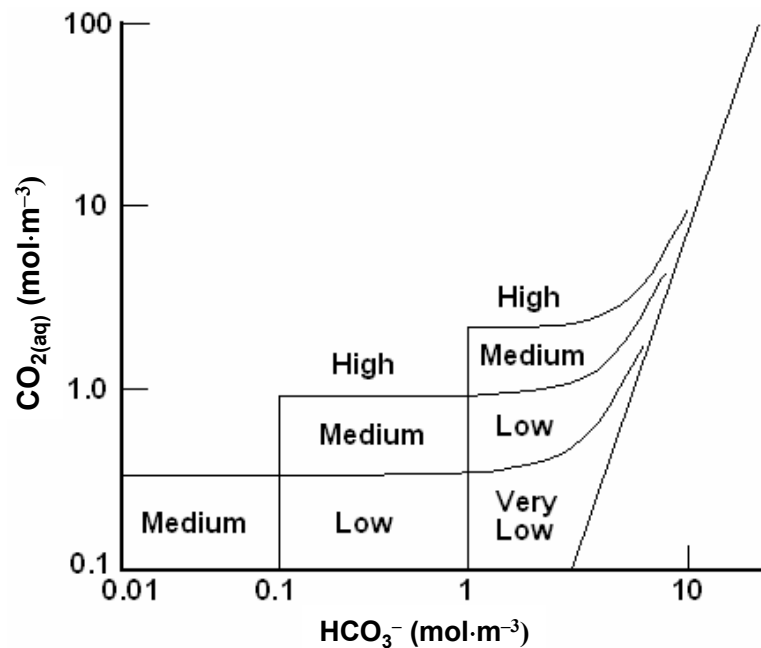


**Figure 4-2. Empirical Correlations Showing the Impact of Natural Waters Containing Dissolved Carbon Dioxide on Portland Cement. Reprinted From Cowie, J. and F.P. Glasser, "The Reaction Between Cement and Natural Waters Containing Dissolved Carbon Dioxide," *Advances in Cement Research*, Vol. 4, pp. 119–134, Copyright® 1992, With Permission From Thomas Telford Publishing.**

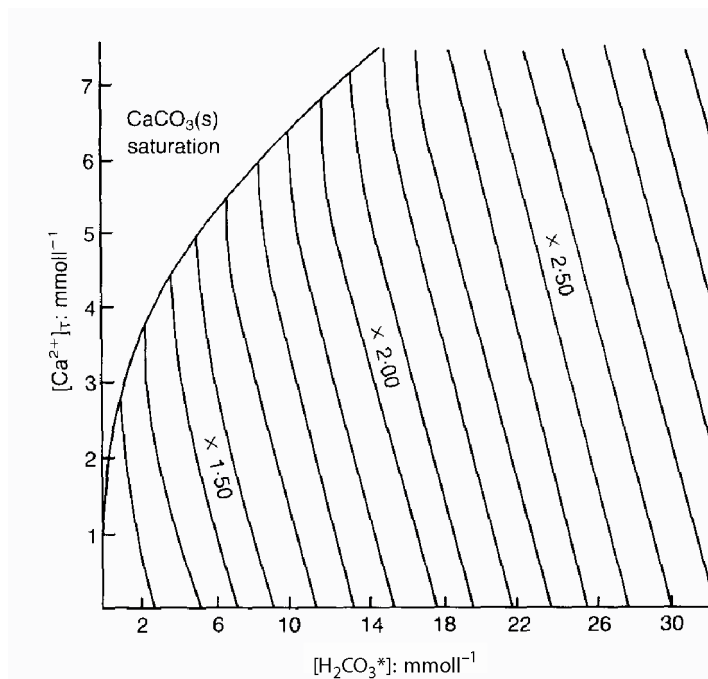


**Figure 4-3. Aggressivity of Groundwater to Cement as a Function of Dissolved Carbon Dioxide ( $\text{H}_2\text{CO}_3^*$ ) Concentration. The Contours Show Dissolving Power of Groundwater for Portlandite Relative to Pure Water at 25 °C [77 °F] and 1 Bar [0.99 Atm] Pressure. Reprinted From Cowie, J. and F.P. Glasser, "The Reaction Between Cement and Natural Waters Containing Dissolved Carbon Dioxide," *Advances in Cement Research*, Vol. 4, pp. 119–134, Copyright © 1992, With Permission From Thomas Telford Publishing.**

On the other hand, the reaction of dissolved  $\text{CO}_2$  with cement-based materials can cause calcium carbonate to precipitate. Because calcium carbonate is several orders of magnitude less soluble than portlandite, a self-healing, semiprotective film of calcite or other calcium carbonate phase can develop on the cement-based material. This situation occurs in many historic structures built with lime mortars. These structures give long service lives in rainy climates despite the high solubility of portlandite (hydrated lime) because portlandite is rapidly converted to the carbonate phase. However, this protection is not universal. Many natural waters containing carbon dioxide dissolve calcite. Thus, the balance between precipitation and dissolution is important in the leaching process. Many empirical treatments of water chemistry have been made to delineate waters giving rise to rapid carbonation attack, but the Cowie and Glasser (1992) model is based on the relevant physical chemistry of carbonation reactions that, in principle, can be coupled to other more general models.

Leaching can have several adverse effects on cement-based materials. It could result in an increased porosity and subsequent loss of strength (Carde and Francois, 1999). The connectivity of the pore spaces can increase, resulting in higher diffusivities of ionic species (Bentz and Garboczi, 1992a). A decrease in pore solution pH due to complete dissolution of portlandite also could cause C-S-H to decalcify and the embedded steel corrosion susceptibility to increase.

The extent of leaching depends on the quality of the cement-based material, the rate at which water percolates through or flows over it, the temperature, and the compositions and concentrations of species in solution (Taylor, 1997). It is a reasonable supposition that cements with reduced calcium contents, such as blends of fly ash and Portland cement, will exhibit better resistance to aggressive CO<sub>2</sub> than plain Portland cement. However, large increases in porosity resulting from attack may still adversely affect hydraulic properties and, as supplementary materials such as fly ash diminish the CaO content of cements, the matrix contains less portlandite to neutralize “aggressive” CO<sub>2</sub>.

The multicomponent character of natural waters and the coupled physical–chemical phenomena involved make it complicated to evaluate the importance of leaching as a degradation mechanism for specific systems. However, various models and computer codes are available to facilitate the calculations (Adenot and Richet, 1997; Carde and Francois, 1999; Garrabrants, et al., 2003; Moranville, et al., 2004; Yokozeki, et al., 2004). These various models are discussed in Section 5.

#### 4.1.4 Corrosion

Corrosion of steel embedded within cement-based materials (e.g., steel reinforcement in concrete vaults and grouted steel tanks) is an electrochemical process that leads to the formation of corrosion products with larger volumes than the parent metal. The volumetric expansion can cause extensive degradation and, possibly, cracking of the cement-based material. Corrosion of the steel can arise from two causes: (i) a general breakdown of the passive oxide film protecting the metal surface resulting from a reduction in the pH of the cement pore solution, predominantly through carbonation (Section 4.1.1), or (ii) a localized breakdown of the passive film by accumulation of chloride ions at the metal surface.

Once the passive oxide film on the steel surface is disrupted, the anodic iron dissolution reaction,



and cathodic oxygen reduction reaction



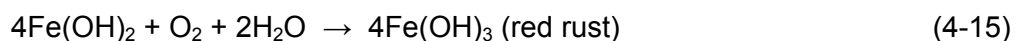
can occur at an accelerated rate. Despite the high alkalinity of the cement-based material, acid production may occur near the anodic sites because of hydrolysis of ferrous ions, as in

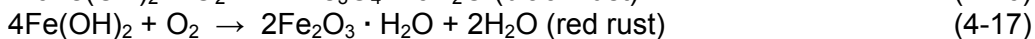
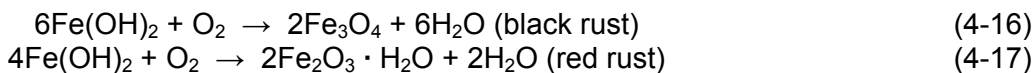


The H<sup>+</sup> ion may be reduced to H<sub>2</sub>(gas) and, along with O<sub>2</sub> reduction at more remote cathodic sites, further stimulate the anodic process. The following reactions also may form ferrous (hydr)oxides



or, if sufficient oxygen is available, ferric or mixed ferrous/ferric (hydr)oxides





As corrosion progresses and iron reacts to form ferrous and ferric (hydr)oxides, the significant increase in volume (by a factor of two to six) can result in pressure buildup at the cement–metal interface, which ultimately could exceed the tensile strength of the cement-based material and cause cracking, spalling, and delaminating of the material (for example, see Figure 4-4).

If chloride ions are present in the cement pore water, these ions may act as a catalyst through additional anodic reactions represented by the following equation



where  $\text{FeCl}_n^{(2-n)}$  are aqueous ferrous chloride complexes ( $n = 1$  to  $4$ ), which subsequently react with hydroxyl ions to form various corrosion products, as in the following reaction



Reaction (4-19) shows that the chloride ions are released and not consumed, such that the process becomes autocatalytic.

Steel corrosion in cement-based materials commonly occurs in two stages—initiation and propagation (Figure 4-5). During the initiation period, the metal is passive with relatively low corrosion rates. Loss of passivity occurs (e.g., due to carbonation or chloride penetration into



**Figure 4-4. Example of Corrosion-Induced Damage of Concrete Structure. The Damage Was Caused by Deicing Salts That Drained From the Highway Pavement, Diffused Through the Concrete Cover of the Support Columns, and Initiated Corrosion of the Reinforcing Steel. The Larger Volume of the Corrosion Products Compared to Steel Caused Cracking and Spalling of the Concrete Cover. Photo Courtesy of Vector Corrosion Technologies, Inc.**

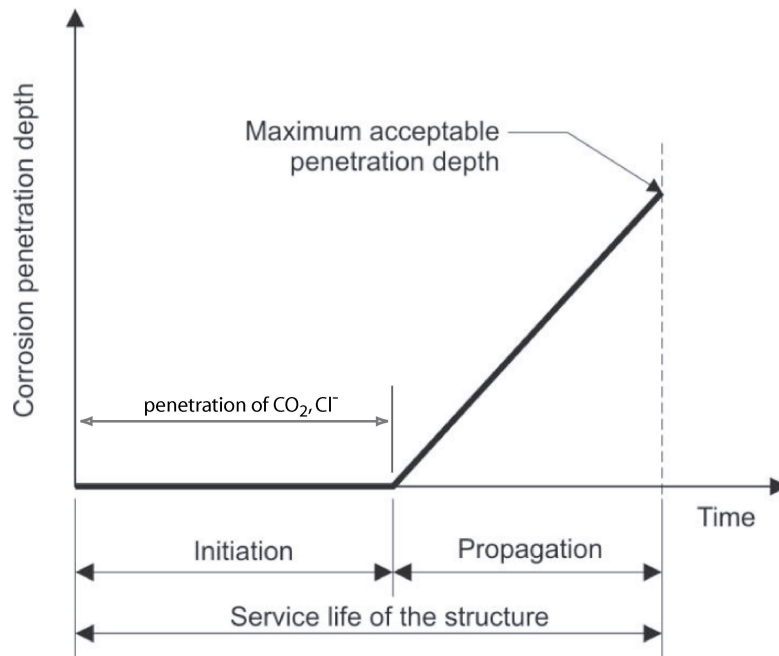


**Figure 4-5. Initiation and Propagation Periods for Corrosion in a Reinforced Cement-Based Structure. Reprinted From Bertolini, L., B. Elsener, P. Pedefferri, and R. Polder, *Corrosion of Steel in Concrete*, Copyright© 2004, With Permission From Wiley-VCH.**

the cement-based material) leading to the propagation period, which ends when a maximum acceptable degree of corrosion is reached (Bertolini, et al., 2004).

As indicated in Section 4.1.1, carbonation causes the pH of the cement pore water to decrease to around 9 where the passive film protecting the steel surface is no longer stable. The factors that influence the rate of CO<sub>2</sub> penetration and carbonation of cement-based materials are discussed in Section 4.1.1. Moreover, chloride ions penetrating into the cement-based material also can locally destroy the protective layer if their concentration at the surface of the metal reaches a critical level. The factors that affect the penetration of chlorides are similar to those for penetration of carbon dioxide, although the former occurs only through the aqueous phase. Carbonation and chloride penetration commonly are modeled as simple diffusion processes, but the processes are actually more complex. For example, chloride ions can be chemically bound (e.g., due to reaction with aluminates) or physical trapped in closed pores in the cement-based material such that some fraction is no longer able to diffuse toward the metal, whereas carbonation is affected by various dissolution and precipitation processes. Some models that account for these complexities are discussed in Section 5.

Although the passive film on the metal surface can remain stable and prevent active corrosion at low chloride concentrations, it breaks down once a critical chloride level is reached and active corrosion can initiate. The chloride could be initially present in the cement components or in the mix water, or could migrate from the service environment. Where cement-based materials are used for waste stabilization and immobilization, the chloride present in the waste also needs to be considered. Many factors affect corrosion initiation such that no single value of chloride

concentration can be used as a threshold concentration. The factors that affect chloride-induced initiation of corrosion include (i) the type and composition of the cement; (ii) water-to-cement ratio; (iii) sulfate content; (iv) curing conditions, age, and environmental history of the cement-based material; (v) degree of carbonation; (vi) temperature and relative humidity of the environment; and (vii) roughness and cleanliness of the steel (Hansson, 1995). The Comité Euro-International du Béton (1989) illustrated the interrelation of some of these factors as shown in Figure 4-6. Chloride threshold levels also depend on the type of metallic material present within the cement-based material. For instance, galvanized steel and stainless steel have much higher threshold levels than carbon steel.

Some researchers have proposed chloride threshold values. Kahhaleh (1994) reported threshold values of 0.14 to 0.35 percent (relative to cement weight) of acid-soluble chlorides based on a thorough literature survey. A value of 0.2 percent acid-soluble chlorides is often reported and recommended (West, et al., 1999). The Comité Euro-International du Béton (1989) (Figure 4-6) suggests that the chloride threshold value in uncarbonated concrete is approximately 0.05 percent by weight of concrete (about 0.4 percent by weight of cement). The U.S. Federal Highway Administration has stated that a chloride ion concentration of 0.15 percent by weight of cement can be tolerated but that 0.3 percent is considered deleterious (Hansson, 1995). However, because some of the chloride that penetrates the cement-based material can be chemically and physically bound in the material, using total chloride content as a threshold value for chloride-induced corrosion can be misleading. Because the chloride threshold value is influenced by various factors, a more broadly accepted methodology for estimating chloride initiation of steel corrosion uses diffusion-based equations similar to ones used for carbonation (see Section 5.1).

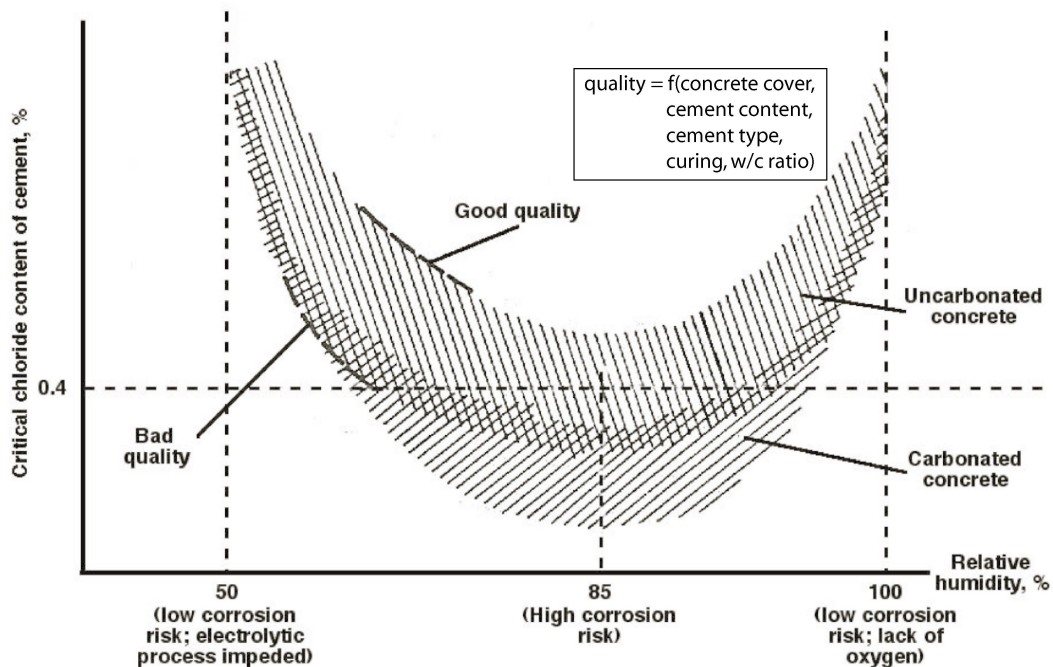


**Figure 4-6. Relationship of Critical Chloride Content to Environmental Conditions and Quality of Concrete Cover (Comité Euro-International du Béton, 1989). Figure Modified From Naus (2007).**

Once the passive film on the steel has been disrupted, the corrosion process can initiate and later propagate provided that water and oxygen are present on the metal surface. The corrosion rate determines the time it will take to reach the minimally acceptable state of the cement-based structure (Figure 4-5). The corrosion rate is affected by several factors including the (i) permeability of the cement-based material, (ii) moisture content of the material, (iii) temperature, and (iv) availability of oxygen. Further, the time required for corrosion to propagate to a level where the cement-based material is damaged will vary depending upon the local climate. For example, a region with a dry climate will have a significantly longer propagation time than a region with a tropical climate due to the lack of moisture in the cement-based material. Typical ranges of corrosion rate of carbon steel in carbonated or chloride-contaminated concrete as a function of relative humidity of the environment are shown in Figure 4-7. For civil engineering applications in which the period of performance is in the tens of years, the corrosion rate can be considered negligible if it is below  $2 \mu\text{m/yr}$  [ $7.9 \times 10^{-5}$  in/yr], low between 2 and  $5 \mu\text{m/yr}$  [ $7.9 \times 10^{-5}$  and  $2.0 \times 10^{-4}$  in/yr], moderate between 5 and  $10 \mu\text{m/yr}$  [ $2.0 \times 10^{-4}$  and  $3.9 \times 10^{-4}$  in/yr], intermediate between 10 and  $50 \mu\text{m/yr}$  [ $3.9 \times 10^{-4}$  and  $2.0 \times 10^{-3}$  in/yr], high between 50 and  $100 \mu\text{m/yr}$  [ $2.0 \times 10^{-3}$  and  $3.9 \times 10^{-3}$  in/yr], and very high for values above  $100 \mu\text{m/yr}$  [ $3.9 \times 10^{-3}$  in/yr] (Bertolini, et al., 2004). For applications with much longer performance periods (e.g., 10,000 years for nuclear waste disposal), these corrosion rates may need to be scaled to lower values.

Numerous researchers have proposed models to predict the rate of reinforcement corrosion [e.g., see review by Raupach (2006)]. Most of these models are based on experiments using laboratory specimens and various parameters, such as properties of the cement-based material (cement content, water to cement ratio, etc.) and exposure conditions (temperature, relative humidity, chloride concentration, etc.).

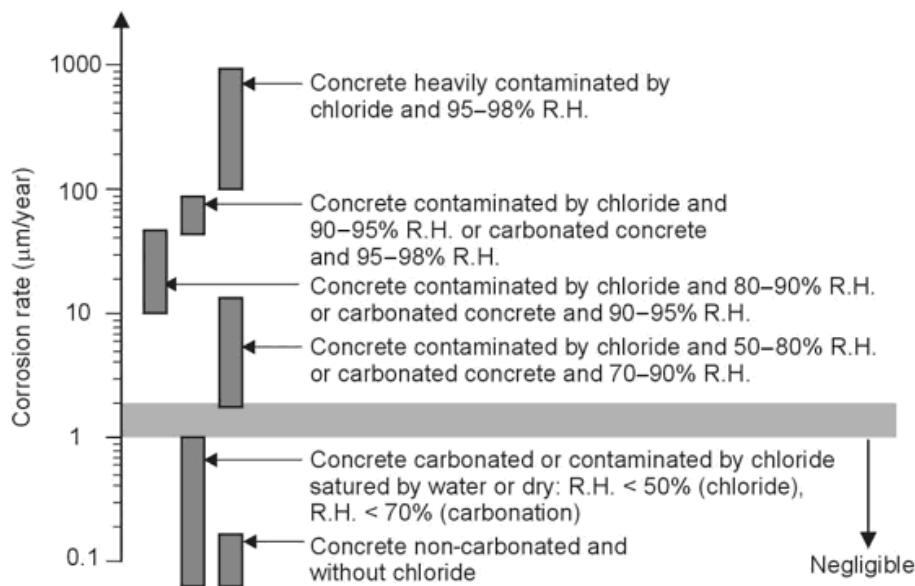


**Figure 4-7. Typical Ranges of Corrosion Rate of Carbon Steel in Concrete Exposed to Different Environmental Conditions. Reprinted From Bertolini, L., B. Elsener, P. Pedefferri, and R. Polder, *Corrosion of Steel in Concrete*, Copyright<sup>®</sup> 2004, With Permission From Wiley–VCH.**

### **4.1.5 Alkali–Silica Reaction**

A fourth chemical degradation mechanism is the reaction that can occur between hydroxyl ions, derived from the alkali hydroxides in the cement pore solutions, and reactive silica constituents of certain aggregates. The reactive forms of silica are opal, chalcedony and tridymite—minerals that occur in opaline or chalcedonic cherts—siliceous limestones, rhyolites and rhyolitic tuffs, dacite and dacite tuffs, andesite and andesite tuffs, and phyllites (Neville, 1996). The reaction causes an alkali–silicate gel to form in the planes of weakness or pores of the aggregate or on the surface of the aggregate particle. The gel imbibes water and swells, increasing in volume and resulting in internal pressures that eventually may lead to expansion, cracking, and disruption of the hydrated cement paste (Neville, 1996). This process is very slow relative to typical laboratory time scales, and its consequences may not be evident until several years after emplacement of the cement-based material.

Alkali–silica reaction occurs only in the presence of water and calcium ions. Higher temperature generally accelerates alkali–silica reaction, due to the lower solubility of portlandite and higher solubility of silica at higher temperatures. However, the total expansion induced by the reaction does not increase with temperature (Neville, 1996).

The best approach to prevent alkali–silica reaction is to avoid aggregates that are susceptible to alkali–silica reaction, which are well known and listed in standards and guidance documents [e.g., ASTM standards C289–03, C1567–04, C586–05 (ASTM International, 2007a,b,c)]. Carbonate aggregates, as pure as possible, are recommended because calcium carbonate does not react with hydroxyl ions to form deleterious expansive gels. Because water is necessary for the reaction to occur, drying out the cement-based material and preventing future contact with water is also an effective method of mitigating alkali–silica reaction.

## **4.2 Physical Degradation Mechanisms**

### **4.2.1 Shrinkage**

Cement-based materials undergo volumetric change as they proceed from the fresh to aged states. Volumetric contraction occurs early in the hydration process while the cement paste is plastic, but the extent of this contraction due to loss of water by hydration is small and is greatly restrained once the hydrating cement paste attains a certain rigidity (Neville, 1996). Evaporation or suction by adjacent dry materials, such as soil or cement, can cause water to leave the surface of the cement-based material that is still in the plastic state. This contraction is referred to as plastic shrinkage. The magnitude of plastic shrinkage is affected by the amount of water lost from the surface of the cement-based material, which in turn is influenced by temperature, ambient relative humidity, and wind velocity (Neville, 1996). Excessive water loss and plastic shrinkage at the surface can cause surface cracking. This process, known as plastic shrinkage cracking, can be mitigated by preventing evaporation immediately after emplacement of the cement-based material. Plastic shrinkage is greater at higher cement content and lower water/cement ratio.

Volume contraction also may occur after setting. This shrinkage, referred to as autogenous shrinkage, arises from withdrawal of water from the capillary pores by hydration of the cement particles and occurs in practice in the interior mass of the cement-based material. Autogenous shrinkage tends to increase at higher temperatures, higher cement content, and possibly with finer cements (Houk, et al., 1969). Autogenous shrinkage has been reported to be lower in

blended cements with higher content of supplementary cement materials like fly ash, but also has been observed to be very high for cement-based materials with a very low water/cement ratio (Neville, 1996). Autogenous shrinkage also is restrained by the rigidity of the already hydrated cement paste and thus tends to be relatively small except at extremely low water/cement ratios. For practical purposes, autogenous shrinkage need not be distinguished from drying shrinkage, which is discussed in the next paragraph.

Drying shrinkage is the observed volume reduction of cement-based materials associated with moisture loss under drying conditions. The initial loss of free water from the cement-based material causes little or no shrinkage, but as drying continues, adsorbed cement gel water is removed and drying shrinkage can occur. Where there is no restraint on the cement-based material, movement can occur freely and no stresses or cracks develop—a hypothetical situation illustrated in Figure 4-8(a). In reality, restraint is always present in cement-based structures and cracks develop when the tensile stress that results from drying shrinkage exceeds the tensile strength of the cement-based material [Figure 4-8(b and c)].

The amount of water per unit volume of cement-based material is one of the important factors affecting shrinkage of the material. Figure 4-9 illustrates the results of tests indicating that drying shrinkage increases with increasing water content. Drying shrinkage also tends to be larger at a higher water/cement ratio because the latter determines the amount of water in the cement paste that can evaporate and the rate at which that water can migrate toward the surface of the cement-based material. In general, higher cement content increases the shrinkage of cement-based materials; the relative shrinkages of neat cement paste, mortar, and concrete may be of the order 5, 2, and 1. Further, aggregates exert an important effect by restraining the amount of shrinkage that can actually occur. The size and grading of aggregates per se do not influence the magnitude of shrinkage, but larger aggregates permit a leaner cement mix (i.e., with a lesser amount of cement) to be used, which would result in lower shrinkage (Neville, 1996). The combined effect of water/cement ratio and aggregate content on shrinkage is illustrated in Figure 4-10.<sup>2</sup>

Carbonation also produces shrinkage. Figure 4-11 shows the amount of drying shrinkage of mortar specimens dried in a CO<sub>2</sub>-free air at different relative humidities and the shrinkage after subsequent carbonation. As discussed in a previous section, carbonation is highest at intermediate relative humidities; thus shrinkage due to carbonation and the total shrinkage due to both drying and carbonation also are highest at intermediate relative humidities. However, once completed, carbonation also reduces the potential for subsequent moisture movement and, therefore, is advantageous from the standpoint of cracking tendency.

The tendency to form cracks depends not only on the potential shrinkage but also on the extensibility of the cement-based material, its strength, and its degree of restraint to the deformation that may lead to cracking (Neville, 1996). Extensibility is the maximum tensile strain that a material can sustain before cracking occurs; a high extensibility of cement-based material enables it to withstand a greater volume change. Restraint in the form of steel

---

<sup>2</sup>Few shrinkage data are available for DOE grout formulations. Harbour (2005) reported values of  $30 \times 10^{-6}$  and  $80 \times 10^{-6}$  for two grout mixes that were studied for the Hanford site. The mixes are composed of Portland cement, blast furnace slag, fly ash, and sand aggregate similar to that used for grouting tanks at the Idaho National Laboratory (see Table 8-1), although the former has a higher water/cement ratio than the latter (0.7 versus 0.6) and has a higher aggregate/cement weight ratio (3.8 versus 3.6). The saltstone waste form at the Savannah River Site also has Portland cement, slag, and fly ash but contains no aggregate; thus its shrinkage is expected to be much greater than the values Harbour (2005) reported.

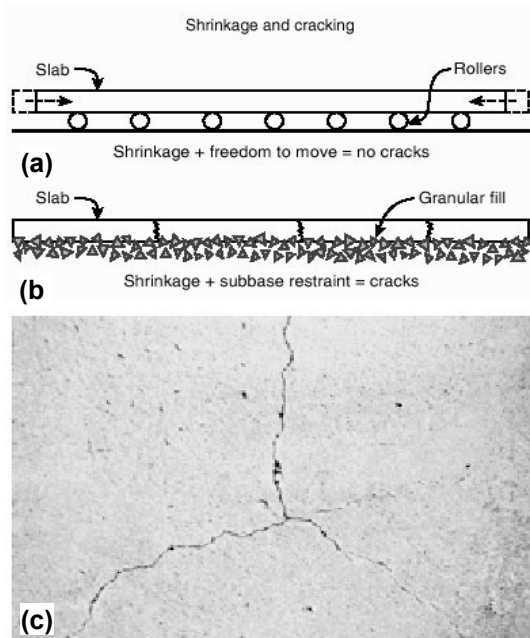


**Figure 4-8. (a) Illustration Showing No Crack Development in Cement-Based Material That Is Free to Shrink (Slab on Rollers). (b) In Reality, a Slab on the Ground Is Restrained by the Subbase, Creating Tensile Stresses and Cracks. (c) Typical Shrinkage Cracks in a Slab on the Ground. Reprinted From Kosmatka, S.H., B. Kerkhoff, and W.C. Panarese, *Design and Control of Concrete Mixtures*, 14th Edition, Copyright© 2002, With Permission From Portland Cement Association.**

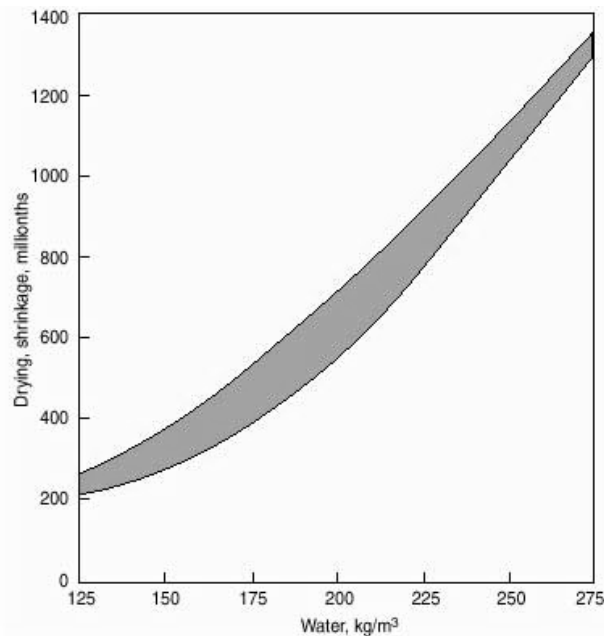


**Figure 4-9. Relationship Between Total Water Content and Drying Shrinkage. The Shaded Area Represents Data on a Large Number of Cement–Aggregate Mixtures With Various Proportions. Reprinted From Kosmatka, S.H., B. Kerkhoff, and W.C. Panarese, *Design and Control of Concrete Mixtures*, 14th Edition, Copyright© 2002, With Permission From Portland Cement Association.**

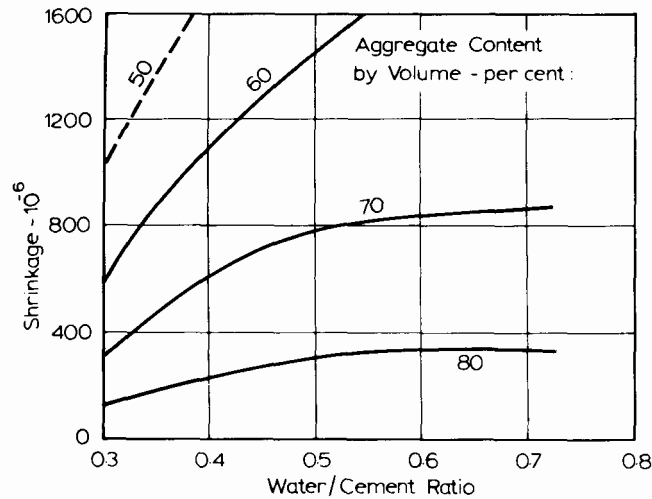


Figure 4-10. Effect of Water/Cement Ratio and Aggregate Content on Shrinkage. Reprinted From Neville, A.M., *Properties of Concrete*, 4<sup>th</sup> Edition. Copyright<sup>®</sup> 1996, With Permission From Pearson Education Limited.

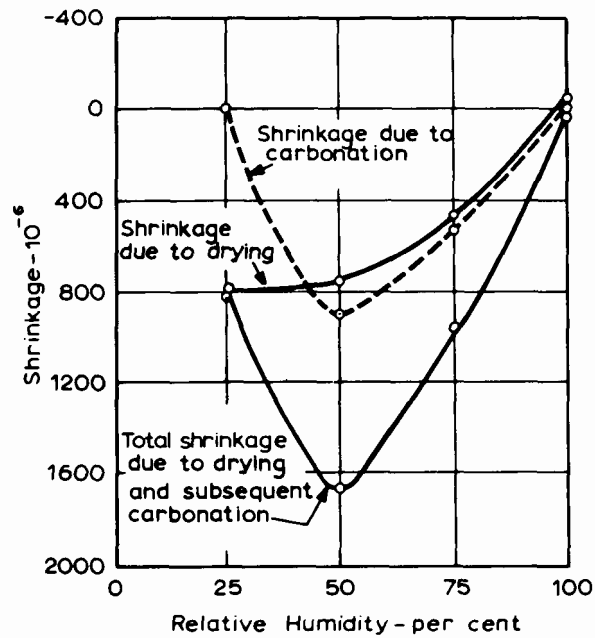


Figure 4-11. Drying Shrinkage and Carbonation Shrinkage of Mortar at Different Relative Humidities. Reprinted From Neville, A.M., *Properties of Concrete*, 4<sup>th</sup> Edition. Copyright<sup>®</sup> 1996, With Permission From Pearson Education Limited.

reinforcing bars or a gradient of stress increases extensibility of cement-based material by allowing strain well beyond that corresponding to maximum stress to develop in the material.

One of the most important factors in cracking due to shrinkage is the water/cement ratio of the mix because a higher water/cement ratio tends to increase shrinkage and, at the same time, to reduce the strength of the cement-based material (Neville, 1996). An increase in cement content also increases shrinkage and, therefore, the cracking tendency, but the effect on strength is positive.

#### **4.2.2 Thermal Cracking**

In the short-term, cement materials liberate heat as they hydrate. Typical modern cements have potential heat liberation of approximately 400 kJ/kg [172 BTU/lb]. Much, perhaps half, of this heat will be liberated within the first 48 hours. Thus, unless heat can readily escape, as occurs spontaneously in cement-based materials with thin cross sections or low-mass shapes, a temperature excursion inevitably will occur, and large masses of cement-based material will harden while still warm or hot. This temperature excursion reduces the durability of the resulting monolith.

The most obvious potential consequence of this temperature excursion is cracking. Like most solids, the hardened, cement-based material shrinks upon cooling and, because of the intrinsic brittleness of the matrix, cracks. Cracks provide conduits that allow the ingress of gas and liquids from the service environment and increase the surface area available for reaction. Another less obvious consequence—and one about which much contention exists—is the extent to which the minerals that form during warm set and hardening become unstable after cooling to ambient temperature and, in the course of phase transformations and recrystallization, contribute to dimensional instabilities. Mineralogical conversions from the “high-temperature” to the stable “low-temperature” phases potentially lead to dimensional instability. Some of these are well recognized [e.g., the formation of “secondary ettringite” (Glasser, 1996)].

The peak temperature resulting from the exothermic excursion can be reduced by adding inert mineral aggregate to cement. The aggregate acts as a heat sink, thereby reducing the peak temperature encountered, other factors being equal, and consequently lessens the physical impacts of thermal excursion. Supplementary cement materials, such as blast furnace slag and fly ash, are also commonly used to reduce the exothermic excursion encountered in large masses of cement. However, care is required to achieve the supposed benefit. For example, the heat of slag hydration is comparable with that of cement on a weight basis. But at or near room temperature, slag hydrates much slower than cement, spreading out the thermal pulse from slag blends over long periods of time and making it more manageable. Rising temperature, however, markedly accelerates the rate of slag hydration. When slag is incorporated in large masses of cementitious matrix, the initial exothermic pulse resulting from cement hydration may be sufficient to activate slag hydration and undo this benefit. Uchikawa (1986) found that the rate of heat release from slag was low at 20 °C [68 °F], but was approximately equal to that of cement at 60–70 °C [140–158 °F]. Thus, geometric factors are an important scale-up effect and cannot be excluded from the design; for this reason, supplementary cement materials are not a universal mitigation of thermal pulses. Moreover, supplementary materials may reduce the pH buffering capacity as will be explained in a later section.

Excessive temperature rise could be avoided by providing cooling (e.g., by embedding cooling coils or by making repeated pours of thin sheets of grout, allowing each to dissipate heat before commencing the next pour). For tank closure applications, the use of cooling coils is not desirable, because of added time and/or expense, so DOE has dealt with the heat evolution problem by diluting Portland cement with large quantities of fly ash and slag and by pouring grout in several layers, at least in the case of the tanks at the Idaho National Laboratory (CH2M–WG Idaho, LLC, 2007). Although the use of fly ash and slag may achieve a short-term objective, it compromises a long-term objective: the presence of sufficient reserve of alkalinity to condition percolating water to high pH.

### **4.2.3 Freezing and Thawing**

Water in the capillary pores of hardened cement paste can freeze, expand by approximately 9 percent, and exert dilating pressure on the surrounding material unless excess water is forced from the pore space. Because of surface tension effects, freezing starts in the largest pores and gradually extends to the smaller ones. As the solution freezes, the remaining liquid water will be forced out of the pore into any available free space. When the dilating pressure produced by these processes exceeds the tensile strength of the cement-based material, physical damage occurs. The damage is exacerbated by alternating freezing and thawing because each cycle of freezing causes liquid water to migrate to previously inaccessible locations where it can freeze. These include fine cracks that are widened by the pressure of the ice and remain widened during the thawing cycle when they become filled with water. If thawing is followed by refreezing, further expansion occurs, so that repeated cycles of freezing and thawing have a damaging cumulative effect.

In addition, freezing, which results in rejection of dissolved salts by newly formed ice, increases the solute concentration of the remaining liquid in the pore space or crack, and causes water to diffuse by osmotic pressure to the local regions with the more concentrated solution. Thus, certain regions or zones of the cement-based material will have higher water content than before freezing occurred, which exacerbates the freezing and thawing effect.

Although the resistance of cement-based material to freezing and thawing depends on its various properties (e.g., strength and extensibility), the main factors are the porosity, pore size distribution, and the degree of water saturation of the material. Partially dry cement-based material has sufficient air-filled pores to allow the freezing pore solution to expand without significantly damaging the material.

Degradation due to freezing and thawing is not expected for cement-based materials used for DOE tank closure and near-surface disposal, because burial depths typically exceed 5 m [16 ft].

## **4.3 Durability and the Composite Nature of Concrete**

Cement often is used as a component of composite constructions. Because hardened cement matrices are mechanically brittle and have low tensile strengths, cement is often reinforced by steel as rods, wire, or fiber. For example, the concrete vaults of the Saltstone Disposal Facility at the Savannah River Site and the cylindrical concrete structures enclosing the underground waste storage tanks at several DOE sites have reinforcing steel bars. The two materials, cement and steel, act in mechanical conjunction to give a composite material. However, in such cases, the durability of construction may relate as much to the steel as to the cement component. Steel normally is passivated against corrosion by cement, and this positive synergy

between the two materials contributes to the success of the composite. Other types of reinforcement are available, including glass and organic polymer fibers, but these are not applied to disposal of radioactive wastes and will not be considered here. To avoid confusion about durability relating specifically to cement, as distinct, for example, from steel, composites are discussed separately in this section.

The composite nature of grout and concrete also extends to the presence of aggregate. Concrete contains mineral aggregate as an important component, typically greater than 50 percent by mass. The mineral aggregate is bound by cement, even though the cement contents may be low, perhaps comprising only 10 to 16 weight percent of concretes used in construction. However, not all mineral aggregates are inert in prolonged contact with cement. Certain aggregates react chemically with cement and, where the reaction is accompanied by dimensional changes (usually expansive in nature), dimensional instability with cracking may result. A common example is alkali-silica reaction, discussed previously in Section 4.1.4, in which hydroxide ions, abundant in the high pH of cement pore fluids, attack and hydrolyze the Si-O-Si bonds of siliceous aggregates. The initial attack degrades the crystallinity of the aggregate, and the degraded product imbibes water with physical expansion. At first, the expansive stress can be contained, and expansion occurs without cracking. But as the accumulated stresses can no longer be accommodated, cracking and disruption of monoliths occur. Alkali-silica reaction is not a problem in structures that can be kept dry, but is observed in structures that are only intermittently wet. In the most well-publicized cases, alkali-silica reaction develops rapidly, within months or years. However, numerous cases are documented in which physical expansion, with visual evidence of cracking, has been noticed only decades after the original construction.

Problems resulting from alkali-silica reaction normally can be avoided by aggregate selection. Thus, specification becomes an important means of ensuring performance lifetime: even where the problem cannot be entirely avoided, specification of cement and aggregate can be used to mitigate the problem. Thus, a useful distinction can be made between those adverse reactions that can be prevented by design and specification and those reactions arising as a consequence of their service environment and that cannot be avoided, although mitigation may still be possible.

Many rapid tests have been proposed to detect aggregates susceptible to alkali-silica reaction. However, serious doubts persist about the predictive ability of these tests. Many aggregates that seem to perform well in practice fail the test. On the other hand, aggregates that pass the test will not necessarily perform well if the period of performance is in the thousands of years. In the present context, it is proposed that the problem of deciding compatibility over a 10,000-year lifetime should be avoided. A very simple means of avoidance is to use limestone aggregates; if the limestone is specified to be low in silica, no significant reaction can occur.

#### **4.4 Role of the Service Environment**

Note that natural environments vary greatly in severity with respect to degradation of cement-based materials. Some environments are broadly protective, whereas others can lead to rapid deterioration. Not surprisingly, performance of cement-based materials in aggressive environments has received the most attention. Thus, by 1900, it was well established that sulfate-rich groundwater, even if near neutral with respect to pH, is deleterious to cement. In this way, from observation and experience, a qualitative picture of the durability of cement-based materials in a broad range of environments has gradually emerged.

Table 4-3 summarizes this experience with respect to geochemically abundant components; manmade aggressive components, such as ammonium nitrate, are excluded from the table.

A short listing like Table 4-3 necessarily simplifies the reactions; the species listed, with the exception of molecular carbon dioxide, cannot occur singly. For example, aqueous sulfate ions must be charge balanced. Aqueous sodium sulfate is commonly used to test sulfate resistance on the grounds that the accompanying cation (sodium) interacts only weakly with cement substances. On the other hand, in many situations (e.g., in seawater), both magnesium and sulfate attack cement, and the attack is mediated by the presence of other ions such as sodium and bicarbonate.

Table 4-4 lists the relative susceptibility of cement-based materials to attack by aggressive chemical species present in service environments. The list, based on a published report by Paul (1994), deals with the effect of single chemicals and does not consider complex chemical interactions that may occur. Therefore, the table should be used only as a guide to help identify potential deleterious reactions in specific service environments and not to determine the performance of cement-based materials.

Table 4-5 tabulates the degree of severity of exposure of cement-based materials specifically to sulfate attack. The list, based on a tabulation in American Concrete Institute (1983), helps evaluate the potential for sulfate attack even if groundwater is not currently present. Thus, the possibility of degradation of buried cement-based materials can be assessed if future pluvial events are anticipated. The table in the original American Concrete Institute (1983) reference was developed for plain Portland cement, but it is probably broadly applicable to cements with fly ash supplementary cement material.

The concentration of aggressive species, listed in Tables 4-4 and 4-5, may be low in site-specific environments. If some factors can be eliminated from consideration, the analysis of future performance of cement-based materials becomes more reliable. Therefore, the most appropriate response to the species listed is not to design against their occurrence, but instead

<b>Table 4-3. Environmentally Abundant Substances Aggressive to Portland Cement</b>		
<b>Species</b>	<b>Reaction</b>	<b>Comment</b>
SO <sub>4</sub> <sup>2-</sup> (sulfate)	Reacts with formation of ettringite and gypsum	Sulfate attack is a worldwide problem experienced in structures at/below grade, in seawater, etc.
Cl <sup>-</sup> (chloride)	Corrosion of embedded steel	Chloride penetration of cement/concrete cover deprives steel of passivation.
CO <sub>2</sub> (carbon dioxide) • gaseous • dissolved	Reduction of pH, acid attack	Carbonation by CO <sub>2</sub> gas, as occurs in air, converts all calcium compounds to calcium carbonate. But dissolved CO <sub>2</sub> can also behave as an acid, leading to dissolution.
Mg <sup>2+</sup> (magnesium)	Ion exchange: Mg <sup>2+</sup> for Ca <sup>2+</sup>	Loss of high pH, physical expansion.
Soil acids	Dissolution	Leaching of calcium and increase in porosity.

<b>Table 4-4. Relative Susceptibility of Cement-Based Materials to Attack by Aggressive Chemical Species Present in Service Environments*</b>			
<b>Degree of Susceptibility</b>	<b>Weak</b>	<b>Moderate</b>	<b>Strong</b>
<b>Water†</b>			
pH	6.5 to 5.5	5.5 to 4.5	4.5 to 4.0
Carbon dioxide (mg CO <sub>2</sub> /L)	15 to 40	40 to 100	>100
Magnesium (mg Mg <sup>2+</sup> /L)	300 to 1,000	1,000 to 3,000	>3,000
Sulfate (mg SO <sub>4</sub> <sup>2-</sup> /L)	200 to 600	600 to 3,000	3,000 to 6,000
<b>Soil</b>			
Degree of acidity	200 mL/kg {20 °C [68 °F] Baumann-Gully}		
Sulfate (mg SO <sub>4</sub> <sup>2-</sup> /L) air dry soil	2,000 to 6,000	6,000 to 12,000	12,000 to 24,000
<p>*Information based on Paul, V. "Performance of Building Materials in Contaminated Land." Report BR 255. Garston, Watford, United Kingdom: Building Research Establishment. 1994.</p> <p>The table applies to static conditions at 20 ± 5 °C [68 ± 9 °F]. Flowing conditions, especially high-velocity waters, require additional protection.</p> <p>The age of the cement-based material prior to contact with aggressive chemical agents should be taken into account. Design aspects (shape) are an important factor.</p> <p>Effects of industrial effluents/pollution, ammonium, sewage, and sulfide oxidation are not included.</p> <p>For buried cement-based materials, the permeability of the soil should be considered as it affects replenishment of water contacting the material. Soil permeability greater than 10<sup>-5</sup> m/s [3.3 × 10<sup>-5</sup> ft/s] may require an upgraded classification.</p> <p>Baumann-Gully determination is carried out by titration with 10<sup>th</sup> normal sodium acetate solution and is a measure of volume of 10<sup>th</sup> normal acid in soil.</p> <p>†1 mg = 2.2 × 10<sup>-6</sup> lb; 1 L = 0.26 gal.</p>			

<b>Table 4-5. Severity of Exposure of Cement-Based Material Subjected to Sulfate Attack*</b>		
<b>Exposure</b>	<b>Water Soluble Sulfate (SO<sub>4</sub><sup>2-</sup>) in Soil (%)</b>	<b>Sulfate (SO<sub>4</sub><sup>2-</sup>) in Water (ppm)</b>
Mild	0.00–0.10	0–150
Moderate†	0.10–0.20	150–1,500
Severe	0.20–2.00	1,500–10,000
Very severe	Greater than 2.00	Greater than 10,000
<p>*American Concrete Institute. "ACI Manual of Concrete Practice Part 1—1983: Materials and General Properties of Concrete". Detroit, Michigan: American Concrete Institute. 1983.</p> <p>†Seawater falls in this category.</p>		

to assess the site-specific data. For example, grouts may be vulnerable to sulfate attack, but if sulfate is not a component of the service environment, nor liable to be a component in the future, this mode of degradation need not be a high design or performance assessment priority.

Note that the values tabulated in Tables 4-4 and 4-5 are based on studies relevant to civil infrastructures whose designed service lifetimes are in tens of years, much shorter than the 10,000-year period of interest when evaluating the performance of cement-based nuclear waste repositories. A species concentration that may cause only little degradation in the short term

may cause, over the course of thousands of years, significant degradation of a cement-based engineered material. Thus, for performance assessment of cement-based nuclear waste repositories, Tables 4-4 and 4-5 are useful as guides, but a temporal factor needs to be included in the assessment (e.g., by applying information derived from degradation models discussed in Section 5). Further studies are needed to determine whether information such as that presented in Tables 4-4 and 4-5 can be scaled to performance periods of interest in cement-based nuclear waste repositories.

#### **4.5 Standards and Standard Methods for Testing Performance in Service Environments**

Determinating performance of cement-based materials and their resistance to aggressive media encountered in service conditions has been the subject of much research directed at standardizing both cements and test methods. For example, in North America, the ASTM International, the American Concrete Institute, and the Canadian Standards Association have actively developed standards, standard test methods, and codes of practice with respect to cement composition, selection, formulation, and emplacement. These standards, available on these organizations' websites, have been developed primarily with the needs of civil engineers and stakeholders in mind and do not necessarily apply directly to nuclear applications. However, the emphasis of these specifications has gradually shifted.

Older specifications tended to be prescriptive, whereas many recent specifications have become permissive or at least allowed permissive options. There must be a balance between not unduly restricting progress by being overly prescriptive and not transferring an undue burden of proof of performance onto potential innovative developments. A knowledge gap has also developed concerning cements modified with supplementary cement materials. This is, of course, particularly relevant as many of the grout formulations proposed for tank closure lie outside the envelope of conventional engineering formulations and experience. If the user is to rely on a permissive specification, performance will need to be demonstrated. This demonstration could be difficult to implement because the unconventional nature of the materials implies that tests designed for "normal" formulations may not be applicable. Hence, the developers of grout formulations are faced with a credibility problem.

Many test specifications have been developed in response to the perceived need to measure the performance of cement-based materials exposed to aggressive environments [e.g., ASTM Standards C1012–04 and C1038–04 (ASTM International, 2007d,e)]. Despite the limitations in transferring the experience gained from these tests to evaluations of performance of grouted tanks and concrete vaults, this body of knowledge is still a valuable resource for guidance. However, the nature of the environments to which cement-based materials have been exposed has proven difficult to characterize and simulate. This difficulty arises because of the following:

- Physical and chemical modes of attack frequently are coupled. For example, a concrete bridge deck may be exposed to salt attack from deicing salts, but salt attack is usually accompanied by damage from freeze–thaw cycles; the two mechanisms are coupled to varying degrees but, overall, it is difficult, if not impossible, to deconvolute the separate effects. Even more complex couplings can occur.
- Chemical attack often is attributed to a specific chemical component but, in practice, a component does not occur alone in solution. For example, sulfate attack is attributed to the presence of sulfate anion in solution, but sulfate must be chemically balanced by a

cation. As discussed in Section 4.1.2, the chemical identity of the cation is also important. For example, if the cation is a proton (e.g., in sulfuric acid), the contribution of the proton to attack is much more significant than that of sulfate. Sodium is less damaging than protons, and for that reason, sodium sulfate usually is used to test the resistance of cement-based materials to sulfate.

Chemical attack, however, does not seem to cause significant degradation of physical properties within the timescale of observations of cement-based structures, except for extreme cases as mentioned earlier. For example, cements react with CO<sub>2</sub> in the atmosphere and in groundwater. As discussed in Section 4.1.1, in the simplest case involving reaction with atmospheric CO<sub>2</sub>, the physical strength and dimensional stability may be little affected. Although carbonation shrinkage can occur, it normally does not disrupt the cement-based material. However, carbonation can reduce the initial high pH of cement pore water, which could disrupt the protective passive oxide film on the surface of embedded steel and may also affect the immobilization potential for radioactive waste species. Thus, carbonation is rightly kept on the list of degradation processes. On the other hand, leaching due to dissolved carbon dioxide can increase the porosity and also affect the mechanical properties such as the compressive strength and the Young's modulus (Yokozeki, et al., 2003) of the cement-based material. The leaching process is very slow, but can be an important degradation mechanism for timescales of interest in nuclear waste disposal.

#### **4.6 Limitations of Tests on Performance of Cement-Based Materials**

Although a phenomenological classification is possible and long experience on the use of cement and concrete confirms the nature and importance of aggressive degradation mechanisms, it does not necessarily lead to quantification. Quantification has proven difficult for a number of reasons. In the present context, the most important reasons are

- Conditions in field exposures frequently fluctuate, and it can be difficult, if not impossible, to determine their precise history.
- The composition of the cement and concrete in historic concretes may be difficult to determine, and conformity with original specification cannot be assured.
- Workmanship and execution may not have achieved the specification, if any.
- Analysis of concrete removed from service is often incomplete: coring, followed by laboratory analysis, readily reveals mass gains (e.g., chloride diffusion profiles), but mass losses generally cannot be inferred.
- Alteration processes in concrete frequently lead to the development of chemically and mineralogically zoned structures. Typically, these structures are graded by depth from the exposed surface. It is difficult, if not impossible, to determine the resulting local changes of porosity and permeability in the zones and to calculate local stress concentrations.
- Much information about kinetics is deduced from both field and controlled exposures. But these usually use Fick's laws to determine effective diffusion coefficients. Fickian calculations assume a homogeneous structure, but the zoned structures so frequently encountered in practice question its appropriateness.

- The expectations of performance time scales also differ according to viewpoint. Civil engineers and stakeholders have become increasingly concerned in recent decades about the social and economic costs of replacing major structures. As a result, performance requirements in the range 80 to 120 years have increasingly been imposed. These long performance lifetime requirements have required a paradigm shift because, previously, low initial cost has been the overriding design priority. But the requirements for conventional structures may be contrasted with nuclear waste cement-based barriers where (i) the time scale for performance is increased by two orders of magnitude, relative to civil expectations, to 10,000 years and (ii) an 80- to 120-year performance lifetime for civil engineering structures is normally subject to periodic inspection and maintenance, which is not usually practical for engineered barriers intended for nuclear waste disposal.

Not surprisingly, scientists and engineers have felt that they enter uncharted territory when attempting quantification of performance lifetimes of nuclear waste barriers formed from cement-based materials. Nevertheless, progress has been made. Parallel studies of other barrier materials (glass, ceramic, metal) suggest possible relevant methodologies and, of course, even the limited expectations and means of assuring performance of civil structures contain valuable guidance. A possible approach for assessing performance lifetimes of cement-based engineered barriers is discussed next.

#### **4.7 Framework for Predicting the Long-Term Behavior of Cement-Based Engineered Barriers**

Much progress in assessing durability of cement-based materials has been made by studying selected aspects of performance; that is, a holistic model was not attempted, but selected degradation processes, usually observed from field studies, were isolated for separate study. These studies, while valuable, do not necessarily link readily into holistic performance models. An agreed framework with which to commission, undertake, evaluate, and assess field observations and research is needed.

A potentially useful framework is based on the ASTM Standard C1174–04 (ASTM International, 2007f), which is intended, with appropriate modification, to apply to all types of barrier materials. Indeed, this common approach to assessing performance is welcome, especially in the knowledge that multiple barriers may interact with each other as well as with their service environment. At the same time, ASTM C1174–04 is clearly not prescriptive: it recognizes the changing and evolving basis of assessment. It is therefore performance-based and makes clear that specialized approaches may be needed for particular materials. However, the ASTM standard provides invaluable guidance to the steps involved and their sequencing in predictive modeling of long-term behavior of materials.

The underlying logic is shown in Figure 4-12. Large portions of the logic chain shown in the figure appear to have been used in past DOE studies. The nature of the data required at each of the five steps—problem definition, modeling, testing, prediction, and confirmation—remains to be user defined, although formal links between steps are clearly indicated. Of special importance to the problem of tank closure is the equality in the rank of testing and modeling, the interactions between the two, and the need to sustain and relate both sets of activities.

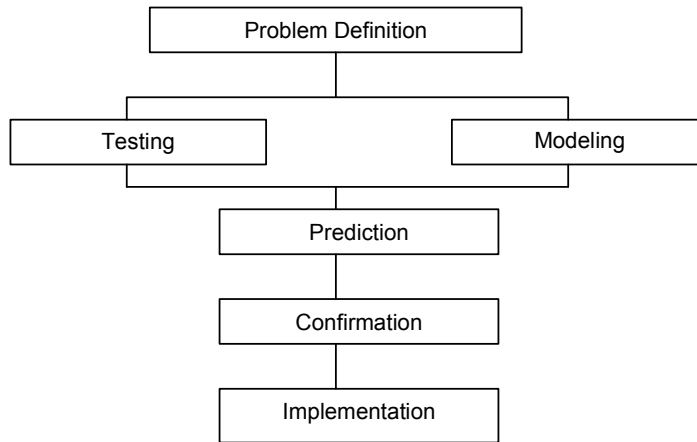


**Figure 4-12. Principal Logic Steps Involved in Predicting the Long-Term Behavior of Materials Based on ASTM Standard C1174–04 (ASTM International, 2007f)**

## 5 APPROACHES TO MODELING THE DEGRADATION OF CEMENT-BASED MATERIALS

As discussed in Section 4, the performance lifetime of cement-based materials can be compromised by a variety of chemical and physical degradation mechanisms. Because cement-based materials generally are thermodynamically unstable in their service environments, chemical processes that cause deterioration or degradation of these materials are especially important, particularly for long periods of performance. Chemical substances that contact the cement-based material can “cause dissolution with mass wastage, neutralize or reduce system pH and Eh buffering capacities, adversely affect the sorption characteristics or affect the physical performance of the system by altering the permeability or by causing significant dimensional changes with cracking or disruption” (Glasser, 1997).

A variety of models for predicting the chemical degradation of cement-based materials has been published in the literature. Several of these models were selected to represent the various types of models available in the literature—from simple diffusion or empirical equations to more complex coupled reactive–transport models—and are reviewed in this section. Modeling the degradation of cement-based materials is an active area of research, and literature describing new approaches continues to be published, precluding a fully comprehensive review. The models reviewed here focus on the degradation mechanisms of carbonation, sulfate attack, and leaching. Alkali–silica reaction was not included in the review. This is because there are no reliable analytical or numerical methods for predicting the future expansion of cement-based structures affected by alkali–silica reaction (Somerville, 2001; Lay, et al., 2003). Corrosion-induced cracking is outside the scope of this report, but recently published papers point to significant progress, particularly in modeling the corrosion-induced cracking of reinforced concrete (Toongoenthong and Maekawa, 2005; Vu and Stewart, 2005; Vu, et al., 2005; Bhargava, et al., 2006a,b; Nguyen, et al., 2006; Isgor and Razaqpur, 2006; El Maaddawy and Soudki, 2007; Li, et al., 2006; Munoz, et al., 2007).

Physical degradation mechanisms, such as shrinkage and thermal cracking, that could cause fractures or cracks to form in the hardened cement-based material also are not included in this review. The processes that contribute to shrinkage of cement-based materials are complex, but have been identified (Stang, et al., 2007). However, the consequences of shrinkage in terms of the timing, spacing, width, and depth of resulting cracks are less amenable to quantification, although progress is being made (Bolander, et al., 2007; Radlinska, et al., 2007; Bamforth, 2007). Structural engineers planning to build cement-based infrastructures are especially concerned about thermal cracking, which could result from thermal gradients and stresses imposed by the exothermic nature of cement hydration. Thus, a significant body of literature has been published on estimating the temperature rise that could result from hydration of cement-based materials (de Schutter and Taerwe, 1995; van Breugel, 1998; Bentz, et al., 1998; Swaddiwudhipong, et al., 2002; Mounanga, et al., 2004; Schindler and Folliard, 2005; Riding, et al., 2006; Bamforth, 2007) and on simulating the stresses and early-age cracking that could result from cement-hydration-induced thermal gradients (de Borst and van den Boogaard, 1994; Nakamura, et al., 1999; Cusson and Repette, 2000; de Schutter, 2002; Fu, et al., 2007;

Bamforth, 2007).<sup>1</sup> The risk of thermal cracking of cement-based materials, as in grouted tanks and concrete vaults, can be mitigated by controlling the temperature rise and temperature gradient that result from cement hydration. Bamforth (2007) discusses these measures. The use of fly ash and blast furnace slag in the U.S. Department of Energy (DOE) grout formulation could significantly reduce the potential for thermal cracking because these supplementary cement materials lower the heat of hydration of the cement-based material. However, because grouting of the tanks and concrete vaults involves sequential grout pours that generate multiple and overlapping heat pulses, evaluation of potential thermal cracking should carefully consider the specific grout pour sequence and geometry.

The degradation models reviewed in this section are explained in sufficient detail to illustrate the derivation and basic assumptions. Several examples are given to illustrate the application of the models and indicate the types of predictions that can be expected from the models.

## 5.1 Carbonation<sup>2</sup>

As discussed in Section 4.1.1, carbonation has an indirect, but important, effect on cement-based materials with embedded steel, such as reinforced concrete: it lowers the pH of the cement pore water, which could destabilize the passive oxide layer on the steel surface and allow steel corrosion. The increase in volume due to the formation of oxidized corrosion products leads to internal stresses within the concrete that could cause cracking and spalling of the concrete cover. Thus, carbonation is an important process that is considered in evaluating the service life<sup>3</sup> of reinforced concrete structures.<sup>4</sup> For example, the service life,  $t_i$ , of reinforced concrete that is subjected to carbonation-induced corrosion can be expressed as the sum of an initiation time and a propagation time as shown in Figure 5-1 (Bertolini, et al., 2004)

$$t_i = t_i + t_p \quad (5-1)$$

where

- $t_i$  — initiation time for corrosion, typically the time needed for the carbonation front to reach the steel surface
- $t_p$  — propagation time (i.e., time to reach a maximum acceptable corrosion penetration of the steel element)

---

<sup>1</sup>The book by Bamforth (2007) includes a CD-ROM with spreadsheet calculators for predicting the temperature rise and thermal gradients in hardening concrete based on a model that accounts for the following factors: (i) cement content, (ii) the use of fly ash or ground granulated blast furnace slag, (iii) mix temperature, (iv) ambient temperature and its daily variation, (v) section thickness, (vi) formwork type, and (vii) time of framework removal. The model was validated by Bamforth (2007) using independent published data on temperature rise for a variety of concrete mixes, element sizes, and mix temperatures.

<sup>2</sup>The models described in this section apply to carbonation in which leaching is unimportant, as discussed in Section 4.1.1.

<sup>3</sup>A commonly used definition of service life is from ASTM E 632–82 (ASTM International, 1996), which defines “the service life of a building component or material” as “the period of time after installation during which all properties exceed the minimum acceptable values when routinely maintained.” Note, however, that it may not be possible to achieve the expectation of this definition—that maintenance is possible.

<sup>4</sup>The effect of carbonation on grouted tanks is discussed in Section 8.5.

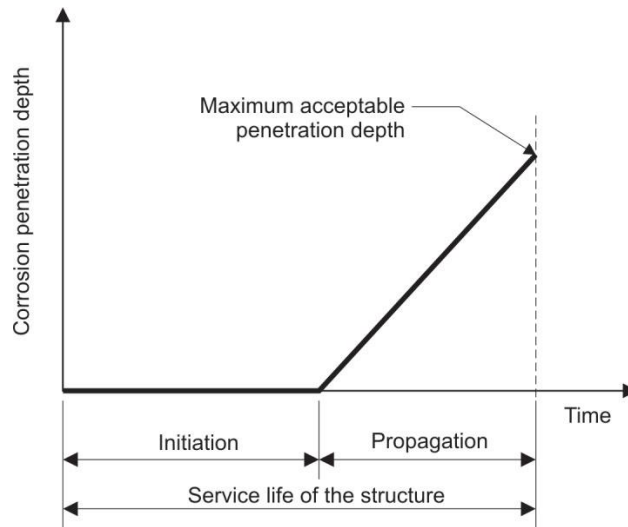


**Figure 5-1. Initiation and Propagation Periods for Corrosion of a Reinforced Concrete Structure. Reprinted From Bertolini, L., B. Elsener, P. Pedferri, and R. Polder, *Corrosion of Steel in Concrete*, Copyright© 2004, With Permission From Wiley–VCH.**

The initiation time,  $t_i$ , will depend on the properties of the concrete, the environment, and the thickness of the concrete covering the steel and can be calculated using models such as those discussed in the following paragraphs. For a given maximum acceptable corrosion penetration of the steel, the propagation time,  $t_p$ , can be calculated from measured or calculated corrosion rates (Lay, et al., 2003). A maximum corrosion penetration of steel that often is accepted for service life calculations of reinforced concrete elements is  $100\ \mu\text{m}$  [ $3.9 \times 10^{-3}$  in] (Bertolini, et al., 2004). Figure 5-2 illustrates the range in corrosion rate of steel in carbonated concrete as a function of relative humidity. The figure is based on data from thousands of measurements taken mainly in Spain (Bertolini, et al., 2004). For civil engineering applications in which the period of performance is in the tens of years, the corrosion rate can be considered negligible if it is below  $2\ \mu\text{m/yr}$  [ $7.9 \times 10^{-5}$  in/yr], low between 2 and  $5\ \mu\text{m/yr}$  [ $7.9 \times 10^{-5}$  and  $2.0 \times 10^{-4}$  in/yr], moderate between 5 and  $10\ \mu\text{m/yr}$  [ $2.0 \times 10^{-4}$  and  $3.9 \times 10^{-4}$  in/yr], intermediate between 10 and  $50\ \mu\text{m/yr}$  [ $3.9 \times 10^{-4}$  and  $2.0 \times 10^{-3}$  in/yr], high between 50 and  $100\ \mu\text{m/yr}$  [ $2.0 \times 10^{-3}$  and  $3.9 \times 10^{-3}$  in/yr], and very high for values above  $100\ \mu\text{m/yr}$  [ $3.9 \times 10^{-3}$  in/yr] (Bertolini, et al., 2004).<sup>5</sup> For applications with much longer performance periods (e.g., 10,000 years for nuclear waste disposal), these corrosion rates may need to be scaled to lower values.

Many of the carbonation models described in this section rely on the concept of a “carbonation front.” This concept derives from the use of phenolphthalein on cement-based materials. Phenolphthalein is an organic indicator that gives a sharp color change from colorless at a pH of 8.0 or lower to deep purplish red at a pH of 9.8 or higher. Because carbonation of a cement-based material has not occurred at a pH of 12.5 to 13 and the cement-based material is fully carbonated at a pH of  $<8$ , the color change observed when phenolphthalein is applied on

<sup>5</sup>Various models for the propagation phase of reinforcement corrosion have been published. These models range from empirical approaches that are based on direct relationships between basic parameters of the cement-based material (water/cement ratio, type of binder, etc.) and the environment (humidity, chloride content, temperature, etc.) to more advanced models that take into account the polarization behavior of anodic and cathodic sites on the steel surface. These different models are reviewed in Raupach (2006).

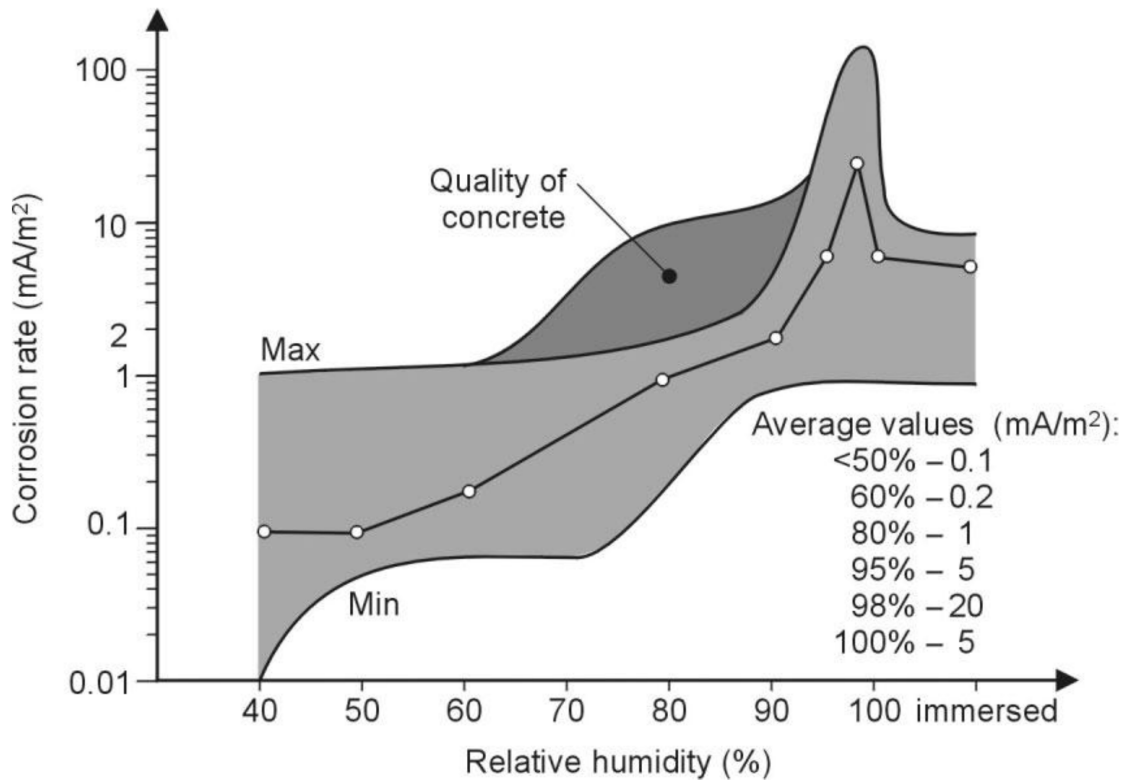


**Figure 5-2. Minimum and Maximum Values of Corrosion Rate of Steel Reinforcement in Carbonated Concrete as a Function of Relative Humidity. A Value of 1 mA/m<sup>2</sup> Corresponds to a Mass Loss Equal to Approximately 9 g/m<sup>2</sup>yr and a Penetration Rate of About 1.17 μm/yr. Reprinted From Bertolini, L., B. Elsener, P. Pedferri, and R. Polder, *Corrosion of Steel in Concrete*, Copyright© 2004, With Permission From Wiley-VCH.**

partially carbonated concrete is often taken as marking the position of the “carbonation front.” However, other instrumental techniques such as thermal analysis and x-ray diffraction show that the “front” is in fact a diffuse zone (Rahman and Glasser, 1989). Glasser and Matschei (2007) provide a more detailed account of the calculated phase changes attending the progressive carbonation of a cement model that indicates the potential existence of 13 zones. However, because the transition between regimes of corrosion and passivation of carbon steel occur at a relatively constant pH, it is acceptable to use the concept of a “carbonation front” by associating its position with the change in pH at the transition between zones that have portlandite and/or C-S-H and zones of lower pH in which these phases are not present.

Most of the current models of cement-based material carbonation are based on Fick’s first law of diffusion (Lay, et al., 2003). The amount of CO<sub>2</sub> that penetrates the cement-based material due to the CO<sub>2</sub> gradient between the external environment and the cement-based material can be expressed by the following equation

$$dm = -D A \frac{C_1 - C_2}{x} dt \quad (5-2)$$

where

$dm$  — mass increment of CO<sub>2</sub> that diffused during the time interval  $dt$  (kg CO<sub>2</sub>)

$D$	—	diffusion coefficient of $\text{CO}_2$ in the carbonated, cement-based material ( $\text{m}^2/\text{s}$ )
$A$	—	surface area ( $\text{m}^2$ )
$c_1$	—	$\text{CO}_2$ concentration in the external environment ( $\text{kg CO}_2/\text{m}^3$ )
$c_2$	—	$\text{CO}_2$ concentration at the carbonation front in the cement-based material ( $\text{kg CO}_2/\text{m}^3$ )
$dt$	—	time interval (s)
$x$	—	depth of carbonated material (m)

At the carbonation front,  $\text{CO}_2$  reacts with the alkaline constituents of the cement-based material to form various types of carbonate phases. The mass of the  $\text{CO}_2$  that reacts can be represented by the following equation

$$dm = a A dx \quad (5-3)$$

where

$dm$	—	mass of $\text{CO}_2$ required for the complete carbonation of the depth increment $dx$ ( $\text{kg CO}_2$ )
$a$	—	$\text{CO}_2$ -binding capacity of noncarbonated, cement-based material ( $\text{kg CO}_2/\text{m}^3$ )
$A$	—	surface area ( $\text{m}^2$ )
$dx$	—	depth increment (m)

A mass balance of diffused  $\text{CO}_2$  and reacted  $\text{CO}_2$  yields

$$x dx = -\frac{D}{a} (c_1 - c_2) dt \quad (5-4)$$

Assuming  $D$ ,  $a$ , and the quantity  $(c_1 - c_2)$  are constant with time and depth, integration of Eq. (5-4) yields

$$x^2 = \frac{2D}{a} (\Delta C_s) (t - t_e) \quad (5-5)$$

where

$t$	—	age of cement-based material at the time of inspection
$t_e$	—	time when the surface was first exposed to $\text{CO}_2$
$\Delta C_s$	—	$(c_1 - c_2)$

Solving for the penetration depth ( $x_c$ ) gives a simple square root of time equation

$$x_c(t) = K \sqrt{(t - t_e)} \quad (5-6)$$

where the effects of the material parameters,  $D$  and  $a$ , and the environmental parameter,  $\Delta C_s$ , are incorporated into the carbonation rate,  $K$ . Usually, the time until the surface was first exposed to  $\text{CO}_2$  is negligible compared to the service life, so  $t_e$  can be set to zero.

Equation (5-6) is a practical approach for calculating carbonation depth for service life predictions. For existing structures, the carbonation depth of any part of the structure can be measured after a certain period of exposure and the value of  $K$ , as well as its spatial variation, can be calculated retrospectively without knowing the environmental conditions or material

properties.<sup>6</sup> By assuming the average exposure conditions will not change in the future, the derived  $K$  can be used to extrapolate the carbonation depth to later times. Values of  $K$  found for real structures exposed to the atmosphere but protected from rain range from 2 to 15 mm/yr<sup>1/2</sup> [0.079 to 0.59 in/yr<sup>1/2</sup>] (Bertolini, et al., 2004). Typical values of  $K$  vary from 2 to 6 mm/yr<sup>1/2</sup> [0.079 to 0.24 in/yr<sup>1/2</sup>] for concrete with low porosity (i.e., well compacted and cured, with low water/cement ratio) whose cement content is above 350 kg/m<sup>3</sup> [590 lb/yd<sup>3</sup>], from 6 to 9 mm/yr<sup>1/2</sup> [0.24 to 0.35 in/yr<sup>1/2</sup>] for concrete of medium porosity, and greater than 9 mm/yr<sup>1/2</sup> [0.35 in/yr<sup>1/2</sup>] for highly porous concrete with cement content less than 250 kg/m<sup>3</sup> [421 lb/yd<sup>3</sup>] (Bertolini, et al., 2004).

Bertolini, et al. (2004) stated that equations like Eq. (5-6) give fairly accurate predictions, although the carbonation penetration for low porosity Portland cement concrete tends to be overestimated, at least for longer times. Values of  $K$  depend on material properties and environmental conditions, which may change nonlinearly with time and in different parts of a structure.

Equation (5-6) does not have explicit parameters to account for the influence on the carbonation rate of environmental factors (humidity, CO<sub>2</sub> concentration, temperature) and the properties of the cement-based material (mainly alkalinity and permeability).<sup>7</sup> Other formulas have been proposed to take into account the effect of these other parameters. For example, Parrott (1994) developed an empirical equation that correlates the depth of carbonation at time  $t$  to the permeability of concrete to air, the calcium oxide content of the hydrated cement matrix that can react with and effectively retard the rate of CO<sub>2</sub> penetration, and the relative humidity of the environment. The parameters used in the equation of Parrot (1994) were based on published data on concrete permeability, calcium oxide content, and carbonation depth. Bakker's (1994) diffusion model takes into account the effect of fluctuating wetting and drying cycles—the carbonation rate is considered negligible and the carbonation front cannot progress during wet conditions, whereas during dry conditions, moisture evaporates and enables further progression of the carbonation front. The model of Steffens, et al. (2002) explicitly accounts for the effects of temperature, relative humidity, and CO<sub>2</sub> concentration on the carbonation rate.

Papadakis, et al. (1991a, 1989) presented a mathematical model for concrete carbonation that accounts for the following processes: (i) diffusion of CO<sub>2</sub> gas in the concrete pores, (ii) dissolution of CO<sub>2</sub> in the aqueous film of these pores, (iii) dissolution of solid Ca(OH)<sub>2</sub> in pore water, (iv) diffusion of dissolved Ca(OH)<sub>2</sub> in pore water and its ultimate reaction with dissolved CO<sub>2</sub>, and (v) reaction of CO<sub>2</sub> with C-S-H and with the unhydrated cement clinker phases dicalcium silicate (Ca<sub>2</sub>SiO<sub>4</sub>) and tricalcium silicate (Ca<sub>3</sub>SiO<sub>5</sub>). The model also accounts for the further hydration of dicalcium and tricalcium silicates and the reduction of concrete porosity resulting from hydration and carbonation.

---

<sup>6</sup>Carbonation of cement-based material in civil infrastructures is easily measured by exposing fresh material and spraying with a phenolphthalein indicator solution. The measurement can be done by breaking away a fresh surface, by coring and splitting, or by cutting the core in the laboratory. The phenolphthalein solution remains clear where the cement-based material is carbonated and turns pink where the material is still alkaline. Petrographic analysis also will reveal carbonated and partially carbonated zones under an optical microscope. These methods can be used for a grouted high-level waste tank if a drill core sample of the grout can be taken and if adequate radiological protection equipment is available. Otherwise, a value of  $K$  for the grout in the tanks may be approximated from laboratory tests using samples of simulated tank grouts exposed to an atmosphere approximating that present inside a grouted tank.

<sup>7</sup>Despite these limitations, Eq. (5-6) could be useful in making order-of-magnitude estimates of carbonation depth versus time for cement-based material (e.g., in tank closure, using calculated or measured  $K$  values).

The mathematical model of Papadakis, et al. (1991a, 1989) applies only to one-dimensional geometry (i.e., to an infinite slab) and to material free of discrete macroscopic cracks, with both surfaces exposed to an atmosphere with CO<sub>2</sub>. However, the model can be extended easily to two- or three-dimensional geometry. The model is based on differential mass balances of gaseous CO<sub>2</sub>, solid and dissolved Ca(OH)<sub>2</sub>, C-S-H, and unhydrated silicates and accounts for diffusion processes and chemical reactions. The mathematical model yields a complex nonlinear system of differential equations in space and time and must be solved numerically for the unknown concentrations of the materials involved. The detailed equations are presented in Papadakis, et al. (1991a,b; 1989). By simplifying the equations and using parameter values typical for concrete, Papadakis, et al. (1991a, 1989) presented the following analytical expression

$$x_c = \sqrt{\frac{2D_{e,CO_2} [CO_2]^0 t}{[Ca(OH)_2]^0 + 3[C-S-H]^0 + 3[C_3S]^0 + 2[C_2S]^0}} \quad (5-7)$$

where

$D_{e,CO_2}$	—	effective diffusivity of CO <sub>2</sub> (g)
$[CO_2]^0$	—	molar concentration of CO <sub>2</sub> in the gas phase at $t = 0$
$[Ca(OH)_2]^0$	—	molar concentration of portlandite at $t = 0$
$[C_2S]^0, [C_3S]^0$	—	molar concentration of dicalcium silicate and tricalcium silicate, respectively, at $t = 0$

The denominator in Eq. (5-7) represents the total molar concentration of CaO in the cement that can undergo carbonation. The effective diffusivity in the numerator applies to fully carbonated cement-based material and is a function of the porosity at time  $t$  and the degree of saturation of the pore, which in turn depends on the ambient relative humidity and on the pore-size distribution.

The use of Eq. (5-7) for predictive purposes requires information on the (i) chemical composition of cement, (ii) ratios of water/cement and aggregate/cement, and (iii) CO<sub>2</sub> concentration and relative humidity of the atmosphere. Details about the synthesis of the previous information to determine the pore-size distribution, the porosity, the degree of saturation of the pores, and ultimately the effective diffusivity of gases in the cement-based material are given in Papadakis, et al. (1991b). Experimental data and calculated values are compared in Figure 5-3, which demonstrates that Eq. (5-7) provides a fairly good description of the experimental results on carbonation depth obtained under indoor normal exposure conditions over a period of several years. However, Eq. (5-7) is not valid for systems at low relative humidity. For example, Figure 5-4 compares calculated versus experimental depth of carbonation as a function of relative humidity. The experimental data show that carbonation depth is maximum at relative humidities near 50 percent. The model results agree well with experimental data at relative humidities above 50 percent but not at lower relative humidities. Note that relative humidity enters Eq. (5-7) only through the effective diffusivity,  $D_{e,CO_2}$ , which increases as relative humidity decreases. Thus, Eq. (5-7) predicts that carbonation depth will continue to increase as relative humidity decreases below 50 percent. However, because the amount of water in the pores becomes small at such low relative humidities, the chemical reactions become the rate-controlling processes instead of CO<sub>2</sub> diffusion, as Eq. (5-7) presumes. This change in rate-controlling process is not accounted for in Eq. (5-7); thus the model was modified to extend

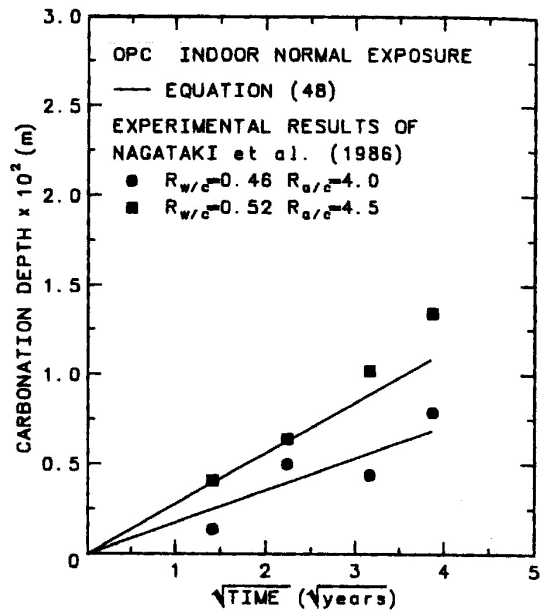


Figure 5-3. Comparison of Carbonation Depth as a Function of Time Calculated Using the Model of Papadakis, et al. (1991a, 1989) and Experimental Data From Nagataki, et al. (1986). Equation (48) Referred to in the Figure Is Analogous to Eq. (5-7) of This Report. The Two Solid Lines in the Figure Were Calculated Using Values of  $D_{e,CO_2}$  That Papadakis, et al. (1989) Measured in the Laboratory on Samples With Water/Cement ( $R_{w/c}$ ) and Aggregate/Cement ( $R_{a/c}$ ) Ratios Similar to Nagataki, et al. (1986). Reprinted From Papadakis, V.G., C.G. Vayenas, and M.N. Fardis, "A Reaction Engineering Approach to the Problem of Concrete Carbonation," *AICHE Journal*, Vol. 35, pp. 1,639-1,650. Copyright© 1989, With Permission From AIChE.

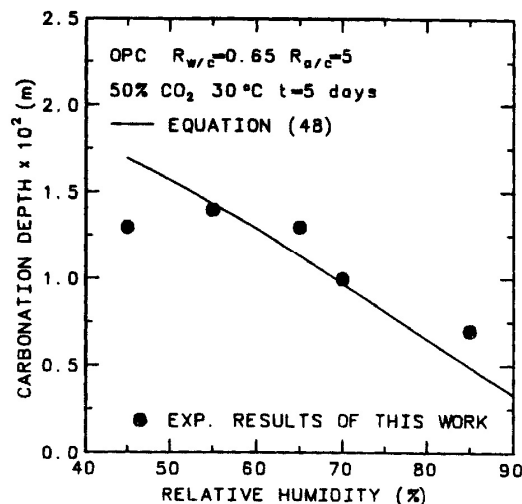


Figure 5-4. Carbonation Depth Calculated as a Function of Relative Humidity Versus Experimental Data. Equation (48) Referred to in the Figure Is Analogous to Eq. (5-7) of This Report.  $R_{w/c}$ —Water/Cement Ratio;  $R_{a/c}$ —Aggregate/Cement Ratio. Reprinted From Papadakis, V.G., C.G. Vayenas, and M.N. Fardis, "A Reaction Engineering Approach to the Problem of Concrete Carbonation," *AICHE Journal*, Vol. 35, pp. 1,639-1,650. Copyright© 1989, With Permission From AIChE.

its validity to relative humidities less than 50 percent. The revised model is presented in Papadakis, et al. (1991c).

The Papadakis, et al. (1991c) model is limited to calculating carbonation in Portland cement paste and concrete. Because it does not account for reactions involving supplementary cement materials such as blast furnace slag and fly ash, it cannot be applied to DOE cement-based formulations used in tank closure and near-surface disposal. To apply the model to such systems, model parameters will need to be derived to account for the effect of supplementary cement materials on the effective diffusivity ( $D_{e,CO_2}$ ) and on the reduced molar concentration of CaO in the cement due to pozzolanic reactions with slag and fly ash.

Note that the carbonation depths calculated with the models described in the preceding paragraphs would apply for all exposed surfaces. If cracks are present, CO<sub>2</sub> can ingress through them such that the carbonation front advances locally from the penetrated cracks.

## 5.2 Sulfate Attack

As discussed in Section 4.1.2, sulfate attack is caused by reaction of sulfate ions in solution with compounds present in hydrated cement leading to disruptive expansion, strength loss, and/or disintegration. This process typically is controlled by diffusion of sulfate ions into the saturated pores of the cement-based material. Models for predicting sulfate attack range from empirical models to mechanistic reactive–transport models.

### 5.2.1 Empirical Correlation

An example of an empirical model for sulfate attack is that of Atkinson and Hearne (1984), who proposed an empirical relation for sulfate attack based on data collected in the Northwick Park (London, United Kingdom) study Harrison and Teychenne (1981) reported. In this study, cement blocks were exposed to Na<sub>2</sub>SO<sub>4</sub> and MgSO<sub>4</sub> solutions. The measured loss of cement at the corners of the blocks after a 5-year exposure to a 0.19 M Na<sub>2</sub>SO<sub>4</sub> solution was 42 mm [1.7 in]. The depth of attack in MgSO<sub>4</sub> solution was observed to be approximately twice that in Na<sub>2</sub>SO<sub>4</sub> and was linear with time. Also, sulfate attack was observed to be greatest on the block of Portland cement with 8 percent tricalcium aluminate (3CaO·Al<sub>2</sub>O<sub>3</sub>). The following empirical equation for predicting sulfate attack was derived based on the assumption that the rate of attack is proportional to the concentrations of sulfate and magnesium in solution and to the tricalcium aluminate content of the cement

$$x = \frac{4.2 C_3}{5 \cdot 8} \frac{([Mg^{2+}] + [SO_4^{2-}]) t}{0.19} \quad (5-8)$$

or

$$x = 0.55 C_3 ([Mg^{2+}] + [SO_4^{2-}]) t \quad (5-9)$$

where

$x$	—	depth of deterioration (cm)
$C_3$	—	weight percent of tricalcium aluminate in unhydrated cement
$[Mg^{2+}], [SO_4^{2-}]$	—	concentration of Mg <sup>2+</sup> and SO <sub>4</sub> <sup>2-</sup> in bulk solution (mole/liter)
$t$	—	time (yr)

Equation (5-9) is consistent with the observed deterioration of old concrete that was exposed in sulfate-bearing clay for about 40 years (Atkinson, et al., 1985). DOE also used the equation to model sulfate and magnesium attack in its degradation analysis of the grouted tank/vault system at the Idaho National Laboratory (DOE–Idaho, 2003, Appendix E). The equation has obvious limitations, especially when applied outside the range of the data used to derive the correlation.<sup>8</sup> It does not consider other factors that affect the sulfate degradation process, such as cement properties (e.g., water/cement ratio, composition) and changes in the diffusivity of the material due to expansive reactions from the sulfate attack. To consider the effects of these other factors, mechanistic reactive–transport models have been proposed in the literature. Some of these models are discussed in the following section.

## 5.2.2 Reactive–Transport Models

### Diffusion–Reaction Models

Atkinson and Hearne (1990) developed a reactive–transport model for sulfate attack and considered sulfate attack as a three-step process: (i) diffusion of sulfate ions into the cement-based material; (ii) reaction of sulfate ions with aluminum-containing phases in the cement; and (iii) internal expansion that causes stress, cracking, and exfoliation (spalling) of the reacted material from the surface. Although sulfate reactions are known to cause an overall increase in solid volume, Atkinson and Hearne (1990) recognized that not all this solid volume increase will appear as a bulk volume expansion, because some, or all, of the extra volume could be accommodated in the pore volume of the cement-based material. Thus, they conducted experiments to measure the bulk linear expansion of thin mortar beams resulting from reaction with sulfate-containing solutions. The experimental results indicated that bulk expansion did not correlate well with the total reacted sulfate or with the total increase in solid volume, but did correlate well with an increase in solid volume associated with ettringite and brucite formation (i.e., gypsum did not contribute to bulk expansion). The results showed that only about one-twentieth of the solid volume increase due to ettringite and brucite formation appeared as a bulk expansion.

Based on the experimental results, Atkinson and Hearne (1990) derived a linear relationship between the amount of ettringite formed ( $C_E$ ) and the expansive strain in the material. This expansive strain induces a compressive stress within the plane of the reaction zone that eventually leads to mechanical rupture and loss of the reaction zone by spallation. Atkinson and Hearne (1990) stated, “the spalling event will be a brittle failure initiating at some critically stressed flaw and propagating as a crack parallel to the surface.” After spallation, a new reaction zone builds up and the cycle is repeated. Atkinson and Hearne (1990) recognized that the reaction of magnesium ions with portlandite [as in Eq. (4-5)] to form brucite and an expansive phase—gypsum—can contribute to the degradation of the cement-based material. However, they simplified their model of sulfate attack by assuming magnesium ions are not present in the aqueous solution. The authors claimed this assumption does not alter the overall conclusions of their study.

The following equations from Atkinson and Hearne (1990) give the thickness,  $X_{\text{spall}}$ , of the layer that spalls off and the time,  $t_{\text{spall}}$ , for the layer to spall

---

<sup>8</sup>Equation (5-9) may not apply to DOE grout formations. The cement-based material compositions used in the tests are different from the DOE grout formulations, and the test solution compositions are likely to be different from those that will interact with the DOE grouts. Nevertheless, because supplementary cement materials used in DOE grout formulations (i.e., blast furnace slag and fly ash) reduce the permeability or hydraulic conductivity of cement-based materials, it is possible Eq. (5-9) could overpredict the depth of sulfate attack if applied to DOE grouts.

$$X_{\text{spall}} = \frac{2 \alpha \gamma (1 - \nu)}{E (\beta C_E)^2} \quad (5-10)$$

$$t_{\text{spall}} = \frac{X_{\text{spall}}^2 C_E}{2 D_i c_0} \quad (5-11)$$

The degradation rate is given by

$$R = \frac{X_{\text{spall}}}{t_{\text{spall}}} = \frac{E \beta^2 c_0 C_E D_i}{\alpha \gamma (1 - \nu)} \quad (5-12)$$

The parameters in Eqs. (5-10) to (5-12) are defined in Table 5-1. Atkinson and Hearne (1990) listed parameter values applicable to ordinary Portland cement and sulfate-resistant Portland cement, and these values also are given in Table 5-1. The latter type of cement has lower alumina content than the former (see Section 4.1.2). The rate of degradation can be estimated by substituting the relevant parameters into Eq. (5-12). Values of  $C_E$ , the concentration of sulfate reacted as ettringite, needed for input into Eq. (5-12) can be calculated from the equation

$$C_E = m \frac{\text{mass of cement}}{\text{volume of cement}} \quad (5-13)$$

whereas  $m$ , the quantity of sulfate reacted with cement, can be derived from the following equation

$$m = m_0 \log_{10} \frac{t c}{t_r c_k} \quad \text{for } m < m'_c \quad (5-14)$$

Depending on the rate of diffusion relative to the rate of reaction, some iteration may be needed to determine  $C_E$  and the degradation rate.

Atkinson and Hearne (1990) provided example calculations indicating the rate of attack for sulfate-resistant Portland cement was approximately 30 percent lower than the rate for ordinary Portland cement. The thickness of the reaction zone at spalling was found to be independent of sulfate concentration and was on the order of a few millimeters, in agreement with the size of debris from sulfate attack observed in their experiments. Calculations using different sulfate concentrations gave degradation rates directly proportional to sulfate concentration, which is consistent with the empirical Eq. (5-9). The degradation rates calculated using Eqs. (5-9) and (5-12) are in relatively good agreement for ordinary Portland cement, but for sulfate-resistant Portland cement, Eq. (5-9) calculates a much lower degradation rate compared to Eq. (5-12). Atkinson and Hearne (1990) concluded the disagreement between the two models is due to the incorrect assumption in Eq. (5-9) in that only tricalcium aluminate contributes to the expansive reaction. Thus, the authors stated Eq. (5-12) likely predicts more accurately the degradation rate compared to Eq. (5-9). They also indicated their model should be more reliable than those that incorporate diffusion and chemical reaction but neglect the mechanical effects of the reaction.

<b>Table 5-1. List of Parameters Used in Sulfate Attack Model*</b>			
<b>Parameter</b>	<b>Description</b>	<b>Value</b>	<b>Units</b>
$c$	Sulfate concentration in liquid		mole/m <sup>3</sup>
$c_k$	Sulfate concentration in kinetic experiments	12.2	mole/m <sup>3</sup>
$c_0$	Sulfate concentration in external solution		mole/m <sup>3</sup>
$C_E$	Concentration of reacted sulfate as ettringite		mole/m <sup>3</sup>
$D_i$	Intrinsic diffusion coefficient	$10^{-12}$	m <sup>2</sup> /s
$E$	Young's modulus	20	GPa
$m$	Quantity of sulfate reacted with cement		mole/kg of anhydrous cement
$m_c$	Value of $m$ for complete reaction	1.24 (OPC)† 1.07 (SRPC)‡	mole/kg of anhydrous cement
$m_0$	Kinetic constant for $m$	0.32 (OPC) 0.16 (SRPC)	mole/kg of anhydrous cement
$R$	Degradation rate		m/s
$t$	Time		s
$t_r$	Characteristic time for reaction	3,577 (OPC) 1,555 (SRPC)	s
$X$	Thickness of reaction zone		m
$\alpha$	Roughness factor for fracture path	1	none
$\beta$	Linear strain caused by one mole of sulfate reacted in 1 m <sup>3</sup>	$1.8 \times 10^{-6}$	m <sup>3</sup> /mole
$\gamma$	Fracture surface energy of cement-based material	10	J/m <sup>2</sup>
$\nu$	Poisson's ratio	0.3	None

\*Atkinson, A. and J.A. Hearne. "Mechanistic Model for the Durability of Concrete Barriers Exposed to Sulphate-Bearing Groundwaters." Materials Research Society Symposium Proceedings 176. V.M. Oversby and P.W. Brown, eds. Pittsburgh, Pennsylvania: Materials Research Society. pp. 149–156. 1990.  
†OPC—ordinary Portland cement  
‡SRPC—sulfate-resistant Portland cement

Atkinson and Hearne (1990) acknowledged their model has limitations because it neglects the relief of stress by creep and the reduction in diffusivity in the reaction zone due to formation of reaction products. The model treats the degraded zone as transparent to fluxes of aggressive substances and ignores the known protective or semiprotective role reaction products in the zone provide. Moreover, the limited volume of solution used in their study resulted in very little dissolution of cement solids relative to realistic scenarios (e.g., in soils) in which the aggressive

solution is replenished as reaction occurs. Dissolution is an important process to consider because damage of cement-based material occurs primarily as a consequence of the larger volume of reaction products relative to the solid precursors and the dissolution process can reduce the stress associated with volume expansion. In spite of its limitations, the Atkinson and Hearne (1990) model was considered state-of-the-art at the time it was developed and still remains an attractive approach because of its simplicity. However, the model has not been tested on cement-based formulations with supplementary cement materials, and parameters that account for the effect of these materials will have to be derived.

Tixier and Mobasher (2003a,b) developed another reactive–transport model to simulate the response of cement-based material exposed to external sulfate solutions. This model applies Fick’s second law to diffusion of sulfate ions and uses a second-order chemical reaction between penetrating sulfates and calcium aluminates, which can lead to expansion of the solid. A schematic of the model is shown in Figure 5-5. There are three major input parameters in the model categorized under (i) initial material parameters, (ii) exposure conditions, and (iii) size and shape of members. The input parameters are used to estimate physical parameters such as diffusivity, strength, concentration of available calcium aluminates, and the volumetric changes resulting from chemical reactions.

The model incorporates several mechanisms for the reaction of calcium aluminates with sulfates to form expansive ettringite. It treats the three distinct, but coupled, problems of sulfate diffusion, calcium aluminate depletion, and crack front propagation as a moving boundary problem as shown in Figures 5-6 and 5-7. With increasing time, sulfates diffuse and react with aluminates, causing ettringite to form and potentially cause cracking. Cracking changes the coefficient of sulfate diffusivity. This change may be linked to a scalar damage parameter  $\omega$  that is defined from the available models for uniaxial stress–strain response (Tixier and Mobasher, 2003a).

The model assumes that the calcium aluminates may be a blend of three reactive phases: tricalcium aluminate, tetracalcium aluminohydrate ( $4\text{CaO}\cdot\text{Al}_2\text{O}_3\cdot 13\text{H}_2\text{O}$ ), and monosulfate ( $3\text{CaO}\cdot\text{Al}_2\text{O}_3\cdot\text{CaSO}_4\cdot 12\text{H}_2\text{O}$ ). In the model, the reaction of these phases with ingressing sulfate is lumped into a global sulfate–aluminate reaction, and the volumetric change is calculated based on stoichiometric amounts. The coupled differential equations for the depletion of both sulfates and aluminates are solved using numerical techniques to account for the (i) limited supply of tricalcium aluminate, (ii) cracking-induced change in sulfate diffusivity, and (iii) degradation effects of the expansive reactions. The amount of ettringite formed as a function of time and space is related to the volumetric strain, from which the constitutive response of the matrix and the expansive stresses are calculated. Microcracks are initiated when the tensile strength of the matrix is reached, leading to changes in the sulfate diffusivity and a reduction in matrix elastic properties. The model predicts the amount of reacted aluminates, the stresses generated, and internal parameters such as damage, expansion levels, weight gain, stiffness degradation, and tensile strength degradation (Tixier and Mobasher, 2003a).

The authors used a variety of literature data on the linear expansion versus time of specimens exposed to sulfate solutions to validate the model (Tixier and Mobasher, 2003b). Using the model, Mobasher and Ferraris (2004) conducted a parametric study to evaluate the effect of several features on the expansion characteristics of the sample: initial sulfate concentration, diffusivity of the material (as affected by cracking or by the use of supplementary cement

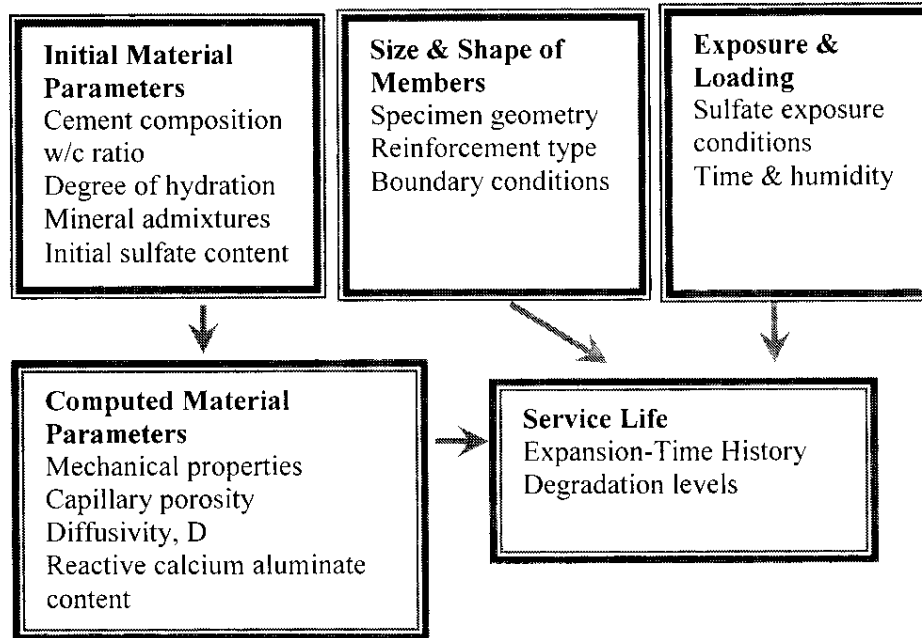


**Figure 5-5. Schematic of the Sulfate Attack Model Tixier and Mobasher (2003a,b) Developed. Reprinted From Tixier, R. and B. Mobasher, "Modeling of Damage in Cement-Based Materials Subjected to External Sulfate Attack. I: Formulation," *Journal of Materials in Civil Engineering*, Vol. 15, pp. 305–313. Copyright® 2003, With Permission From American Society of Civil Engineers.**

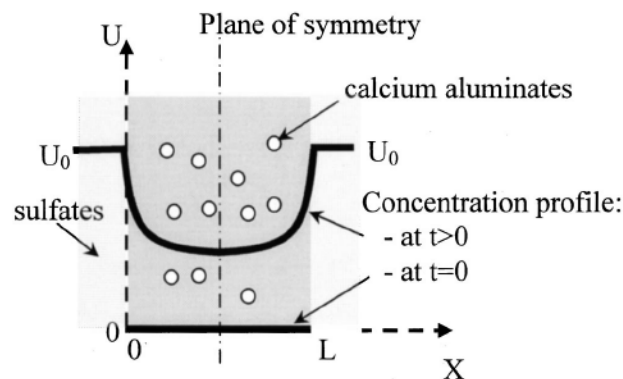


**Figure 5-6. Schematic Representation of Sulfate Penetration and Reaction Showing Profiles of Sulfate Concentration ( $U$ ) at Times  $t = 0$  and  $t > 0$  in a Specimen of Length  $L$  Exposed to a Sulfate Solution. Reprinted From Tixier, R. and B. Mobasher, "Modeling of Damage in Cement-Based Materials Subjected to External Sulfate Attack. I: Formulation," *Journal of Materials in Civil Engineering*, Vol. 15, pp. 305–313. Copyright® 2003, With Permission From American Society of Civil Engineers.**

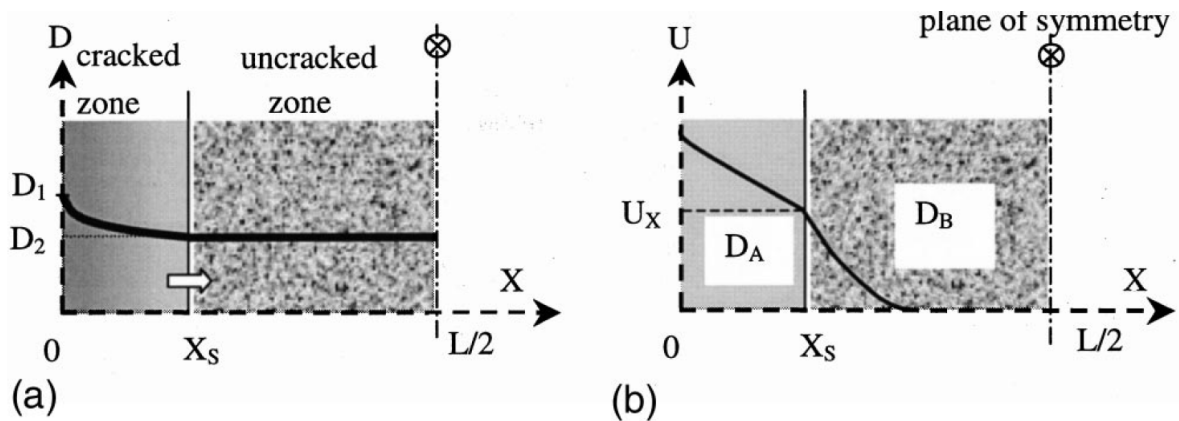


**Figure 5-7. Schematic Representation of (a) Diffusivity Profile and (b) Sulfate Concentration Profile for a Cracked ( $D_A$ ) and Uncracked ( $D_B$ ) Specimen. The Region  $D_B$  Has a Constant Diffusion Coefficient,  $D_2$ , Whereas  $D_A$  Has a Variable Diffusion Coefficient. Reprinted From Tixier, R. and B. Mobasher, "Modeling of Damage in Cement-Based Materials Subjected to External Sulfate Attack. I: Formulation," *Journal of Materials in Civil Engineering*, Vol. 15, pp. 305–313. Copyright® 2003, With Permission From American Society of Civil Engineers.**

materials), and amount of sulfate phase (e.g., gypsum) initially present in the material. Figure 5-8 shows the results of a parametric study of the effect of diffusivity on the expansion-time curves for specimens with varying degrees of damage due to cracking. In

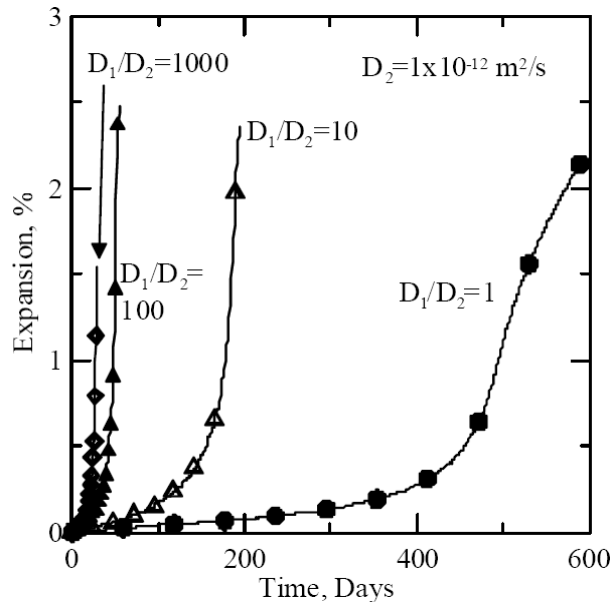


**Figure 5-8. Effect of Diffusivity on the Expansion of a Cement-Based Material With Different Levels of Damage Due to Sulfate-Induced Cracking. The Level of Damage Is Represented by  $D_1/D_2$ , Where  $D_2$  Is the Diffusivity of the Uncracked Material. Reprinted From Mobasher, B. and C.F. Ferraris, "Simulation of Expansion in Cement Based Materials Subjected to External Sulfate Attack," *Advances in Concrete Through Science and Engineering*, J. Weiss, K. Kovler, J. Marchand, and S. Mindess, eds., pp. 1–12, Copyright® 2004, With Permission From RILEM Publications S.A.R.L.**

this figure, the initial diffusivity,  $D_2$ , of the specimen is assumed to be  $1 \times 10^{-12} \text{ m}^2/\text{s}$  [ $1.1 \times 10^{-11} \text{ ft}^2/\text{s}$ ] and the range in degree of damage due to cracking is represented by the ratio  $D_1/D_2$ . A parameter  $D_1/D_2 = 10$  means that the cracked material would have its diffusivity increase from  $1 \times 10^{-12} \text{ m}^2/\text{s}$  [ $1.1 \times 10^{-11} \text{ ft}^2/\text{s}$ ] to 10 times that value. The results shown in Figure 5-8 indicate that as time increases, an increased diffusivity due to cracking would directly result in faster rates of expansion. The expansion and degradation would occur faster (the curves are steeper) at higher  $D_1/D_2$  ratio. Mobasher and Ferraris (2004) also inferred that slower expansion and lower degradation rates resulted from using supplementary cement materials, such as fly ash and blast furnace slag, and from a lower water/cement ratio because these lead to lower diffusivity. Figure 5-9 shows the results of a parametric study on the effect of initial gypsum content on the expansion of sulfate-attacked specimens. The results indicate that an increase in the amount of initial gypsum in the cement-based material increases the potential for damage and degradation.

Tixier and Mobasher (2003b) identified possible improvements to their model, including (i) accounting for the effect of decalcification on the diffusion, the mechanical properties, and the damage parameter  $\omega$ ; (ii) incorporating other expansive reactions (e.g., formation of gypsum in addition to ettringite); (iii) incorporating the effect of supplementary cement materials on the diffusivity parameter; and (iv) extending the model to handle cases of wetting and drying.

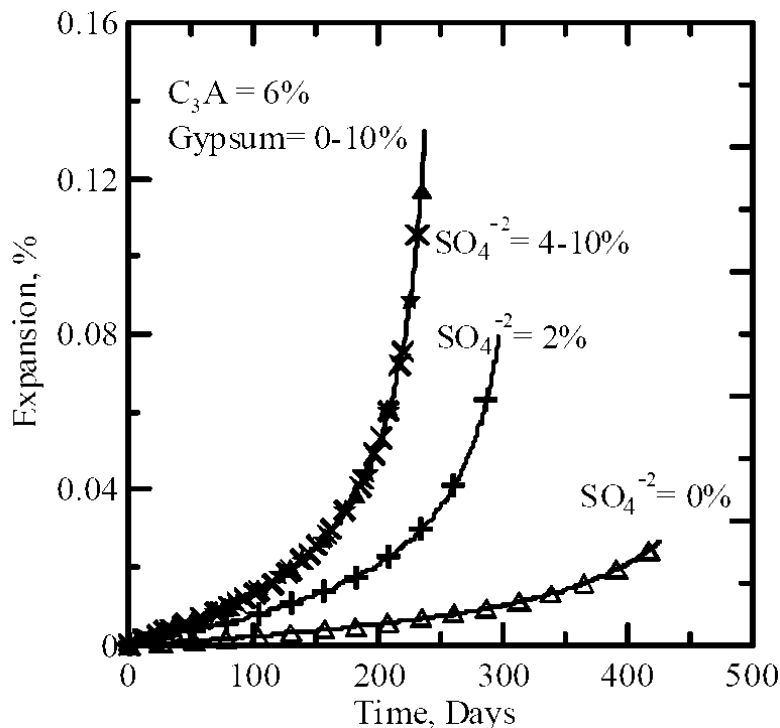


**Figure 5-9. Effect of Initial Gypsum Content (Labeled as  $\text{SO}_4^{2-}$ ) on the Sulfate Reaction-Induced Expansion of a Specimen Containing 6 Percent Tricalcium Aluminate ( $\text{C}_3\text{A}$ ). Reprinted From Mobasher, B. and C.F. Ferraris, "Simulation of Expansion in Cement Based Materials Subjected to External Sulfate Attack," *Advances in Concrete Through Science and Engineering*, J. Weiss, K. Kovler, J. Marchand, and S. Mindess, eds., pp. 1-12, Copyright© 2004, With Permission From RILEM Publications S.A.R.L.**

The models described in preceding paragraphs are concerned with sulfate attack under fully saturated hydrologic conditions. However, in many cases, sulfate attack will occur under unsaturated conditions. Modeling flow and transport under unsaturated conditions involves different and complex definitions of transport parameters and inevitably is more complicated than under saturated conditions. Nevertheless, significant progress has been made in implementing degradation models in unsaturated conditions as discussed next.

### Diffusion–Advection–Reaction Models

Marchand, et al. (1999) developed a reactive–transport model more elaborate than the one by Tixier and Mobasher (2003a,b) to predict the degradation of cement-based material subjected to external sulfate attack. The Marchand, et al. (1999) model differs from the Tixier and Mobasher (2003a,b) model in its applicability to hydrologically unsaturated conditions, inclusion of advective transport of ionic species in addition to diffusive transport, and the electrical coupling between the various ionic species diffusing in the solution. The electrical coupling of ionic species ensures electrical neutrality is preserved and more accurately describes the ionic transport process in the material. Similar to the model of Tixier and Mobasher (2003a,b), the model of Marchand, et al. (1999) accounts for the chemical interaction of dissolved species with the hydrated phases in the cement paste and the effects of the chemically induced microstructural alterations on the transport properties of the material. But in contrast to the model of Tixier and Mobasher (2003a,b), the model of Marchand, et al. (1999) also can account for the effect of leaching (i.e., dissolution of portlandite and decalcification of C-S-H).

Coupled diffusive and advective ionic transport in the model of Marchand, et al. (1999) is represented by the following equation (for a one-dimensional system)

$$F_i = -D_i \left( \frac{\partial c_i}{\partial x} + \frac{z_i F}{RT} c_i \frac{\partial V}{\partial x} \right) - c_i \left( D_w \frac{\partial \theta_w}{\partial x} \right) \quad (5-15)$$

where

$F_i$	—	flow of ionic species $i$ (mol/m <sup>2</sup> ·s)
$x$	—	distance from the interface between the cement-based material and the source of external sulfate (m)
$D_i$	—	diffusion coefficient of ionic species $i$ in the porous cement-based material (m <sup>2</sup> /s)
$D_w$	—	diffusion coefficient of water in the porous cement-based material (m <sup>2</sup> /s)
$c_i$	—	ion concentration (mol/m <sup>3</sup> )
$z_i$	—	ionic charge
$\theta_w$	—	water content (m <sup>3</sup> of water/m <sup>3</sup> of cement-based material)
$T$	—	temperature (K)
$V$	—	local electrical potential (Volt)
$R$	—	gas constant (8.3143 J/mol/K)
$F$	—	Faraday constant (9.64846 × 10 <sup>4</sup> C/mol)

The mass balance equation for each ionic species is represented by the equation

$$(1 - \phi) \frac{\partial C_{is}}{\partial t} + \rho_s \alpha \kappa \frac{\partial c_{ia}}{\partial t} + \frac{\partial (\theta_w c_i)}{\partial t} \quad (5-16)$$

$$-\frac{\partial}{\partial x} \left[ \theta_w D_i \left( \frac{\partial c_i}{\partial x} + \frac{z_i F}{RT} c_i \frac{\partial V}{\partial x} \right) + \theta_w c_i \left( D_w \frac{\partial \theta_w}{\partial x} \right) \right] = 0$$

where

$\phi$	—	porosity of the cement-based material
$\alpha$	—	specific surface area of the cement-based material (m <sup>2</sup> /kg)
$\kappa$	—	thickness of water layer adsorbed on the pore wall (m)
$\rho_s$	—	density of the cement-based material (kg/m <sup>3</sup> )
$c_{is}$	—	concentration of species i in the solid phase (mol/m <sup>3</sup> )
$c_{ia}$	—	concentration of species i adsorbed on the solid (mol/m <sup>3</sup> )

The advection–diffusion represented by Eq. (5-16) has to be solved for all the ionic species considered in a particular system. For modeling sulfate attack, Marchand, et al. (1999) limited the number of ionic species to four: (i) sulfate; (ii) sodium; (iii) calcium; and (iv) hydroxyl ions, although magnesium ions had to be included in some systems. It was also assumed the only hydrated phases present are hydrogarnet, portlandite, ettringite, and gypsum, and the chemical reactions are fast compared to the transport process such that ionic binding can be considered to be an equilibrium process. To solve Eq. (5-16), the terms  $\partial c_{is}/\partial t$  and  $\partial c_{ia}/\partial t$  must be defined for each ionic species considered. The term  $\partial c_{is}/\partial t$  accounts for the formation or the dissolution of solid phases during sulfate attack (e.g., formation of ettringite or dissolution of portlandite). The term  $\partial c_{ia}/\partial t$  models the physical interaction of ions on (or near) the pore wall. The complete mathematical treatment of  $\partial c_{is}/\partial t$  and  $\partial c_{ia}/\partial t$  is described in Marchand, et al. (1999).

Chemical reactions, such as dissolution of portlandite and decalcification of C-S-H, significantly alter the microstructure of the solid and affect the rate at which ionic species can diffuse through the pore structure of the cement-based material. The model of Marchand, et al. (1999) uses the following equation from Bentz and Garboczi (1992a,b) to relate the diffusion coefficient,  $D_i$ , of a given ionic species in an undamaged hydrated cement to the porosity,  $\phi$

$$\frac{D_i}{D_{i0}} = 0.001 + 0.07\phi^2 + 1.8(\phi - 0.18)^2 H(\phi - 0.18) \quad (5-17)$$

where  $D_{i0}$  is the diffusion coefficient of the species in pure water and  $H(x)$  is the Heaviside function [ $H(x = \phi - 0.18) = 1$  for  $x > 0$  and  $H(x = \phi - 0.18) = 0$  for  $x \leq 0$ ]. In the model, changes in porosity resulting from sulfate attack are calculated from the amount and density of cement phases that dissolve or precipitate. The complex system of nonlinear equations in the model is solved numerically. The spatial discretization of the coupled system is performed through a finite element method, and the set of nonlinear equations is solved with the Newton-Raphson algorithm.

Marchand, et al. (1999) conducted numerical simulations to predict sulfate and magnesium ion penetration in a concrete slab over a 50-year period. Figure 5-10 shows a schematic representation of a concrete slab {11.5 cm [4.52 in] thick and initially undamaged} contacting soil containing sulfate, sodium, and magnesium ions. The simulations provided information on the formation of ettringite, dissolution of portlandite, and decalcification of C-S-H in the concrete slab after being exposed to different sodium and magnesium sulfate solutions. The results for two concrete mixtures with water/cement ratios of 0.45 and 0.65 (with corresponding total

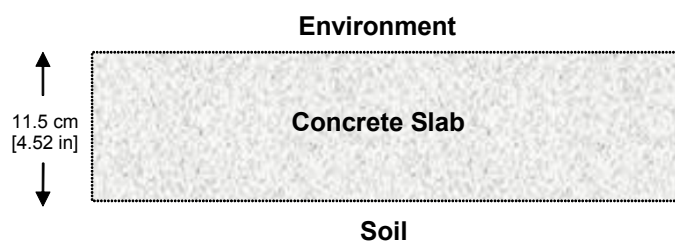


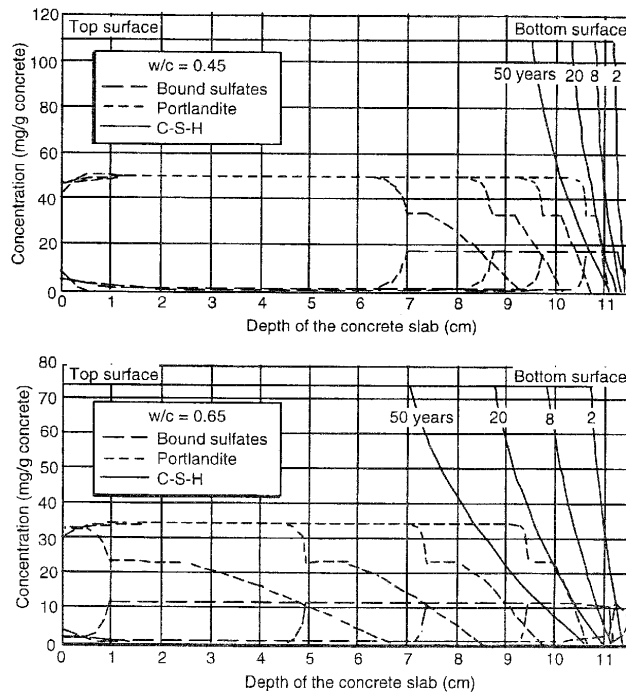
**Figure 5-10. Schematic Representation of a Concrete Slab Marchand, et al. (1999) Considered in Numerical Simulations of Sulfate Attack**

porosity of 11.7 and 13 percent, respectively) are shown in Figure 5-11. The results indicate sulfate attack causes a major reorganization of the hydrated cement paste microstructure: new sulfate-bearing solids are formed and the dissolution of portlandite, as well as decalcification of C-S-H, is significantly increased. As shown in Figure 5-11, the model predicts the progression of a degradation front from the bottom of the concrete slab (in contact with the sulfate-containing soil) to the center of the slab. The degradation front penetrated faster in the slab with the 0.65 water/cement ratio compared to the slab with the 0.45 water/cement ratio because of the higher porosity in the former that allowed faster transport of moisture and ions within the material. This result supports the requirement in some building codes [e.g., CSA A23.1-04 (Canadian Standards Association, 2004); ACI 201.2R (American Concrete Institute, 2006)] that limits the maximum water/cement ratio for any concrete exposed to a severe sulfate environment at 0.45.

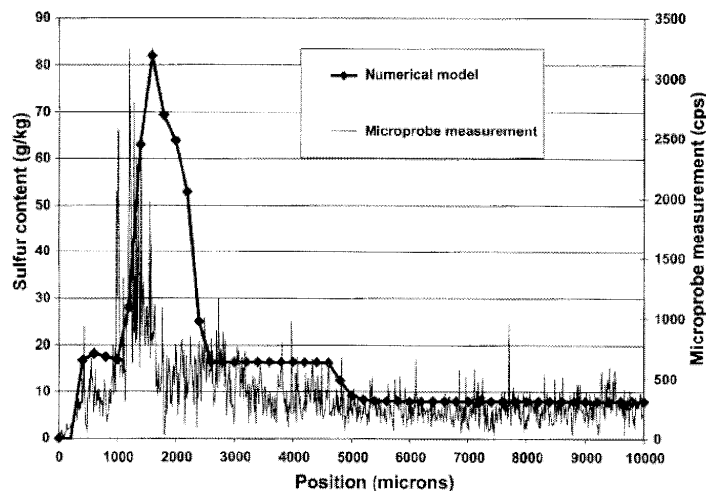
The model Marchand, et al. (1999) described was later improved and called the STADIUM model (Marchand, et al., 2002). STADIUM has an expanded set of ionic species and solid phases such that multiple degradation processes of hydrated cement paste (e.g., chloride penetration, external sulfate and magnesium attack, and leaching) can be evaluated. The model can simulate transport by diffusion as well as by advection under saturated or unsaturated conditions. The model considers eight ionic species— $K^+$ ,  $Na^+$ ,  $Mg^{2+}$ ,  $Ca^{2+}$ ,  $SO_4^{2-}$ ,  $OH^-$ ,  $Al(OH)_4^-$ , and  $Cl^-$ —and nine solid phases—portlandite, C-S-H, ettringite ( $3CaO \cdot 3CaSO_4 \cdot Al_2O_3 \cdot 32H_2O$ ), gypsum ( $CaSO_4 \cdot 2H_2O$ ), mirabilite ( $Na_2SO_4 \cdot 10H_2O$ ), halite (NaCl), brucite [ $Mg(OH)_2$ ], hydrogarnet ( $3CaO \cdot Al_2O_3 \cdot 6H_2O$ ), and Friedel's salt ( $3CaO \cdot CaCl_2 \cdot Al_2O_3 \cdot 10H_2O$ ). The decalcification of poorly crystallized C-S-H, which is represented in the model by a combination of  $Ca(OH)_2$  and  $CaH_2SiO_4$ , is assumed to proceed by dissolution of the  $Ca(OH)_2$  part, leaving behind a  $CaH_2SiO_4$  with a Ca/Si ratio of 1.0. As with other reactive-transport models, the transport equations are solved separately from the chemical reaction equations. To account for changes in porosity resulting from dissolution or precipitation on transport, a correction factor that is a function of porosity is used to modify the diffusion coefficient of ionic species.

Figure 5-12 compares the sulfur profile Maltais, et al. (2004) calculated using STADIUM with that determined experimentally on a sample exposed to a sodium sulfate solution for 3 months under saturated conditions. As the figure shows, the model correctly predicts the location of the gypsum (sulfur) peak at 1,000 to ~2,500  $\mu m$  [0.039 to ~0.098 in] and the thickness of the ettringite layer that ranges from ~2,500 to 5,000  $\mu m$  [~0.098 to 0.20 in].

Marchand, et al. (2002) also compared analytical results of field samples with simulation results. Vertical cores of 11.5-cm [4.5-in]-thick concrete garage slabs that had been exposed to



**Figure 5-11. Results of Simulations of Sulfate Attack Showing the Penetration of Degradation Front in a Concrete Slab (Represented in Figure 5-10) as a Function of Time. Reprinted From Marchand, J., E. Samson, and Y. Maltais, "Modeling Microstructural Alterations of Concrete Subjected to External Sulfate Attack," *Materials Science of Concrete: Sulfate Attack Mechanisms*, J. Marchand and J.P. Skalny, eds., pp. 211–257. Copyright© 1999, With Permission From Wiley.**



**Figure 5-12. Comparison of Measured Sulfur Profile in Cement Sample Exposed to a 0.05 mol/L  $\text{Na}_2\text{SO}_4$  Solution for 3 Months With the Sulfur Profile Calculated Using STADIUM. Reprinted From Maltais, Y., J. Marchand, and E. Samson, "Predicting the Durability of Portland Cement Systems in Aggressive Environments—Laboratory Validation," *Cement and Concrete Research*, Vol. 34, pp. 1,579–1,589. Copyright© 2004, With Permission From Elsevier.**

sulfate-bearing soils for 8 years were taken and analyzed with a scanning electron microscope and energy-dispersive spectrometry. For each core, the locations of the ettringite formation layer, portlandite dissolution front, C-S-H decalcification zone, and gypsum precipitation layer were determined. Numerical simulations of the concrete slab degradation were conducted using STADIUM. Table 5-2 compares the electron microscope results with the simulation results. This comparison indicates that the model correctly predicts the depth of penetration of the ettringite precipitation layer and the thickness of the portlandite-depleted zone in the slab.

Note that the models discussed in the preceding paragraphs do not address a form of sulfate attack variously termed “internal sulfate attack” or “delayed ettringite formation.” The problem of delayed ettringite formation is sufficiently important to warrant a recent book by Scrivener and Skalny (2004). When cement-based materials are subjected to a thermal excursion during the course of early hydration, the solid phase mineralogy that develops can be affected. The initial temperature excursion may be deliberate, such as when concrete is warm cured, or may be fortuitous, such as when the escape of exothermic heat of hydration is prevented. The latter situation most often is encountered in large pours of grout or concrete. With increasing temperature up to 40–50 °C [104–122 °F], the solid phase mineralogy remains substantially unchanged from the ambient temperature assemblage. However, with further increases in temperature, the mineralogy exhibits progressively greater changes. The mineralogy developed during the course of high temperature cure is unstable at lower temperatures; thus during cooling, it gradually reverts to the more stable low-temperature assemblage. For instance, ettringite formed during early hydration decomposes at high temperatures but spontaneously reforms at lower temperatures. Diffusion into or out of the system is not necessary—the process is isochemical. The transformation in mineralogy may be a slow process requiring months or even years to complete, but it is characterized by a volume expansion. For instance,

<b>Table 5-2. Comparison of Scanning Electron Microscopy Observations and STADIUM Simulation Results*</b>		
	<b>Depth of Penetration (mm)</b>	
	<b>Scanning Electron Microscopy Observations</b>	<b>Simulation Results†</b>
Ca(OH) <sub>2</sub> dissolution	From 12 to 35	20, 19, 25
C-S-H decalcification	From 6 to 12	11, 10, 14
Ettringite formation	From 12 to 35	32, 32, 12 to 28
Gypsum formation	From 0 to 12	20, 18, 2 to 20
Brucite formation	—	—, —, 18
Carbonation‡	From 5 to 17	—, —, —

\*Marchand, J., E. Samson, Y. Maltais, R.J. Lee, and S. Sahu. “Predicting the Performance on Concrete Structures Exposed to Chemically Aggressive Environment—Field Validation.” *Materials and Structures*. Vol. 35. pp. 623–631. 2002.  
†Some parameters were varied between different simulations  
‡Not predicted by the actual version of the STADIUM model

ettringite has a lower specific density {1.77 g/cm<sup>3</sup> [0.064 lb/in<sup>3</sup>] than other cement minerals, typically >2 g/cm<sup>3</sup> [>0.072 lb/in<sup>3</sup>]} and its reformation upon cooling gives rise to the observed expansion. Delayed ettringite formation has not been modeled, simply because it is best to avoid its occurrence (e.g., by controlling the increase in grout temperature in large pours).

## 5.3 Leaching

As discussed in Section 4.1.3, in leaching, a liquid dissolves and removes the soluble components of a material. Leaching is potentially an important mechanism for gradual degradation of cement-based engineered barriers because of the large chemical gradient between the groundwater and the components of the cement-based material. The solid phases in the hydrated cement are stable under the alkaline pH condition of the cement pore waters, but are susceptible to dissolution when exposed to waters with much lower pH.

Various models for calculating the effects of leaching on the properties of cement-based materials have been published in the literature. These models vary from purely chemical approaches that neglect transport processes to more complex reactive–transport models that account for the coupling between chemical and transport processes. Several of these models are discussed in the following sections.

### 5.3.1 Chemical Models of Leaching

An example of a purely chemical approach to modeling the leaching of cement-based materials is the thermodynamic model of Berner (1992a), which was used to evaluate the evolution of system chemistry during degradation of cement in a radioactive waste repository. In this model, the basic assumptions include

- The cement is fully hydrated (i.e., no unreacted clinker phases), and all solid phases can be modeled using the concepts of thermodynamic equilibrium.
- The chemical behavior of cement can be modeled adequately using a subset of solids typically present in hydrated cement. The subset of solids used by Berner (1992a) comprises C-S-H, portlandite [Ca(OH)<sub>2</sub>], brucite [Mg(OH)<sub>2</sub>], potassium hydroxide (KOH), and sodium hydroxide (NaOH).
- The rates of chemical reactions between cement and leachant (groundwater) are much faster than transport rates.

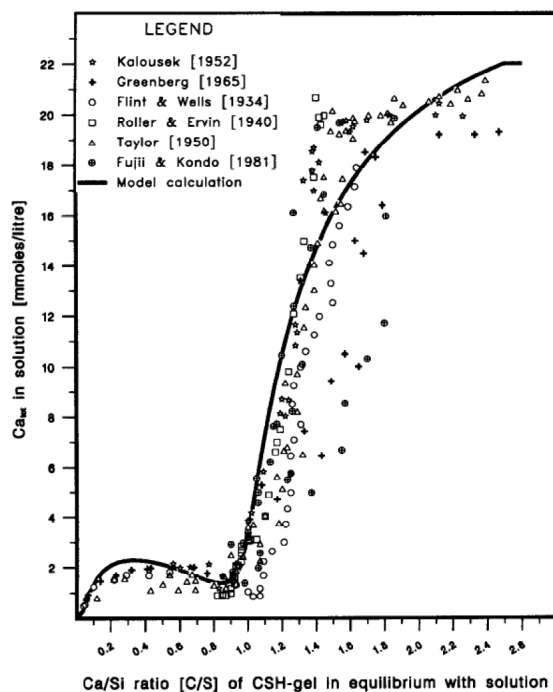
An advantage of the purely chemical approach is that it can be implemented using widely available geochemical equilibrium computer codes, such as MINEQL (Westall, et al., 1976), EQ3/6 (Wolery, 1992), PHREEQE (Parkhurst, et al., 1980), Geochemist's Workbench<sup>®</sup> (Bethke, 1996), and GEMS-PSI (Kulik, et al., 2004). Berner (1992a) used MINEQL to implement his model. However, calculating the solubility of the C-S-H phase using a geochemical equilibrium code is difficult because C-S-H has a nontrivial, incongruent solubility behavior that is not handled by standard geochemical codes. Thus, Berner (1992a) used a nonideal mixture of two model solids to represent the C-S-H phase in each of three ranges of Ca/Si ratio, as listed in Table 5-3. Although the model solids Berner (1992a) used are different from the well-known chemical compounds with the same composition, the use of these fictive components allowed calculations of solubility and pore water pH over the entire range of C-S-H Ca/Si ratio. The calcium concentrations and pHs of solutions in equilibrium with C-S-H are illustrated in

Figures 5-13 and 5-14, respectively. As shown in the figures, the values calculated using Berner's model agree very well with experimental data taken from the literature.

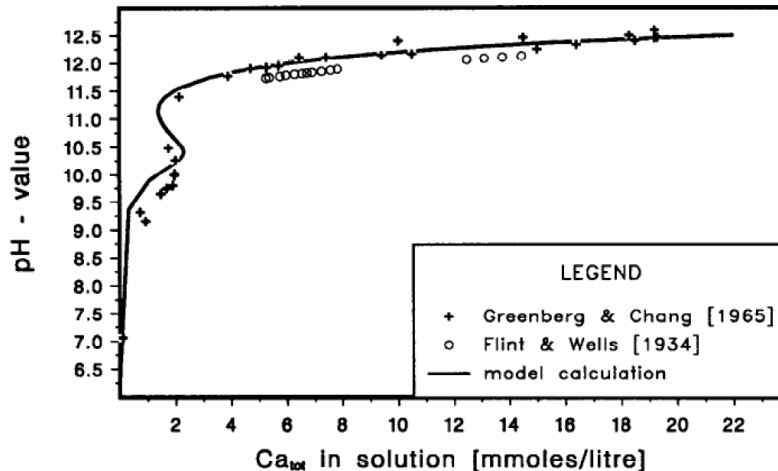
Berner (1992a) used his thermodynamic model to estimate how the chemical inventory of a cement-based structure evolves with time in a given groundwater environment. The

Table 5-3. Selected Model Solids Berner Used To Describe the Solubility Behavior of C-S-H at Varying Ca/Si Ratio*	
Ca/Si Range	Model Solids
Ca/Si = 0	SiO <sub>2</sub> †
0 < Ca/Si ≤ 1	SiO <sub>2</sub> and CaH <sub>2</sub> SiO <sub>4</sub>
1 < Ca/Si ≤ 2.5	Ca(OH) <sub>2</sub> and CaH <sub>2</sub> SiO <sub>4</sub> †
Ca/Si > 2.5	Ca(OH) <sub>2</sub> † and CaH <sub>2</sub> SiO <sub>4</sub> †

\*Berner, U.R. "Evolution of Pore Water Chemistry During Degradation of Cement in a Radioactive Waste Repository Environment." *Waste Management*. Vol. 12. pp. 201–219. 1992.  
 †Model solids marked with a † are assigned fixed solubility products; unmarked solids have solubility products that vary with the Ca/Si ratio of the C-S-H phase. Values or equations for the solubility product of the model solids are given in Berner (1992).



**Figure 5-13. Calcium Concentration of Solutions in Equilibrium With C-S-H Berner (1992a) Calculated, Compared With Experimental Data. Reprinted from Berner, U.R., "Evolution of Pore Water Chemistry During Degradation of Cement in a Radioactive Waste Repository Environment," *Waste Management*, Vol. 12, pp. 201–219. Copyright© 1992, With Permission From Elsevier.**



**Figure 5-14. pH of Solutions in Equilibrium With C-S-H Berner (1992a) Calculated, Compared With Experimental Data. Reprinted from Berner, U.R., "Evolution of Pore Water Chemistry During Degradation of Cement in a Radioactive Waste Repository Environment," *Waste Management*, Vol. 12, pp. 201–219. Copyright© 1992, With Permission From Elsevier.**

calculations used a mixing tank approach in which a normalized quantity of hydrated cement was reacted with a volume of leachant equal to the total porosity of the hydrated cement. The amount of solids that dissolved or precipitated was used to recalculate how much of the initial solids remained in the cement and how much the porosity changed. After each calculation step, the equilibrated pore solution was replaced with a fresh volume of leachant. The calculations, which were done using MINEQL, were repeated until complete leaching of the cement inventory was achieved. Some of the leaching simulation results of Berner (1992a) are shown in Figures 5-15 and 5-16. Figure 5-15 illustrates the evolution of pore water composition of a sulfate-resistant Portland cement degrading in a marl-type groundwater (with ionic constituents comprised predominantly of  $\text{Na}^+$ ,  $\text{Ca}^{2+}$ ,  $\text{SO}_4^{2-}$ ,  $\text{Cl}^-$  and  $\text{HCO}_3^-$ ), and Figure 5-16 shows the evolution of the solid phase inventory of a pozzolanic cement degrading in a similar type of groundwater. The evolution of pore water pH is of particular interest because it is a useful indicator of the "lifetime" of cement. Figure 5-17 compares the modeled pH evolution of pore water in sulfate-resistant Portland cement degrading in pure water and in marl-type groundwater. The figure illustrates that it takes ~4,500 to 7,500 cycles to completely degrade the hydrated cement and that reactions with carbonate-bearing marl-type groundwater result in faster degradation than reactions with pure water due to the transformation of hydrated cement minerals to calcite.

The results plotted in Figures 5-15, 5-16, and 5-17 are expressed in terms of pore water exchange cycles, which are independent of both the size of the system and time. The number of cycles can be converted to time using the porosity of the hydrated cement (21 percent for the sulfate-resistant Portland cement and 26 percent for the pozzolanic cement) and an assumed value for the volumetric flow rate. Neall (1996) used the modeling approach of Berner (1992a) to simulate groundwater leaching of a column of hydrated cement/concrete and plotted the evolution of pore water pH as a function of number of cycles of pore water exchange and of time based on a groundwater flow rate of  $4 \times 10^{-12} \text{ m}^3/\text{m}^2\cdot\text{s}$  [ $1.3 \times 10^{-11} \text{ ft}^3/\text{ft}^2\cdot\text{s}$ ].

Diagrams such as Figure 5-17 are useful in illustrating the effect of various parameters (e.g., concentration of cement and groundwater constituents, mixing ratios of blended cements) on cement performance. However, Berner (1992a) acknowledged using the mixing tank

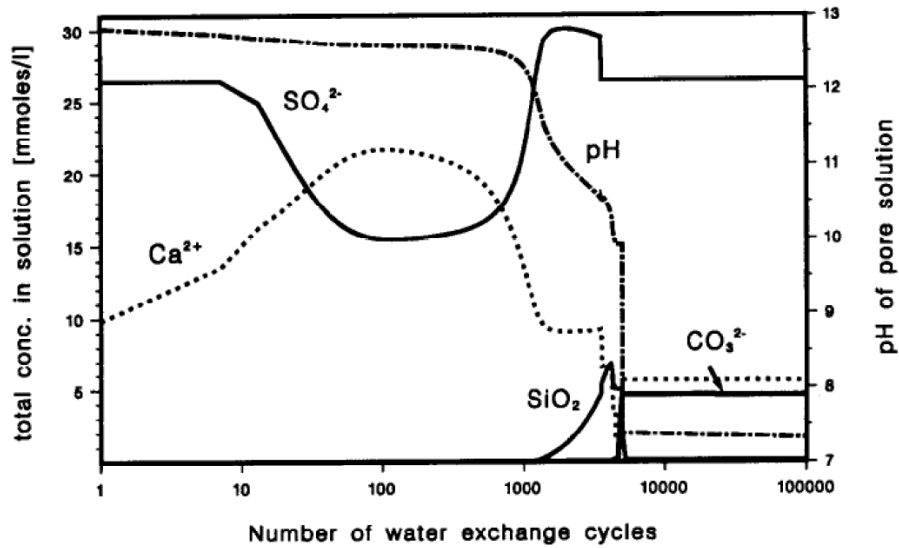


Figure 5-15. Calculated Evolution of Pore Water Composition of a Sulfate-Resistant Cement Degrading in a Marl-Type Groundwater. Reprinted from Berner, U.R., "Evolution of Pore Water Chemistry During Degradation of Cement in a Radioactive Waste Repository Environment," *Waste Management*, Vol. 12, pp. 201–219. Copyright© 1992, With Permission From Elsevier.

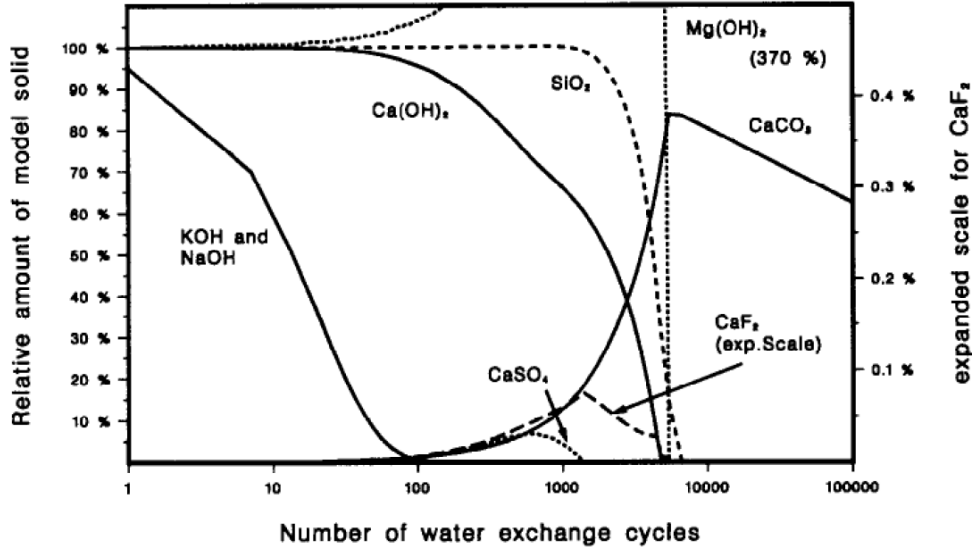
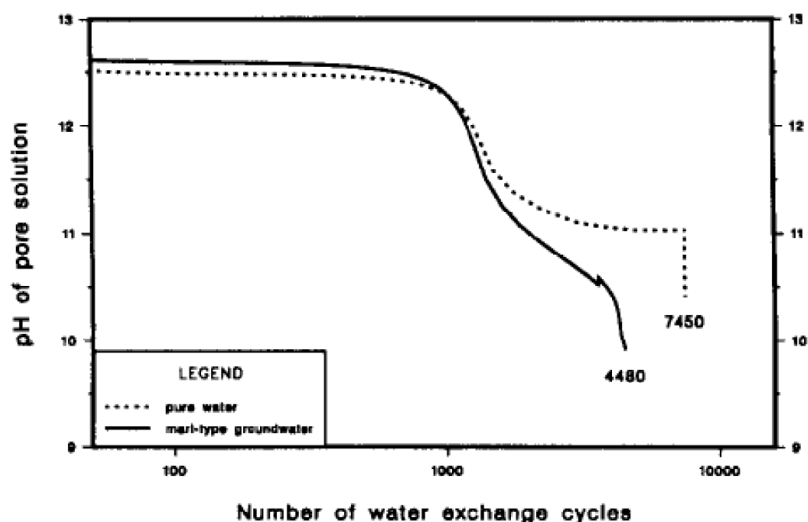


Figure 5-16. Calculated Evolution of the Solid Phase Inventory of a Pozzolanic Cement Degrading in a Marl-Type Groundwater. The Amount of Each Solid Plotted in the Figure Is Relative to Its Initial Amount in the Hydrated Cement. Reprinted from Berner, U.R., "Evolution of Pore Water Chemistry During Degradation of Cement in a Radioactive Waste Repository Environment," *Waste Management*, Vol. 12, pp. 201–219. Copyright© 1992, With Permission From Elsevier.



**Figure 5-17. Evolution of Pore Water pH in a Sulfate-Resistant Portland Cement Degrading in Pure Water and in a Marl-Type Groundwater. Reprinted from Berner, U.R., "Evolution of Pore Water Chemistry During Degradation of Cement in a Radioactive Waste Repository Environment," *Waste Management*, Vol. 12, pp. 201–219. Copyright© 1992, With Permission From Elsevier.**

approach is limited because the temporal evolution of chemistry, hence degradation, is not expressed in terms of real time but in water exchange cycles. Relating cycles with real time requires additional information (e.g., the amount of groundwater entering the system per unit time). Also, other processes are not considered, such as mass transport, spatial and temporal heterogeneities of processes, and kinetically controlled reactions.

Glasser and coworkers (Glasser, et al., 1988; Atkins, et al., 1994, 1991, 1990; Bennett, et al., 1992) identified an important limitation of the approach used in studies similar to that of Berner (1992a) and other studies that assume reactions involving early formed cement phases dominate the chemical evolution of the system, particularly for long time periods. The solid phase composition of a cement paste aged over laboratory time scales will almost certainly be thermodynamically metastable and will be quite different than that of cement pastes aged for 100 or 1,000 years. Thus, other properties, such as pore water composition and microstructure of the material, also may be quite different, which would make predictions of long-term behavior based on short-term data misleading. For cements blended with supplementary materials such as fly ash and blast furnace slag, the difference between short- and long-term properties likely would be greater because these additives hydrate much more slowly than Portland cement. Thus, Glasser and coworkers developed a normative chemical model for predicting the solid phase assemblage following complete hydration of blended cements based on the bulk oxide composition of the unhydrated components.

The model is based on simplifying cement to the six-component  $\text{CaO-SiO}_2\text{-Al}_2\text{O}_3\text{-SO}_4\text{-MgO-H}_2\text{O}$  system, which constitutes greater than 95 percent of most cement formulations (Atkins, et al., 1992a; Bennett, et al., 1992). The model and associated database were derived from (i) observations on phase development in cement blends aged under controlled conditions, (ii) extensive phase compatibility experiments using synthetic mixtures of pure phases, (iii) literature data, (iv) solubility measurements on single phases, and (v) thermodynamic

modeling (Atkins, et al., 1994). It is implemented using the CEMCHEM code (Atkins, et al., 1992a,b) and is applicable to blends of ordinary Portland cement with up to ~90 percent blast furnace slag or ~30 percent fly ash. An example of phase assemblages calculated using CEMCHEM for a blend of ordinary Portland cement and blast furnace slag is illustrated in Figure 5-18. The resulting solid phase assemblage derived from CEMCHEM and the known solubility constants of the solids subsequently can be used to predict the composition of the aqueous phase in equilibrium with the cement-based material. For example, Atkins, et al. (1992a) used the geochemical code PHREEQE to calculate the pore fluid compositions in equilibrium with ordinary Portland cement and its mixture with blast furnace slag and fly ash. The predicted fluid compositions are compared in Table 5-4 with measured values for pore fluids extracted from 5-year-old cements. The model predictions for calcium and aluminum in most cases are relatively close to the measured values, which is also true for sulfate in Portland cement and in the Portland cement–blast furnace slag blend. However, the predicted sulfate concentration in the Portland cement–fly ash blend and the predicted silica concentration in the blends of Portland cement with blast furnace slag and fly ash are much higher than the observed values. The authors acknowledged their model has limitations due to the sorption and solid solution processes that are not accounted for and suggested further research into these processes (Atkins, et al., 1992a).

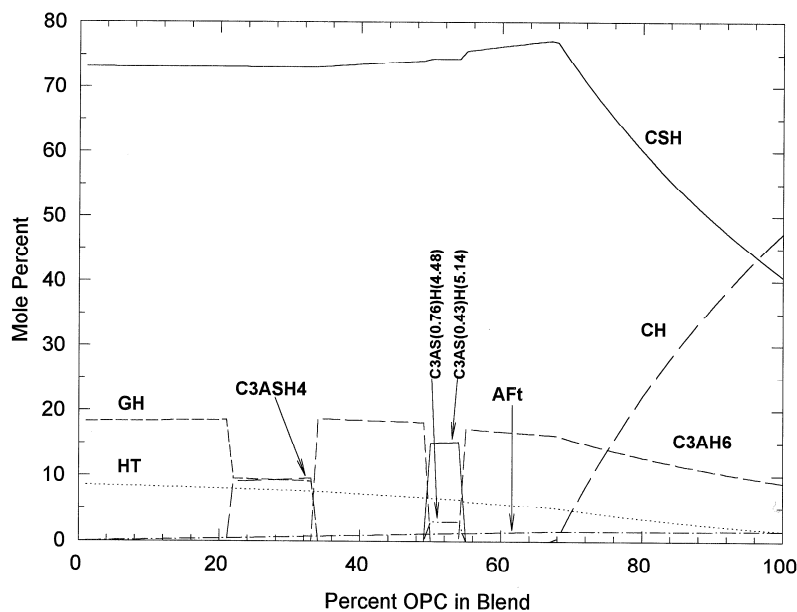


**Figure 5-18. Distribution of Solid Phases in Blends of Ordinary Portland Cement and Blast Furnace Slag Calculated Using CEMCHEM (Atkins, et al., 1992a,b).**  
 GH—Gehlenite Hydrate ( $2\text{CaO}\cdot\text{Al}_2\text{O}_3\cdot\text{SiO}_2\cdot 8\text{H}_2\text{O}$ ); HT—Hydrotalcite ( $4\text{MgO}\cdot\text{Al}_2\text{O}_3\cdot 10\text{H}_2\text{O}$ );  
 C3ASH4—Siliceous Hydrogarnet ( $3\text{CaO}\cdot\text{Al}_2\text{O}_3\cdot\text{SiO}_2\cdot 4\text{H}_2\text{O}$ );  
 C3AS(0.76)H(4.48)— $3\text{CaO}\cdot\text{Al}_2\text{O}_3\cdot 0.76\text{SiO}_2\cdot 4.48\text{H}_2\text{O}$ ;  
 C3AS(0.43)H(5.14)— $3\text{CaO}\cdot\text{Al}_2\text{O}_3\cdot 0.43\text{SiO}_2\cdot 5.14\text{H}_2\text{O}$   
 AF<sub>t</sub>—Ettringite ( $3\text{CaO}\cdot 3\text{CaSO}_4\cdot\text{Al}_2\text{O}_3\cdot 32\text{H}_2\text{O}$ ); C3AH6—Hydrogarnet ( $3\text{CaO}\cdot\text{Al}_2\text{O}_3\cdot 6\text{H}_2\text{O}$ );  
 CH—Portlandite [ $\text{Ca}(\text{OH})_2$ ]; CSH—Calcium Silicate Hydrate. Note: OPC = Ordinary Portland Cement.

Cement†		pH	Concentration (mmol/L)					
			Na	K	Ca	Al	Si	SO <sub>4</sub>
OPC†	measured	13.6	87	512	0.84	—	—	1.95
	calculated	—‡	—	—	0.6	0.92	6.7	1.26
30 % BFS–OPC†	measured	13.5	106	181	0.77	0.92	0.59	2.83
	calculated	—	—	—	0.65	0.93	6.95	0.96
30 % FA–OPC†	measured	13.5	120	233	1.23	2.33	4.6	6.15
	calculated	—	—	—	0.1	0.8	36.1	75.5

\*Atkins, M., D.G. Bennett, A.C. Dawes, F.P. Glasser, A. Kindness, and D. Read. "A Thermodynamic Model for Blended Cements." *Cement and Concrete Research*. Vol. 22. pp. 497–502. 1992.  
†OPC—ordinary Portland Cement; BFS—blast furnace slag; FA—fly ash.  
‡Not measured or calculated.

Glasser, et al. (1999) also used PHREEQE to calculate the pore solution chemistry of ordinary Portland cement and its mixture with blast furnace slag and fly ash in equilibrium with groundwater. The predicted values, which are listed in Table 5-5, are the resultant chemistries following complete equilibration of cement blends with groundwaters. To derive information on the gradual progression of the chemistry due to leaching by groundwater, Glasser, et al. (1999) used mixing calculations implemented with PHREEQE. In this approach, cement-equilibrated pore water was mixed with groundwater in varying proportions. An example of mixing calculation results is shown in Figure 5-19. The figure, which plots the saturation indices of different minerals, indicates the likely minerals that could precipitate from the interaction of groundwater and cement-equilibrated pore water. Glasser, et al. (1999) acknowledged the mixing approach does not consider space or time dimensions, but claimed the results provide a basis from which to select key chemical reactions for more detailed coupled chemical transport modeling.

Note that although CEMCHEM can be used to calculate the solid phase assemblage resulting from hydration of cement blends of Portland cement and blast furnace slag, the reducing oxidation potential, or low Eh, of the hydrated slag–cement blend cannot be calculated with CEMCHEM. The CEMCHEM model does not account for the sulfide phase—inferred to be the Tc<sub>3</sub>S<sub>10</sub> compound based on a study by Lukens, et al. (2005)—in the blast furnace slag that gives the slag–cement blend its reducing Eh condition.

Cement degradation models, purely chemical or otherwise, generally do not account for changes in the Eh of the system. Although Eh is a variable that is included in existing geochemical codes, its calculation for cement–slag–water systems would require adding the thermodynamic properties of Tc<sub>3</sub>S<sub>10</sub> in the thermodynamic database of the geochemical code. The thermodynamic properties of Tc<sub>3</sub>S<sub>10</sub>, however, are currently unknown. Some geochemical modeling studies have used reduced iron minerals, such as magnetite, to constrain the Eh of slag–cement mixtures to low values (de Windt, et al., 2004). A thermodynamic modeling study

Table 5-5. Calculated Pore Solution Composition (Columns 3–5) of Cements at Equilibrium With Groundwater (Initial Composition Given in Column 2)*				
Element in Solution (mol/L)	Groundwater	OPC†	75% BFS–OPC†	60% FA–OPC†
Ca	$2.85 \times 10^{-2}$	$5.62 \times 10^{-4}$	$8.53 \times 10^{-4}$	$4.79 \times 10^{-4}$
Mg	$6.30 \times 10^{-3}$	$7.43 \times 10^{-11}$	$8.95 \times 10^{-10}$	$5.20 \times 10^{-11}$
Na	$3.71 \times 10^{-1}$	$3.63 \times 10^{-1}$	$3.63 \times 10^{-1}$	$3.63 \times 10^{-1}$
K	$3.90 \times 10^{-3}$	$3.9 \times 10^{-3}$	$3.9 \times 10^{-3}$	$3.9 \times 10^{-3}$
Si	$4.81 \times 10^{-7}$	$3.23 \times 10^{-4}$	$2.73 \times 10^{-4}$	$3.53 \times 10^{-4}$
Al	—‡	$1.54 \times 10^{-3}$	$1.74 \times 10^{-4}$	$3.14 \times 10^{-3}$
Cl	$4.42 \times 10^{-1}$	$2.74 \times 10^{-2}$	$2.47 \times 10^{-4}$	$1.84 \times 10^{-2}$
C ( $\text{CO}_3^{2-}$ )	$1.55 \times 10^{-3}$	$4.42 \times 10^{-2}$	$3.76 \times 10^{-5}$	$2.01 \times 10^{-3}$
S ( $\text{SO}_4^{2-}$ )	$1.30 \times 10^{-2}$	$2.35 \times 10^{-4}$	$5.56 \times 10^{-4}$	$2.02 \times 10^{-4}$
pH	7.31	13.4	12.2	13.4

\*Glasser, F.P., M. Tyrer, K. Quillin, D. Ross, J. Pedersen, K. Goldthorpe, D.G. Bennett, and M. Atkins. "The Chemistry of Blended Cements and Backfills Intended for Use in Radioactive Waste Disposal." R&D Technical Report P98. Bristol, United Kingdom: U.K. Environment Agency, 1999.  
†OPC—ordinary Portland cement, BFS—blast furnace slag, FA—fly ash.  
‡Not measured.

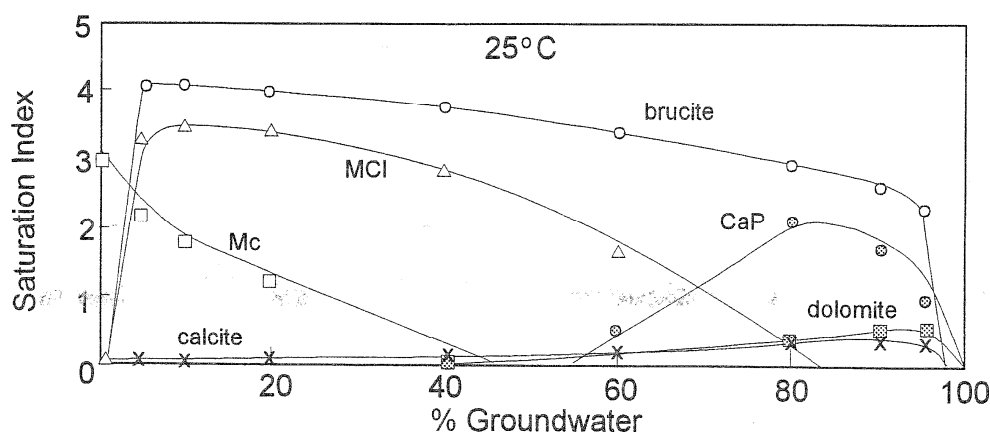


**Figure 5-19. Results of PHREEQE Calculations of Mixing Cement Pore Water and Groundwater (Composition Given in Table 5-5). From Glasser, et al. (1999). MCI—Friedel’s Salt ( $3\text{CaO}\cdot\text{CaCl}_2\cdot\text{Al}_2\text{O}_3\cdot 10\text{H}_2\text{O}$ ); MC—Calcium Monocarboaluminate; CaP—Calcium Zeolite.**

by Berner (1992b) used the redox potential of an anoxic corroding iron ( $E_h < -450$  mV) or of groundwater in a Swiss repository ( $E_h \sim -200$  mV) as boundary conditions in evaluating the effect of redox conditions on radionuclide release. However, such approximations are unlikely to accurately represent the  $E_h$  evolution during degradation of slag–cement systems.

Chemical modeling of the leaching of cement-based materials also has been handicapped by the lack of thermodynamic data on phases important to the constitution of blended cement (e.g., siliceous hydrogarnet and strätlingite) and the lack of data at temperatures other than 25 °C [77 °F]. However, a new and internally consistent database for a wide range of cement substances and covering the temperature range 1 to 99 °C [34 to 210 °F] has been published and should enable thermodynamic treatment over wider ranges of composition and temperature than was previously possible (Matschei, et al., 2007).

### 5.3.2 Reactive–Transport Leaching Models

#### Diffusion Leaching Models

Models for calculating the effects of leaching typically consider diffusion as controlling the degradation process based on the assumptions that the cement-based material is saturated, advective flow is negligible, and the rates of chemical reactions are much faster than diffusion rates. In the case of leaching of ordinary Portland cement, a simple assumption is that leaching is controlled mainly by the chemistry of the external water and by the calcium content of the pore solution, which itself is controlled by the dissolution of portlandite. Thus, leaching can be calculated using a shrinking core model (e.g., Atkinson and Hearne, 1984), which can be described by the following equations

$$N = -D_i \frac{C_i - C_{gw}}{X} \quad (5-18)$$

$$\frac{dX}{dt} = \frac{D_i}{X} \frac{C_i - C_{gw}}{C_s} \quad (5-19)$$

$$X = \left( 2D_i \frac{C_i - C_{gw}}{C_s} t \right)^{1/2} \quad (5-20)$$

where

$C_i$	—	concentration of $\text{Ca}^{2+}$ in cement pore water (moles/cm <sup>3</sup> )
$C_s$	—	bulk concentration of $\text{Ca}^{2+}$ in cement solid (moles/cm <sup>3</sup> )
$D_i$	—	intrinsic diffusion coefficient of $\text{Ca}^{2+}$ in degraded cement (cm <sup>2</sup> /s)
$C_{gw}$	—	concentration of $\text{Ca}^{2+}$ in external (or ground) water (moles/cm <sup>3</sup> )
$X$	—	penetration depth (cm)
$N$	—	molar flux (moles/cm <sup>2</sup> ·s)
$t$	—	time (s)

For civil engineering applications, service life can be equated to the time it takes to reach a critical value of the penetration depth,  $X_c$ . For example, concrete that has lost one-third of the initial portlandite can be considered to be degraded, and no credit is taken for the degraded concrete when calculating the residual load capacity of the concrete element (Clifton, et al., 1995). Thus, leaching will reduce the thickness of the concrete element by  $X_c$ . The magnitude of  $X_c$  will depend on the structural design of the concrete element.

The model represented by Eqs. (5-18) through (5-20) is very simplified and does not consider other factors that give the zonal pattern illustrated in Figure 4-1, such as (i) dissolved species other than  $\text{Ca}^{2+}$ ; (ii) other cement phases, such as C-S-H; and (iii) changes in material properties as degradation proceeds. Adenot and Richet (1997) developed a more elaborate diffusion-controlled leaching model, referred to as the DIFFUZON model, to evaluate the

long-term degradation of cement pastes and concretes in contact with an aggressive solution. In the model, the degraded section of the hardened cement paste is divided into several zones with constant mineralogy separated by moving fronts of dissolution or precipitation (Figure 5-20). By applying Fick's second law for diffusion transport, a material balance over a unit volume element in a zone  $j$  gives

$$\frac{\partial C_i}{\partial t} = D_{ij} \frac{\partial^2 C_{ij}}{\partial x^2} - \frac{1}{\phi_j} \frac{\partial S_{ij}}{\partial t} \quad (5-21)$$

where

- $C_{ij}$  — solution concentration of species  $i$  (moles per unit volume of liquid)
- $D_{ij}$  — diffusion coefficient of species  $i$  in zone  $j$
- $S_{ij}$  — solid phase concentration of species  $i$  in zone  $j$  (moles per unit volume of solid + liquid)
- $\phi_j$  — porosity in zone  $j$
- $x$  — distance from the surface (m)
- $t$  — time (s)

Equation (5-21) has to be solved for the  $n$  diffusing species simultaneously with the chemical equilibrium equations for the different solid phases at every point in each zone. At each dissolution or precipitation front  $j$ , conservation of mass of  $n$  components gives

$$(S_{ij^-} - S_{ij^{+1}}) \frac{dl_j}{dt} = \phi_{sj} D_{ij} \frac{\partial C_{ij^-}}{\partial x} - \phi_{s_{j+1}} D_{ij+1} \frac{\partial C_{ij^{+1}}}{\partial x} \quad (5-22)$$

where

- $C_{ij^-}$  and  $S_{ij^-}$  — concentrations of species  $i$  in liquid and solid phases *left* of front  $j$
- $C_{ij^+}$  and  $S_{ij^+}$  — concentrations of species  $i$  in liquid and solid phases *right* of front  $j$
- $\phi_{sj}$  and  $\phi_{s_{j+1}}$  — porosities in zones  $j$  and  $j+1$
- $l_j$  — front  $j$  position at time  $t$
- $D_{ij}$  and  $D_{ij+1}$  — diffusion coefficient of species  $i$  in zones  $j$  and  $j+1$

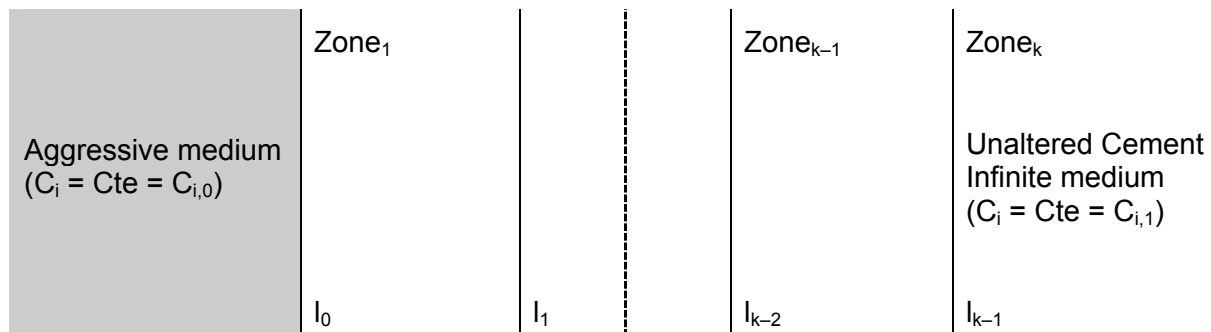


**Figure 5-20. Representation of the Leaching Model of Adenot and Richet (1997), Which Is Made up of Zones of Constant Mineralogy**

Equation (5-22) also has to be simultaneously solved for  $n$  diffusing species with chemical equilibrium equations for the different solid phases present.

The boundary and initial conditions are described mathematically as follows:

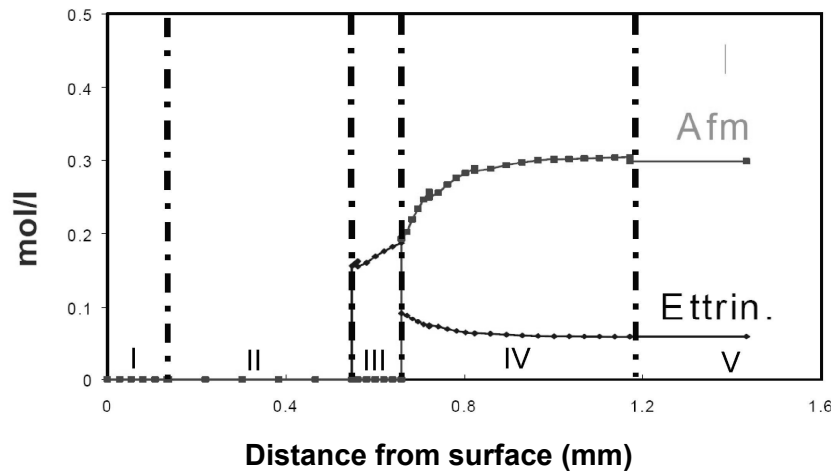
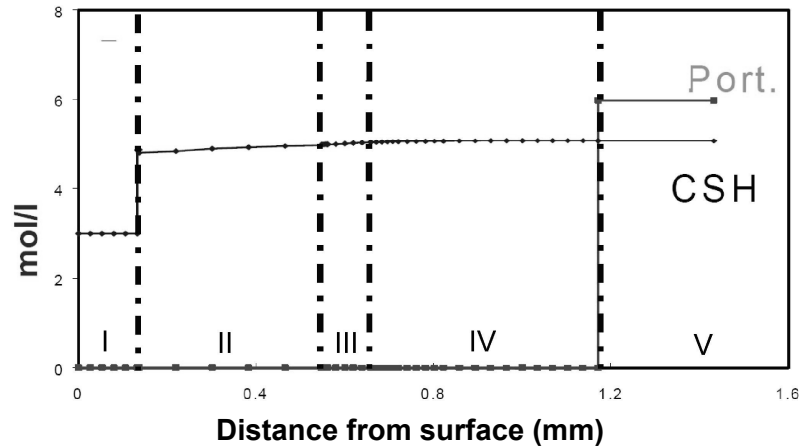
- Boundary condition ( $x = 0$ ):  $C_i = C_{i,0}$  for  $t > 0$
- Initial condition ( $t = 0$ ):  $C_i = C_{i,j}$  for  $x > 0$

The composition of the aggressive solution (pH, type, and concentration of aggressive ions) and the type of material (cement composition, water/cement ratio) are DIFFUZON-model-required input variables. For output, the model produces the concentration profiles in the solid and liquid phases, the porosity profile, the diffusion coefficient profile, the mineral assemblage, and the degraded thickness at a given time. The porosity in each zone is calculated from the mean concentration, molar volume, and density of the solid phases present in the zone, but the increase in porosity due to decalcification of C-S-H is considered negligible compared to the initial porosity of the material. An empirical equation relating diffusion coefficients to porosity uses different water/cement ratios. The solid phases considered in the unaltered cement are portlandite, ettringite, monosulfate, and a C-S-H with a CaO-to-SiO<sub>2</sub> molar ratio of 1.65. To model the incongruent dissolution of C-S-H, the C-S-H composition in each zone is approximated by a solid solution comprising two C-S-H phases with different CaO-to-SiO<sub>2</sub> molar ratios.

Figure 5-21 gives examples taken from Adenot, et al. (1997) of calculated composition profiles in the solid phase after 8.5 months of leaching by a solution at pH 11.5. The figure shows (i) a portlandite dissolution front separates the unaltered portion (Zone V) from the degraded portion of the cement; (ii) dissolution of monosulfate and precipitation of secondary ettringite occur in the zone consisting of monosulfate, ettringite, and C-S-H (Zone IV); (iii) ettringite precipitation is coincident with monosulfate dissolution, indicating the latter releases aqueous species that promote the former; (iv) dissolution of ettringite occurs in the zone consisting of ettringite and C-S-H (Zone III); and (v) the amount of C-S-H in Zones II to V is nearly constant before it is converted to silica gel in Zone I.

Adenot, et al. (1997) also compared the thicknesses of the degraded section calculated using the model with experimental data. The calculated and experimental values are listed in Table 5-6 and show that the thicknesses derived from the model are in relatively good agreement with values derived from the experiment. Adenot, et al. (1997) also calculated the degraded thicknesses at 300 and 1,000 years, which are listed in Table 5-7.

Moranville, et al. (2004) developed a three-dimensional model to understand, at the microstructural scale, the evolution of a Portland cement paste subjected to leaching. The model accounts for the interactions between the solid constituents of the cement paste and the pore solution and the interactions of the pore solution with the external aqueous environment. Similar to the model Adenot and Richet (1997) developed, the Moranville, et al. (2004) model assumes (i) the cement paste porosity is fully saturated with pore solution such that ionic fluxes are mainly diffusive and (ii) chemical reactions are instantaneous relative to diffusive processes such that local chemical equilibrium is attained at each simulation timestep. The latter assumption enables the diffusion calculation to be decoupled from the reaction calculation. The system of equations in the model is numerically solved in three stages: (i) ionic diffusion calculation, (ii) chemical reaction calculation, and (iii) calculation of transport parameters from the volume balance of dissolved or precipitated solid phases. The diffusive species included in the model are calcium, silica, aluminum, sulfate, sodium, and potassium. The first four species



Zone	I	II	III	IV	V
Mineralogical Composition	Silica gel	C-S-H	Ettringite C-S-H	Monosulfate Ettringite C-S-H	<i>Unaltered Cement:</i> Portlandite Monosulfate Ettringite C-S-H

**Figure 5-21. Profiles Adenot, et al. (1997) Calculated of Ettringite, Monosulfate, Portlandite, and C-S-H After 8.5 Months of Degradation by a pH 11.5 Solution. The Solid Phase Concentration Is Given in Units of Moles Per Liter of Ordinary Portland Cement With an Initial Water/Cement Ratio of 0.38. For Comparison, the Zonation Typically Observed in Leached Cement (Adenot and Richet, 1997) Also Is Shown. The Top Two Figures Were Taken From Richet, et al. (2004; Figure 3.14) and Modified. Port—Portlandite; Ettrin—Ettringite; Afm—Monosulfate.**

<b>Table 5-6. Comparison of Calculated and Measured Degraded Thickness*</b>			
	<b>pH 11.5 Degraded Thickness After 8.5 Months</b>	<b>pH 8.5 Degraded Thickness After 2.8 Months</b>	<b>pH 4.5 Degraded Thickness After 2.8 Months</b>
Experimental	1.91 mm [0.075 in]	1.4 mm [0.055 in]	1.43 mm [0.056 in]
Calculated	1.47 mm [0.058 in]	1.13 mm [0.044 in]	1.12 mm [0.044 in]
*Adenot, F., C. Richet, and P. Faucon. "Long-Term Prediction of Concrete Durability in Radioactive Waste Management: Influence of the pH of the Aggressive Solution." International Conference on Engineering Materials, Ottawa, Canada, June 8–11, 1997. Ottawa, Canada: Canadian Society for Civil Engineering. pp. 117–128. 1997.			

<b>Table 5-7. Degraded Thickness After 300 and 1,000 Years Calculated*</b>			
	<b>pH 11.5</b>	<b>pH 8.5</b>	<b>pH 4.5</b>
300 years	30 mm [1.2 in]	40 mm [1.6 in]	40 mm [1.6 in]
1,000 years	55 mm [2.2 in]	75 mm [3.0 in]	75 mm [3.0 in]
*Adenot, F., C. Richet, and P. Faucon. "Long-Term Prediction of Concrete Durability in Radioactive Waste Management: Influence of the pH of the Aggressive Solution." International Conference on Engineering Materials, Ottawa, Canada, June 8–11, 1997. Ottawa, Canada: Canadian Society for Civil Engineering. pp. 117–128. 1997.			

are involved in the dissolution or precipitation of the following solids included in the model: C-S-H, portlandite, ettringite, and calcium monosulfate. The apparent diffusion coefficient of the dissolved species in the cement paste is calculated using an equation similar to Eq. (5-17), and the chemical reactions are calculated with the PHREEQC geochemical code (Parkhurst and Appelo, 1999).

The study domain in the Moranville, et al. (2004) model can be represented by a rectangular prism subdivided into cubic cells that represent either a volume of cement paste or an aggressive external solution (Figure 5-22). The cells representing the cement paste are derived from microstructures generated by the three-dimensional hydration model CEMHYD3D, which was developed at the National Institute of Standards and Technology (Bentz, 2000, 1997). In the x direction, the first two cells represent aggressive solutions and the other cells represent cement paste. The equations representing the model are developed and solved numerically in three dimensions, although for the example calculations Moranville, et al. (2004) presented, the problem was made one-dimensional by considering all cells in a section perpendicular to the x direction to be identical. The results of these calculations are shown in Figures 5-23 to 5-25.

Calculated pore solution pH and calcium concentration are plotted in Figure 5-23 as functions of time and depth from the surface. In Figure 5-23, the initial pH close to 13.3 is due to the presence of alkali ions, which need to be charge-balanced by hydroxide ions. After depletion of the alkali ions, a pH close to 12.5 (and calcium concentration equal to  $20 \times 10^{-3}$  mol/L) is attained, buffered by the dissolution of portlandite. The drop in pH from 12.5 to 11.8, which is

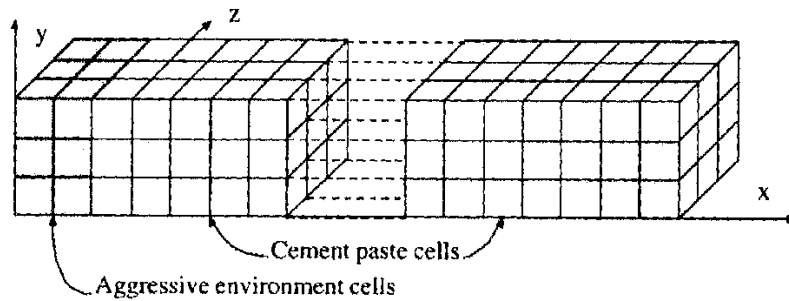


Figure 5-22. Study Domain Moranville, et al. (2004) Used in Modeling Cement Leaching. Each Cell Represents Either an Aggressive Aqueous Environment or a Cement Paste Cell Composed of the Pore Solution and a Microstructure Generated by the CEMHYD3D Model. Reprinted From Moranville, M., S. Kamali, and E. Guillon, "Physicochemical Equilibria of Cement-Based Materials in Aggressive Environments—Experiment and Modeling," *Cement and Concrete Research*, Vol. 34, pp. 1,569–1,578. Copyright© 2004, With Permission From Elsevier.

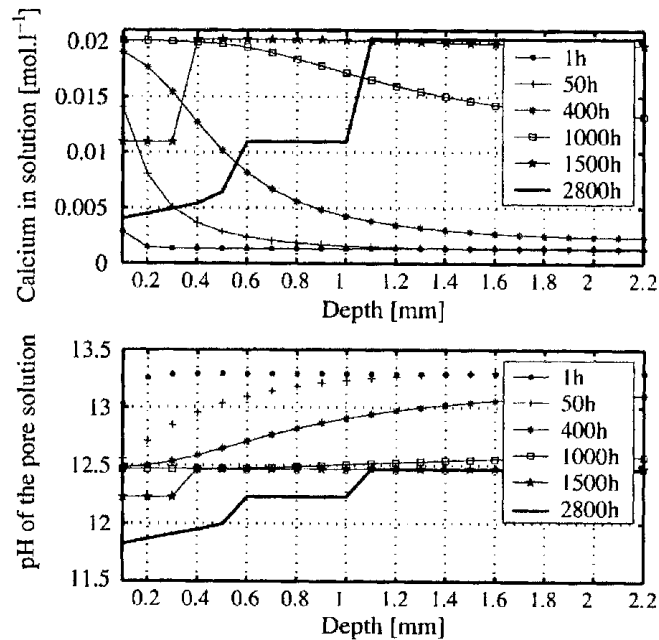
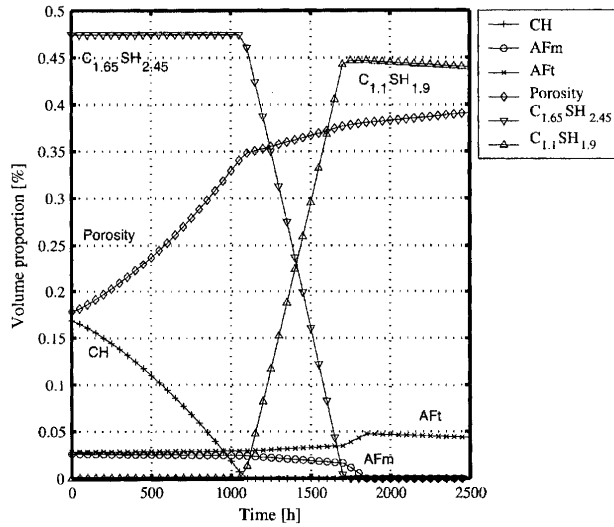
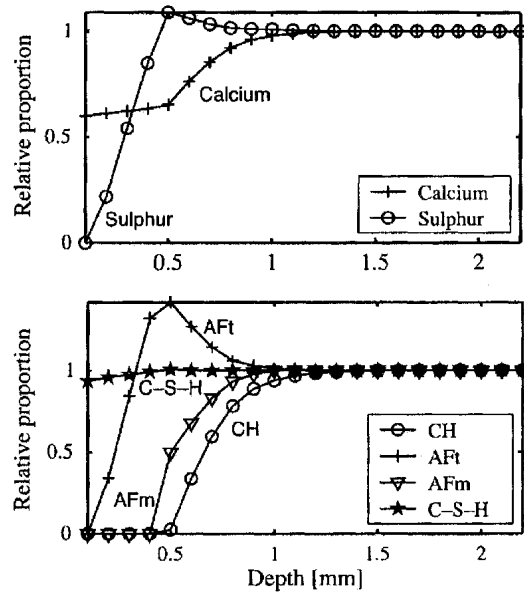


Figure 5-23. Calculated pH and Calcium Concentration Profiles Within Degrading Portland Cement Paste at Different Timesteps. Reprinted From Moranville, M., S. Kamali, and E. Guillon, "Physicochemical Equilibria of Cement-Based Materials in Aggressive Environments—Experiment and Modeling," *Cement and Concrete Research*, Vol. 34, pp. 1,569–1,578. Copyright© 2004, With Permission From Elsevier.



**Figure 5-24. Evolution With Time of Porosity and Volume Proportion of Solids in Degrading Portland Cement Paste Moranville, et al. (2004) Calculated.**  
 CH—Portlandite; AF<sub>m</sub>—Monosulfate; AF<sub>t</sub>—Ettringite. Reprinted From Moranville, M., S. Kamali, and E. Guillon, “Physicochemical Equilibria of Cement-Based Materials in Aggressive Environments—Experiment and Modeling,” *Cement and Concrete Research*, Vol. 34, pp. 1,569–1,578. Copyright© 2004, With Permission From Elsevier.



**Figure 5-25. Relative Quantities of Solid Phases and of Calcium and Sulfur in Those Solids Versus Depth of Portland Cement Paste After 1,286 Hours of Simulated Leaching by Pure Water. The Plotted Values Are Relative to Undegraded Material (Value of 1 in the Y Axis). CH—Portlandite; AF<sub>t</sub>—Ettringite; AF<sub>m</sub>—Monosulfate.** Reprinted From Moranville, M., S. Kamali, and E. Guillon, “Physicochemical Equilibria of Cement-Based Materials in Aggressive Environments—Experiment and Modeling,” *Cement and Concrete Research*, Vol. 34, pp. 1,569–1,578. Copyright© 2004, With Permission From Elsevier.

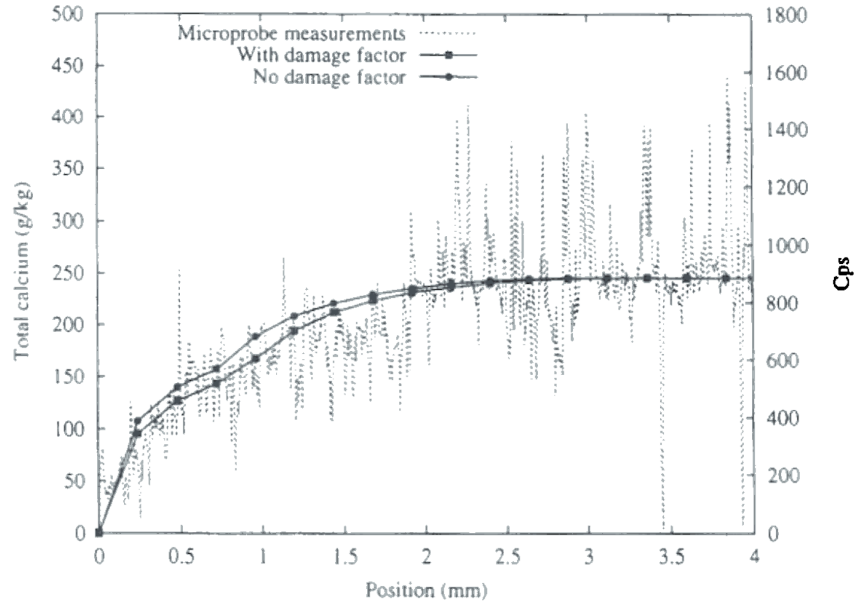
coincident with a decrease in solution concentration of calcium from  $20 \times 10^{-3}$  to  $5 \times 10^{-3}$  mol/L, corresponds to a depletion of portlandite.

Figure 5-24 shows the evolution with time of the volume proportion of the solid phases in the degrading cement paste the model of Moranville, et al. (2004) calculated. The results shown in the figure confirm that portlandite is the first solid phase to dissolve completely. After depletion of portlandite, dissolution of  $C_{1.65}SH_{2.45}$  and precipitation of  $C_{1.1}SH_{1.9}$  occur, as a consequence of the decalcification of C-S-H. Figure 5-24 also allows the increase in porosity that accompanies dissolution of the cement solids. Figure 5-25 is a plot of the relative quantities of the solid phases and the calcium and sulfur in those solids after 1,286 hours of simulated leaching of Portland cement past by pure water. The zoning in mineralogy typically observed in experiments and other modeling results is evident in the bottom figure of Figure 5-25.

### **Diffusion–Advection Leaching Models**

The STADIUM model of Marchand, et al. (2002), discussed previously in Section 5.2.2 in regard to modeling sulfate attack, also has been used to simulate leaching of cement-based materials. Marchand, et al. (2001) investigated the effect of leaching (i.e., dissolution of portlandite) on the transport of ions and water in hydrated cement pastes. Portlandite dissolution is a concern for the durability of cement-based materials because it could increase the porosity and decrease the materials' resistance to penetration by aggressive ions. It also can adversely affect the engineering properties of cement-based structures. The Marchand, et al. (2001) study used the CEMHYD3D code, which the National Institute of Standards and Technology (Bentz, 2000) developed, to model the microstructure and diffusivity of hydrated cement paste at varying degrees of portlandite dissolution, and STADIUM to predict the transport of ions in the porous medium and to account for the effect of dissolution and precipitation reactions on the transport processes. To validate the results of the numerical simulations, experiments also were conducted by reacting hydrated cement pastes (cured for 18 months) with deionized water in a  $CO_2$ -free environment at a relative humidity close to 65 percent. Some of the simulation results are shown in Figure 5-26, where the calculated total calcium concentrations are compared with calcium concentrations determined by electron microprobe analyses. The curve labeled “with damage factor” corresponds to the calculations that accounted for the effect of portlandite dissolution on the transport properties of the hydrated cement paste. The figure shows that the calcium profile the model predicted is in good agreement with the profile the microprobe analysis obtained. The results of calculations that accounted for the effect of leaching on the transport property of the porous medium are only slightly different from the results that did not account for this effect. Marchand, et al. (2001) explained that the small difference was due to the short duration (3 months) of the experiments, which limited the extent of leaching and its effect on transport.

Yokozeiki, et al. (2004) proposed another diffusion–advection leaching model for evaluating the long-term durability of engineered barriers used in underground radioactive waste disposal facilities. The model is applicable only to leaching of calcium, which is the element of highest proportion in cement hydrates and has the most influence on the degradation of cement-based materials that result from leaching. The model accounts for the effect of aggregate on the tortuosity of the mass transfer path and also for the increase in porosity as calcium is leached. To validate the model, the authors studied the degradation due to leaching observed in core samples taken from 34- to 104-year-old concrete structures in Japan. The numerical model



**Figure 5-26. Comparison of Total Calcium Profile Determined Using an Electron Microprobe (in CPS, Counts per Second) With the Total Calcium Profile (in Grams of Calcium Per Kilogram of Solid) Calculated Using STADIUM. The Cement Sample Was Reacted With Deionized Water for 3 Months in a CO<sub>2</sub>-Free Atmosphere. The Curve Labeled “With Damage Factor” Represents Simulation Results That Account for the Effect of Leaching on the Transport Property of the Porous Medium. Reprinted From Marchand, J., D.P. Bentz, E. Samson, and Y. Maltais, “Influence of Calcium Hydroxide Dissolution on the Transport Properties of Hydrated Cement Systems,” *Materials Science of Concrete: Calcium Hydroxide in Concrete*, J.P. Skalny, J. Gebauer, and I. Odler, eds., Special Vol., pp. 113–129. Copyright© 2001, With Permission From Wiley.**

simulated the measured values very well. The model was used in a parametric study to evaluate the effect of several factors, such as water/cement ratio, cement calcium oxide content, fine-sized fraction of the aggregate, temperature, and hydraulic gradient, on leaching behavior. The degradation depth increased significantly with the water/cement ratio due to the higher porosity at a higher water/cement ratio and increased only slightly at a higher cement calcium oxide content in cement. Degradation depth also increased with an increase in the relative amount of fine-sized aggregate and increased, almost linearly, with temperature {from 20 to 80 °C [68 to 176 °F]}. The hydraulic gradient did not have a large effect on degradation depth, because the effect of diffusion is larger than that of advection. Yokozeki, et al. (2004) also simulated the leaching of calcium from concrete contacting water or bentonite.

Figure 5-27(a) shows the calculated degradation depths of concrete in contact with water, and Figure 5-27(b) shows the results for concrete in contact with bentonite. The degradation depth of concrete obeys the  $t^{1/2}$  law and is smaller for the concrete contacting bentonite compared to that contacting water. In both cases, the simulation indicates that most of the C-S-H in the cement will not have deteriorated after 2,000 years.

An important process that was not explicitly considered in the previously discussed diffusion–advection leaching models is the interaction of the cement-based material with groundwater rich in dissolved carbonate that will cause calcite precipitation and affect the permeability and diffusivity of the system. Pfingsten (2002, 2001) applied the two-dimensional MCOTAC code to evaluate the effect of that process on the temporal evolution of the near field

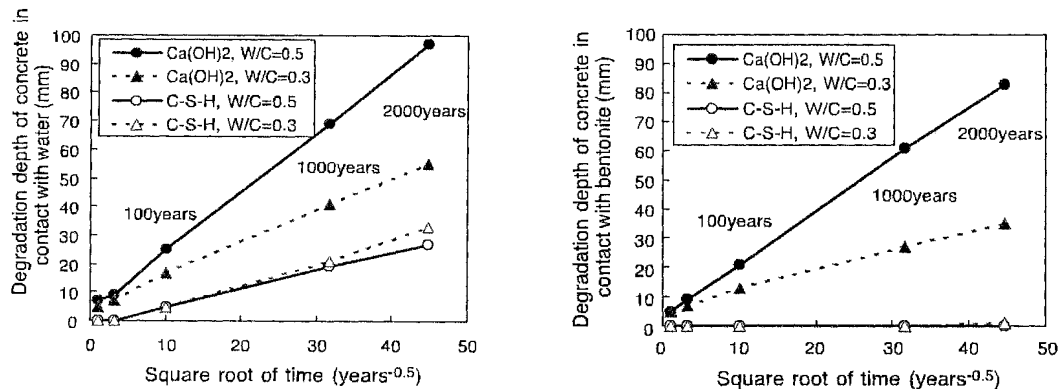


**Figure 5-27. Calculated Degradation Depth of Concrete in Contact With (a) Water and (b) Bentonite. The Curves Indicated as Ca(OH)<sub>2</sub> Are Depths at Which the Solid-Phase Calcium Concentration Begins to Drop, Whereas the Curves Indicated as C-S-H Are Depths at Which the Solid-Phase Calcium Concentration Drops Steeply to Near Zero (i.e., C-S-H Disappears). Reprinted From Yokozeki, K., K. Watanabe, N. Sakata, and N. Tosuki, "Modeling of Leaching From Cementitious Materials Used in Underground Environment," *Applied Clay Science*, Vol. 26, pp. 293–308. Copyright<sup>©</sup> 2004, With Permission From Elsevier**

of a cementitious nuclear waste repository. The MCOTAC code has modules for hydraulic, transport, and chemical models that are coupled sequentially with the option of iterating between the modules. The hydraulic module describes stepwise stationary flow, including sources and sinks, in a heterogeneous porous medium. The transport module accounts for advection, diffusion, and linear sorption, as well as decay for a single species, and source and sink terms due to external pumping and/or chemical reaction. Assumptions Pfingsten (2002, 2001) used include local chemical equilibrium, constant head or flux conditions at the boundaries, constant external sources or sinks, as well as constant porosity and hydraulic conductivity during a single timestep. The hydraulic conductivity was derived using the Kozeny-Carman equation (Bear, 1972) that directly relates the hydraulic conductivity to porosity, which is recalculated at each timestep based on the mineral composition. The chemistry module includes aqueous complexation, sorption, and mineral reactions. The solid phases considered are limited to SiO<sub>2</sub>, CaCO<sub>3</sub>, CaF<sub>2</sub>, and C-S-H [represented by Ca(OH)<sub>2</sub> and CaH<sub>2</sub>SiO<sub>4</sub> based on the Berner (1992a) model], although other solids (e.g., those relevant to slag and fly ash) can be added if thermodynamic parameters are available. The code accounts for changes in porosity, hydraulic conductivity, and diffusivity that result from mineral dissolution and precipitation. Both the chemistry of the cement and the geometry of the near field were simplified, as illustrated in Figure 5-28. Some of the results are shown in Figure 5-29 for the case in which fluoride-containing groundwater flow is dominated by diffusion. Figure 5-29(a) represents the initial solid and porosity distribution within the modeled area. As time evolves, portlandite and C-S-H dissolve and a calcite and fluorite (CaF<sub>2</sub>) precipitation front appears around the cement. Within 2,000 years, portlandite has nearly dissolved or transformed into CaH<sub>2</sub>SiO<sub>4</sub> [Figure 5-29(b)]. The amount of precipitated calcite and the resulting decrease in porosity in the first 1,000 years is larger compared to the second 1,000 years [Figure 5-29(c)] due to decreasing chemical gradients and decreasing porosity around the cement, where calcite precipitation forms a barrier of low porosity.

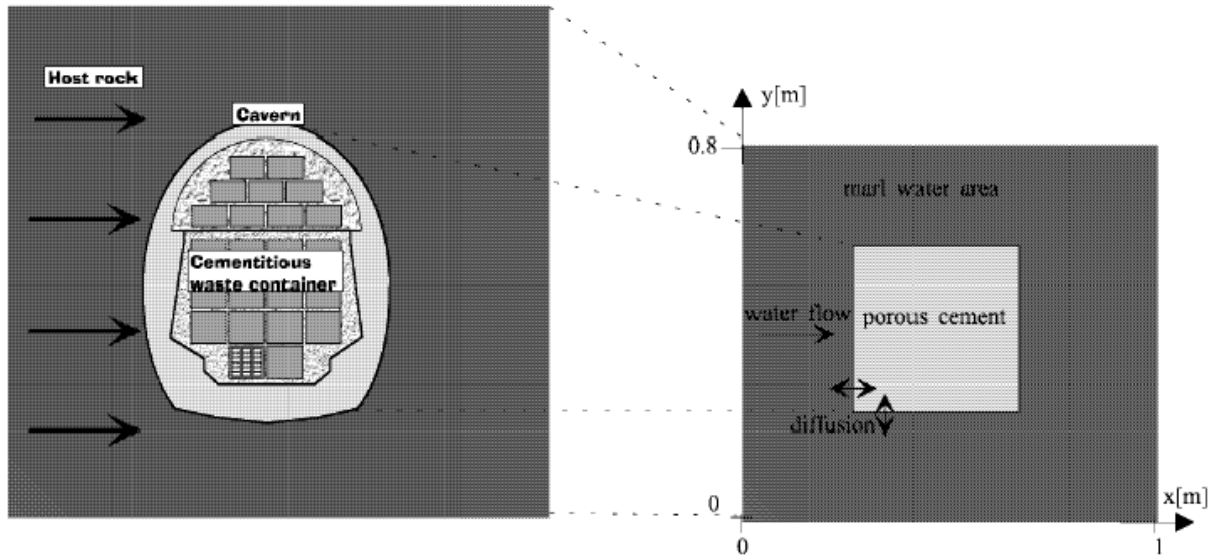


**Figure 5-28. Cross Section Through the Near Field of a Cementitious Repository and Its Simplified Representation in the MCOTAC Model. The Groundwater Flow Field, Defined Initially by a Hydraulic Gradient, Changes With Time Due to Mineral Reactions and Changes in Hydraulic Conductivity (From Pfingsten, 2001).**

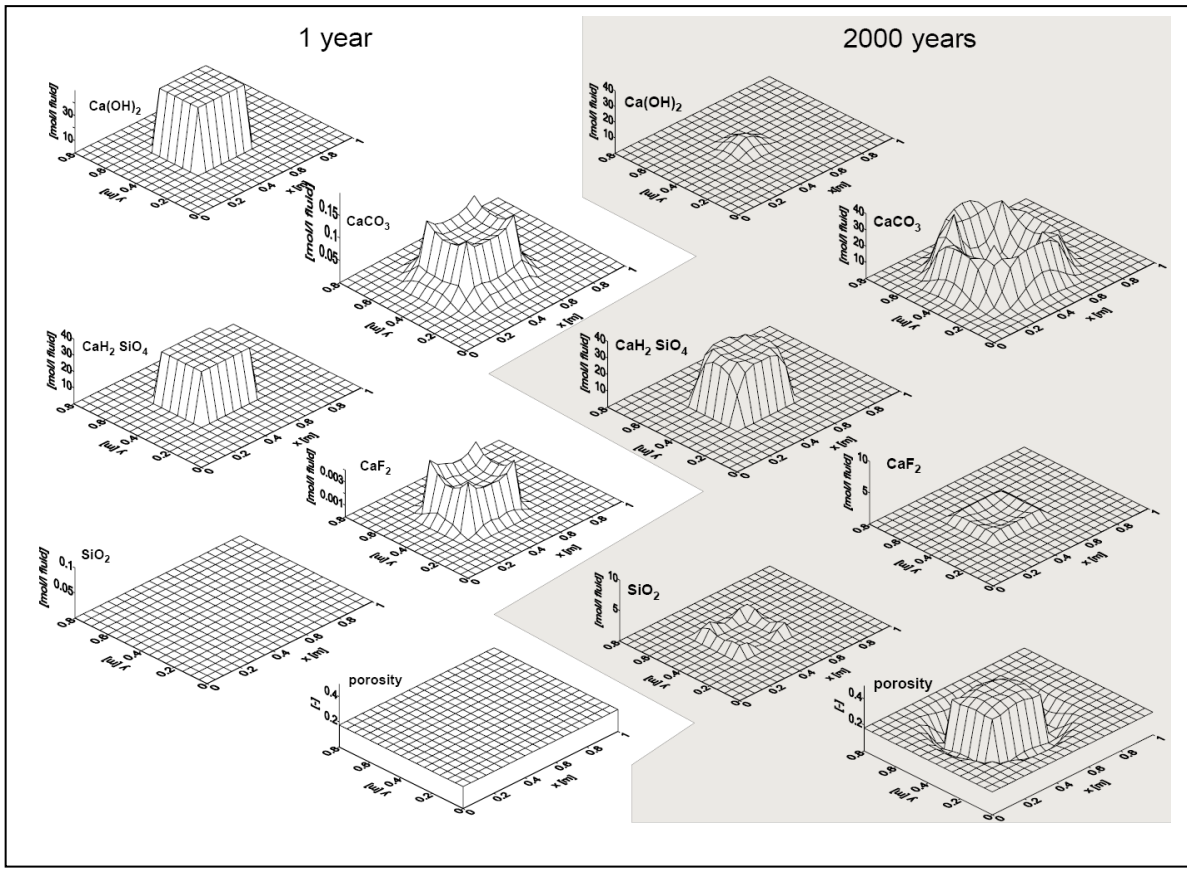
The MCOTAC code applies only to water-saturated systems and does not consider the kinetic reactions and precipitation of metastable minerals. It is also limited by long run times; simple calculations take only minutes to complete, but simulations of more complex, finely discretized, and fully coupled systems take hours or days to finish.

### Diffusion–Advection–Fracture Leaching Models

The models discussed in preceding sections focused on the chemical degradation of uncracked cement-based materials and did not explicitly consider the effect of fractures or cracks on the degradation process. Cracks provide a preferential flow pathway for groundwater and can have several effects on the performance of cement-based engineered barriers, including (i) concentration of chemical interactions to particular regions of the barrier, (ii) reduction in the

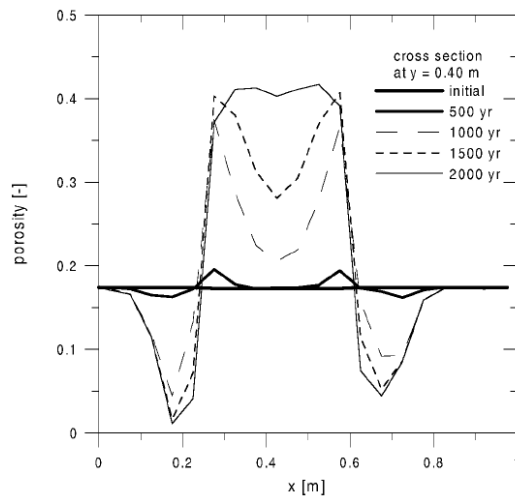
volume of cement-based material that interacts with the groundwater, and (iii) increase in flow velocity through the cement-based engineered barrier. These processes potentially could affect the release of radionuclides from cementitious waste forms or cement-based repositories, as discussed in Section 7.

Harris, et al. (1997) described a model for evaluating the chemical buffering performance of a deep geologic repository with cement-based materials that considers the effects of crack size and distribution, groundwater flow velocity, and the formation of reaction layers on crack surfaces. The model focused on the evolution of the chemistry of groundwater within cracks and was implemented using the computer code CHEQFRAQ, which is an application of the one-dimensional coupled transport and chemical equilibrium code CHEQMATE to a two-dimensional problem. The CHEQMATE code uses a finite difference method to



(a)

(b)



(c)

**Figure 5-29. Concentration of Model Solids and Porosity Changes Calculated for (a) 1 Year and (b) 2,000 Years of Interaction of Cement Vault With Groundwater. The Temporal Evolution of Porosity Along a Cross Section in the Direction of Groundwater Flow Is Shown in (c). Figures Taken from Pfingsten (2001).**

solve the transport equations for advection, dispersion, diffusion, and electromigration in a one-dimensional, heterogeneous porous medium. The transport and chemical processes are solved separately and sequentially in CHEQMATE. The fracture flow model as implemented in the CHEQFRAC code allows the transport processes to occur in either of two directions: (i) through the porous matrix perpendicular to the crack (leading to a flux of ions into or out of the crack) and (ii) along the crack itself. Typically, transport through the porous matrix is by diffusion, whereas transport in the crack itself occurs by both diffusion and advection. The model accounts for mineral precipitation and dissolution within the crack and for the effect of reaction layers within the crack, but is limited to simulating the chemistry of groundwater flowing through a porous medium with equally spaced cracks that have sides parallel to the direction of flow. Leaching of the cement-based material is assumed to occur by the dissolution of a solid solution comprising two endmembers— $\text{Ca}(\text{OH})_2$  and  $\text{CaH}_2\text{SiO}_4$ —based on the work of Berner (1992a). Local chemical equilibrium is assumed, and the transport and chemical equations are solved separately and sequentially. A schematic illustration of the finite difference grid required for the CHECFRAC code is shown in Figure 5-30. In this illustration, the unaltered material is represented by medium 2 and the reaction zone adjacent to the crack by medium 1. The effect of reaction layers is modeled by assigning a different value (typically smaller) of intrinsic diffusion coefficient and porosity to a layer, and the values for the reaction layers and the matrix are invariant with time. Crack properties also are assumed to be constant.

Figure 5-31 shows some of the results of the CHEQFRAC simulations Harris, et al. (1997) conducted to evaluate the effect of precipitated reaction layers. For these simulations, the repository cross section was assumed to be a 20-m [66-ft] square with an array of parallel cracks with spacing of 1 m [3.3 ft], width of 5 mm [0.20 in], length of 0.5 m [1.6 ft], and crack aperture area of  $1.9 \text{ m}^2$  [ $20.5 \text{ ft}^2$ ]. One or two reaction layers, which have diffusivities one or two orders of magnitude lower than unaltered material, were included in the simulations. Figure 5-31 illustrates the predicted pH profiles along a crack after 1 year for flow rates of  $4 \times 10^{-6}$  and  $4 \times 10^{-7} \text{ m/s}$  [ $1.3 \times 10^{-5}$  and  $1.3 \times 10^{-6} \text{ ft/s}$ ]. At the lower flow velocity, the pH at the end of the crack is about 12.5, approximately the value expected for static dissolution of portlandite. The presence of one protective layer (layer 1 in Figure 5-31) has a negligible effect on the pH at the end of the crack, which was still  $\sim 12.5$ . However, the presence of a more protective reaction layer (layer 2 in Figure 5-31) reduces the pH at the end of the crack to 10.7.

At the higher flow rate and without a reaction layer present, the pH at the end of the crack is about 12, indicating the dissolution of portlandite is not reaching saturation. The presence of a reaction layer at the higher flow rate causes the pH at the end of the crack to decrease to less than 10, well below the pH buffered by dissolution of portlandite, demonstrating the effect of protective layers in controlling the pH of the percolating aqueous phase is enhanced at higher flow velocities.

Harris, et al. (1997) also used CHECFRAQ to evaluate the effect of crack parameters. Crack widths of 1, 10, or 20 mm [0.04, 0.39, or 0.79 in] and a constant crack spacing of 1 m [3.3 ft] were assumed, along with an intrinsic diffusion coefficient of  $4 \times 10^{-11} \text{ m}^2/\text{s}$  [ $4 \times 10^{-10} \text{ ft}^2/\text{s}$ ]. The results showed that for a 10-mm [0.39-in]-wide crack, an increase in the groundwater flow velocity by an order of magnitude results in a pH decrease at a given location along the crack by about one pH unit. The flow velocity for a constant groundwater discharge through the repository is inversely proportional to the crack width. The model predicts that changes in the crack width, for a constant specific discharge, have no effect on the pH buffering in the crack because the increased dilution in wider cracks is balanced by a reduction in the flow velocity.

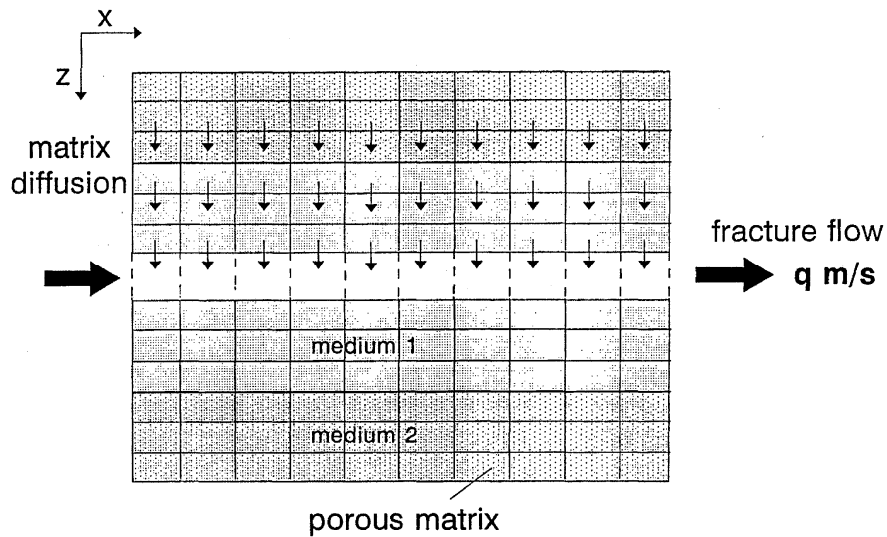
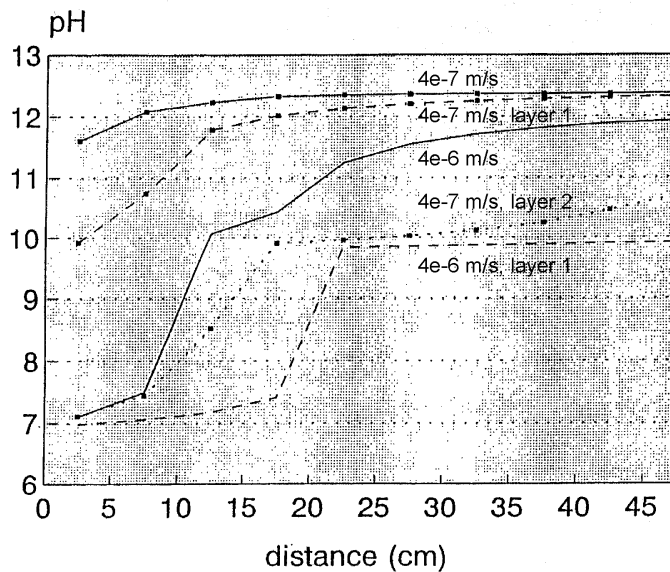


**Figure 5-30. Schematic Illustration of CHEQMATE Cells Used in the CHEQFRAC Model (From Harris, et al., 1997). The Unaltered Material Is Represented by Medium 2 and the Reaction Zone Adjacent to the Crack by Medium 1. The Effects of Reaction Layers Can Be Simulated by Assigning Different Transport and Chemical Properties to the Various Media.**



Layer 1,  $D_i = 4 \times 10^{-12} \text{ m}^2\text{s}^{-1}$   
 Layer 2,  $D_i = 4 \times 10^{-13} \text{ m}^2\text{s}^{-1}$

**Figure 5-31. pH of Groundwater Versus Distance in the Crack of a Cement-Based Backfill of a Nuclear Waste Repository. Values of pH Were Calculated Using CHEQFRAC as a Function of the Reaction Layer Properties and Groundwater Flow Rate (From Harris, et al., 1997).**

Additional analyses by Harris, et al. (1997) using an analytical model based on a simplified crack geometry indicated that an increase in the number of cracks (and therefore a decrease in crack spacing) results in a reduced ability of the repository to buffer the groundwater pH.

Note that the Harris, et al. (1997) results shown in Figure 5-31 are based on the assumption that the entire discharge of groundwater through the backfilled part of the repository is partitioned into cracks. Harris, et al. (1997) considered the annual flow rates of 126 and 12.6 m/yr [414 and 41.4 ft/yr] used in their analysis to be “high” and “more realistic,” respectively, for their repository. However, both flow rates are much higher than those anticipated for DOE sites for tank closure and near-surface disposal because the DOE sites are located mostly above the water table and because engineered caps are planned to be emplaced over the cement-based structures.

The results of Harris, et al. (1997) demonstrate that the presence of cracks can effectively reduce the time period during which the groundwater flowing through the cracks and interacting with the cement-based material is buffered to a high pH. This reduction is due to the depletion of buffering phases from a zone adjacent to each crack such that further dissolution of cement phases in the matrix is limited by diffusion of aqueous species through the depleted zone. The precipitation of relatively insoluble minerals such as calcite along the crack walls also reduces the interaction of groundwater with the cement-based material. Harris, et al. (1997) noted that their study did not consider the effects of the increased porosity resulting from extensive leaching and dissolution of minerals, which may counter the effects of precipitation and formation of reaction layers. Also, the authors stated the application of the CHEQFRAC code is only feasible for calculations covering relatively short time scales.

Note that reactive-transport models more sophisticated than CHEQFRAC have been developed, including MULTIFLO<sup>TM</sup> (Painter and Seth, 2003), TOUGHREACT (Xu, et al., 2004), and FLOTRAN (Lichtner, 2001). These other models potentially can be used to simulate the effect of fractures or cracks on the degradation of cement-based materials, but have not been applied to this problem. MULTIFLO, TOUGHREACT, and FLOTRAN are dual-continuum models (i.e., individual fractures are not explicitly represented). Rather, the hydraulic and mass transport properties of the fracture network are averaged over the volume represented by a model grid node (or cell) such that the fracture network is treated as a continuum. The physical properties of the individual fractures can be represented in the fracture continuum by assigning appropriate values of hydraulic conductivity and by using statistical representations of the fracture network to deduce equivalent hydraulic conductivities. The models can be applied to one-, two-, or three-dimensional porous and fractured media with physical and chemical heterogeneity, although the current implementation of the dual-continuum approach in FLOTRAN is limited to one-dimensional problems.<sup>9</sup> Carey and Lichtner (2007) recently used FLOTRAN to simulate carbonation and sulfate attack on cement and demonstrated that the simulation results are consistent with reaction features observed in a core of wellbore cement taken from a West Texas enhanced-oil recovery field.

Note, however, that the thermodynamic database associated with these reactive-transport codes may have to be expanded if the thermodynamic parameters for phases relevant to cement-based systems are not in the current version of the codes. Also, reactive-transport models are complex and computationally expensive and require the modeler to have a good knowledge of both the physical and chemical attributes of the system. Further, the data

---

<sup>9</sup>Lichtner, P. “Question Regarding FLOTRAN.” Personal communication (June 28) to R. Pabalan, Center for Nuclear Waste Regulatory Analyses. Los Alamos, New Mexico: Los Alamos National Laboratory. 2007.

requirements of these codes, such as field data and thermodynamic and kinetic properties, can be burdensome.

## 5.4 Summary

A number of modeling approaches for predicting the degradation of cement-based materials by carbonation, sulfate attack, and leaching have been published in the literature. Several of these models, ranging from simple diffusion or empirical equations to complex coupled reactive–transport models, were reviewed in this section (a summary list is given in Table 5-8), and examples of model results and comparisons with measured data were presented. Modeling the degradation of cement-based materials is an active area of research, and literature describing new approaches continues to be published, precluding a fully comprehensive review. For carbonation, a practical equation for calculating carbonation depth as a function of time is the simple diffusion equation, Eq. (5-6). For existing structures, the carbonation depth of any part of the structure can be measured after a certain period of exposure and the carbonation rate,  $K$ , as well as its spatial variation, can be calculated retrospectively without knowing the environmental conditions or material properties. Such a method can be used for a grouted high-level waste tank if a drill core sample of the tank grout can be taken. Otherwise,  $K$  can be approximated from laboratory tests using simulated tank grouts exposed to an atmosphere approximating that present inside a grouted tank. By assuming the average exposure conditions will not change in the future, the derived  $K$  can be used to extrapolate the carbonation depth to later times. The equation does not have explicit parameters to account for the influence on the carbonation rate of environmental factors and of the cement-based material properties, which may change nonlinearly with time and in different parts of a structure. Nevertheless, it is useful for making order-of-magnitude estimates of carbonation depth versus time.

Other carbonation models explicitly take into account the effect of environmental factors and material properties on the carbonation rate. The Papadakis, et al. (1991a, 1989) model is based on differential mass balances of gaseous  $\text{CO}_2$  and solid and dissolved  $\text{Ca}(\text{OH})_2$ , C-S-H, and unhydrated silicates, and accounts for diffusion processes and chemical reactions. For a one-dimensional geometry, a simple analytical expression gives the evolution of the carbonation front location with time in terms of the effective  $\text{CO}_2$  diffusivity in the cement-based material and of the total molar concentration of CaO that can undergo carbonation. However, the model is limited to calculating carbonation in Portland cement paste and concrete. To apply the model to DOE grouts, model parameters will need to be derived to account for the effect of supplementary cement materials on the effective  $\text{CO}_2$  diffusivity and on the reduced molar concentration of CaO in the cement due to pozzolanic reactions with blast furnace slag and fly ash.

For sulfate attack, the degradation depth as a function of time can be calculated using an empirical equation Atkinson and Hearne (1984) developed that requires as input the concentration of sulfate and magnesium in solution and the tricalcium content of the cement. The equation is based on laboratory tests that exposed ordinary Portland cement blocks to  $\text{Na}_2\text{SO}_4$  and  $\text{MgSO}_4$  solutions for 5 years. The equation does not explicitly consider factors that affect the sulfate degradation process, such as cement properties (e.g., water/cement ratio, composition) and changes in the diffusivity of the material due to expansive reactions from the sulfate attack. Thus, the equation may not be applicable to DOE grout formulations, which have compositions different from the cement blocks used in the tests and will be exposed to solution compositions different from those of the test solutions. However, because the DOE grout

<b>Table 5-8. Reviewed Chemical Degradation Models</b>	
<b>Chemical Degradation Mechanism</b>	<b>Modeling Approach and References*</b>
Carbonation†	Diffusion–reaction model <ul style="list-style-type: none"> <li>• Lay, et al. (2003)</li> <li>• Papadakis, et al. (1991a,b,c; 1989)</li> </ul>
Sulfate attack	Empirical correlation <ul style="list-style-type: none"> <li>• Atkinson and Hearne (1984)</li> </ul> Diffusion–reaction model <ul style="list-style-type: none"> <li>• Atkinson and Hearne (1990)</li> <li>• Tixier and Mobasher (2003a,b)</li> </ul> Diffusion–advection–reaction model <ul style="list-style-type: none"> <li>• Marchand, et al. (1999)</li> <li>• STADIUM (Marchand, et al., 2002; Maltais, et al., 2004)</li> </ul>
Leaching	Chemical model <ul style="list-style-type: none"> <li>• Berner (1992a)</li> <li>• CEMCHEM/PHREEQE (Glasser, et al., 1999, 1988; Atkins, et al., 1994, 1992a,b, 1991, 1990; Bennett, et al., 1992)</li> </ul> Diffusion–reaction model <ul style="list-style-type: none"> <li>• Atkinson and Hearne (1984)</li> <li>• DIFFUZON (Adenot and Richet, 1997; Adenot, et al., 1997)</li> <li>• Moranville, et al. (2004)</li> </ul> Diffusion–advection–reaction model <ul style="list-style-type: none"> <li>• Marchand, et al. (1999)</li> <li>• STADIUM (Marchand, et al., 2002, 2001; Maltais, et al., 2004)</li> <li>• Yokozeke, et al. (2004)</li> <li>• MCOTAC (Pfungsten, 2002, 2001)</li> </ul> Diffusion–advection–fracture model <ul style="list-style-type: none"> <li>• CHEQFRAC (Harris, et al., 1997)</li> </ul>
*Note: Refer to reference section of this report for full references.	
†The models apply to carbonation in which leaching is unimportant, as discussed in Section 4.1.1.	

formulations contain blast furnace slag and fly ash that reduce the permeability or hydraulic conductivity of the cement-based material, it is possible the Atkinson and Hearne (1984) empirical equation could overpredict and, thus, provide an upper bound on the depth of sulfate attack if applied to DOE grouts.

The Atkinson and Hearne (1990) reactive–transport model for sulfate attack has relatively simple equations that account for sulfate ion diffusion and for expansive ettringite formation that could cause cracking and spallation. The model has parameters applicable to ordinary Portland cement and sulfate-resistant Portland cement derived from measurements of bulk linear expansion of thin mortar beams exposed to sulfate solutions. Atkinson and Hearne (1990) stated this model likely is more accurate than simple diffusion equations and models that account for chemical reactions but neglect the mechanical effect of the reactions. However, the authors acknowledged their model has limitations because it neglects the relief of stress by creep, the protective or semiprotective role of reaction products, and the contribution of dissolution on the degradation process. Also, the model has not been tested on cement-based formulations with supplementary cement materials, and parameters that account for the effect of

these materials will have to be derived if the model is to be applied to degradation modeling of DOE grouts.

The Tixier and Mobasher (2003a,b) reactive–transport model for sulfate attack also accounts for sulfate ion diffusion and expansive ettringite formation. Microcracks are initiated in the model when the expansive stress exceeds the tensile strength of the matrix, which increases sulfate diffusivity. The model predicts the amount of reacted calcium aluminates, the stresses generated, and internal parameters such as damage, expansion levels, weight gain, stiffness degradation, and tensile strength degradation. The Marchand, et al. (1999) reactive–transport model also accounts for expansive reactions of ingressing sulfate ions with cement phases that lead to changes in the microstructure and transport properties of the cement-based material. This model differs from that of Tixier and Mobasher (2003a,b) in that it includes both diffusive and advective transport, can account for the effect of leaching (i.e., dissolution of portlandite and decalcification of C-S-H), and can be applied to hydrologically unsaturated conditions. The Marchand, et al. (1999) model was later improved and called STADIUM (Marchand, et al., 2002).

For leaching, purely chemical models can be used to evaluate the evolution of system chemistry during degradation of cement-based materials. For example, Berner (1992a) and Glasser, et al. (1999) both used mixing calculations to estimate how the chemical inventory of a cement-based structure and the pore solution composition evolve with time in a given groundwater environment. A major advantage of the purely chemical approach to modeling leaching is that it can be implemented using widely available geochemical computer codes; however, a major disadvantage is its neglect of mass transport and spatial and temporal heterogeneities of the degradation process. The main limitation of Berner's (1992a) mixing tank approach is the use of water exchange cycles, instead of real time, to express the temporal evolution of chemistry. Relating cycles to real time requires additional information (e.g., the amount of groundwater entering the system per unit time) that may not be available nor well constrained.

A particularly useful chemical model for cement formulations with supplementary cement materials like fly ash and blast furnace slag is CEMCHEM. The solid phase composition of a cement-based material aged over laboratory time scales is likely to be quite different than that of a material aged for 100 or 1,000 years. Thus, other properties, such as pore water composition and material microstructure, also may be quite different, which would make predictions of long-term behavior based on short-term data misleading. CEMCHEM, which was developed by Glasser and coworkers, predicts the solid phase assemblage following complete hydration of blended cements based on the bulk oxide composition of the unhydrated components. The resulting solid phase assemblage derived from CEMCHEM and the known solubility constants of the solids can be used to predict the composition of the aqueous phase in equilibrium with the cement-based material. CEMCHEM, however, does not account for the reduced sulfide phase in blast furnace slag and cannot be used to model the evolution of the redox potential in slag–cement systems.

Some reactive–transport models for leaching consider diffusion as controlling the degradation process based on the assumptions that the cement-based material is saturated, advective flow is negligible, and the rates of chemical reactions are much faster than diffusion rates. The Atkinson and Hearne (1984) shrinking core model for leaching of ordinary Portland cement further assumes that leaching is controlled mainly by the external water chemistry and by the calcium concentration in the pore solution, which itself is controlled by portlandite dissolution. This model requires only the diffusion coefficient of calcium ions in the degraded cement, the calcium ion concentration gradient between the groundwater and cement pore water, and the

bulk concentration of calcium in cement solids. This model is simple to apply, but it does not consider factors such as dissolved species other than  $\text{Ca}^{2+}$ , other cement phases (e.g., C-S-H), and changes in material properties as degradation proceeds.

More complex reactive–transport leaching models have been developed to explicitly account for the coupling between chemical reactions and transport processes. These coupled reactive–transport models, including those developed by Adenot and Richet (1997); Moranville, et al. (2004); Marchand, et al. (2002); Pfingsten (2002, 2001); and Yokozeki, et al. (2004), vary in degree of complexity but generally account for changes in transport parameters that result from dissolution or precipitation reactions. The models by Adenot and Richet (1997) and Moranville, et al. (2004) model only diffusive transport, whereas Marchand, et al. (2002); Pfingsten (2002, 2001); and Yokozeki, et al. (2004) model both diffusive and advective transport. However, none of these models have been applied to cement-based materials with compositions similar to DOE grouts and parameters will need to be developed to apply these models to those systems.

None of the chemical degradation models in the reviewed published literature have been applied to simulations of the evolution of the redox condition or Eh of cement pore waters or of groundwaters interacting with cement-based materials. However, existing geochemical models and coupled reactive–transport models generally enable calculation of Eh or of oxygen fugacity, which is related to Eh. Blast furnace slag is a supplementary cement material that DOE uses to impose a reducing environment in grouted waste tanks and concrete vaults and to mitigate the release of redox sensitive radionuclides, such as technetium-99. Therefore, it would be useful to modify existing geochemical models or coupled reactive–transport codes and associated thermodynamic databases to add the capability to simulate the Eh evolution in systems containing slag–cement blends.

Simple diffusion or empirical models are useful in providing gross estimates of performance of cement-based materials, particularly when applied to civil infrastructures for which the intended service life is in the tens of years (Lay, et al., 2003; Bertolini, et al., 2004). However, such models make simplifying assumptions about the degradation process and ignore the effect of various parameters that may affect the degradation rate, such as the presence of cracks that can accelerate the ingress of deleterious chemical species. Also, these simpler models focus on a specific degradation mechanism such that a separate effects analysis using two or more models is required if more than one degradation process is anticipated. A separate effects analysis, however, can be limited by its lack of consideration of the coupling that could occur between different degradation mechanisms. Such coupling may either reinforce the effect of different processes and accelerate degradation or counteract the effect of different processes and reduce degradation. For example, carbonation reactions that precipitate calcite and reduce the permeability of the cement-based material could enhance the resistance of the material to sulfate attack and leaching.

For explicit consideration of coupling between different chemical degradation mechanisms and between chemical reactions and transport processes, a coupled reactive–transport model is required. Several coupled reactive–transport models have been applied successfully to modeling degradation of cement-based materials, and many features of cement degradation observed in laboratory experiments or in field samples have been reproduced using these models. Several examples presented in this section that show good agreement between modeling results and laboratory or field sample data provide a good degree of confidence in the predictive ability of coupled reactive–transport models. However, the degradation periods experienced by the laboratory or field samples are relatively short compared to the time period

of interest in performance evaluations of cement-based engineered barriers so that predictions to longer time periods still have considerable uncertainties. In addition, Carey and Lichtner (2007) pointed out some of the more difficult problems with making long-term predictions using coupled reactive–transport models, including (i) uncertainties in the pore-scale geometries that govern the exposed surface area (hence, the effective reaction rate) of minerals and the tortuosity of the cement-based material and (ii) many systems to be modeled are not in equilibrium, but the kinetic parameters required to simulate such systems are not available. Further studies are needed to determine how coupled reactive–transport models can be applied to the long timeframes of interest in radioactive waste disposal. Parameter values also need to be developed if the models are to be applied to DOE grouts.

Most of the chemical degradation models reviewed in this section do not account explicitly for the effect of fractures or cracks on the chemical degradation process. However, the Harris, et al. (1997) study, which used a two-dimensional model that explicitly considered crack size, crack distribution, and formation of reaction layers on crack surfaces, clearly demonstrated the effect of these parameters on the chemical-buffering performance of a cement-based repository. Fractures or cracks could provide fast or bypassing pathways for the transport of chemically reactive gaseous or aqueous species or for the migration of radionuclides from cement-based waste forms. Thus, it is important to consider the presence of fractures or cracks in models used to evaluate the performance of cement-based engineered barriers. Codes that potentially can be used for this evaluation are dual-continuum, coupled reactive–transport codes, such as MULTIFLO, TOUGHREACT, and FLOTRAN. Conceptual and mathematical models that can be used to evaluate the potential influence of fast pathways and bypassing pathways in engineered barriers on radionuclide releases are discussed in the next section.

## **6 CONCEPTUAL AND MATHEMATICAL MODELS OF POTENTIAL FAST AND BYPASSING PATHWAYS ASSOCIATED WITH *IN-SITU* TANK CLOSURES**

An important component of the plan for tank closure at U.S. Department of Energy (DOE) sites is the creation of an engineered barrier to radionuclide migration (in addition to preexisting barriers that were part of the original tank design) by filling the tanks and any external tank penetrations (such as fill lines) with a cement-based grout. Subsequently, an engineered cover will be placed over the tanks to act as an additional barrier to limit infiltration of meteoric water and to restrict human and biological intrusion into contaminated materials. The ability of the engineered barriers to mitigate the release and migration of radionuclides could be reduced if fast pathways and bypassing pathways develop. For the purposes of this section, fast pathways refer to features that allow fluids (i.e., water or gas) and associated radionuclides and chemical constituents to flow at rates significantly faster than those estimated to occur through the bulk engineered barrier. Bypassing pathways refer to features that may allow (i) dissolved radionuclides to bypass chemical barriers or (ii) meteoric water or environmental gases to bypass engineered barriers and either contact the waste form or accelerate the degradation of engineered barriers. Bypassing pathways also could divert environmental fluids around the waste form.

This section describes conceptual and mathematical models that can be used to evaluate the potential influence of fast pathways and bypassing pathways in engineered barriers on radionuclide releases from radioactive waste processing tanks that are closed in place as well as from other cement-based near-surface disposal sites for nuclear waste (e.g., saltstone). Although this section is not specific to any one DOE tank closure plan, DOE-specific tank designs and closure plans are used to develop classifications and conceptual models of potential fast pathways and bypassing pathways that may affect the performance of *in-situ* grouted tanks in general.

### **6.1 Identification and Classification of Potential Fast and Bypassing Pathways**

Despite the generally low permeability of cement-based materials, cement-based structures have expansion joints and cracks that are potential pathways for water and gas movement. For example, groundwater seepage into basements through cracks, joints, and utility penetrations is a common occurrence in humid climates, as is radon vapor intrusion in some areas. Seepage of water into concrete vaults used for secondary containment of waste tanks has been observed at the West Valley Nuclear Services site (e.g., Elmore and Henderson, 2001). Infiltration of meteoric water through cracks and joints in concrete vaults containing waste handling tanks also is suspected to have occurred at the Idaho National Laboratory site (DOE–Idaho, 2006a). Although these examples of water and gas movement through concrete structures illustrate the physical process, they are not good analogs for movement of fluids through large, grouted tanks at DOE sites, because of significant differences in the size, shape, composition, and structure of the grouted tanks.

Figures 6-1 and 6-2 show schematic cross sections of as-built tank constructions at the Idaho National Laboratory Site and the Savannah River Site, respectively. Common characteristics of the tanks at each site are a metal tank with penetrations for fluid transfer piping and equipment access (such as the center riser in Figure 6-2). The tank interiors contain various metal pipes, cooling coils, and metal support structures. The photographs in Figure 6-3 show the cooling

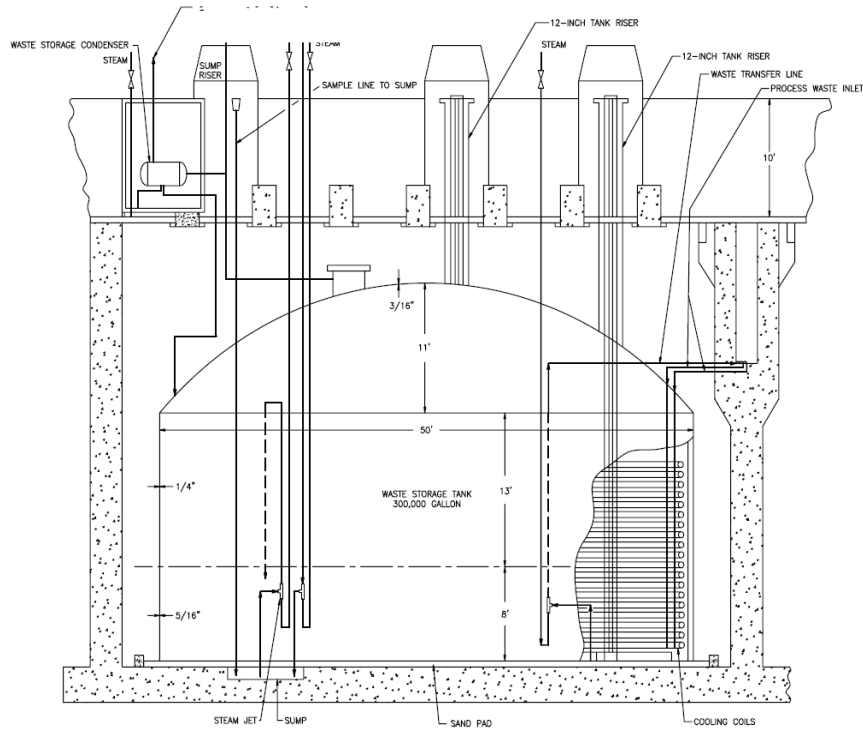


**Figure 6-1. Cross Section of a Typical Tank With Cooling Coils at the Idaho National Laboratory (From DOE–Idaho, 2006a)**

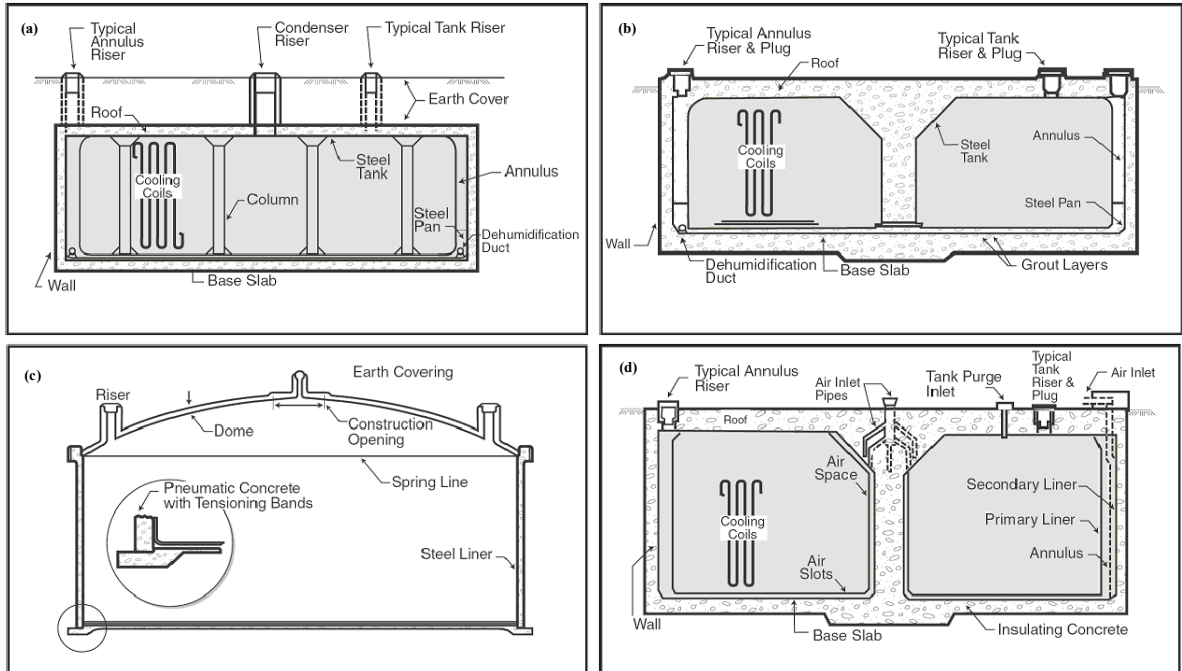


**Figure 6-2. Tank Configurations at the Savannah River Site: (a) Cooled Waste Storage Tank, Type I; (b) Cooled Waste Storage Tank, Type II; (c) Uncooled Waste Storage Tank, Type IV (Prestressed Concrete Walls); and (d) Cooled Waste Storage Tank, Type III (Stress Relieved Primary Liner). Figures Taken From DOE–Savannah River Site (2002).**

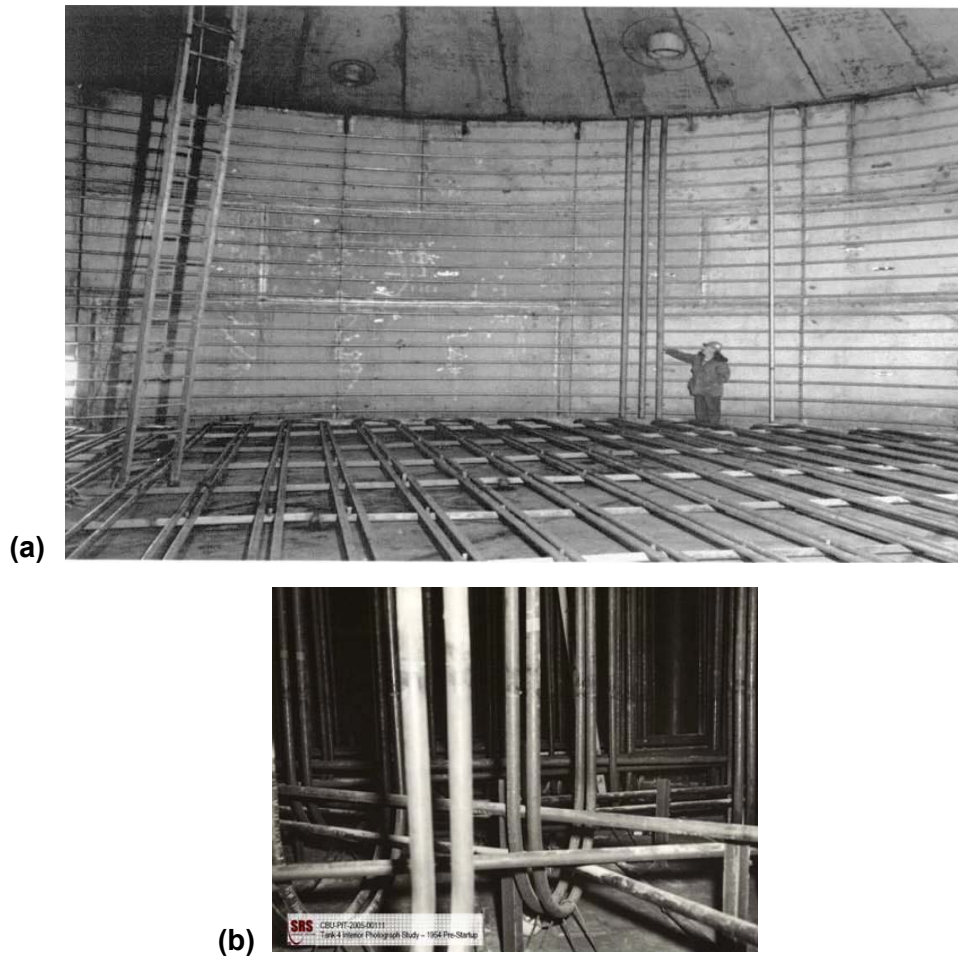


**Figure 6-3. (a) Photograph Showing the Internal Structure and Cooling Coils of Tank WM-185 During Construction at the Idaho National Laboratory Tank Farm Facility [From DOE–Idaho (2006a)] and (b) Photograph Showing the Network of Cooling Coils in the Interior of a Savannah River Site Type I Tank Prior to Receipt of Wastes. Reprinted With Permission From National Academies Press, Copyright<sup>®</sup> 2006, National Academy of Sciences.**

coils in the tank interiors at Idaho National Laboratory Site and at Savannah River Site. The metal walls of the tanks and the cooling coils are constructed with either carbon steel, as at Savannah River Site, or stainless steel, as at the Idaho National Laboratory Site. A significant difference between the tanks shown in Figures 6-1 and 6-2 is that the Idaho National Laboratory Site tanks are freestanding metal structures housed within reinforced concrete vaults, whereas the Savannah River Site tanks have a metal liner encased in reinforced concrete for structural support. Additionally, some of the Idaho National Laboratory Site tanks, illustrated in Figure 6-1, sit on a base of bedding sand connected to an overflow collection sump, whereas the Savannah River Site tanks sit on a concrete base with drainage channels connected to a collection sump.<sup>1</sup>

The conceptual plan for in-place closure of these tanks is to fill the tanks with a cement-based grout having a composition suitable for immobilizing or encapsulating residual radioactive

<sup>1</sup>Not all tanks at the Idaho National Laboratory Site have sand pads. Tanks shown in Figure 6-1 are intended to illustrate the variety of engineered structures that may be present in and around a tank.

materials. At the Savannah River Site, the tanks might be filled with two types of grout: (i) a reducing grout to chemically immobilize the waste and (ii) a strong grout to act as an intruder barrier, as illustrated in Figure 6-4. At the Idaho National Laboratory Site, both the tank and the vault have been filled with grout, as illustrated in Figure 6-5. The amount of reducing grout at the Idaho National Laboratory Site was limited to the lower portion of the tanks. Although the grout placed in the tanks may mix with the residual waste, complete mixing may not occur, leaving some of the waste as discrete layers or lenses, described in DOE–Idaho (2006a) as “...trapped between grout layers, and some encapsulated between the tank structure and the grout.”

With respect to the overall tank construction geometry and environmental setting, the domed tanks at the Idaho National Laboratory Site (Figure 6-1) and the Savannah River Site (Type IV tanks, Figure 6-2) may have a greater potential to divert infiltrating meteoric water from the waste form than the tanks with flat roofs, such as the Savannah River Site Types I, II, and III tanks shown in Figure 6-2. Some tanks at the Savannah River Site are located within the saturated zone in direct contact with groundwater (National Research Council, 2006). The tanks at the Idaho National Laboratory Site are all located high above the water table so that downward percolation of infiltrating meteoric water is the most likely way that water would contact the waste form.

Although the tank construction and specific in-place closure procedure may vary from site to site, Figures 6-1 to 6-5 adequately identify the types of features that could act as fast or bypassing pathways. These features can be categorized generally as cracks and conduits. Cracks are two-dimensional features that form due to mechanical failure of a material, such as grout or concrete structures. As used here, conduits will refer to discrete fluid pathways that may be present or develop along specific engineered features (e.g., annular spaces between grout and a corroded pipe or rebar) or voids in pipes and cooling coils not accessed by the emplaced grout. Specific pathways within each of these categories are listed in Table 6-1 and discussed in detail in the following sections.

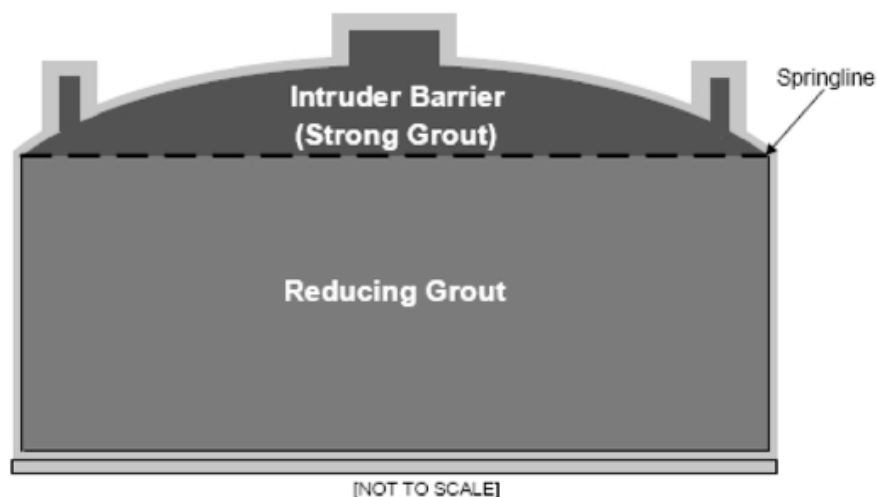


**Figure 6-4. Conceptual Illustration of Grouted Tank at the Savannah River Site (From DOE–Savannah River Site, 2005)**

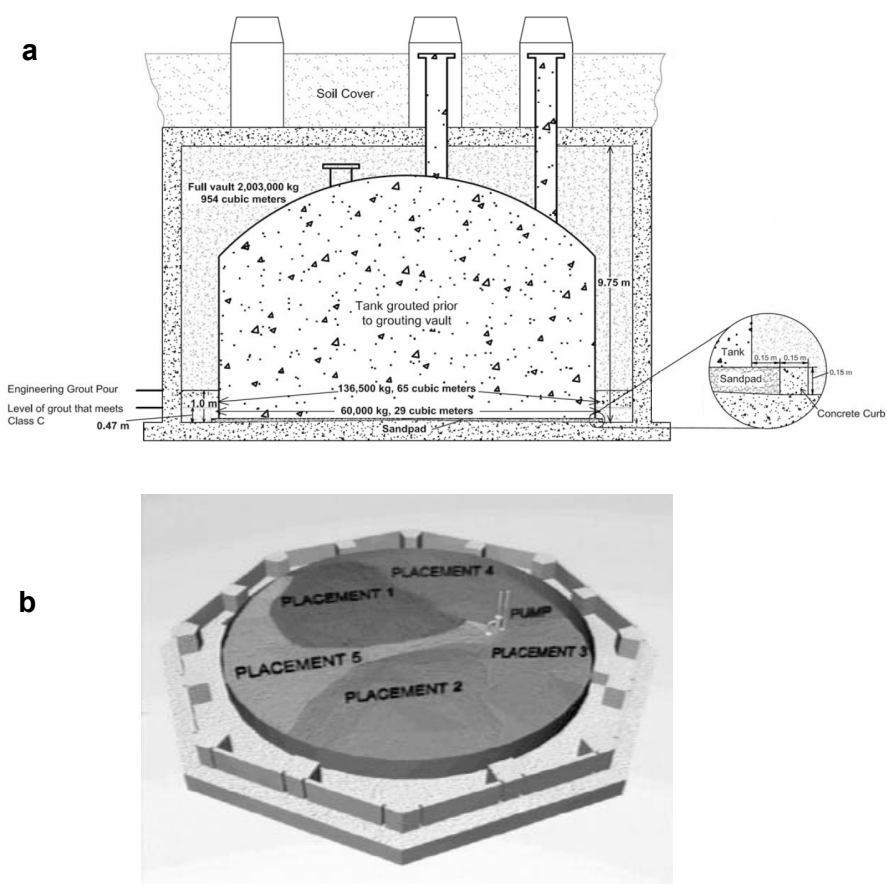


**Figure 6-5. Illustration of (a) Grouted Tank and Vault (From DOE–Idaho, 2005) and (b) Placement of Reducing Grout During Engineered Pours at the Idaho Nuclear Technology and Engineering Center Tank Farm Facility (From DOE–Idaho, 2006b)**

<b>Table 6-1. Categories and Features That May Act as Fast or Bypassing Pathways Associated With In-Place Tank Closures</b>	
<b>Category</b>	<b>Feature</b>
Cracks	Microcracks in grout monolith
	Macrocracks in grout monolith
	Microcracks in external grout and concrete surrounding tanks
	Macrocracks in external grout
	Cracked and corroded seams/joints in metal tank walls
	Macrocracks in concrete tank and vault walls
Conduits	Annular spaces between grout and pipes, coiling coils, and tank walls
	Annular spaces due to metal pipe corrosion
	Discontinuities in grout pours
	Corroded rebar in concrete vault walls and footings
	Annular spaces between grout and external pipes and risers
	Liquid collection systems external to tanks
	Voids in pipes and cooling coils not filled with grout

### 6.1.1 Cracks in Grout and Concrete Structures

For the purposes of this report, cracks in grout used to fill tanks, associated piping and risers, and concrete structures associated with the tanks (such as external concrete support, footings, and vault walls) can be classified as microcracks and macrocracks. Microcracks are microscopic cracks disseminated throughout a concrete matrix that probably exist in all cement-based structures due to plastic shrinkage, heat of hydration drying shrinkage, and mechanical stress (Young, 1988; Hearn, 1999). Neville (1996) characterized microcracks as cracks with apertures less than 0.1 mm [less than 0.02 in]. Macrocracks are discrete fractures in a cement-based material that are often visible to the naked eye.

#### Microcracks

Various types of microcracks are illustrated in Figure 6-6. These microcracks have been described as bond cracks and mortar cracks (Hearn, 1999). As illustrated in Figure 6-6(a), bond cracks occur when the mortar separates from the aggregate during drying.<sup>2</sup> Thus, simple bond cracks are not likely to form interconnected pathways through the grout. Mortar cracks form in the mortar between the aggregate and may form interconnected networks through the concrete matrix as well as interconnecting bond cracks [Figure 6-6(b)]. Hearn (1999) also identified drying-shrinkage cracks, illustrated in Figure 6-6(c), which can be described as a combination of bond and mortar cracks. The formation of drying-shrinkage cracks was ascribed to the heterogeneity of the constituents of the cement-based material, which causes stresses strong enough to cause cracking (Hearn, 1999). In the process of drying, the difference in the moduli of elasticity between hydrated cement paste and clinker residue, hydrated cement paste and fine aggregate, and mortar and coarse aggregate causes circumferential and radial cracking in the cement-based material [Figure 6-6(c)]. Drying-shrinkage cracks may intersect throughgoing mortar cracks.

Due to their ubiquitous nature in concrete, microcracks affect the bulk permeability and diffusion properties of apparently intact concrete materials. For this reason, the influence of microcracks on fluid permeation and chemical diffusion is likely to be included with uncracked mortar properties in laboratory measurements of concrete permeability and diffusion coefficients (e.g., Young, 1988; Boulfiza, et al., 2003; Hearn, et al., 1994) if the laboratory curing process is similar to that of a large-scale structure. Viewed on a macroscopic scale, microcracks would not be described as fast or bypassing pathways in calculations of bulk water, gas, or chemical transport through a grout monolith.<sup>3</sup> Combining the influence of microcracks with the matrix may not always be appropriate, however, for modeling radionuclide release because:

- Preferential flow through microcracks may reduce the residence time of fluids in the matrix.
- Transport of dissolved radionuclides from the uncracked mortar to fluids in the microcracks may be diffusion limited, and radionuclide concentrations in fluids flowing through the microcracks would be overestimated.

---

<sup>2</sup>Although aggregate is typically viewed as the very coarse crushed rock added to concrete, grout also contains fine aggregate, such as sand and supplementary cement materials.

<sup>3</sup>As used in Section 6 of this report, monolith refers to an intact, continuous cement-based structure, such as a grout-filled tank, a cell within a saltstone vault, or a continuous section of grout within a pipe.

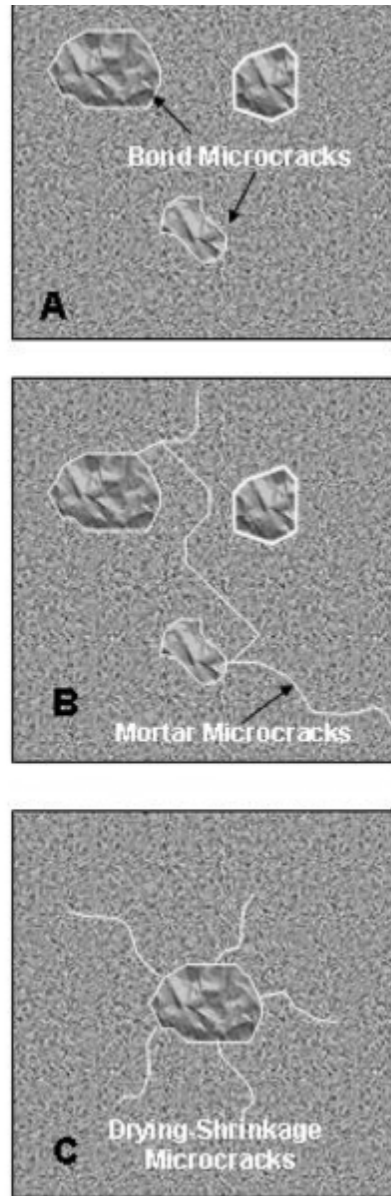


**Figure 6-6. Illustration of Types of Microcracks in a Concrete Matrix: (a) Bond Microcracks, (b) Mortar Microcracks, and (c) Drying-Shrinkage Microcracks (After Hearn, 1999)**

- Radionuclides traveling through the microcracks may not be immobilized, because chemical equilibrium with reactants in the mortar or aggregate is not achieved.
- Because laboratory measurements of flow and transport properties probably include the effect of microcracks in the matrix, it would be inappropriate to adjust laboratory measured parameters to account for microcracks when modeling the matrix as a single continuum. If microcracks are explicitly represented in the model, then the flow and transport parameters of the mortar should be adjusted with respect to laboratory measurements on matrix materials, most likely to lower values.

- Transport of environmental fluids and reactants (water, dissolved species, and atmospheric gases) from the microcracks to the uncracked mortar or aggregate may be diffusion limited so that degradation of the mortar or aggregate would be overestimated.

Because simulating local flow and transport through microcracks may not be feasible in field-scale models, subscale calculations may be required to determine the extent to which the matrix (mortar and microcracks) can be treated as a single continuum.

### **Macrocracks in Grout and Other Concrete Structures**

Macrocracks in grout and concrete generally form after the cement-based material has hardened and are usually the result of thermomechanical stress (Wang, et al., 1996) or the mechanical stress in large concrete monoliths (e.g., Copen, 1974; Zhang, et al., 2003). Macrocracks can also form when preexisting microcracks expand due to mechanical stress, water freezing, and salt precipitation and hydration. By their nature, macrocracks are more widely spaced and have much larger apertures than microcracks. The spacing and aperture for macrocracks can vary significantly depending on the composition of the cement-based material, size and shape of the structure, mechanical loading, and environmental exposure.

Laboratory tests on concrete core samples with mechanically induced macrocracks indicate that single or simple branching cracks can increase the average water permeability of the test specimen by many orders of magnitude. For example, the Wang, et al. (1996) test results indicate hydraulic conductivities on the order of  $10^{-16}$  m/s [ $3 \times 10^{-16}$  ft/s] for concrete samples without macrocracks. Freedman (1974) reported values of hydraulic conductivity ranging from approximately  $4 \times 10^{-13}$  to  $3 \times 10^{-11}$  m/s [ $1 \times 10^{-12}$  to  $1 \times 10^{-10}$  ft/s] based on aged  $46 \times 46$ -cm [ $18 \times 18$ -in] concrete specimens from various concrete dams. Tests on 10-cm [4-in]-diameter cores with macrocracks with apertures of approximately 0.05 cm [0.02 in] had hydraulic conductivities as high as  $10^{-4}$  m/s [ $3 \times 10^{-4}$  ft/s] (Wang, et al., 1996). Aldea, et al. (1999) reported similar findings. For comparison, the hydraulic conductivity of concrete without macrocracks is equivalent to an intrinsic permeability of approximately  $10^{-16}$  m<sup>2</sup> [ $10^{-15}$  ft<sup>2</sup>], which is about two orders of magnitude higher than the lower range of matrix permeabilities estimated for welded tuffs at Yucca Mountain, Nevada (Bechtel SAIC Company, LLC, 2004). The hydraulic conductivities for cracked concrete Wang, et al. (1996) and Aldea, et al. (1999) reported represent the hydraulic conductivity of the crack weighted by the surface area of the concrete core and are only meaningful if converted to the hydraulic conductivity of the crack itself. For example, a single crack with an aperture of 0.5 mm [0.02 in] in a 10-cm [4-in]-diameter concrete core would have a hydraulic conductivity of approximately  $2 \times 10^{-2}$  m/s [ $7 \times 10^{-2}$  ft/s]. Even if the uncracked matrix was impervious, the apparent hydraulic conductivity of the sample would be approximately  $1 \times 10^{-4}$  m/s [ $3 \times 10^{-4}$  ft/s] based on the ratio of the surface area of the crack to the surface area of the sample. Thus, values of hydraulic conductivity or permeability reported for cement-based materials are very scale dependent. These scale effects must be clearly understood before using reported values in flow and transport calculations.

Due to the much higher permeability of macrocracks than the grout or concrete matrix,<sup>4</sup> most fluid flow through the grout monolith and external concrete structures will occur through macrocracks, if present, rather than through the grout or concrete matrix. Macrocracks in the grout monolith could act as fast pathways for environmental fluids (infiltrating water and air) to

---

<sup>4</sup>The grout or concrete matrix refers to the grout or concrete mass between macrocracks that consists of mortar and aggregate and that may contain microcracks.

contact the grout matrix and any radionuclides incorporated in the matrix. If radionuclides are present as segregated layers, lenses, or pockets in the grout monolith, the macrocracks could act as fast pathways for radionuclide migration through the grout monolith and as bypassing pathways limiting radionuclide contact with grout matrix constituents intended to reduce radionuclides mobility. Alternatively, macrocracks in the grout monolith where radionuclides are incorporated in the grout matrix will act as bypassing pathways, limiting the percolating water contact with the waste. Macrocracks will also shorten the diffusion path length from the matrix to mobile fluids in the cracks.

### 6.1.2 Conduits

Conduits are distinguished from cracks in this report because they may occur as discrete pathways that are initially present or may develop along specific engineered features, rather than as disseminated pathways throughout a grout or concrete monolith, as is the case for cracks. Various types of potential conduits are listed in Table 6-1 and are illustrated in Figure 6-7. The conduits illustrated in Figure 6-7 can act as pathways for fast movement of environmental fluids (water and air) into the waste form (such as the corroded pipe pathway in Figure 6-8), as fast pathways from the waste form to the environment (such as the corroded tank pathway out of the waste form in Figure 6-8), or as bypassing pathways that divert environmental fluids away from the waste form (e.g., the tank annulus pathway past the waste form in Figure 6-8). Alternatively, seepage along the tank walls may result in preferential contact with the waste form if radionuclides are concentrated on the walls and floor of the tank.

Conduits formed around preexisting engineering structures (e.g., pipes, tank walls) can be described as annular spaces. Figure 6-9 illustrates two types of annular spaces that could exist inside a grout-filled pipe. In Figure 6-9(a), the annulus is open (i.e., a gap exists between the pipe and the grout). Such a gap could occur when grout shrinks from the pipe wall during curing or result from corrosive degradation of the pipe. Figure 6-9(b) illustrates an annulus filled with a porous material, such as the oxidized residue of a corroded metal pipe. A similar situation could

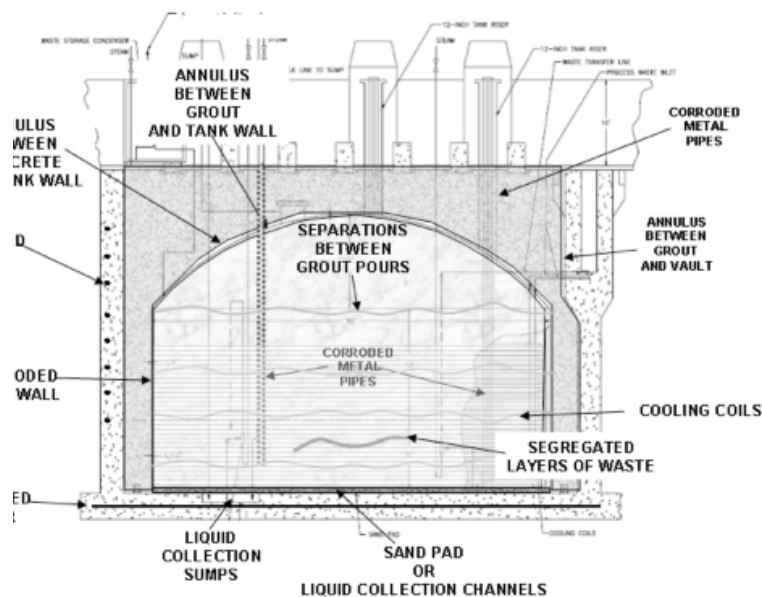


**Figure 6-7. Features That May Act As Conduits in a Typical Tank at the Idaho National Laboratory (Conduits Superimposed on Tank Cross Section From DOE-Idaho, 2006a)**

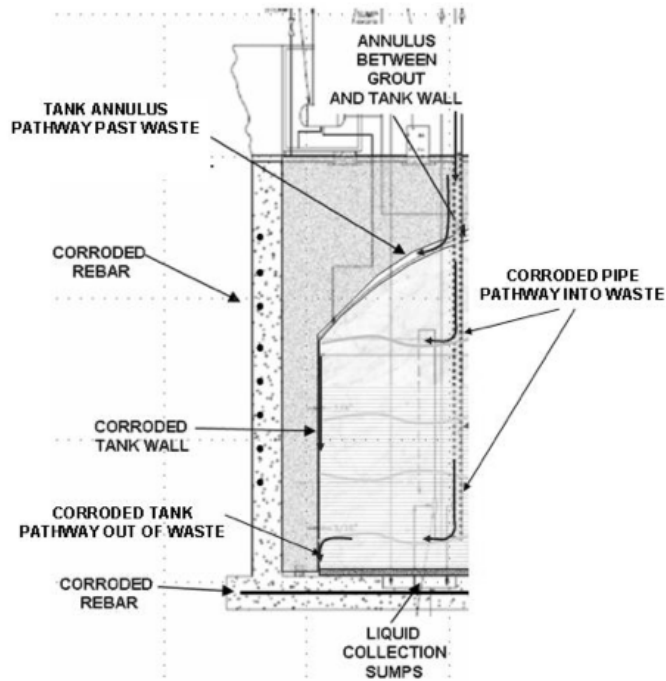


**Figure 6-8. Illustration of Fast and Bypassing Conduit Pathways. Corroded Pipe May Act as Fast Pathway to the Waste Form. Corroded Tank Wall May Act as Either a Pathway Bypassing the Waste Form or a Fast Pathway From the Waste Form to the Environment (Based on Tank Cross Section From DOE-Idaho, 2006a).**

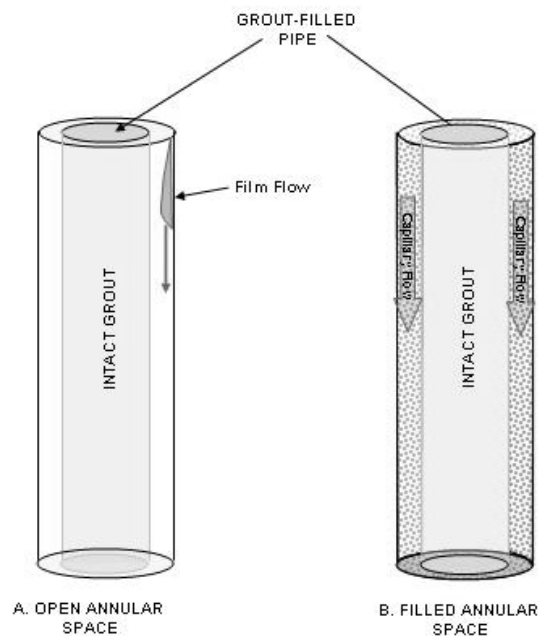


**Figure 6-9. Liquid Flow Regimes in an Annular Space Around a Grouted Pipe: (a) Film Flow in an Open Annular Space With Large Aperture and (b) Capillary Flow in an Annular Space Filled With Corrosion Products or With Small Aperture**

occur when corrosion products form and expand, resulting in cracks or a permeable annulus around the pipe. In either case, the processes for fluid and mass exchange between the conduit and the matrix are fundamentally the same as for a crack in the grout (Figure 6-10). Liquid exchange between the conduit and the matrix is controlled by the hydraulic gradient between the matrix and the wetted surface of the annulus (Walton and Seitz, 1991; Kapoor, 1994; Tokunaga and Wan, 1997; Tokunaga, et al., 2000).

Mass transport between the fluid in the conduit and the matrix can be by advection, diffusion, or both. If the conduit and matrix are both water saturated so that there is no hydraulic gradient to drive advection, transport will be diffusion dominated. If the aperture of the conduit is much larger than the representative pore size in the matrix and the matrix is not saturated, then advective transport from the conduit to the matrix can occur in the presence of diffusion either into or out of the matrix. Even when the matrix is generally unsaturated, advective transport from the matrix to the conduit can occur where locally saturated conditions are present, such as at long interfaces between higher and lower permeability grout or at contacts with engineered structures.

As indicated in Figure 6-7, other types of conduits could exist that would not be described as annular spaces, such as pipes and cooling coils not filled with grout, corroded reinforcing bars (rebars) in concrete vault walls and footings, internal structural supports, and liquid collection systems beneath the tanks and within the vaults. These types of conduits would generally be exterior to the waste form in the tank, although the sand pad at one Idaho National Laboratory tank is known to be contaminated with radioactive materials, and would potentially affect radionuclide releases either by acting as fast pathways from the waste to the environment or fast pathways for environmental fluids into the waste form. In some cases, however, conduits could act as bypassing pathways that divert percolating water around the waste form, as illustrated in Figure 6-11.

Finally, interfaces between grout pour layers or lenses of segregated residual waste also could act as conduits, as illustrated in Figure 6-12. Liquid flow and mass transport processes in such a conduit would be similar to those for macrocracks. Whether or not such layering or waste segregation is present in the grout monolith will depend on the properties and manner of grout emplacement.

## **6.2 Movement of Fluids Through Potential Fast and Bypassing Pathways**

Cracks and conduits are likely to act as the primary pathways by which environmental fluids, such as infiltrating water and atmospheric gases, can contact the waste form. These environmental fluids can affect radionuclide releases by carrying radionuclides and conveying chemical reactants that (i) physically degrade the grout or engineered structures or (ii) change the chemical properties of the grout and chemical environment of the waste form thus increasing radionuclide mobility. This section discusses the physical structure and properties that determine the mathematical description of fluid flow through the pathways described in Section 6.1 and the way such flow could be modeled. Data on the permeability of

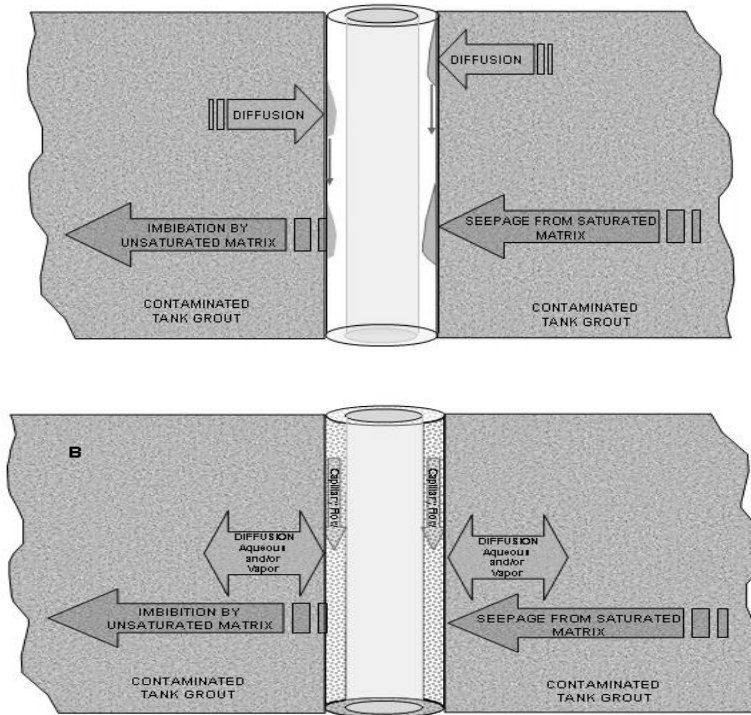


Figure 6-10. Fluid and Mass Transport Processes in Annular Spaces: (a) Open Annular Space and (b) Filled Annular Space

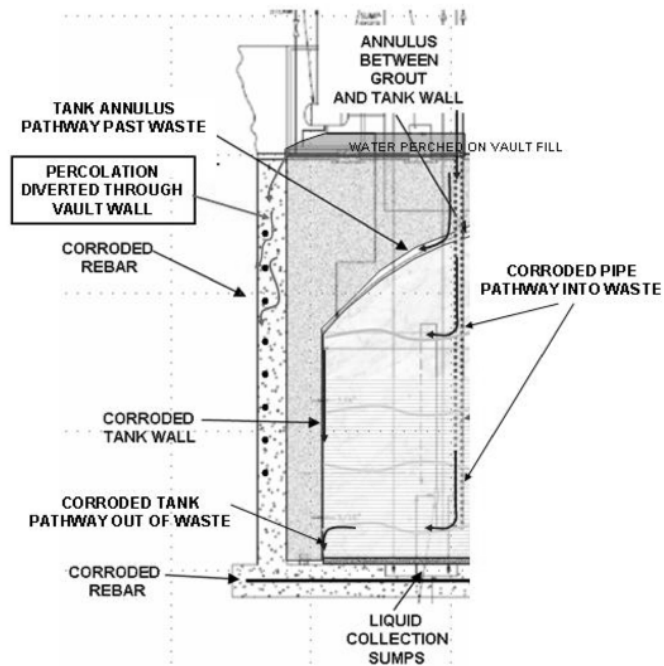
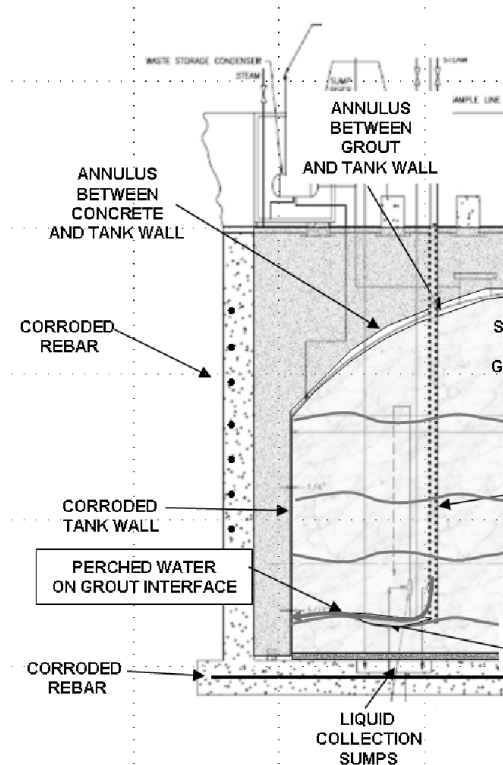


Figure 6-11. Illustration of (i) Percolation Diverted Away From Waste Form Through Cracks and Conduits in Vault Wall and (ii) Flow Into the Waste Form Through a Conduit (Based on Tank Cross Section From DOE-Idaho, 2006a)



**Figure 6-12. Conduit Flow Along a Grout Pour Interface Due to Perching on a Grout Layer (Based on Tank Cross Section From DOE-Idaho, 2006a)**

cement-based materials is presented in Appendix A. The mathematical description of mass transport processes is discussed in Section 6.3.

### 6.2.1 Fluid Flow in Cracks

Although macrocracks, by definition, have larger apertures than microcracks, the same fluid dynamic principles usually are applied in calculating fluid flow through both macrocracks and microcracks. Assuming that the macrocrack is fully saturated and flow is laminar, the velocity distribution within the macrocrack will be the same as those illustrated for microcracks in Figure 6-13. Features of unsaturated flow in cracks and conduits, such as film flow, are discussed later in this section.

As discussed in Section 6.1.1, microcracks form in grout and concrete due to shrinkage and mechanical stress and are likely an intrinsic part of the grout or concrete matrix. As such, the effect of microcracks on water and gas flow through the monolith is generally incorporated into estimates of the bulk permeability of the matrix (e.g., Young, 1988; Boulfiza, et al., 2003; Hearn, et al., 1994), and bulk flow through the monolith is computed using Darcy's Law. Measured permeability and diffusion properties of small, laboratory-prepared specimens, however, may not adequately represent the matrix properties of a large grout monolith, because of differences in the curing history of the small specimens and the large monolith. Viewed in this way, microcracks would not be treated as fast or bypassing pathways. On the other hand, fluids in microcracks would not necessarily be in hydraulic or chemical equilibrium with the mortar or aggregate.

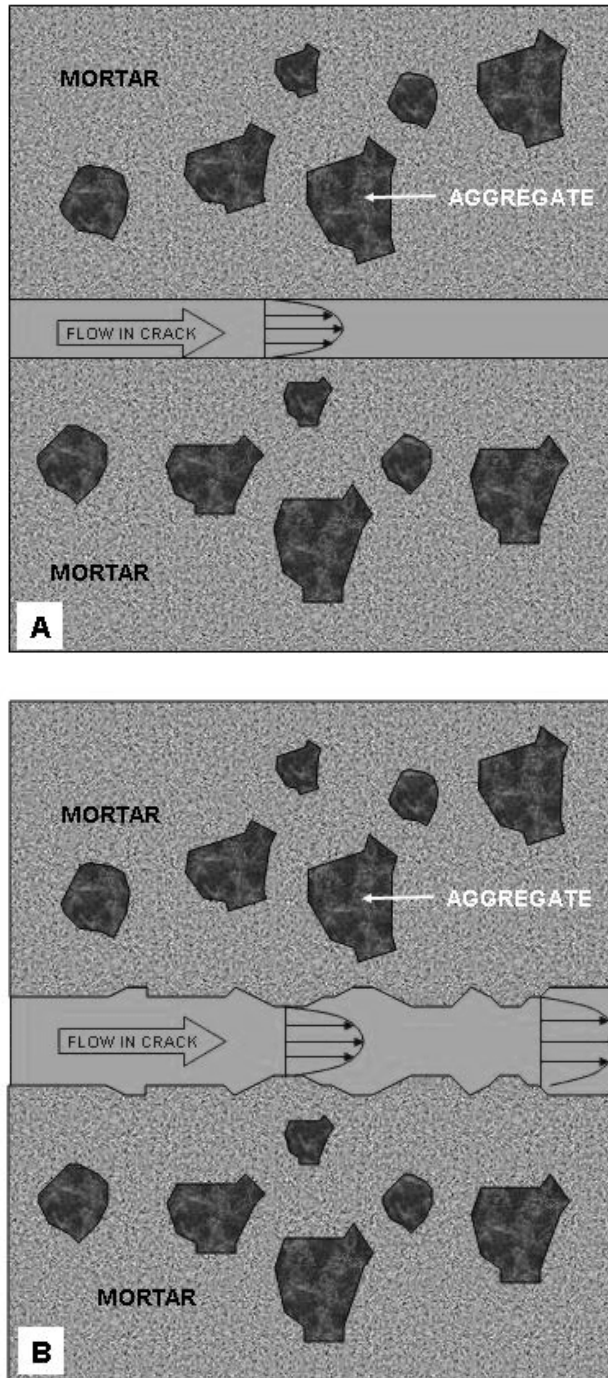


**Figure 6-13. Illustration of Capillary Flow Through a Microcrack in a Porous Matrix: (a) Smooth Crack Walls and (b) Rough Crack Walls**

If the interaction of fluids in the microcracks with the mortar or aggregate is important to radionuclide mobility, then microcracks should be treated as pathways bypassing the mortar and aggregate, and flow through the microcracks would need to be modeled to evaluate engineered barrier performance. In the simplest case, flow through microcracks can be considered as capillary flow between parallel plates, as illustrated in Figure 6-13(a), where the

fluid velocity has a parabolic distribution perpendicular to the crack walls. This simple case assumes that there is no fluid flow between the crack and the matrix, although chemical mass transfer can occur between the crack and the matrix. The effect of this simple type of mass transfer between the crack and matrix has been studied extensively in the chemical engineering literature (e.g., Bird, et al., 1960), and various solutions can estimate the chemical interaction between the fluid in the crack and the matrix. In reality, crack surfaces are rough and the crack walls are not parallel [Figure 6-13(b)]. In this case, the velocity distribution in the crack needs to be computed numerically using the Navier-Stokes equation (e.g., Thompson, 1991) if the microscopic variations in velocity are important for evaluating mass transport. Mass transport in microcracks is discussed in Section 6.3.1.

Fluid flow through saturated macrocracks and microcracks with relatively small apertures usually is described by capillary flow equations in which crack permeability is related to the cube of the fracture aperture (e.g., Bird, et al., 1960). The so-called cubic law relationship is derived from viscous flow equations for closely spaced parallel plates (Couette Flow). In reality, crack surfaces are rough and opposing crack surfaces are not strictly parallel, which complicates the relationship between crack permeability and crack aperture. Nevertheless, research has indicated that permeability can be assigned to a crack that is proportional to the cube of the crack aperture (e.g., Walton and Seitz, 1991; Oron and Berkowitz, 1998) so that flow through the crack can be described by Darcy's Law

$$K_c = \alpha \frac{\rho g}{12\mu} b^3 \quad (6-1)$$

and

$$q_c = -K_c \frac{dH}{ds} \quad (6-2)$$

where

$K_c$	—	saturated hydraulic conductivity of the crack [L/t]
$\alpha$	—	factor that accounts for the crack roughness [dimensionless]
$\rho$	—	fluid density [M/L <sup>3</sup> ]
$g$	—	gravity [L/t <sup>2</sup> ]
$\mu$	—	fluid dynamic viscosity [M/L-t]
$b$	—	crack aperture [L]
$q_c$	—	average fluid velocity in the crack [L/t]
$dH/ds$	—	is the hydraulic gradient along the crack [L/L]

Walton and Seitz (1991) cite values of  $\alpha$  between 0.3 and 0.5.

Using Darcy's Law to describe fluid flow in fully saturated cracks is a common approach when the detailed velocity distribution in the crack is not important to the analysis (e.g., Walton and Seitz, 1991; Boulfiza, et al., 2003; National Council on Radiation Protection and Measurements, 2005). Applying Darcy's Law to flow in cracks that are not fully saturated is more complex, however, because the effective hydraulic conductivity will vary with the degree of saturation, as it does in porous media. Boulfiza, et al. (2003) developed an analytical relationship between crack saturation and relative hydraulic conductivity assuming a lognormal distribution of crack apertures. Their analysis indicated that single macrocracks or widely spaced macrocracks would be more conductive than the concrete matrix until the crack saturation dropped below

about 10 percent. At that point, the matrix would become more conductive. Where this transition occurs in real cement-based materials depends on the specific properties of cracks and matrix. The hydraulic properties of partially saturated cracks also can be described using relationships between saturation, capillary pressure, and relative permeability that have been developed for partially saturated porous media. These relationships will be described in a later discussion of dual continuum models for fractured materials. Ultimately, flow in discrete fractures is difficult to accurately simulate because of uncertainty in the constitutive relationships between fracture water content, wetted surface area, and variations in aperture. Unsaturated flow through cracks also can be episodic and display chaotic behavior (Glass and Yarrington, 2003).

Fluid flow in large aperture cracks also could occur as film flow, as illustrated in Figure 6-9 for a large aperture conduit, or could, theoretically, be nonlaminar and thus cannot be described by Eq. (6-1) or Darcy's Law. Cook, et al. (2005) considered film flow through macrocracks in a performance assessment for the saltstone vaults at the Savannah River Site. Film flow with respect to flow in conduits will be discussed further in Section 6.2.2.

Even though macrocracks may be more conductive than the matrix, in general, the volumetric flow of either water or gas through a cement-based monolith depends on the surface area and water saturation of the macrocracks and matrix. Because macrocracks constitute a very small fraction of the surface area and volume of a cement-based structure [generally less than 1 percent (Walton, et al., 1990)], their contribution to flow through the structure will be less than the permeability ratio between the cracks and the matrix implies. In addition, the water content and saturation of the grout or concrete matrix will generally be higher than those of the macrocracks, except when water is actively being applied to the monolith surface. This is because the macrocracks drain more rapidly than the matrix and the matrix has a much higher water retention capacity than the macrocracks due to its small pore size. As a result, the relative proportions of flow through the macrocracks and the matrix will vary with time, as will fluid exchange between the cracks and the matrix (Boufiza, et al., 2003). These conclusions about flow through macrocracks may not apply to microcracks, because microcracks have much smaller apertures and are more prevalent than macrocracks. Thus, the water saturation of microcracks generally will be higher than that in macrocracks at a given bulk water content of the monolith.

The application of Darcy's Law to flow through cracks can be extended to multiple cracks disseminated throughout the monolith using either discrete fracture or dual-continuum models. Both of these approaches have been used extensively to model fluid flow and mass transport, including those of radionuclides, through naturally fractured rocks (e.g., Andersson and Thunvik, 1986; Huyakorn, et al., 1983).

In discrete fracture models, flow and transport in individual fractures is explicitly represented in the model along with fluid exchange with the matrix, as illustrated in Figure 6-14. Flow in the fractures usually is computed using Darcy's Law, and adjustments are made for partially saturated conditions, if necessary. Examples of discrete fracture models that include matrix interactions are SOLFRAC (Bodin, et al., 2007), TOUGH2 using specially constructed discrete fracture grids (Ito and Seol, 2003), and PORFLOW (Analytical & Computational Research, Inc., 2004). SOLFRAC uses a random walk method to simulate flow and transport through a fracture system. Although TOUGH2 (Pruess, et al., 1999) usually is used to perform dual-continuum simulations of fracture flow and transport, Ito and Seol (2003) developed a special mesh generator (FRACMESH) that generates discrete fracture grids for use with TOUGH2. PORFLOW is a single-continuum flow and transport model based on the finite element method

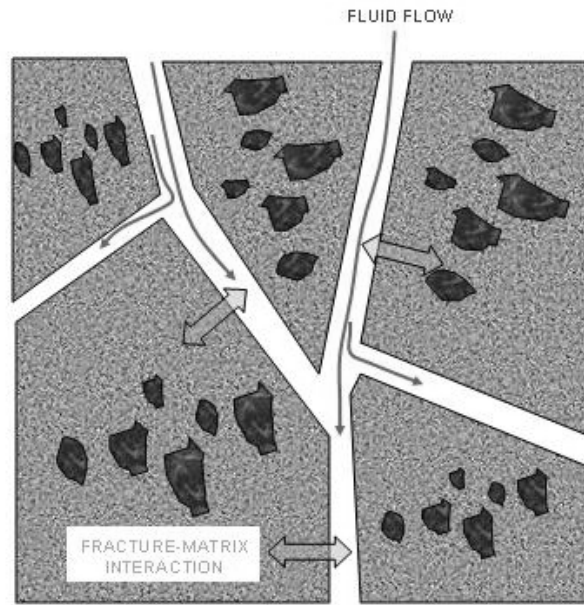


**Figure 6-14. Illustration of Discrete Fracture and Transport Model**

that represents discrete two-dimensional features such as fractures (Analytical & Computational Research, Inc., 2004). Some other finite element codes, such as FEFLOW (Diersch, 2005), include similar provisions to represent discrete features using line and plane elements. Other discrete fracture simulation models, which range from those that simply simulate fluid flow to those that simulate mass transport with matrix interactions, have been reported in the literature. Generally, these have been specialized codes developed for specific research objectives and, thus, are not discussed here.

The concept behind dual continuum models is illustrated in Figure 6-15. In dual-continuum models, individual fractures are not explicitly represented. Rather, the hydraulic and mass

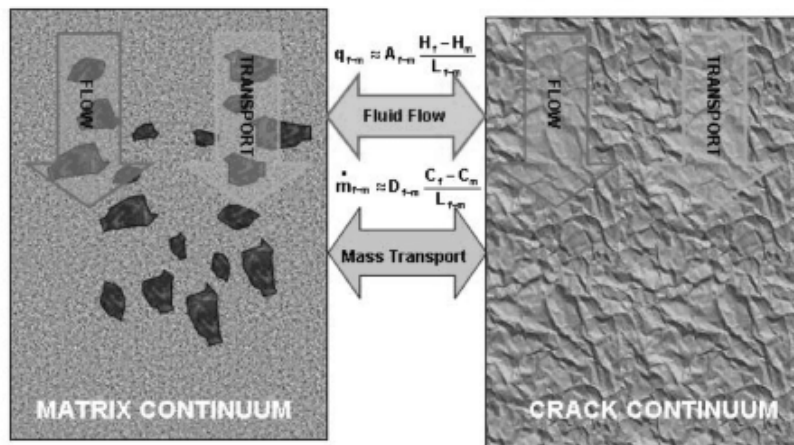


**Figure 6-15. Conceptual Illustration of Flow and Transport Coupling in a Dual Porosity Continuum Model [Symbols Defined in Eqs. (6-3) and (6-16)]**

transport properties of the fracture network are averaged over the volume represented by a model grid node (or cell) so that the fracture network is treated as a continuum. The actual physical properties of the individual fractures can be represented in the fracture continuum by assigning appropriate values of hydraulic conductivity based on Eq. (6-1) and by using statistical representations of the fracture network to deduce equivalent hydraulic conductivities. The effects of partial saturation of the fracture network are accounted for by using constitutive relationships between fracture saturation, fracture capillary pressure, and relative permeability. Exchange of fluid between the fracture continuum and the matrix continuum is computed using a linear transfer function. For example, water flow between the fracture and the matrix is computed by

$$q_{f-m} = A_{f-m}(H_f - H_m) \quad (6-3)$$

where

$q_{f-m}$	—	water flux between the crack and the matrix [L/t]
$A_{f-m}$	—	hydraulic conductance term [1/t]
$H_f$	—	hydraulic head in the crack [L]
$H_m$	—	hydraulic head in the matrix [L]

The hydraulic conductance term usually must be determined by calibration because it can only be estimated from fundamental material properties. Calibration of a grout-filled tank or vault model would be difficult or impossible because it would require monitoring of the response to infiltration events. Additionally, the hydraulic properties of the crack and matrix are likely to change as the cement-based material ages.

TOUGH2 and MULTIFLO (Painter, et al., 2001) are examples of numerical models that have been used extensively to perform dual-continuum simulations of fractured rocks. Either of these models could be used to simulate flow through macrocracks in a partially saturated, cement-based monolith.

The hydraulic properties of a partially saturated fracture continuum are generally described using semiempirical relationships between water saturation, capillary pressure, and hydraulic conductivity or permeability.

One popular approach to describing the partially saturated fracture hydraulic properties is to use relationships van Genuchten (1980) developed, which relate capillary pressure, matrix saturation, and hydraulic conductivity. The relationship between saturation and capillary pressure in the fracture continuum is

$$P_{cf} = \frac{1}{\alpha_p m} [S_{ef}^{1/2} - 1]^{1/m} \quad (6-4)$$

and

$$m = 1 - 1 / \lambda_f \quad (6-5)$$

where

- $P_{cf}$  — capillary pressure in the fracture continuum (taken as positive)  
 $S_{ef}$  — effective saturation of the matrix continuum  
 $\alpha_p$  and  $\lambda_f$  — fitting parameters

The effective saturation is defined as

$$S_{ef} = \frac{S_f - S_{rf}}{1 - S_{rf}} \quad (6-6)$$

where

- $S_f$  — actual fracture continuum saturation  
 $S_{rf}$  — irreducible fracture saturation

The effective permeability ( $k_{ef}$ ) for water flow in the fracture continuum is then

$$k_{ef} = k_{rf} k_f \quad (6-7)$$

where  $k_f$  is the permeability of the fracture continuum and  $k_{rf}$  is the relative permeability, which is assumed to be a function of the matrix saturation. The water relative permeability of the fracture continuum is described using van Genuchten's (1980) model

$$k_{rf} = S_{ef}^{1/2} \left[ 1 - \left( 1 - S_{ef}^{1/\lambda} \right) \right]^2 \quad (6-8)$$

The partially saturated hydraulic properties of the matrix continuum are described by similar relationships.

The hydraulic properties of the fracture continuum also can be described using the active fracture model of Liu, et al. (1998). The active fracture conceptual model was developed to represent phenomena inferred to occur in fractured rock where the number of fractures actually conducting water varies with the saturation of the fracture network. This concept also is applicable to networks of cracks, not all of which are conducting water at any particular time. According to the active fracture model, the capillary pressure/saturation relationship is given by

$$P_{cf} = \frac{1}{\alpha_f} \left[ S_{ef}^{(\gamma-1)/\lambda_f} - 1 \right]^{1/m} \quad (6-9)$$

and the relative permeability/saturation relationship by

$$k_{rf} = S_{ef}^{(1+\gamma)/2} \left[ 1 - \left( 1 - S_{ef}^{(1-\gamma)/\lambda_f} \right)^{\lambda_f} \right]^2 \quad (6-10)$$

where  $\gamma$  is the activity factor that varies from zero to one. The activity factor scales the fraction of fractures conducting water to the effective saturation of the fracture network based on an empirical power law relationship between effective saturation and fraction of active fractures (Liu, et al., 1998). When  $\gamma$  is zero, the model devolves into the conventional fracture model.

Increasing values of  $\gamma$  cause the relative permeability of the fracture continuum to be higher at a given saturation of the fracture network. The constitutive relationship given by Eqs. (6-6) and (6-7) are still based on the van Genuchten (1980) porous media models in which  $k_f$  is the permeability of the fracture continuum and  $k_{rf}$  is the relative permeability, which is assumed to be a function of the fracture saturation. The relative permeability for the fracture–matrix conductance is then

$$k_{rf-m} = S_{ef}^{(1+\gamma)} k_{rf} \quad (6-11)$$

where  $k_{rf-m}$  is the fracture–matrix relative permeability. Eqs. (6-4) to (6-11) also can be applied to flow through discrete macrocracks if it is assumed that the fracture interior behaves more or less like a two-dimensional porous medium. This assumption is likely to be valid for cracks with rough surfaces (e.g., Boulfiza, et al., 2003). It may not be appropriate for cracks with smooth surfaces for which an analytical approach to computing the rate of flow through the crack should be used.

In practice, the parameters required to apply Eqs. (6-3) to (6-11) to simulate flow through cracks using a dual-continuum model need to be determined empirically because they cannot be determined from first principles. Unfortunately, the literature review conducted for this report did not find any studies of crack properties in large grout monoliths that are representative of grout-filled tanks.

The advective flow of gases into and out of partially saturated cracked grout or concrete can be modeled using the same basic principles as those described previously for water flow. For example, the relative gas permeability of the cracks and matrix is related to the relative water permeability at a given water saturation by (Bear, 1972)

$$k_{rg} = 1 - k_{rw} \quad (6-12)$$

where  $k_{rg}$  is the relative gas permeability and  $k_{rw}$  is the relative water permeability, such as computed using Eqs. (6-7) or (6-8). The gas permeability is then

$$k_g = k_{rg} k \quad (6-13)$$

where  $k$  is the intrinsic permeability of the crack or matrix [ $L^2$ ].

Some analytical and numerical models developed for the flow of liquids through discrete fractures or fractured continua can be applied to the flow of gases with an appropriate substitution of fluid properties (density and viscosity). Other models developed specifically for water flow may incorporate assumptions that are not appropriate for simulating the flow of gases. TOUGH2 and MULTIFLO are examples of numerical models specifically developed to handle the flow of both water and gas through dual porosity materials. With respect to the movement of gases through cement-based materials, most research has focused on diffusion. Gas phase diffusive transport through cracks and conduits will be discussed in Section 6.3.

## 6.2.2 Flow Through Conduits

Although fluid flow through conduits is fundamentally the same as flow through cracks, the discrete nature and geometry of many types of conduits could require using different

mathematical models than those used to simulate flow through cracks. Flow in annular-type conduits in which the liquid completely bridges the annular space or flows through an annular space filled with porous material, as in Figure 6-9(b), would be similar to Darcian flow through a discrete crack. However, models derived for flow through planar cracks in a porous matrix would need to be modified to account for radial flow into the matrix to be applied to an annulus around a pipe.

In the case of an annular space of large aperture, liquid flow could occur as isolated drops or as films [Figure 6-9(a)]. Film flow and mass transfer has received considerable attention in the chemical engineering literature because of its importance to various chemical processing technologies. Bird, et al. (1960) provide the following simple expression for the laminar flow of a film on a smooth, inclined surface

$$q = \frac{\rho g \delta^3 \cos \theta}{3\mu} \quad (6-14)$$

where

$q$	—	liquid flux [L/t]
$\rho$	—	liquid density [M/L <sup>3</sup> ]
$g$	—	gravitational acceleration [L/t <sup>2</sup> ]
$\delta$	—	film thickness [L]
$\theta$	—	angle from the vertical
$\mu$	—	fluid viscosity [M/L-t]

Equation (6-14) can be applied to curved annular spaces if the liquid does not completely bridge the space and there is no imbibition into the matrix. Equation (6-14) also applies to macrocracks with large apertures. Or and Tuller (2000) developed an approach for calculating film flow on a rough porous surface and for calculating an equivalent unsaturated hydraulic conductivity as a function of roughness and matric suction of the porous medium. Cook, et al. (2005) used the Or and Tuller (2000) approach to estimate the influence of macrocracks on fluid flow through the saltstone vaults at the Savannah River Site. Kapoor (1994), Tokunaga and Wan (1997), and Tokunaga, et al. (2000) developed models for laminar film flow in fractures and rough surfaces in porous materials that can be used to estimate film flow rates through macrocracks and conduits with large apertures. Their solutions would require some modification for application to flow through annuli around pipes, but would be appropriate for flow through annuli between the metal wall of a tank and the grout matrix where the radius of curvature of the tank is large.

Flow through large aperture cracks and conduits can finger and be episodic or pulsating under unsaturated conditions, causing only a portion of the crack or conduit surface area to wet at any particular time (e.g., Glass and Yarrington, 2003). Although these flow phenomena undoubtedly occur, predicting their significance with respect to flow and transport in grout-filled tanks would be difficult without site-specific data. In practice, and for applications involving long-term scenarios, these processes may be best characterized using empirical approximations, such as the active fracture modeling approach described previously.

These mathematical models apply only to laminar flow of liquids. As noted earlier, conduits, as well as macrocracks, can act as pathways for atmospheric and soil gas to move into a grout monolith and for gas phase radionuclides to move out of the waste form. With respect to

movement of atmospheric gases into concrete, most research has focused on carbon dioxide transport by diffusion and its effect on concrete carbonation (e.g., Odeh, et al., 2006; Meier, et al., 2007; Monlouis-Bonnaire, et al., 2004) and oxygen diffusion and its effect on the corrosion of reinforcing steel (e.g., Kranc and Sagues, 2006). Thunvik and Braesler (1990) modeled advective-diffusive flow of subsurface gases through fractured rock to investigate gas flow and hydrogen transport from submarine geologic radioactive waste repositories. Although no studies specifically related to advective transport of gas through conduits in cement-based materials were identified in the literature, the physics of gas flow through pipes and other open spaces are well understood. The potential for gas and associated contaminants to migrate through conduits in concrete building slabs and foundations is also well known (e.g., New York State Department of Health, 2006). Simple models have been developed for estimating gas and contaminant vapor flow through cracks in building slabs (e.g., Johnson and Ettinger, 1991); these models could estimate gas flow through discrete, planar conduits into a grout monolith or waste form. Similar approaches could be used to estimate gas flow through annular conduits, either from the soil surrounding a tank or vault or from the atmosphere. Although rarely studied, the effects of atmospheric barometric pressure changes on gas flow into and out of the monolith through conduits need to be considered to evaluate the effect of atmospheric and soil gases on the degradation of cement-based materials and the migration of gas phase radionuclides out of the waste form. An approach similar to that of Rossabi and Falta (2002) could be used to estimate barometrically induced gas flow through conduits into a grout monolith.

Whether or not barometrically induced advective gas transport is a significant process for inducing reactive gases, such as oxygen and carbon dioxide, into the waste form or for facilitating release of gaseous contaminants from the waste form depends on a number of factors. First, significant advective gas flow requires that the crack or conduit be well connected not only to the atmosphere, but also to the outside the tank or vault so that a pressure gradient can exist and persist to induce gas flow. Without such a continuous connection, little advective flow will occur. Second, the magnitude of barometrically induced flow depends on the gas permeability of the structures and materials on the outside of the grout. If the materials on the outside of the grout are highly permeable, then changes in atmospheric pressure will propagate rapidly through these materials as well as through any open conduits in the interior of the grout, in which case the pressure gradient between the conduits and the exterior of the grout will be small and little advective flow will result. If the exterior materials have relatively low gas permeability, then larger pressure gradients and more advective flow can result. Finally, the importance of barometrically induced gas flow increases with the thickness of the unsaturated zone beneath the tank or vault. A thicker unsaturated zone allows for more storage of soil gas, a slower response of the soil to barometric pressure changes, and a potential for larger pressure gradients between interior conduits and the exterior of the grout.

### **6.3 Mass Transport Processes Related to Fast and Bypassing Pathways**

Section 6.2 focused on the physics and models of fluid flow (water and gas) through cracks and conduits in the grout monolith and associated concrete structures (e.g., vault walls). This section considers mass transport processes associated with these flows that may affect the release of radionuclides to the environment, including processes affecting the degradation of physical and chemical barriers. The mass transport processes important to evaluating the influence of cracks and conduits on radionuclide releases from in-place closure of waste tanks are

- Transfer of radionuclides between the grout matrix and fluids in the cracks and conduits

- Advective, diffusive, and dispersive transport of radionuclides through the cracks and conduits
- Advective, diffusive, and dispersive transport of environmental reactants through the cracks and conduits
- Sorption of radionuclides within the cracks and conduits
- Decay and ingrowth of radionuclides within the cracks and conduits

### 6.3.1 Mass Transport in Microcracks

As discussed in Section 6.1.1, microcracks are ubiquitous in cement-based structures and their influence on mass transport is often treated as part of the bulk properties of the concrete matrix (e.g., Young, 1988; Boulfiza, et al., 2003; Hearn, et al., 1994). Lumping the effects of microcracks with the bulk properties of the matrix may not be appropriate if the fluids in the microcracks are not in chemical equilibrium with the grout mortar and aggregate. If this is the case, the microcracks can be viewed as bypassing pathways even if they do not behave as fast pathways. Figure 6-16 illustrates such a scenario where the fluid in a microcrack is not in chemical equilibrium with reductants from blast furnace slag added to reduce the mobility of Tc-99. This scenario is similar to that Esh, et al. (2006) considered.

The fluid flow and mass transport processes in a cement-based monolith containing microcracks are similar to those that have been studied in multiporosity geologic materials, such as soil and rock containing macro- and microporosity. Fluid flow and transport in such materials

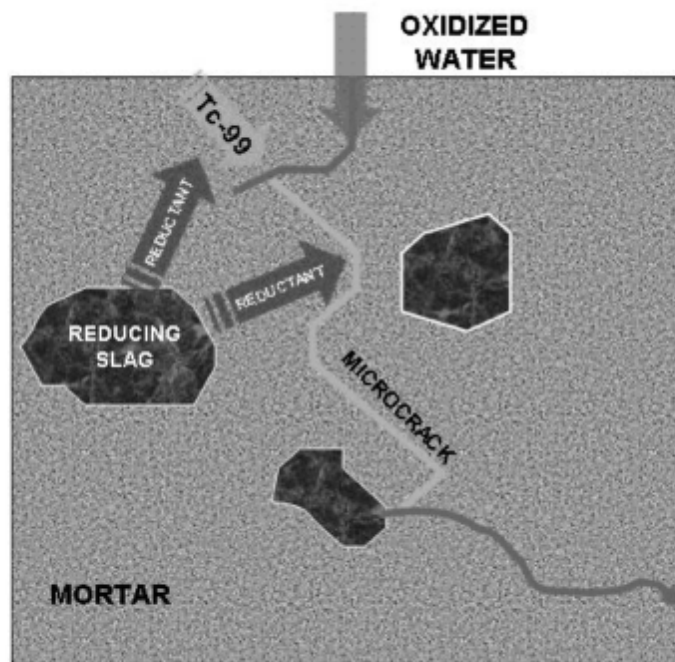


**Figure 6-16. Conceptual Illustration of Chemical Disequilibrium Between Fluid in a Microcrack and a Reducing Aggregate**

can occur in both the macro- and micropores, although advective transport in the macroporous, high permeability material typically dominates. Most analytical and numerical models of dual-porosity media use linear functions to represent fluid flow and mass transfer between a high permeability medium, such as a crack, and a low permeability medium, such as a grout matrix as illustrated in Figure 6-15. For example, water flow at each location is represented by Eq. (6-3) and diffusive mass transfer by equations of the form

$$\dot{m} = D_{f-m}(C_f - C_m) \quad (6-15)$$

where

$\dot{m}$	—	mass flux [M/L <sup>2</sup> -t]
$D_{f-m}$	—	fracture–matrix diffusion conductance term [L/t]
$C_f$	—	concentration in the crack [M/L <sup>3</sup> ]
$C_m$	—	concentration in the matrix [M/L <sup>3</sup> ]

Advective transport between the crack and matrix is represented by

$$\dot{m}_a = q_{f-m} C_{up} \quad (6-16)$$

where

$q_{f-m}$	—	water flux between the crack and matrix [L/t]
$C_{up}$	—	upstream concentration, which can be either in the crack or matrix depending on the direction of flow [M/L <sup>3</sup> ]

Such formulations do not consider pressure or concentration gradients in the matrix; rather, the values in the matrix at a given location are assumed to be uniform or an average within the matrix. This approach may not be appropriate for simulating transient fluid flow over short time periods or, more importantly, for simulating sharp concentration gradients due to sorption or chemical reactions within the matrix.

Transport through dual-porosity materials has been studied extensively, and both analytical and numerical models have been developed for simulating the fluid flow and mass transport processes in such materials on a macroscopic scale (e.g., van Genuchten and Wierenga, 1976; Rasmussen and Neretnieks, 1981; Narasimhan, 1982; Corapcioglu and Wang, 1999; Huang and Hu, 2001). Multiporosity fluid flow and mass transport calculations also are included in numerical models such as HYDRUS (Simunek, et al., 1999), MULTIFLO (Painter, et al., 2001), and the TOUGH2 family of codes (Pruess, et al., 1999). For example, HYDRUS can simulate aqueous advective dispersion of a six-member decay chain with nonlinear sorption through a dual porosity medium in which water is treated as immobile in the matrix.

The TOUGH2 family of codes includes capabilities to simulate advective dispersion with sorption and chemical reaction in multiporosity media. Moridis, et al. (1999) published a module for TOUGH2 that simulates transport with chain decay of an n—1 daughter product sequence. However, TOUGH2 is a complex set of process modules, and not all processes relevant to radionuclide release from cement-based materials can be simulated simultaneously. For example, radioactive chain decay cannot be simulated with multicomponent chemical reactions.

An interesting capability of TOUGH2 is its ability to simulate multiple interacting continua (Pruess, et al., 1999); this concept is illustrated in Figure 6-17. Multiple interacting continua allow the matrix to be represented as multiple overlapping continua in which fluid pressures and concentration gradients can be simulated. This approach could be useful for simulating chemical reaction zones in a cementitious matrix surrounding microcracks or dispersed macrocracks. The multiple interacting continua approach might also be very well suited for simulations involving chemical reactions between the mortar matrix and aggregate within the mortar.

MULTIFLO (Painter, et al., 2001) can simulate simultaneous flow of water and gas with chemical reactions in dual-porosity media and could be used to simulate flow and transport through a grout monolith with microcracks or dispersed macrocracks. MULTIFLO cannot, however, simulate radioactive chain decay or multiple interacting continua grid structures. Painter, et al. (2006) recently developed a fluid particle-based methodology for simulating radionuclide transport through discrete fracture networks in porous media. Their methodology, termed Particle on Random Streamline Segment (PORSS), includes the effects of matrix diffusion and chain decay. PORSS is potentially applicable for simulating radionuclide transport through networks of micro- and macrocracks, as well as through conduits.

### 6.3.2 Mass Transport in Macrocracks

Mass transport through a cement-based monolith containing macrocracks can be modeled using either the dual-porosity approach or a discrete fracture pathway approach. Determining which approach is most appropriate depends on how widely the macrocracks are dispersed through the monolith and the purpose of the calculation. The dual-porosity approach would be

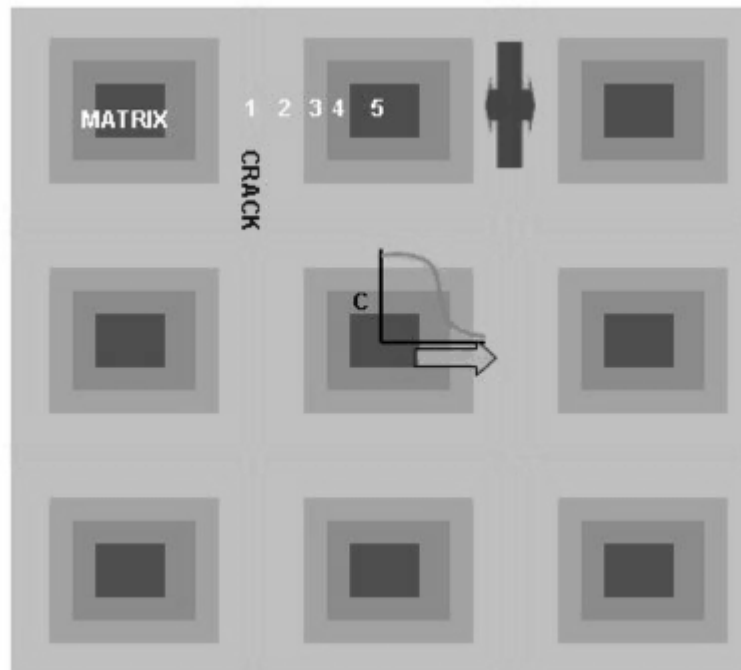


**Figure 6-17. Conceptual Illustration of the Multiple Interacting Continua (MINC) Modeling Approach**

appropriate if the macrocracks are relatively closely spaced and well connected and steep concentration gradients are not expected in the matrix. Discrete fracture models would be better suited to simulate flow through widely spaced cracks and transport with steep concentration gradients in the matrix. Because the dual-porosity models discussed in Section 6.3.1 for microcracks are equally applicable to macrocracks, the dual-porosity approach will not be discussed further.

Nearly all of the fluid flow and mass transport processes associated with the influence of macrocracks on radionuclide release and migration from in-place tank closure have been investigated in the context of matrix diffusion in porous geologic materials containing discrete fractures (e.g., Grisak and Pickens, 1980; Sudicky and Frind, 1982; Zhang and Woodbury, 2000; Sun and Buscheck, 2003; Neretnieks, 2006; Houseworth, 2006). Walton and Seitz (1991) and Walton (1992) applied some of these concepts to evaluating the performance of cracked concrete barriers for radioactive waste isolation. Mainguy, et al. (2001) applied similar matrix diffusion concepts to analyze concrete degradation due to leaching of calcium by water flowing through macrocracks. Roden and Scheibe (2005) used a one-dimensional modeling approach applicable to a discrete crack to study reductive immobilization of uranium(VI) in fractured soil.

Except for the work of Mainguy, et al. (2001) and Roden and Scheibe (2005), matrix diffusion mass transport studies have focused on attenuating contaminant concentrations, particularly radionuclides, due to diffusion from the fracture into the rock or soil matrix. Some of these models consider decay of only a single constituent (e.g., Grisak and Pickens, 1980), while others consider chain decay (e.g., Sun and Buscheck, 2003; Neretnieks, 2006). Although the analytical models developed from such studies are applicable to the transport of radionuclides through microcracks in initially uncontaminated grout or concrete, they do not directly represent leaching of radionuclides from grout or concrete. Some of the simpler analytical models can be applied to contaminated grout or concrete leaching with a relatively simple change in variables. For example, for a single constituent that is linear in terms of the concentration in the fluid flowing into the fracture,  $C_o$ , and the initial concentration in the matrix,  $C_1$ , an analytical solution applies to either the case where the fluid entering the fracture is contaminated,  $C_o > 0$ , and the matrix is uncontaminated,  $C_1 = 0$ , or vice versa. The more complex models, such as those that include chain decay (e.g., Sun and Buscheck, 2003; Neretnieks, 2006), may not be easily adapted to the leaching problem, although the mathematical methods on which these models are based can be applied to leaching.

### **6.3.3 Mass Transport in Conduits**

Mass transport in conduits involves the same fundamental processes as mass transport through macrocracks. Analytical and numerical models developed for flow and transport through discrete cracks also can be used to model flow and transport through planar conduits and, to a good approximation, flow and transport through annular spaces with large radii of curvature, such as along tank walls. However, models derived for mass transport through planar cracks in a porous matrix would need to be modified to account for radial flow into the matrix to be applied to an annulus around a pipe. The difference in transport geometry between a planar crack and an annulus around a pipe is illustrated in Figure 6-18.

Numerical models developed for fractured, dual-porosity media (e.g., TOUGH2 and MULTIFLO) can be used also to simulate transport processes between conduits and the matrix if the fluid flow in the conduit can be assumed to be laminar or steady. If flow through cracks in the matrix surrounding a conduit is not important, single-continuum flow and transport models also can be

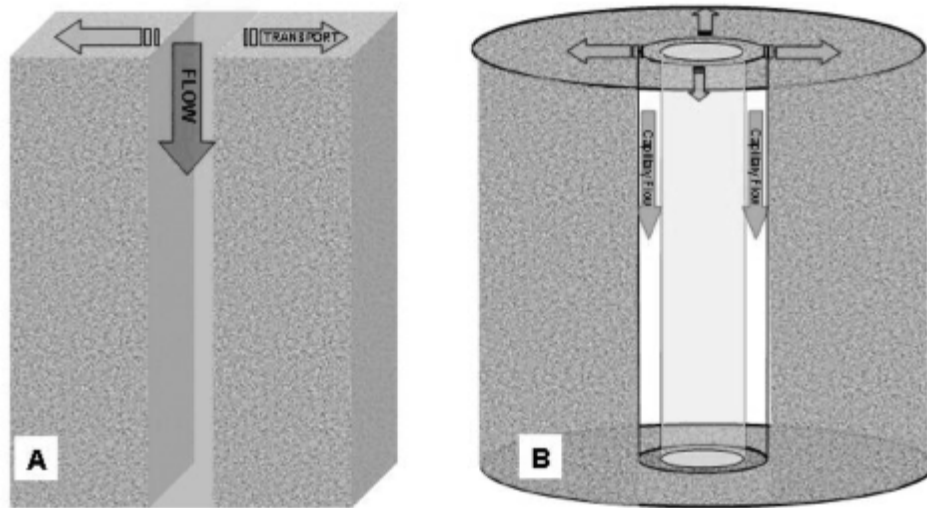


**Figure 6-18. Illustration of Difference in Flow and Transport Geometry Between a Fracture and a Small Conduit: (a) Linear Flow and Transport From a Fracture and (b) Radial Flow and Transport Away From a Cylindrical Conduit**

used to simulate conduits. For example, Kaplan, et al. (2005) used PORFLOW (Analytical & Computational Research, Inc., 2004) to simulate water flow and oxygen transport through large aperture, symmetric cracks in a tank grout monolith and oxygen transport from the cracks to the grout. Because PORFLOW assumes a single, porous continuum, the cracks were treated as discrete elements and were assumed to be filled with a porous material so that Darcy's Law applied, even though the cracks were assumed to have apertures ranging from 1.5 to 3 cm [0.6 to 1.2 in].

### 6.3.4 Representation of Microcrack/Mortar Interactions

An overarching question has been raised with respect to representation of the cementitious matrix containing microcracks and reactive mortar and aggregate in mathematical models: to what extent can the matrix be treated as a single continuum? In other words, can the influence of microcracks on flow and transport be lumped with the hydraulic and mass transport properties of the mortar? As discussed in previous sections, experimental measurements of the hydraulic and mass transport properties of cement-based materials are likely to represent the bulk matrix, including the microcracks and mortar. Whether water or gas bulk fluid flow, treating the matrix as a single continuum is likely to yield reasonably accurate estimates of total flow and the details of flow in the microcracks and mortar will be of little importance.

This may not be the case for mass transport, however, in which the extent of interaction between solutes in the microcracks and in the mortar could determine solute mobility. The extent of mass transfer between microcracks and mortar is likely to be controlled by molecular diffusion in the mortar due to the low permeability of the mortar.<sup>5</sup> First-order estimates of the

<sup>5</sup>In addition to diffusion due to chemical concentration gradients, described by Fick's Law, nonadvective mass transport also can be driven by temperature gradients (Soret Effect) and electrical potential gradients (electrophoresis), as described by the Onsager reciprocity relationships (e.g., Haase, 1969; Martys, 1995).

importance of diffusion-limited mass transfer between microcracks and mortar can be made by comparing the rate of diffusive mass transfer in the mortar to the rate of advective mass transfer through the crack. To make this comparison, consider two limiting cases: Case 1, the time for a stagnant or slow-moving fluid in the crack to chemically equilibrate with the mortar and vice versa, and Case 2, the time for the mortar to equilibrate with a fast moving fluid in the crack.

### Case 1: Slow Flow in a Crack

Diffusion in the limiting case of a stagnant fluid in a crack can be described in terms of the rate of mass accumulation in a well-mixed reservoir of finite volume in contact with a porous medium through which diffusion occurs. If the volume of the reservoir is small in comparison to the volume of the porous medium (as would be the case for a microcrack in mortar), the rate of mass accumulation or depletion in the crack is given by Eq. (6-17) (Crank, 1975, p. 58) and illustrated in Figure 6-19

$$M_R = \frac{M_t}{M_\infty} = (1 + \beta) \left\{ 1 - \frac{\beta}{\pi^{1/2} T^{1/2}} + \frac{\beta^3}{2\pi^{1/2} T^{3/2}} - \frac{3\beta^5}{4\pi^{1/2} T^{5/2}} \dots \right\} \quad (6-17)$$

where

- $M_R$  — relative mass in the crack at time  $t$  [ $M$ ]
- $M_t$  — mass in the crack at time  $t$  [ $M$ ]
- $M_\infty$  — mass in the crack at infinite time [ $M$ ]

and

$$\beta = \frac{a}{RW} \quad (6-18)$$

$$T = \frac{\phi D_e t}{RL_c^2} \quad (6-19)$$

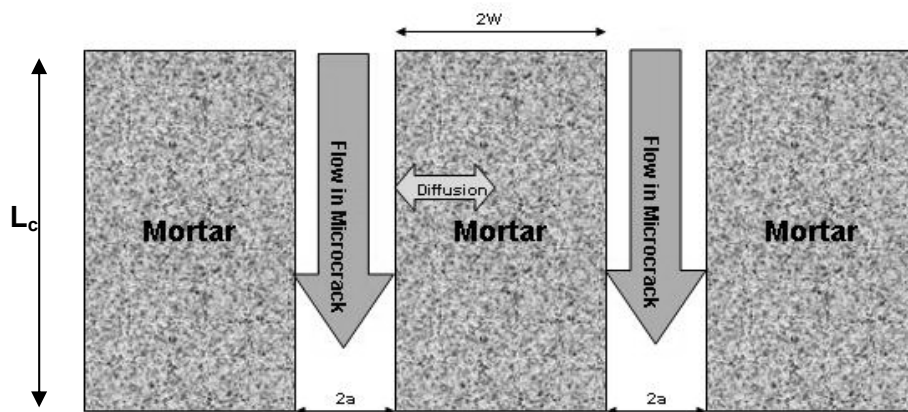


**Figure 6-19. Conceptual Model of Advective Flow Through Microcracks With Diffusion in Mortar**

where

- $a$  — half-aperture of the crack [L]
- $R$  — retardation factor in the mortar
- $W$  — crack half-spacing in the mortar [L]
- $\phi$  — porosity of the mortar
- $D_e$  — effective diffusion coefficient in the mortar [ $L^2/t$ ]
- $L_c$  — characteristic length of the crack [L]

For small  $\beta$ , only the first term in the summation of the right-hand side of Eq. (6-17) is significant and Eq. (6-17) can be solved for time to give

$$t_e = \frac{RW^2}{\pi D_e} \left\{ \frac{\beta(1+\beta)}{M_R - (1+\beta)} \right\}^2 \quad (6-20)$$

where

- $t_e$  — time to reach a relative mass of  $M_R$

To approximate the extent of equilibration between the fluid in the crack and in the mortar, consider the case where  $M_R = 0.9$  (i.e., the crack is 90 percent equilibrated with the mortar).

This time is given by Eq. (6-20) and can be compared to the advective travel time through the crack. For a water-filled crack under gravity flow, the advective travel time can be approximated by

$$t_t = L_c / K_c \quad (6-21)$$

where

- $K_c$  — characteristic crack hydraulic conductivity [L/t]

The characteristic crack hydraulic conductivity can be estimated using Eq. (6-1) with  $\alpha = 1$ . If  $t_e/t_t$  is less than one, the flow in the crack is fast with respect to the equilibration time and it may not be acceptable to treat the crack and mortar as a single continuum for mass transport calculations.

Figure 6-20 shows values of  $t_e/t_t$  as a function of crack aperture and retardation factor assuming  $D_e = 10^{-8}$  cm<sup>2</sup>/s [ $1.6 \times 10^{-9}$  in<sup>2</sup>/s],  $\phi = 0.3$ , and  $L_c = 1$  cm [0.4 in]. The figure indicates that for cracks with aperture greater than 20  $\mu$ m [ $3.9 \times 10^{-5}$  in] and retardation factors

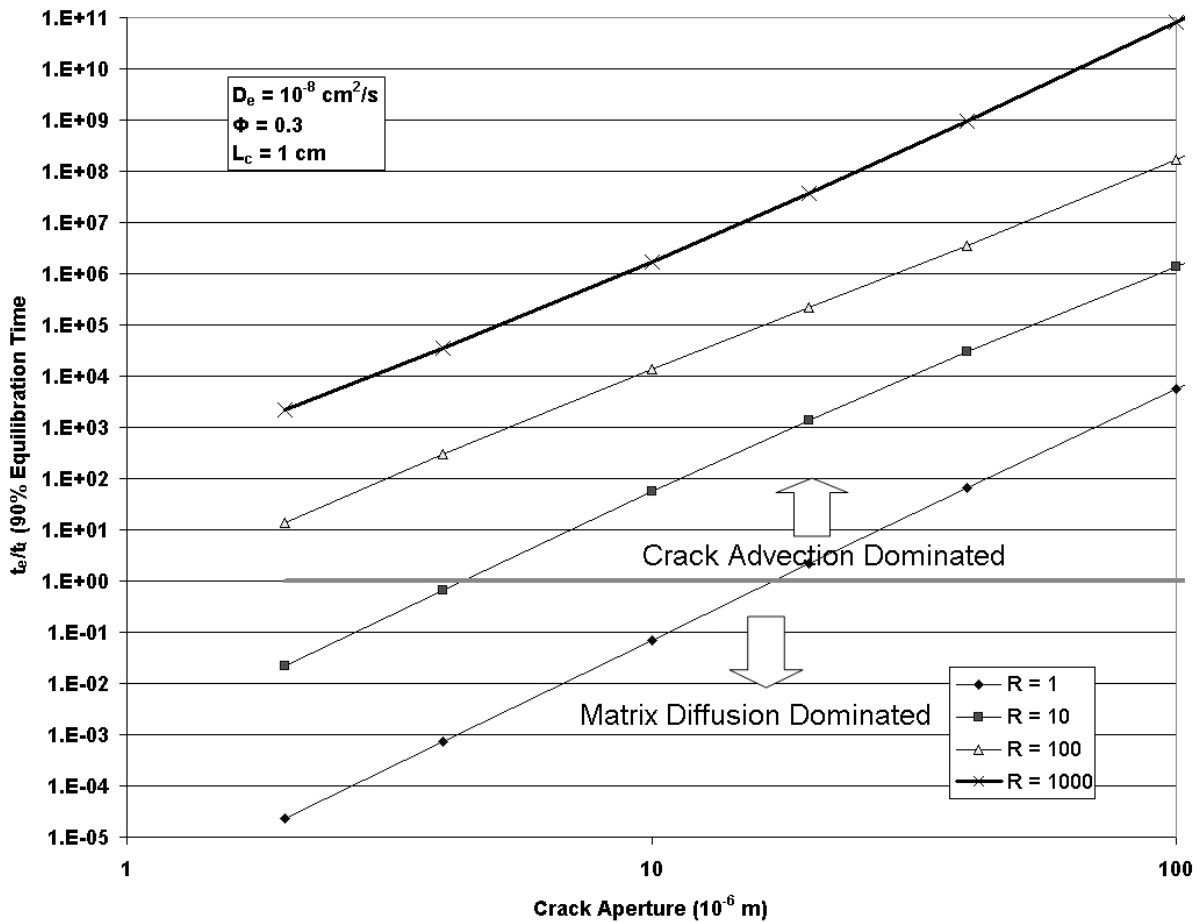


**Figure 6-20. Ratio of Time for Mass in a Crack to Exchange 90 Percent of Mass With Mortar by Diffusion to Advective Travel Time Through a Crack Assuming an Effective Diffusion Coefficient ( $D_e$ ) of  $1 \times 10^{-8}$  cm<sup>2</sup>/s [ $1.6 \times 10^{-9}$  in<sup>2</sup>/s], Mortar Porosity of 0.3, and Crack Length of 1 cm [0.4 in]**

greater than 1, advective flow in the crack is much faster than the equilibration time such that the fluid in the crack is unlikely to be equilibrated with the mortar on the scale of 1 cm [0.4 in].

### Case 2: Fast Flow in a Crack

The case of a rapidly moving fluid in a crack represents the other mass transport endmember. In this case, the fluid in the crack is assumed to be replenished rapidly with respect to the rate of diffusion into or out of the mortar so that the crack concentration remains nearly constant. Thus, the extent of interaction between the crack and the mortar can be characterized by the “penetration depth” of a solute into the mortar after a given residence time in the crack. The penetration depth is defined as the distance into the mortar that, assuming a concentration equal to that in the crack, would contain the same mass that had diffused into the mortar after

time  $t_t$  (Bird, 1960; Neretnieks, 1980). The concept of the penetration depth is illustrated in Figure 6-21. The penetration depth is given by

$$\bar{d} = \frac{2}{\pi^{1/2}} \left( \frac{\phi D_e t}{R} \right)^{1/2} \cong 1.13 \left( \frac{\phi D_e t}{R} \right)^{1/2} \quad (6-22)$$

To characterize the penetration depth as a function of crack aperture, the time,  $t$ , in Eq. (6-22) can be taken as the 1-cm [0.4-in] travel time,  $t_t$ , from Eq. (6-21). The resulting penetration depth is plotted versus crack aperture in Figure 6-22. The penetration depth decreases with increasing crack aperture (faster flow) and with increasing retardation in the mortar. When the penetration depth is less than 10 percent of the crack spacing, equilibration between the crack and mortar fluids is limited. As the microcrack spacing decreases, equilibration between the fluid in the crack and the mortar becomes more complete. Neville (1996) characterized microcracks as cracks with apertures less than 0.1 mm [ $4 \times 10^{-3}$  in] and presented data indicating microcrack lengths were less than 1 cm [0.4 in]. Because microcracks are not simple, linear features and have a complex connectivity, the calculations presented here may underestimate the travel time in the cracks and the extent of crack/mortar interaction.

#### 6.4 Summary and Recommendations

As discussed in Section 6.1, microcracks, macrocracks, and conduits can act as

- Pathways for relatively rapid movement of environmental fluids (water, atmospheric gases, and soil gases) into the waste form and surrounding cement-based materials (grout and concrete structures)
- Fast pathways for radionuclide transport from these materials to the environment
- Bypassing pathways that either divert environmental fluids away from the waste form or create a condition of chemical disequilibrium with the waste form

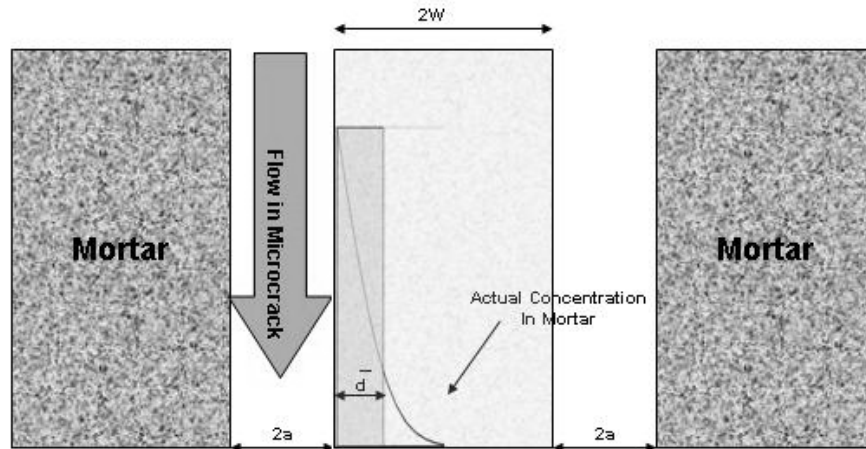


**Figure 6-21. Illustration of Concept of Penetration Depth in Mortar With Fast-Moving Fluid in Crack**

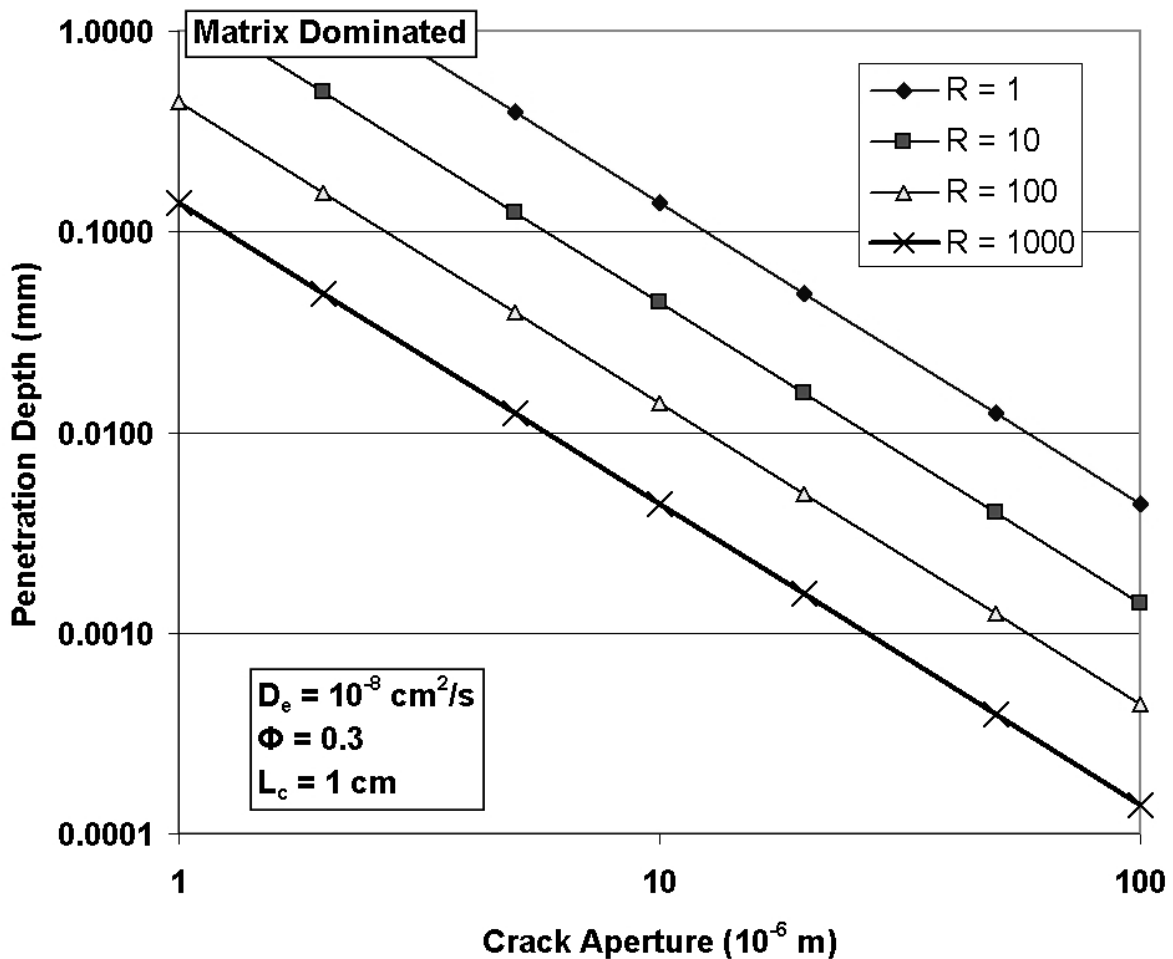


Figure 6-22. Diffusion Penetration Depth as a Function of Crack Aperture Based on Advective Travel Time Through a 1-cm [0.4-in]-Long Crack Assuming an Effective Diffusion Coefficient ( $D_e$ ) of  $1 \times 10^{-8}$   $\text{cm}^2/\text{s}$  [ $1.6 \times 10^{-9}$   $\text{in}^2/\text{s}$ ] and a Mortar Porosity ( $\phi$ ) of 0.3

Although the effect of these features on radionuclide releases to the environment will be site specific, some general observations about their potential effects can be made from basic principles of mass transport in fractured and porous media and on studies of cement-based materials in general.

Because microcracks form primarily during the curing process of a cement-based monolith, they can be expected to be present in the grout used to fill a former waste tank or annular spaces around a tank. Most engineering studies of concrete materials, including studies of intrusion of water and chemicals that can degrade the concrete, have included the effect of microcracks in matrix properties. These studies have shown that the matrix permeability is very low {saturated hydraulic conductivity less than  $1 \times 10^{-10}$   $\text{m/s}$  [ $3 \times 10^{-10}$   $\text{ft/s}$ ] in intact concrete structures. Thus, microcracks are not likely to act as fast pathways for bulk fluid flow through or from a grout or concrete matrix. Care should be taken in applying the results of these studies to large grout monoliths because most of these studies used small specimens specially prepared in the laboratory. The matrix structure of those specimens may be different than that in a large grout monolith due to differences in curing temperature and stress history. Microcracks could,

however, contain fluids and radionuclides that are not in chemical equilibrium with the mortar or aggregate. Chemical reactions occurring in the matrix are important for immobilization of radionuclides, such as in the maintenance of reducing conditions to limit the mobility of Tc-99. The extent to which such chemical equilibrium can be achieved depends on the residence time in the microcracks and can be estimated using existing analytical and numerical models for diffusive and reactive transport through fractured, porous media.

Macrocracks that develop in a cement-based monolith after it hardens are the features most likely to act as fast pathways between the waste form and the environment, although they also could act as bypassing pathways that limit the contact of environmental fluids with the waste form and other engineered barriers. Fluid flow and mass transport through macrocracks in cement-based structures are closely analogous to flow and transport through fractured geologic materials. Many of the same modeling methods used to simulate contaminant transport through fractured geologic media can and have been used to simulate the effects of environmental chemicals (chloride and carbon dioxide) on the degradation of concrete structures. With the exception of relatively simple discrete fracture diffusion models (e.g., Walton, 1992), these modeling approaches have not been applied to study radionuclide releases from in-place tank closures or the effect of environmental fluids on long-term grout integrity. In addition, fluids conveying radionuclides in macrocracks may not be in chemical equilibrium with the chemical environment of the matrix and aggregate, and this disequilibrium may affect radionuclide mobility in the macrocrack.

Fluid flow and mass transport through a grout monolith or concrete structure containing macrocracks can be modeled using either dual-porosity or discrete fracture models. The application of these modeling approaches to a specific in-place tank closure depends on the purpose of the study and the nature of the macrocracks. For example, many processes affecting radionuclide releases from a grout monolith with many well-connected macrocracks per unit volume might be adequately modeled using analytical or numerical dual porosity models. In the absence of a well-connected crack network, discrete fracture models would be necessary. Despite extensive research over the past 30 years on mass transport through fractured, porous geologic media, no single model or modeling approach could simulate all processes of interest in evaluating potential radionuclide releases from a fractured grout monolith. Existing models or slightly modified models could simulate many of the important processes relevant to the effect of microcracks on radionuclide release from in-place tank closures. The results of these process-level models could then be abstracted and integrated into a system-level modeling platform such as GoldSim (Goldsim Technology Group, LLC, 2004) (e.g., Esh, et al., 2006).

Conduits were distinguished from cracks as a separate type of pathway because they represent discrete fluid pathways that may be present or may develop along specific engineered features with known locations, such as annular spaces between grout and a corroded pipe or rebar. Fluid flow and mass transport through conduits is fundamentally similar to those through discrete macrocracks, and many of the same modeling approaches would be applicable to conduit flow and transport. The flow geometry around small conduits, such as annular spaces around pipes, is different than that for cracks, which are roughly planar features, and this difference in geometry needs to be considered in model selection.

Although models and modeling approaches exist for simulating most of the flow and transport processes associated with fast and bypassing pathways, these models are of limited value without estimates of the nature, extent, and properties of the pathways. Information on cracks in concrete structures is available in the literature. However, most studies have focused on

reinforced concrete structures of interest in civil engineering projects. These studies may be of limited value in estimating the nature, extent, and properties of cracks in a grout monolith inside a former process tank. Even less information may be available to estimate the properties of conduits. With respect to cracks in the monolith, mechanical models could be used to estimate the extent of cracking for performance assessment (e.g., DeBorst, et al., 2004), and chemical weathering models (e.g., Boddy, et al., 1999; Mainguy, et al., 2001; Yoon, et al., 2000; Boulfiza, et al., 2003) could extrapolate how these cracks might evolve and affect the integrity of the grout.

## 7 EVALUATION OF RADIONUCLIDE RELEASE MECHANISMS FOR CEMENT-BASED WASTE FORMS

### 7.1 Introduction

The other sections of this report discuss the processes leading to degradation of, and water availability to, cement-based materials used in the two disposal concepts the U.S. Department of Energy (DOE) proposed to address tank cleanup activities under the Ronald W. Reagan National Defense Authorization Act for Fiscal Year 2005: grouted tanks and cement-based monoliths. This section summarizes and evaluates models and data available for estimating how radionuclides will be released from these cement-based waste forms over the long time scales relevant to performance assessments supporting the DOE waste determinations. This section does not promote the use of particular model approaches or specific codes; rather, this section is intended to provide staff with background information on radionuclide release models and relevant data that will help staff evaluate DOE performance assessments. This section should not be interpreted as endorsing any particular model approach or data source for DOE use, nor does this section constitute a consultative review of any specific DOE model, performance assessment, or waste determination.

Groundwater-pathway, dose-based performance assessment models depend on water-facilitated radionuclide release from the waste form. Release is a complex process that is dependent on the hydrologic, structural, and chemical environment of the waste form. For example, the rate of water flow through the waste form will affect the release, but the specific nature of flow (e.g., fracture versus matrix) also has a direct influence. The presence of fast flow pathways due to structural features such as pipes and through-going cracks may enhance release. The chemical environment can affect not only waste form degradation, but also radionuclide mobility. Release models need to consider these factors and use appropriate data in quantifying predictions. Uncertainties in data and models may be addressed by adopting conservative approaches—that is, generally, approaches that will tend to overpredict the rates of radionuclide releases from the waste form.

This section will, as appropriate, emphasize those radioelements suggested to be potentially important in previous DOE performance assessments supporting waste determinations (DOE-Idaho, 2003; Cook, et al., 2005), including technetium, selenium, iodine, strontium, uranium, neptunium, and plutonium. Data from other elements (e.g., cesium) will be discussed when they shed light on release mechanisms and contribute to model development and quantification.

The two relevant disposal concepts present contrasting conditions for release. For tank closure at Idaho National Laboratory and the Savannah River Site F-Area Tank Farm, DOE is washing the tank to remove residues and then filling the tank with grout. The grout immediately above the remaining tank-bottom residue will be designed to provide a chemically reducing environment; its major constituents will be sand, fly ash, blast furnace slag, and ordinary Portland cement. Saltstone, in contrast, is produced at Savannah River Site by mixing waste salt solutions with a dry mix of fly ash, slag, and Portland cement and pumping the grout mix into cement vaults for disposal. Radionuclides will therefore be distributed throughout the grout waste form. In both cases, relatively small masses of admixtures such as superplasticizers and set retarders may be added during grout preparation (Section 8.2.8).

This section will not evaluate the potential role of colloids in facilitating radionuclide release in cement-based systems. There is a lack of relevant literature and site-specific data on this process, preventing quantification of its effects. Colloidal effects may be negligible if highly alkaline conditions are maintained in cement-based systems (Wieland, et al., 2004).

## **7.2 Radionuclide Release Models For Cementitious Systems**

Because cement-based material has been viewed as a favorable waste form for many years, extensive literature exists on contaminant release models. In addition, DOE has developed release models as part of performance assessments supporting waste determinations at Idaho National Laboratory (grouted tanks) and the Savannah River Site (grouted tanks and saltstone). This section describes the conceptual approaches to these models and the chemical and physical settings in which they are applied, emphasizing the Idaho National Laboratory and Savannah River Site disposal systems.

### **7.2.1 Key Chemical and Physical Characteristics of the System**

#### **7.2.1.1 Brief Descriptions of Grouted Tank and Saltstone Systems**

In grouted tanks at Idaho National Laboratory and the Savannah River Site, radionuclides will be associated with a thin layer of presumably insoluble residue at the bottom interior of steel tanks after cleaning (e.g., DOE–Idaho, 2006a). A reducing grout containing slag will be poured over the residue, followed by a structural grout that provides structural integrity and intruder barrier characteristics for the closed tank. DOE–Idaho performance assessment models assumed that residual waste was mixed with the bottom 15 cm [6 in] of grout (DOE–Idaho, 2003), with a sensitivity analysis evaluating the effect of no mixing between the grout and waste. How well that mixing will be accomplished is uncertain (NRC, 2006; see also Kauschinger, et al., 1998). The mineralogical and aqueous disposition of any radionuclides remaining in the residue after cleaning and the extent of mixing of residue with grout have not been well established from site-specific studies at either site. Gilbertson (2006) concluded that the results of a large-scale grout mock-up at Idaho National Engineering and Environmental Laboratory (1999) indicated vertical mixing of waste residuals with reducing grout poured in five successive placements engineered to mobilize remaining waste residuals to pumps for additional waste removal.

In either tank closure case, the reducing grout influences the chemistry of water flowing through the tanks to the contaminated zone. Evolution of the chemical environment for radionuclide release, therefore, is dependent on the degradation history of the grout. As discussed in Appendix B, the tank residue itself is unlikely to strongly affect water chemistry. Chemical control by reducing grout can be compromised not only by general grout degradation, but also by the existence of fast pathways such as cracks and interfaces with in-tank components such as pipes. These pathways, which may also eventually include the tank bottom, provide potential access to the contaminated zone by waters that are not thoroughly conditioned by reducing grout (e.g., they may contain oxygen). Other sections of this report discuss degradation mechanisms and models, as well as the potential for and consequences of crack formation in the tank grouts.

For saltstone disposal, the chemical environment is also dependent on grout performance and would be affected by crack formation. In this case, however, the cement-based material is also the waste form. Radionuclide behavior at the source is therefore better understood than in grouted tanks in light of the extensive literature on cement-based waste forms. For example, it is

it is not clear that a release model based on cement-based material  $K_d$  values (see Section 7.2.2.3) is applicable if tank residue has not mixed with reducing grout (NRC, 2006), but such a model deserves consideration in the case of saltstone. In addition, in grouted tanks the contaminant source is concentrated at a potential fast pathway (the tank bottom), whereas in saltstone the contaminants are homogeneously dispersed throughout the monolith.

For both grouted tanks and saltstone, therefore, the chemical environment for radionuclide release is tied directly to the evolution of cement-based material pore waters as the material degrades (with the possible exception of preferential bypassing pathways through the tank system). As the cumulative volume of water contacting the material increases with time, the pH buffering and redox poisoning capacity of the reducing grout will be weakened and water chemistry will increasingly reflect the oxidizing character of infiltrating unsaturated zone waters. This evolution can be broadly characterized as resulting in a lowering of pH and a raising of Eh. Again, this process may be accelerated at the margins of the tanks or saltstone monolith, or along cracks.

### **7.2.1.2 Literature Information on Chemical Conditions**

A number of studies in the literature have provided conceptual or quantitative models of this water chemistry evolution. An oft-cited representation of this evolution by Bradbury and Sarott (1995), based in part on experimental work by Atkinson, et al. (1988), can be summarized as follows:

- Region I—Initially high pH at 12.5 to 13.5, controlled by sodium and potassium hydroxides
- Region II—Portlandite [ $\text{Ca}(\text{OH})_2$ ] control of pH at 12.5 after removal of Na and K
- Region III—Steady decrease of pH after exhaustion of portlandite and domination of the solid phase by calcium–silicate–hydrate (C-S-H) gels; pH will evolve toward the ambient groundwater value

In the presence of carbon dioxide, cement carbonation is an important process, driving the water to lower pH as C-S-H is exhausted; calcite will buffer pH at less than 9 (Section 8). Ultimately, the pH buffering capacity of the grout or waste form will be exhausted and percolating groundwaters will be little changed by their interactions with the disposal system. The Bradbury and Sarott (1995) model did not specify the oxidation-reduction character of the water, which is dependent on site-specific characteristics. As discussed in Appendix B for Idaho National Laboratory and Savannah River Site settings, however, Eh is expected to gradually increase toward more oxidizing values as pH decreases.

This pH evolution has been corroborated by laboratory studies of cement compounds as they are leached in various waters (e.g., Ochs, et al., 2006, 2002; Sugiyama and Fujita, 2006, 1999; Harris, et al., 2002). Other critical features of this aqueous evolution are a decrease in dissolved calcium concentration and in the aqueous Ca/Si ratio. These studies have typically stressed the behavior of ordinary Portland cement to the exclusion of slag and fly ash, which are important constituents of Idaho National Laboratory and Savannah River Site grouts. There is no evidence, however, that the broad outlines of chemical evolution described here will differ for blends rich in slag and fly ash. For example, in hydrothermal alteration experiments, Sugiyama and Fujita (1999) reported that alteration assemblages for 9:1 slag-to-cement blends differed from pure cement assemblages mainly in the absence of portlandite, which will be eventually

exhausted in either case, leading to pH control by C-S-H phases. Studies on blast furnace slag alone show that it will contribute to C-S-H formation at pH above 11.5 (Song and Jennings, 1999), such that C-S-H will control subsequent chemical evolution. Therefore, blends of cement and slag will have similar long-term effects on chemical conditions as cements alone. An exception to this similarity is the role of slag in maintaining reducing conditions but, as discussed in Section 8, the long-term Eh poisoning capacity of slag-containing blends is uncertain. With regard to pH evolution, both fly ash and slag will most significantly affect grout by likely shortening the period of high pH buffering. This effect comes about through both dilution of portlandite and reaction between portlandite and the other components (Section 8.2.1).

Berner (1992a,b); Sugiyama and Fujita (2006, 1999); and Matschei, et al. (2007), among others, have reported quantitative thermodynamic modeling of pore water evolution, with comparison to and validation by laboratory studies. Directly coupled modeling of radionuclide behavior during the degradation process is less common; modeling of individual element behavior over a range of conditions defined by degradation models is more common (e.g., Berner, 1992b).

Less is known about the chemical effects of common cement admixtures (see Section 8.2.8). Studies on radionuclide behavior in the presence of these typically organic substances do not emphasize overall effects on chemistry; these data will therefore be addressed in Section 7.3. Glaus and van Loon (2004) point out that lack of thermodynamic data prevents quantitative prediction of solubility and sorption effects of most admixtures.

The chemical evolution of cement pore waters has implications for the physical environment for radionuclide release. Grout and saltstone porosity and permeability affect diffusivity and advective water flow rates. While dissolution of C-S-H phases can increase porosity (Haga, et al., 2005; Yokozeki, et al., 2004), calcite precipitation due to carbonation could close pores and cracks (Pfingsten, 2002; Andersson and Nilsson, 2000). Carbonation effects on crack formation and apertures are even less certain (e.g., Andersson and Nilsson, 2000; Langton, 2007). Other sections of this report have more information on the physical state of degrading cement-based materials.

### **7.2.1.3 Chemical Evolution as Represented in Grouted Tank and Saltstone Performance Assessments**

Performance assessments for Idaho National Laboratory tanks and Savannah River Site saltstone have not directly implemented the previously described changing chemical environment for radionuclide release. For tank closure at Idaho National Laboratory, DOE–Idaho (2003) used a surface rinsing model that, for release from the grouted tank bottom, employed radionuclide  $K_d$  values from Region II in Bradbury and Sarott (1995). This region corresponds to the period when portlandite controls pH to around 12.5. Region III conditions, during which pH decreases as C-S-H solids degrade, were not modeled on the basis that these conditions would not be attained during the performance period of 1,000 years evaluated in DOE performance assessments. (Lower  $K_d$  values were, however, evaluated in sensitivity analyses.) The model for release of most radionuclides from saltstone likewise used Region II  $K_d$  values (Cook, et al., 2005; Rosenberger, et al., 2005).

A conceptual model developed for a potential performance assessment for tank closure at the Savannah River Site F-Area Tank Farm, however, explicitly links the waste form chemical environment to the degradation state and hydraulic characteristics of the reducing grout overlying the contaminated zone (Denham, 2007). In contrast to the earlier performance

assessments, in this approach, conditions are primarily defined based on redox conditions rather than pH. As shown in Figure 7-1, four conditions are assumed in the model:

- Condition 1: Initial condition with the steel tank liner intact, such that no radionuclides are released.
  - Condition 2: The liner has failed and water flows along preferential pathways (e.g., through-going cracks), such that the accessible grout-reducing capacity is quickly exhausted.
  - Condition 3: General advective flow through the intact grout, or through grout fractured enough so that it may be modeled as a continuum.
  - Condition 4: The same as Condition 3, except that the reducing capacity has been exhausted.
- Condition 2 may be skipped, depending on grout conditions after steel liner failure.

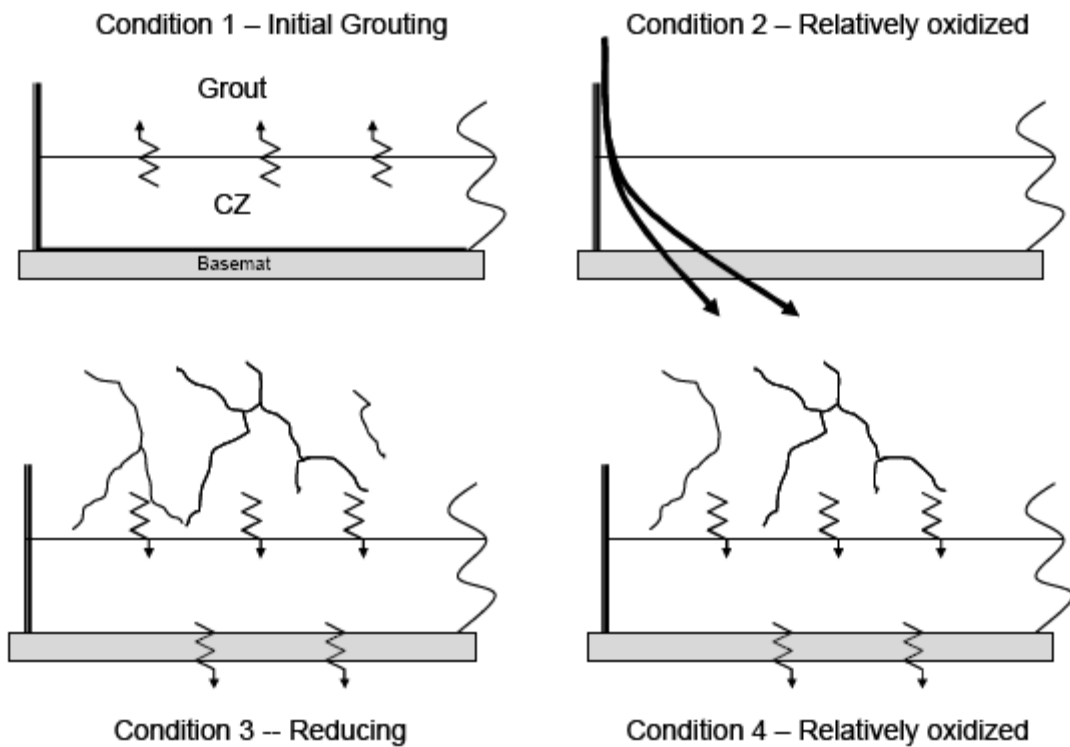


**Figure 7-1. Four Modeled Conditions for Radionuclide Release From Grouted Tanks in the Closure Concept for F-Area Tank Farm at Savannah River Site (From Denham, 2007, Figure 1). “CZ” Refers to the Contaminated Zone Containing the Tank Residue; the Upward Arrows in the Condition 1 Diagram Indicate Migration of Residual Liquid Into the Reducing Grout. The Vertical Double Lines Represent the Tank Wall.**

In the Denham (2007) model, two sets of chemical characteristics are defined for each condition, corresponding to Regions II and III of Bradbury and Sarott (1995). Denham (2007) presented a thermodynamic model of reducing grout chemical evolution during infiltrate flushing that used pyrrhotite (FeS) oxidation to simulate the longevity of the grout-reducing capacity and used C-S-H phase reactions to calculate the pH associated with the hydrated grout solid assemblage.

## **7.2.2 Overview of Conceptual Models**

Models for aqueous radionuclide release from cement-based waste forms typically focus on diffusion. This approach is often based on the assertion that chemical degradation of these materials is too slow for waste form dissolution to cause release (e.g., Riley and Lo Presti, 2001). The validity of this approach is related to the applicable timeframe; as the system degrades, advection may become more important. Another process often invoked is solid–liquid partitioning using the  $K_d$  coefficient. The processes of diffusion, advection, and partitioning can be combined in hydrologic transport models based on advection–dispersion relations. Furthermore, aqueous concentrations can be limited by solid phase solubilities (Appendix B). We discuss here how these processes have been incorporated into models for radionuclide release in cement-based systems. These models are most directly applicable to the saltstone case, in which radionuclides are encased in the cement-based material. Applicability to grouted tanks depends on the degree of mixing of tank residues and grout and will also be discussed (DOE–Idaho, 2003; Denham, 2007).

### **7.2.2.1 Waste Form Dissolution With Congruent Release**

A review of the literature shows a large number of models for dissolution of cement-based materials (Section 5 of this report; Berner, 1992b; Harris, et al., 2002; DOE–Idaho, 2003; Sugiyama, et al., 2007; Matschei, et al., 2007), but none have been found that explicitly and mechanistically couple radionuclide release mechanisms with material degradation. If these studies addressed radionuclide release, then chemical and mineralogical outputs of the degradation model were used as inputs to separate release models. Examples of this approach are discussed in the following sections in the context of the modeled release mechanism.

#### **7.2.2.2 Diffusion**

Diffusion tends to dominate aqueous radionuclide release from relatively unmodified cement-based waste forms because the material's low hydraulic conductivity makes advective release ineffectively slow. Diffusive transport depends on the chemical characteristics of the contaminant and water, the physical characteristics of the medium, and the nature of concentration gradients necessary for driving diffusion (NRC, 2005). Development and application of diffusion release models have, therefore, been common for cement-based systems (e.g., Furhmann, et al., 1990; Pescatore, 1991; Andersson and Nilsson, 2000; Riley and Lo Presti, 2001; Kosson, et al., 2002). The relevant physical characteristics that can affect diffusion are tortuosity, porosity, permeability, and mineralogy. The effects of degradation on diffusion depend on how these characteristics, especially permeability, evolve (Section 7.2.1.2).

Researchers recognize, however, that diffusion alone is only applicable to elements that are transported conservatively without sorption or solubility limit in a given setting (e.g., Serne, et al., 1992). In addition, a simple diffusion model does not account for advection if the water flow velocity becomes nonnegligible. Therefore, diffusion is most commonly applied in combination with sorption or a solubility limit, or in combined advection–diffusion models (Section 7.2.2.5).

(Section 7.2.2.5). Another potential mechanism that is not addressed by a diffusion model is early radionuclide release from a waste liquid phase that was not bound in the grout waste form.

### **7.2.2.3 Surface Rinse**

In a “surface rinse” (DOE–Idaho, 2006a, 2003) or “reverse  $K_d$ ” or “desorption  $K_d$ ” release model (Jones and Serne, 1995), the aqueous concentration of a contaminant is calculated from the solid concentration using a distribution coefficient, or  $K_d$ . This model assumes that the radionuclide is reversibly available to the solution and is not explicitly dependent on waste form dissolution. (Here, this model is distinguished from the incorporation of sorption into advection–diffusion or diffusion models.) For the Idaho National Laboratory grouted tank performance assessment, surface rinsing was applied using the DUST-MS code (DOE–Idaho, 2003). This approach was adopted because the performance assessment assumed that (i) release would not occur until the grout had degraded and (ii) at that point, the hydraulic conductivity of the grout was high enough that advection effectively transported radionuclides through the grout. As the radionuclide is transported through the contaminated grout zone at the bottom of the tank, equilibrium  $K_d$  partitioning is maintained in the model.

### **7.2.2.4 Solubility Control**

The limitation of a dissolved radionuclide concentration during release at the waste form by the solubility of a solid phase (Appendix B) is mostly applied in combination with other processes. From an equilibrium thermodynamic perspective, the use of a well-chosen solubility value as an upper limit to aqueous concentration is justifiable. There are examples, however, of using solubility to define the aqueous concentration of a given radionuclide on release from the source. Berner (1992b) calculated uranium solubility for a set of conditions defined from the outputs of a degradation model for a cement-based waste form. Similarly, Criscenti, et al. (1996) calculated cement degradation using a coupled reaction/transport code and used the time-dependent outputs to calculate uranium solubility-limited concentrations. Solubility limits have been used in two cases for modeling release from tank residues. Kienzler, et al. (2000) interpreted uranium release data from full-scale, cement-based waste forms in terms of uranium pure-phase solubility. Deutsch, et al. (2006), after concluding that mechanistic models for radionuclide release from tank sludges could not be well constrained, applied an empirical “solubility” model using laboratory sludge leachate concentrations. In this model, the measured dissolved radionuclide concentrations are used to define the model dissolved concentrations. Denham (2007) presents a conceptual model for release from a thin tank-bottom residue that uses calculated solubility limits for defining the source aqueous concentration. (The varying chemical conditions for these calculations were discussed in Section 7.2.1.3.)

### **7.2.2.5 Combined Models**

In recognizing the complex interplay of mechanisms, modelers often apply radionuclide release models that combine processes such as diffusion, sorption, advection, and solubility. In interpreting laboratory leach data (Section 7.3.1), workers note that measured diffusion coefficients can indicate the possible influence of sorption or some other solid retention mechanism. Mathematical expressions for different definitions of the diffusion coefficient are discussed in Appendix A. Here, will adopt the nomenclature of Appendix A, such that the term “effective diffusion coefficient” applies to the measured intrinsic parameter that includes combined effects such as tortuosity and sorption. The “effective diffusion coefficient” is the property most commonly reported from leach studies of cement-based waste forms. Based on studies such as Atkinson, et al. (1986), a contaminant with a high sorption coefficient will

apparently diffuse more slowly than a nonsorbing contaminant, but in a predictable way given knowledge of its sorption properties. The authors showed that, to a reasonable approximation, the same construction works if the contaminant concentration is limited by solubility rather than sorption. Nonsorbing or non-solubility-limited constituents should diffuse identically in a given medium.

Kim, et al. (1995) describe a similar approach to combining diffusion with a pore water concentration limited by sorption or solubility. [Note that the term “effective diffusion coefficient” is not consistently applied in the literature. In contrast to the Atkinson, et al. (1986) usage described earlier, Phifer, et al. (2006) identify the coefficient that includes sorption effects as the “apparent diffusion coefficient.”] Fuhrmann, et al. (1990) illustrated the subtle differences in leach curves that result from the interaction of diffusion and partitioning versus diffusion alone. A more empirical approach to modeling release has been developed (Cote, et al., 1987; Plecas and Dimovic, 2005a) that combines the effects of sorption, diffusion, and long-term, kinetically controlled release from waste form degradation. This approach has not been widely used.

Combined advection–diffusion models, including sorption, are applied with codes such as PORFLOW (e.g., saltstone performance assessment, Cook and Fowler, 1992; see also Walton, 1994). An advection–diffusion model directly ties transport to water flow conditions, and it is not necessary to exclude one process or the other. As Cook, et al. (2005, p. A–46) stated, with regard to saltstone release modeling

“When the facility is intact, the predominant contaminant release mechanism is diffusion. As time goes on, the closure cap, the drain layer and the Saltstone flow properties degrade to cause more water percolating through the closure cap and Saltstone monolith. Convective transport becomes increasingly important as indicated by the increasing water velocity through the Saltstone.”

In this saltstone model, the sorption  $K_d$  is used to set the pore water radionuclide concentration at the source and to model retardation during advective transport. As discussed in NRC (2005), the main uncertainty in using this advection–diffusion model approach is in accounting for material property changes (e.g., diffusion coefficient, hydraulic conductivity, sorption coefficients) over time as the medium degrades.

### **7.3 Review of Relevant Literature Data**

There is extensive literature on laboratory and field data relevant to modeling radionuclide release from cement-based materials. We do not intend to provide a detailed analysis of all data, but rather an overview of what is available, emphasizing site-specific data for the Idaho National Laboratory and Savannah River Site grouted tank facilities and saltstone.

#### **7.3.1 Leaching Data**

The common approach to studying radionuclide association with and release from cement-based waste forms has been the leach test. (Here, we emphasize tests on radionuclides, rather than on cement material major components that reveal information on degradation.) Leach tests, such as ANSI/ANS–16.1 (American Nuclear Society, 2003), are most commonly applied to determine an effective diffusion coefficient; this parameter will be the focus of this section. As discussed in Section 7.2.2.5, the term “effective diffusion coefficient” is used here to refer to measured data and may include sorption effects.

Approaches to measuring diffusion coefficients are discussed in Appendix A. The ANSI/ANS-16.1 (American Nuclear Society, 2003) leach test is a useful example of the type of test commonly applied to radioactive waste forms of various types. A small cylinder of waste is held in distilled water, and at specified time intervals, the leachate is removed for analysis and completely replaced. An effective diffusion coefficient may be interpreted from the leachate data assuming that the radionuclide is freely available to the solution and sorption has not taken place; nevertheless, the effective diffusion coefficient so derived may reflect the influence of sorption. Data analysis assumes a semi-infinite plane diffusion model; in the test, geometric effects on constituent release to the surrounding solution can be neglected if less than 20 percent of the radionuclide has been removed. Comparisons by Mattigod, et al. (2001) showed that the ANSI/ANS-16.1 (American Nuclear Society, 2003) “dynamic” leach test yielded higher (i.e., more conservative) effective diffusion coefficients than a “static” test in which leachate was not completely replaced. This is because, in the dynamic test, leachant is periodically replaced such that a higher concentration gradient from the solution surrounding the sample is maintained. In static leach tests, leachant is not replaced and the concentration gradient between the sample and solution continuously diminishes. Dynamic tests may more realistically simulate the case of infiltrating water reacting with a waste form.

#### **7.3.1.1 Site-Specific Data**

Site-specific data for Idaho National Laboratory and Savannah River Site tank grouts and saltstone are most relevant. However, leaching or diffusion coefficient data have only been reported for saltstone (see Table A3-6 for effective diffusion coefficients). Phifer, et al. (2006) summarized available data on saltstone and recommended a value for an effective diffusion coefficient for nonsorbing species of  $5 \times 10^{-9} \text{ cm}^2/\text{s}$  [ $8 \times 10^{-10} \text{ in}^2/\text{s}$ ], in line with earlier recommendations for the saltstone performance assessment (Cook and Fowler, 1992; Cook, et al., 2005, 2002). Oblath (1984) reported leached fractions of nitrate, technetium, cesium, and strontium from an early saltstone formulation that did not contain slag, using a leach test generally similar to ANSI/ANS-16.1 (American Nuclear Society, 2003). Technetium leached as efficiently as nitrate, suggesting that it was not sorbed or retained in the medium. Cesium and strontium did not leach as completely as technetium. Barnes, et al. (1985) reported effective diffusion coefficients of  $9 \times 10^{-11}$  to  $2 \times 10^{-9} \text{ cm}^2/\text{s}$  [ $1 \times 10^{-11}$  to  $3 \times 10^{-10} \text{ in}^2/\text{s}$ ] on nonradioactive components of an early saltstone formulation, observing higher diffusivity with higher water/cement ratio (Table A3-6). The studies did show an appreciable fraction released early that did not have diffusion characteristics; Barnes, et al. (1984) interpreted this more rapid early release as resulting from surface washoff. Cesium through-diffusion tests by Kumar, et al. (1985) yielded an effective diffusion coefficient of  $2 \times 10^{-9} \text{ cm}^2/\text{s}$  [ $3 \times 10^{-10} \text{ in}^2/\text{s}$ ] for the then-current reference formulation; the tests revealed a strong dependence on water/cement ratio.

Langton (1986) used a modified ANSI/ANS-16.1 (American Nuclear Society, 2003) method to measure approximately  $5 \times 10^{-9} \text{ cm}^2/\text{s}$  [ $8 \times 10^{-10} \text{ in}^2/\text{s}$ ] on nitrate in slag-containing saltstone; this formed the basis for the adopted performance assessment value (Cook and Fowler, 1992). The maximum effective diffusion coefficient measured for technetium,  $6 \times 10^{-10} \text{ cm}^2/\text{s}$  [ $2 \times 10^{-9} \text{ in}^2/\text{s}$ ], is an order of magnitude lower than the nitrate value, demonstrating that the added slag had reduced technetium to the less mobile Tc(IV) oxidation state. The strontium data did not fit diffusion models well. Langton, et al. (1988) obtained a somewhat higher value of  $1 \times 10^{-8} \text{ cm}^2/\text{s}$  [ $2 \times 10^{-9} \text{ in}^2/\text{s}$ ] for nitrate in saltstone without slag using a similar method. Oblath (1989) reported the  $5 \times 10^{-9} \text{ cm}^2/\text{s}$  [ $8 \times 10^{-10} \text{ in}^2/\text{s}$ ] value from the saltstone immersion tests, but also showed that, in unsaturated conditions, the effective diffusion coefficient did not drop appreciably

drop appreciably until the saturation level dropped below 8 percent. Oblath (1989) therefore concluded that diffusion coefficients measured under saturated conditions were applicable to partially saturated conditions. More recently, Harbour and Aloy (2007), using the ANSI/ANS-16.1 (American Nuclear Society, 2003) protocol, measured an effective diffusion coefficient of  $5 \times 10^{-9} \text{ cm}^2/\text{s}$  [ $8 \times 10^{-10} \text{ in}^2/\text{s}$ ] for selenium in slag-containing saltstone when air was not excluded from the sample. A lower, but highly uncertain, value of  $5 \times 10^{-12} \text{ cm}^2/\text{s}$  [ $8 \times 10^{-13} \text{ in}^2/\text{s}$ ] was obtained for technetium, demonstrating the reducing action of the slag. Crushed sample leach tests confirmed this strong technetium retention; in the absence of slag, however, nearly all technetium was released to solution.

The range of nitrate effective diffusion coefficients for saltstone Langton (1986), Langton, et al. (1988), and Oblath (1989) reported was a relatively narrow  $5 \times 10^{-9} \text{ cm}^2/\text{s}$  to  $1 \times 10^{-8} \text{ cm}^2/\text{s}$  [ $8 \times 10^{-10}$  to  $2 \times 10^{-9} \text{ in}^2/\text{s}$ ] (Table A3-6). Kumar, et al. (1985), in contrast, measured a large range of values for cesium in saltstone by varying the water/cement ratio (Table A3-6). At the lowest water/cement ratio (0.41) the effective diffusion coefficient was  $2 \times 10^{-9} \text{ cm}^2/\text{s}$  [ $3 \times 10^{-10} \text{ in}^2/\text{s}$ ], while at the highest water/cement ratio (1.8), it was  $4 \times 10^{-7} \text{ cm}^2/\text{s}$  [ $6 \times 10^{-8} \text{ in}^2/\text{s}$ ]. Barnes, et al. (1985) reported a similar contrast in nitrate diffusion coefficients, with a value of  $4 \times 10^{-10} \text{ cm}^2/\text{s}$  [ $6 \times 10^{-11} \text{ in}^2/\text{s}$ ] at a water/cement ratio of 0.45 and  $2 \times 10^{-9} \text{ cm}^2/\text{s}$  [ $3 \times 10^{-10} \text{ in}^2/\text{s}$ ] at a water/cement ratio of 2.8 (Table A3-6). Barnes, et al. (1985) attributed the difference to "a higher porosity and greater fraction of large pores" in the higher water/cement ratio formulation. This effect of increasing effective diffusion coefficients with higher water/cement ratios may need to be considered if higher water/cement ratios are observed or occur in microenvironments (e.g., due to addition of flush water during grouting operations).

As noted earlier in this section, DOE has concluded that, taken together, these studies corroborate the use of an effective diffusion coefficient for nonsorbing species of  $5 \times 10^{-9} \text{ cm}^2/\text{s}$  [ $8 \times 10^{-10} \text{ in}^2/\text{s}$ ] for the saltstone formulation (Cook and Fowler, 1992; Cook, et al., 2005, 2002; Phifer, et al., 2006). The diffusion data also demonstrate the relative immobility of redox-sensitive technetium in fresh slag-containing saltstone; this capability will, however, be affected on long time scales by saltstone degradation. The diffusion behavior of emplaced saltstone may be variably affected by factors such as the presence of cracks, process variability, and effects of additives.

There are no site-specific leach data for reducing grouts proposed for Savannah River Site tank closure. Phifer and Dixon (2007) recommended an effective diffusion coefficient of  $8 \times 10^{-7} \text{ cm}^2/\text{s}$  [ $1.2 \times 10^{-7} \text{ in}^2/\text{s}$ ] for Savannah River Site tank farm reducing fill grout, based on the analysis of Phifer, et al. (2006). In the absence of site-specific data, this value was from the high (i.e., conservative) end of the range for low-quality concretes in Phifer, et al. (2006).

Because degraded grout was assumed and a surface rinse release model was adopted, no value for diffusion coefficient was recommended for the Idaho National Laboratory grouted tank performance assessment (DOE-Idaho, 2003).

Site-specific hydraulic conductivity data are also relevant to release models and are discussed in Appendix A.

### 7.3.1.2 Literature Data

Radionuclide-relevant leach tests on cement-based waste forms examined in the literature include Bernard, et al. (1982); Atkinson, et al. (1986); Gilliam, et al. (1990); Seveque, et al. (1992); Kim, et al. (1995); Harris, et al. (1997); Brodda (1988); Jakob, et al. (1999); Biddle, et al. (2000); Kienzler, et al. (2000); Tognazzi, et al. (2000); El-Kamash, et al. (2006, 2002); Plecas (2003); Plecas and Dimovic (2005b); and Chambers, et al. (2006). Studies from the DOE complex that are not specific to Idaho National Laboratory and Savannah River Site tank grouts and saltstone include Kauschinger, et al. (1998); Walter, et al. (1988); Serne, et al. (1996, 1992); Jones and Serne (1995); Last, et al. (1995); McConnell, et al. (1997); Mattigod, et al. (2001); and Spence and Mattus (2004). Notable results from these leach studies are highlighted. When effective or intrinsic diffusion coefficients were reported in these studies, none exceeded the reducing grout value of  $8 \times 10^{-7} \text{ cm}^2/\text{s}$  [ $1.2 \times 10^{-7} \text{ in}^2/\text{s}$ ] adopted for the Savannah River Site tanks (Phifer and Dixon, 2007), confirming that it appears to be a conservative value. Selected effective diffusion coefficient literature data most relevant to saltstone and tank grouts are included in Tables A3–6 and A3–7.

Certain studies at Oak Ridge National Laboratory (e.g., Kauschinger, et al., 1998; Spence and Mattus, 2004) looked at leaching from thorough mixtures of grout and radioactive sludges (such as might occur at the bottom of tanks). Radionuclide leaching was not markedly enhanced over rates from purely cement-based materials in any case. While these data may provide some insight into Idaho National Laboratory and Savannah River Site grouted tank processes, grout and tank residue have not been shown to mix thoroughly.

Results from ANSI/ANS–16.1 (American Nuclear Society, 2003) and similar tests commonly showed the effects of sorption or other retention mechanisms. For example, cesium and strontium sorption were evident in the Kim, et al. (1995) study and actinide release was slowed by apparent sorption in the Serne, et al. (1992) test. In many cases, sorption coefficients can be estimated from diffusion coefficient measurements. Another common phenomenon in these tests was an initial rapid leaching period, followed by more steady-state, diffusive behavior (Barnes, et al., 1985; El-Kamash, et al., 2006; Lewis, et al., 1981; Sugiyama, et al., 2007; Mattigod, et al., 2001). This phenomenon has also been seen in full-scale leach tests (Bernard, et al., 1982).

There is ample evidence corroborating the saltstone results demonstrating the technetium-immobilizing capability of slag-containing grouts (e.g., Brodda, 1988; Gilliam, et al., 1990), at least at the time scales of laboratory experiments.

In performance assessments, the effect of grout or saltstone degradation on radionuclide release is uncertain. While we found no studies of radionuclide leaching from strongly degraded cement-based materials, a number of workers have reported the formation of carbonates on samples during testing. This mineralization has accompanied a reduction in effective diffusion coefficients, presumably through a reduction in porosity and permeability (Seveque, et al., 1992; Harris, et al., 1997; Guerrero and Gofii, 2002). Serne, et al. (1992) saw visible evidence for carbonation but did not observe any effect on diffusion behavior. On the other hand, studies and models of cement degradation in the absence of  $\text{CO}_2$  (i.e., with carbonates unable to form) show porosity increases that would lead to more rapid diffusion (Haga, et al., 2005; Yokozeki, et al., 2004; Yokozeki, 2007).

The potentially beneficial effects on radionuclide release of carbonation (e.g., Smith and Walton, 1991; Langton, 2007) are difficult to quantify confidently in performance assessments,

particularly in light of the potentially detrimental role of cracks. Aside from the potential fast pathways from through-going meso-cracks in tank grouts or saltstone (Section 6), smaller cracks may affect material diffusivity. Tognazzi, et al. (2000) conducted through-diffusion experiments using tritiated water on cracked mortar discs. The cracks resulted in an increase in effective diffusion coefficient by up to a factor of two.

Hydraulic conductivity data are also relevant to release models; applicable literature data are discussed in Appendix A.

### **7.3.2 Solubility Data**

Solubility limit data for relevant radionuclides are discussed in depth in Appendix B. As mentioned in Section 7.2.2.4, the latest conceptual model for release from Savannah River Site grouted tanks assumes solubility-controlled release from the tank residue, with the overlying reducing grout controlling chemical conditions (Denham, 2007). Some leach test data are discussed in Appendix B (e.g., Deutsch, et al., 2006) because they are more applicable to considerations of solubility release models.

### **7.3.3 Other Data on Radionuclide/Waste Form Partitioning**

In contrast to leaching studies, partitioning experiments look at the uptake of radionuclides onto cement-based materials, whether in a static system or as the material forms or alters. Binding mechanisms that may influence uptake include (i) precipitation, (ii) solid solution or coprecipitation, (iii) surface complexation, and (iv) ion exchange (e.g., Wieland and van Loon, 2003). The precise uptake mechanism is often not known (e.g., Harfouche, et al., 2006). Sorption experiments reflect processes that associate dissolved radionuclides with host surfaces and, therefore, do not necessarily provide information on release of radionuclides originally bound to a host matrix. Experiments that observe both adsorption and desorption provide additional information on how the radionuclide/host association may respond to changing geochemical conditions. This section does not provide an exhaustive catalog of relevant partitioning data for cement-based systems (such as Bradbury and Sarott, 1995, or Wieland and van Loon, 2003), but does provide a sense of the variety of data and their implications for model approaches.

#### **7.3.3.1 Site-Specific Partitioning Data**

Radionuclide-cement partitioning data directly applicable to Idaho National Laboratory and Savannah River Site grouted tanks and Savannah River Site saltstone are sparse. For saltstone radionuclide  $K_d$  values in the PORFLOW release model in the saltstone performance assessment (Rosenberger, et al., 2005), DOE used the Region II reducing values from the Bradbury and Sarott (1995) literature review (see Section 7.2.1.3). As discussed in NRC (2005), DOE sensitivity analyses demonstrated the importance to predicted dose of the use of a technetium  $K_d$  based on reducing conditions (Westinghouse Savannah River Company, 2005). Model assumptions regarding the persistence of reducing conditions in saltstone and grouted tanks are critical to dose predictions (Section 8). Given the geochemical conditions, however, the selection of appropriate  $K_d$  values is also important, because they would reflect the sorptive properties particular to conditions in the waste form (reducing effects and surface characteristics).

Until recently, no site-specific sorption data existed for tank grouts proposed for closure at the Savannah River Site F-Area Tank Farm. Kaplan and Coates (2007) have recently revised the set of recommended grout radionuclide  $K_d$  values for performance assessment, partially based on new laboratory measurements on the actual proposed formulation. These parameters may not be needed for the tank reducing grout if, as suggested in Denham (2007), a solubility release model is applied for the tank-bottom residue. While the data and conclusions are preliminary, a subset of the results is shown in Table 7-1. Partition coefficients are shown for iodine, neptunium, technetium, and uranium, which Kaplan and Coates (2007) identified as important to risk, measured on two of the three studied materials: fresh reducing cement and old structural concrete cement. The third material, results from which are not shown in Table 7-1, was aerated reducing cement.

Two different solutions were used in experiments: (i) saturated in portlandite [ $\text{Ca}(\text{OH})_2$ ] and held in an argon atmosphere and (ii) saturated in calcite ( $\text{CaCO}_3$ ) and held in air. These two solutions were intended to represent early and late stages in cement-based material degradation and are analogous to Regions II and III of Bradbury and Sarott (1995). In Table 7-1, these new data are compared to analogous, previously recommended values from Kaplan (2006). In most, but not all, cases, the measurements exceed the previously recommended values. The exceptions, however (e.g., uranium), point to the importance of site-specific data obtained under appropriate conditions.

Similarly, site-specific grout sorption data were not available for the performance assessment supporting the Idaho National Laboratory grouted tank waste determination (DOE-Idaho, 2003). Values were selected from the literature (Portage Environmental, Inc., 2005). As discussed in NRC (2006, Sections 4.2.6.4 and 4.2.7.1), these selected values were not all demonstrably conservative, but DOE sensitivity analyses suggested that using, for example, a lower  $K_d$  for technetium reflecting oxidizing conditions did not result in calculated doses exceeding performance objectives.

Fuhrmann, et al. (2006) reported batch iodine and technetium sorption data on two slag-containing grouts proposed for tank closure at the West Valley Demonstration Project. The experiments were conducted under air in a pH 12.3,  $\text{Ca}(\text{OH})_2$ -KOH solution intended to simulate relatively fresh cement pore water. Both elements were poorly sorbed to the grouts, yielding

<b>Table 7-1. Selected Preliminary Measured and Previously Recommended <math>K_d</math> Values (mL/g) for the Reducing Grout Formulation for Savannah River Site F-Area Tank Farm</b>				
	<b>Measured Reducing Grout <math>\text{Ca}(\text{OH})_2</math> Solution ("Young")*</b>	<b>Previously Recommended Early Stage Reducing†</b>	<b>Measured 40-Year-Old Cement <math>\text{CaCO}_3</math> Solution ("Old")*</b>	<b>Previously Recommended Late Stage Oxidizing†</b>
Iodine(-1)	6.2 ± 0.2	8–20	14 ± 7	0
Neptunium(+5)	3,900 ± 600	2,000	1,300 ± 800	200
Technetium(+7)	Not reported	5,000	1.4 ± 5.8	0
Uranium(+6)	2,000 ± 2,000	5,000	170 ± 70	70

\*Kaplan, D. and J. Coates. "Concrete  $K_d$  Values Appropriate for the Tank Closure Performance Assessment." WSRC-RP-2007-01122. Aiken, South Carolina: Savannah River National Laboratory. 2007.  
†Kaplan, D.I. "Geochemical Data Package for Performance Assessment Calculations Related to the Savannah River Site." WSRC-TR-2006-00004. Rev. 0. Aiken, South Carolina: Westinghouse Savannah River Company. 2006.

iodine  $K_d$ s of 0.7 and 0.8 mL/g and technetium values of 0.5 and 0.7 mL/g. Tests on slag components showed that Portland cement was the chief iodine sorber, while blast furnace slag most effectively sorbed technetium. The data may indicate the poor retention of iodine and technetium even in fresh grout when air contact is possible.

### 7.3.3.2 Literature Partitioning Data

Partitioning data surveyed from the literature include Jakubick, et al. (1987); Atkins and Glasser (1990); Altenhein-Haese, et al. (1994); Shrivastava and Verma (1995); Curti (1999); Sugiyama and Fujita (2003, 1999); Matzen, et al. (2000); Zhao, et al. (2000); Sylwester, et al. (2000); Shrivastava and Shrivastava (2001); Bonhoure, et al. (2002); Ochs, et al. (2006, 2002); Baur and Johnson (2003); Tits, et al. (2006a,b, 2004); Pointeau, et al. (2006, 2004); Dario, et al. (2004); Glaus and van Loon (2004); Harfouche, et al. (2006); Cowper, et al. (2006); Mace, et al. (2007); and Wieland, et al. (2008).

The data, in general, point to the importance of C-S-H phases and other secondary minerals in sorbing radionuclides. For example, selenium studies by Sugiyama and Fujita (1999), Ochs, et al. (2002), and Baur and Johnson (2003) showed strong sorption of selenite to C-S-H and the sulfates ettringite and monosulfate, and possible solid solution of selenate with the sulfates. In studying hydrothermally altered cements, Sugiyama and Fujita (1999) and Mace, et al. (2007) associated a decrease in selenite sorption at higher temperature with a decrease in surface area as C-S-H became more crystalline. C-S-H solids were also indicated as important to sorption of strontium (Shrivastava and Verma, 1995; Shrivastava and Shrivastava, 2001; Tits, et al., 2006a), actinides (Altenhein-Haese, et al., 1994; Tits, et al., 2003; Sugiyama and Fujita, 2003), cesium (Ochs, et al., 2006), and radium (Tits, et al., 2006b), while calcium aluminate sulfates are important for iodine (Atkins and Glasser, 1990). For example, Shrivastava and Shrivastava (2001) showed that strontium release rates decreased by up to three orders of magnitude as ordinary Portland cement was replaced by 40 percent tobermorite, which is an analogue for C-S-H solids.

These studies may suggest that cements that have degraded to the point of portlandite removal have not necessarily lost a great deal of their sorptive properties. In fact, Cowper, et al. (2006) showed that degraded Portland cement, dominated by C-S-H, more effectively sorbed thorium and americium than fresh Portland cement. These results were consistent, Cowper, et al. (2006) said, with the known sorption affinity of C-S-H for actinides. Pointeau, et al. (2004) noted an increase in uranium sorption as cement degraded and pH decreased; they attributed this behavior to the C-S-H abundance of the degraded cement, but could not reach a conclusion on the specific uranium sorption mechanism. Pointeau, et al. (2006) observed stronger selenium sorption in degraded cement (pH 11.9) than in fresh cement (pH 13.2), which they suggested could result from the positive surface charge in the degraded cement producing a higher affinity for anionic selenite. The literature suggests that the use of sorption data from fresh cements may not be useful for predicting long-term cement radionuclide retention.

In a system in communication with air, calcite formation is also an important degradation mechanism. Curti (1999) used laboratory data and modeling to predict the potential for radionuclide coprecipitation as calcite forms in aging cements. He found that, while trivalent and tetravalent actinides will be strongly associated with calcite, strontium and radium will not. This study contrasts with the earlier Smith and Walton (1991) conclusion that strontium coprecipitation with calcite will decrease release through cement-based barriers. The work of Gutierrez, et al. (1996) also supports stronger strontium retention on carbonation.

Radionuclide behavior in cracked cement-based materials, although perhaps one of the most important factors in understanding the persistence of reducing conditions in grouted tanks and monolithic waste forms, has received little experimental attention. Chambers, et al. (2006) speculated that microcracks may have provided paths for faster diffusion of tritiated water in through-diffusion experiments in cement blends, complicating interpretation of the results in terms of simple diffusion. Gutierrez, et al. (1996) suggested that more rapid diffusion of radioelements other than strontium from carbonated cement was due to development of microcracks. Matzen, et al. (2000) studied uranium and neptunium transport through a concrete column that was fractured and hydrothermally altered. In flow-through experiments, the fractured concrete effectively retained uranium, neptunium, and synthetic colloids. This was attributed to the growth of C-S-H and clays on the free fracture surface, providing a particularly sorptive surface. In a companion batch sorption study, Zhao, et al. (2000) found that hydrothermal alteration made concrete less sorptive for uranium and neptunium. The favorable influence of a fracture in the Matzen, et al. (2000) study does not consider the potential for unfavorable effects on redox-sensitive elements such as technetium if the fracture allows rapid oxidation.

A limited number of studies have looked at the effects of organic cement admixtures on radionuclide partitioning. As discussed in Section 8.2.8, Glaus and van Loon (2004) concluded that no effects were observed on radionuclide sorption onto hardened cement paste in the presence of organic-based admixtures, despite the potential for radionuclide complexation with the organic substances. Glaus and van Loon (2004) explained this lack of effect as resulting from strong sorption onto surface sites by the admixture compounds, such that aqueous complexant concentrations were sharply reduced. Dario, et al. (2004) obtained inconclusive results on the effects of several admixtures on actinide analogue Eu(III) sorption, and effects on selenium were minor in the presence of gluconic acid (Pointeau, et al., 2006). A study of gluconic acid complex stability constants showed that effects on uranium mobility were likely to be minor, apparently because of weak complexation of gluconic acid with U(VI) (Warwick, et al., 2006).

### **7.3.4 Evaluation of Models in Light of Data**

The literature on measured radionuclide release rates from cement-based materials provides two types of data: empirical release rates (e.g., in fraction released per time, or mass released per area per time) and interpreted effective diffusion coefficients. The former type of release rate is highly specific to laboratory scale and conditions and does not provide an intrinsic parameter that may be applied directly in performance assessments in a meaningful way. There is no clear way to compare a modeled release rate from a grouted tank or saltstone monolith to laboratory data, nor are there appropriate, applicable full-scale data available. Effective diffusion coefficients, on the other hand, are intrinsic parameters that can be incorporated into release models, but the spatial and temporal effects of diffusion depend on the specific model scenario. We will not, therefore, discuss direct comparisons between measured release rates and model predictions. Applicability of conceptual models to performance assessment can, however, be assessed in light of empirical studies.

The applicability of radionuclide release models based on diffusion and sorption on long time scales is brought into question by several factors:

- Physical characteristics change as degradation progresses, in terms of both sorptive properties and water flow characteristics.

- Pore water chemistry changes as degradation progresses.
- When processes other than diffusion take place during leach tests, extrapolations in time may be inaccurate even if that process is accounted for in models.
- The effects of the specific sorption mechanism (e.g., surface complexation versus coprecipitation) can differ strongly over time.

A number of leaching studies have stressed the limitations of simple diffusion or diffusion/sorption models based on small-scale leach tests (e.g., Fuhrmann, et al., 1990; Pescatore, 1991; Serne, et al., 1992; McConnell, et al., 1997; Kim, et al., 1995; Jakob, et al., 1999). For example, diffusive release from a finite shape such as a cylinder is actually more rapid than from a semi-infinite plane geometry, which is assumed in the ANSI/ANS-16.1 equation for deriving the diffusion coefficient from cylinder leach tests. Interpreting diffusion from a cylindrical sample requires that less than 20 percent of the constituent be depleted so that the semi-infinite plane assumption is not significantly violated (Section 7.3.1). Mathematical approaches to explicit geometric modeling (Fuhrmann, et al., 1990; Pescatore, 1991) are typically neglected in leaching studies. If leach fractions higher than 20 percent are reached, neglect of geometric effects means the diffusion coefficient may be overestimated.

Similarly, equations used for calculating the diffusion coefficient do not always explicitly include sorption or solubility limits. Fuhrmann, et al. (1990) gave an example of an alternative calculation of release when a sorbed fraction is assumed to be unavailable for diffusion; the resulting comparative curves are reproduced in Figure 7-2. While the partitioning model fits the data better, use of the diffusion interpretation would predict higher release rates.

From a risk perspective, these limitations on interpreting diffusion coefficients from leach tests typically lead to overpredicting radionuclide release rates. Likewise, the use of a reversible sorption model when coprecipitation is the actual mechanism (e.g., Shrivastava and Shrivastava, 2001; Sugiyama and Fujita, 2003) will overpredict release. The increasing use of tools for understanding the coordination environment of surface-associated radionuclides will help delineate actual mechanisms (e.g., Harfouche, et al., 2006).

As discussed in Section 7.3.1.2, many investigators have noted an “instantaneous washoff,” or initially rapid leaching rate, that flattens out and gives way to more demonstrably diffusive behavior. Because this release fraction is clearly not controlled by diffusion, it is not included in calculations of effective diffusion coefficient. Although this fraction—which is highly specific to particular sample preparation and test conditions and may result from surface concentrations of contaminants—is likely not useful for predicting long-term behavior, it may be important to consider in performance assessments. If, for instance, excess bleed water persists after saltstone emplacement, the possibility exists for a significant early release of radionuclides. Such a scenario depends on facility conditions and will not be informed by laboratory tests on small samples.

Experiments on radionuclide release from crushed waste samples can provide information on relative release behavior, demonstrate a lack of solubility control, or provide minimum estimates of achievable dissolved concentrations (e.g., Harbour and Aloy, 2007; Atkinson, et al., 1986; Serne, et al., 1996). This type of test does not, in general, provide intrinsic parameters that may be translated directly to models and, for reasons discussed in Appendix B, this type of test may not necessarily provide a quantitative solubility limit. It is perhaps for these reasons that release tests on crushed samples are not common in the literature. More commonly, crushed

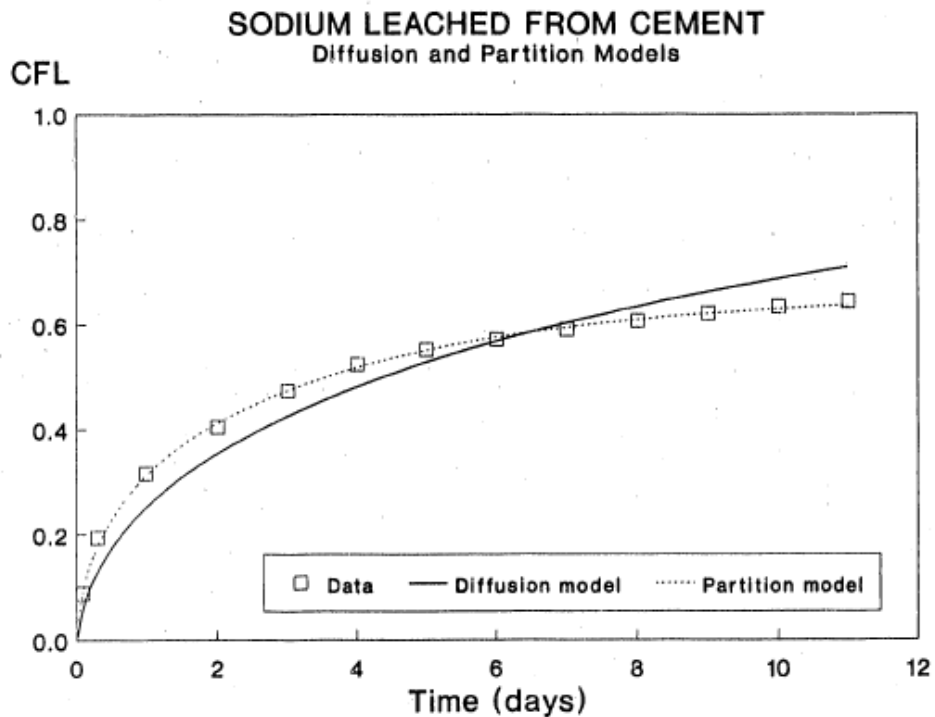


**Figure 7-2. Two Different Fits to Leaching Data on Sodium From a Portland Cement (From Fuhrmann, et al., 1990, Figure A1). “CFL” Means Cumulative Fraction Leached. A Partitioning Model That Treats a Sorbed Fraction as Permanently Unavailable Matches the Data Better Than a Simple Diffusion Model.**

cement-based materials are used in sorption tests to evaluate radionuclide transport through the material (see Section 7.3.3); these tests do not provide direct information on release rates from the waste form.

An interesting effort to match long-term Sr-90 release data from cement-based waste forms is shown in Figure 7-3 (McConnell, et al., 1997). The radioactive waste samples were loaded resins and zeolite encased in Portland cement and vinyl ester-styrene. The samples were placed in field lysimeters in Oak Ridge and Argonne National Laboratory soils for 10 years, and the leachate data were modeled using an earlier version of the DUST-MS code used at Idaho National Laboratory (DOE-Idaho, 2003). McConnell, et al. (1997) compared the Sr-90 lysimeter data to four different DUST-MS release submodels: (i) governed by only diffusion with no sorption, (ii) held at a constant fractional rate with no sorption, (iii) governed by sorption and dispersion, and (iv) held at a constant solubility limit concentration with no sorption. The figure shows how well the different release models fit the observed cumulative released Sr-90. In both cases, the sorption model gave the worst fit to the shape of the observed release curve. Note that the released fractions are very low, such that applicability of the model curves beyond the 10- to 100-year timeframe is uncertain. These data are also highly site-specific and clearly cannot be directly applied in a grouted tank or saltstone vault setting.

The foregoing discussion suggests that, in performance assessments for cement-based waste forms such as saltstone, it is not necessary to choose from among conceptual release models invoking processes such as diffusion, advection, sorption, and solubility limits. For example,

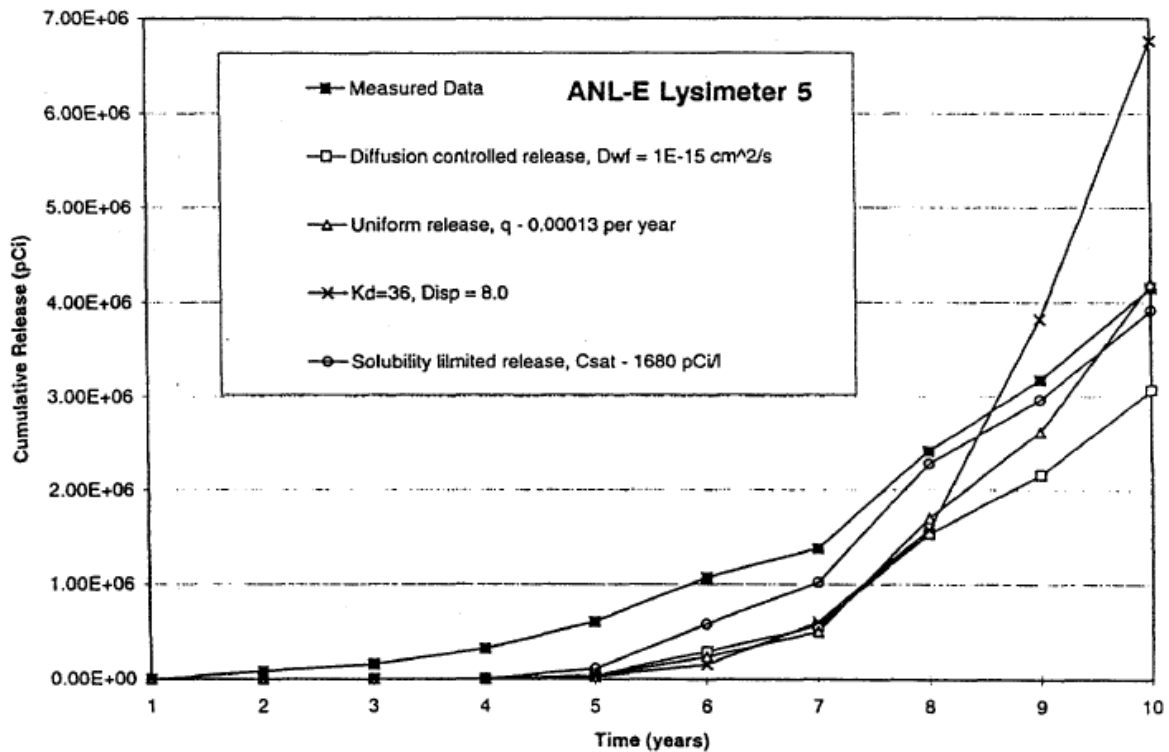
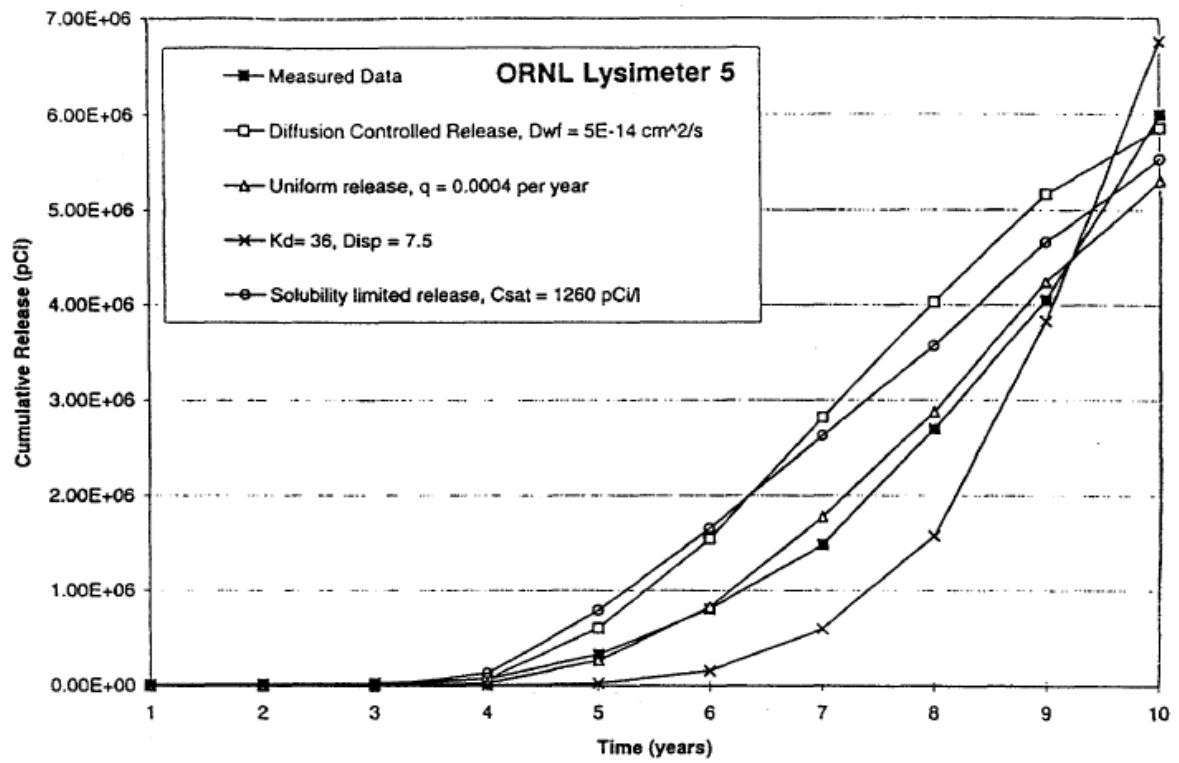


Figure 7-3. Fits of Various Release Models to Data on Sr-90 From Field Lysimeters at Oak Ridge and Argonne National Laboratories (From McConnell, et al., 1997, Figure 3)

while diffusion has proven useful in interpreting leach data, results often point to the need to include sorption. Advection and diffusion are typically combined in mass transport models, and solubility limits can be invoked in models involving the other processes. The effects of waste form degradation can be simulated by changing parameters such as hydraulic conductivity and sorption coefficient. With regard to modeling dissolved radionuclide concentrations in waste form pore waters, the use of a well-considered solubility limit is clearly conservative if other processes that could limit concentration are active. Setting dissolved concentrations using partition coefficients based on sorption experiments is not always as conservative and should be invoked only when based on understanding of contaminant-host interactions or on material- and site-specific measured released radionuclide concentrations.

For a system in which a tank residue is overlain by, and does not effectively mix with, a grout fill, there appears to be limited support for conceptualizing a release model based on data from studies of cement-based waste forms. Although the overlying grout will certainly be important to the chemical and hydrologic environment, the contaminant source is discrete from the grout and will have its own release characteristics. Released contaminants will not be transported through the tank grout. In the absence of definitive information on the chemical and mineralogic characteristics of the residue—and supporting release test data—a solubility-limited release model may be an appropriate approach. (These statements do not apply to modeling transport through the underlying concrete basemat, for which sorption studies are clearly relevant.)

While the literature provides a great deal of fundamental data on radionuclide behavior in cement-based systems, more focused studies on specific conditions and expected processes are needed. Useful information may be obtained, for example, by (i) studying radionuclide leaching behavior in incomplete mixtures of grout and tank residue, (ii) conducting flow-through release experiments on degraded saltstone, or (iii) observing chemical changes in waters flowing through cracks in reducing grout. There is also a need to better constrain the potentially beneficial and detrimental effects on sorption and leaching of cement degradation (e.g., Pointeau, et al., 2006, 2004) and crack formation (e.g., Tognazzi, et al., 2000; Matzen, et al., 2000), using data from materials with appropriate characteristics such as mineralogy and surface area.

Strong conclusions cannot yet be drawn concerning the effects of carbonation on radionuclide mobility. Carbonation will be an important process in grouted tank and saltstone settings. Carbonation could lower porosity and fill cracks, inhibiting transport, or could enhance mobility by promoting crack formation and increasing bulk permeability (e.g., Andersson and Nilsson, 2000; Langton, 2007). Similarly, calcite replacement of C-S-H could either reduce or enhance the sorption environment for radionuclides (e.g., Curti, 1999).

The need for material-specific data is also highlighted by the potential effects of organic-based cement admixtures, which as also suggested in Section 8.2.8, are uncertain.

While these variations and uncertainties exist and direct coupling of cement-based material degradation and radionuclide release has not yet been achieved in models, hydrologic transport tools (e.g., Cook and Fowler, 1992; Walton, 1994) can provide useful results if mechanisms and parameters are conservatively chosen.

### **7.3.5 Relative Importance of Diffusive and Advective Release**

As the preceding discussions show, literature data on radionuclide release from cement-based waste forms has focused on (i) obtaining intrinsic parameters such as diffusion coefficients,

sorption coefficients, and solubility limits and (ii) observing semi-quantitative information on release behavior. Less common is an emphasis on site-specific experiments shedding light on what the likely release mechanisms may be. [An example exception to this neglect is the lysimeter study of McConnell, et al. (1997) which, nevertheless, cannot be generally applied to other disposal settings.] For grout monolith disposal, and in cases in which tank residues mix with grout fill, release of radionuclides from the waste form will be accommodated by either diffusion or advection.

An important consideration in predicting long-term behavior is the relative degree to which diffusion and advection contribute to release. A useful construct for this consideration is the Peclet number, which indicates the relative contributions to mass transport of diffusion and advection. The Peclet number  $P_e$  can be defined by the following equation

$$P_e = \frac{Lv}{D_e} \quad (7-1)$$

where  $L$  is the characteristic length (say, in cm),  $v$  is the flow velocity (cm/s), and  $D_e$  is the effective diffusion coefficient (cm<sup>2</sup>/s). For a cement-based system, flow velocities will initially be low and may increase as degradation proceeds; under this assumption,  $P_e$  would increase with time. When the value of  $P_e$  exceeds one, advection may be considered to begin dominating transport.

Assuming saturated, vertical, gravity-driven seepage, Eq. (7-1) may be rewritten as

$$P_e = \frac{LK_e}{\theta_e D_e} \quad (7-2)$$

where  $K_e$  is the effective hydraulic conductivity (cm/s) and  $\theta_e$  is the effective porosity (dimensionless). For undegraded grout, a reasonable median value for the saturated hydraulic conductivity is 10<sup>-8</sup> cm/s [4 × 10<sup>-9</sup> in/s] (Figure A3-2) and for the effective diffusion coefficient of a conservative constituent is 10<sup>-8</sup> cm<sup>2</sup>/s [2 × 10<sup>-9</sup> in/s] (Figure A3-5). Assuming an effective porosity of 0.1, Eq. (7-2) then becomes

$$P_e = 10 L \quad (7-3)$$

For  $L$  less than 0.1 cm [0.4 in],  $P_e$  is less than 1. Therefore, diffusion in a water-saturated grout system would be effective only at length scales less than 1 cm [0.4 in] at the margins of the grout-based monolith or along the walls of cracks. Thus, in a bulk sense, diffusion is ineffective at mobilizing radionuclides from throughout an intact grout monolith. Advection would be the dominant process in the bulk of the body, but it is ineffective at such a low transport velocity of 10<sup>-7</sup> cm/s [4 × 10<sup>-8</sup> in/s] {approximately 3 cm/yr [1.2 in/yr]}. Cracks through the monolith, however, may provide pathways along which diffusion is effective at releasing radionuclides into the more rapid flow pathways along the cracks; this points to the importance of fracture spacing in understanding release.

To investigate the impacts of fractures on performance of a cement-based waste form, Walton (1992) modeled radionuclide release rates from a concrete monolith with regularly spaced cracks bounding intact matrix blocks. Diffusion was the only release process modeled for the intact concrete matrix. Walton (1992) defined three types of release behavior, based on water percolation rates. At very low percolation rates, release is controlled by diffusion only and is not

affected by crack spacing or percolation rate. At a moderate range of percolation rates, release rate is independent of crack spacing but is a strong function of percolation rate; this is because contaminant concentration is nearly the same in matrix and cracks, such that the system behaves as an equivalent porous medium. At the highest percolation rates, in contrast, release depends strongly on crack spacing but not on percolation rate; this is because contaminants that diffuse into cracks are quickly diluted and removed, such that concentrations are very low in the cracks. Diffusion into the cracks, therefore, dominates the release rate.

Returning to the Peclet number analysis, under unsaturated conditions, the effective hydraulic conductivity in Eq. (7-2) would be very much lower than the saturated hydraulic conductivity (see Figure A2-2), but  $D_e$  will be similar unless water contents are very low (say, less than about 8 percent; Section 7.3.1.1). The Peclet number would therefore be lower, increasing the length scale of diffusion dominance, and advection will be even less effective at mass transport. The lower the unsaturated-zone percolation rate, the less effective is advection, even in the presence of cracks. Even if cracks provide the primary pathways for fluid flow under unsaturated conditions, the rate of mass release will still be diffusion limited. At very low saturations in the cracks, the effective hydraulic conductivity of the cracks may be lower than that in the matrix, and the matrix will become the primary medium for fluid flow, but diffusion from the matrix to the surrounding environment may still dominate.

With time, hydraulic conductivity of the cement-based material may increase, such that the Peclet number will increase, increased flow velocity will enhance advective transport, and diffusion will become less important. Under these conditions, the role of cracks will also diminish, in a relative sense, as transport through the grout monolith will be more effective.

In a grouted tank with minimal mixing between radioactive residue and reducing grout, essentially all radionuclide release and transport takes place at the tank bottom, such that transport through the tank grout is not relevant. Considerations of diffusive and advective release, therefore, would not apply within the source area.

## **7.4 Summary and Recommendations**

Section B2 discusses the preferred conceptual model for the time-varying chemical environment for radionuclide release. Radionuclide release models for grouted tanks or saltstone should account for this evolution, as well as for the associated solid phase changes, chiefly characterized by the sequence portlandite–C–S–H phases–carbonate. Selection of sorption parameters for this sequence should be based on site-specific and condition-specific data and, if that is impractical, on a comprehensive view of the literature. Uncertainty in mechanisms and parameters should be addressed by favoring the choice that results in higher predicted release rates.

This review demonstrates that simple diffusion models are inadequate to describe radionuclide release from cement-based waste forms on long time scales. Diffusion, however, can be appropriately incorporated in hydrologic flow and transport codes that account for the dependence of the extent of advective and diffusive contributions on water flow rate and that incorporate sorption mechanisms. This is the approach adopted for the saltstone performance assessment (Cook, et al., 2005). Models should include appropriate links between material degradation and changing physical and chemical characteristics directly affecting release. For example, cracks and other fast pathways should be incorporated as much as practical, if their formation cannot be excluded, with respect to both flow rates and grout oxidation. Fast pathways can provide not only locally high flow rates, they can also potentially serve as oxidized

source regions. More explicit linkage between degradation and release should help reduce uncertainty and the need for large degrees of conservatism. Approaches for modeling ionic transport and degradation in concrete (e.g., Samson and Marchand, 2007) may prove useful in efforts to develop coupled models for cement-based radioactive waste disposal systems.

Nevertheless, it is possible to evaluate how reasonable and bounding models are in the absence of such direct linkage between release and degradation processes. In light of uncertainties, the conservative release approach adopted for the Idaho National Laboratory tank performance assessment—assuming hydraulic degradation of tank grout at an early time—is appropriate. That model, however, assumed that radionuclide sources were embedded in grout. If grout and tank residue do not mix, cement-based materials provide only the chemical, not physical, environment for release. Grouted tank models also need to consider how long the grout-reducing capacity persists at the bottom of the tank and along fast pathways that could be providing the bulk of the water to the source region. Another consideration in models is the potential for early release of radionuclides associated with a free liquid phase that represents salt waste solution that was not bound in the waste form.

The most useful models for radionuclide release would directly couple the chemistry and hydrology of material degradation with release mechanisms. Lacking such models, if the predictive capabilities of existing models are to be improved, more data of the following types should be obtained:

- Sorption, diffusion, leaching, and solubility data that account for a representative range of cement mixture components
- Sorption, diffusion, leaching, and solubility data that account for multiple stages of material degradation history for specific disposal environments
- The physical and mineralogical evolution of cracks
- Appropriate radionuclide aqueous concentrations at the source, including those for tank residues that do not mix with grout

## 8 ASSESSMENT OF FACTORS IMPORTANT TO PERFORMANCE OF GROUTED TANKS AND CONCRETE VAULTS AT U.S. DEPARTMENT OF ENERGY SITES

The issue of tank closure at the Savannah River Site, Idaho National Laboratory, and Hanford has been discussed in previous literature (e.g., DOE–Idaho, 2005; DOE–Savannah River Site, 2005; National Research Council, 2006). Briefly, large-volume tanks have been used to contain radioactive process liquids. The tanks were built from the 1940s through the 1980s, have capacities ranging from 50 to more than 3,800 m<sup>3</sup> [13,000 to more than 1,000,000 gal], are inside reinforced concrete structures, and are buried. The tanks are of various constructions; most are fabricated of carbon steel, either single- or double-walled, and others are stainless steel. A schematic diagram of a typical tank and vault system at the Idaho National Laboratory tank farm facility is shown in Figure 8-1. The configurations of the different types of tanks at the Savannah River Site are illustrated in Figure 8-2.

As mentioned in Section 1, the tank closure process involves waste removal; cleaning of the tanks, piping, and ancillary equipment; and stabilization of the tank configuration and ancillary equipment. Some residual sludge, as well as adherent coatings of solids on tank bottoms and on tank walls, likely will not be removed by the cleaning process and will remain in the tank along with some residual liquid. The tank system will be stabilized by filling the system with grout. The U.S. Department of Energy (DOE) generally plans to decontaminate process lines

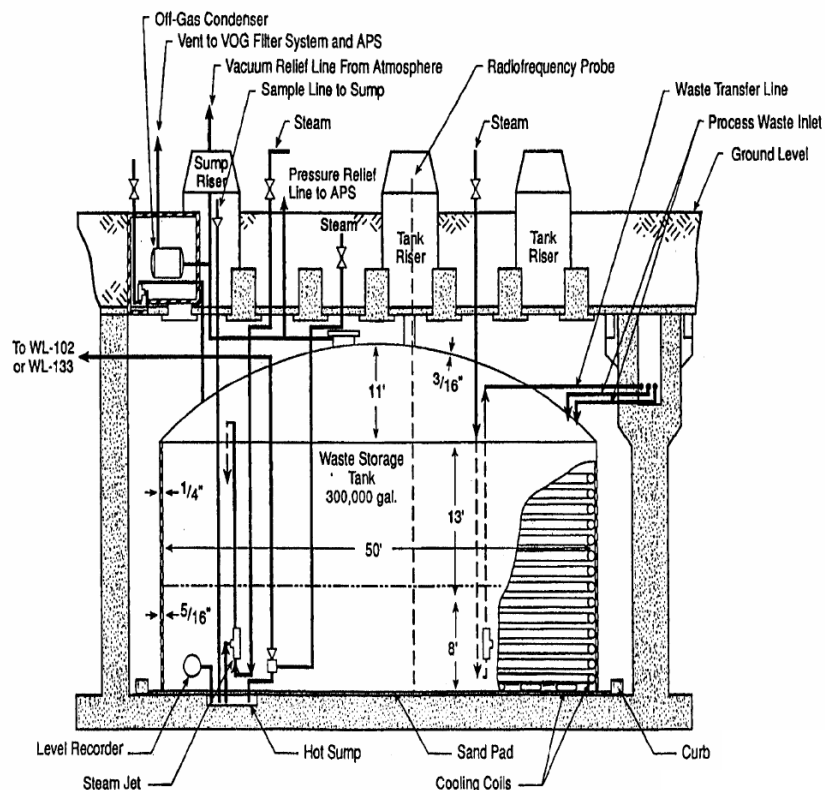


**Figure 8-1. Typical Tank and Vault Layout and Dimensions at the Idaho National Laboratory Tank Farm Facility (From DOE–Idaho, 2003)**

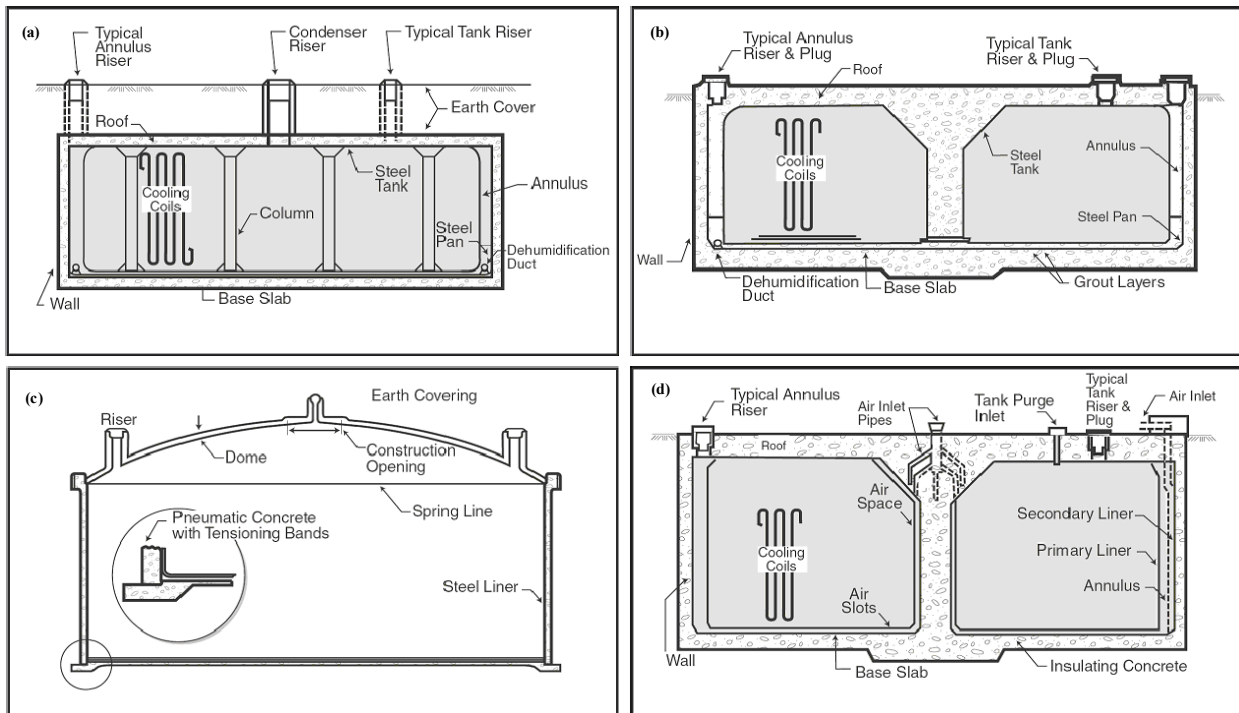


**Figure 8-2. Tank Configurations at the Savannah River Site: (a) Cooled Waste Storage Tank, Type I; (b) Cooled Waste Storage Tank, Type II; (c) Uncooled Waste Storage Tank, Type IV (Prestressed Concrete Walls); and (d) Cooled Waste Storage Tank, Type III (Stress Relieved Primary Liner). Figures Taken From DOE–Savannah River Site (2002).**

and to grout and cap lines that provide a pathway to the tanks (e.g., DOE–Idaho, 2005). A schematic of a grout-filled tank and concrete vault at the Idaho National Laboratory is shown in Figure 8-3.

DOE selected a cement-based material for filling the tank system and pipework for several reasons (Harbour, 2005; National Research Council, 2006; Langton, et al., 2007).

- The material has sufficient mechanical rigidity to prevent collapse of the tank and vault system and protect against inadvertent intrusion.
- The high pH will slow steel corrosion (especially carbon steel) and provide additional chemical immobilization potential for radioactive species present in the residual waste.
- Its low permeability will largely exclude groundwater percolation during the postclosure phase.
- Adding blast furnace slag to the grout formulation helps establish a reducing environment that could mitigate the release of redox-sensitive radionuclides, such as Tc-99.

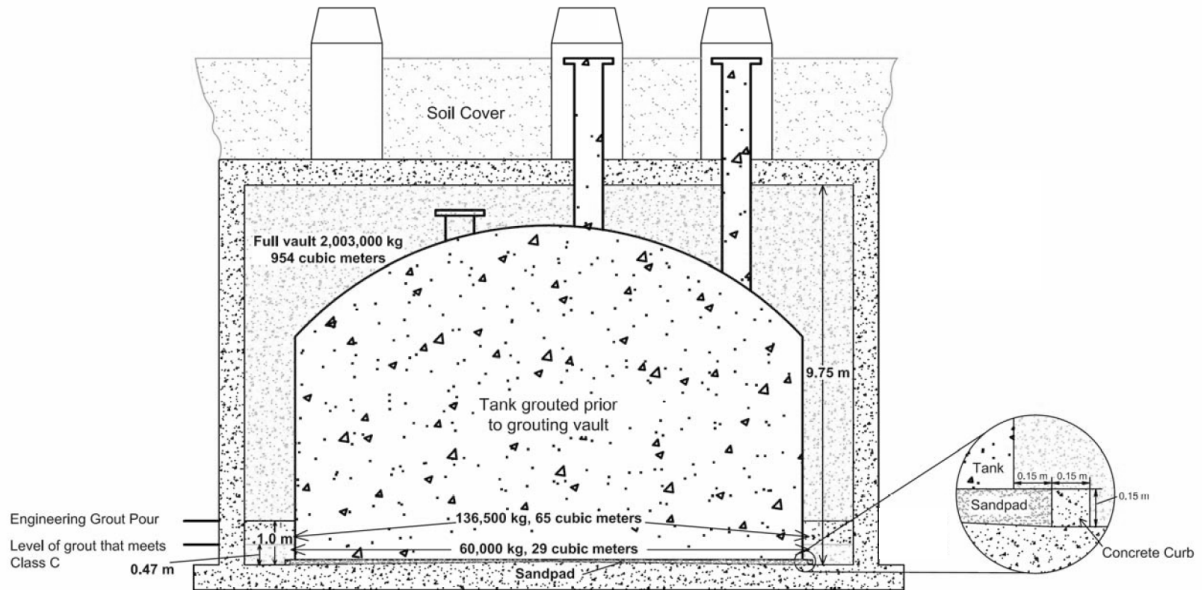


**Figure 8-3. Schematic of a Grout-Filled Tank and Vault at the Idaho National Laboratory Tank Farm Facility Showing the Vault Volume and the Grout Mass (From DOE–Idaho, 2005, Figure 16)**

- Cement and cement-based materials are persistent in the natural environment for relatively long exposure times, although not necessarily for 10,000 years for manmade cements and concretes.
- Cementation can be implemented using proven and remote technologies.

These advantages are considerable and, despite uncertainties, make it likely that the use of cement-based materials will remain the preferred option.

Three types of grouts could be used for tank closure. Figure 8-4, taken from a National Research Council (2006) report, shows that tank bottoms are emplaced with a “stabilizing grout,” above which is a “structural grout,” and finally a “capping grout.” Figure 8-4 is a schematic, but structural grout likely will comprise the bulk of the grout volume. The structural grout is intended to be a low-strength, low-permeability formulation; the capping grout will have similar low permeability, but will have higher strength to discourage intrusion. The stabilizing grout contributes to space filling, provides physical and chemical stabilization of residual waste at the bottom of the tank (“tank heel”), and combines with any residual water in the tank. All three grouts are intended to remain sufficiently alkaline, pH approximately >11, to reduce steel corrosion. Note that the schematic in Figure 8-4 is for grout-filled tanks at the Hanford site; tanks at other DOE sites could have a different design. The grout mix formulations used for grouting tanks and vaults at the Idaho National Laboratory Tank Farm Facility are listed in Table 8-1. No decision has yet been made on specific formulations for closing tanks at other DOE facilities, but based on the direction of previous DOE-funded research, preference likely will be given to a “ternary” grout (i.e., a grout consisting of three solid components: Portland cement, slag, and fly ash).

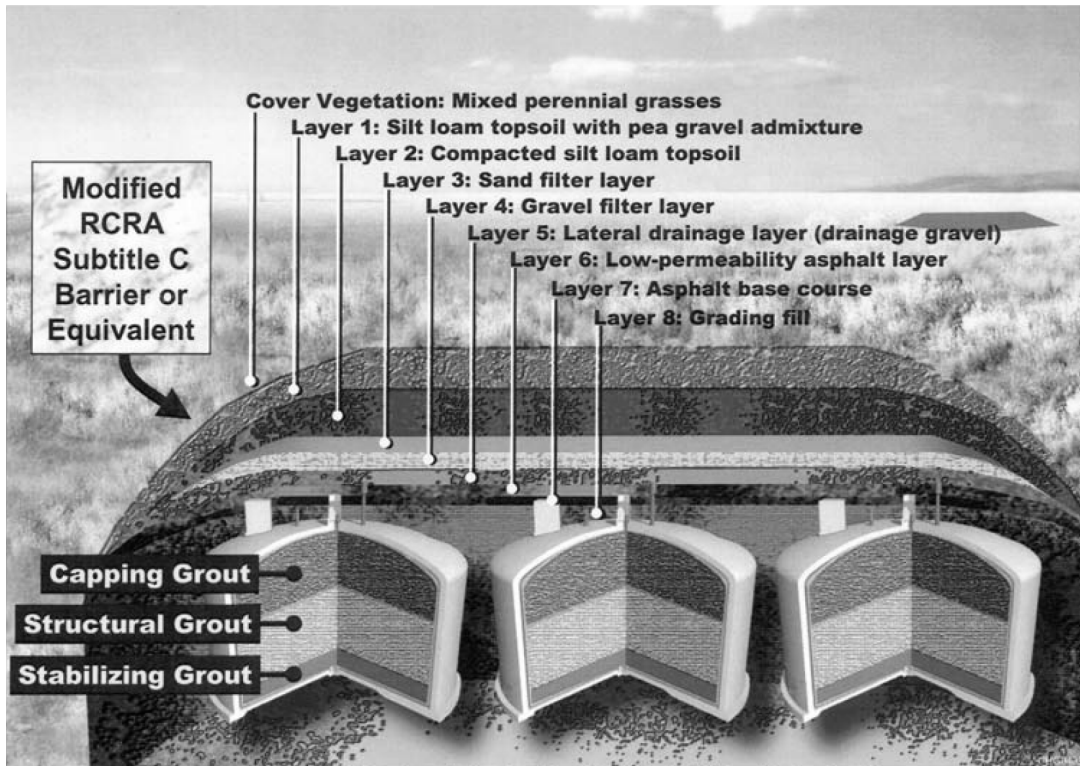


Figure 8-4. Schematic of an Engineered Barrier System To Close Tanks at the Hanford Site. A Similar Plan of Engineered Grout Layers Plus a Cap System Is Adopted at the Savannah River Site and the Idaho National Laboratory. (From National Research Council, 2006, Figure V-1.) Reprinted With Permission From the National Academies Press, Copyright® 2006, National Academy of Sciences.

Table 8-1. Grout Mix Formulations for Closing of Tanks and Vaults at the Idaho National Laboratory Tank Farm Facility		
Component	Stabilizing Grout* (Amount Per Cubic Yard of Grout Mix)	Structural Grout† (Amount Per Cubic Yard of Grout Mix)
Portland cement, Types I-II	230 lb	300-415 lb
Blast furnace slag	352 lb	—
Class F fly ash	118 lb	200 lb
Fine aggregate (sand)	2,500 lb	Adjusted according to final cement requirement
Water	Up to 400 lb (48 gal)	320-400 lb
High-range water reducer	Up to 32 oz or as required to obtain slump and flow	As required to produce 20-30 percent air content

\* CH2M-WG Idaho, LLC. "Specifications for INTEC Grout and CLSM Supply Project." SPC-763, Revision 1. Idaho Falls, Idaho: CH2M-WG Idaho, LLC. 2007.  
†Thorne, D. "Evaluation of Grout Formulations for Tank Farm Facility Closure." PEI-EDF-1033. Rev. 0. Idaho Falls, Idaho: Portage Environmental, Inc. 2007.

DOE-funded research on grout formulation for tank closure relies mainly on empirical knowledge, but is supported by laboratory studies (e.g., Langton, 1987a,b, 1986; Langton, et al., 2007, 1988; Lorier, et al., 2003) and, to a lesser extent, by large-scale trials (Idaho National Engineering and Environmental Laboratory, 1999; Langton, et al., 2003). The general bases for the development of DOE grout formulations are summarized in Table 8-2. The selection of materials and proportioning for DOE tank grouts has involved a compromise between the properties of fresh and hardened grout. Fly ash has been added to (i) reduce the exothermic heat of cement hydration, (ii) maintain good flow properties of fresh grout at low water contents, and (iii) reduce the intrinsic permeability of the hardened grout. Ground, glassy, iron blast furnace slag was introduced to create and maintain a chemically reducing matrix and help attain low initial heat evolution and low final permeability. A short-term consideration is the need to achieve good flow and self-leveling of fresh material inside the tank and the space between the tank and concrete vault. Moreover, grout has to flow freely into the associated pipes and vents and be suitable for pumping and emplacement without an excess of water that would contribute to bleed or segregation. Thus, water-reducing admixture also has been included in the grout formulation to achieve good flow with a low water-to-cement ratio of the grout mix to achieve a sufficiently low porosity and permeability of the hardened cement-based material. Other admixtures such as viscosity-modifying admixtures and set retarders also have been used on some grout formulations (e.g., Langton, et al., 2007).

DOE has conducted performance assessments to demonstrate that disposal actions at its sites (e.g., Idaho National Laboratory and the Savannah River Site) will meet specified performance objectives. The demonstration of compliance has included a reliance on the ability of cement-based materials to serve as a barrier to groundwater influx and to mitigate radionuclide release and transport (DOE–Idaho, 2003; Cook, et al., 2005). The following sections assess factors, as well as features, events, and processes, that are important to consider when evaluating the performance of cement-based engineered barriers at DOE sites. Much of the discussion is focused on grouted tanks and concrete vaults, but in many respects, the assessment applies also to the cementitious waste form—saltstone—that will be disposed in the Saltstone Disposal Facility at the Savannah River Site.

## 8.1 General Considerations

Cements have distinctive features setting them apart from other engineered barrier materials. All barrier materials have low permeability in common, but only cements furnish a chemical

<b>Table 8-2. General Bases for the Design and Development of the U.S. Department of Energy Grout Formulations</b>	
<b>Criteria</b>	<b>Basis</b>
Materials selection	Reliance on conventional civil engineering codes and experience
Materials proportioning	Laboratory experiments and property measurement; compatibility with soluble but inactive waste components (e.g., leading to the development of Saltstone)
Grout properties	Measurements done on laboratory formulations
Scale effects	Limited number of large-scale trials undertaken

immobilization potential. However, as noted in previous sections, hydrated Portland cement matrices are generally unstable in their service environment. Their action as an engineered barrier material characteristically reflects this instability. In the fresh and unaltered state, the chemical reactivity of cements enables cement-based materials to react with a range of radionuclides, and the resulting impact on radionuclide release is determined by the binding potential, generally expressed as a sorption coefficient or defined based on the solubility of the solubility-controlling solid phase.<sup>1</sup> Reaction is not confined to radioactive components, and many of the nonradioactive constituents in waste streams and in groundwaters also will react with cement and compete for binding sites. Therefore, it is not sufficient to determine the mechanisms and strengths of radionuclide binding in cement during the fresh state; they must also be determined during the period when cement is undergoing alteration.

Cement, by virtue of the slight solubility of its components, can condition infiltrating water pH. The resulting pH, normally above 12 for fresh cements, also helps protect embedded steel against corrosion. Very simple considerations show that cement should not be too insoluble if it is to maintain these functions over prolonged periods. For example, a pH of 12 corresponds approximately to a solution about 0.01 molar with respect to its hydroxide ion concentration. This concentration is achieved by a solution 0.005 molar with respect to calcium hydroxide [each mole of  $\text{Ca}(\text{OH})_2$  dissociates to yield two moles of  $\text{OH}^-$ ]. Thus, the solubility of cement components is sufficient to achieve high pH, but because the solubility is not too high, pH conditioning can be achieved over a relatively long performance lifetime in conditions of low groundwater flow and large mass of cement. Natural analogs, such as that at Maqarin, Jordan, confirm the pH-conditioning ability of cementlike matrices (Alexander, et al., 1992). At the Maqarin site, hyperalkaline groundwaters are present as a result of leaching of an assemblage of natural cement minerals produced by high temperature/low pressure metamorphism of marls and limestones. The simple considerations described previously benchmark other more sophisticated calculations.

In most tank closure applications, cement grouts will not be directly and continuously exposed to water. With few exceptions, the tanks being closed are physically situated in horizons above the water table such that contact with water will be infrequent (e.g., in the course of a pluvial phase or when the engineered covers designed to prevent water infiltration to the cement-based barriers fail). There is general agreement that a prolonged lack of contact with permeating groundwater would cause conditions that are benign with respect to performance of cement-based materials. Perhaps on this account, little has been published about cement deterioration in moist environments. However, when evaluating a 10,000-year performance lifetime, deterioration in humid environments needs consideration. This point is elaborated on later in this section.

In addition, performance in the postclosure phase is strongly influenced by formulation and construction. Hence, it is not a digression to briefly consider these aspects, because they will affect the robustness of the assessment. Experience of cementation in other civil engineering applications enables some of the potential problems of construction and constructability to be anticipated and solutions to be developed. While direct translation of civil engineering experience to nuclear waste disposal may not be practicable, much experience on different types of construction suggests that different considerations have to be made between fresh grout properties and those of hardened grouts. Table 8-3 examines these considerations in the context of a 10,000-year performance lifetime.

---

<sup>1</sup> A review of radionuclide solubility, sorption, and release in cement-based systems is provided in Section 7 and Appendix B of this report.

<b>Table 8-3. Desired Short- and Long-Term Grout Properties</b>	
<b>Short Term (0 to 10 years)</b>	
Rheological properties of fresh grout	Acceptable for emplacement (fluidity, self-compaction, freedom from segregation and bleeding)
Hardening	Develop strength progressively without long-term regression
Heat evolution	Preferably low
Robustness	Good envelope of performance with variations in grout composition
<b>Long Term (&gt;10 years)</b>	
Internal chemistry	Specified pH and Eh targets maintained by adequate buffering/poising reserves
Permeability	Good resistance to percolation by groundwater
Mechanical response	No long-term regression of strength in the absence of degradation
Compatibility	Provides protection against corrosion and does not react adversely with other engineered/natural barriers
Aging	Capable of limited plasticity and/or ability to self-heal cracks

In the context of this long period of performance, “short term” is defined by the period of human or instrumental observation—typically a few years or at most, a few decades. In Table 8-3, the distinction between “short” and “long” term is arbitrarily fixed at 10 years assuming that this number of years will be the longest practicable period of observation and monitoring of laboratory simulations. Note that the grout formulations thus far proposed for tank closure use materials familiar to civil engineers, but contain these materials in unconventional proportions. The added restriction listed in Table 8-3 regarding strength regression allows for the possibility that some unknown mechanism, which could lead to a loss of strength, could occur as the matrix ages and that the first sign of distress is a strength regression.

Furthermore, performance needs to be evaluated in the context of different timeframes. A time scale up to 1 or 2 years can be used to benchmark a reference state. Within this time period, the grouts should mature sufficiently to attain relatively constant properties and allow the properties derived from laboratory tests to be compared with larger scale tests made in the field. In the longer term, reactions will continue within the grout, but without further self-generated thermal excursions. The property data obtained after 1 to 2 years’ cure duration probably can be extended by a factor of 10. But features, events, and processes that can occur at longer timeframes, up to 10,000 years, also need to be considered. It is suggested that “snapshots” be developed for 100, 1,000, and 10,000 years.

It is currently possible to anticipate the features, events, and processes relevant to performance of grouted tanks and vaults, but mostly it is not possible to say over what time scale these features, events, and processes will occur and how they will affect grout properties. However, a quantification basis can be outlined and probabilistic assessment can be used to project the range of potential impacts from degradation processes and identify important uncertainties that

need to be mitigated. The features, events, and processes can be divided into two classes: closed system and open system. As the term implies, closed-system features, events, and processes will occur without an interchange of mass between the grout and the service environment. Open systems permit interactions with the external environment. Truly closed-system reactions are unlikely, but where they occur but do not significantly affect grout properties, a simplified approach facilitates a better mechanistic understanding. Several key features, events, and processes in closed and in open systems are examined in Sections 8.2 and 8.3, respectively.

## **8.2 Key Features, Events, and Processes in Closed Systems**

### **8.2.1 Evolution of Grout pH**

In the absence of environmentally assisted alteration, the pH evolution will be dependent mainly on the composition of the individual grout components and on the mix proportions. As noted in Section 2, the composition of Portland cements lies within a relatively narrow envelope, so it can be assumed all Portland cements will behave similarly, at least for scoping purposes.

#### **Effect of Blast Furnace Slag on pH**

Blast furnace slag is a byproduct of iron- and steelmaking—processes that involve using a blast furnace to produce metallic iron from oxides. The preferred reducing agent for these processes is carbon, usually as coke. The iron oxides contain impurities, notably silica and alumina, which are removed at this stage. The coke, and to a lesser extent the iron ore, introduces sulfur, which also needs to be removed. A good solvent system is achieved by (i) adding lime and magnesia to the batch and (ii) operating the process at high temperature. At the operating temperature, usually about 1,550 °C [2,822 °F], both slag and metal are molten and the fluid phases are immiscible or nearly so. The slag, having a lower density than crude iron, floats on top. This slag is occasionally removed. If the molten slag is allowed to cool, it will spontaneously crystallize, so it is air quenched or water quenched if intended for use as a supplementary cement material. If the molten slag is rapidly quenched with water, the slag solidifies to a glassy state with little or no crystallization and forms sand-size (or fritlike) fragments. The resulting granulate is readily dewatered and subsequently is ground to a high specific surface area to further enhance its reactivity. The ground granulated blast furnace slag has cementitious properties that make it a suitable partial replacement for or additive to Portland cement.

The compositions of commercial slag range over somewhat wider limits than Portland cement, but this variation is not important for the present purposes. Slag, like cement, is rich in calcium oxide (~36 to 40 weight percent in slag; 65 to 70 weight percent in Portland cement) compared to other supplementary cement materials like fly ash and silica fume. The silica content of slag is higher than that of cement (~30 to 36 percent versus only 22 to 24 percent for cement). If slag is hydrated on its own, it will generally elevate the pH of the aqueous solution to 10 or 11, controlled by the concentration of alkali ions in solution. But the elevation of pH would be less than that achieved with portlandite (pH approximately 12.4); portlandite is absent from the solid hydration products of slag.

With these facts, one can apply nonaqueous acid–base concepts to predict the future course of reaction, if any, to cement–slag mixtures. On this acid–base scale, cement is strongly basic,

whereas slag is weakly to moderately basic. Thus, when slag and cement are mixed, differences in basicity can drive a pozzolanic reaction. Because of the broad similarity in slag and cement composition, the pH reduction resulting from the pozzolanic reaction might be acceptable in the present context, particularly if slag were added at low replacement levels. Complete hydration of a modern Portland cement tends to yield about 25 percent portlandite, which provides a robust buffer system for pH. However, if slag is blended with cement and assuming the slag reacts completely, the portlandite content of the mix will decrease. This decrease occurs for two reasons. First, the Portland cement is diluted and the resulting amount of portlandite decreases because it is not produced from hydration of slag. Second, most slag actually will consume portlandite in the course of hydration. As a good first approximation, it can be assumed the pH does not depend on the amount of portlandite—only on its presence or absence. The full extent of the reduction in portlandite content is often not easy to ascertain, because practically, much of the slag persists without reaction over the normal period of observation (up to a decade). Thus, dilution of the cement with slag is observed to affect the portlandite content, but the full chemical potential of slag to react with portlandite is not achieved, because only a fraction of the slag will have reacted. The remaining unhydrated slag acts in the short term as an inert diluent, but over millennia, the continued persistence of unhydrated slag cannot be assured. In fact, complete reaction likely will occur over long time periods leading to the reduction or even elimination of portlandite.

Present knowledge of the mineral balance achieved in hydrated slag–cement matrices is insufficient to calculate quantitatively the potential of slag to reduce pH in the long term. But scoping studies indicate that the potential for portlandite consumption also will be sensitive to slag composition. However, it can be concluded that the full potential of slag to reduce the portlandite content is not well established from DOE research undertaken thus far. The apparent persistence of portlandite, and hence the high pH of the blends, arises in part or even entirely from the metastable persistence of unreacted slag.

### **Effect of Fly Ash on pH**

Fly ash compositions vary widely, but ASTM classification suggests a bimodal distribution of fly ash chemistries into the so-called Class C and Class F ashes. Class F ash is a pozzolanic fly ash normally produced from burning anthracite or bituminous coal, whereas Class C ash is a pozzolanic and cementitious fly ash normally produced from burning lignite or subbituminous coal. DOE information indicates that grout formulations used or proposed for tank closure or included in the DOE program utilize Class F ash. Class F ashes are rich in alumina and silica, which together often comprise 70 percent or more of the total mass of the fly ash. On that account, Class F ashes have much greater potential than blast furnace slag to undergo a pozzolanic reaction with portlandite. The effect on pH of a pozzolanic reaction acts in conjunction with the effect of dilution for both slag and fly ash, but the overall effect is proportionally much greater for Class F ash than for slag. However, this effect for Class F ash is achieved only slowly because of (i) the low reactivity of the glassy phase in fly ash and (ii) the combination of alumina and silica into crystalline phases including mullite. Mullite, nominally  $3\text{Al}_2\text{O}_3 \cdot 2\text{SiO}_2$ , is slowly reactive with cement at elevated temperature {85 °C [185 °F]} (Gordon, 2004) but, in the absence of evidence to the contrary, must be presumed to react with Portland cement over 10,000 years. The amount of fly ash needed to consume the portlandite in cement depends on the assumptions made about the reactivity of its component phases, but it is likely that 20- to 25-percent Class F fly ash is sufficient to completely consume the portlandite generated by cement (see Section 8.5.1).

Based on the discussion presented in the preceding paragraphs, the long-term pH of grouts formulated with high replacement levels of Portland cement by slag and fly ash will be less than those obtained by short-term tests because portlandite likely will be consumed by reactions with slag and fly ash. Although the C-S-H phase can also condition a high pH, the complete consumption of portlandite marks a transition between a regime of constant high pH buffered by the presence of portlandite to one of steadily decreasing pH buffered by the presence of C-S-H, which has a variable Ca/Si ratio. Thus, for preliminary calculations regarding the persistence of an alkaline pH, the presence of portlandite in the grout is a useful reference state.

## 8.2.2 Evolution of Grout Redox Potential

Previous studies have demonstrated the importance of maintaining a reducing chemical environment in the grout. The main benefits are (i) reduction of the corrosion rates of metallic components due to the low redox potential and (ii) conversion of redox-sensitive radionuclides, such as Tc-99 (discussed in Section 8.4), to a lower and normally less soluble oxidation state. For example, the reducing capacity of the tank grout was an important factor considered in DOE performance assessments to support onsite waste disposal at the Savannah River Site and the Idaho National Laboratory. Thus, it is important to understand the processes that could affect the long-term evolution of Eh in cement–fly ash–slag grouts.

### Effect of Blast Furnace Slag on Redox Potential

Blast furnace slag is viewed as the most effective carrier of chemically reduced species capable of generating a low redox potential in blends with other cementitious components. Table 8-4 compares the Eh and poisoning capacity (the capacity to maintain a particular reduction potential level) determined for Portland cement and a slag–cement blend. The Eh measured in the slag–cement blend, about –300 mV (versus standard hydrogen electrode), is much more reducing than the Eh in cement, although cement kilns sometimes may be operated under reducing conditions such that an occasional low Eh cement product may be obtained. Note that if slag and cement are mixed in equal weight ratios, the Eh measured after 1 day of hydration tends to be about the same as that of unblended cement. This observation is due to the slow hydration of slag; most of the sulfide sulfur remains locked up in unreacted slag. But at longer times, perhaps by 28 days, the Eh will decrease abruptly (Atkins and Glasser, 1992).

The origin of slag discussed in Section 8.2.1 helps explain why its reducing power is variable. The reducing potential in the slag arises from two sources: (i) the small quantity of metallic iron dissolved in the oxide slag and (ii) dissolved sulfur, which is strongly concentrated in the slag.

**Table 8-4. Poisoning Capacity and Eh in Cement Blends**

<b>Material</b>	<b>Eh mV (SHE)*</b>	<b>Poisoning Capacity</b>	<b>Comment</b>
Portland cement	+100 to +200	low	Cements occasionally give low Eh
Blast furnace slag–cement blend	–200 to –350	moderate	Eh obtained in blends with Portland cement activator

\*SHE = Standard hydrogen electrode, 25 °C [77 °F]

The glass structure of quenched slag consists of an incomplete network of (Al,Si)O<sub>4</sub> tetrahedra in which some of the oxide ions are replaced by sulfide. Thus, sulfide sulfur is invariably present and homogeneously distributed on an atomic scale, albeit in varying amounts depending on the slag source.

Note that sulfide sulfur is the main source of the reducing potential of slag. However, the sulfide content of slag is not specified, except as a maximum, by existing standards (e.g., ASTM C-989), and the commercial product may vary in the amount of sulfide. Most North American and European slag contains sulfur (as sulfide) in the range 0.6 to 1.0 weight percent. However, the modern tendency to use preprocessed iron feed stocks and “clean” coals results in the sulfur content of modern slag tending toward lower values. As a consequence, without a batch analysis and confirmation that the sulfur in the slag is present as sulfide, it is not possible to estimate the amount of the sulfide sulfur reserve and, hence, the poisoning capacity potentially available to maintain a low Eh.

If slag is mixed with CO<sub>2</sub>-free water (no cement added), the pH of the aqueous phase will gradually increase, perhaps reaching 10 to 11. However, the fraction of reacted slag will remain low unless an activator is present. Commonly used activators include Portland cement, gypsum, and portlandite. Because Portland cement is the activator in DOE grout formulations—fly ash is not an activator of slag—it is an essential component for activating the Eh control envisioned in tank closure performance assessments. Portland cement normally will contain several weight percent of sulfur [usually shown in the chemical analysis as sulfur(VI) oxide, SO<sub>3</sub>]. Apart from this sulfur(VI) content, the cement itself does not appear to contain other components capable of reacting with sulfide species to change the oxidation state. For that reason, even the low content of sulfide sulfur in slag dominates the redox effect.

But the reaction between sulfur(VI) and sulfide (S<sup>2-</sup>) causes intermediate sulfur species to form, specifically thiosulfate (S<sub>2</sub>O<sub>3</sub><sup>2-</sup>). Thus, the sulfur balance can be represented by



The Eh poisoning couples are set by the equilibrium of thiosulfate with either sulfate or sulfide, depending on mass balances. The presence of thiosulfate has been confirmed by ion chromatographic analysis of pore fluid extracted under nitrogen from mature slag-cement pastes. Based on its general chemistry, thiosulfate participates readily in a wide range of oxidation-reduction reactions. For example, thiosulfate reduces aqueous hexavalent chromium rapidly and quantitatively to trivalent chromium.

Unfortunately, the literature disagrees on the thermodynamics of sulfur in alkaline aqueous media. The Pourbaix atlas (Pourbaix, 1974) shows two versions of the sulfur-water system: one with and the other without a stability field for thiosulfate. During oxidation of pyrite present in Boom Clay, which is a geologic formation being studied for geological disposal of high-level waste and is present in the subsurface of a characterization facility in Mol, Belgium, both sulfite (SO<sub>3</sub><sup>2-</sup>) and thiosulfate (S<sub>2</sub>O<sub>3</sub><sup>2-</sup>) form. These uncertainties about the nature of the redox controls raise uncertainties in estimating the Eh poisoning capacity of slag-cement blends. When considering the evolution of the grout redox potential for long time periods, important questions arise regarding the possible speciation of sulfur and whether continued formation of thiosulfate can be assured as slag hydrates slowly, perhaps over centuries or more, and continues to release chemically reduced sulfur. For the present assessment, thiosulfate is assumed to control Eh, but additional studies are needed to demonstrate the validity of this Eh control and to

determine the poisoning capacity of slag–cement formulations proposed for tank closure use. These studies could include a redetermination of thiosulfate stability in aqueous alkaline media.

Uncertainties about the long-term Eh in slag–cement blends also arise because of the potential for reduced sulfur species to react with the iron oxide component of Portland cement. For example, ferric iron ( $\text{Fe}^{3+}$ ), normally present in Portland cement, could be reduced to ferrous iron ( $\text{Fe}^{2+}$ ), or the products of iron and steel corrosion could react with sulfide sulfur to form sulfide minerals. The cement also may contain manganese, probably as  $\text{Mn}^{3+}$ , which could participate in redox reactions with sulfide. Thus, important questions remain to be answered concerning the origin, controls, and long-term poisoning of Eh in grout formulations proposed for tank closure.

### **Effect of Fly Ash on Redox Potential**

Fly ash is also a potential source of reducing species. Commercial fly ashes are more “reduced” than cements. Very high temperatures may be achieved during coal combustion, resulting in an iron oxide component with mixed (ferrous and ferric) oxidation states. Thus magnetite, a solid solution between  $\text{Fe}_3\text{O}_4$  and  $\gamma\text{-Fe}_2\text{O}_3$ , is frequently recorded as present at several weight percent. Moreover, fly ash may contain unburned carbon. The form of this unburned carbon is variable, ranging from essentially amorphous to poorly crystallized graphite. There are no formal limits, other than indirect restrictions, on the content of unburned carbon in fly ash permitted by standards or specifications [e.g., ASTM C618–05 (ASTM International, 2007g)]. The indirect restriction arises because unburned carbon would increase the amount of water needed to reach a given consistency. However, it is likely that commercial fly ashes with up to 4 to 5 weight percent carbon will be passed as acceptable for cement blending conducted under industrial standards. In experiments up to 1 to 2 years’ duration, fly ash containing carbon did not appear to affect the Eh of cement–fly ash blends (Atkins, et al., 1989). Whether the reducing potential of carbon will become operative over a 10,000-year time scale is not known.

### **Effect of Steel Components on Redox Potential**

The corrosion of steel components, such as the tanks, cooling coils, and process lines, potentially could affect the evolution of the grout redox potential. Steel embedded in cement normally will corrode slowly—measured rates of corrosion in the absence of significant inward diffusion of oxygen are on the order of 1 to 2  $\mu\text{m}$  [ $3.9$  to  $7.9 \times 10^{-5}$  in] per year (Saqoe-Crenstil and Glasser, 1989a,b). But as discussed in Section 4.1.4, higher corrosion rates can arise from a general breakdown of the passive oxide layer protecting the metal surface due a reduction in the pH of the cement pore solution, predominantly through carbonation, or from a localized breakdown of the passive film by ingressing chloride ions. Under the alkaline pH conditions of cement pore waters, the dominant cathodic reaction is oxygen reduction [Eq. (4-11)]. Because the steel tank surrounds the inner grout, oxygen consumption during steel tank corrosion (see Section 4.1.4) may help conserve the reducing potential generated by the presence of slag in the inner tank fillings. Reduction of water to  $\text{H}_2(\text{gas})$  also occurs, although this reaction is very slow and significant only at very low corrosion potentials. However, the  $\text{H}_2(\text{gas})$  produced may extend and spread the envelope of reduced grout.

### **Effect of Radiolysis on Redox Potential**

Radiolysis of water also could affect the grout redox potential. Radiolysis is the dissociation of molecules by radiation. The primary products of the radiolysis of water molecules include the

radicals  $e_{aq}^-$ , H, OH, and  $HO_2$  (or an ionic form of the radicals); molecular hydrogen ( $H_2$ ); and molecular hydrogen peroxide ( $H_2O_2$ ) (Spinks and Woods, 1990). The radicals  $e_{aq}^-$  and H are reducing radicals because they bring about reduction in inorganic solutes. Conversely, OH,  $HO_2$ , and  $H_2O_2$  are oxidizing products because of their ability to oxidize inorganic solutes. Therefore, radiolysis can locally modify the redox condition of the system.

For grouted tanks, radiolysis likely will be confined to the contact zone between cement grout and residual waste at the tank bottom or tank wall. The peroxide species arising from radiolysis can be contained in plain cement, but almost certainly will interact strongly with chemically reduced sulfur species furnished by slag. Thus, a relatively thin zone of grout, but one critical to the solubilization of radionuclides, may more rapidly deplete reductants than the bulk of the tank filling material. For cementitious waste forms such as saltstone, radiolysis and the consequent depletion in reductants likely will occur more homogeneously in the cement-based material.

### 8.2.3 Shrinkage

Portland cement-based materials, including grouts, mortars, and concretes, tend to shrink in the course of setting and hardening. An important consequence of shrinkage in the present context is cracking. Cement is an intrinsically brittle material and has low tensile strength such that its natural response to shrinkage, in the absence of restraint, is to crack. Cracks potentially can serve as fast or bypassing pathways to exchange matter between the external environment and the cement-based material or waste form (see Sections 6 and 8.3.1). Thus, a concern when evaluating the performance of cement-based engineered barriers is that the low permeability, as measured on uncracked laboratory specimens, may not be attained in scaled-up emplacements and that the permeation properties derived from small-scale tests cannot be applied to predictions of the long-term evolution of grout masses.

The processes that contribute to shrinkage of Portland cement are complex but have been identified (Stang, et al., 2007). However, as mentioned in Section 5, the consequences of shrinkage in terms of the timing, spacing, width, and depth of resulting cracks are less amenable to quantification, although progress is being made (Bolander, et al., 2007; Radlinska, et al., 2007; Bamforth, 2007). The difficulty arises partly as a consequence of physical scale; large masses of cement-based material behave differently than laboratory-sized samples and undergo a heterogeneous thermal excursion during hardening. Other processes such as bleed, segregation, and compaction also cause heterogeneity that inevitably is greater at the bottom of the mass of cement-based material than at the top.

Some general principles applicable to the hardening process of Portland cement-based materials also apply to the grout that is emplaced in waste tanks and concrete vaults. Tank grouting is initiated by mixing essentially dry powders with water at a batch plant. Thereafter, the fluid grout has to be transported and emplaced into the waste tanks and vaults, perhaps by pumping or trucking or some combination of transport. At the emplacement stage but before significant chemical reaction has occurred, the total volume of the fluid grout system is composed of liquid water and the solid grains of cement, supplementary cement materials (i.e., fly ash and blast furnace slag), and aggregate particles (i.e., sand). However, chemical reaction begins within minutes of emplacement such that as hydration proceeds, the volume fractions of liquid water and reactive components diminish while the volume fraction of solid hydration products increases. The hardening process also results in a rapid physical set (i.e., the mass becomes more rigid and is progressively less capable of undergoing plastic

deformation on ordinary time scales). However, the conversion of liquid water into bound water (i.e., contained in the structure of the solid cement hydrates) is such that the effective volume fraction of the hydrates formed is less than that of the reactants. This reduction in volume, referred to as chemical shrinkage, is characteristic of all Portland cement-based materials.

Chemical shrinkage is essentially irreversible and, therefore, tends to be an important parameter contributing to early age cracking. The magnitude of the chemical shrinkage and the resulting potential for stress accumulation are influenced by cement fineness as well as by the amount and particle size of any supplementary cement material. Experience in using a particular grout formulation often is used as a guide to the approximate shrinkage that could occur. However, the grout formulations DOE used or plans to use for tank grouting are not commonly used in industry, resulting in insufficient experience to estimate potential shrinkage of the tank grouts. Thus, shrinkage measurements for the specific tank grout formulation appear to be necessary to provide such estimates. In addition, although good progress has been made in relating shrinkage to accumulated strain (Biernacki, et al., 2007; Lura and Jensen, 2007), basic data that can be used in modeling strain and shrinkage is lacking for the DOE tank grout compositions.

At longer ages and in the posthardened state, other shrinkage mechanisms can become operative. For example, wet–dry cycles also induce dimensional change in hardened grouts. However, unlike chemical shrinkage, wet–dry cycling tends to result in reversible or nearly reversible dimensional changes, with shrinkage occurring during the drying phase and dilation occurring upon rewetting. As mentioned in the preceding paragraph, no specific studies regarding the initial chemical shrinkage of the grout proposed for tank closure appear to have been conducted nor do the impacts of wet–dry cycling on dimensional stability of the grout mass appear to have been evaluated.

With respect to shrinkage potentially separating hardened grout and steel (e.g., tank walls or steel pipes), it is not common to observe such separation in old, steel-reinforced structures that have been demolished. This lack of separation arises because in such structures, the reinforcements typically have relatively close spacing such that shrinkage between bars is relatively small. Also, reinforcement bars are deliberately patterned to increase adhesion between the bars and the matrix. Although bars are not always in good physical contact with the matrix, this observation typically is ascribed to the uneven quality of the original construction (e.g., inadequate compaction or presence of local excess of water permitting aggregates to settle under gravity in a still-fluid mix). In a grouted tank, the pipes are not spaced optimally to constrain shrinkage such that stresses that may lead to physical loss of coherence between the hardened grout and steel components are more likely in this system than in reinforced concrete structures. Furthermore, separation of hardened grout from steel depends on the strength of the bond that develops between the two materials. If, for example, the steel surface was oily or had a layer of contaminants or corrosion products, the bond would be poor and at least some of the shrinkage would be expressed in the formation of a gap between the grout and steel. Thus, the steel–cement interface potentially could be irregular and provide a fast pathway for the movement of fluids.

#### **8.2.4 Cracking Due to Thermal Effects**

The processes discussed in the preceding subsection operate under isothermal conditions, but an important characteristic of cement-based materials is the liberation of heat during hydration and setting. This heat can be substantial; for example, Odler (1998) gives the heat of hydration of tricalcium silicate, which comprises about 60 percent of a modern Portland cement, as

520 kJ/kg [224 BTU/lb].<sup>2</sup> This self-heating commonly is not evident in small-scale laboratory simulations, but it is characteristic of scaled-up grout pours. Thus, although grout will be emplaced in DOE tanks and vaults at or near ambient temperature, the exothermic hydration reactions will cause the setting grout mass to experience a temperature rise. Because much of this heat is liberated within the first few to tens of days of hydration, if the heat is effectively contained, a thermal excursion is expected to be superimposed on the maturing grout.

The magnitude of the temperature rise will depend upon the grout formulation, size and geometry of the pour, and the rate at which the evolved heat can be dissipated. Inert aggregate, such as sand, will act as a heat sink and decrease the exothermic reaction of the cementitious portions, and thus reduce the thermal excursion. The reaction of fly ash and slag with cement also is exothermic, but the rates of reaction and heat release are much slower than for Portland cement hydration resulting in a thermal pulse from cement blends that is spread out over a longer period of time. On the other hand, the large volume of individual grout pours<sup>3</sup> and the buried nature of the tanks and vaults reduce the opportunity for heat to escape. Normally, as in isothermal hydration, the reactions of fly ash and slag do not contribute markedly to heat flow. Indeed, these supplementary cement materials behave as semi-inert diluents because of their slow reaction with cement. But the kinetics of fly ash and slag reaction are very temperature dependent such that isothermal data may significantly underpredict the potential for short-term heat release and, hence, the magnitude of the resulting thermal excursion. These kinetics are very dependent on the specific reactivity, as well as the particle size distribution, of the material, and it is not practical to estimate the temperature rise without knowing the exact characteristics of the cementitious components, the initial pour temperature, and the capability of the surrounding concrete vaults and soils to act as thermal sinks or insulators. Without adequate data, it is difficult to assess the magnitude of the thermal excursion arising in the course of tank grouting.

A number of computer programs are available to calculate the thermal excursion in mass concrete. It is necessary to input a particular geometry—not difficult in the case of tanks—and the magnitude and time dependence of the exothermic heat output of the grout. It is largely these latter data that are lacking, although the spreadsheet model of Bamforth (2007) allows the option of calculating the thermal excursion for a cement–fly ash–slag mixture. In any event, such calculations should be made before the final grout formulation is selected and the pour schedule specified as part of a deliberate effort to control cracking and thermal stress during tank grout hydration. Using such calculations, the grout formulation can be optimized and the pour schedule modified, if necessary.

Once cement is set and hardened in warm conditions and subsequently cools, thermal contraction is inevitable. At the outset of cooling, the thermal stresses generated by cooling are accommodated in the concrete matrix. But as cooling continues, stress accumulation exceeds the tensile strength of the matrix and the matrix cracks. The nature and the geometry of cracking occur partly in response to the transient thermal gradients arising during the thermal excursion and partly to the intrinsic properties of the matrix at early ages, including chemical shrinkage (Radlinska, et al., 2007). Low strength grouts characteristically crack readily because the critical stress to cracking is low. Stress typically is relieved by forming a network of fine cracks. However, tanks have some restraint (e.g., from tank walls and internal pipework).

---

<sup>2</sup>If a standard steel drum {200 L [53 gal]} is filled with a cement–water slurry and allowed to dissipate heat through the drum walls into air at 20 °C [68 °F], the centerline temperature in the drum will reach 100 °C [212 °F] within 10 to 18 hours.

<sup>3</sup>The tank grout is emplaced in several layers. At the Idaho National Laboratory, the volume of each grout layer emplaced in the large tanks is on the order of 268 to 344 m<sup>3</sup> [350 to 450 yd<sup>3</sup>].

Moreover, the complex history of grout pours (size, geometry, time between successive pours, etc.) makes it impossible to exactly calculate the thermal regime. Data to even commence this task are not available and, in any event, there is little practical experience with the DOE grout formulations with which to benchmark calculations.

Large-scale trials could allow cracking to be measured. The basic goals of large-scale trials should comprise more than a feasibility demonstration. Thermal cycling affects cracking and, partly for that reason, laboratory-scale products often achieve significantly better permeation properties than nominally identical products made to full scale. For tank-filling grouts, differences in scale strongly influence the permeation properties of the hardened product. In addition, the layered sequence of tank grouting could impose additional stress if there is a sufficiently high thermal gradient between a new and warm grout pour and a preceding, already cool grout layer. If cracking occurs in response to the coupled impacts of chemical shrinkage and thermal excursion, it should be apparent within a month. Note that if a badly cracked grout product is obtained, the analysis of postcooling features and processes in grout becomes somewhat simpler because other features and processes in the postclosure period leading to additional small increases in permeability diminish in importance: the crack network developed during the initial cycle of heating and cooling would dominate subsequent flow and mass transport. Additional cracking arising from wet–dry cycling might well make only a minor impact on the permeation properties of an already badly cracked matrix.

Furthermore, published literature on warm-cured cement products discloses that the minerals formed at elevated temperatures are unstable at lower temperatures {15 to 25 °C [59 to 77 °F]}. The main feature of this process, or at least its most damaging aspect, arises from the dissolution or partial dissolution at elevated temperature of ettringite, a hydrated calcium sulfoaluminate phase. However, the dissolution reaction of ettringite is slowly reversible with decreasing temperature. The ettringite reformation process has been termed “delayed ettringite formation.” This process tends to result in physical expansion; ettringite has a notably higher molar volume than its precursors. The industry lacks guidance on elevated temperature cure, and several expert groups are presently drafting codes of practice for warm-cured cement products. These recommendations will apply to constructional concretes, not grouts. While final reports from these groups are not yet available, the general approach seems to be to recommend a maximum upper cure temperature, or range of temperatures, depending on cement composition. For normal Portland cements, this temperature is likely to be limited to a maximum of 50–60 °C [122–140 °F]. This range in maximum temperature is much lower than the values given in DOE reports on grout trials (e.g., Shaw, 2006) where the upper temperature limit has been variously given as 70–80 °C [158–176 °F].

### **8.2.5 Cracking Due to Moisture Changes**

As noted previously, cement compositions require a minimum amount of water to achieve sufficient workability. The workability requirements for tank closure are not onerous by conventional grouting standards. The fresh mix will have to be emplaced, most likely by pumping, but emplacement is complicated by the need to fill annular spaces, such as the space between the tank and the concrete vault wall, and to flow around and into pipes and ducts. A weight ratio of water to cementitious material in the range 0.45 to 0.55 or higher likely will be required to achieve the required consistency. Thus, more water will be added than is required for complete hydration of the solid components of the grout (assuming a mixture of Portland cement, fly ash, and slag). The excess water will be trapped in the pores of the hardened grout. Given that permeability measurements of hardened grouts show that low permeability is achieved (see Appendix A), the pores thus generated must be relatively isolated from each

other. Nevertheless, much water will remain trapped in the hardened grout. The amount of trapped water is difficult to estimate without knowing the formulation and the hydration kinetics of its components. If Portland cement hydration is taken as a benchmark, 80 to 90 percent hydration probably will be achieved within 90 days, but fly ash and slag will hydrate much more slowly. Fly ash also will contain a substantial content of solid that is unreactive with cement, and no reliable means are presently available to estimate the reactive content. Thus, it appears likely that in the absence of rigorous drying, the grout pore network will continue to be at least partially water filled. If water is conserved, an additional source of shrinkage—self-desiccation (discussed next)—is avoided.

Spontaneous migration of liquid water through hardened matrices is not necessarily negligible, especially if a mixture of filled and unfilled pores persists. The potential for heat evolution and thermal excursion in large grout masses was noted previously. The resulting thermal gradients tend to drive the migration of water from warm to cool regions. The peak heat evolution occurs well before the grout matures such that the matrix can be expected to be permeable. Thus, considerable moisture transport can be expected to occur during the immediate period after grout emplacement. In the longer term, moisture transport also will continue to be driven by residual thermal gradients, as well as by coupling and moisture transport between the grout and its service environment as externally driven wet–dry cycles occur. Long-term dimensional changes will occur in the grout in response to the inhomogeneous water distributions, and these gradients will contribute to cracking.

The literature broadly describes two mechanisms of cracking in response to moisture changes. One such mechanism, self-desiccation, operates mainly in low permeability, low water content matrices. Matrices prone to self-desiccation typically are formulations with low ratios of water to cementitious materials, and shrinkage of the cement-based material occurs primarily in response to depletion of pore water as hydration approaches completion (Jensen, 2005). Modern “high performance” cement matrices afford an excellent example: the high potential to resist internal migration and diffusion from the service environment is compromised by spontaneous crack development. At higher water contents where pores remain partly water filled, a second shrink–swell mechanism may be operative (Benbovdjema, et al., 2007). However, this process, which results from inhomogeneous water distributions, and its potential to generate stresses that can only be relieved by cracking are not well understood.

Insufficient information is available on the DOE grout formulations to determine whether they are inherently likely to undergo self-desiccation. But there is little doubt that the physical consequences of inhomogeneous water distributions, whether created during fabrication or generated subsequently as a consequence of the natural evolution in the service environment, ultimately will be an important factor in the evolution of cracks and changes in the physical properties of the grout. A potential complicating factor in the evaluation of these changes is the presence of bleed water and the addition to the emplaced grout of flush water, which is used to rinse the grout delivery system after grout emplacement. These waters could locally increase the water-to-cement ratio and the permeability of the hardened cement-based material.

## **8.2.6 Grout Curing Conditions**

Cement–fly ash–slag grouts require adequate cure conditions to achieve the intended benefit of low permeability. Typically, at least 6 months of moist cure at 20 °C [68 °F] is required to reasonably indicate long-term properties. The conditions encountered in tank closure are generally favorable to ensure a good cure: the grouts will be emplaced into closed tanks, pipes, and vaults with little opportunity for escape of moisture, except when the tank farm ventilation

system is kept on during grout emplacement and curing. Where significant escape of moisture is possible, shrinkage cracking is a potential concern. For example, in a full-scale grout test pour conducted at a field site at the Idaho National Laboratory Tank Farm Facility, visible cracks with approximately 1-m [3.3-ft] spacing were observed (Figure 8-5).<sup>4</sup> On the other hand, hardened grout inside tanks at the Idaho National Laboratory Tank Farm Facility observed through in-tank video cameras indicated no visible surface cracking (Flanders, 2007).

Even though sequential emplacement of large volumes may require some time, the sequence can and should be managed to minimize evaporation at any free interfaces. The one problem area that requires management is the interface between the grout and the concrete vault wall. If the vault walls are dry and porous, considerable water may be lost from the fresh, fluid grout to this concrete. Given that the thickness of the grout in the annular space between the vault wall and the steel tank is relatively narrow {e.g., ~60 cm [~24 in]} in some Savannah River Site tanks (National Research Council, 2006)} and that the performance of the annular grout is depended

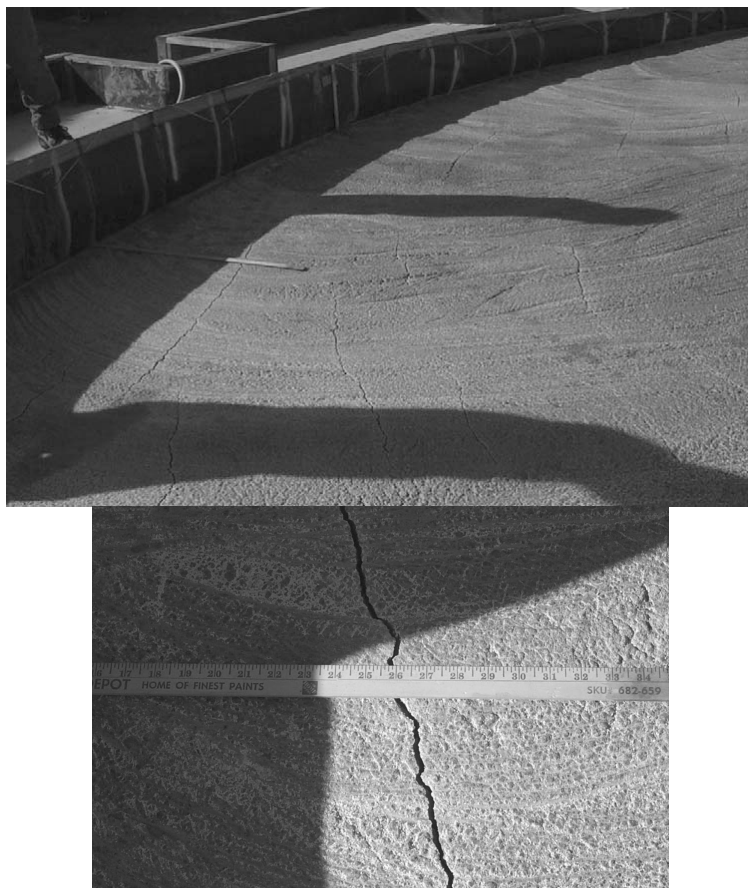


**Figure 8-5. Photographs Taken After a Test Grout Pour at the Idaho National Laboratory Tank Farm Facility Showing Visible Cracks at Approximately 1-m [3.3-ft] Spacing. Photographs Taken From DOE–Idaho (2006b).**

<sup>4</sup>The grout mix design used in the test comprised Portland cement {Types I and II, 145 kg [320 lb]}, Class F fly ash {290 kg [640 lb]}, sand {998 kg [2,200 lb]}, and water {up to 196 kg [433 lb]} per cubic yard of grout, plus high and medium range water reducing admixtures to enhance workability of the grout mixture without increasing the water content (Idaho National Engineering and Environmental Laboratory, 1999).

upon to control corrosion of carbon steel tank shells, the curing history of this portion of the grout acquires special significance in the overall performance model and requires special assessment if potential degradation (e.g., by sulfate attack) exists.

### 8.2.7 Waste–Grout Interaction

Interactions between the waste components and the grout can affect the setting, hardening, and strength development of the cement-based material. Studies have shown that a number of inorganic constituents, such as those listed in Table 8-5, interfere with the solidification of cement-based materials (Conner, 1990). For example, lead and zinc salts, phosphates, and borates are strong retarders of setting and hardening (Taylor, 1997). Sulfates also are known to strongly affect set—calcium sulfate commonly is added to clinker to control the early age hydration rate. But if sulfate is present in significant amounts in the waste, delayed ettringite formation can occur in the hardened cement-based material that could lead to cracking and

<b>Table 8-5. Inorganic Constituents That Affect Solidification of Cement-Based Materials*†</b>	
<b>Inorganics, General</b>	<b>Inorganics, Specific</b>
Acids	Calcium chloride
Bases	Copper nitrate
Borates	Gypsum, hydrate
Calcium compounds	Gypsum, semihydrate
Chlorides	Lead nitrate
Chromium compounds	Sodium borate
Heavy metal salts	Sodium hydroxide
Iron compounds	Sodium sulfate
Lead compounds	Sulfur
Magnesium compounds	Zinc nitrate
Salts, general	
Silicas	
Sodium compounds	
Sulfates	
Sulfides	
Tin compounds	
Zinc compounds	

\*Bone, B.D., L.H. Barnard, D.I. Boardman, P.J. Carey, C.D. Hills, H.M. Jones, C.L. MacLeod, and M. Tyrer. "Review of Scientific Literature on the Use of Stabilisation/Solidification for the Treatment of Contaminated Soil, Solid Waste and Sludges." Science Report SC980003/SR2. Bristol, United Kingdom: Environment Agency. 2004.  
† Conner, J.R. *Chemical Fixation and Solidification of Hazardous Wastes*. New York City, New York: Van Nostrand Reinhold. 1990.

matrix disruption. Nitrates of barium, copper, nickel, zinc, chromium, lead, and cadmium reduced cement hydration by up to 50 percent but also reduced the porosity of the hardened cement paste by up to 60 percent (Ouki and Hills, 2002). Calcium chloride and magnesium salts accelerate both the setting and hardening of Portland cement, whereas others, such as carbonates, can either accelerate or retard set depending on the concentration. Most organics also can retard or accelerate early hydration of cement, although in a Hills, et al. (1995) study, mature samples of cement mixed with organics displayed a similar phase composition to samples without organics and the observed effects on setting times and strength were small.

The interactions between waste constituents and the grout are complex, and the interference effects on cement hydration have been ascribed to various mechanisms, including precipitation or dissolution of cement phases, flocculation of the colloidlike solids, changes in the pH of the cement pore solution, precipitation of new solids, and sorption onto cement phases (van Eijk, 2001). The chemical form of the constituent can affect the mode of interference. For example, cadmium oxide acts as a retarder, but other cadmium compounds are recognized as retarders, accelerators, or have no effect (Stegemann, et al., 2000). Whether a particular waste constituent will interfere with the setting or hardening process depends not only on its amount but also on the other constituents present in the mixture. Some constituents that retard at low concentrations may accelerate setting at higher concentrations, and a constituent that by itself does not affect setting may cause problems when combined with other compounds (Hills and Pollard, 1997).

Because these interactions are complex, the consequences to the long-term performance of cement-based materials incorporating waste constituents are difficult to predict. For grouting of tanks with only small amounts of residual waste, such as the Idaho National Laboratory waste tanks, the consequence will be insignificant given the relatively large volume of grout that is emplaced compared to the volume of residual waste. However, for disposal concepts such as the Saltstone Disposal Facility at Savannah River Site in which radionuclide-bearing salt solution is mixed with cementitious materials to form a grout (saltstone) monolith, the interaction between the waste components and the grout must be considered. The Savannah River Site waste salt solutions have high concentrations of  $\text{NaNO}_3$ ,  $\text{NaNO}_2$ , and  $\text{NaOH}$  and lesser concentrations of  $\text{Na}_2\text{CO}_3$ ,  $\text{NaAl(OH)}_4$ , and  $\text{Na}_2\text{SO}_4$ . Heavy metals in the waste solutions, such as chromium, lead, zinc, mercury, and tin, are present only in trace amounts (parts per million level) (Cook and Fowler, 1992) and are unlikely to significantly affect the setting and hardening of the grout. But sulfate concentrations in the waste are sufficiently high that expansive reactions due to delayed ettringite formation are a potential concern. Laboratory studies (e.g., Langton, 1987a,b; Malek, et al., 1985) have been conducted to characterize the cured saltstone waste form (i.e., compressive strength, hydraulic conductivity, porosity, mineralogy, pore solution composition, and Toxicity Characteristic Leaching Procedure leaching). However, the short duration and the small scale of these tests make it unlikely that the effects of delayed ettringite formation on the physical properties of the cement-based material have been captured. In addition, no information is available on the potential effects of organic constituents unique to some of the Savannah River Site wastes (such as tetraphenylborates) on the physical properties, leaching characteristics, and long-term durability of the grouted waste form. These potential issues need to be evaluated.

### **8.2.8 Effect of Chemical Admixtures**

Chemical admixtures generally are mixed with Portland cement, water, and aggregate to improve the workability of cement and alter its physical properties such as compressive strength, durability, or setting time. There are five general classes of chemical admixtures

(Portland Cement Association, 2008): (i) water reducing, (ii) plasticizers (superplasticizers), (iii) retarding, (iv) accelerating, and (v) air entraining. Water-reducing admixtures usually reduce the required water content for a cement-based mixture by 5–10 percent and enable the cement-based material to achieve a required slump with less water. Superplasticizers, also known as plasticizers or high-range water reducers, reduce water content by 12–30 percent and enable the use of low water-to-cement ratio to make a high-slump flowing cement mixture that can be placed with little or no vibration or compaction. Retarding admixtures slow the setting rate of concrete, whereas accelerating admixtures increase the rate of early strength development, reduce the time required for proper curing and protection, and speed up the start of finishing operations. Air-entraining admixtures are used to purposely place microscopic air bubbles into concrete, which results in cement-based material that is highly resistant to severe frost action and cycles of wetting and drying or freezing and thawing. Specialty admixtures are those whose functions include corrosion inhibition, shrinkage reduction, alkali–silica reactivity reduction, workability enhancement, bonding, damp proofing, and coloring.

Grout formulations used or proposed for use in grouting tanks at DOE sites include superplasticizers (e.g., CH2M–WG Idaho, LLC, 2007; Langton, et al., 2007; Thorne, 2007). The superplasticizer enhances the workability of the grout mixture without increasing the water content, which determines the porosity of the material and thereby influences the mobility of radionuclides. A potential concern in the use of admixtures in tank grouts is their potential effect on the long-term grout performance. Based on available literature, Rixom and Mailvaganam (1999) concluded that superplasticizers will not have a deleterious effect on the physical properties of cement-based material. They stated that, in general, superplasticizers will not adversely effect strength or strength development of cement-based materials and, in fact, several studies have shown that an increase in strength may occur. Rixom and Mailvaganam (1999) also noted that most studies indicate cement-based materials with superplasticizers have shrinkage, creep characteristics, and resistance to sulfate attack similar to plain material.

An additional concern regarding admixtures is their effect on the sorption of radionuclides on cement solids or on radionuclide solubility in cement pore waters. After hydration of the cement-based material, admixtures that remain dissolved in the cement pore water may form soluble complexes with radionuclides (Greenfield, et al., 1998). For example, lignosulfonates, a type of water-reducing admixture, have chemical structures similar to humic substances, which form aqueous complexes with radionuclides. Gluconate, another water-reducing admixture, also forms aqueous complexes with radionuclides. In addition, sorption of admixtures on the cement surface may decrease the sorption of radionuclides on cement phases. Thus, admixtures could enhance the release of radionuclides from cement-based waste forms. There is very little experimental data regarding the effect of admixtures on radionuclide sorption or solubility. The Greenfield, et al. (1998) study indicated that the solubility of plutonium, uranium(IV), and americium is one to two orders of magnitude higher in cement-equilibrated water with admixture compared to water without additives. The result was ascribed to the formation of aqueous complexes of the radionuclides with the admixture and hydroxyl ions. On the other hand, a Glaus and van Loon (2004) study showed that admixtures did not affect the sorption of Ni(II), Eu(III), and Th(IV) on hardened cement paste. This result was ascribed to the sorption of admixtures onto the hardened cement paste, which decreased the concentration of admixtures in the pore water to levels at which radionuclide complex formation was no longer important.

Studies that have been conducted on admixtures involved tests of short duration. Also, relatively little is known about the ultimate fate of admixtures in cement-based materials, although sulphonated melamine formaldehyde, a superplasticizer, eventually becomes

denatured at high pH and undergoes irreversible precipitation into an insoluble form (Atkins and Glasser, 1992). Thus, it is not possible to draw conclusions about the effects of admixtures on the long-term performance of grouted tanks and cement-based waste forms. Additional studies to address this issue are warranted.<sup>5</sup>

### 8.2.9 Effect of Fly Ash Selection

DOE grout formulations do not impose any special restrictions on fly ash composition other than general suitability for grout making. However, highly variable results have been reported on the sulfate resistance of fly ash concretes, even if inadequately cured concretes are excluded from consideration. In this connection, Dunstan (1980, 1976) examined a series of fly ash concretes made using U.S. fly ashes, all of which were certified for concrete making. Large differences in sulfate resistance were found over a 5-year test program. Dunstan (1976) defined a factor, R, as

$$R = (C-5)/F \quad (8-2)$$

where C is the calcium oxide content and F is the iron oxide content of the ash, as determined from chemical analysis. Thus, high calcium oxide contents, above 5 weight percent, are adverse to performance, whereas high iron oxide contents are desirable. A series of expansion tests, which involved soaking test specimens in a sulfate-bearing solution and measuring the change in length of the specimen, was made up to 1,200 days using 25 percent replacement of cement by fly ash and with plain Portland cement as a control. These tests showed that sulfate resistance was greatly improved using ash having an R value less than 0.75, whereas moderate improvement was obtained at R values between 0.75 and 1.5. No significant change in sulfate resistance was observed for R values between 1.5 and 3.0, whereas the benefit of fly ash replacement was reduced at R >3.0.

The theoretical explanation for Dunstan's correlations is not clear. At the time of that work, fly ash characterization was relatively immature, so many questions about the mineralogy of the ash and the distribution of calcium and iron oxides remain unknown. Nevertheless, the empirical correlations are inescapable and were subsequently incorporated into the U.S. Bureau of Reclamation specifications, together with other safeguards regarding the selection of cement types (Pierce, 1982; Dunstan, 1984). It is apparent, therefore, that if sulfate attack is a potential problem at any of the tank closure sites and if fly ash grouts are used for cementation, then fly ash composition may be a crucial variable in the prediction of sulfate resistance.

With respect to the selection and durability of fly ash, Helmuth (1987) wrote

“The characterization of fly ashes for concrete unsoundness and durability is probably the most challenging of the technical problems, unless we choose to provide wide margins of safety. To assure long term durability of concretes that will be exposed to sulfate (and other aggressive) solutions in service, we need to be able to predict from the results of performance tests or from material characteristics, or both, that concretes made from these materials will have a satisfactory service life under these conditions. However, even for Portland cements, neither rapid test methods nor chemical compositions always rank

---

<sup>5</sup>Testing is necessary to ensure that grout formations containing admixtures mix properly and attain the required physical property. For example, in a laboratory study of grout formulations for tank closure at the Savannah River Site, a problem was encountered in initial tests using a viscosity modifying admixture with a high-range water reducing polycarboxylate admixture (Langton, et al., 2007). The authors indicated that further testing of admixtures is needed for full-scale production proportioning and mixing of the tank grouts.

different cements in the same order, nor do either always agree with experience. The inherent variability of fly ashes further complicates prediction of performance of concretes.”

Although these words were written more than 20 years ago and apply to conventional concretes rather than tank-filling grouts, they are entirely appropriate with respect to the present application.

### **8.3 Key Features, Events, and Processes in Open Systems**

Although many of the DOE tanks are located physically above the local groundwater table and an engineered cover likely will be emplaced above the grouted tanks and vaults to prevent meteoric water infiltration, interactions of the grouted engineered barrier with the external environment cannot be precluded when evaluating a 10,000-year performance lifetime. Thus, open-system features, events, and processes need to be considered.

#### **8.3.1 Fast Pathways and Bypassing Pathways**

As discussed in Section 6.0, despite the generally low permeability of cement-based materials (see Appendix A), cement-based structures, including those at DOE sites, have potential pathways for movement of fluids. For example, meteoric water has seeped into the concrete vaults used for secondary containment of waste tanks at the West Valley Nuclear Services site (e.g., Elmore and Henderson, 2001) and at the Idaho National Laboratory Tank Farm Facility (Cahn, et al., 2006). The exact pathway through which seepage occurred at these sites is not known. At the Savannah River Site Saltstone Disposal Facility, seepage of contaminated bleed water from saltstone during cure has occurred through cracks and construction joints in the reinforced concrete vault (Haney, 1994; Flanders, 2008).

These pathways, whether as construction joints or as cracks and conduits formed through mechanisms discussed in Section 8.2, are likely to be the primary avenues through which environmental fluids, such as infiltrating water and atmospheric gases, can interact with the grouted waste form and other engineered barriers. These environmental fluids can affect radionuclide releases by transporting radionuclides and by conveying chemical reactants that degrade the grout and engineered structures or change the chemical environment of the waste form thus increasing radionuclide mobility.

As discussed in Section 6, macrocracks that develop in the cement-based monolith after it hardens are the features most likely to act as fast pathways between the grouted waste form and the environment, although they also could act as bypassing pathways that limit the contact of environmental fluids with the grouted waste form and other engineered barriers. Conduits, which represent discrete fluid pathways that may be present or may develop along specific engineered features with known locations such as annular spaces between grout and a corroded tank, pipe, or rebar (see Figures 6-6 and 6-7), also could act as fast pathways or as bypassing pathways.

The mere presence of macrocracks and conduits in the grouted tanks and vaults does not determine whether environmental fluids will enter or leave the system. Rather, the flow of fluids through the system will be controlled by the boundary conditions. These external boundary conditions include the

- Degree of hydraulic saturation of the soil overlying and surrounding the grouted tank and vault
- Permeability contrasts between the grouted tank and vault and the surrounding soil
- Changes in water table elevation that may result in saturated conditions intersecting the tanks

Because the occurrence of these conditions is strongly site specific, their possible influence on the ability of macrocracks and conduits to serve as fast and bypassing pathways can only be discussed in general terms, as in the following paragraphs.

### **Effect of Degree of Hydraulic Saturation**

In theory, water from a partially saturated soil will enter a crack or conduit only if the capillary pressure in the crack or conduit is less (more negative) than that in the soil. The capillary pressure in the soil is determined by the pore size distribution of the soil and the degree of saturation in the soil. The capillary pressure in the crack or conduit is determined by the aperture distribution and degree of saturation in the crack or conduit. The smaller the soil pore or crack/conduit aperture, the less the capillary pressure at a given saturation. Assuming that the particle grain size in soil is roughly equivalent to the pore size, loamy soils would have pore diameters ranging predominantly from 1 to 100  $\mu\text{m}$  [ $4 \times 10^{-5}$  to  $4 \times 10^{-3}$  in] (e.g., Hillel, 1982). The size of crack apertures in cement-based materials can have a wide range—from microscopic microcracks to visible macrocracks. Neville (1996) characterized microcracks as cracks with apertures less than 100  $\mu\text{m}$  [ $4 \times 10^{-3}$  in]. Macrocracks are discrete fractures in a concrete material that may be visible to the naked eye and, based on Neville's criterion, would have apertures greater than 100  $\mu\text{m}$  [ $4 \times 10^{-3}$  in]. Because the capillary pressure in the soil is controlled by the smaller pores, water would not be expected to be imbibed by the crack or conduits from the soil except under relatively high water saturations in the soil.

This ideal situation may not be realized under actual conditions, because soils are not homogeneous, even in engineered soil covers, and may contain cracks, root tubes, and animal burrows (such as worm and invertebrate tubes as well as macrovertebrate burrows). These macroscopic soil features have much larger diameters than the soil pores and, thus, would be preferential pathways for water percolation. If these soil features contact macrocracks or conduits in the cement-based material, water may be directly imbibed from the soil. However, it is more likely that percolation through the soil heterogeneities would lead to saturated lenses or films of water on an intact, cement-based structure that could flow into macrocracks and conduits. Such perched water conditions are discussed in the next subsection.

### **Effect of Permeability Contrasts**

The tanks and vaults such as those at the Idaho National Laboratory and the Savannah River Site (Figures 8-1 and 8-2) have lower water permeability than the soil in the overlying engineered cover or the surrounding native soil. These structures are also very large in terms of their surface area in contact with the overlying soil that may be used in engineered covers. Thus, these structures have large footprints to intercept percolation through soil heterogeneities, which would result in locally saturated conditions and promote water percolation into macrocracks and conduits of the cement-based structure. Even in the absence of soil heterogeneities, the large surface area would result in increased water saturations above the

tank or vault due to diffuse water movement through the soil. This effect is illustrated in Figure 8-6. Asperities associated with tank external penetrations and structures also could act as focal points for increased saturation and percolation into cracks and conduits. In addition, saturated conditions may develop on concrete foundations below the tank if water percolates through the annular space (if present) between the tank and vault. Such perched water could enter the tank and contact the waste form from below rather than above the tank.

### Effect of Changing Water Table Elevation

A rising water table could cause water to flow into the vaults and tanks from below rather than above the tank or vault. If the water table rises above the base of the tank, water can contact the grouted waste form under saturated conditions. Under this condition, the flow through cracks and conduits will be controlled by their saturated hydraulic conductivity and the hydraulic gradient. Entry of groundwater into the grouted waste form also could be enhanced by the presence of sand beds and other drainage layers below the tanks.

If the water table falls, the reverse sequence of events would occur. Some portion of the water that entered the grouted waste form through cracks and conduits would be retained in the grout matrix and in the cracks and conduits, depending on their initial saturation. It is possible that sand beds or drainage layers beneath the tanks could act as a capillary barrier to flow during a falling water table. The mitigation effects of the sand or drainage layers would likely be small, however, because the highest water flow from the waste form will occur under saturated, rather than unsaturated, hydrologic conditions.

Conceptual and mathematical models that can evaluate the potential influence of fast pathways and bypassing pathways in engineered barriers on radionuclide release are discussed in

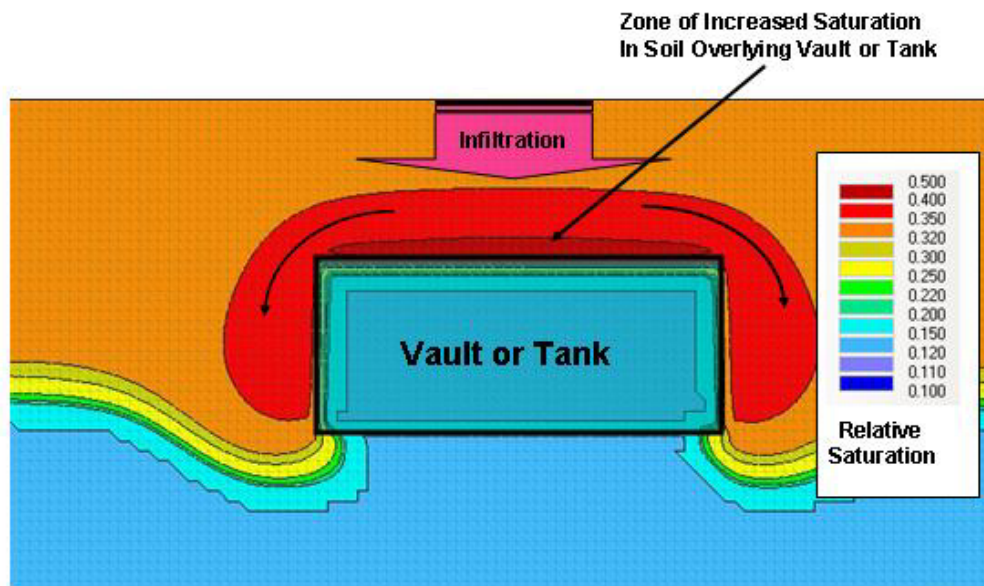


**Figure 8-6. Illustration of Water Flow in the Hydrologically Unsaturated Zone Around a Vault or Tank Due to Increased Saturation Above the Vault or Tank**

Section 6. But as pointed out in that section, with the exception of relatively discrete fracture diffusion models, these modeling approaches have not been applied to study radionuclide releases from grouted tanks or the effect of environmental fluids on long-term grout integrity. Models for simulating flow and transport associated with fast and bypassing pathways are of limited value without estimates of the nature, extent, and properties of pathways that may be present or form in grouted tanks and concrete vaults. Such information is not available for DOE grouted tanks and vaults and precludes a quantitative evaluation of the influence of these pathways to radionuclide release from these tanks and vaults. Large-scale experiments designed to simulate physical processes and features that may result in macrocracks and conduits in tank grout monoliths, including potential separation of grout from tank walls and tank pipes, could provide useful information and would be useful to pursue.

### 8.3.2 Carbonation of Tank Grouts

As mentioned previously, many of the tanks are physically located above the local groundwater table and an engineered cover likely will be emplaced above the grouted tanks and vaults to prevent infiltration of meteoric water. As long as this situation holds and the tank grouts are protected from direct contact with liquid water, the grouts will not be subject to leaching and mass exchange between the grouts and their service environment will be confined principally to reactions involving vapor transport. Under this scenario, carbonation would be the likely mechanism of tank grout degradation. As discussed in Section 4.1.1, the potential consequences of grout carbonation are twofold: (i) the pH of the grout pore water diminishes to values that accelerate steel corrosion and (ii) the grout shrinks.

Table 8-6 identifies some of the environmental factors affecting carbonation that require characterization. Of particular importance is the thickness of the grout cover protecting the steel

<b>Table 8-6. Environmental Factors Affecting the Interaction Between Soil Gases and Cement–Steel Composites</b>	
<b>Soil</b>	<b>Engineered Barriers (Cement, Steel)</b>
<i>Steady State</i>	<i>Steady State</i>
$p\text{CO}_2$ , $p\text{O}_2$ Rate of $\text{CO}_2$ production Gas transport characteristics Moisture state	Slow matrix and diffusion rate changes for gas ( $\text{CO}_2$ , $\text{H}_2\text{O}$ , $\text{O}_2$ ) Dimensional changes and crack growth Quantification of $\text{CO}_2$ and pH/Eh buffering/poising reserves
<i>Perturbing Effects</i>	<i>Perturbing Effects</i>
Construction disturbance	Engineered cover failure and changed water regime
Climate change, vegetation, and land use changes Groundwater level fluctuations	Carbonation front reaches the steel reinforcement of the concrete vault or the steel tank: onset of rapid corrosion regime*
*Carbonation through the thickness of the grout cover over carbon steel is taken as the initiation period for steel reinforcement corrosion (for concrete vault degradation analysis) or for steel tank corrosion (for grouted tank degradation analysis). For the latter, the thickness of the grout in the annular space separating the steel tank and the concrete vault provides an additional grout cover. In some Savannah River Site tanks, the annular space is 60 cm [24 in] (National Research Council. "Tank Waste Retrieval, Processing, and On-site Disposal at Three Department of Energy Sites: Final Report." Washington, DC: National Academy Press. 2006.). The U.S. Department of Energy tanks and vaults have different constructions, and the thickness of the grout cover will vary.	

reinforcement (of concrete vaults) or steel tank from corrosion. The grout cover will experience inward diffusion of carbon dioxide and, once the initial high pH is neutralized, steel can corrode rapidly. Because the annular space between the concrete vault and the tank will be grouted, this annular grout will afford additional protection of the steel tank from corrosion, although this protection could be reduced if preferential pathways for carbon dioxide diffusion develop along the interface of the grout with process/transfer lines that penetrate the vault, annular grout, and steel tank (e.g., Figures 6-6 and 6-7).

While some of the factors listed in Table 8-6 must be derived from onsite studies, such as determining the present level of biotic activity leading to CO<sub>2</sub> generation, other factors may require expert elicitation (for example, the impact of future climate states on rates of CO<sub>2</sub> generation), whereas others require research, such as the evolution of cracking in the specialized grout formulations. Probably the main effort should be to understand and quantify the steady state factors; an attempt is made to assess grout degradation predominantly by carbonation in Section 8.5.2.

### **8.3.3 Environmental Effects on Redox Potential**

An important issue particularly with an open system that allows interaction of the grout with its service environment is the long-term persistence of the reducing capabilities of the grout. As pointed out in the National Research Council (2006) report, although the use of cement-based materials in the construction industry has provided some understanding of the mechanisms of reduction in pH of cement pore waters over time, no such information is available to provide an understanding of the persistence of reducing Eh over time. With respect to externally imposed changes in redox potential, the oxidant of most concern is oxygen, which could react with and reduce the Eh poisoning capacity of slag. Experimental data indicate that slag oxidation is a fast reaction (Lukens, et al., 2005). Oxygen can be present in the gas phase or dissolved in infiltrating water, and the relative importance of each phase will depend on the flow pathways through the grout, the hydrologic saturation condition, and the flow rate of infiltrating water. The presence of cracks or conduits could facilitate the oxygen influx into the grouted system, but slow oxygen diffusion into the grout matrix could limit redox changes to areas along the interface of the crack or conduit with the grout. Additional considerations with respect to environmental effects on the grout redox potential listed in Table 8-6 include the properties of the near field, such as the character of gases diffusing inward and possible changes in gas composition with time; for example, climate change or future land use, or both, could affect the situation.

### **8.3.4 Leaching and Wet–Dry Cycling**

All DOE tank farm sites have relatively old (up to ~60 years) concrete constructions, and it is likely that it would be evident if highly aggressive waters are present at the sites. In the absence of such evidence and because most of the tanks are above the local groundwater table, Section 8.5.2 focuses on carbonation as the degradation mechanism. However, in some DOE sites, the elevation of the groundwater table is above that of the tank floor, which could degrade and result in the tank heel contacting groundwater that has not been substantially altered by the chemically tailored grout atop the tank heel (National Research Council, 2006). Moreover, failure of the engineered cover, as well as episodic flooding, also may occur and allow water to infiltrate and contact the grouted tanks and concrete vaults. In such scenarios, degradation is likely to occur by a combination of leaching, carbonation, and wet–dry cycling.

In this context, note that the solubility of calcite is generally several orders of magnitude less than that of portlandite. Thus, carbonation may actually have a favorable influence on performance if the grout is not also required to provide a high local pH.

### 8.3.5 Sulfate Attack

Sulfate attack also could contribute to grout degradation if the sulfate concentration in the groundwater is sufficiently high. Available groundwater chemistry data for the Savannah River Site indicate low sulfate concentrations [ $<15$  ppm (Prikryl and Pickett, 2007; Table 2-1)]. Under those conditions, grout degradation due to sulfate attack is unlikely to be significant in the short term (see Table 4-5), although a quantitative assessment is necessary to determine its significance to grout performance in a 10,000-year period. Analyses of perched and aquifer water samples collected at the Idaho National Laboratory also show low sulfate concentrations [ $\sim 20$  ppm (Prikryl and Pickett, 2007; Table 3-3)]. However, samples taken from wells tapping into the Snake River Plain aquifer underlying the Idaho National Laboratory show sulfate concentrations can be moderately high [the range is 2 to 220 ppm (Prikryl and Pickett, 2007; Table 3-2)] such that grout degradation due to sulfate attack is more likely at this site than at the Savannah River Site.

## 8.4 Immobilization of Technetium in Tank Grouts

One of the radioelements present in tank waste heels is technetium (Tc). This radioelement is of special concern because of its radiotoxicity and its mobility under oxidized conditions. It is one of the radionuclides that dominate the long-term risk to the public from disposed tank waste (Cook, 2005). Thus, it is detailed in this section. The solubility of technetium and other selected radioelements in environments expected in DOE cement-based disposal facilities also is discussed in Appendix B. Technetium is a synthetic element and, on that account, no geochemical data are available on its long-term behavior in nature. Laboratory studies disclose the existence of two principal oxidation states, Tc(IV) and Tc(VII), depending on the redox conditions. Tc(IV) and its complexes and compounds form at Eh values below about 220 mV in neutral pH conditions, whereas at Eh values above this, they occur in the Tc(VII) state as the pertechnetate anion ( $\text{TcO}_4^-$ ) over the complete pH range of natural waters (Brookins, 1988; Sparkes and Long, 1988). The Tc(VII) state is relatively soluble and, as pertechnetate, interacts only weakly with mineral surfaces (Palmer and Meyer, 1981; Walton, et al., 1986), making it very mobile in oxidizing environments. The Tc(IV) state is relatively immobile; it is strongly sorbed to mineral surfaces and forms sparingly soluble solids, reported variously as  $\text{TcO}_2$ ,  $\text{TcO}_2 \cdot n\text{H}_2\text{O}$ , and  $\text{Tc}_2\text{O}_7$  (Rard, et al., 1999).

Technetium has no stable isotopes and, therefore, much of its chemistry has been deduced by studies on fully active samples and by analogy with the chemistry of rhenium (Re). Similar to other relevant parts of the periodic table, a close relationship undoubtedly exists between the two; for example, there is direct experimental verification of the Tc(IV) and Tc(VII) states, both of which would be predicted from rhenium chemistry, and of the ease of the oxidation of Tc(IV) to Tc(VII) as well as the reverse reduction reaction. But the numerical value of the redox potential for the reversible reaction for technetium cannot be deduced from that of rhenium and, moreover, direct determination of potentials in this system has been handicapped by instability of the electrode system. Rard, et al. (1999, pp. 74–92, and Appendix A) provided an extended discussion of the many uncertainties affecting knowledge of technetium chemistry. Although Rard, et al. (1999) gives recommended values, considerable uncertainty must be attached to the numerical values.

Further uncertainties arise concerning the application of technetium data to alkaline systems and cementitious media. These uncertainties are principally (i) the composition and crystallinity (or lack thereof) of the solid Tc(IV) reaction products obtained at high pH; (ii) possible aqueous complexation of technetium by carbonate and its impact on speciation and solubility; and (iii) possible interactions between technetium, especially Tc(IV), and sulfur species. As discussed in previous sections, blast furnace slags are used in DOE-proposed grout formulations to provide redox controls for technetium by reducing Tc(VII) to Tc(IV). It has been suggested that at high sulfide activities and low Eh, technetium will not be precipitated as an oxide or hydrous oxide but instead as the sulfide  $\text{TcS}_2$  under reducing conditions, but at higher Eh, as  $\text{Tc}_2\text{S}_7$  (Rard, et al., 1999). A recent study using extended x-ray absorption fine structure spectroscopy (Lukens, et al., 2005) indicated that the compound generally referred to in the literature as " $\text{Tc}_2\text{S}_7$ " has a stoichiometry corresponding to  $\text{Tc}_3\text{S}_{10}$ , consistent with a structure consisting of triangular clusters of Tc(IV) centers linked together through a combination of disulfide and sulfide bridges, as in  $\text{MoS}_3$ .

From the perspective of waste form performance, there appears to be abundant experimental evidence that, whereas technetium is readily leachable from ordinary Portland cement matrices, slag-rich cement matrices significantly reduce leaching of technetium (Smith and Walton, 1993; Aloy, et al., 2007). Thus, slag is an effective supplementary cement material. Differences in cement matrix performance with and without slag are too great to be explained simply by a matrix permeability reduction; chemical factors also must operate. Thus, the ability of slag cements to react with and greatly reduce the solubility of technetium has been experimentally verified. However, thermodynamic data necessary to model technetium are not available or have insufficient accuracy to venture firm predictions.

As cement barriers age, the most important factors relevant to maintaining the immobilization potential for technetium are

- Low Eh. However, the threshold Eh that, if exceeded, allows reoxidation of technetium to occur is not well established. Many soils appear to have sufficiently low Eh to maintain technetium as Tc(IV), at least in waterlogged conditions (Tagami and Uchida, 1995), and it is possible to envision sites in which technetium, once reduced, will remain in the reduced and less soluble state. It is doubtful, however, whether the unsaturated conditions near many of the tanks would favor reducing conditions. In addition, physical degradation (i.e., cracking and fracturing) of the cement-based material could allow diffusion of oxygen or infiltration of oxygenated water and significantly enhance technetium release.
- Carbonation. Fresh cement reduces the activity of  $\text{CO}_2$  by combining it as calcium carbonate and other phases. Thus, carbonate complexes of technetium are unlikely to form unless stable at very low carbonate activities. However, the buffering capacity of the cement for  $\text{CO}_2$  is limited, and resolubilization of technetium in carbonated cement remains a possibility.
- Impact of radiolysis on the course of reoxidation. The ability of the cement system to locally resist reoxidation resulting from radiolysis is uncertain. Radiolysis, by generating oxygen and peroxide, could possibly lead to a gradual rise of Eh in the grout.

## 8.5 Scoping Assessments of Tank Grout Degradation

As noted previously, there is uncertainty about the long-term performance of DOE tank grouts and their ability to sustain a chemical environment that is conducive to mitigating the release and transport of radionuclides from the grouted waste form. This section discusses scoping assessments of tank grout degradation. Because grout degradation depends on numerous factors, including the environment in which degradation occurs, and will vary from site to site, the discussion necessarily is generic in nature and not site specific. Also, although the DOE grout formulations for tank closure typically are ternary mixtures of fly ash, blast furnace slag, and Portland cement, for the purpose of the present analysis, it is prudent to take a generic approach to the grout formulation and focus the assessment on unmodified Portland cement, which has more data and can provide a more confident evaluation. Such an assessment should be treated as a benchmark against which the performance of other grout formulations can be evaluated.

Furthermore, a useful indicator of grout degradation is the degree to which the ability of the grout to buffer the chemical environment in the system is lost. Thus, much of the scoping assessments focus on the ability of the grout to sustain an alkaline pore water pH, which is necessary to mitigate the carbon steel corrosion and the radionuclide release and transport. In this context, the principal factors thus far identified as leading to a decline in grout pore water pH are reactions involving

- Supplementary cementing materials added to Portland cement, including slag and fly ash, which reduce the pH buffering reserves inherent in the hydration products of Portland cement
- Acidic or reactive waste components and metals (e.g., steel), which during corrosion, behave as an acid toward cement grout
- Components of the near-field service environment, of which mobile gaseous components (e.g., carbon dioxide) are the most important
- Contact with water resulting in leaching, which dissolves the cement substance, increases the porosity, and increases the transport of aggressive species

Three scenarios are discussed in the following sections. Section 8.5.1 discusses the first factor in the list, which concerns the evolution of grout pH in the absence of interactions with the external environment. This factor is considered separately from other factors because the formulation of the grout is engineered and, in the absence of interactions with the external environment, it should be possible to assure the maintenance of high internal pH by design. On the other hand, some factors are not well defined for assessment purposes. For example, there is uncertainty in the potential inventory of acidic or reactive aqueous components remaining in individual tanks at the start of grouting. Thus, the second factor listed is not considered in the scoping assessments. In Section 8.5.2, a scenario is discussed in which water infiltration is limited and carbonation due to influx of carbon dioxide is the dominant degradation mechanism. Section 8.5.3 discusses a scenario in which infiltration is important and there is extensive interaction with the environment.

### 8.5.1 Scenario 1: No Interaction With the External Environment

This section evaluates a scenario in which no interaction of the cement-based material with the external environment occurs, but which serves as a benchmark for scenarios in which external fluxes affect the grout. In this respect, sufficient information is available only on Portland cement, and the analysis presented in this section will assume that the grout is composed only of Portland cement.

Portland cement can cause percolating water to have high pH as a consequence of (i) soluble alkalis, which are present in cement mainly as sodium and potassium hydroxides; (ii) the low, but significant, solubility of portlandite, a source of hydroxide ions; and (iii) the pH-conditioning ability of other cement solids, the most important of which is C-S-H, the gellike binding phase that comprises perhaps 60 mass percent or more of a hydrated Portland cement paste. Concerning these sources of high pH, the alkali content of cements is not guaranteed and, in any event, is low (on the order of 1 percent or less). Its high solubility ensures its tendency to be depleted in the early stages of cement degradation. On that basis, alkalis are not included in this assessment, which is consistent with other conservative assessments (e.g., Atkinson, et al., 1989; Reardon, 1992).

Portlandite is formed abundantly in Portland cement. It comprises about 25 mass percent of the solids and is well distributed throughout the hardened cement paste. Portlandite has essentially constant composition, and its chemical and physical properties are well established. It dissolves congruently in a wide range of environments and is not prone to developing protective films of product phases that might isolate it from its environment and lead to sluggish reaction kinetics. Consequently, performance scenarios based on portlandite generally are considered to be robust.

Once portlandite is either exhausted or becomes unavailable for reaction and dissolution, C-S-H is available to buffer the pH, initially to the same value as calcium hydroxide. However, C-S-H has a variable composition, and because it is Ca/Si molar ratio (initially in the range 1.7 to 2.0) and decreases during continued reaction with percolating water, its pH conditioning ability also diminishes. This is evidenced by a decline in cement pore water pH such that the low calcium C-S-H may not condition pHs above about 10 (i.e., pHs may become sufficiently low that embedded steel no longer is passivated). The literature is not in complete agreement about the factors that control the evolution of pH as the C-S-H composition is changed, but suffice it to say that scenarios based on pH-conditioning by C-S-H are less robust than those based on portlandite: small losses of calcium from C-S-H significantly diminish its pH conditioning ability. C-S-H is also incongruently soluble, and leaching of its outer layers can lead to development of siliceous films that passivate its surfaces; ongoing reactions involve transport, mainly of calcium and hydroxyl ions, through a thickening layer of reaction products.

The impact of fly ash on Portland cement is considered here by performing scoping calculations. Without specific knowledge about the reactivity of the fly ash and the content of unreactive minerals in grout formulations to be used for tank closure, the calculations do not justify great precision at this stage. Mixtures of Portland cement with Class F fly ash (an ASTM designation for an aluminosilicate-rich ash) could be used, as in the closure of the tank farm facility at the Idaho National Laboratory (CH2M-WG Idaho, LLC, 2007; Thorne, 2007). Qian, et al. (1989) found that the glass phase of Class F fly ash had approximately the same composition as the bulk ash, except for carbon and a slight iron oxide depletion and alkali enrichment in the glass phase. If it is further assumed that the (i) sum of chemical alumina and silica in the bulk fly ash is about 75 percent (as may readily be verified by a bulk chemical analysis); (ii) products of

reaction of fly ash glass and cement have poor abilities for conditioning the pH above the threshold for steel corrosion; and (iii) fly ash is two-thirds glass, a calculation can be done as follows. Each gram of fly ash glass can react with approximately 1 g of portlandite<sup>6</sup> (the formula weights of CaO and SiO<sub>2</sub> are nearly equal and are 56 and 60, respectively), and the approximate reaction stoichiometry is



represented by Figure 8-7 shows the consequences of cement dilution by fly ash, as well as the reaction stoichiometry, and predicts the decrease of portlandite content. As indicated in the figure, about 27 percent fly ash is sufficient to consume the free portlandite, which would mark the end of pH buffering by portlandite.<sup>7</sup> The sample calculation is open to refinement, but its general conclusion remains: the reaction of fly ash in mixtures with Portland cement is remarkably effective in eliminating free portlandite. This reaction highlights a serious potential problem affecting the ability of DOE grouts to condition pH in the long term.

Helmuth (1987) reports a more sophisticated model of reaction between cement and fly ash. The main reaction was described by the equation



After reaction, the molar ratio of CaO/SiO<sub>2</sub> in C-S-H was equal to 1.0. This molar ratio is equivalent to a CaO/SiO<sub>2</sub> weight ratio of 0.93. The effect of the significant alumina content of a class F fly ash was included by reacting the alumina with sufficient portlandite, silica, and water to form gehlenite hydrate, corresponding to the mineral strätlingite, 2CaO·Al<sub>2</sub>O<sub>3</sub>·SiO<sub>2</sub>·8H<sub>2</sub>O.<sup>8</sup>

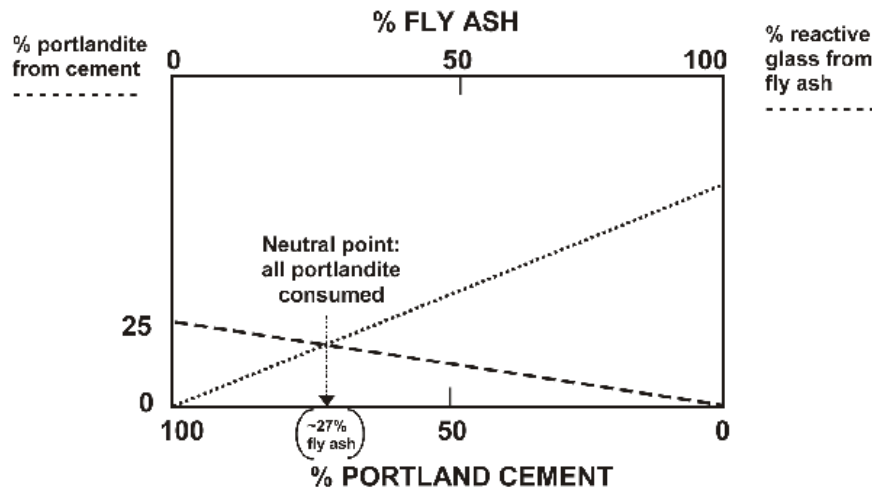


**Figure 8-7. Nomograph Showing the Decrease of Portlandite in Portland Cement–Fly Ash Blends After Reaction Is Completed. See Text for Assumptions Underlying the Calculation.**

<sup>6</sup>1 g = 2.2 × 10<sup>-3</sup> lb

<sup>7</sup>The amount of fly ash required to consume Portlandite would be lower in a ternary grout comprising Portland cement, fly ash, and blast furnace slag because slag also would react with Portlandite.

<sup>8</sup>The formation of strätlingite can be represented by the following reaction:  

$$2\text{Ca(OH)}_2 + \text{Al}_2\text{O}_3 + \text{SiO}_2 + 6\text{H}_2\text{O} \rightleftharpoons 2\text{CaO} \cdot \text{Al}_2\text{O}_3 \cdot \text{SiO}_2 \cdot 8\text{H}_2\text{O}$$
 portlandite alumina silica strätlingite

Strätlingite has a  $\text{CaO}/(\text{Al}_2\text{O}_3 + \text{SiO}_2)$  molar ratio of 1.0, which is equivalent to a  $\text{CaO}/\text{Al}_2\text{O}_3$  of 0.55. Assuming the reactive silica and alumina contents of fly ash were 50 and 30 weight percent, respectively (i.e., there would be 0.5 kg of  $\text{SiO}_2$ <sup>9</sup> and 0.3 kg of  $\text{Al}_2\text{O}_3$  in 1 kg of fly ash), the amount of fly ash required to complete the reaction with  $\text{Ca}(\text{OH})_2$  in cement would be

$$(0.5 \times 0.93) + (0.3 \times 0.55) = 0.63 \text{ kg CaO/kg fly ash} \quad (8-5)$$

or

$$1.59 \text{ kg fly ash/kg CaO} = 1.20 \text{ kg fly ash/kg Ca}(\text{OH})_2 \quad (8-6)$$

or 55 percent fly ash in a fly ash–portlandite mixture (i.e., 0.55 kg fly ash per 1.0 kg of fly ash–portlandite mixture).

The calculation presented in Figure 8-7 differs from this calculation in several respects, but the former calculation is based on a Portland cement composition and a further assumption that the cement can supply 25-percent CaO [converted to  $\text{Ca}(\text{OH})_2$  in the calculation]. Thus, the two sets of calculations, although employing different assumptions, give the same approximate conclusion: on reacting with the available alumina and silica, the portlandite furnished by Portland cement hydration is depleted by fly ash. These calculations can be further refined using compositions specific to grouts used in tank closure.

A rationale for replacing Portland cement with fly ash in the grout formulation is to lower the heat of reaction in the initial phase of grout hydration. The grout pore solution would still have high pH in the short term because of the slow reactivity of fly ash with cement. Various studies have shown that pozzolanic reactions involving fly ash are much slower compared to the hydration reactions of Portland cement and that only after curing for several weeks does substantial reaction occur (Helmuth, 1987; Stefanovic, et al., 2007). However, the prognosis for long-term retention of high pH is not good. But, at present, there is insufficient data to predict the long-term pH evolution of the DOE formulations that contain mixtures of Portland cement, fly ash, and slag.

### 8.5.2 Scenario 2: Limited Infiltration of Water; Carbonation as Dominant Degradation Mechanism

Many of the tanks physically are located above the local groundwater table, and an engineered cover likely will be emplaced above the grouted tanks and vaults to prevent infiltration of meteoric water. Thus, reactions of the grout with its service environment will be confined principally to those involving vapor transport. Under this scenario, carbonation would be the likely mechanism of tank grout degradation. To commence scenario development, the tank grouts are classified as shown in Table 8-7. The grout might be homogeneous on a centimeter scale, but its service environment can be heterogeneous on that scale. For that reason, a logic scheme similar to one shown in Table 8-7 is desirable to focus the analysis on key features and processes affecting tank grout performance.

Each grout type will have to be treated separately, although certain common functions and mechanisms can be identified. Considering the cross section of a grouted tank system, degradation by external agents likely will occur sequentially, so that annular grout and capping

---

<sup>9</sup>1 kg = 2.2 lb

<b>Grout Location/ Designation</b>	<b>Function of Grout</b>	<b>Processes Affecting Grout Performance</b>
Annular grout	Passivates steel tank liners and gives mechanical stabilization.	Leaching, carbonation, cracking from steel corrosion.
Capping grout	Prevents intrusion and sheds percolating water.	Leaching, carbonation, cracking.
Structural grout	Provides mechanical stabilization of tanks. Comprises the bulk of the grout by mass.	Leaching, carbonation, cracking, but attack delayed by remaining life of steel shell and by cap and annular grouts.
Stabilizing grout	At/near interface with solid heel. Buffers pH and poises Eh; sorbs and precipitates radionuclides.	Reaction with residual aqueous solution and heel solids. Radiolysis and gas production.
Pipe and vent fillings	Prevents fast pathways and bypassing pathways. Inhibits corrosion, stabilizes residual waste deposits.	Leaching, carbonation, cracking from steel corrosion.

grout performance will be described first and with the assumption that Portland cement is taken as a benchmark.

Subsequent to the dissipation of heat from initial exothermic reactions, the grout emplaced in the space between the steel tank and the concrete vault (the annulus<sup>10</sup>) will be exposed to an environment with high humidity and very nearly constant temperature. The high humidity is initially caused by the excess of mix water in the grout formulation, but in the longer term, the humidity will tend toward that of the near-field materials (soil/subsoil/unconsolidated sediments). No site-specific data on the state and condition of the near-field materials are available, but typically the pores will be filled with gas. The gas will be humid and have a CO<sub>2</sub> partial pressure somewhat exceeding normal atmospheric CO<sub>2</sub> partial pressure (10<sup>-3.5</sup> atm).

The impact of these environmental conditions on steel corrosion is described as follows. The component most vulnerable to corrosion is the steel tank. In the original construction, there is an air gap<sup>11</sup> between the tank and an outer concrete wall. After the annular space is grouted, the air gap will be lost, but the steel will continue to afford physical separation between the annular grout and the structural grout (see Table 8-7). At or near the tank bottom, the steel shell also separates the concrete vault floor from the stabilizing grout. In the majority of tanks, the steel barrier is carbon steel.

In a few of the carbon steel tanks, the steel will already have become perforated, but even if the shell is intact at the time of grouting, perforations could develop early in the postclosure evolution. However, the cross-sectional area of the perforations likely will be small relative to intact steel, and this relative geometry will continue for prolonged periods. Therefore, the evolution of the annular grout can be assessed separately from that of the structural grout,

<sup>10</sup>The tank system design varies; not all systems have an annulus or the annular space varies with design.

<sup>11</sup>60 cm [24 in] in some Savannah River Site tanks (National Research Council, 2006).

although with increasing time, the degree of difference in the evolution of the two grouts will decrease. Thus, in the early stages of degradation, the barriers of a grouted tank from outside (referring to near-field materials) are

- The concrete vault wall (part of the original construction)
- Annular grout, filling the annulus between the concrete vault and steel tank and emplaced during tank closure; assumed to be 60 cm [24 in] thick for the purpose of this analysis
- Steel tank shell (part of the original construction)
- Structural grout (possibly layered) added during tank closure

The capping grout, added above the structural grout during tank closure, is not considered in this set of scoping calculations.

The present quality and condition of the concrete vaults at DOE sites are not known. Presumably, the original concrete specification exists and could be consulted but, because the construction occurred approximately between 30 and 60 years ago, deterioration already may have progressed. The concrete possibly could be sampled by coring to determine its present state, but coring and intrusion may cause more problems than it solves. Thus, for the subsequent analysis, a conservative approach is taken, and the role of this concrete is neglected. If desirable, the role of this concrete could be included in the scope of a future assessment.

The corrosion rate of the steel tank shell in the postclosure period is determined largely by the performance of the 60-cm [24-in] grout barrier and the supply of aggressive agents from the near-field environment. In the absence of chemical degradation, the grout is assumed to behave like a normal cement composition maintaining a high internal pH (close to 12.5). Under these conditions, steel corrosion will be slow, at a rate of 1 to 2  $\mu\text{m}$  [ $3.9$  to  $7.9 \times 10^{-5}$  in] per year. In this ideal scenario and assuming uniform, steady state corrosion, a 20-mm [0.79-in] shell thickness<sup>12</sup> would approach total corrosion after about 10,000 years. Of course, some of the tanks are already perforated and, moreover, corrosion in the postclosure phase is unlikely to be uniform. But scoping calculations suggest that the perforation does not play a significant role in gas-induced corrosion and that tank metal will persist over long periods, perhaps approaching the 10,000-year performance timeframe. However, this scoping calculation does not allow for grout degradation, which is considered in the following paragraph.

Table 8-8 lists the most probable causes of grout degradation for scenarios in which percolation of meteoric water is limited. In the normal postclosure state, gas migration through near-field materials will contribute to the decline of grout performance. The composition of gas in near-field materials is presently unknown but, in common with most unconsolidated media, it is probably depleted in oxygen and enriched in  $\text{CO}_2$  relative to standard atmosphere. Therefore, it is potentially able to facilitate carbonation of the grout matrix. Relative humidities in the near-field materials remain to be established, but are probably favorable for carbonation (i.e., they range from 40 to 80 percent).

---

<sup>12</sup>The exact thickness, if known, could be used; 20 mm [0.79 in] is used for scoping calculation.

<b>Causes</b>	<b>Consequences</b>	<b>Remarks</b>
Coupling of grout to near-field materials occurs mainly by gas transport	Carbonation of grout	Predicted to be the normal mode of attack
Intermittent flooding but with long intervals between episodic flooding	As above, but with episodic suction of CO <sub>2</sub> -saturated water into grout pores followed by slow dewatering	Difficult to evaluate because of non-steady-state conditions
Continuous flooding	Carbonation occurs via the liquid phase as well as dissolution of solids	Some tanks at/below water table; climate change could affect status of tanks

Scenario 2 can be evaluated for grouts based on Portland cement as follows. Glasser and Matschei (2007) calculated the mineralogical development of a model hydrated cement paste as a function of added CO<sub>2</sub> in grams per 100 g<sup>13</sup> of hydrated cement paste. Results of the calculation are shown in Figures 8-8 and 8-9 and supplemented by Table 8-9. The most rapid changes are predicted to occur at low CO<sub>2</sub> additions and are shown in Figure 8-9. However, most cements contain sufficient carbonate present as an impurity or gained in the course of handling and emplacement such that the early-stage reactions shown in Figure 8-9 are already completed. Thus, these early-stage reactions will occur during initial hydration and strength gain and may not be relevant to elucidating the potential for volume change in the postclosure phase. The predicted course of reaction simulates experimental observations made on commercial cements during laboratory investigations and field experience.<sup>14</sup>

Portland cement hydration results in mixtures of mainly four solids: portlandite, C-S-H, and two calcium sulfoaluminate hydrates—monosulfoaluminate and ettringite. These are shown in Figure 8-9 at the left-hand side, which corresponds to zero CO<sub>2</sub>. But, as noted, most cements will contain at least a little CO<sub>2</sub> so that commercial cements are apt to start near the left-hand side, but not at zero CO<sub>2</sub>.

Besides the solids, additional liquid water, exceeding that required to hydrate the cement solids, will persist because the calculation was directed to start at a water/cement weight ratio equal to 0.5 (i.e., an excess of liquid water was present). This value is probably realistic for free-flowing grouts made without superplasticizers; it leaves a permanent excess of water that is present as pore water. The pore water is held in micron-sized pores in the solid cement matrix where it is in intimate contact with the solids.

The model used for calculation does not include the iron oxide content of cement, typically 5 to 10 percent of the cement by mass. However, during hydration, much of the iron forms hydrated iron oxide, which does not participate in subsequent reactions with CO<sub>2</sub>. Some iron also substitutes for aluminum in the AFt and AFm phases, but is neglected. Alkalis, often present in cement at the 1 percent level, also are not included in the scope of the calculation: they are mainly dissolved in pore fluid, effectively as hydroxides. Thus, with minor simplifications, the

<sup>13</sup>1 g = 2.2 × 10<sup>-3</sup> lb

<sup>14</sup>Ibid.

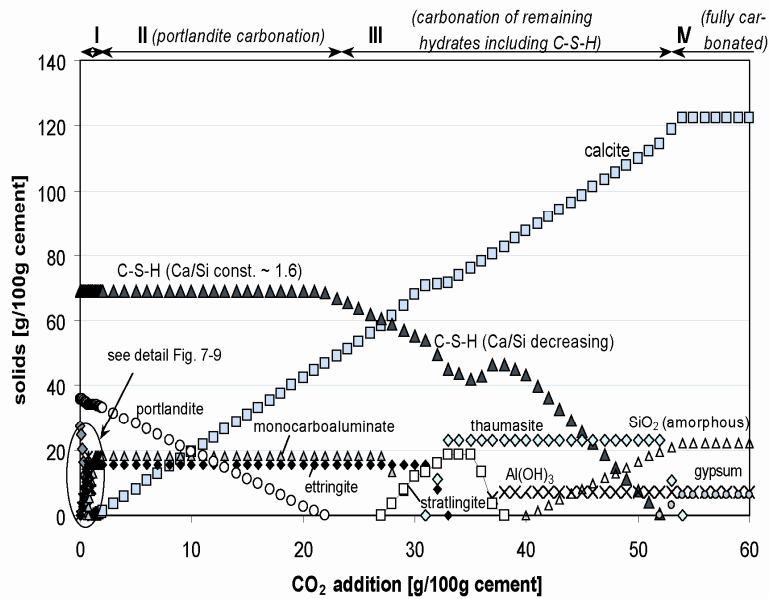


**Figure 8-8. Impact of Carbonation on Mass-Balance of Hydrated Model Cement Paste at 25 °C [77 °F] at Saturated Relative Humidity (From Glasser and Matschei, 2007). Note That the Calculated Phase Distribution Is a Function of CO<sub>2</sub> Addition; Thus, the Diagram Represents the Sequence of Different Zones, Not Their Relative Physical Thicknesses. [1 g = 2.2 × 10<sup>-3</sup> lb]**

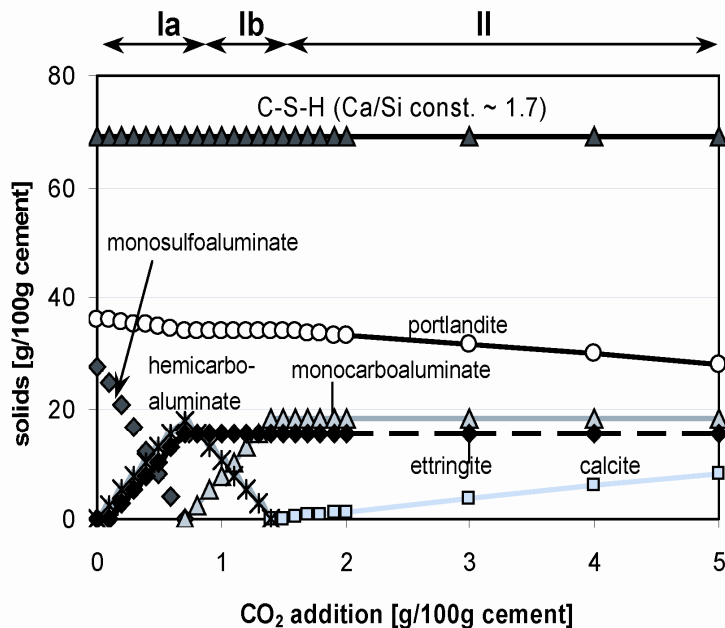


**Figure 8-9. Impact of Carbonation on Mass-Balance of Hydrated Model Cement Paste (Enlarged Detail From Figure 8-8). Zones (Top) Are Defined in Table 8-9. From Glasser and Matschei (2007). [1 g = 2.2 × 10<sup>-3</sup> lb]**

<b>Table 8-9. Calculated Phase Assemblages in the Course of Carbonation at 25 °C [77 °F]*</b>	
<b>Zone (and Mass of CO<sub>2</sub>, Grams Per 100 g of Cement, to Complete the Stage)†</b>	<b>Solid Phase Assemblage‡</b>
<b>0</b> Intact core zone (~2)	C-S-H§ (Ca/Si ~1.65), portlandite, monosulfoaluminate (ss)
<b>I</b> Early stages (~22)	(a) C-S-H (Ca/Si ~1.65), portlandite, monosulfoaluminate ↓, hemicarboaluminate ↑, ettringite ↑
	(b) C-S-H (Ca/Si ~1.65), portlandite, hemicarboaluminate ↓, monocarboaluminate ↑, ettringite
<b>II</b> Portlandite carbonation (22.5)	C-S-H (Ca/Si ~1.65), portlandite ↓, monocarboaluminate, ettringite, calcite ↑
<b>III</b> Transition zone: carbonation of remaining hydrates (~52)	(a) C-S-H (Ca/Si ~1.65→1.4) ↓, monocarboaluminate, ettringite, calcite ↑
	(b) C-S-H (Ca/Si ~1.4→1.3) ↓, monocarboaluminate ↓, ettringite, strätlingite ↑, calcite ↑
	(c) C-S-H (Ca/Si ~1.3) ↓, ettringite ↑, calcite ↑, strätlingite ↑, thaumasite ↑
	(d) C-S-H (Ca/Si ~1.3→1.1) ↓, calcite ↑, strätlingite, thaumasite
	(e) C-S-H (Ca/Si ~1.1→1.0) ↑, calcite ↑, strätlingite ↓, thaumasite, Al(OH) <sub>3</sub> ↑
	(f) C-S-H (Ca/Si ~1.0→0.83) ↓, calcite ↑, thaumasite, Al(OH) <sub>3</sub>
	(g) C-S-H (Ca/Si ~0.83) ↓, calcite ↑, thaumasite, Al(OH) <sub>3</sub> , SiO <sub>2</sub> (amorphous) ↑
	(h) SiO <sub>2</sub> (amorphous), calcite ↑, thaumasite ↓, Al(OH) <sub>3</sub> , gypsum ↑
<b>IV</b> Fully carbonated (~52)	SiO <sub>2</sub> (amorphous), calcite, Al(OH) <sub>3</sub> , gypsum

\*Glasser, F.T. and T. Matschei. "Interactions Between Portland Cement and Carbon Dioxide." Proceedings of the XII International Congress on the Chemistry of Cements, Montreal, Canada, July 8–13, 2007. Published on CD-ROM. 2007.  
†1 g = 2.2 × 10<sup>-3</sup> lb.  
‡In addition, an aqueous phase also is present in all assemblages; ↑ increasing and ↓ decreasing amounts.  
§Calcium silicate hydrate.

calculation concerning carbonation in the posthardened state, after hydration is finished, discloses a complex system of mineralogical changes. Table 8-9 shows these changes and the mineralogical zonation as functions of the local CO<sub>2</sub> concentration (which is equated with the partial pressure of CO<sub>2</sub>). The mass of CO<sub>2</sub> cumulatively necessary to achieve a given degree of carbonation is also shown in the table. Note that a zoned structure is predicted to develop.

The progress of carbonation is marked by a slight but continuing increase in the volume of solids. If water is included in the volume calculation, the increase in specific volume is large. But entrapment of water seems unlikely: if reaction is to continue, CO<sub>2</sub> must diffuse inward and this is extremely slow in a water-saturated pore network. So, it is likely that inward diffusion of CO<sub>2</sub> will be accompanied also by outward diffusion of water liberated during hydration reactions.

Applying these data to reach a mass balance is facilitated by the fact that during vapor phase carbonation, as is predicted to occur in tank grouts, mass transport is limited to only two species—CO<sub>2</sub> and H<sub>2</sub>O; leaching is not a factor. This enables calculation to proceed like a

titration: incremental portions of CO<sub>2</sub> are added, and mass balances are recalculated in terms of changing water content of the solids, mineralogy, and specific volume of each constituent phase as reaction proceeds. In the present context, it is also useful to calculate the pore fluid pH because the resulting decline in pH from carbonation initiates a change of regimes, from one of high pH that passivates embedded steel (Stages I and II in Figure 8-10) to a lower pH regime of possible active corrosion.

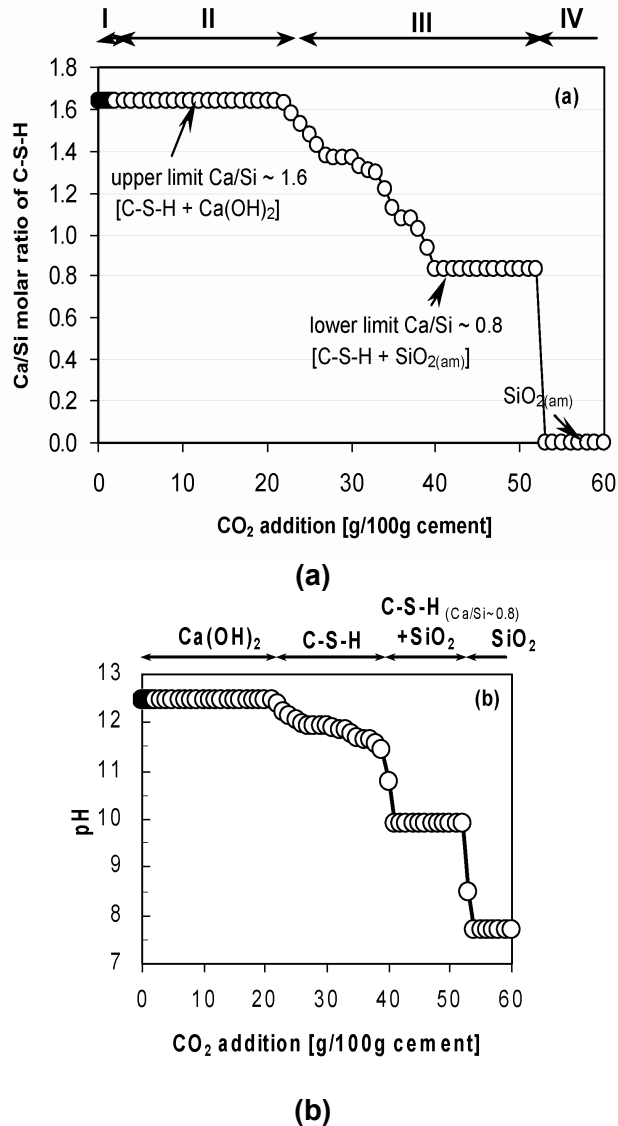


**Figure 8-10. Evolution of the (a) Ca/Si Molar Ratio of C-S-H and (b) Pore Water pH in a Model Cement Undergoing Carbonation. The Roman Numerals Correspond to Those in Table 8-9. The Aqueous pH Conditioning Ability Remains Constant at ~12.5 at 20 °C [68 °F], Until the End of Stage II, Corresponding to ~22 g CO<sub>2</sub> per 100 g [22 lb CO<sub>2</sub> per 100 lb] Cement. This Point, Marking the End of the Robust Buffering Reserve and the Start of pH Lowering, Is Coincident With Exhaustion of the Ca(OH)<sub>2</sub> (Portlandite) Content. From Glasser and Matschei (2007). [1 g = 2.2 × 10<sup>-3</sup> lb]**

In the example calculation, carbonation was envisioned to commence at a gas–solid (cement) surface and propagate inward with time and continued CO<sub>2</sub> uptake. The mineralogical development becomes spontaneously graded as tabulated in Table 8-9 and graphically illustrated in Figures 8-9 and 8-10. Initially, the partial pressure of CO<sub>2</sub> within the hydrated cement is low (on the order of 10<sup>-15</sup> atm). However, atmospheric CO<sub>2</sub> pressures are about 11 orders of magnitude greater and similar pressure is believed to occur in the near-field materials. At approximately 20 °C [68 °F], surface reaction between cement and the atmosphere is rapid at humidities in the range of 40 to 80 percent. The kinetics are affected by humidity because the first stage of reaction requires CO<sub>2</sub> gas to dissolve in water. Because this water also dissolves cement substances and becomes alkaline, the hydroxide ions react with CO<sub>2</sub> and form bicarbonate and carbonate ions. These species in turn react with cement solids. The figures show the progress of carbonation as a function of (mass of CO<sub>2</sub>)/(mass of cement). Each of the reactions shown in Table 8-9 requires a specific mass of CO<sub>2</sub> for completion. This mass is related to reaction stoichiometry, as detailed in Table 8-9. A series of buffering reactions occur, with each stepwise change in CO<sub>2</sub> activity enabling sorption of a definite mass of CO<sub>2</sub>. The consequences of the buffering reactions to corrosion control can be elucidated from Figure 8-10a, where the pH of the pore fluid solution is shown as a function of added CO<sub>2</sub>. Figure 8-10 is compatible with Figures 8-8 and 8-9 and with Table 8-9. As shown in the figure, the decline in pH with added CO<sub>2</sub> occurs in a stepwise manner.

A performance lifetime of the cement can be estimated as follows. An exact value for the regime transition between passivation and active corrosion of embedded steel is not available, but the sharp decline in pH from greater than 11.5 to less than 10.5 must include this regime change and is an appropriate point at which to fix the transition. Therefore, the steep pH decline occurring at about 32 g CO<sub>2</sub> per 100 g<sup>15</sup> cement marks the end of effective buffering capacity for steel passivation; it includes the neutralization of Ca(OH)<sub>2</sub> and the more calcium-rich C-S-H. The calculation has been done only for one cement, but back-of-the-envelope calculations made using a range of commercial Portland cement compositions suggest that the relevant capacity is unlikely to be less than about 30 g CO<sub>2</sub> per 100 g cement and not more than 35 g CO<sub>2</sub> per 100 g of cement. It is suggested that 30 g CO<sub>2</sub> per 100 g cement be used in subsequent calculations. If the barrier grout contains inert material (e.g., inert mineral aggregate), the cement content—usually expressed in kg/m<sup>3</sup>—is an important design parameter and will be known, so an appropriate dilution factor can be applied. For reference, 60 cm [24 in] of cement-only grout, with a density of 2,200 kg/m<sup>3</sup> [137 lb/ft<sup>3</sup>], have a cement content of 1,320 kg/m<sup>2</sup> [270 lb/ft<sup>2</sup>] of surface.

However, the grouts presently proposed for tank closure are complex mixtures of cement with both reactive and inert components. Moreover, the distinction between “reactive” and “inert” is not clear cut; fly ash, for example, contains significant quantities of both categories. In these complex mixtures, the ultimate mineralogy achieved by reaction amongst the reactive components is not known. Thus, the scheme used to perform calculations for Portland cement may not be immediately applicable to these complex grouts; the basis of the calculation will change. This is not to conclude that the problem cannot be solved, only that the data necessary to enable calculations have not been obtained. But qualitative calculations disclose that the most robust case will inevitably rest on the continued presence of portlandite, and it appears this cannot be assured in grouts with high cement replacement levels by fly ash and slag.

The preceding analysis shows that if the annular grout is Portland cement, the transfer of about 30 g CO<sub>2</sub> per 100 g cement is sufficient to reduce the pH conditioning ability of the grout and

---

<sup>15</sup>1 g = 2.2 × 10<sup>-3</sup> lb

deprive steel of passivation and protection from corrosion. The onset of active corrosion will lead to cracking and acceleration of barrier deterioration. The data on the rate of CO<sub>2</sub> generation and CO<sub>2</sub> transport parameters in near-field materials necessary to evaluate the rate of CO<sub>2</sub> delivery and effective partial pressure are not available. However, attention is directed to the proposals to use fly ash and slag in grout formulations. By reacting with Ca(OH)<sub>2</sub> and reducing the pH buffering reserve, fly ash and slag will reduce the time required to neutralize grout pH and, thereby, decrease the time to the onset of active corrosion.

### **8.5.3 Scenario 3: Infiltration Scenario**

This section discusses a scenario in which significant infiltration of water can occur. This evaluation uses a tank and vault layout illustrated in Figure 8-1, with emplaced grout in the annular space between the tank and vault and inside the tank. In the absence of site-specific information and data on the postclosure state or condition of the tank and vault, only a qualitative evaluation of the scenario is presented. A normal future rainfall also is assumed, although occasional wet episodes are part of the normal distribution. Wet episodes would temporarily saturate the adjacent soil and possibly cause a rise in groundwater levels adjacent to the tanks.

An engineered cover (e.g., see Figure 8-4), will protect the grouted tank and vault from direct impingement of percolating meteoric water, but the effectiveness of this cover will decrease with time. Thus, impingement of percolating water on the grouted tank and vault eventually will be significant, although the timeframe at which this occurs will depend on the degradation rate of the engineered cover, which is unknown. On the other hand, occasional flooding and perhaps water table elevation will allow groundwater to migrate laterally and impinge on the grouted tank and vault, thereby avoiding the protection the engineered cover provides.

The concrete vault surrounding the grouted tank also will serve as a barrier to water infiltration. The performance lifetime of this vault will depend on (i) the success of the engineered cover in diverting percolating meteoric water; (ii) the design of the vault, including concrete quality and thickness of cover over carbon steel reinforcements; and (iii) the incidence of flooding that bypasses the engineered cover. However, based on observations of seepage water in the underground concrete vaults at the West Valley Nuclear Services site (Elmore and Henderson, 2001) and at the Idaho National Laboratory tank farm facility (Cahn, et al., 2006), the infiltration barrier afforded by the concrete vault likely will be short-lived. Potential flow pathways through the vault include construction joints and contacts, annular spaces between the concrete and the pipes penetrating the vault roof, and cracks induced by shrinkage and by corrosion of steel reinforcements and pipes. Thus, water will contact the annular grout between the steel tank and vault not too long after the engineered cover fails.

The annular grout between the tank dome and vault roof will be contacted by percolating meteoric water and be subjected to leaching, carbonation, wet-dry cycling, and possibly sulfate attack. Periodic elevation of the water table would expose the annular grout along the tank bottom and sides to similar degradation processes. It is likely that upon its first contact with the annular grout, infiltrating water will be oxidizing due to dissolved oxygen and will contain dissolved carbon dioxide. The water will contain dissolved salts, although the salinity likely will be low, and also organic acids derived from the overlying and surrounding soil, which would enhance leaching of the grout.

Percolating water will frequently contact the annular grout above the tank, but contact the steel tank less often, mostly through shrinkage cracks in the annular grout. Nevertheless, the local

humidity near the tank will always be high. The most rapid process, assisted by high humidity and dissolved oxygen, will be corrosion of the carbon steel tank. This corrosion is unlikely to be uniform—corrosion near the top of the tank will be most rapid along the interface between the annular grout and tank where water first infiltrates. The oxygen in permeating water will be depleted during corrosion of the steel, thus reducing the potential for corrosion of steel at some distance from the point of first contact. But the volume of corrosion products generated is markedly larger than that of the steel consumed, resulting in steel corrosion that will stress the grout matrix, which will respond by cracking. Once cracking is initiated, it becomes self-sustaining. Thus, tank corrosion would enhance crack formation in the annular grout. Eventually, water percolating through crack zones in the annular grout will attack the steel tank until perforation occurs.

Too many unknowns persist to enable placing time scales on most of the features and processes identified, but perforation of the steel tanks and channeling of permeating water into the tank filling grout could occur somewhere between 100 and 1,000 years after closure. The failure process leading to water infiltration will be gradual. At first, the quantities of water entering the grouted tank will be small, but will increase progressively with time. Moreover, the design is such that water reaching the tank filling grout may not readily escape; the intact portions of the tank shell could act as a vessel and retain water.

Previous large-scale trials (e.g., Idaho National Engineering and Environmental Laboratory, 1999) demonstrated that it is not practicable to emplace crack-free tank grout on a large scale. Therefore, it is reasonable to assume that the tank grout will contain large (mm size) and continuous but widely spaced cracks forming in approximately concentric vertical rings. Also, the interface between successive pours could crack in the horizontal plane owing to differential stresses between successive pours, although direct evidence for this occurrence is not available. The resulting network of horizontal and vertical cracks could develop within the first few months of tank filling. The tank grout initially will not be subject to infiltrating water, but when infiltration does occur, the crack network will quickly and effectively distribute any entering water throughout the tank-filling grout. If the tank bottom does not perforate, or if its perforation is long delayed, accumulation of water against the heel and tank bottom will result until the tank bottom also perforates. However, the junction between the tank sides and bottom is vulnerable to corrosion such that ponding of water by this mechanism and its impact may not be significant.

As explained previously in Section 8.5.1, it is unlikely that the tank-filling grouts will maintain high internal pH over long time periods. The soluble alkalis will be depleted in the early stages of cement degradation and the fly ash and slag slowly will react with the cement phases that buffer high pH [mainly  $\text{Ca}(\text{OH})_2$  and calcium-rich C-S-H], with the result that the internal pH of the grout is likely to be in the range 10 to 11 by the time perforation occurs. Carbonation, induced by percolating water, will further lower the pH to about 9. At first, the lower pH zones will develop along permeable channels formed by the crack network. Thus, the originally homogeneous grout mass will become subdivided into faceted blocks. These blocks will have unaltered interiors, but their facets will become carbonated and leached. The Eh of the faceted surfaces also will rise to that of the infiltrating water, although the interior of the faceted blocks may retain its low Eh, conditioned by slag, for a much longer time period.

The state of the grout/tank interface is less certain. A potential concern is shrinkage of the grout and separation from the steel, leaving an empty annular space. This empty zone deprives steel of its passivation against corrosion. Basically, shrinkage data are not available for the DOE grout formulations. The separate contributions of thermal dilational change and chemical shrinkage cannot be deconvoluted on the basis of currently available information. Large-scale

trials should be used to provide this type of information. If an annular space between the grout and steel shell is going to develop, it should be apparent from inspection within a few days or weeks. Results that could guide an assessment of crack evolution and the development of an annular space between grout and steel currently are not available.

Pipework (e.g., process/transfer lines, cooling coils) present inside grouted tanks could act to some extent as restraints, which may aid in controlling cracking, but also could subsequently undergo corrosion, contributing to grout cracking or serving as flow pathways. Without knowledge of (i) the intrinsic propensity of the grout to crack; (ii) the thermal regime that is partially determined by the grout placement schedule; and (iii) the size, position, and distribution of these pipes, it is not possible to predict how the pipes will influence cracking. However, it can be assumed that once the tanks are perforated, percolating water will reach these components quickly and, if constructed of carbon steel, these components will corrode.

Thus, tank-filling grout properties can be visualized as being controlled largely by the incidence and geometry of cracking. The fact that very low saturated hydraulic conductivity has been obtained in laboratory test formulations is not necessarily relevant to their overall tank grout performance. Once the tank is perforated, water will quickly percolate the grout, initially through the coarse crack and void network. While the interior of blocks of grout will remain unaffected for long periods of time, perhaps 10,000 years or more, the grout will not significantly condition the pH of infiltrating waters because (i) its interior portions are physically decoupled from the fast flow pathways and (ii) the grout is likely to lose its ability to condition a high pH due to leaching of soluble alkalis and to internal reactions, as discussed in Section 8.5.1. If tank bottom perforation is long delayed, liquid water may accumulate in the bottom layers of grout, in contact with the tank heel. This combination of features could result in a pulse of released radionuclides. In this scenario, ponding of water precedes perforation of the sides and bottom of the tank, allowing water conditioned to a pH of about 10 to equilibrate with the tank heels and, as perforations develop, to discharge, producing a period of radioactive release at some point in the future.

## **8.6 Summary and Recommendations**

The stabilization and permanent closure of tank systems at the Savannah River Site, the Idaho National Laboratory, and the Hanford site involve filling the tanks, pipework, and concrete vaults with grout—a cement-based material. The benefits for tank closure provided by cement-based materials, particularly blends of Portland cement, fly ash, and blast furnace slag, include mechanical rigidity, high pH pore water, low permeability, a reducing environment, persistence in the natural environment, and proven technologies for emplacement. These benefits are considerable and make it likely that these materials will continue to be the preferred option for closing tank systems at DOE sites.

The ability of cement-based materials to serve as a barrier to groundwater influx and to release and transport of radionuclides is an important factor in performance assessments DOE conducted to demonstrate that tank closure and low-activity waste disposal in near-surface disposal facilities will meet the appropriate performance objectives. In these performance assessments, assumptions are made regarding the physical integrity (e.g., hydraulic conductivity) and chemical condition (e.g., pH and Eh affecting radionuclide solubility and sorption) of the cement-based material. Because performance assessment calculations typically are carried out to peak dose within 10,000 years, assumptions also are made regarding changes to the material properties to account for degradation that is expected to occur with time.

Several features, events, and processes—broadly classified into closed-system type and open-system type—are important to consider when evaluating the long-term performance of cement-based materials. In a closed system where no interchange of mass occurs between the cement-based material and the service environment, the grout pore water pH—an important factor influencing embedded steel corrosion and radionuclide release and transport—will depend mainly on the grout component composition and proportion. The high replacement levels of Portland cement by fly ash and blast furnace slag in the DOE grout formulations imply that the high pH conditioned by the presence of portlandite may not persist in the long term, because fly ash and slag both react with portlandite. Although the C-S-H phase can also condition a high pH, a complete consumption of portlandite marks a transition from a chemical environment of constant high pH buffered by the presence of portlandite to one of steadily decreasing pH buffered by the presence of C-S-H.

In a closed system, the grout redox potential—another important factor affecting the corrosion of metallic components and the solubility and sorption of redox-sensitive radionuclides—will depend on the sulfide sulfur content of the blast furnace slag. But the sulfide content of commercial blast furnace slag varies, typically from 0.6 to 1.0 weight percent, and is not specified, except as a maximum, by existing standards (e.g., ASTM C-989). Also, the modern tendency to use preprocessed iron feed stocks and “clean” coals results in the slag sulfur content tending toward lower values. Thus, chemical analysis of the slag used in tank grouts would be necessary to ensure that the amount of the sulfide sulfur is sufficient to achieve a low Eh.

Although the presence of a reducing environment in slag-cement blends is supported by experimental data and is ascribed to the sulfide sulfur in slag, uncertainties remain about the nature of the redox control in a slag-cement grout, particularly regarding the possible speciation of sulfur in the alkaline pore water. It is possible that thiosulfate species control the Eh, but studies to validate this Eh control are needed, possibly including a redetermination of thiosulfate stability in aqueous alkaline media. Measurements also are needed of the redox-poising capacity of DOE slag-cement formulations proposed for tank closure to complement the data from slag chemical analysis and to confirm that the redox-poising capacity is sufficient to maintain a low Eh in the long term.

Cement-based materials tend to shrink in the course of setting and hardening, which could lead to cracking. Experience in using a particular grout formulation often is used as a guide to the approximate shrinkage that could occur. However, the DOE grout formulations are not commonly used in industry, resulting in insufficient experience to estimate the potential shrinkage of tank grouts. Thus, shrinkage measurements for specific tank grout formulations appear to be necessary to provide such estimates. In addition, although published literature indicates that good progress has been made in relating shrinkage to accumulated strain, basic data that can be used in modeling strain and shrinkage are limited for DOE tank grout compositions.

However, even if such data are available for DOE grouts, the consequences of shrinkage in terms of the timing, spacing, width, and depth of resulting cracks are difficult to quantify, particularly for large masses of tank grout material. These masses behave differently than the laboratory-sized samples used in shrinkage and hydraulic conductivity measurements, undergo a heterogeneous thermal excursion during hardening, and develop differential stresses during cooling that could contribute to cracking. Other processes also complicate the analysis of potential cracking in a large mass of cement-based material, such as bleed, segregation, and

compaction, which cause heterogeneity that inevitably is greater at the bottom of the hardened material than at the top. In addition, the layered sequence of tank grouting could impose additional stress if there is a sufficiently high thermal gradient between a new and warm grout pour and a preceding, already cool grout layer. Large-scale trials using DOE grout formulations could provide information on the effects of scale on crack formation.

Although grout will be emplaced in DOE tanks and vaults at or near ambient temperature, the exothermic hydration reactions will cause the setting grout mass to experience a temperature rise. The magnitude of the temperature rise will depend upon the grout formulation, size and geometry of the pour, and the rate at which the evolved heat can be dissipated. Inert aggregate (such as sand) and supplementary cement materials (such as fly ash and slag) that react slowly with cement will decrease the exothermic reaction of the cementitious portions and thus reduce the thermal excursion. However, the large volume of individual grout pours and the buried nature of the tanks and vaults will reduce the opportunity for heat to escape. It is not practical to estimate the temperature rise without knowing the characteristics of the cementitious components, the initial pour temperature, and the capability of the surrounding concrete vaults and soils to act as thermal sinks or insulators. If adequate data are available, a number of computer programs are available to calculate the thermal excursion in mass cement-based material, although the uncertainty in the result can be significant for materials of variable particle-size distribution and composition such as slag and fly ash. Such calculations should be made before the final grout formulation is selected and the pour schedule specified as part of a deliberate effort to control thermal stress and cracking during tank grout hydration. The calculations could be used to optimize the grout formulation and modify the pour schedule, if warranted.

The conditions encountered in tank closure are generally favorable to ensure a good cure: the grouts will be emplaced into closed tanks, pipes, and vaults with little opportunity for escape of moisture, except when the tank farm ventilation system is kept on during grout emplacement and curing. The sequence of tank grout emplacement should be managed to minimize evaporation at any free interfaces. A potential problem area that may require attention is the interface between the grout and the concrete vault wall. If the vault walls are dry and porous, considerable water may be lost from the fresh, fluid grout to this concrete.

Grout-waste interactions are complex, and their consequences to the long-term performance of cement-based materials incorporating waste constituents are difficult to predict. For grouting of tanks with only small amounts of residual waste, such as the Idaho National Laboratory waste tanks, the consequence likely will be small given the relatively large volume of grout that is emplaced compared to the volume of residual waste. However, for disposal concepts such as the Saltstone Disposal Facility at the Savannah River Site in which radionuclide-bearing salt solution is mixed with cementitious materials to form a grout (saltstone) monolith, the interaction between the waste components and the grout must be considered. Sulfate concentrations in the Savannah River Site waste are sufficiently high that expansive reactions due to delayed ettringite formation are a potential concern. Although laboratory characterization of the saltstone waste form has been conducted, the short duration and the small scale of these tests make it unlikely that the effects of delayed ettringite formation on the physical properties of the cement-based material have been captured. In addition, no information is available on the potential effects of organic constituents unique to some of the Savannah River Site wastes (such as tetraphenylborates) on the physical properties, leaching characteristics, and long-term durability of the grouted waste form. These potential issues need to be evaluated.

Grout formulations used or proposed for use in grouting tanks at DOE sites include chemical admixtures such as superplasticizers. Data that can be used to determine the effects of admixtures on the long-term performance of grouted tanks and cement-based waste forms are limited. Additional studies to address this issue, including experiments to evaluate the effect of admixtures on the solubility of radionuclides (as recommended in Appendix B), also are warranted.

For open systems in which interactions could occur between the grout and the external environment, there are additional features, events, and processes important to consider when evaluating the long-term performance of cement-based materials. Despite the generally low permeability of cement-based materials (see Appendix A), cement-based structures, including those at DOE sites, have potential pathways through which environmental fluids, such as infiltrating water and atmospheric gases, can interact with the grouted waste form and other engineered barriers. Macrocracks that develop in the cement-based monolith after it hardens are the features most likely to act as fast pathways between the grouted waste form and the environment, although they also could act as bypassing pathways that limit the contact of environmental fluids with the grouted waste form and other engineered barriers. Conduits, which represent discrete fluid pathways that may be present or may develop along specific engineered features with known locations such as annular spaces between grout and a corroded tank, pipe, or rebar, also could act as fast pathways or as bypassing pathways. However, the flow of fluids through the macrocracks and conduits and through the grouted system will be controlled more by the boundary conditions including (i) the degree of hydraulic saturation of the soil surrounding the grouted tank and vault, (ii) the permeability contrasts between the grouted tank and vault and the surrounding soil, and (iii) the changes in water table elevation that may result in saturated conditions intersecting the tanks. The occurrence of these conditions and their possible influence on the ability of macrocracks and conduits to serve as fast and bypassing pathways will depend on site-specific conditions.

Many of the DOE tanks are physically located above the local groundwater table, and an engineered cover likely will be emplaced above the grouted tanks and vaults to prevent infiltration of meteoric water. As long as the tank grouts are protected from direct contact with liquid water, the grouts will not be subject to leaching and mass exchange between the grouts and their service environment will be confined principally to reactions involving vapor transport. Under this scenario, carbonation would be the likely mechanism of tank degradation. Carbonation could decrease the grout pore water pH to values that accelerate steel corrosion and also cause grout shrinkage.

In some DOE sites, however, the groundwater elevation is above that of the tank floor, which could degrade and result in the tank heel contacting the groundwater, or failure of the engineered cover, as well as episodic flooding, may occur and allow water to infiltrate and contact the grouted tanks and concrete vaults. In such scenarios, degradation is likely to occur by a combination of leaching, carbonation, and wet-dry cycling. However, because the solubility of calcite is several orders of magnitude less than that of portlandite, carbonation may actually have a favorable influence on performance if the grout is not also required to provide a high local pH. Sulfate attack also could contribute to degradation if the sulfate concentration in the groundwater that interacts with the grout is sufficiently high. Available groundwater chemistry data for the Savannah River Site and the Idaho National Laboratory show low sulfate concentrations, indicating grout degradation due to sulfate attack is unlikely to be significant in the short term. However, because of a performance period that may be as long as 10,000 years, a quantitative assessment is necessary to ascertain that sulfate attack will not significantly affect grout performance in the long term.

An important issue—particularly with an open system that allows interaction of the grout with the service environment—is the long-term persistence of the reducing capabilities of the grout. As pointed out in Appendix B, the solubility of redox-sensitive radioelements such as selenium and technetium depends markedly on the ability of the cement-based material to maintain strongly reducing conditions for an extended period of time. The oxidant of most concern is oxygen, which could react with and reduce the Eh poisoning capacity of slag. Oxygen can be present in the gas phase or dissolved in infiltrating water, and the relative importance of each phase will depend on the flow pathways through the grout, the hydrologic saturation condition, and the flow rate of infiltrating water. The presence of cracks or conduits could facilitate the oxygen influx into the grouted system, but slow oxygen diffusion into the grout matrix could limit redox changes to areas along the interface of the crack or conduit with the grout. Little information is available to assess the long-term persistence of reducing Eh of DOE grouts; thus degradation experiments and modeling studies are warranted to address this issue.

The various features, events, and processes were placed into context by providing in Section 8.5 a scoping assessment of tank grout degradation covering three scenarios. Scenario 1 involves no interaction of the cement-based material with the external environment and serves as a benchmark for scenarios in which external fluxes affect the grout. Simple calculations for Scenario 1 determined the consequence of dilution of Portland cement with fly ash and indicated that the prognosis for long-term retention of high pH by DOE grouts is not good. But additional data are needed to predict the long-term pH evolution of the DOE formulations that contain mixtures of Portland cement, fly ash, and blast furnace slag. Scenario 2 involves an open system where external fluxes can occur but groundwater infiltration is not significant. Under this scenario, carbonation is indicated to be the likely mechanism of degradation of tank grouts, which would shorten the time period during which carbon steel components would be passivated and protected from corrosion. Scenario 3 is a stylized scenario in which infiltration of water, through percolation of meteoric water or due to a rise in water table, occurs. Under this scenario, several processes are considered including shrinkage and corrosion-induced cracking, carbonation, leaching, wet–dry cycling, and sulfate attack.

Although the scoping assessment of tank grout degradation presented in Section 8.5 is only qualitative in nature, a more quantitative assessment may be possible using the approaches for modeling carbonation, sulfate attack, and leaching reviewed in Section 5. These approaches range from simple diffusion or empirical equations to complex reactive–transport models. The simple diffusion or empirical models are useful in providing gross estimates of performance of cement-based materials; however, these models make simplifying assumptions about the degradation process, ignore the effects of various parameters that may affect the degradation rate, and neglect the couplings that may occur between different processes. Also, the diffusion or empirical models discussed in Section 5 have not been validated for use on DOE grout formulations, thus parameter values will need to be determined if those models are to be applied to DOE grout degradation. The coupled reactive–transport models reviewed in Section 5 can explicitly account for the couplings between different chemical degradation mechanisms and between chemical reactions and transport processes. Several of the models are supported by good agreement between model results and laboratory or field sample data. However, the laboratory or field tests are much shorter than the time period of interest in cement-based engineered barrier performance evaluations so that predictions for longer time periods still have considerable uncertainties. Thus, further studies are needed to determine how coupled reactive-transport models can be applied to the long time frames of interest in radioactive waste disposal.

As indicated in a preceding paragraph, macrocracks and conduits can act as fast pathways between the grouted waste form and the service environment, or as bypassing pathways that limit the contact of environmental fluids with the grouted waste form and other engineered barriers. Literature information discussed in Section 5 supports the importance of considering the presence of fractures or cracks when evaluating the performance of cement-based engineered barriers. Because fluid flow and mass transport through macrocracks and conduits in cement-based structures are closely analogous to flow and transport through fractured geologic media, methods used to simulate contaminant transport through fractured geologic media (e.g., dual-porosity and discrete fracture models) would be applicable to simulation of fluid flow and mass transport through a grout monolith or concrete structure containing macrocracks and conduits. However, the applicability of these flow and transport models likely will be limited by a lack of sufficient information on the nature, extent, and properties of the pathways in cement-based engineered barriers. Although literature information on cracks in concrete structures is available, most of the studies have focused on reinforced-concrete civil engineering structures; thus the information may have limited value when estimating the nature, extent, and properties of macrocracks or conduits in a grouted tank or concrete vault. As pointed out in a preceding paragraph, large-scale trials using DOE grout formulations could provide information on crack formation in grouted tanks and concrete vaults at DOE sites.

## 9 REFERENCES

- Adenot, F. and C. Richet. "Modeling of the Chemical Degradation of a Cement Paste." *Mechanisms of Chemical Degradation of Cement-Based Systems*. K.L. Scrivener and J.F. Young, eds. London, United Kingdom: E & FN Spon. pp. 341–349. 1997.
- Adenot, F., C. Richet, and P. Faucon. "Long-Term Prediction of Concrete Durability in Radioactive Waste Management: Influence of the pH of the Aggressive Solution." International Conference on Engineering Materials, Ottawa, Canada, June 8–11, 1997. Ottawa, Canada: Canadian Society for Civil Engineering. pp. 117–128. 1997.
- Aldea, C.-M., S.P. Shah, and A. Karr. "Permeability of Cracked Concrete." *Materials and Constructions*. Vol. 32. pp. 370–376. 1999.
- Alexander, W.R., R. Dayal, K. Eagleson, J. Eikenberg, E. Hamilton, C.M. Linklater, I.G. McKinley, and C.J. Tweed. "A Natural Analogue of High pH Cement Pore Waters From the Maqarin Area of Northern Jordan—II: Results of Predictive Geochemical Calculations." *Journal of Geochemical Exploration*. Vol. 46. pp. 133–146. 1992.
- Aloy, A., E.N. Kovarskaya, J.R. Harbour, C.A. Langton, and E.W. Holtzscheiter. "Pretreatment of Tc-Containing Waste and Its Effect on Tc-99 Leaching From Grouts." Materials Research Society Symposium Proceedings 985. D.S. Dunn, C. Poinssot, and B. Begg, eds. Warrendale, Pennsylvania: Materials Research Society. pp. 367–372. 2007.
- Altenhein-Haese, C., H. Bischoff, L. Fu, J. Mao, and G. Marx. "Adsorption of Actinides on Cement Compounds." *Journal of Alloys and Compounds*. Vols. 213–214. pp. 554–556. 1994.
- American Concrete Institute. *Guide to Durable Concrete*. ACI 201.2R. Farmington Hills, Michigan: American Concrete Institute. 2006.
- . "ACI Manual of Concrete Practice Part 1—1983: Materials and General Properties of Concrete." Detroit, Michigan: American Concrete Institute. 1983.
- American Nuclear Society. "Measurement of the Leachability of Solidified Low-Level Radioactive Wastes by a Short-Term Test Procedure." ANSI/ANS-16.1. La Grange Park, Illinois: American Nuclear Society. 2003.
- Analytical & Computational Research, Inc. *PORFLOW Version 5.0 User's Manual*. Rev. 5. Los Angeles, California: Analytical & Computational Research, Inc. 2004.
- Andersson, A. and L.O. Nilsson. "Prediction of the Long-Term Release of Hazardous Substances From Cement-Based Materials to Water." Materials Research Society Symposium Proceedings 608. R.W. Smith and D.W. Shoosmith, eds. Warrendale, Pennsylvania: Materials Research Society. pp. 313–318. 2000.
- Andersson, J. and R. Thunvik. "Predicting Mass Transport in Discrete Fracture Networks With the Aid of Geometrical Field Data." *Water Resources Research*. Vol. 22. pp. 1,941–1,950. 1986.

ASTM International. ASTM C289–03, “Standard Test Method for Potential Alkali–Silica Reactivity of Aggregates (Chemical Method).” West Conshohocken, Pennsylvania: ASTM International. 2007a.

———. ASTM C1567–04, “Standard Test Method for Determining the Potential Alkali–Silica Reactivity of Combinations of Cementitious Materials and Aggregate (Accelerated Mortar-Bar Method).” West Conshohocken, Pennsylvania: ASTM International. 2007b.

———. ASTM C586–05, “Standard Test Method for Determining the Potential Alkali–Silica Reactivity of Carbonate Rocks as Concrete Aggregates (Rock-Cylinder Method).” West Conshohocken, Pennsylvania: ASTM International. 2007c.

———. ASTM C1012–04, “Standard Test Method for Length Change of Hydraulic-Cement Mortars Exposed to a Sulfate Solution.” West Conshohocken, Pennsylvania: ASTM International. 2007d.

———. ASTM C1038–04, “Standard Test Method for Expansion of Hydraulic Cement Mortar Bars Stored in Water.” West Conshohocken, Pennsylvania: ASTM International. 2007e.

———. ASTM C1174–04, “Standard Practice for Prediction of the Long-Term Behavior of Materials, Including Waste Forms, Used in Engineered Barrier Systems (EBS) for Geological Disposal of High-Level Radioactive Waste.” West Conshohocken, Pennsylvania: ASTM International. 2007f.

———. ASTM C628–04, “Standard Specification for Coal Fly Ash and Raw or Calcined Natural Pozzolan for Use in Concrete.” West Conshohocken, Pennsylvania: ASTM International. 2007g.

———. ASTM E632–82, “Standard Practice for Developing Accelerated Tests to Aid Prediction of the Service Life of Building Components and Materials.” West Conshohocken, Pennsylvania: ASTM International. 1996.

Atkins, M. and F.P. Glasser. “Application of Portland Cement-Based Materials to Radioactive Waste Immobilization.” *Waste Management*. Vol. 12. pp. 105–131. 1992.

———. “Encapsulation of Radioiodine in Cementitious Waste Forms.” Materials Research Society Symposium Proceedings 176. V.M. Oversby and P.W. Brown, eds. Pittsburgh, Pennsylvania: Materials Research Society. pp. 15–22. 1990.

Atkins, M., D. Damidot, and F.P. Glasser. “Performance of Cementitious Systems in the Repository.” Materials Research Society Symposium Proceedings 333. A. Barkatt and R. Van Konynenburg, eds. Pittsburgh, Pennsylvania: Materials Research Society. pp. 315–326. 1994.

Atkins, M., D.G. Bennett, A.C. Dawes, F.P. Glasser, A. Kindness, and D. Read. “A Thermodynamic Model for Blended Cements.” *Cement and Concrete Research*. Vol. 22. pp. 497–502. 1992a.

———. “Thermodynamic Modeling for Blended Cements.” Report DOE/HMIP/PR/92/005. Aberdeen, Scotland: Aberdeen University. 1992b.

Atkins, M., F.P. Glasser, and A. Kindness. "Phase Relations and Solubility Modeling in the CaO-SiO<sub>2</sub>-Al<sub>2</sub>O<sub>3</sub>-MgO-SO<sub>3</sub>-H<sub>2</sub>O System: For Application to Blended Cements." *Materials Research Society Symposium Proceedings* 212. T.A. Abrajano, Jr. and L.H. Johnson, eds. Pittsburgh, Pennsylvania: Materials Research Society. pp. 387–394. 1991.

Atkins, M., J. Cowie, F.P. Glasser, T. Jappy, A. Kindness, and C. Pointer. "Assessment of the Performance of Cement-Based Composite Material for Radioactive Waste Immobilization." *Materials Research Society Symposium Proceedings* 176. V.M. Oversby and P.W. Brown, eds. Pittsburgh, Pennsylvania: Materials Research Society. pp. 117–127. 1990.

Atkins, M., D.E. Macphee, and F.P. Glasser. "Chemical Modeling in Blended Cement Systems." *Proceedings of the Third International Conference—Fly Ash, Silica Fume, Slag, and Natural Pozzolans in Concrete*, Trondheim, Norway. V.M. Malhotra, ed. Special Publication SP-114. Farmington Hills, Michigan: American Concrete Institute. pp. 73–96. 1989.

Atkinson, A. and J.A. Hearne. "Mechanistic Model for the Durability of Concrete Barriers Exposed to Sulphate-Bearing Groundwaters." *Materials Research Society Symposium Proceedings* 176. V.M. Oversby and P.W. Brown, eds. Pittsburgh, Pennsylvania: Materials Research Society. pp. 149–156. 1990.

———. "An Assessment of the Long-Term Durability of Concrete in Radioactive Waste Repositories." AERE-R-11465. Harwell, United Kingdom: U.K. Atomic Energy Authority. 1984.

Atkinson, A., N.M. Everitt, and R.M. Guppy. "Time Dependence of pH in a Cementitious Repository." *Materials Research Society Symposium Proceedings* 127. W. Lutze and R.C. Ewing, eds. Pittsburgh, Pennsylvania: Materials Research Society. pp. 439–446. 1989.

———. "Evolution of pH in a Radwaste Repository: Internal Reactions Between Concrete Constituents." AERE-R12939. Harwell, United Kingdom: United Kingdom Atomic Energy Authority. 1988.

Atkinson, A., K. Nelson, and T.M. Valentine. "Leach Test Characterization of Cement-Based Nuclear Waste Forms." *Nuclear and Chemical Waste Management*. Vol. 6. pp. 241–253. 1986.

Atkinson, A., D.J. Goult, and J.A. Hearne. "An Assessment of the Long-Term Durability of Concrete in Radioactive Waste Repositories." *Materials Research Society Symposium Proceedings* 50. L.O. Werme, ed. Pittsburgh, Pennsylvania: Materials Research Society. pp. 239–246. 1985.

Bakker, R.F.M. "Prediction of Service Life of Reinforcements in Concrete Under Different Climatic Conditions at a Given Cover." R. Swamy, ed. Sheffield, United Kingdom: Sheffield Academic Press. 1994.

Bamforth, P.B. *Early-Age Thermal Crack Control in Concrete*. London, United Kingdom: CIRIA. 2007.

Barnes, M.W., C.A. Langton, and D.M. Roy. "Leaching of Saltstone." *Materials Research Society Symposium Proceedings 44*. C.M. Jantzen, J.A. Stone, and R.C. Ewing, eds. Pittsburgh, Pennsylvania: Materials Research Society. pp. 865–873. 1985.

Barr, C., X. Yin, C.L. Dinwiddie, L.D. Howard, R.T. Pabalan, and D. Pickett. "U.S. Nuclear Regulatory Commission Review of U.S. Department of Energy Non-High-Level Waste Determination for Idaho National Laboratory Tank Farm Facility." *Waste Management Conference (WM'07)*, Tucson, Arizona, February 25–March 1, 2007. Tucson, Arizona: Waste Management Symposia, Inc. 2007.

Baur, I. and C.A. Johnson. "Sorption of Selenite and Selenate to Cement Minerals." *Environmental Science and Technology*. Vol. 37. pp. 3,442–3,447. 2003.

Bear, J. *Dynamics of Fluids in Porous Media*. New York City, New York: American Elsevier Publishing Company. 1972.

Bechtel SAIC Company, LLC. "Calibrated Properties Model." MDL–NBS–HS–000003. Rev. 02. Las Vegas, Nevada: Bechtel SAIC Company, LLC. 2004.

Benbovdjema, F., F. Meftabi, and J.-M. Toyrenti. "A Viscoelastic Approach for the Assessment of the Drying Shrinkage Behavior of Cementitious Materials." *Materials and Structures*. Vol. 40. pp. 163–174. 2007.

Bennett, D.G., D. Read, M. Atkins, and F.P. Glasser. "A Thermodynamic Model for Blended Cements II: Cement Hydrate Phases; Thermodynamic Values and Modeling Studies." *Journal of Nuclear Materials*. Vol. 190. pp. 315–325. 1992.

Bentz, D.P. "CEMHYD3D: A Three-Dimensional Cement Hydration and Microstructure Development Modeling Package, Version 2.0." Gaithersburg, Maryland: National Institute of Standards and Technology. 2000.

———. "Three-Dimensional Computer Simulation of Portland Cement Hydration and Microstructure Development." *Journal of the American Ceramic Society*. Vol. 80. pp. 3–21. 1997.

Bentz, D.P. and E.J. Garboczi. "Modeling the Leaching of Calcium Hydroxide from Cement Paste: Effects on Pore Space Percolation and Diffusivity." *Materials and Structures*. Vol. 25. pp. 523–533. 1992a.

———. "Computer Simulation of the Diffusivity of Cement-Based Materials." *Journal of Material Science*. Vol. 27. pp. 2,083–2,902. 1992b.

Bentz, D.P., V. Waller, and F. de Larrard. "Prediction of the Adiabatic Temperature Rise in Conventional and High-Performance Concretes Using a 3-D Microstructural Model." *Cement and Concrete Research*. Vol. 28. pp. 285–297. 1998.

Bernard, A., J.C. Nomine, G. Cornec, A. Bonnet, and L. Farges. "Long-Term Leaching Tests on Full-Scale Blocks of Radioactive Wastes." *Nuclear and Chemical Waste Management*. Vol. 3. pp. 161–168. 1982.

- Berner, U.R. "Evolution of Pore Water Chemistry During Degradation of Cement in a Radioactive Waste Repository Environment." *Waste Management*. Vol. 12. pp. 201–219. 1992a.
- . "Thermodynamic Modeling of Cement Degradation: Impact of Redox Conditions on Radionuclide Release." *Cement and Concrete Research*. Vol. 22. pp. 465–475. 1992b.
- Bertolini, L., B. Elsener, P. Pedeferri, and R. Polder, eds. *Corrosion of Steel in Concrete: Prevention, Diagnosis, Repair*. Weinheim, Germany: Wiley-VCH Verlag GmbH & Co. 2004.
- Bethke, C.M. *Geochemical Reaction Modeling, Concepts, and Applications*. New York City, New York: Oxford University Press. 1996.
- Bhargava, K., A.K. Ghosh, Y. Mori, and S. Ramanujam. "Analytical Model for Time to Cover Cracking in RC Structures Due to Rebar Corrosion." *Nuclear Engineering and Design*. Vol. 236. pp. 1,123–1,139. 2006a.
- . "Model for Cover Cracking Due to Rebar Corrosion in RC Structures." *Engineering Structures*. Vol. 28. pp. 1,093–1,109. 2006b.
- Biddle, P., K.A. Boulton, M.D. Gale, J.G. Godfrey, and N.S. Stone. "Equilibrium Leach Testing of Low Level Waste. Part 2: Long-Term Tests on the Effects of Cementitious Grouts." AEAT/ERRA-0075 Issue 1. Harwell, United Kingdom: AEA Technology. 2000.
- Biehl, K. "Destruction of Concrete by Active Carbonic Acid." *Zement*. Vol. 17. pp. 1,102–1,105. 1928.
- Biernacki, J.J., S.E. Mikel, C.J. Parnham, R. Wang, J. Bai, T. Watkins, M.J. Lance, and C. Hubbard. "Direct Phase-Resolved Strain Measurements in Cementitious Materials." *Transport Properties and Concrete Quality*. B. Mobasher and J. Skalny, eds. Westerville, Ohio: The American Ceramic Society. pp. 57–72. 2007.
- Bin-Shafique, M., J. Walton, N. Gutierrez, R. Smith, and A. Tarquin. "Influence of Carbonation on Leaching of Cementitious Wasteforms." *Journal of Environmental Engineering*. Vol. 124. pp. 463–467. 1998.
- Bird, R.B., W.E. Stewart, and E.N. Lightfoot. *Transport Phenomena*. New York City, New York: John Wiley & Sons. 1960.
- Boddy, A., E. Bentz, M.D.A. Thomas, and R.D. Hooton. "An Overview and Sensitivity Study of a Multimechanistic Chloride Transport Model." *Cement and Concrete Research*. Vol. 29. pp. 827–837. 1999.
- Bodin, J., G. Porel, F. Delay, F. Ubertosi, S. Bernard, and J.-R. de Deuzy. "Simulation and Analysis of Solute Transport in 2D Fracture/Pipe Networks: The SOLFRAC Program." *Journal of Contaminant Hydrology*. Vol. 89. pp. 1–28. 2007.
- Bolander, J., Z. Li, and M. Yip. "Restraint and Cracking During Non-Uniform Drying of Cement Composites." *Transport Properties and Concrete Quality*. B. Mobasher and J. Skalny, eds. Westerville, Ohio: The American Ceramic Society. pp. 123–140. 2007.

Bonhoure, I., A.M. Scheidegger, E. Wieland, and R. Dähn. "Iodine Species Uptake by Cement and C-S-H Studied by I K-Edge X-Ray Absorption Spectroscopy." *Radiochimica Acta*. Vol. 90. pp. 647–651. 2002.

Boufiza, M., K. Sakai, N. Banthia, and H. Yoshida. "Prediction of Chloride Ions Ingress in Uncracked and Cracked Concrete." *ACI Materials Journal*. Vol. 100. pp. 38–48. 2003.

Bradbury, M.H. and F.A. Sarott. "Sorpton Databases for the Cementitious Near-Field of a L/LLW Repository for Performance Assessment." PSI Bericht 95-06. Würenlingen and Villigen, Switzerland: Paul Scherrer Institut. 1995.

Brodda, B.G. "Leachability of Technetium From Concrete." *The Science of the Total Environment*. Vol. 69. pp. 319–345. 1988.

Brookins, D.G. *Eh/pH Diagrams for Geochemistry*. Berlin, Germany: Springer-Verlag. 1988.

Brouwers, H.J.H. "The Work of Powers and Brownyard Revisited: Part 1." *Cement and Concrete Research*. Vol. 34. pp. 1,697–1,716. 2004.

Cahn, L.S., M.L. Abbott, J.F. Keck, P. Martian, A.L. Schafer, and M.C. Swenson. "Operable Unit 3-14 Tank Farm Soil and Groundwater Remedial Investigation/Baseline Risk Assessment." Idaho Falls, Idaho: DOE Idaho Operations Office. 2006.

Canadian Standards Association. "Concrete Materials and Methods of Concrete Construction/Methods of Test for Concrete." CSA A23.1–04/A23.2–04. Mississauga, Ontario: Canadian Standards Association. 2004.

Carde, C. and R. Francois. "Modeling the Loss of Strength and Porosity Increase Due to the Leaching of Cement Pastes." *Cement and Concrete Composites*. Vol. 21. pp. 181–188. 1999.

Carey, J.W. and P.C. Lichtner. "Calcium Silicate Hydrate (C-S-H) Solid Solution Model Applied to Cement Degradation Using the Continuum Reactive Transport Model FLOTRAN." *Transport Properties and Concrete Quality*. B. Mobasher and J. Skalny, eds. Westerville, Ohio: The American Ceramic Society. pp. 73–106. 2007.

CH2M-WG, LLC. "Compliance and Monitoring Plan for Performing Grouting at the INTEC Tank Farm Facility Closure Project." PLN-2309. Rev. 2. Idaho Falls, Idaho: CH2M-WG Idaho, LLC. 2007.

Chambers, A.V., A. Green, A.W. Harris, T.G. Heath, F.M.I. Hunter, M.C. Manning, and S.J. Williams. "The Diffusion of Radionuclides Through Waste Encapsulation Grouts." *Materials Research Society Symposium Proceedings 932*. P. Van Iseghem, ed. Warrendale, Pennsylvania: Materials Research Society. pp. 705–712. 2006.

Clifton, J.R., J.M. Pommersheim, and K. Snyder. "Long-Term Performance of Engineered Concrete Barriers." NISTIR 5690. Gaithersburg, Maryland: National Institute of Standards and Technology. 1995.

Comité Euro-International du Béton. "Durable Concrete Structures—CEB Design Guide." *Bulletin D'Information No. 182*. Lausanne, Switzerland: Comité Euro-International du Béton. 1989.

Conner, J.R. *Chemical Fixation and Solidification of Hazardous Wastes*. New York City, New York: Van Nostrand Reinhold. 1990.

Cook, J.R. "Estimated All Pathways and Inadvertent Intruder Doses From Saltstone Disposal Using Updated Salt Waste Compositions." WSRC-RP-2005-01402. Rev. 0. Aiken, South Carolina: Westinghouse Savannah River Company. 2005.

Cook, J.R. and J.R. Fowler. "Radiological Performance Assessment for the Z-Area Disposal Facility (U)." WSRC-RP-92-1360. Rev. 0. Aiken, South Carolina: Westinghouse Savannah River Company. 1992.

Cook, J.R., E.L. Wilhite, R.A. Hiergesell, and G.A. Flach. "Special Analysis: Revision of the Saltstone Vault 4 Disposal Limits (U)." WSRC-TR-2005-00074. Aiken, South Carolina: Westinghouse Savannah River Company. 2005.

Cook, J., D. Kocher, L. McDowell-Boyer, and E. Wilhite. "Special Analysis: Reevaluation of the Inadvertent Intruder, Groundwater, Air, and Radon Analyses for the Saltstone Disposal Facility." WSRC-TR-2002-00456. Rev. 0. Aiken, South Carolina: Westinghouse Savannah River Company. 2002.

Copen, M.D. "Concrete Dams." *Handbook of Concrete Engineering*. M. Fintel, ed. New York City, New York: Van Nostrand Reinhold Company. 1974.

Corapcioglu, M.Y. and S. Wang. "Dual-Porosity Groundwater Contaminant Transport in the Presence of Colloids." *Water Resources Research*. Vol. 35. pp. 3,261-3,273. 1999.

Cote, P.I.L., T.W. Constable, and A. Moreira. "An Evaluation of Cement-Based Waste Forms Using the Results of Approximately Two Years of Dynamic Leaching." *Nuclear and Chemical Waste Management*. Vol. 7. pp. 129-139. 1987.

Cowie, J. and F.P. Glasser. "The Reaction Between Cement and Natural Waters Containing Dissolved Carbon Dioxide." *Advances in Cement Research*. Vol. 4. pp. 119-134. 1992.

Cowper, M.M., S. Baker, A.V. Chambers, T.G. Heath, M. Mihara, and S.J. Williams. "The Sorption of Thorium and Americium Onto Fresh and Degraded Ordinary Portland Cement and Onto Green Tuff." *Materials Research Society Symposium Proceedings 932*. P. Van Iseghem, ed. Warrendale, Pennsylvania: Materials Research Society. pp. 925-932. 2006.

Crank, J. *The Mathematics of Diffusion*. New York City, New York: Oxford University Press. 1975.

Criscenti, L.J., R.J. Serne, K.M. Krupka, and M.I. Wood. "Predictive Calculations To Assess the Long-Term Effect of Cementitious Materials on the pH and Solubility of Uranium(VI) in a Shallow Land Disposal Environment." PNNL-11182. Richland, Washington: Pacific Northwest National Laboratory. 1996.

Curti, E. "Coprecipitation of Radionuclides With Calcite: Estimation of Partition Coefficients Based on a Review of Laboratory Investigations and Geochemical Data." *Applied Geochemistry*. Vol. 14. pp. 433-445. 1999.

Cusson, D. and W. Repette. "Early-Age Cracking in Reconstructed Concrete Bridge Barrier Walls." *ACI Materials Journal*. Vol. 97. pp. 438–446. 2000.

Dario, M., M. Molera, and B. Allard. "Effects of Cement Additives on Radionuclide Mobility." Materials Research Society Symposium Proceedings 807. V.M. Oversby and L.O. Werme, eds. Warrendale, Pennsylvania: Materials Research Society. pp. 639–644. 2004.

de Borst, R. and A.H. van den Boogaard. "Finite-Element Modeling of Deformation and Cracking in Early-Age Concrete." *Journal of Engineering Mechanics*. Vol. 120. pp. 2,519–2,534. 1994.

de Borst, R., J.J.C. Remmers, A. Needleman, and M.-A. Abellan. "Discrete vs Smearred Crack Models for Concrete Failure: Bridging the Gap." *International Journal for Numerical and Analytical Methods in Geomechanics*. Vol. 28. pp. 583–607. 2004.

Denham, M.E. "Conceptual Model of Waste Release From the Contaminated Zone of Closed Radioactive Waste Tanks." WSRC–STI–2007–00544. Aiken, South Carolina: Savannah River National Laboratory. 2007.

de Schutter, G. "Finite Element Simulation of Thermal Cracking in Massive Hardening Concrete Elements Using Degree of Hydration Based Material Laws." *Computers and Structures*. Vol. 80. pp. 2,035–2,042. 2002.

de Schutter, G. and L. Taerwe. "General Hydration Model for Portland Cement and Blast Furnace Slag Cement." *Cement and Concrete Research*. Vol. 25. pp. 593–604. 1995.

Deutsch, W.J., K.M. Krupka, M.J. Lindberg, K.J. Cantrell, C.F. Brown, and H.T. Schaefer. "Hanford Tank 241–C–106: Impact of Cement Reactions on Release of Contaminants From Residual Waste." PNNL–15544. Richland, Washington: Pacific Northwest National Laboratory. 2006.

de Windt, L., D. Pellegrini, and J. van der Lee. "Coupled Modeling of Cement/Claystone Interactions and Radionuclide Migration." *Journal of Contaminant Hydrology*. Vol. 68. pp. 165–182. 2004.

Diersch, H.-J.G. "FEFLOW—Finite Element Subsurface Flow and Transport Simulation System Reference Manual." Berlin, Germany: WASY GmbH Institute for Water Resources Planning and Systems Research. 2005.

DOE. DOE/EIS–0287, "Record of Decision for the Idaho High-Level Waste and Facilities Disposition Final Environmental Impact Statement." Washington, DC: DOE. 2005.

DOE–Idaho. DOE/NE–ID–11226, "Basis for Section 3116 Determination for the Idaho Nuclear Technology and Engineering Center Tank Farm Facility." Idaho Falls, Idaho: DOE–Idaho. 2006a.

———. "Response to Request for Additional Information on the Draft Section 3116 Determination Idaho Nuclear Technology and Engineering Center Tank Farm Facility." ICP/EXT–06–01204. Rev. 1. Idaho Falls, Idaho: DOE–Idaho. 2006b.

———. DOE/NE-ID-11226, “Draft Section 3116 Determination Idaho Nuclear Technology and Engineering Center Tank Farm Facility—Draft.” Rev. 0. Idaho Falls, Idaho: DOE-Idaho. 2005.

———. DOE/ID-10966, “Performance Assessment for the Tank Farm Facility at the Idaho National Engineering and Environmental Laboratory.” Rev. 1. Errata December 2, 2003. Idaho Falls, Idaho: DOE-Idaho. 2003.

DOE-Savannah River Site. DOE-WD-2005-002, “Draft Section 3116 Determination for Closure of Tank 19 and 18 at the Savannah River Site.” Rev. 0. Aiken, South Carolina: DOE-Savannah River Site. 2005.

———. DOE/EIS-0303, “Savannah River Site High-Level Waste Tank Closure Final Environmental Impact Statement.” Aiken, South Carolina: DOE-Savannah River Site. 2002.

Dow, C. and F.P. Glasser. “Calcium Carbonate Efflorescence on Portland Cement and Building Materials.” *Cement and Concrete Research*. Vol. 33. pp. 147–154. 2003.

Dunstan, E.R. “Fly Ash and Fly Ash Concrete.” Report REC-EPC-82-1. Denver, Colorado: U.S. Bureau of Reclamation. 1984.

———. “A Possible Method for Identifying Fly Ashes That Will Improve the Sulphate Resistance of Concrete.” *Cement, Concrete, and Aggregates (ASTM)*. Vol. 2. pp. 20–30. 1980.

———. “Performance of Lignite and Sub-Bituminous Fly Ash in Concrete—A Progress Report.” Report REC-EPC-76-1. Denver Colorado: U.S. Bureau of Reclamation. 1976.

El-Kamash, A.M., M.R. El-Naggar, and M.I. El-Dessouky. “Immobilization of Cesium and Strontium Radionuclides in Zeolite-Cement Blends.” *Journal of Hazardous Materials*. Vol. 136. pp. 310–316. 2006.

El-Kamash, A.M., A.M. El-Dakrouy, and H.F. Aly. “Leaching Kinetics of <sup>137</sup>Cs and <sup>60</sup>Co Radionuclides Fixed in Cement and Cement-Based Materials.” *Cement and Concrete Research*. Vol. 32. pp. 1,797–1,803. 2002.

El Maaddawy, T. and K. Soudki. “A Model for Prediction of Time from Corrosion Initiation to Corrosion Cracking.” *Cement and Concrete Composites*. Vol. 29. pp. 168–175. 2007.

Elmore, M. and C. Henderson. “West Valley High-Level Waste Tank Lay-up Strategies.” PNNL-13902. Richland, Washington: Pacific Northwest National Laboratory. 2001.

Esh, D.W., A.C. Ridge, and M. Thaggard. “Development of Risk Insights for Regulatory Review of a Near-Surface Disposal Facility for Radioactive Waste.” Proceedings of the Waste Management '06 Symposium, Tucson, Arizona, February 26–March 2, 2006. Tucson, Arizona: Waste Management Symposia, Inc. 2006.

Flanders, S. “Nuclear Regulatory Commission Onsite Observation Report for the Savannah River Site Saltstone Production and Disposal Facilities.” Letter (January 31, 2008) to L. Ling, Department of Energy Savannah River Operations Office. Washington, DC: NRC. 2008.

———. “Nuclear Regulatory Commission Onsite Observation Report for the Idaho National Laboratory Idaho Nuclear Technology and Engineering Center Tank Farm Facility.” Letter (September 25, 2007) to K. Lockie, DOE. Washington, DC: NRC. 2007.

Freedman, S. “Properties of Materials for Reinforced Concrete.” *Handbook of Concrete Engineering*. M. Fintel, ed. New York City, New York: Van Nostrand Reinhold Company. 1974.

Fu, Y.F., Y.L. Wong, C.S. Poon, and C.A. Tang. “Numerical Tests of Thermal Cracking Induced by Temperature Gradient in Cement-Based Composites Under Thermal Loads.” *Cement and Concrete Composites*. Vol. 29. pp. 103–116. 2007.

Fuhrmann, M., J. Heiser, and J. Gillow. “Behavior of Radionuclides and RCRA Elements in Tank Backfill Grouts.” Waste Management '06 Conference, Tucson, Arizona, February 26–March 2, 2006. Tucson, Arizona: Waste Management Symposia, Inc. 2006.  
<<http://www.wmsym.org/abstracts/2006/pdfs/6455.pdf>> (11 March 2008).

Fuhrmann, M., J.H. Heiser, R. Pietrzak, E.M. Franz, and P. Colombo. “Users’ Guide for the Accelerated Leach Test Computer Program.” BNL–52267. Upton, New York: Brookhaven National Laboratory. 1990.

Garrabrants, A.C., F. Sanchez, and D.S. Kosson. “Leaching Model for a Cement Mortar Exposed to Intermittent Wetting and Drying.” *AIChE Journal*. Vol. 49. pp. 1,317–1,333. 2003.

Gilbertson, M.A. “Response to Request for Additional Information No. 17 on Concentration Averaging and Waste Classification.” Letter (May 31) to S.C. Flanders, NRC. Washington, DC: DOE. 2006.

Gilliam, T.M., R.D. Spence, W.D. Bostick, and J.L. Shoemaker. “Solidification/Stabilization of Technetium in Cement-Based Grouts.” *Journal of Hazardous Materials*. Vol. 24. pp. 189–197. 1990.

Glass, R.J. and L. Yarrington. “Mechanistic Modeling of Fingering, Nonmonotonicity, Fragmentation, and Pulsation Within Gravity/Buoyant Destabilized Two-Phase/Unsaturated Flow.” *Water Resources Research*. Vol. 39. pp. 7-1 to 7-10. 2003.

Glasser, F.P. “Chemical Attack on Cement in Nuclear Repositories.” *Mechanisms of Chemical Degradation of Cement-Based Systems*. K.L. Scrivener and J.F. Young, eds. London, United Kingdom: E & FN Spon. pp. 323–330. 1997.

———. “The Role of Sulfate Mineralogy and Cure Temperature in Delayed Ettringite Formation.” *Cement and Concrete Composites*. Vol. 18. pp. 187–193. 1996.

———. “Coexisting Solid and Aqueous Phase in Portland Cement.” Hydration and Setting of Cements—Proceedings of the International RILEM Workshop. A. Nonat and J.C. Mutin, eds. London, United Kingdom: E & FN Spon. pp. 101–123. 1992.

Glasser, F.P. and T. Matschei. “Interactions Between Portland Cement and Carbon Dioxide.” Proceedings of the XII International Congress on the Chemistry of Cements, Montreal, Canada, July 8–13, 2007. Published in CD-ROM. 2007.

Glasser, F.P., M. Tyrer, K. Quillin, D. Ross, J. Pedersen, K. Goldthorpe, D.G. Bennett, and M. Atkins. "The Chemistry of Blended Cements and Backfills Intended for Use in Radioactive Waste Disposal." R&D Technical Report P98. Bristol, United Kingdom: U.K. Environment Agency. 1999.

Glasser, F.P., D. Macphee, and E.E. Lachowski. "Modeling Approach to the Prediction of Equilibrium Phase Distribution in Slag-Cement Blends and Their Solubility Properties." Materials Research Society Symposium Proceedings 112. M. Apter and R. E. Westerman, eds. Pittsburgh, Pennsylvania: Materials Research Society. pp. 117–127. 1988.

Glaus, M.A. and L.R. van Loon. "A Generic Procedure for the Assessment of the Effect of Concrete Admixtures on the Retention Behaviour of Cement for Radionuclides: Concept and Case Studies." PSI Report Number 04–02. Villigen, Switzerland: Paul Scherrer Institute. 2004.

GoldSim Technology Group, LLC. "GoldSim Probabilistic Simulation Environment." Issaquah, Washington: GoldSim Technology Group, LLC. 2004.

Gordon, L.E. "Impact of Prolonged Warm (40 °C and 85 °C) Moist Cure on Fly Ash/Portland Cement Paste." M.Sc. Thesis. University of Aberdeen, Aberdeen, Scotland: United Kingdom. 2004.

Greenfield, B.F., D.J. Ilett, M. Ito, R. McCrohon, T.G. Heath, and C.J. Tweed. "The Effect of Cement Additives on Radionuclide Solubilities." *Radiochimica Acta*. Vol. 82. pp. 27–32. 1998.

Grisak, G.E. and J.F. Pickens. "Solute Transport Through Fractured Media. 1—The Effect of Matrix Diffusion." *Water Resources Research*. Vol. 16. pp. 719–730. 1980.

Guerrero, A. and S. Goñi. "Efficiency of a Blast Furnace Slag Cement for Immobilizing Simulated Borate Radioactive Liquid Waste." *Waste Management*. Vol. 22. pp. 831–836. 2002.

Gutierrez, N., M.D.S. Bin-Shafique, J.C. Walton, A. Tarquin, R. Smith, P. Sheeley, M. Rodriguez, and R. Andrade. "Effects of Carbonation on the Long-Term Leaching Performance of Cementitious Wasteforms." Proceedings of the 1996 HSRC/WERC Joint Conference on the Environment. L.E. Erickson, D.L. Tillison, S.C. Grant, and J.P. McDonald, eds. Albuquerque, New Mexico: Hazardous Substance Research Center and Waste-Management Education and Research Consortium. 1996.  
<<http://www.engg.ksu.edu/HSRC/96Proceed/gutierrez.pdf>> (9 July 2008).

Haase, R. *Thermodynamics of Irreversible Processes*. Reading, Massachusetts: Addison-Wesley Publishing Co. 1969.

Haga, K., M. Shibata, M. Hironaga, S. Tanaka, and S. Nagasaki. "Change in Pore Structure and Composition of Hardened Cement Paste During the Process of Dissolution." *Cement and Concrete Research*. Vol. 35. pp. 943–950. 2005.

Haney, L.C. "Information Requested by SCDHEC Regarding the Z-Area Saltstone Facility (IWP-217)(U)." Letter (October 11, 1994) to J. Schnabel, South Carolina Department of Health and Environment Control. Aiken, South Carolina: Westinghouse Savannah River Company. 1994.

Hansson, C.M. "Concrete: The Advanced Industrial Material of the 21st Century." *Metallurgical and Materials Transactions B*. Vol. 26B. pp. 417–437. 1995.

Harbour, J.R. "Summary of Grout Development and Testing for Single Shell Tank Closure at Hanford." WSRC–TR–2005–00195, Rev. 0. Aiken, South Carolina: Savannah River National Laboratory. 2005.

Harbour, J.R. and A.S. Aloy. "International Program: Summary Report on the Properties of Cementitious Waste Forms." WSRC–STI–2007–00056. Rev. 0. Aiken, South Carolina: Savannah River National Laboratory. 2007.

Harfouche, M., E. Wieland, R. Dähn, T. Fujita, J. Tits, D. Kunz, and M. Tsukamoto. "EXAFS Study of U(VI) Uptake by Calcium Silicate Hydrates." *Journal of Colloid and Interface Science*. Vol. 303. pp. 195–204. 2006.

Harris, A.W., M.C. Manning, W.M. Tearle, and C.J. Tweed. "Testing of Models of the Dissolution of Cements—Leaching of Synthetic C-S-H Gels." *Cement and Concrete Research*. Vol. 32. pp. 731–746. 2002.

Harris, A.W., A. Atkinson, G.B. Cole, A. Haworth, A.K. Nickerson, and A.C. Smith. "The Performance of Cementitious Barriers in Repositories." NSS/R389. Harwell, United Kingdom: AEA Technology. 1997.

Harrison, W.H. and D.C. Teychenne. "Sulphate Resistance of Buried Concrete: Second Interim Report on Long Term Investigation at Northwick Park." London, United Kingdom: Building Research Establishment, Her Majesty's Stationery Office. 1981.

Hearn, N. "Effect of Shrinkage and Load-Induced Cracking on Water Permeability of Concrete." *ACI Materials Journal*. Vol. 96. pp. 234–241. 1999.

Hearn, N., R.J. Detwiler, and C. Sframeli. "Water Permeability and Microstructure of Three Old Concretes." *Cement and Concrete Research*. Vol. 24. pp. 633–640. 1994.

Helmuth, R. "Fly Ash in Cement and Concrete." Publication No. SP040.01T. Skokie, Illinois: Portland Cement Association. 1987.

Hillel, D. *Introduction to Soil Physics*. San Diego, California: Academic Press. 1982.

Hills, C.D. and S.J.T. Pollard. "The Influence of Interference Effects on the Mechanical, Microstructural, and Fixation Characteristics of Cement-Solidified Hazardous Waste Forms." *Journal of Hazardous Materials*. Vol. 52. pp. 171–191. 1997.

Hills, C.D., C.J. Sollars, L.C. Koe, and R. Perry. "A Calorimetric Study of the Effect of Organic Compounds on the Initial Behaviour of Cement-Based Solidified Wastes." *Waste Management Research*. Vol. 13. pp. 21–36. 1995.

Houk, I.E., O.E. Borge, and D.L. Houghton. "Studies of Autogenous Volume Change in Concrete for Dworshak Dam." *Journal of the American Concrete Institute*. Vol. 66. pp. 560–568. 1969.

Houseworth, J.E. "An Analytical Model for Solute Transport in Unsaturated Flow Through a Single Fracture and Porous Rock Matrix." *Water Resources Research*. Vol. 42. W01416. 2006.

Huang, H. and B.X. Hu. "Nonlocal Reactive Transport in Heterogeneous Dual-Porosity Media with Rate-Limited Sorption and Interregional Mass Diffusion." *Water Resources Research*. Vol. 37. pp. 639–647. 2001.

Huyakorn, P.S., B.H. Lester, and J.W. Mercer. "An Efficient Finite Element Technique for Modeling Transport in Fractured Porous Media. 2—Nuclide Chain Transport." *Water Resources Research*. Vol. 19. pp. 1,286–1,296. 1983.

Idaho National Engineering and Environmental Laboratory. "Idaho Nuclear Technology and Engineering Center Tank Farm Facility (TFF) Closure TFF WM-182 Grout Mock-Up." INEEL/EXT-99-01067. Rev. 0. Idaho Falls, Idaho: Idaho National Engineering and Environmental Laboratory. 1999.

International Atomic Energy Agency. "Long-Term Behavior of Low and Intermediate Level Waste Packages Under Repository Conditions." TECDOC Series No.1397. Vienna, Austria: International Atomic Energy Agency. 2004.

———. "Predisposal Management of Radioactive Waste, Including Decommissioning. Safety Requirements. Safety Standards Series." WSR- 2. Vienna, Austria: International Atomic Energy Agency. 2000.

———. "Near-Surface Disposal of Radioactive Waste. Safety Requirements. Safety Standards Series." WS-R-1. Vienna, Austria: International Atomic Energy Agency. 1999.

Isgor, O.B. and A.G. Razaqpur. "Advanced Modeling of Concrete Deterioration due to Reinforcement Corrosion." *Canadian Journal of Civil Engineering*. Vol. 33. pp. 707–718. 2006.

Ito, K. and Y. Seol. "A 3-Dimensional Discrete Fracture Network Generator to Examine Fracture-Matrix Interaction Using TOUGH2." Proceedings of the TOUGH Symposium 2003, Berkeley, California, May 12–14, 2003. Berkeley, California: Lawrence Berkeley National Laboratory. 2003.

Jakob, A., F.-A. Sarott, and P. Spieler. "Diffusion and Sorption on Hardened Cement Pastes—Experiments and Modelling Results." PSI-Bericht 99-05. Villigen, Switzerland: Paul Scherrer Institute. 1999.

Jakubick, A.T., R.W. Gilham, I. Kahl, and M. Robin. "Attenuation of Pu, Am, Cs, and Sr Mobility in Concrete." Materials Research Society Symposium Proceedings 84. J.K. Bates and W. Seefeldt, eds. Pittsburgh, Pennsylvania: Materials Research Society. pp. 355–368. 1987.

Jensen, O.M. *Autogenous Phenomena in Cement-Based Materials*. Copenhagen, Denmark: Aalborg University. 2005.

Johnson, P.C. and R.A. Ettinger. "Heuristic Model for the Intrusion Rate of Contaminant Vapors into Buildings." *Environmental Science and Technology*. Vol. 25. pp. 1,445–1,452. 1991.

Jones, T.L. and R.J. Serne. "Contaminant Release From Solidified Radioactive-Wastes Buried in Unsaturated Sediments—Lysimeter Study." *Journal Of Environmental Quality*. Vol. 24. pp. 1,063–1,073. 1995.

Kahhaleh, K.Z. "Corrosion Performance of Epoxy Coated Reinforcement." Ph.D. dissertation. The University of Texas at Austin. Austin, Texas. 1994.

Kamali, S., M. Moranville, E. Garboczi, S. Prené, and B. Gérard. "Hydrate Dissolution Influence on the Young's Modulus of Cement Pastes." Fifth International Conference on Fracture Mechanics of Concrete and Concrete Structures, Vail, Colorado, April 12–16, 2004. Detroit, Michigan: American Concrete Institute. 2004.

Kaplan, D.I. "Geochemical Data Package for Performance Assessment Calculations Related to the Savannah River Site." WSRC–TR–2006–00004. Rev. 0. Aiken, South Carolina: Westinghouse Savannah River Company. 2006.

Kaplan, D. and J. Coates. "Concrete  $K_d$  Values Appropriate for the Tank Closure Performance Assessment." WSRC–RP–2007–01122. Aiken, South Carolina: Savannah River National Laboratory. 2007.

Kaplan, D.I., T. Hang, and S.E. Aleman. "Estimated Duration of the Reduction Capacity Within a High-Level Waste Tank (U)." WSRC–RP–2005–01674. Rev. 0. Aiken, South Carolina: Westinghouse Savannah River Company, LLC. 2005.

Kapoor, V. "Water Film Flow in a Fracture in Unsaturated Porous Medium." San Antonio, Texas: CNWRA. 1994.

Kauschinger, U.L., R.D. Spence, and B.E. Lewis. "*In-Situ* Grouting Technology Demonstration and Field Specifications Overview for Hot Deployment of the Multi-Point-Injection™ System in Gunite and Associated Tank TH-4." ORNL/TM–13710. Oak Ridge, Tennessee: Oak Ridge National Laboratory. 1998.

Kienzler, B., P. Vejmelka, H.-J. Herbert, H. Meyer, and C. Altenhein-Haese. "Long-Term Leaching Experiments of Full-Scale Cemented Waste Forms: Experiments and Modeling." *Nuclear Technology*. Vol. 129. pp. 101–118. 2000.

Kim, C.L., C.H. Cho, and H.J. Choi. "Equilibrium Concentration and Diffusion Controlled Leaching Model for Cement-Based Waste Forms." *Waste Management*. Vol. 15. pp. 449–455. 1995.

Komarneni, S. and D.M. Roy. "Mechanisms of Immobilization of Nuclear Waste Elements by Cement Minerals, Cement and Mortar." *Cement and Concrete Research*. Vol. 11. pp. 789–794. 1981.

Kosmatka, S.H., B. Kerkhoff, and W.C. Panarese. *Design and Control of Concrete Mixtures*. 14<sup>th</sup> Edition. Skokie, Illinois: Portland Cement Association. 2002.

Kosson, D.S., H.A. van der Sloot, F. Sanchez, and A.C. Garrabrants. "An Integrated Framework for Evaluating Leaching in Waste Management and Utilization of Secondary Materials." *Environmental Engineering Science*. Vol. 19, No. 3. 2002.

- Kranc, S.C. and A.A. Sagues. "A Numerical Method for the Recovery of Local Potentials and Currents Due to Corrosion of Steel in Concrete." *Journal of ASTM International*. Vol. 3. Paper: JAI11788. 2006.
- Kulik, D., U. Berner, and E. Curti. "Modeling Chemical Equilibrium Partitioning With the GEMS-PSI Code." B. Smith and B. Gschwend, eds. PSI Scientific Report 2003/Volume IV, Nuclear Energy and Safety. Villigen, Switzerland: Paul Scherrer Institute. pp. 109–122. 2004.
- Kumar, A., D.M. Roy, P.H. Licastro, and C.A. Langton. "Effective Diffusion Coefficients for Several Saltstone Waste Forms." Memo DPST–85–528. Aiken, South Carolina: Savannah River Laboratory. 1985.
- Lagerblad, B. "Leaching Performance of Concrete Based on Studies of Samples From Old Concrete Constructions." TR–01–27. Stockholm, Sweden: Swedish Nuclear Fuel and Waste Management Company. 2001.
- Langmuir, D. *Aqueous Environmental Geochemistry*. Upper Saddle River, New Jersey: Prentice Hall. 1997.
- Langton, C.A. "Chemical Degradation Assessment of Cementitious Materials for the HLW Tank Closure Project (U)." WSRC–STI–2007–00607. Rev. 0. Aiken, South Carolina: Savannah River National Laboratory. 2007.
- . "Physical Properties of Slag Saltstone." DPST 87–673. Aiken, South Carolina: Savannah River Laboratory. 1987a.
- . "EP and TCLP Test Results for Slag Saltstone." DPST 87–869. Aiken, South Carolina: Savannah River Laboratory. 1987b.
- . "Slag-Substituted Concrete for Saltstone Vault Construction." DPST–86–830. Aiken, South Carolina: Savannah River Laboratory. 1986.
- Langton, C.A., A. Ganguly, C.A. Bookhamer, M. Koval, and W.L. Mhyre. "Grout Formulations and Properties for Tank Farm Closure (U)." WSRC–STI–2007–00641. Rev. 0. Aiken, South Carolina: Savannah River National Laboratory. 2007.
- Langton, C.A., J.R. Harbour, D.H. Miller, W.L. Mhyre, C.N. Shramek, J. Carroll, E. Johnson, and A.L. Furgeson. "Grout Placement and Property Evaluation for Closing Hanford High-Level Waste Tanks—Scale-Up Testing." WSRC–TR–2003–00556. Rev. 0. Aiken, South Carolina: Westinghouse Savannah River Company. 2003.
- Langton, C.A., S.B. Oblath, D.W. Pepper, and E.L. Wilhite. "Waste Salt Disposal at the Savannah River Plant." *Chemical Engineering Communications*. Vol. 66. pp. 189–199. 1988.
- Last, G.V., R.J. Serne, and V.L. LeGore. "Field Lysimeter Studies for Performance Evaluation of Grouted Hanford Defense Wastes." PNL–10166. Richland, Washington: Pacific Northwest National Laboratory. 1995.
- Lay, S., P. Schiebl, and J. Cairns. "Probabilistic Service Life Models for Reinforced Concrete Structures." Report D3.2. Munich, Germany: Technical University of Munich. 2003.

- Lewis, E.L., J.W. Doty, R.F. Herbert, and P.D. Bantz. "Factors Influencing Leachability in a Pelletized Cement Waste Form." *Nuclear and Chemical Waste Management*. Vol. 2. pp. 109–111. 1981.
- Li, C.Q., R.E. Melchers, and J.J. Zheng. "An Analytical Model for Corrosion Induced Crack Width in Reinforced Concrete Structures." *ACI Structural Journal*. Vol. 103. pp. 479–487. 2006.
- Lichtner, P.C. "FLOTRAN User Manual." LA–UR–01–2349. Los Alamos, New Mexico: Los Alamos National Laboratory. 2001.
- Liu, H.H., C. Doughty, and G.S. Bodvarsson. "An Active Fracture Model for Unsaturated Flow and Transport in Fractured Rocks." *Water Resources Research*. Vol. 34. pp. 2,633–2,646. 1998.
- Lorier, T.H., D.H. Miller, J.R. Harbour, C.A. Langton, and W.L. Mhyre. "Grout Formulations for Closing Hanford High-Level Waste Tanks—Bench-Scale Study." WSRC–TR–2003–00447. Rev. 0. Aiken, South Carolina: Westinghouse Savannah River Company. 2003.
- Lukens, W.W., J.I. Bucher, D.K. Shuh, and N.M. Edelstein. "Evolution of Technetium Speciation in Reducing Grout." *Environmental Science and Technology*. Vol. 39. pp. 8,064–8,070. 2005.
- Lura, P. and O.M. Jensen. "Measuring Techniques for Autogenous Strain of Cement Paste." *Materials and Structures*. Vol. 40. pp. 431–440. 2007.
- Mace, N., C. Landesman, and C. Pointeau. "Characterization of Thermally Altered Cement Pastes—Influence on Selenite Sorption." *Advances in Cement Research*. Vol. 19. pp. 157–165. 2007.
- Macias, A., A. Kindness, and F.P. Glasser. "Impact of Carbon Dioxide on the Immobilization Potential of Cemented Wastes: Chromium." *Cement and Concrete Research*. Vol. 27. pp. 215–222. 1997.
- Mainguy, M., F.-J. Ulm, and F.H. Henkamp. "Similarity Properties of Demineralization and Degradation of Cracked Porous Materials." *International Journal of Solids and Structures*. Vol. 38. pp. 7,079–7,100. 2001.
- Malek, R., D.M. Roy, M.W. Barnes, and C.A. Langton. "Slag Cement—Low-Level Waste Forms at Savannah River Plant." DP-MS-85-9. Aiken, South Carolina: E.I. du Pont de Nemours and Company. 1985.
- Maltais, Y., J. Marchand, and E. Samson. "Predicting the Durability of Portland Cement Systems in Aggressive Environments—Laboratory Validation." *Cement and Concrete Research*. Vol. 34. pp. 1,579–1,589. 2004.
- Marchand, J., E. Samson, Y. Maltais, R.J. Lee, and S. Sahu. "Predicting the Performance on Concrete Structures Exposed to Chemically Aggressive Environment—Field Validation." *Materials and Structures*. Vol. 35. pp. 623–631. 2002.

Marchand, J., D.P. Bentz, E. Samson, and Y. Maltais. "Influence of Calcium Hydroxide Dissolution on the Transport Properties of Hydrated Cement Systems." J.P. Skalny, J. Gebauer, and I. Odler, eds. *Materials Science of Concrete: Calcium Hydroxide in Concrete, Special Volume*. Westerville, Ohio: American Ceramic Society. pp. 113–129. 2001.

Marchand, J., E. Samson, and Y. Maltais. "Modeling Microstructural Alterations of Concrete Subjected to External Sulfate Attack." *Materials Science of Concrete: Sulfate Attack Mechanisms*. J. Marchand and J.P. Skalny, eds. Westerville, Ohio: American Ceramic Society. pp. 211–257. 1999.

Martys, N.S. "Survey of Concrete Transport Properties and Their Measurement." NISTIR–5592. Gaithersburg, Maryland: National Institute of Standards and Technology. 1995.

Matschei, T., B. Lothenbach, and F.P. Glasser. "Thermodynamic Properties of Portland Cement Hydrates in the System  $\text{CaO-Al}_2\text{O}_3\text{-SiO}_2\text{-CaSO}_4\text{-CaCO}_3\text{-H}_2\text{O}$ ." *Cement and Concrete Research*. Vol. 37. pp. 1,379–1,410. 2007.

Mattigod, S.V., P.F. Martin, G.A. Whyatt, K.E. Schwab, R.J. Serne, and M.I. Wood. "Diffusion and Leaching of Selected Radionuclides (Iodine-129, Technetium-99, and Uranium) Through Category 3 Waste Encasement Concrete and Soil Fill Material." PNNL–13639. Richland, Washington: Pacific Northwest National Laboratory. 2001.

Matzen, S.L., J.M. Beiriger, P.C. Torretto, P. Zhao, and B.E. Viani. "Uranium(VI) and Neptunium(V) Transport Through Fractured, Hydrothermally Altered Concrete." *Radiochimica Acta*. Vol. 88. pp. 657–664. 2000.

McConnell, Jr., J.W., R.D. Rogers, J.D. Jastrow, W.E. Sanford, S.R. Cline, T.M. Sullivan, and M. Fuhrmann. "Results After Ten Years of Field Testing Low-Level Radioactive Waste Forms Using Lysimeters." ANL/ER/CP–95275. Idaho Falls, Idaho: Idaho National Engineering Laboratory. 1997.

Meier, S.A., M.A. Peter, and M. Bohn. "A Two-Scale Modeling Approach to Reaction–Diffusion Processes in Porous Materials." *Computational Materials Science*. Vol. 39. pp. 29–34. 2007.

Mobasher, B. and C.F. Ferraris. "Simulation of Expansion in Cement Based Materials Subjected to External Sulfate Attack." *Advances in Concrete Through Science and Engineering*. J. Weiss, K. Kovler, J. Marchand, and S. Mindess, eds. Bagnaux, France: RILEM. pp. 1–12. 2004.

Monlouis-Bonnaire, J.P., J. Verdier, and B. Perrin. "Prediction of the Relative Permeability of Gas Flow of Cement-Based Materials." *Cement and Concrete Research*. Vol. 34. pp. 737–744. 2004.

Moranville, M., S. Kamali, and E. Guillon. "Physicochemical Equilibria of Cement-Based Materials in Aggressive Environments—Experiment and Modeling." *Cement and Concrete Research*. Vol. 34. pp. 1,569–1,578. 2004.

Moridis, G.J., Y.-S. Wu, and K. Pruess. "EOS9nT: A TOUGH2 Module for the Simulation of Water Flow and Solute/Colloid Transport in the Subsurface." LBNL–42351. Berkeley, California: Lawrence Berkeley National Laboratory. 1999.

- Mounanga, P., A. Khelid, and G. Bastian. "Experimental Study and Modeling Approaches for the Thermal Conductivity Evolution of Hydrating Cement Paste." *Advances in Cement Research*. Vol. 16. pp. 95–103. 2004.
- Munoz, A., C. Andrade, and A. Torres. "Corrosion Products Pressure Needed To Crack the Concrete Cover." C.U. Grosse, ed. *Advances in Construction Materials 2007*. Berlin, Germany: Springer. pp. 359–370. 2007.
- Nagataki, S., H. Ohga, and E.K. Kim. "Effect of Curing Conditions on the Carbonation of Concrete with Fly Ash and the Corrosion of Reinforcement in Long-term Tests." Proceedings of the International Conference on the Use of Fly Ash, Silica Fume, Slag, and Natural Pozzolans in Concrete, Madrid, Spain. American Concrete Institute Special Publication 91. Vol. 1. Farmington Hills, Michigan: American Concrete Institute. pp. 521–540. 1986.
- Nakamura, H., S. Hamada, T. Tanimoto, and M. Miyamoto. "Estimation of Thermal Crack Resistance for Mass Concrete Structures with Uncertain Material Properties." *Structural Journal*. Vol. 96. pp. 509–518. 1999.
- Narasimhan, T.N. "Multidimensional Numerical Simulation of Fluid Flow in Fractured Porous Media." *Water Resources Research*. Vol. 18. pp. 1,235–1,247. 1982.
- National Council on Radiation Protection and Measurements. "Performance Assessment of Near-Surface Facilities for Disposal of Low-Level Radioactive Waste." Report No. 152. Bethesda, Maryland: National Council on Radiation Protection and Measurements. 2005.
- National Research Council. "Tank Waste Retrieval, Processing, and On-site Disposal at Three Department of Energy Sites: Final Report." Washington, DC: National Academy Press. 2006.
- . "The State of Development of Waste Forms for Mixed Wastes." Washington, DC: National Academy Press. 1999.
- . "Guide to the Compounds of Interest in Cement and Concrete Research." Highway Research Board Special Report 127. Washington, DC: National Research Council. 1972.
- Naus, D.J. NUREG/CR-6927, "Primer on Durability of Nuclear Power Plant Reinforced Concrete Structures—A Review of Pertinent Factors." Oak Ridge, Tennessee: Oak Ridge National Laboratory. 2007.
- Neall, F.B. "Modeling the Long-Term Chemical Evolution of Cement-Groundwater Systems." Materials Research Society Symposium Proceedings 412. W.M. Murphy and D.A. Knecht, eds. Pittsburgh, Pennsylvania: Materials Research Society. pp. 483–490. 1996.
- Neretnieks, I. "Fast Method for Simulation of Radionuclide Chain Migration in Dual Porosity Fracture Rocks." *Journal of Contaminant Hydrology*. Vol. 88. pp. 269–288. 2006.
- . "Diffusion in the Rock Matrix: An Important Factor in Radionuclide Retardation?" *Journal of Geophysical Research*. Vol. 85, No. B8. pp. 4,379–4,397. 1980.
- Neville, A.M. *Properties of Concrete*. New York City, New York: John Wiley & Sons. 1996.

New York State Department of Health. "Guidance for Evaluating Soil Vapor Intrusion in the State of New York." New York City, New York: New York State Department of Health, Center for Environmental Health, Bureau of Environmental Exposure Investigation. 2006.

Nguyen, Q.T., A. Millard, S. Caré, V. L'Hostis, and Y. Berthaud. "Fracture of Concrete Caused by the Reinforcement Corrosion Products." *Journal de Physique IV France*. Vol. 136. pp. 109–120. 2006.

NRC. "U.S. Nuclear Regulatory Commission Technical Evaluation Report for the U.S. Department of Energy Idaho National Laboratory Site Draft Section 3116 Waste Determination for Idaho Nuclear Technology and Engineering Center Tank Farm Facility." Washington, DC: NRC. 2006.

\_\_\_\_\_. "U.S. Nuclear Regulatory Commission Technical Evaluation Report for the U.S. Department of Energy Savannah River Site Draft Section 3116 Waste Determination for Salt Waste Disposal." Washington, DC: NRC. 2005.

Oblath, S.B. "Leaching From Solidified Waste Forms Under Saturated and Unsaturated Conditions." *Environmental Science and Technology*. Vol. 23. pp. 1,098–1,102. 1989.

\_\_\_\_\_. "Relative Release Rates of Nitrate, Tc, Cs and Sr From Saltstone." Memo (July 20) to G.T. Wright, Savannah River Laboratory. Report DPST–84–620. Aiken, South Carolina: Savannah River Laboratory Technical Division. 1984.

Ochs, M., I. Pointeau, and E. Giffaut. "Caesium Sorption by Hydrated Cement as a Function of Degradation State: Experiments and Modelling." *Waste Management*. Vol. 26. pp. 725–732. 2006.

Ochs, M., B. Lothenbach, and E. Giffaut. "Uptake of Oxo-Anions by Cements Through Solid-Solution Formation: Experimental Evidence and Modeling." *Radiochimica Acta*. Vol. 90. pp. 639–646. 2002.

Odeh, A.M., W. Abu-El-Sha'r, and R. Al-Ruzouq. "Gas Transport Through Concrete Slabs." *Building and Environment*. Vol. 41. pp. 492–500. 2006.

Odler, I. "Hydration, Setting and Hardening of Portland Cement." P.C. Hewlitt, ed. *Lea's Chemistry of Cement and Concrete*. 4<sup>th</sup> Edition. London, United Kingdom: Arnold. pp. 241–298. 1998.

Or, D. and M. Tuller. "Flow in Unsaturated Fractured Porous Media: Hydraulic Conductivity of Rough Surfaces." *Water Resources Research*. Vol. 36. pp. 1,165–1,177. 2000.

Oron, A.P. and B. Berkowitz. "Flow in Rock Fractures: The Local Cubic Law Assumption Reexamined." *Water Resources Research*. Vol. 34. pp. 2,811–2,825. 1998.

Ouki, S.K. and C.D. Hills. "Microstructure of Portland Cement Pastes Containing Metal Nitrate Salts." *Journal of Waste Management*. Vol. 22. pp. 147–151. 2002.

Painter, S.C. and M.S. Seth. "MULTIFLO User's Manual Two-Phase Nonisothermal Coupled Thermal-Hydrologic-Chemical Flow Simulator: MULTIFLO Version 2.0." San Antonio, Texas: CNWRA. 2003.

Painter, S.L., V. Cvetkovic, and O. Pensado. "Time-Domain Random Walk Algorithms for Simulating Radionuclide Transport in Fractured Porous Rock." Proceedings of the 11<sup>th</sup> International High-Level Radioactive Waste Management Conference, Las Vegas, Nevada, April 30–May 4, 2006. La Grange Park, Illinois: American Nuclear Society. 2006.

Painter, S., P.C. Lichtner, and M.S. Seth. "MULTIFLO User's Manual Two-Phase Nonisothermal Coupled Thermal-Hydrologic-Chemical Flow Simulator MULTIFLO Version 1.5." San Antonio, Texas: CNWRA. 2001.

Palmer, D.A. and R.E. Meyer. "Adsorption of Technetium on Selected Inorganic Ion Exchange Materials and on a Range of Naturally Occurring Minerals Under Oxidic Conditions." *Journal of Inorganic and Nuclear Chemistry*. Vol. 43. pp. 2,979–2,984. 1981.

Papadakis, V.G., C.G. Vayenas, and M.N. Fardis. "Fundamental Modeling and Experimental Investigation of Concrete Carbonation." *ACI Materials Journal*. Vol. 88. pp. 363–373. 1991a.

———. "Physical and Chemical Characteristics Affecting the Durability of Concrete." *ACI Materials Journal*. Vol. 88. pp. 186–196. 1991b.

———. "Experimental Investigation and Mathematical Modeling of the Concrete Carbonation Problem." *Chemical Engineering Science*. Vol. 46. pp. 1,333–1,338. 1991c.

———. "A Reaction Engineering Approach to the Problem of Concrete Carbonation." *AIChE Journal*. Vol. 35. pp. 1,639–1,650. 1989.

Parkhurst, D.L. and C.A.J. Appelo. "User's Guide to PHREEQC (Version 2)—A Computer Program for Speciation, Batch-Reaction, One-Dimensional Transport, and Inverse Geochemical Calculations." U.S. Geological Survey Water Resources Investigations Report 99-4259. 1999.

Parkhurst, D.L., D.C. Thorstenson, and L.N. Plummer. "PHREEQE: A Computer Program for Geochemical Calculations." U.S. Geological Survey Water Resources Investigations Report 80-96. 1980.

Parrot, L.J. "Design for Avoiding Damage Due to Carbonation-Induced Corrosion." SP-145: Durability of Concrete—Proceedings of the Third CANMET–ACI International Conference, Nice, France, May 22–27, 1994. V.M. Malhotra, ed. Detroit, Michigan: American Concrete Institute. pp. 283–298. 1994.

Paul, V. "Performance of Building Materials in Contaminated Land." Report BR-255. Garston, Watford, United Kingdom: Building Research Establishment. 1994.

Pescatore, C. "Leach Rate Expressions for Performance Assessment of Solidified, Low-Level Radioactive Waste." *Waste Management*. Vol. 11. pp. 223–229. 1991.

Pfingsten, W. "Experimental and Modeling Indications for Self-Sealing of a Cementitious Low- and Intermediate-Level Waste Repository by Calcite Precipitation." *Nuclear Technology*. Vol. 140. pp. 63–82. 2002.

———. "Indications for Self-Sealing of a Cementitious L&ILW Repository." PSI Report 01-09. Villigen, Switzerland: Paul Scherrer Institute. 2001.

Phifer, M.A. and K.L. Dixon. "Recommended Effective Diffusion Coefficient for FTF Base Mat Surrogate and Tank Grouts." SRNL-ESB-2007-00034. Aiken, South Carolina: Savannah River National Laboratory. 2007.

Phifer, M.A., M.R. Millings, and G.P. Flach. "Hydraulic Property Data Package for the E-Area and Z-Area Soils, Cementitious Materials, and Waste Zones." WSRC-STI-2006-00198. Rev. 0. Aiken, South Carolina: Washington Savannah River Company. 2006.

Pierce, J.S. "Use of Fly Ash in Combating Sulfate Attack in Concrete." Proceedings of the 6<sup>th</sup> International Symposium on Fly Ash Utilization, Reno, Nevada, March 1982. DOE/METC/82-52. pp. 208-231. 1982.

Pisters, H. "Reaction of Corrosive Water With Cement." *Vom Wasser*. Vol. 30. pp. 208-221. 1963.

Plecas, I. "Immobilization of <sup>137</sup>Cs and <sup>60</sup>Co in Concrete Matrix." *Annals of Nuclear Energy*. Vol. 30. pp. 1,899-1,903. 2003.

Plecas, I. and S. Dimovic. "Immobilization of <sup>137</sup>Cs and <sup>60</sup>Co in Concrete Matrix—Part 2: Mathematical Modeling of Transport Phenomena." *Annals of Nuclear Energy*. Vol. 32. pp. 1,509-1,515. 2005a.

\_\_\_\_\_. "Immobilization of Radioactive Evaporator Concentrate in Mortar Matrix." *Progress in Nuclear Energy*. Vol. 46. pp. 151-157. 2005b.

Plummer, L.N. and E. Busenberg. "The Solubilities of Calcite, Aragonite, and Vaterite in CO<sub>2</sub>-H<sub>2</sub>O Solutions Between 0 and 90 °C and an Evaluation of the Aqueous Model for the System CaCO<sub>3</sub>-CO<sub>2</sub>-H<sub>2</sub>O." *Geochimica et Cosmochimica Acta*. Vol. 46. pp. 1,011-1,040. 1982.

Pointeau, I., D. Hainos, N. Coreau, and P. Reiller. "Effect of Organics on Selenite Uptake by Cementitious Materials." *Waste Management*. Vol. 26, Issue 7. pp. 733-740. 2006.

Pointeau, I., C. Landesman, and E. Giffaut. "Reproducibility of the Uptake of U(VI) Onto Degraded Cement Pastes and Calcium Silicate Hydrate Phases." *Radiochimica Acta*. Vol. 92. pp. 645-650. 2004.

Portage Environmental, Inc. "Analysis of Sorption Coefficient (K<sub>d</sub>) Values Supplemental Report for the Tank Farm Facility Preliminary Assessment." PEI-EDF-1023. Rev. 1. Aiken, South Carolina: Westinghouse Savannah River Company. 2005.

Portland Cement Association. "Chemical Admixtures." 2008.  
<[http://www.cement.org/basics/concretebasics\\_chemical.asp](http://www.cement.org/basics/concretebasics_chemical.asp)> (28 January 2008).

Pourbaix, M. "Atlas of Electrochemical Equilibria in Aqueous Solutions." Houston, Texas: NACE International. 1974.

Prikryl, J.D. and D.A. Pickett. "Recommended Site-Specific Sorption Coefficients for Reviewing Non-High-Level Waste Determinations at the Savannah River Site and Idaho National Laboratory." San Antonio, Texas: CNWRA. 2007.

Pruess, K., C. Oldenburg, and G. Moridis. "TOUGH2 User's Guide, Version 2.0." LBNL-43124. Berkeley, California: Lawrence Berkeley National Laboratory. 1999.

Qian, J.C., E.E. Lachowski, and F.P. Glasser. "The Microstructure of National Bureau of Standards Fly Ashes." *Materials Research Society Symposium Proceedings* 136. R.T. Hemmings, E.E. Berry, G.J. McCarthy, and F.P. Glasser, eds. Pittsburgh, Pennsylvania: Materials Research Society. pp. 86-97. 1989.

Radlinska, A., B. Pease, and J. Weiss. "A Preliminary Numerical Investigation on the Influence of Material Variability in the Early Age Cracking Behavior of Restrained Concrete." *Materials and Structures*. Vol. 40. pp. 375-386. 2007.

Rahman, A.A. and F.P. Glasser. "Comparative Studies of the Carbonation of Hydrated Cements." *Advances in Cement Research*. Vol. 2. pp. 49-54. 1989.

Rard, J.A., M.H. Rand, G. Anderegg, and H. Wanner. "Chemical Thermodynamics—Volume 3: Chemical Thermodynamics of Technetium." Amsterdam, The Netherlands: Elsevier. 1999.

Rasmussen, A. and I. Neretnieks. "Migration of Radionuclides in Fissured Rock: The Influence of Micropore Diffusion and Longitudinal Dispersion." *Journal of Geophysical Research*. Vol. 86. pp. 3,749-3,758. 1981.

Raupach, M. "Models for the Propagation Phase of Reinforcement Corrosion—An Overview." *Materials and Corrosion*. Vol. 57. pp. 605-613. 2006.

Reardon, E.J. "Problems and Approaches to the Prediction of the Chemical Composition in Cement/Water Systems." *Waste Management*. Vol. 12. pp. 221-239. 1992.

Richet, C., C. Galle, P. LeBescop, H. Peycelon, S. Bejaoui, I. Toven, I. Poiteau, V. L'Hostis, and P. Overa. "Synthesis of Knowledge on the Long-Term Behaviour of Concretes: Applications to Cemented Waste Packages." CEA-R-6050. Gif-sur-Yvette Cedex, France: Commissariat à l'Énergie Atomique-France. 2004.

Riding, K.A., J.L. Poole, A.K. Schindler, M.C.G. Juenger, and K.J. Folliard. "Evaluation of Temperature Prediction Methods for Mass Concrete Members." *ACI Materials Journal*. Vol. 103. pp. 357-365. 2006.

Riley, R.G. and C.A. Lo Presti. "Data Catalog for Models Simulating Release of Contaminants From Hanford Site Waste Sources." PNNL-13666. Richland, Washington: Pacific Northwest National Laboratory. 2001.

Rixom, R. and N. Mailvaganam. *Chemical Admixtures for Concrete*. 3<sup>rd</sup> Edition. London, United Kingdom: E & FN Spon. 1999.

Roden, E.E. and T.D. Sheibe. "Conceptual and Numerical Model of Uranium(VI) Reductive Immobilization in Fractured Subsurface Sediments." *Chemosphere*. Vol. 59. pp. 617-628. 2005.

Roger, D.E. "Determination of Carbon Dioxide and Aggressive Carbon Dioxide in Waters." *New Zealand Journal of Sciences*. Vol. 16. pp. 875-893. 1973.

- Rosenberger, K.H., B.C. Rogers, and R.K. Cauthen. "Saltstone Performance Objective Demonstration Document (U)." CBU-PIT-2005-00146. Rev. 0. Aiken, South Carolina: Westinghouse Savannah River Company. 2005.
- Rossabi, J. and R.W. Falta. "Analytical Solution for Subsurface Gas Flow to a Well Induced by Surface Pressure Fluctuations." *Ground Water*. Vol. 40. pp. 67-75. 2002.
- Samson, E. and J. Marchand. "Modeling the Transport of Ions in Unsaturated Cement-Based Materials." *Computers and Structures*. Vol. 85. pp. 1,740-1,756. 2007.
- Saqoe-Crenstil, K.K. and F.P. Glasser. "Steel in Concretes—Part 1: A Review of Electrochemical and Thermodynamic Aspects." *Magazine of Concrete Research*. Vol. 41. pp. 205-212. 1989a.
- . "Steel in Concretes—Part 2: Electron Microscopy Analysis." *Magazine of Concrete Research*. Vol. 41. pp. 213-220. 1989b.
- Schindler, A.K. and K.J. Folliard. "Heat of Hydration Models for Cementitious Materials." *ACI Materials Journal*. Vol. 102. pp. 24-33. 2005.
- Scrivener, K. and J. Skalny, eds. *RILEM Proceedings PRO035: Internal Sulfate Attack and Delayed Ettringite Formation*. Bagnoux, France: RILEM Publications. 2004.
- Serne, R.J., D. Rai, P.F. Martin, A.R. Felmy, L. Rao, and S. Ueta. "Leachability of Nd, U, Th, and Sr, From Cements in a CO<sub>2</sub> Free Atmosphere." Materials Research Society Symposium Proceedings 412. W.M. Murphy and D.A. Knecht, eds. Pittsburgh, Pennsylvania: Materials Research Society. pp. 459-467. 1996.
- Serne, R.J., R.O. Lokken, and L.J. Criscenti. "Characterization of Grouted Low-Level Waste to Support Performance Assessment." *Waste Management*. Vol. 12. pp. 271-287. 1992.
- Seveque, J.L., M.D. de Cayeux, M. Elert, and H. Nouguiet. "Mathematical Modeling of Radioactive Waste Leaching." *Cement and Concrete Research*. Vol. 22. pp. 477-488. 1992.
- Shaw, P. "Grout/CLSM Testing and Selection for the INTEC Tank Farm Closure." EDF-6715, Rev. 0. Idaho Falls, Idaho: Idaho National Engineering and Environmental Laboratory. 2006.
- Shrivastava, O.P. and R. Shrivastava. "Sr<sup>2+</sup> Uptake and Leachability Study on Cured Aluminum-Substituted Tobermorite-OPC Admixtures." *Cement and Concrete Research*. Vol. 31. pp. 1,251-1,255. 2001.
- Shrivastava, O.P. and T. Verma. "Sr<sup>2+</sup> Sorption and Leach Rate Studies on Synthetic Calcium Silicate Hydroxy Hydrate." *Advanced Cement Based Materials*. Vol. 2. pp. 119-124. 1995.
- Simunek, J., M. Sejna, and M.T. van Genuchten. "The HYDRUS-2D Software Package for Simulating the Two-Dimensional Movement of Water, Heat, and Multiple Solutes in Variably-Saturated Media." Washington, DC: U.S. Department of Agriculture, U.S. Salinity Laboratory, Agricultural Research Service. 1999.

Smith, R. and J.C. Walton. "The Role of Oxygen Diffusion in the Release of Technetium From Reducing Cementitious Waste Forms." Materials Research Society Symposium Proceedings 294. C.G. Interrante and R.T. Pabalan, eds. Pittsburgh, Pennsylvania: Materials Research Society. pp. 247–253. 1993.

———. "The Effects of Calcite Solid Solution Formation on the Transient Release of Radionuclides From Concrete Barriers." Materials Research Society Symposium Proceedings 212. T. Abrajano, Jr. and L.H. Johnson, eds. Pittsburgh, Pennsylvania: Materials Research Society. pp. 403–409. 1991.

Somerville, G., ed. "CONTECVET: A Validated Users Manual for Assessing the Residual Service Life of Concrete Structures—Manual for Assessing Structures Affected by ASR." EC Innovation Programme IN309021. Crowthorne, United Kingdom: British Cement Association. 2001.

Song, S. and H.M. Jennings. "Pore Solution Chemistry of Alkali-Activated Ground Granulated Blast-Furnace Slag." *Cement and Concrete Research*. Vol. 29. pp. 159–170. 1999.

Sparkes, S.T. and S.E. Long. "The Chemical Speciation of Technetium in the Environment—A Literature Survey." AERE R12743. Harwell, Oxon, United Kingdom: U.K. Atomic Energy Authority. 1988.

Spence, R.D. and A.J. Mattus. "Laboratory Stabilizations/Solidification of Tank Sludges: MVST/BVEST." *Journal of Environmental Management*. Vol. 70. pp. 189–202. 2004.

Spinks, J.W. and R.J. Woods. *An Introduction to Radiation Chemistry*. 3<sup>rd</sup> Edition. New York City, New York: John Wiley & Sons. 1990.

Stang, H., J.F. Olesen, P.N. Poulsen, and L. Dick-Nielsen. "On the Application of Cohesive Crack Modeling in Cementitious Materials." *Materials and Structures*. Vol. 40. pp. 365–374. 2007.

Stefanovic, G., Z. Sekulic, L. Cojbasic, and V. Javanovic. "Hydration of Mechanically Activated Mixtures of Portland Cement and Fly Ash." *Ceramics–Silikaty*. Vol. 51. pp. 160–167. 2007.

Steffens, A., D. Dinkler, and H. Ahrens. "Modeling Carbonation for Corrosion Risk Prediction of Concrete Structures." *Cement and Concrete Research*. Vol. 32. pp. 935–941. 2002.

Stegemann, J.A., A.S.R. Perera, C. Cheeseman, and N.R. Buenfeld. "1/8 Factorial Study of Metal Effects on Acid Neutralization by Cement." *Journal of Environmental Engineering*. Vol. 126. 2000.

Sudicky, E.A. and E.O. Frind. "Contaminant Transport in Fractured Porous Media: Analytical Solutions for a System of Parallel Fractures." *Water Resources Research*. Vol. 18. pp. 1,634–1,642. 1982.

Sugiyama, D. and T. Fujita. "A Thermodynamic Model of Dissolution and Precipitation of Calcium Silicate Hydrates." *Cement and Concrete Research*. Vol. 36. pp. 227–237. 2006.

\_\_\_\_\_. “Modelling the Sorption of Actinides Onto Cement: An Approach With the Surface Co-Precipitation Model.” *Materials Research Society Symposium Proceedings* 757. R.J. Finch and D.B. Bullen, eds. Warrendale, Pennsylvania: Materials Research Society. pp. 705–710. 2003.

\_\_\_\_\_. “Sorption of Radionuclides Onto Cement Materials Altered by Hydrothermal Reactions.” *Materials Research Society Symposium Proceedings* 556. D.J. Wronkiewicz and J.H. Lee, eds. Warrendale, Pennsylvania: Materials Research Society. pp. 1,123–1,130. 1999.

Sugiyama, D., T. Fujita, T. Chida, and M. Tsukamoto. “Alteration of Fractured Cementitious Materials.” *Cement and Concrete Research*. Vol. 37. pp. 1,257–1,264. 2007.

Sun, Y. and T.A. Buscheck. “Analytical Solutions for Reactive Transport of N-Member Radionuclide Chains in a Single Fracture.” *Journal of Contaminant Hydrology*. Vols. 62–63. pp. 695–712. 2003.

Swaddiwudhipong, S., D. Chen, and M.H. Zhang. “Simulation of the Exothermic Hydration Process of Portland Cement.” *Advances in Cement Research*. Vol. 14. pp. 61–69. 2002.

Sylwester, E.R., P.G. Allen, P. Zhao, and B.E. Viani. “Interactions of Uranium and Neptunium With Cementitious Materials Studied by XAFS.” *Materials Research Society Symposium Proceedings* 608. R.W. Smith and D.W. Shoesmith, eds. Warrendale, Pennsylvania: Materials Research Society. pp. 307–312. 2000.

Tagami, K. and S. Uchida. “Influence of Microbial Activity on Technetium Behaviour in Soil Under Waterlogged Conditions.” *Materials Research Society Symposium Proceedings* 353. T. Murakami and R.C. Ewing, eds. Pittsburgh, Pennsylvania: Materials Research Society. pp. 973–979. 1995.

Taylor, H.F.W. *Cement Chemistry*. 2<sup>nd</sup> Edition. London, United Kingdom: Thomas Telford. 1997.

\_\_\_\_\_. “A Method for Predicting Alkali Ion Concentrations in Cement Pore Fluids.” *Advances in Cement Research*. Vol. 1. pp. 5–16. 1987.

Thiéry, M. “Modélisation de la Carbonatation Atmosphérique des Matériaux Cimentaires.” Ouvrage d’art OA52—Etudes et Recherches des Laboratoires des Ponts et Chaussées. Paris, France: Laboratoire des Ponts et Chaussées. 2006.

Thompson, M.E. “Numerical Simulation of Solute Transport in Rough Fractures.” *Journal of Geophysical Research*. Vol. 96B. pp. 4,157–4,166. 1991.

Thorne, D. “Evaluation of Grout Formulations for Tank Farm Facility Closure.” PEI-EDF-1033. Rev. 0. Idaho Falls, Idaho: Portage Environmental, Inc. 2007.

Thunvik, R. and C. Braesler. “Gas Migration in Discrete Fracture Networks.” *Water Resources Research*. Vol. 26. pp. 2,425–2,434. 1990.

Tian, B. and M.D. Cohen. “Does Gypsum Formation During Sulfate Attack on Concrete Lead to Expansion?” *Cement and Concrete Research*. Vol. 30. pp. 117–123. 2000.

Tits, J., E. Wieland, and C.J. Muller. "Strontium Binding by Calcium Silicate Hydrates." *Journal of Colloid and Interface Science*. Vol. 300. pp. 78–87. 2006a.

Tits, J., K. Lijima, and E. Wieland. "The Uptake of Radium by Calcium Silicate Hydrates and Hardened Cement Paste." *Radiochimica Acta*. Vol. 94, Issue 9-11. pp. 637–643. 2006b.

Tits, J., E. Wieland, J.-P. Dobler, and D. Kunz. "The Uptake of Strontium by Calcium Silicate Hydrates Under High pH Conditions: An Experimental Approach To Distinguish Adsorption From Co-Precipitation Processes." *Materials Research Society Symposium Proceedings 807*. V.M. Oversby and L.O. Werme, eds. Warrendale, Pennsylvania: Materials Research Society. pp. 689–694. 2004.

Tits, J., T. Stumpf, T. Rabung, E. Wieland, and T. Fanghänel. "Uptake of Cm(III) and Eu(III) by Calcium Silicate Hydrates: A Solution Chemistry and Time-Resolved Laser Fluorescence Spectroscopy Study." *Environmental Science and Technology*. Vol. 37. pp. 3,568–3,573. 2003.

Tixier, R. and B. Mobasher. "Modeling of Damage in Cement-Based Materials Subjected to External Sulfate Attack. I: Formulation." *Journal of Materials in Civil Engineering*. Vol. 15. pp. 305–313. 2003a.

———. "Modeling of Damage in Cement-Based Materials Subjected to External Sulfate Attack. II: Comparison with Experiments." *Journal of Materials in Civil Engineering*. Vol. 15. pp. 314–322. 2003b.

Tognazzi, C., J.-M. Torrenti, M. Carcasses, and J.-P. Ollivier. "Coupling Between Diffusivity and Cracks in Cement-Based Systems." *Materials Research Society Symposium Proceedings 608*. R.W. Smith and D.W. Shoesmith, eds. Warrendale, Pennsylvania: Materials Research Society. pp. 325–330. 2000.

Tokunaga, T.K. and J. Wan. "Water Film Flow Along Fracture Surfaces of Porous Rock." *Water Resources Research*. Vol. 33. pp. 1,287–1,295. 1997.

Tokunaga, T.K., J. Wan, and S.R. Sutton. "Transient Film Flow on Rough Fracture Surfaces." *Water Resources Research*. Vol. 36. pp. 1,737–1,746. 2000.

Toongoenthong, K. and K. Maekawa. "Simulation of Coupled Corrosive Product Formation, Migration into Crack and Propagation in Reinforced Concrete Sections." *Journal of Advanced Concrete Technology*. Vol. 3. pp. 253–265. 2005.

Uchikawa, H. "Effect of Blending Components on Hydration and Structure Formation." 8th International Congress on the Chemistry of Cement. Rio de Janeiro. pp. 249–280. 1986.

van Breugel, K. "Prediction of Temperature Development in Hardening Concrete." *Prevention of Thermal Cracking in Concrete at Early Ages, RILEM Report 15*. R. Springenschmid, ed. London, United Kingdom: E & FN Spon. pp. 51–75. 1998.

van Eijk, R.J. "Hydration of Cement Mixtures Containing Contaminants—Design and Application of the Solidified Product." Ph.D. dissertation. University of Twente. The Netherlands. 2001.

van Genuchten, M.T. "A Closed-Form Equation for Predicting the Hydraulic Conductivity of Unsaturated Soils." *Soil Science Society of America Journal*. Vol. 44. pp. 892–898. 1980.

van Genuchten, M.T. and P.J. Wierenga. "Mass Transfer Studies in Sorbing Porous Media: Analytical Solutions." *Soil Science Society of America Journal*. Vol. 40. pp. 473–479. 1976.

Vu, K.A.T. and M.G. Stewart. "Predicting the Likelihood and Extent of Reinforced Concrete Corrosion-Induced Cracking." *Journal of Structural Engineering*. Vol. 131. pp. 1,681–1,689. 2005.

Vu, K.A.T., M.G. Stewart, and J.A. Mullard. "Corrosion-Induced Cracking: Experimental Data and Predictive Models." *ACI Structural Journal*. Vol. 102. pp. 719–726. 2005.

Walter, M.B., R.J. Serne, D.L. Johnstone, and D.R. Yonge. "Chemical Characterization, Leach and Adsorption Studies of Solidified Low-Level Wastes." *Nuclear and Chemical Waste Management*. Vol. 8. pp. 55–67. 1988.

Walton, F.B., J. Paquette, J.P.M. Ross, and W.E. Lawrence. "Tc(IV) and Tc(VII) Interactions With Iron Oxyhydroxides." *Nuclear Chemistry and Waste Management*. Vol. 6. pp. 121–126. 1986.

Walton, J.C. "Leaching From Cementitious Waste Forms in Belowground Vaults." *Journal of Environmental Engineering*. Vol. 120. pp. 1,507–1,523. 1994.

———. NUREG/CR–5445, "Performance of Intact and Partially Degraded Concrete Barriers in Limiting Mass Transport." Washington, DC: NRC. June 1992.

Walton, J.C. and R.R. Seitz. NUREG/CR–5614, "Performance of Intact and Partially Degraded Concrete Barriers in Limiting Fluid Flow." Washington, DC: NRC. July 1991.

Walton, J.C., L.E. Plansky, and R.W. Smith. NUREG/CR–5542, "Models for Estimation of Service Life of Concrete Barriers in Low-Level Radioactive Waste Disposal." Washington, DC: NRC. September 1990.

Wang, K., D.C. Jensen, S.P. Shah, and A.F. Karr. "Permeability of Cracked Concrete." Technical Report No. 46. Research Triangle Park, North Carolina: National Institute of Statistical Sciences. 1996.

Warwick, P., N. Evans, and S. Vines. "Studies on Metal Gluconic Acid Complexes." Materials Research Society Symposium Proceedings 932. P. Van Iseghem, ed. Warrendale, Pennsylvania: Materials Research Society. pp. 959–966. 2006.

West, J.S., C.J. Larosche, B.D. Koester, J.E. Breen, and M.E. Kreger. "State-of-the-Art Report About Durability of Post-Tensioned Bridge Substructures." Research Report 1405-1. Austin, Texas: The University of Texas at Austin. 1999.

Westall, J.C., J.L. Zachary, and F.M. Morel. "MINEQL—A Computer Program for the Calculation of Chemical Equilibrium Compositions of Aqueous Systems." M.I.T. Technical Note TN–18. Cambridge, Massachusetts: Parsons Laboratory, Massachusetts Institute of Technology. 1976.

Westinghouse Savannah River Company. "Response to Action Items From Public Meetings Between NRC and DOE To Discuss RAI for the Savannah River Site." CBU-PIT-2005-00203. Rev. 1. Aiken, South Carolina: Westinghouse Savannah River Company. 2005.

Wieland, E. and L.R. Van Loon. "Cementitious Near-Field Sorption Data Base for Performance Assessment of an ILW Repository in Opalinus Clay." PSI Bericht 03-06. Villigen, Switzerland: Paul Scherrer Institute. 2003.

Wieland, E., J. Tits, and D. Kunz. "Strontium Uptake by Cementitious Materials." *Environmental Science & Technology*. Vol. 42. pp. 403-409. 2008.

Wieland, E., J. Tits, and M.H. Bradbury. "The Potential Effect of Cementitious Colloids on Radionuclide Mobilisation in a Repository for Radioactive Waste." *Applied Geochemistry*. Vol. 19. pp. 119-135. 2004.

Wolery, T.J. "EQ3/6, A Software Package for Geochemical Modeling of Aqueous Systems." UCRLMA-110662-PT I-IV. Livermore, California: Lawrence Livermore National Laboratory. 1992.

Xu, T., E. Sonnenthal, N. Spycher, and K. Pruess. "TOUGHREACT User's Guide: A Simulation Program for Non-Isothermal Multiphase Reactive Geochemical Transport in Variably Saturated Geologic Media." LBNL-55460. Berkeley, California: Lawrence Berkeley National Laboratory. 2004.

Yokozeki, K. "Leaching From Cementitious Materials Used in Radioactive Waste Disposal Sites." *Thermodynamics, Solubility and Environmental Issues*. T.M. Letcher, ed. Amsterdam, The Netherlands: Elsevier, Inc. pp. 169-186. 2007.

Yokozeki, K., K. Watanabe, N. Sakata, and N. Otsuki. "Modeling of Leaching from Cementitious Materials Used in Underground Environment." *Applied Clay Science*. Vol. 26. pp. 293-308. 2004.

———. "Prediction of Changes in Physical Properties Due to Leaching of Hydration Products From Concrete." *Journal of Advanced Concrete Technology*. Vol. 1. pp. 161-171. 2003.

Yoon, S., K. Wang, W.J. Weiss, and S.P. Shah. "Interaction Between Loading, Corrosion, and Serviceability of Reinforced Concrete." *ACI Materials Journal*. Vol. 97. pp. 637-644. 2000.

Young, J.F. "A Review of the Pore Structure of Cement Paste and Concrete and Its Influence on Permeability." *Permeability of Concrete*. D. Whiting and A. Walitt, eds. ACI SP-108. Detroit, Michigan: American Concrete Institute. 1988.

Zhang, K. and A.D. Woodbury. "The Arnoldi Reduction Technique for Efficient Direct Solution of Radionuclide Decay Chain Transport in Dual-Porosity Media." *Journal of Contaminant Hydrology*. Vol. 44. pp. 387-416. 2000.

Zhang, G.X., B.F. Zhu, and N.X. Guo. "Thermal Stress Simulation and Possible Crack Analysis of Mianhuatan RCC Dam." Proceedings of the 4th International Symposium on Roller Compacted Concrete Dams, Madrid, Spain, November 17-19, 2003. Lisse, Netherlands: A.A. Balkema Publishers. 2003.

Zhao, P., P.G. Allen, E.R. Sylwester, and B.E. Viani. "The Partitioning of Uranium and Neptunium Onto Hydrothermally Altered Concrete." *Radiochimica Acta*. Vol. 88. pp. 729–736. 2000.

## **APPENDIX A**

# PERMEABILITY AND DIFFUSION PROPERTIES OF CEMENTITIOUS MATERIALS

## A1 INTRODUCTION

This appendix presents data related to the permeability and diffusion properties of cementitious materials. These data may be relevant to evaluating aqueous and vapor phase mass transport processes in engineered barriers to radionuclide releases from radioactive waste processing tanks that may be closed in place. The U.S. Department of Energy (DOE) has proposed *in-situ* disposal of residual radioactive materials contained in liquid storage tanks formerly used to process radioactive materials at the Savannah River Site (Savannah River Site) and the Idaho National Laboratory pursuant to Section 3116 of the Ronald W. Reagan National Defense Authorization Act for Fiscal Year 2005. An important component of the disposal plan at these sites is creation of an engineered barrier to radionuclide migration (in addition to preexisting barriers that were part of the original tank design) by filling the tanks with a cement-based grout and sealing any external tank penetrations (such as fill lines). Tanks also exist at the DOE Hanford, Washington, site and at the West Valley Nuclear Services site in New York State that may be closed in a similar manner. In addition to the grout that may be used to fill the tanks and fillings, preexisting concrete materials in tank walls, vaults, and footings may form part of the engineered barrier.

## A2 CONCEPTS AND DEFINITION OF TERMS

Most studies of the transport properties of cementitious materials have evaluated the durability of concrete structures used in civil engineering projects, but have not determined properties such as hydraulic conductivity or aqueous diffusion coefficients to evaluate chemical or radionuclide mass transport into and out of cementitious materials. These properties are important not only for estimating radionuclide release from the material, but also for estimating degradation of the material due to intrusion of environmental chemicals. Most published data on these properties is found in the civil engineering and material science literature, whereas members of the earth and environmental sciences community (such as soil scientists, hydrologists, and geochemists) conduct most radionuclide transport studies. For this reason, the terminology used to describe the transport properties of cementitious materials is not always consistent or transparent. This section discusses the concepts of fluid permeability and molecular diffusion and defines relevant parameters that are important for interpreting the permeability and diffusivity data reported in Section A3.

### A2.1 Permeability and Hydraulic Conductivity

For this report and for fluid (gas or liquid) flow modeling of cementitious materials, intrinsic permeability refers to the coefficient that relates the volumetric fluid flux to the fluid pressure gradient in a porous material according to Darcy's Law (e.g., Bird, et al., 1960; Bear, 1972)

$$q = - \frac{k}{\mu} \frac{dP}{ds} \quad (A2-1)$$

where

$q$	—	volumetric flux [L/t]
$k$	—	intrinsic permeability [L <sup>2</sup> ]
$\mu$	—	dynamic viscosity [M/L-t]
$P$	—	fluid pressure [M/L-t <sup>2</sup> ]
$s$	—	macroscopic distance in the direction of flow [L]
$\frac{dP}{ds}$	—	pressure gradient in the direction of flow pressure [M/L <sup>2</sup> -t <sup>2</sup> ]

As its name indicates,  $k$  is an intrinsic property of the porous material whose value is determined by the size distribution and shape of the void space (pores) and by the porosity. Although Darcy's Law and permeability strictly apply to a porous medium, similar relationships can be applied to fractured materials. Equation (A2-1) applies to a material saturated with a single fluid phase, such as water or air. In the case of water, Eq. (A2-1) can also be written in terms of a hydraulic conductivity and hydraulic head as

$$q = -\frac{k}{\mu} \frac{dP}{ds} = -\frac{\rho g k}{\mu} \frac{dH}{ds} = -K \frac{dH}{ds} \quad (\text{A2-2})$$

where

$\rho$	—	fluid density [M/L <sup>3</sup> ]
$g$	—	gravitational acceleration [L/t <sup>2</sup> ]
$K$	—	hydraulic conductivity [L/t]
$H$	—	hydraulic head [L]

The hydraulic conductivity,  $K$ , in Eq. (A2-2) depends on the properties of the fluid as well as the intrinsic properties of the material. Although not strictly correct, the terms permeability and hydraulic conductivity are sometimes used interchangeably in the technical literature on cementitious materials. In some cases, "permeability" refers to the hydraulic conductivity. In this report, the term permeability generally refers to the fluid-conducting property of the cementitious material, and the terms intrinsic or relative permeability and hydraulic conductivity will refer to measured values. If the material is not fully saturated with the mobile fluid, then the permeability or hydraulic conductivity is reduced due to the decreased pore space available for flow. Modifications to Eqs. (A2-1) and (A2-2) to account for this effect are discussed later.

Permeability is a bulk property of a porous material, and its value can depend on the volume of material tested or the volume of material to which Darcy's Law is being applied. Cementitious materials are typically multiporous, multipermeable materials because they consist of porous and permeable mortar (consisting of cement paste and sand-sized aggregate) and contain permeable micro- and macrocracks (e.g., Young, 1988; Martys, 1995; Garboczi and Bentz, 1996; Boulfiza, et al., 2003), as illustrated in Figure A2-1. The influence of these porous and permeable features on a reported value of permeability or hydraulic conductivity depends on the spatial scale of the measurement. Typically, a sample of uncracked mortar will have a lower permeability than a sample containing microcracks, and the permeability of a large sample containing macrocracks will have a higher permeability than a sample with only mortar and microcracks (e.g., Wang, et al., 1996). When choosing a value of permeability to use in a transport simulation, the value should be selected considering the scale of the processes being simulated and the scale of the measurement being relied on.

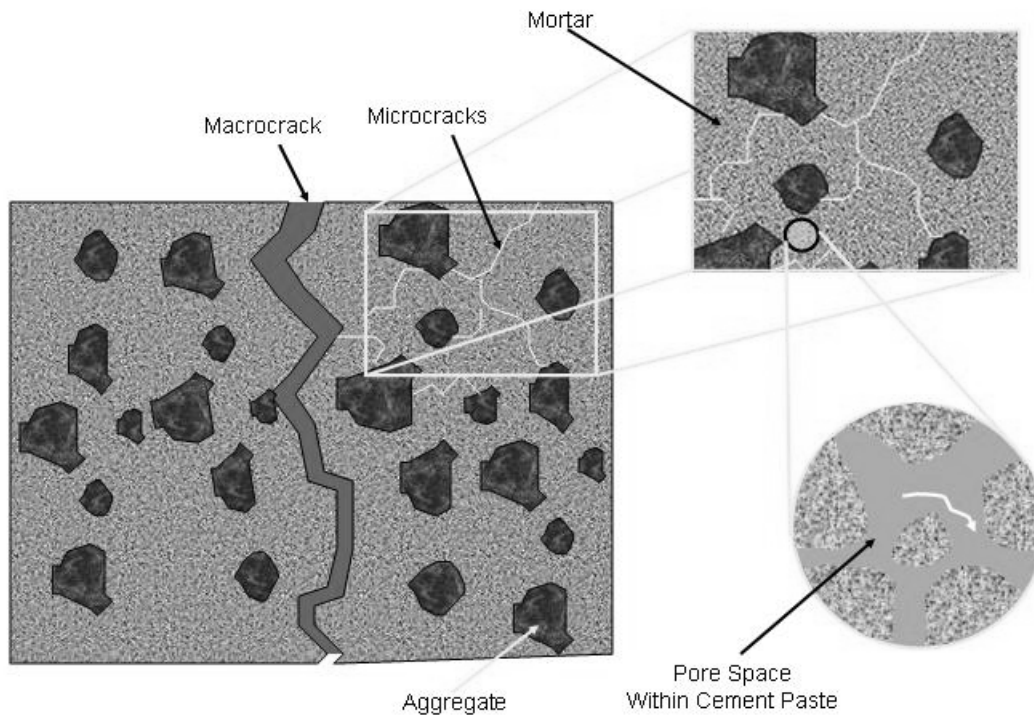


**Figure A2-1. Illustration of the Heterogeneous Pore Structure of Cementitious Materials**

If the cementitious material is not fully saturated with a single fluid, not all of the pore space is available to conduct the fluid. In this case, the permeability becomes a function of the fluid content, and Darcy's Law is usually expressed as (e.g., Bear, 1972)

$$q = -\frac{k_R(\theta)k}{\mu} \frac{dP}{ds} = -K(\theta) \frac{dH}{ds} \quad (\text{A2-3})$$

where

- $\theta$  — fluid (water) content [dimensionless]
- $k_R$  — relative permeability at fluid content  $\theta$  [dimensionless]
- $K(\theta)$  — unsaturated hydraulic conductivity at fluid content  $\theta$  [L/t]

In the case of cementitious materials used in tank closures, water is usually the fluid of interest, although it could also be air. The values of relative permeability and unsaturated hydraulic conductivity of porous and fractured materials can vary by orders of magnitude with the fluid content (e.g., Bear, 1972; Boulfiza, et al., 2003). Thus, the conditions under which a

permeability value was measured must be known to correctly interpret its meaning. Typical laboratory methods for measuring concrete water permeability assume that the sample is water saturated (e.g., Wang, et al., 1996). Claisse, et al. (1999) presented data showing the effect of drying and water content on air and water permeability values derived from *in-situ* testing methods.

Various empirical models have been presented in the soil science, hydrology, and petroleum engineering literature to describe the unsaturated hydraulic properties of porous materials (e.g., Brooks and Corey, 1966; van Genuchten, 1980). These models relate the relative permeability or hydraulic conductivity to the free water content of the material. The most commonly used model for soils or porous rock is that of van Genuchten (1980)

$$P_c = \frac{1}{\alpha_p} [S_e^{-1/m} - 1]^{1/n} \quad (\text{A2-4})$$

and

$$m = 1 - 1/n \quad (\text{A2-5})$$

where

$P_c$	—	capillary pressure (taken as positive)
$S_e$	—	effective saturation
$\alpha_p, n$	—	fitting parameters

The parameters  $\alpha_p$  and  $n$  are determined empirically.

The effective saturation is defined as

$$S_e = \frac{S - S_r}{1 - S_r} \quad (\text{A2-6})$$

where

$S$	—	actual saturation
$S_r$	—	irreducible saturation

The effective permeability ( $k_e$ ) for water flow is then

$$k_e = k_r k \quad (\text{A2-7})$$

where  $k_r$  is the relative permeability, which is assumed to be a function of the matrix saturation. The water relative permeability of the porous medium is described using van Genuchten's (1980) model by

$$k_r = S_e^{1/2} [1 - (1 - S_e^{1/m})^m]^2 \quad (\text{A2-8})$$

Although cementitious materials are not usually fully saturated (Martys, 1995), this study found very limited reports of measurements of the unsaturated hydraulic properties of cementitious materials. Yu, et al. (1993) measured the relative permeability of cementitious materials consisting of concrete from vaults and saltstone from Savannah River Site and reported values of  $\alpha$  and  $n$  for use in Eq. (A2-8). Dixon and Phifer (2007) reported values for grout materials considered for use in Savannah River Site tank closures. Figure A2-2 shows the unsaturated hydraulic conductivity as a function of water saturation calculated using Eq. (A2-8) and the parameters Dixon and Phifer (2007) reported. Figure A2-2 illustrates that the effective hydraulic conductivity of cementitious materials can change by many orders of magnitude with small changes in effective water saturation. For example, the effective hydraulic conductivity of the strong grout Dixon and Phifer (2007) tested increases by nearly two orders of magnitude with an increase in effective saturation from 80 percent to 90 percent. Thus, values of effective hydraulic conductivity used in estimating or simulating performance of a cementitious waste form or barrier can be very sensitive to uncertainty in the *in-situ* state of water saturation.

Given the very small pore sizes typical of concrete mortar {typically less than  $5 \times 10^{-8}$  m [ $2 \times 10^{-7}$  ft]; e.g., Halamickova, et al., 1995} relative to the pore size of typical soil that might

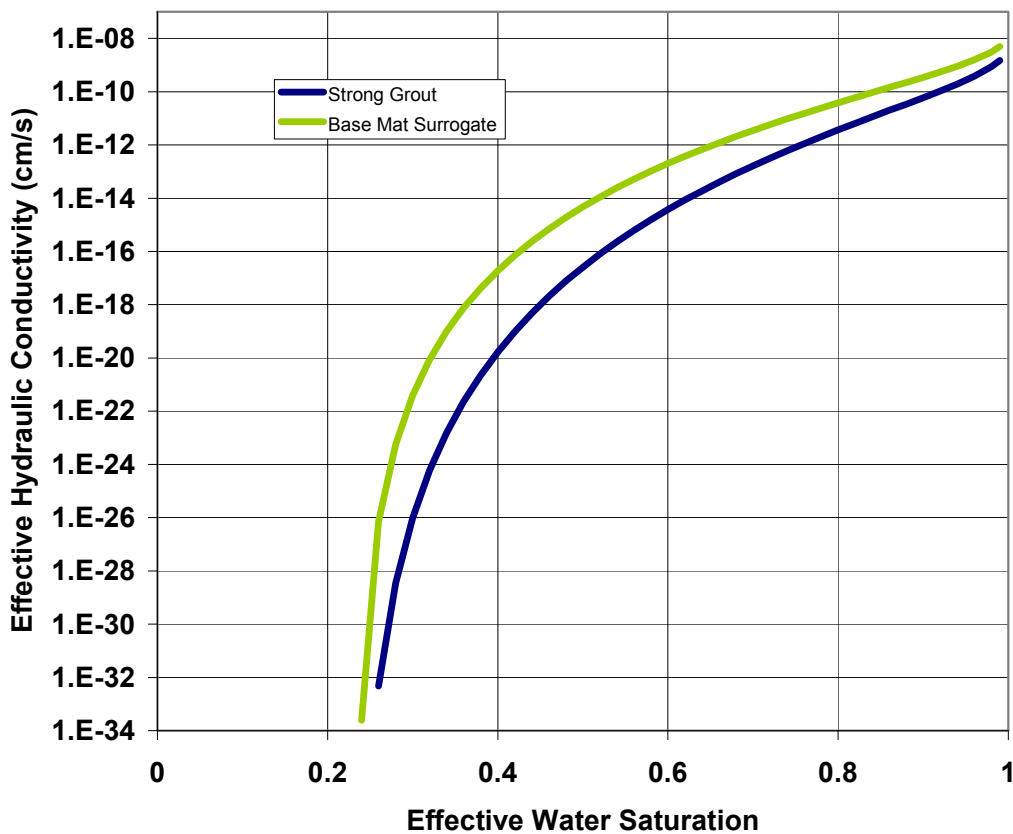


**Figure A2-2. Variation of Hydraulic Conductivity of Strong Grout and Base Mat Surrogate With Effective Water Saturation Based on Parameters Dixon and Phifer (2007) Reported**

surround an in-place tank {typically greater than  $1 \times 10^{-7}$  m [ $3 \times 10^{-7}$  ft] for a loam soil; e.g., Marshall, et al., 1996}, the cement-based material used in a tank closure and concrete vault can be expected to absorb water from the soil. Therefore, the water saturation of these cementitious materials is not likely to be extremely low and will probably be greater than 50 percent. For example, Wong, et al. (2007) found the water saturation of Portland cement exposed to air with 55 percent relative humidity and higher to be greater than 45 percent. Because the relative humidity of soil in the unsaturated zone is very high [greater than 90 percent (Hillel, 1982)], the saturation of cementitious materials used in tank closures should be relatively high whether at arid, semi-arid, or humid climate sites.

Mattson, et al. (2006) measured the unsaturated hydraulic conductivity of controlled low-strength material grout considered for use at Savannah River Site. They found that this material had a relatively high saturated hydraulic conductivity on the order of  $10^{-5}$  cm/s [ $3 \times 10^{-7}$  ft/s], which decreased to approximately  $10^{-7}$  cm/s [ $3 \times 10^{-9}$  ft/s] at approximately 60 percent saturation (porosity is 0.35). Tests on components-in-grout trenches grout material indicated saturated hydraulic conductivities as high as  $10^{-4}$  cm/s [ $3 \times 10^{-6}$  ft/s], which decreased to approximately  $10^{-7}$  cm/s [ $3 \times 10^{-9}$  ft/s] at 97 percent saturation. Mattson, et al. (2006) attributed the high saturated hydraulic conductivity and rapid decrease with saturation to the presence of macropores in the samples.

Conca and Wright (2006) measured the unsaturated hydraulic conductivity of “ordinary” concrete and “porous” grout, but gave no details regarding the specific materials tested. The hydraulic conductivity for the ordinary concrete ranged from approximately  $5 \times 10^{-5}$  cm/s [ $1.5 \times 10^{-6}$  ft/s] at 100 percent saturation to  $2 \times 10^{-5}$  cm/s [ $6 \times 10^{-7}$  ft/s] at 80 percent saturation. The hydraulic conductivity of the porous grout ranged from approximately  $5 \times 10^{-4}$  cm/s [ $1.5 \times 10^{-5}$  ft/s] at 100 percent saturation to  $2 \times 10^{-9}$  cm/s [ $6 \times 10^{-11}$  ft/s] at 35 percent saturation.

Various methods have been used to measure the permeability of cementitious materials. The most common method for measuring the water-saturated permeability is to place a cylinder of the material, which could be either a specially molded specimen or a core from a larger sample, into a permeability cell, schematically illustrated in Figure A2–3, and force a flow of water through the specimen. The permeability is calculated based on the measured flow rate and pressure gradient using Darcy’s Law. To minimize or prevent flow short-circuiting through the contact between the specimen and the pressure cell wall, sealants may be placed between the sample and the cell wall, or the sample placed in a rubber sleeve to which confining pressure is applied (ASTM International, 2003). This method is generally restricted to samples only a few tens of centimeters (a few inches) in diameter and a few centimeters 2.5 to 5.1 cm [1 to 2 in] thick. If the annulus between the specimen and the pressure cell wall is not adequately sealed, artificially high values of permeability may be calculated. Likewise, if the sample contains cracks that fully penetrate its thickness, the calculated permeability will be higher than that of a thicker specimen or structure that does not contain through-going cracks.

To measure permeability under unsaturated conditions, a pressure plate apparatus is commonly used (ASTM International, 1972), as illustrated in Figure A2–4 (Schaap, et al., 2003). The hydraulic conductivity at a given saturation can be determined by applying a partial vacuum to the specimen and measuring the flow rate after the water content of the specimen stabilizes. This can also be determined by measuring the specimen saturation at various applied pressures, fitting the saturation-pressure data to a model, such as Eq. (A2–4), and then using Eq. (A2–8) and a measured value of the saturated permeability to compute the unsaturated permeability.

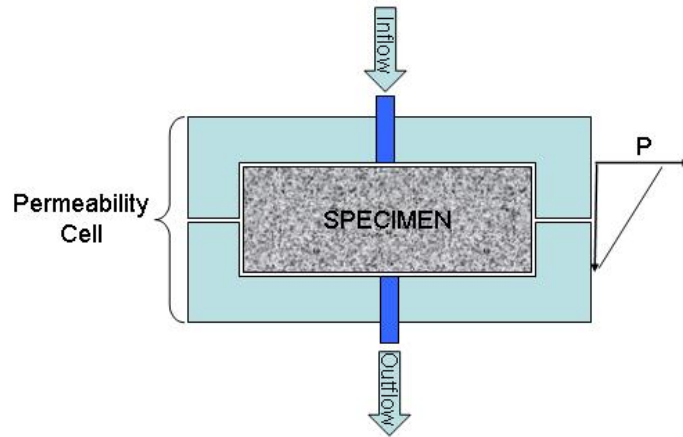


**Figure A2-3. Schematic Illustration of a Permeability Cell**

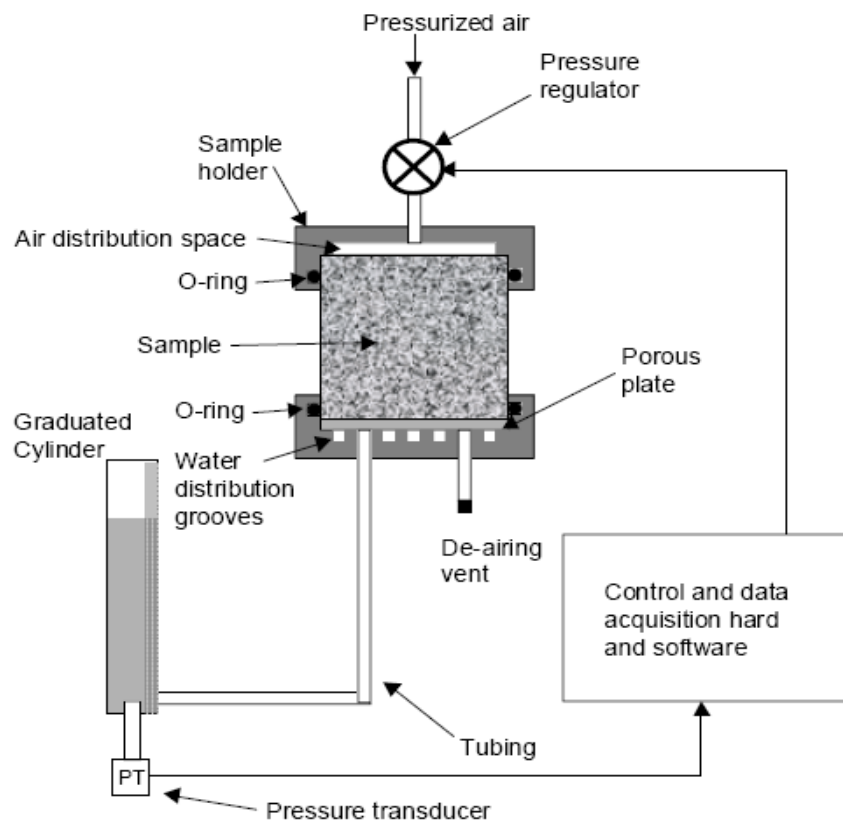


**Figure A2-4. Schematic Illustration of a Pressure Plate Apparatus Used To Measure Unsaturated Hydraulic Properties (Schaap, et al., 2003)**

Unsaturated permeability can also be determined by placing the specimen in a centrifuge and measuring the saturation decrease as the applied centrifugal force is increased (ASTM International, 2001; Dixon and Phifer, 2007). These methods are all limited to relatively small samples and are affected by the same scale effects as the saturated permeability measurements.

Scherer (2007) reported on a number of new methods for determining the permeability of cementitious materials. These include

- Pressure–permeability relationships
- Beam bending
- Thermopermeametry
- Dynamic pressurization

These methods have been developed to more rapidly measure the permeability of very low permeability cementitious materials than the conventional methods described previously. These innovative methods have not been generally applied, and no data based on them was identified for this report.

In addition to direct measurements of permeability or hydraulic conductivity, measurements of “sorptivity” of cementitious materials, a parameter related to permeability, have been reported in the technical literature. Sorptivity is determined from the rate of uptake of water by an unsaturated material using the following equation (e.g., Hillel, 1982; Martys, 1995; Claisse, et al., 1997)

$$V(t) = S_p t^{1/2} \quad (\text{A2-9})$$

where

- |       |   |   |
|-------|---|---|
| $V$   | — | cumulative water uptake per unit area [L] |
| $S_p$ | — | sorptivity [ $L/t^{1/2}$ ]                |
| $t$   | — | time                                      |

The sorptivity is the slope of the cumulative uptake plotted versus the square root of time. The sorptivity is related to the permeability, porosity, and pore size distribution of the porous material. Claisse, et al. (1997) developed the following approximate relationship between intrinsic permeability and sorptivity

$$S_p = \frac{ks\phi}{\gamma\mu} \quad (\text{A2-10})$$

where

- |          |   |                                |
|----------|---|--------------------------------|
| $s$      | — | surface tension [ $M/t^2$ ]    |
| $\phi$   | — | porosity                       |
| $\gamma$ | — | characteristic pore radius [L] |

Equation (A2-10) assumes linear flow of a sharp wetting front into the material. Computing the intrinsic permeability from Eq. (A2-10) requires estimating a characteristic pore radius that determines the capillary suction, which is the driving force for the water uptake. Because most

porous materials, including cementitious materials, consist of a range of pore sizes, the characteristic radius will depend on those pores that are not saturated at the initial water content of the test. Thus, although sorptivity indicates the relative permeability of materials, it cannot be directly used to determine permeability or hydraulic conductivity. For this reason, sorptivity data are not presented in this report.

Finally, the technical literature on cementitious materials contains many references to “permeability” measurements based on the “rapid chloride permeability test.” This is a standard method (ASTM C1202, AASHTO T277) for characterizing the ability of chloride and other salts to penetrate concrete in place of ponding tests that could take days or weeks to perform. The test is performed on concrete cores that are placed between solutions of sodium chloride and sodium hydroxide, as schematically illustrated in Figure A2–5. A 60-volt electric potential is applied between the negative (sodium chloride) and positive (sodium hydroxide) sides of the test cell. The value of “chloride permeability” is reported as the total charge (in coulombs) that flows through the circuit in 6 hours. As Martys (1995) pointed out, this test is actually an electrically driven diffusion test and does not directly measure the hydraulic permeability of the sample. For this reason, the results of the rapid chloride permeability test are not presented in this report.

## A2.2 Diffusion Coefficients

The diffusion coefficient of a specific chemical or isotopic species in a cementitious material is a function not only of the material but also of the chemical and physical properties of the species and the fluids in the material. For the case of aqueous diffusion of a dissolved species, most

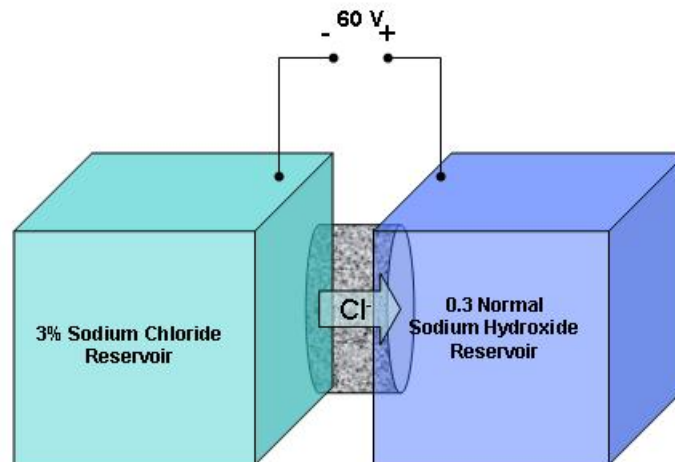


Figure A2–5. Schematic Illustration of the Rapid Chloride Permeability Test

experimental data for cementitious materials have been collected assuming the material is water-saturated. The meaning of the measured values can vary, however, depending on the nature of the measurement, the method of analyzing the data, and the definition of the “effective diffusion coefficient” the investigator uses.

Fick’s Law is the basis for all diffusion simulations and interpretations of experimental results. For diffusion of a nonsorbing species through a water-saturated porous medium, it can be written as

$$J_D = -\phi\alpha D_0 \frac{dC_a}{dx} \quad (\text{A2-11})$$

where

- $\alpha$  — matrix factor accounting for microscopic, tortuous paths and other factors related to pore geometry
- $C_a$  — aqueous concentration [M/L<sup>3</sup>]
- $D_0$  — free aqueous diffusion coefficient [L<sup>2</sup>/t]
- $\frac{dC_a}{dx}$  — macroscopic aqueous concentration gradient [M/L<sup>4</sup>]

The parameter  $\alpha$  in Eq. (A2–11) is an empirical factor that accounts for the effect of the tortuous microscopic path within the porous medium and other physical factors that interfere with diffusion, such as constrictions in the porous space (e.g., van Brakel and Heertjes, 1974) and, possibly, ion exclusion at pore throats (e.g., Graham-Bryce, 1963). The porosity in Eq. (A2–11) accounts solely for the reduced area for diffusion, although it is often expressed as a function of porosity (e.g., Hillel, 1982).

The most common definition of the effective diffusion coefficient in the soil science, material science, and chemical engineering literature is

$$D_e = \phi\alpha D_0 \quad (\text{A2-12})$$

The effective diffusion coefficient defined in Eq. (A2–12) depends on both the pore structure of the material and the diffusion properties of the chemical or radionuclide under consideration. It has also been called the “apparent effective diffusion coefficient” (Martys, 1995) or the “apparent diffusion coefficient” (e.g., Neretnieks, 1980) to distinguish it from the diffusion coefficient within the microscopic pores. An additional definition of the effective diffusion coefficient accounts for sorption of the diffusing species. For the case of a sorbing species whose sorption can be described by a linear isotherm

$$C_s = K_d C_a \quad (\text{A2-13})$$

- $C_s$  — sorbed concentration [M/M]
- $K_d$  — distribution coefficient [L<sup>3</sup>/M]

A retardation factor can be defined as (e.g., Bear, 1979)

$$R = 1 + \frac{\rho_b K_d}{\phi} \quad (\text{A2-14})$$

where

$\rho_b$  — dry bulk density [M/L<sup>3</sup>]

An effective diffusion coefficient including the effects of sorption can then be defined as

$$D_e = \frac{\phi \alpha}{R} D_0 \quad (\text{A2-15})$$

The effective diffusion coefficient defined by Eq. (A2-15) is the value measured and reported in most experimental studies of cementitious materials and is species and material specific. Although not explicitly represented in Eq. (A2-15), any ion exclusion effects are included in the matrix factor,  $\alpha$ .

Only one experimental study reviewed for this report (Tits, et al., 2003) reported values of the effective aqueous diffusion coefficient based on Eq. (A2-12). The data for gaseous diffusion includes both definitions. Unless specifically indicated, the diffusion coefficients presented in this report will be the effective diffusion coefficient as defined by Eq. (A2-15).

Although other physical and chemical processes can influence the release of radionuclides from cementitious materials, such as precipitation/dissolution, electrical potential gradients, and radioactive decay, the effect of these processes is not properly included in the definition of the effective diffusion coefficient. The effect of these processes would cause the time history of release or concentration gradient used to compute the effective diffusion coefficient to deviate from that of a simple diffusion process with retardation. Thus, their effect would not be incorporated into the diffusion coefficient in a properly interpreted experiment.

The effective aqueous diffusion coefficient is affected by the degrees of water saturation. As the saturation decreases, so does the effective aqueous diffusion coefficient due to (i) a decrease in the cross-sectional area of water-filled pores through which dissolved species can diffuse and (ii) an increase in the tortuosity of the water-filled channels through which diffusion occurs (i.e., an increase in the diffusion path length). The converse is true for vapor phase diffusion. As the water saturation decreases, the cross-sectional area available for vapor phase diffusion increases and the tortuosity of the vapor phase diffusion paths decreases resulting in an increase in the effective vapor phase diffusion coefficient with decreasing water saturation.

The most common methods for measuring aqueous diffusion coefficients are with a diffusion cell and the dynamic leach test. The diffusion cell method is fundamentally similar to that described for the rapid chloride permeability test (Figure A2-5) in which a sample of the material is placed between two reservoirs, one with a high concentration of the diffusing substance and one with a lower concentration, except that an electric current is not applied. The rate of increase in concentration in the low concentration reservoir is used, along with an appropriate mathematical model, to estimate the diffusion coefficient in the sample (e.g., Tits, et al., 2003).

A wide variety of diffusion cell designs can be found in the technical literature, but they all work on this same principle.

In the dynamic leach test, a cylindrical specimen presaturated with a species of interest is placed in a well-mixed solution of a lower concentration (see Figure A2–6) (e.g., Mattigod, et al., 2001). As the species of interest diffuses or leaches out of the specimen, its concentration in the external solution increases. The diffusion coefficient is estimated from the rate of increase in concentration in the external solution.

A less common method for measuring the diffusion coefficient is to place one end of a specimen in a concentrated solution of the species of interest and then to measure the concentration profile in the specimen after a given time. This method requires either destructive sampling and chemical analysis of the specimen, or use of a non-destructive method to measure the concentration profile (e.g., Jenneson, et al., 1998).

Measurements of gas-phase diffusion through cementitious materials have mostly been made using diffusion cells with gas as the conducting fluid rather than water (e.g., Nielson, et al., 1997). However, Culot, et al. (1976) developed a flux method for measuring the radon flux (attributed to gas-phase diffusion) through concrete walls.

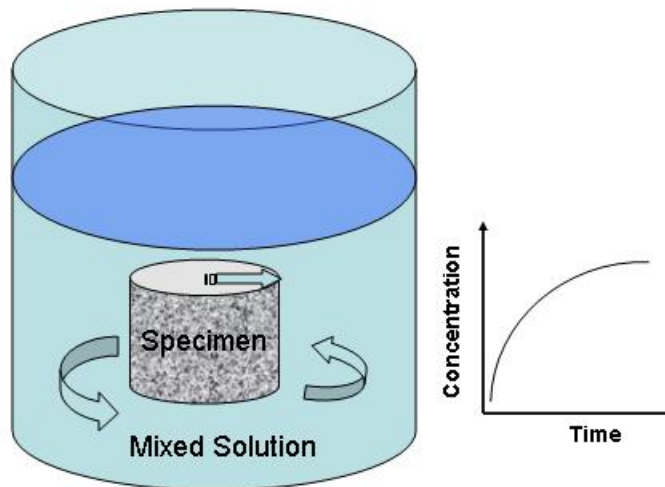


**Figure A2–6. Schematic Illustration of the Dynamic Leach Test for Determining Effective Diffusion Coefficient. Diffusion from Specimen Results in Increasing Concentration in Mixed Solution. Rate of Increase in Concentration is Used to Compute Effective Diffusion Coefficient.**

## A3 PERMEABILITY AND DIFFUSION COEFFICIENT DATA

This section presents technical literature data on the permeability and diffusivity of cementitious materials. The data are presented in terms of permeability and hydraulic conductivity measured using water as a working fluid, gas permeability (typically using air as the working fluid), aqueous effective diffusion coefficients for inorganic species, and vapor phase diffusion coefficients.

### A3.1 Water Permeability and Hydraulic Conductivity

Table A3–1 summarizes measurements of intrinsic permeability and saturated hydraulic conductivity of cementitious materials without macrocracks using water as a working fluid. The reported data are, for the most part, based on laboratory measurements on specially prepared specimens. The values are reported only to one significant figure even if the source of the data reported more significant figures. This was done for ease of comparison and to avoid implying that the reported values have more accuracy than they deserve given the variability of the materials tested and sources of data. For example, some sources presented experimental results only in graphical form, in which case the values listed in Table A3–1 had to be estimated from the graphs, whereas other sources presented results in tabular form.

Values reported in the primary source with units of length squared are presented as intrinsic permeability in meters squared and feet squared and marked with a “P” in the basis column. In these cases, a value of saturated hydraulic conductivity was computed using the relationship between intrinsic permeability and hydraulic conductivity in Eq. (A2–2) assuming a water density of  $1 \text{ gm/cm}^3$  [ $62.4 \text{ lb/ft}^3$ ], dynamic viscosity of  $0.01 \text{ gm/cm-s}$  [ $2.42 \text{ lb/ft-hr}$ ], and gravitational acceleration of  $9.81 \text{ m/s}^2$  [ $32.4 \text{ ft/s}^2$ ]. The value of hydraulic conductivity is qualified with an “S” to indicate it is a secondary or derived value. In cases where the source reported values of hydraulic conductivity, the reverse procedure was followed to derive a value for the intrinsic permeability.

The values of permeability presented in Table A3–1 cover a wide range of cementitious materials—from cement paste to construction concrete. The reported values for materials that did not contain macrocracks span approximately 9 orders of magnitude from  $10^{-14}$  to almost  $10^{-5} \text{ cm/s}$  [ $3 \times 10^{-15} \text{ ft/s}$  to almost  $3 \times 10^{-8} \text{ ft/s}$ ]. Figure A3–1 shows a cumulative frequency plot of the values for samples without macrocracks. The different symbols in Figure A3–1 indicate the general types of material tested. The data from Table A3–1 attributed to Mattson, et al. (2006) have not been included in Figure A3–1, because the authors indicated the permeability measurements may have been biased to high values by macrocracks or channels in the samples. Although Figure A3–1 suggests a median value for all cementitious materials of  $10^{-9} \text{ cm/s}$  [ $3 \times 10^{-11} \text{ ft/s}$ ], care should be taken in drawing any strong statistical inference because the number of samples in each material type was uneven.

The data on grout hydraulic conductivity Dixon and Phifer (2007) reported are plotted separately in Figure A3–2 along with the values for other grout and flowable cementitious materials listed in Table A3–1. Figure A3–2 indicates that the hydraulic conductivity of grouts Dixon and Phifer (2007) tested for possible use at Savannah River Site falls in a relatively narrow range with a median value of approximately  $10^{-8} \text{ cm/s}$  ( $3 \times 10^{-10} \text{ ft/s}$ ), although values as low as  $10^{-10} \text{ cm/s}$  ( $3 \times 10^{-12} \text{ ft/s}$ ) were measured. Figure A3–3 shows the data of Dixon and Phifer (2007) and the data of Naik, et al. (2001) for flowable grouts plotted versus the water to cement plus pozzolan

<b>Material Description</b>	<b>Measurement Conditions*</b>	<b>Intrinsic Permeability† (k)(m<sup>2</sup>)</b>	<b>Basis‡</b>	<b>Saturated Hydraulic Conductivity† (cm/s)§</b>	<b>Basis  </b>	<b>Comments</b>	<b>Source</b>
Low water-to-cement ratio cement paste	Reported	1.E-22	P	1.E-13	S	Values could not be traced to a particular source	Martys, N.S. "Survey of Concrete Transport Properties and Their Measurement." NISTIR 5592. Washington, DC: National Institute of Standards. 1995.
Typical concrete	Reported	1.E-18	P	1.E-09	S	Values could not be traced to a particular source	Martys (1995).
Concrete, Type I cement, uncracked	Laboratory	1.E-18	S	1.E-09	P	Sample prepared in laboratory	Wang, J., D.C. Jansen, S.P. Shah, and A.F. Karr. "Permeability of Cracked Concrete." Report No. 46. Research Triangle Park, North Carolina: National Institute of Statistical Sciences. 1996.
Concrete, ordinary Portland cement, water cured	Laboratory	3.E-17	P	3.E-08	S	Confinement flow through permeability, triaxial	Claisse, P.A., H.I. Elsayad, and I.G. Shaaban. "Test Methods for Measuring Fluid Transport in Cover Concrete." <i>Journal of Materials in Civil Engineering</i> . Vol. 11. pp. 138-143. 1999.
Concrete, ordinary Portland cement, air cured	Laboratory	3.E-16	P	3.E-07	S	Confinement flow through permeability, triaxial	Claisse, et al. (1999).
Concrete, low water cement, water cured	Laboratory	4.E-18	P	4.E-09	S	Confinement flow through permeability, triaxial	Claisse, et al. (1999).

**Table A3-1. Water Permeability (continued)**

<b>Material Description</b>	<b>Measurement Conditions*</b>	<b>Intrinsic Permeability† (k)(m<sup>2</sup>)</b>	<b>Basis‡</b>	<b>Saturated Hydraulic Conductivity† (cm/s)§</b>	<b>Basis  </b>	<b>Comments</b>	<b>Source</b>
Concrete, low water cement, water cured	Laboratory	2.E-17	P	2.E-08	S	Confinement flow through permeability, triaxial	Claisse, et al. (1999).
Portland cement mortar, no sand, 45% hydration, 0.4 water/cement	Laboratory	1.E-18	P	1.E-09	S	Values estimated from graph	Halamickova, P., R.J. Detwiler, D.P. Bentz, and E.J. Garboczi. "Water Permeability and Chloride Ion Diffusion in Portland Cement Mortars: Relationship to Sand Content and Critical Pore Diameter." <i>Cement and Concrete Research</i> . Vol. 25. pp. 790-802. 1995.
Portland cement mortar, no sand, 60% hydration, 0.4 water/cement	Laboratory	5.E-21	P	5.E-12	S	Values estimated from graph	Halamickova, et al. (1995).
Portland cement mortar, 45% sand, 57% hydration, 0.4 water/cement	Laboratory	5.E-19	P	5.E-10	S	Values estimated from graph	Halamickova, et al. (1995).
Portland cement mortar, 55% sand, 72% hydration, 0.4 water/cement	Laboratory	8.E-19	P	8.E-10	S	Values estimated from graph	Halamickova, et al. (1995).
Portland cement mortar, no sand, 60% hydration, 0.5 water/cement	Laboratory	1.E-17	P	1.E-08	S	Values estimated from graph	Halamickova, et al. (1995).
Portland cement mortar, no sand, 56% hydration, 0.5 water/cement	Laboratory	2.E-19	P	2.E-10	S	Values estimated from graph	Halamickova, et al. (1995).
Portland cement mortar, 45% sand, 72% hydration, 0.5 water/cement	Laboratory	1.E-19	P	1.E-10	S	Values estimated from graph	Halamickova, et al. (1995).
Portland cement mortar, 55% sand, 73% hydration, 0.5 water/cement	Laboratory	5.E-19	P	5.E-10	S	Values estimated from graph	Halamickova, et al. (1995).

Table A3-1. Water Permeability (continued)

Material Description	Measurement Conditions*	Intrinsic Permeability† (k)(m <sup>2</sup> )	Basis‡	Saturated Hydraulic Conductivity† (cm/s)§	Basis	Comments	Source
Concrete from Savannah River Site (SRS) Saltstone Vault 1B (fluid viscosity = 2.39 cp)	Laboratory	2.E-19	P	9.E-11	S	Sample provided as block, age not specified	Yu, A.D., C.A. Langton, and M. Serrato. "Physical Properties Measurement Program (U)." WSRC-RP-93-894. Aiken, South Carolina: Westinghouse Savannah River Company. 1993.
Concrete from SRS Saltstone Vault 5B	Laboratory	2.E-18	P	2.E-09	S	Sample provided as block, age not specified	Yu, et al. (1993).
Concrete from SRS Saltstone Vault 7B	Laboratory	1.E-18	P	1.E-09	S	Sample provided as block, age not specified	Yu, et al. (1993).
Concrete from SRS E-Area Vault 2E	Laboratory	7.E-22	P	7.E-13	S	Sample provided as block, age not specified	Yu, et al. (1993).
Concrete from SRS E-Area Vault 4E	Laboratory	1.E-21	P	1.E-12	S	Sample provided as block, age not specified	Yu, et al. (1993).
Concrete from SRS E-Area Vault 7E	Laboratory	1.E-21	P	1.E-12	S	Sample provided as block, age not specified	Yu, et al. (1993).
SRS Saltstone 1 (Fluid viscosity = 2.39 cp)	Laboratory	7.E-21	P	6.E-12	S	Sample provided as block, age not specified	Yu, et al. (1993).
SRS Saltstone 3A (Fluid viscosity = 2.39 cp)	Laboratory	5.E-21	P	5.E-12	S	Sample provided as block, age not specified	Yu, et al. (1993).
SRS Saltstone 4 (Fluid viscosity = 2.39 cp)	Laboratory	1.E-21	P	1.E-12	S	Sample provided as block, age not specified	Yu, et al. (1993).
Concrete with vinylester styrene binder	Laboratory	2.E-19	S	2.E-10	P	Laboratory test specimen	Heiser, J.H. and L.W. Milian. "Laboratory Evaluation of Performance and Durability of Polymer Grouts for Subsurface Hydraulic/Diffusion Barriers." BNL-61292. Long Island, New York: Brookhaven National Laboratory. 1994.

**Table A3-1. Water Permeability (continued)**

<b>Material Description</b>	<b>Measurement Conditions*</b>	<b>Intrinsic Permeability† (k)(m<sup>2</sup>)</b>	<b>Basis‡</b>	<b>Saturated Hydraulic Conductivity† (cm/s)§</b>	<b>Basis  </b>	<b>Comments</b>	<b>Source</b>
Concrete with polyester styrene binder	Laboratory	2.E-19	S	2.E-10	P	Laboratory test specimen	Heiser and Milian (1994).
Concrete with furan binder	Laboratory	5.E-20	S	5.E-11	P	Laboratory test specimen	Heiser and Milian (1994).
Concrete with acrylic binder	Laboratory	1.E-20	S	1.E-11	P	Laboratory test specimen, reported value less than $2 \times 10^{-10}$ cm/s	Heiser and Milian (1994).
Concrete with sulfur polymer cement	Laboratory	2.E-19	S	2.E-10	P	Laboratory test specimen	Heiser and Milian (1994).
Concrete with bitumen binder	Laboratory	1.E-20	S	1.E-11	P	Laboratory test specimen, reported value less than $2 \times 10^{-10}$ cm/s	Heiser and Milian (1994).
Concrete with Portland Type II cement	Laboratory	4.E-20	S	4.E-11	P	Laboratory test specimen	Heiser and Milian (1994).
Mortar with vinylester styrene binder	Laboratory	3.E-19	S	3.E-10	P	Laboratory test specimen	Heiser and Milian (1994).
Mortar with polyester styrene binder	Laboratory	3.E-19	S	3.E-10	P	Laboratory test specimen	Heiser and Milian (1994).
Mortar with acrylic binder	Laboratory	7.E-19	S	7.E-10	P	Laboratory test specimen	Heiser and Milian (1994).
Mortar with furan binder	Laboratory	3.E-17	S	3.E-08	P	Laboratory test specimen	Heiser and Milian (1994).
Mortar with sulfur polymer cement	Laboratory	5.E-20	S	5.E-11	P	Laboratory test specimen	Heiser and Milian (1994).
Mortar with bitumen binder	Laboratory	1.E-20	S	1.E-11	P	Laboratory test specimen, reported value less than $2 \times 10^{-10}$ cm/s	Heiser and Milian (1994).
Cracked concrete element after 5 years of exposure	Reported	1.E-19	S	1.E-10	P	Values could not be traced to a particular source	Boulfiza, M., K. Sakai, N. Banthia, and H. Yoshida. "Prediction of Chloride Ions Ingress in Uncracked and Cracked Concrete." <i>ACI Materials Journal</i> . Vol. 100. pp. 38-48. 2003.

Table A3-1. Water Permeability (continued)

Material Description	Measurement Conditions*	Intrinsic Permeability† (k)(m <sup>2</sup> )	Basis‡	Saturated Hydraulic Conductivity† (cm/s)§	Basis	Comments	Source
High performance concrete	Reported	2.E-23	S	2.E-14	P	Value traced to McGrath, P.F. "Development of Test Methods for Predicting Chloride Ingress Into High Performance Concrete." Doctor of Philosophy Thesis. Department of Civil Engineering, University of Toronto. Toronto, Canada. 1996.	Boddy, A., E. Bentz, M.D.A. Thomas, and R.D. Hooton. "An Overview and Sensitivity Study of a Multimechanistic Chloride Transport Model." <i>Cement and Concrete Research</i> . Vol. 29. pp. 827-837. 1999.
Typical bridge deck	Reported	1.E-20	S	1.E-11	P	Value traced to McGrath (1996)	Boddy, et al. (1999).
Roller-compacted concrete (RCC)	Laboratory	5.E-20	S	5.E-11	P	Test 1 using permeability cell	Pelletier, B. and E. Ouellet. "Evaluation of Water Permeability in a Roller Compacted Concrete (RCC) and a Conventional Concrete." 2005. < <a href="http://www.cement.ca/cement.nsf/eee9ec7bbd630126852566c40052107b/e662f65f76044afb852570900066d94e/\$FILE/English%20Report%20-%20Final.pdf">http://www.cement.ca/cement.nsf/eee9ec7bbd630126852566c40052107b/e662f65f76044afb852570900066d94e/\$FILE/English%20Report%20-%20Final.pdf</a> > (14 June 2007).
	Laboratory	1.E-21	S	1.E-12	P	Test 2 using permeability cell	Pelletier and Ouellet (2005).
Conventional concrete	Laboratory	1.E-19	S	1.E-10	P	Test 1 using permeability cell	Pelletier and Ouellet (2005).
	Laboratory	9.E-20	S	9.E-11	P	Test 2 using permeability cell	Pelletier and Ouellet (2005).

Table A3-1. Water Permeability (continued)

Material Description	Measurement Conditions*	Intrinsic Permeability† (k)(m <sup>2</sup> )	Basis‡	Saturated Hydraulic Conductivity† (cm/s)§	Basis	Comments	Source
20% cementitious material with 70% slag replacement	Laboratory	2.E-17	S	2.E-08	P	Hydraulic conductivity results with mix proportions showing least values	Opdyke, S.M. and J.C. Evans. "Slag-Cement-Bentonite Slurry Walls." <i>Journal of Geotechnical and Geoenvironmental Engineering</i> . Vol. 131. pp. 673-681. 2005.
15% cementitious material with 80% slag replacement	Laboratory	2.E-17	S	2.E-08	P	Hydraulic conductivity results with mix proportions showing least values	Opdyke and Evans (2005).
Fly ash slurry mixture with 0% foundry sand	Laboratory	1.E-14	S	1.E-05	P	Representative values estimated from graph	Naik, T.R., S.S. Singh, and B.W. Ramne. "Performance and Leaching Assessment of Flowable Slurry." <i>Journal of Environmental Engineering</i> . Vol. 127, No. 4. pp. 359-368. 2001.
Fly ash slurry mixture with 30% foundry sand	Laboratory	5.E-15	S	5.E-06	P	Representative values estimated from graph	Naik, et al. (2001).
Fly ash slurry mixture with 50% foundry sand	Laboratory	8.E-15	S	8.E-06	P	Representative values estimated from graph	Naik, et al. (2001).
Fly ash slurry mixture with 70% foundry sand	Laboratory	1.E-14	S	1.E-05	P	Representative values estimated from graph	Naik, et al. (2001).
Fly ash slurry mixture with 85% foundry sand	Laboratory	7.E-14	S	7.E-05	P	Representative values estimated from graph	Naik, et al. (2001).

**Table A3-1. Water Permeability (continued)**

<b>Material Description</b>	<b>Measurement Conditions*</b>	<b>Intrinsic Permeability† (k)(m<sup>2</sup>)</b>	<b>Basis‡</b>	<b>Saturated Hydraulic Conductivity† (cm/s)§</b>	<b>Basis  </b>	<b>Comments</b>	<b>Source</b>
Controlled low strength material	Laboratory	1.E-14	S	1.E-05	P	Low	Mattson, E.D., K.L. Dixon, M.A. Phifer, and K.M. Gibbs. "Novel Methods To Characterize Cementitious Material for Performance Assessment Calculations." Poster for Cementitious Materials for Waste Treatment, Disposal, Remediation and Decommissioning Workshop, December 12-14, 2006. Aiken, South Carolina: Westinghouse Savannah River Company. 2006.
Controlled low strength material	Laboratory	1.E-13	S	1.E-04	P	High	Mattson, et al. (2006).
Concrete for Hanford Site	Laboratory	4.E-19	S	4.E-10	P	Properties not reported	Rockhold, M.L., M.J. Fayer, and P.R. Heller. "Physical and Hydraulic Properties of Sediments and Engineered Materials Associated With Grouted Double-Shell Tank Waste Disposal at Hanford." PNNL-8813. Richland, Washington: Pacific Northwest National Laboratory. 1993.
Double-shell slurry feed grout	Laboratory	1.E-17	S	1.E-08	P		Rockhold, et al. (1993).
26-year-old concrete, saturated	Laboratory	1.E-19	S	1.E-10	P	Typical value for seven samples aged in saturated condition	Hearn, N., R.J. Detwiler, and C. Sframeli. "Water Permeability and Microstructure of Three Old Concretes." <i>Cement and Concrete Research</i> . Vol. 24, No. 4. pp. 633-640. 1994.
Portland cement paste, coarse	Laboratory	3.E-20	S	3.E-11	P	Average for four samples	Powers, T.C., L.E. Copeland, J.C. Hayes, and H.M. Mann. "Permeability of Portland Cement Paste." <i>Journal of the American Concrete Institute</i> . Vol. 51. pp. 285-298. 1954.

**Table A3-1. Water Permeability (continued)**

<b>Material Description</b>	<b>Measurement Conditions*</b>	<b>Intrinsic Permeability† (k)(m<sup>2</sup>)</b>	<b>Basis‡</b>	<b>Saturated Hydraulic Conductivity† (cm/s)§</b>	<b>Basis  </b>	<b>Comments</b>	<b>Source</b>
Portland cement paste, fine	Laboratory	1.E-19	S	1.E-10	P	Average for four samples	Powers, et al. (1954).
Strong grout, mix B2000-X-0-0-BS	Laboratory	2.8E-17	S	2.8E-08	P	7.62-cm [3-in] diameter mold sample	Dixon, K. and M. Phifer. "Hydraulic and Physical Properties of Tank Grouts and Base Mat Surrogate Concrete for FTF Closure." WSRC-STI-2007-00369. Aiken, South Carolina: Westinghouse Savannah River Company. 2007.
Strong grout, mix B2000-X-0-0-BS	Laboratory	2.5E-17	S	2.5E-08	P	7.62-cm [3-in] diameter mold sample	Dixon and Phifer (2007).
Strong grout, mix B2000-X-0-0-BS	Laboratory	2.9E-17	S	2.9E-08	P	7.62-cm [3-in] diameter mold sample	Dixon and Phifer (2007).
Strong grout, mix B2000-X-0-0-BS	Laboratory	9.5E-18	S	9.4E-09	P	7.62-cm [3-in] diameter mold sample	Dixon and Phifer (2007).
Strong grout, mix B2000-X-0-0-BS	Laboratory	6.9E-18	S	6.8E-09	P	7.62-cm [3-in] diameter mold sample	Dixon and Phifer (2007).
Strong grout, mix B2000-X-0-0-BS	Laboratory	2.7E-17	S	2.7e-08	P	7.62-cm [3-in] diameter mold sample	Dixon and Phifer (2007).
Reducing grout OPDEXE-X-P-0-BS	Laboratory	1.0E-17	S	1.0E-08	P	7.62-cm [3-in] diameter mold sample	Dixon and Phifer (2007).
Reducing grout OPDEXE-X-P-0-BS	Laboratory	8.6E-17	S	8.5E-08	P	7.62-cm [3-in] diameter mold sample	Dixon and Phifer (2007).
Reducing grout OPDEXE-X-P-0-BS	Laboratory	1.0E-17	S	1.0E-08	P	7.62-cm [3-in] diameter mold sample	Dixon and Phifer (2007).
Reducing grout OPDEXE-X-P-0-BS	Laboratory	5.3E-17	S	5.2E-08	P	7.62-cm [3-in] diameter mold sample	Dixon and Phifer (2007).

**Table A3-1. Water Permeability (continued)**

<b>Material Description</b>	<b>Measurement Conditions*</b>	<b>Intrinsic Permeability† (k)(m<sup>2</sup>)</b>	<b>Basis‡</b>	<b>Saturated Hydraulic Conductivity† (cm/s)§</b>	<b>Basis  </b>	<b>Comments</b>	<b>Source</b>
Reducing grout OPDEXE-X-P-0-BS	Laboratory	4.4E-17	S	4.3E-08	P	7.62-cm [3-in] diameter mold sample	Dixon and Phifer (2007).
Reducing grout OPDEXE-X-P-0-BS	Laboratory	1.7E-17	S	1.7E-08	P	7.62-cm [3-in] diameter mold sample	Dixon and Phifer (2007).
Reducing grout OPDEXE	Laboratory	9.1E-20	S	9.0E-11	P	2.54-cm [1-in] diameter mold sample	Dixon and Phifer (2007).
Reducing grout OPDEXE	Laboratory	4.1E-19	S	4.0E-10	P	2.54-cm [1-in] diameter mold sample	Dixon and Phifer (2007).
Reducing grout OPDEXE	Laboratory	5.1E-19	S	5.0E-10	P	2.54-cm [1-in] diameter mold sample	Dixon and Phifer (2007).
Reducing grout OPDEXE	Laboratory	5.1E-19	S	5.0E-10	P	2.54-cm [1-in] diameter mold sample	Dixon and Phifer (2007).
Reducing grout 1A	Laboratory	8.3E-18	S	8.2E-09	P	7.62-cm [3-in] diameter mold sample	Dixon and Phifer (2007).
Reducing grout 1A	Laboratory	9.6E-18	S	9.5E-09	P	7.62-cm [3-in] diameter mold sample	Dixon and Phifer (2007).
Reducing grout 1B	Laboratory	1.0E-17	S	1.0E-08	P	7.62-cm [3-in] diameter mold sample	Dixon and Phifer (2007).
Reducing grout 1B	Laboratory	1.5E-17	S	1.5E-08	P	7.62-cm [3-in] diameter mold sample	Dixon and Phifer (2007).
Reducing grout 1B	Laboratory	1.4E-17	S	1.4E-08	P	7.62-cm [3-in] diameter mold sample	Dixon and Phifer (2007).
Reducing grout 1B	Laboratory	1.3E-17	S	1.3E-08	P	7.62-cm [3-in] diameter mold sample	Dixon and Phifer (2007).

Table A3-1. Water Permeability (continued)

Material Description	Measurement Conditions*	Intrinsic Permeability† (k)(m <sup>2</sup> )	Basis‡	Saturated Hydraulic Conductivity† (cm/s)§	Basis	Comments	Source
Reducing grout 2	Laboratory	6.4E-18	S	6.3E-09	P	7.62-cm [3-in] diameter mold sample	Dixon and Phifer (2007).
Reducing grout 2	Laboratory	5.6E-18	S	5.5E-09	P	7.62-cm [3-in] diameter mold sample	Dixon and Phifer (2007).
Reducing grout 2	Laboratory	6.7E-18	S	6.6E-09	P	7.62-cm [3-in] diameter mold sample	Dixon and Phifer (2007).
Reducing grout 2	Laboratory	8.2E-18	S	8.1E-09	P	7.62-cm [3-in] diameter mold sample	Dixon and Phifer (2007).
Base mat surrogate	Laboratory	1.6E-17	S	1.6E-08	P	7.62-cm [3-in] core of concrete slab	Dixon and Phifer (2007).
Base mat surrogate	Laboratory	3.1E-17	S	3.1E-08	P	7.62-cm [3-in] core of concrete slab	Dixon and Phifer (2007).
Base mat surrogate	Laboratory	6.1E-17	S	6.0E-08	P	7.62-cm [3-in] core of concrete slab	Dixon and Phifer (2007).
Base mat surrogate	Laboratory	3.3E-17	S	3.3E-08	P	7.62-cm [3-in] core of concrete slab	Dixon and Phifer (2007).

\*Measurement conditions are reported as "laboratory" if measured in a laboratory environment; "field" if an *in-situ* field measurement; "reported" if the value is derived from an unspecified secondary source

†Values measured on water-saturated samples unless noted

‡Basis—P indicates primary value reported as intrinsic permeability; S indicates secondary value from hydraulic conductivity assuming water density of 1 g/cm<sup>3</sup>, viscosity of 1 cp, and gravity of 9.8 m/s<sup>2</sup>—conversion is  $k = K/9.8 \times 10^6$

§Conversion Factors:  
 1 cm/s approximately equal to  $9.81 \times 10^6$  m<sup>2</sup>  
 0.093 m<sup>2</sup> = 1 ft<sup>2</sup>  
 30.5 cm/s = 1 ft/s

||Basis—P indicates primary value reported as hydraulic conductivity; S indicates secondary value from intrinsic permeability assuming water density of 1 g/cm<sup>3</sup>, viscosity of 1 cp, and gravity of 9.8 m/s<sup>2</sup>.

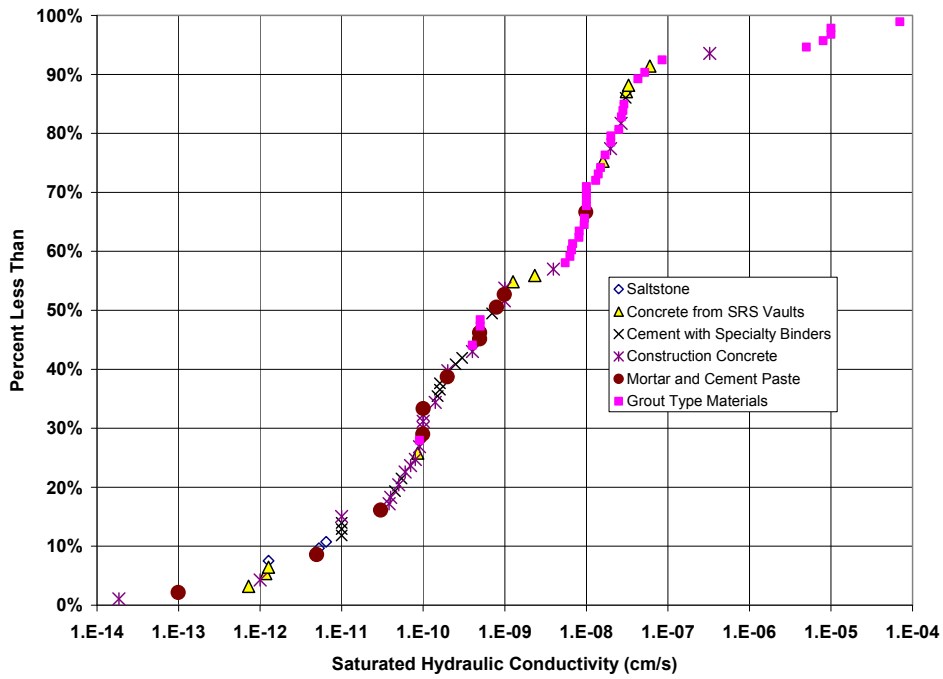


**Figure A3-1. Cumulative Distribution Plot of Hydraulic Conductivity Reported for Cementitious Materials Without Macrocracks**

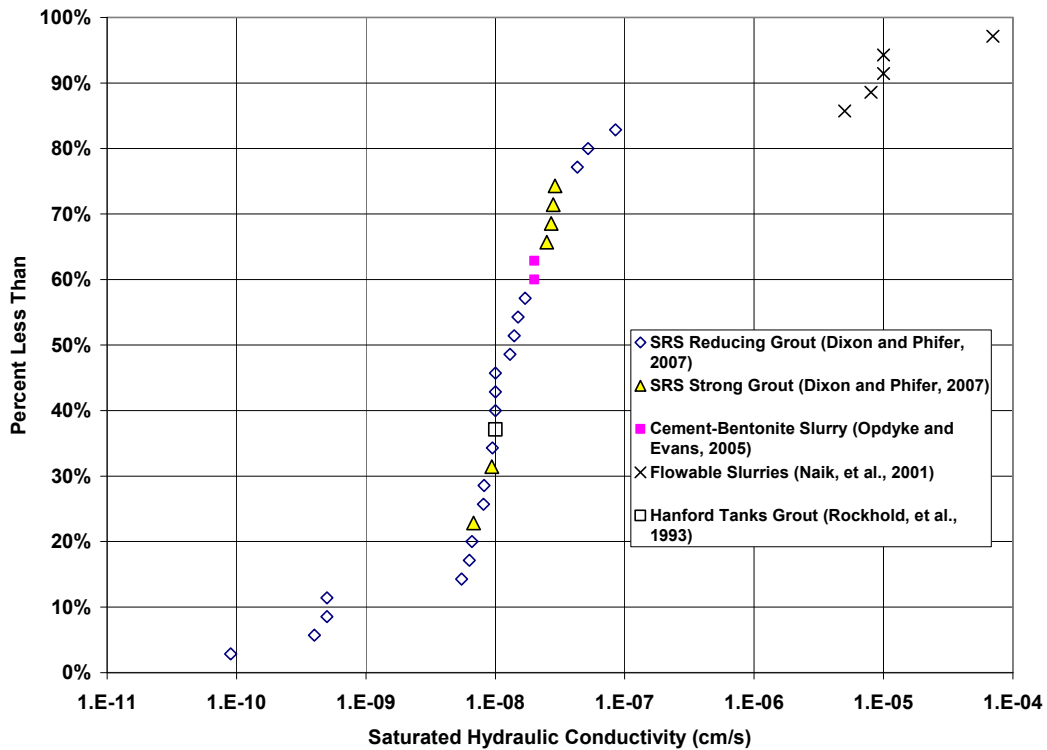


**Figure A3-2. Cumulative Distribution Plot of Hydraulic Conductivity Reported for Grout-Type Materials**

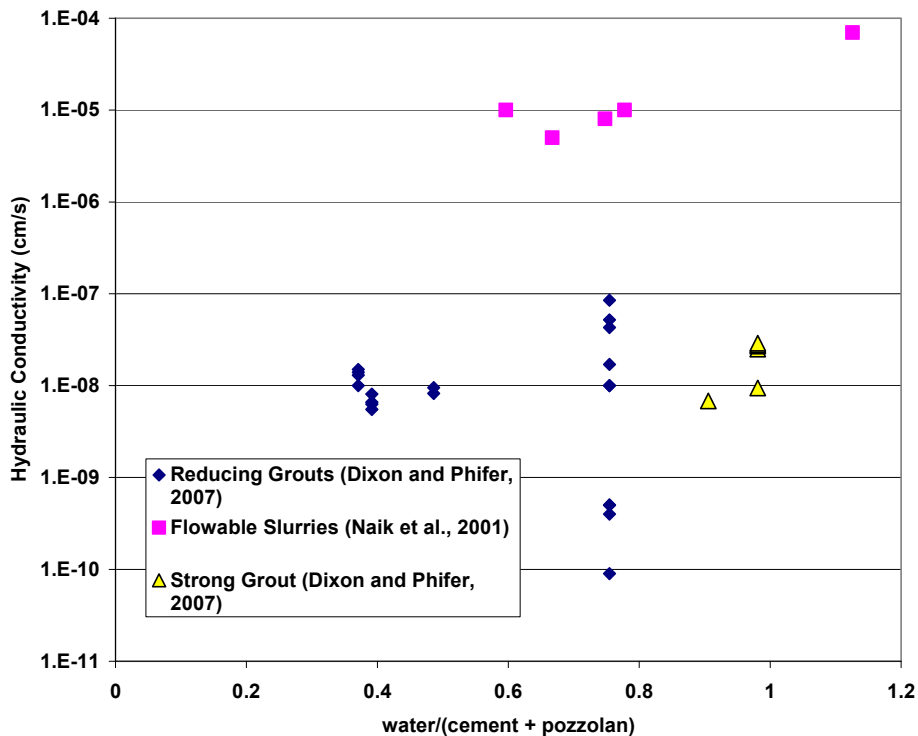


**Figure A3-3. Grout Hydraulic Conductivity Versus Water to Cement Plus Pozzolan Ratio**

ratio. For the grouts Dixon and Phifer (2007) studied, the pozzolan is fly ash and slag. For the Naik, et al. (2001) grouts, the pozzolan is only fly ash. Figure A3-3 does not indicate any clear relationship between the water-cement-pozzolan ratio and hydraulic conductivity for either data set. The values of hydraulic conductivity Dixon and Phifer (2007) reported cluster around  $10^{-8}$  cm/s ( $3 \times 10^{-10}$  ft/s), whereas the values Naik, et al. (2001) reported cluster around  $10^{-5}$  cm/s ( $3 \times 10^{-7}$  ft/s) despite similar water-cement-pozzolan ratios. The difference between the two data sets may be associated with the use of foundry sand by Naik, et al. (2001) and silica sand by Dixon and Phifer (2007). The grout mixes Dixon and Phifer (2007) tested also contained additives, such as a plasticizer and high-range water reducer.

The previously presented permeability data relate to cementitious materials that did not contain macrocracks, although these materials probably contain microcracks that are ubiquitous in cementitious materials as a result of drying and shrinkage (e.g., Young, 1988; Hearn, 1999). Several studies reviewed for this report presented data on the permeability of concrete containing macrocracks, and these data are discussed here.

Wang, et al. (1996) reported data on the saturated hydraulic conductivity of concrete containing discrete macrocracks of various apertures (Table A3-2). As would be expected, the permeability of the concrete increased dramatically with the aperture of the crack. Aldea, et al. (1999a,b) presented additional data on the effect of crack width on hydraulic conductivity showing a similar trend.

**Table A3-2. Intrinsic Permeability and Saturated Hydraulic Conductivity of Cracked Concrete Samples\***

<b>Material Description</b>	<b>Measurement Conditions†</b>	<b>Intrinsic Permeability‡ (k)(m<sup>2</sup>)</b>	<b>Basis§</b>	<b>Saturated Hydraulic Conductivity‡ (cm/s)¶</b>	<b>Basis¶</b>	<b>Comments</b>
Concrete, Type I cement, uncracked	Laboratory	1.E-18	S	1.E-09	P	Sample prepared in laboratory*
Concrete, Type I cement, 150-micron macrocrack	Laboratory	1.E-17	S	1.E-08	P	Value estimated from graph
Concrete, Type I cement, 200-micron macrocrack	Laboratory	8.E-16	S	8.E-07	P	Value estimated from graph
Concrete, Type I cement, 350-micron macrocrack	Laboratory	1.E-13	S	1.E-04	P	Value estimated from graph

\*Wang, J., D.C. Jansen, S.P. Shah, and A.F. Karr. "Permeability of Cracked Concrete." Report No. 46. Research Triangle Park, North Carolina: National Institute of Statistical Sciences. 1996.

†Measurement conditions are reported as "laboratory" if measured in a laboratory environment; "field" if an *in-situ* field measurement; "reported" if the value is derived from an unspecified secondary source.

‡Values measured on water-saturated samples unless noted.

§Basis—P indicates primary value reported as intrinsic permeability; S indicates secondary value from hydraulic conductivity assuming water density of 1 g/cm<sup>3</sup>, viscosity of 1 cp, and gravity of 9.8 m/s<sup>2</sup>.

¶Conversion Factors:  
 1 cm/s approximately equal to 9.81 × 10<sup>6</sup> m<sup>2</sup>  
 0.093 m<sup>2</sup> = 1 ft<sup>2</sup>  
 30.5 cm/s = 1 ft/s

¶Basis—P indicates primary value reported as hydraulic conductivity; S indicates secondary value from intrinsic permeability assuming water density of 1 g/cm<sup>3</sup>, viscosity of 1 cp, and gravity of 9.8 m/s<sup>2</sup>.

Hearn (1999) presented data on laboratory concrete specimens prepared with various water/cement ratios and subjected to various levels of unconfined stress. Hearn's data are summarized in Table A3-3 in terms of hydraulic conductivity, water/cement ratio, and applied stress. The samples that were tested were either never dried after they set or were oven dried prior to loading and then resaturated for permeability testing. Based on the data presented in Table A3-3, Hearn (1999) observed that the samples that were never dried and rewetted showed a much greater range in hydraulic conductivity (approximately three orders of magnitude) than the samples that were dried, stressed, and resaturated for permeability testing (approximately one order of magnitude). The variability in the Hearn (1999) data is illustrated in Figure A3-4. This behavior was attributed to stress-induced cracks that were healed before the permeability testing.

Comparing the data in Table A3-3 with those in Table A3-1 and Figure A3-1 for uncracked materials indicates that even the stressed and most permeable specimens in Hearn (1999) had hydraulic conductivities in the lower range of those of the uncracked materials. The Hearn (1999) data are for construction concrete and provide little insight into the hydraulic properties of monolithic grout materials that might be used in tank closures. The Hearn (1999) data may have some relevance to the hydraulic properties of tank walls, footings, and vaults.

When evaluating the permeability data for cracked cementitious materials, note that the samples tested had diameters of a few centimeters and thicknesses of 2.5 to 5.1 cm [1 to 2 in]. In a large concrete structure, the contribution of the cracks to the average permeability of the structure would depend on the number of cracks per unit area and their depth of penetration; thus the permeability data for cracked samples cannot be directly applied to a specific concrete structure. Given information on the intensity of cracking and penetration depth of the cracks in a cementitious structure, the laboratory data could be used to estimate areal and volumetric average permeability. Annuli that formed around pipes and at tank walls would also increase water flow and increase the apparent hydraulic conductivity of a grout monolith, as discussed in Section 6.

Five sources of data on the unsaturated cementitious materials were identified that presented values of the van Genuchten parameters ( $\alpha$  and  $n$ ) needed to compute the unsaturated hydraulic conductivity using Eq. (A2-8). These data are listed in Table A3-4. Yu, et al. (1993) reported values for concrete and saltstone from the Savannah River Site. Green, et al. (1995) reported values for Portland cement used in laboratory experiments. Rockhold, et al. (1993) reported values for concrete and grout used at the Hanford site. Savage and Janssen (1997) reported values for various Portland cement concretes. Finally, Dixon and Phifer (2007) reported values for grout formulations considered for tank closures at Savannah River Site.

### **A3.2 Permeability to Gas**

The limited data found on the gas permeability of cementitious materials are listed in Table A3-5. These data all relate to the permeability of concrete without macrocracks. The gas permeabilities of the laboratory-prepared specimens listed in Table A3-5 (data from de Beer, et al., 2005; Roux, et al., 1996) fall in the midrange of intrinsic water permeabilities for cementitious materials listed in Table A3-1. The single value for concrete that had been in service (Lampacher and Blight, 1998) is five orders of magnitude higher than that of the laboratory-prepared specimens and falls at the upper end of the range for water

Table A3-3. Summary of Hydraulic Conductivity of Stressed Concrete Samples\*

		Hydraulic Conductivity (cm/s)†									
Specimen Condition	Stress Level‡	w/c§ = 0.42	w   = 200 kg/m <sup>3</sup>	w/c§ = 0.56	w   = 200 kg/m <sup>3</sup>	w/c§ = 0.77	w   = 200 kg/m <sup>3</sup>	w/c§ = 0.56	w   = 240 kg/m <sup>3</sup>	w/c§ = 0.56	w   = 150 kg/m <sup>3</sup>
		Minimum	Maximum	Minimum	Maximum	Minimum	Maximum	Minimum	Maximum	Minimum	Maximum
Never dried	0	1.0E-10	1.0E-10	1.5E-11	1.0E-9	3.0E-12	3.7E-12	9.0E-11	1.6E-9	2.0E-11	5.0E-11
	0.3	1.4E-11	1.4E-10	2.5E-11	2.6E-9	1.1E-10	8.5E-10	—	—	2.0E-11	9.0E-10
	0.5	3.0E-12	1.7E-11	1.5E-10	4.5E-9	3.4E-10	7.2E-10	—	—	2.0E-11	1.0E-10
	0.7	2.0E-12	6.0E-11	1.4E-9	3.0E-9	1.7E-11	3.5E-10	4.7E-11	1.8E-10	3.5E-11	1.5E-10
	0.8	2.0E-12	—	5.0E-11	8.0E-10	4.2E-11	4.2E-10	2.0E-11	4.5E-9	2.0E-12	8.0E-12
Oven dried	0	5.1E-9	6.8E-9	1.4E-8	2.7E-8	4.0E-9	4.8E-9	1.1E-8	1.4E-8	—	—
	0.3	3.4E-9	7.6E-9	1.0E-8	3.5E-8	1.1E-8	1.2E-8	—	—	—	—
	0.5	4.3E-9	7.6E-9	1.0E-8	4.0E-8	6.4E-9	1.3E-8	—	—	—	—
	0.7	1.8E-9	2.2E-9	1.0E-8	6.0E-8	1.3E-9	6.4E-9	—	—	—	—
	0.8	3.6E-9	6.0E-9	3.5E-8	4.8E-8	1.1E-8	1.2E-8	3.6E-8	1.6E-8	—	—

\*Hearn, N. "Effect of Shrinkage and Load-Induced Cracking on Water Permeability of Concrete." *ACI Materials Journal*. Vol. 96. pp. 234-241. 1999.

†3.05 cm/s = 1 ft/s

‡Ratio of maximum applied stress to unconfined failure stress

§w/c is water/cement ratio

||w is water content

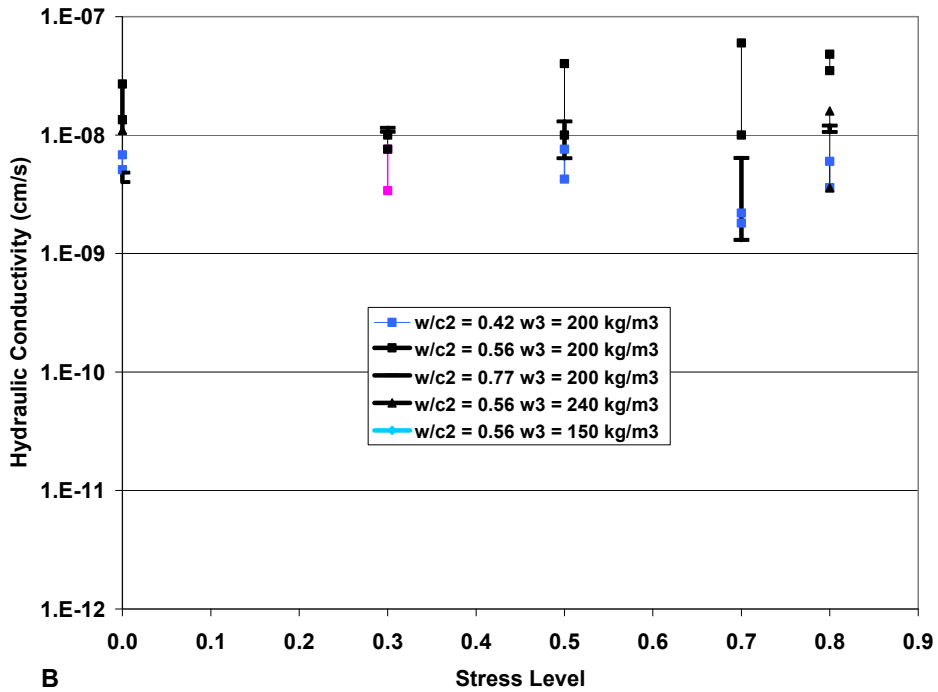
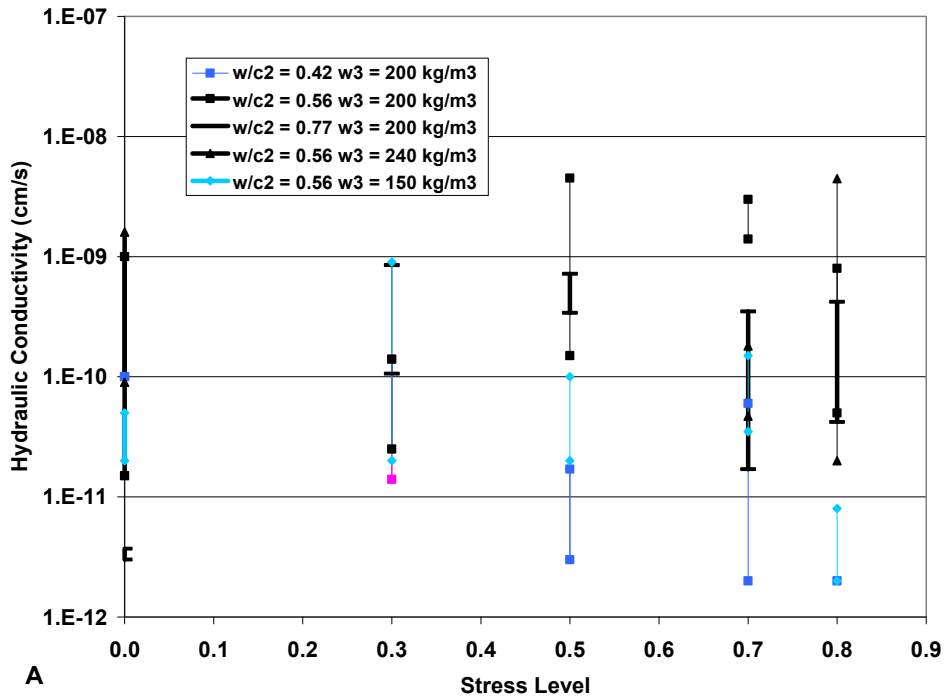


**Figure A3–4. Hydraulic Conductivity of Stressed Concrete Samples for Hearn (1999): (A) Never Dried Samples; (B) Oven Dried Samples**

**Table A3-4. Summary of Unsaturated Hydraulic Properties of Cementitious Materials**

<b>Material Description</b>	<b>Saturated Hydraulic Conductivity (cm/s)*</b>	<b>Irreducible Saturation</b>	<b>van Genuchten Alpha (1/cm water)</b>	<b>van Genuchten</b>	<b>Source</b>
Concrete from Savannah River Site (SRS) E-Area Vault 7E	1.E-12	0.98	5.98E-04	3.43	Yu, A.D., C.A. Langton, and M. Serrato. "Physical Properties Measurement Program (U)." WSRC-RP-93-894. Aiken, South Carolina: Westinghouse Savannah River Company. 1993.
Concrete from SRS Saltstone Vault 7B	1.E-09	0.83	4.70E-04	2.62	Yu, et al. (1993).
SRS Saltstone 4 (fluid viscosity = 2.39 cp)	1.E-12	0.94	5.39E-04	2.36	Yu, et al. (1993).
Cement C3—Type 1 Portland Cement	Not Reported	0.05	6.23E-05	1.37	Green, R.T., F.T. Dodge, S.J. Svedeman, R.D. Manteufel, G. Rice, K.A. Meyer, and R.G. Baca. NUREG/CR-6348, "Thermally Driven Moisture Redistribution in Partially Saturated Porous Media." Washington, DC: NRC. December 1995.
Concrete from Hanford Site	4.E-10	0.00	7.61E-06	1.39	Rockhold, M.L., M.J. Fayer, and P.R. Heller. "Physical and Hydraulic Properties of Sediments and Engineered Materials Associated With Grouted Double-Shell Tank Waste Disposal at Hanford." PNNL-8813. Richland, Washington: Pacific Northwest National Laboratory. 1993.
Double-shell slurry feed grout	1.E-8	0.00	1.08E-05	1.65	Rockhold, et al. (1993).

**Table A3-4. Summary of Unsaturated Hydraulic Properties of Cementitious Materials (continued)**

<b>Material Description</b>	<b>Saturated Hydraulic Conductivity (cm/s)*</b>	<b>Irreducible Saturation</b>	<b>van Genuchten Alpha (1/cm water)</b>	<b>van Genuchten</b>	<b>Source</b>
Concrete mixture, w/c = 0.4, M60 sample	9.E-10	0.01	2.47-06	1.72	Savage, B.M. and D.J. Janssen. "Soil Physics Principles Validated for Use in Predicting Unsaturated Moisture Movement in Portland Cement Concrete." <i>ACI Materials Journal</i> . Vol. 94. pp. 63-70. 1997.
Concrete mixture, w/c = 0.4 M64 sample	6.E-10	0.01	2.26E-06	1.75	Savage and Janssen (1997).
Concrete mixture, w/c = 0.45 M69 sample	3.E-10	0.00	2.89E-06	1.66	Savage and Janssen (1997).
Concrete mixture, w/c = 0.4 M87 sample	4.E-10	0.01	2.36E-06	1.74	Savage and Janssen (1997).
Strong grout	Not Reported for Specific Specimen	0.234	0.0060	1.1539	Dixon, K. and M. Phifer. "Hydraulic and Physical Properties of Tank Grouts and Base Mat Surrogate Concrete for FTF Closure." WSRC-STI-2007-00369. Aiken, South Carolina: Westinghouse Savannah River Company. 2007.
Reducing fill grout	Not Reported for Specific Specimen	0.245	0.006	1.202	Dixon and Phifer (2007).
Reducing fill grout	Not Reported for Specific Specimen	0.215	0.00733	1.2290	Dixon and Phifer (2007).
Reducing fill grout	Not Reported for Specific Specimen	0.233	0.0104	1.229	Dixon and Phifer (2007).
Alternative reducing grout 1A (Top)	Not Reported for Specific Specimen	0.078	0.0085	1.1414	Dixon and Phifer (2007).

**Table A3-4. Summary of Unsaturated Hydraulic Properties of Cementitious Materials (continued)**

<b>Material Description</b>	<b>Saturated Hydraulic Conductivity (cm/s)*</b>	<b>Irreducible Saturation</b>	<b>van Genuchten Alpha (1/cm water)</b>	<b>van Genuchten</b>	<b>Source</b>
Alternative reducing grout 1A (bottom)	Not Reported for Specific Specimen	0.109	0.0114	1.1926	Dixon and Phifer (2007).
Alternative reducing grout 1B (top)	Not Reported for Specific Specimen	0.167	0.0120	1.2677	Dixon and Phifer (2007).
Alternative reducing grout 1B (bottom)	Not Reported for Specific Specimen	0.157	0.0182	1.2635	Dixon and Phifer (2007).
Alternative reducing grout 2	Not Reported for Specific Specimen	0.162	0.0137	1.2081	Dixon and Phifer (2007).
Base mat surrogate (top)	Not Reported for Specific Specimen	0.023	0.0137	1.772	Dixon and Phifer (2007).
Base mat surrogate (bottom)	Not Reported for Specific Specimen	0.040	0.0101	1.2573	Dixon and Phifer (2007).

\*Hydraulic conductivity computed from intrinsic permeability assuming water density of 1 g/cm<sup>3</sup>, viscosity of 1 cp, and gravity of 9.8 m/s<sup>2</sup>  
1 ft/s = 30.5 cm/s

Table A3-5. Summary of Gas Permeability Data

Material Description	Measurement Conditions	Gas	Intrinsic Permeability (k)(m <sup>2</sup> )*	Comments	Source
Concrete, 0.7 water/cement, 21 days curing	Laboratory	Oxygen	2.E-17	Value estimated from graph	de Beer, F.C., J.J. le Roux, and E.P. Kearsley. "Testing the Durability of Concrete With Neutron Radiography." <i>Nuclear Instruments and Methods in Physics Research</i> . Vol. A, No. 542. pp. 226-231. 2005.
Concrete, 0.5 water/cement, 21 days curing	Laboratory	Oxygen	1.E-17	Value estimated from graph	de Beer, et al. (2005).
Concrete, in service, reinforced	Laboratory	Oxygen	2.E-11	Value estimated from graph, converted to m <sup>2</sup>	Lampacher, B.J. and G.E. Blight. "Permeability and Sorption Properties of Mature Near-Surface Concrete." <i>Journal of Materials in Civil Engineering</i> . Vol. 10. pp. 21-25. 1998.
Low cement content concrete (C30) after 5 days at 122 °F [50 °C]	Laboratory	Air	3.E-17	30-mm [1.2-in]-thick concrete samples	Roux, N., C. Andrade, and M.A. Sanjuan. "Experimental Study of Durability of Reactive Powder Concretes." <i>Journal of Materials in Civil Engineering</i> . Vol. 8, No. 1. pp. 1-6. 1996.
Very high strength concrete (C80) after 5 days at 122 °F [50 °C]	Laboratory	Air	3.E-19	30-mm [1.2-in]-thick concrete samples	Roux, et al. (1996).
Very high strength concrete (C80) after 30 days at 176 °F [80 °C]	Laboratory	Air	1.E-16	30-mm [1.2-in]-thick concrete samples	Roux, et al. (1996).
Reactive powder concrete (RPC200) after 30 days at 176 °F [80 °C]	Laboratory	Air	3.E-18	30-mm [1.2-in]-thick concrete samples	Roux, et al. (1996).
3 parts pulverized blast furnace slag/1 part ordinary Portland cement	Laboratory	Air	1.E-18	20-mm [0.8-in]-thick disc with microcracks, 85% water saturation	Roux, et al. (1996).
<p>*Conversion Factors:            Dynamic viscosity = 0.000201 gm/cm-s            Gas constant = 82.057 cm<sup>3</sup>-atm/mole-K            Temperature = 293 K            Molecular weight = 32 gm/cm<sup>3</sup>            Gravity = 987 cm/s<sup>2</sup>            0.093 m<sup>2</sup> = 1 ft<sup>2</sup>            Conversion from cm/s to m<sup>2</sup> = 0.000153007; 25 mm = 1 in</p>					

permeability data. The value of the permeability data provided in these studies is limited by the lack of information on the change in effective gas permeability with water content. The permeability to gas decreases with increased water saturation in roughly the same way that water effective permeability decreases with decreased water saturation.

### A3.3 Aqueous Diffusion Data

Data on the effective diffusion coefficient for inorganic, ionic species in cementitious materials collected from the technical literature are provided in Tables A3–6 and A3–7. The effective diffusion coefficients listed in these tables are based on the definition of the effective diffusion coefficient given in Eq. (A2–15) and include the effects of porosity, tortuosity, sorption, and chemical interaction, if any, with the cement. Table A3–6 contains values of the effective diffusion coefficient reported for a variety of cementitious materials under a variety of experimental conditions. Table A3–7 contains values for an extensive list of species based on leach tests on four waste forms mixed with grout considered for use in concrete vault closures at the Hanford site (Serne, et al., 1992). The range of effective diffusion coefficients Serne, et al. (1992) reported is also illustrated in Figure A3–5

The diffusion data Serne, et al. (1992) reported for grouts at the Hanford site may have limited transferability to grout formulations considered for tank closures at other sites. For example, the water/cement plus pozzolan ratios of the grouts Serne, et al. (1992) tested were approximately 1.2—much higher than those of the reducing grouts considered for use at the Savannah River Site (Dixon and Phifer, 2007). Also, the phosphate–sulfate grouts Serne, et al. (1992) tested contained fly ash and clay, whereas the grouts considered for use at the Savannah River Site contained sand, fly ash, and slag. Thus, the effective diffusion coefficients Serne, et al. (1992) reported may have limited transferability for cationic species that exchange with clay minerals. In general, however, the Serne, et al. (1992) data indicate that species with the greatest sorptive potential, such as plutonium and americium, have much lower effective diffusion coefficients than more mobile species, such as technetium.

The values listed in Tables A3–6 and A3–7 all relate to specimens without macrocracks. Although the values reported in Tables A3–6 and A3–7 span nearly 12 orders of magnitude, the values for most species are likely to be strongly influenced by sorption or chemical reactions. Of the various species for which diffusion coefficients are reported, only a few, such as chloride, iodide, and nitrate, are likely to reflect only the geometric properties of the cementitious materials.

Extensive literature exists on the diffusion of chloride in cementitious materials because of its importance to corrosion of metal rebar in concrete structures. Table A3–6 contains a representative sample of these data. The distribution of effective diffusion coefficients for chloride and iodine-125, presumably both nonsorbing species, is shown in Figure A3–6. For reference, the tracer diffusion coefficients of both chloride and iodide in water (free aqueous diffusion coefficient) are approximately  $2 \times 10^{-5} \text{ cm}^2/\text{s}$  [ $2 \times 10^{-8} \text{ ft}^2/\text{s}$ ] (Thibodeux, 1996). Figure A3–2 indicates that the median value of the reported chloride diffusion coefficients is approximately  $1 \times 10^{-7} \text{ cm}^2/\text{s}$  [ $1 \times 10^{-10} \text{ ft}^2/\text{s}$ ] or a factor of 200 less than the free aqueous diffusion coefficient. The effective diffusion coefficients for iodine-125 are even lower. Assuming a porosity of a cementitious material of approximately 0.4, the matrix factor in Eq. (A2–15) would be approximately 0.01, which is much lower than that expected for a typical porous medium (e.g., 0.1 to 0.8 in van Brakel and Heertjes, 1974). This low value of the matrix factor is consistent with the formation factor for chloride Sato (2000) reported for sodium

**Table A3-6. Aqueous Diffusion**

<b>Material Description</b>	<b>Measurement Conditions*</b>	<b>Species</b>	<b>Effective Diffusion Coefficient† (cm<sup>2</sup>/s)‡</b>	<b>Comments</b>	<b>Source</b>
Phosphogypsum, 30% Portland cement in seawater	Laboratory	Calcium	1.8E-12	Leaching study with chemical reactions, lowest value reported	Guo, T., A.S. Hawke, and K.A. Rusch. "Determination of Calcium Diffusion Coefficients as an Estimator of the Long-Term Dissolution Potential of Phosphogypsum: Cement:Lime Composites." <i>Environmental Science and Technology</i> . Vol. 33, No. 18. pp. 3,185-3,192. 1999.
Phosphogypsum, 10% lime in seawater	Laboratory	Calcium	3.3E-09	Leaching study with chemical reactions, highest value reported	Guo, et al. (1999).
Concrete with sand/cement = 1.5	Laboratory	Cesium-137	6.5E-10	Using 50-mm-thick concrete mixture	Plecas, I. and S. Dimovic. "Immobilization of 137Cs and 60Co in Concrete Matrix." <i>Journal of Porous Media</i> . Vol. 9, No. 2. pp. 181-184. 2006.
Concrete with sand/cement = 1.9	Laboratory	Cesium-137	3.7E-10	Using 50-mm [2-in]-thick concrete mixture	Plecas and Dimovic (2006).
Concrete with sand/cement = 1.3	Laboratory	Cesium-137	8.8E-10	Using 50-mm [2-in]-thick concrete mixture	Plecas and Dimovic (2006).
Concrete with sand/cement = 1.7	Laboratory	Cesium-137	9.7E-10	Using 50-mm [2-in]-thick concrete mixture	Plecas and Dimovic (2006).
Saltstone waste forms, water/cementitious solids = 0.41	Laboratory	Cesium ion	2.1E-09	Lowest value measured on potential Saltstone mixture	Kumar, A., D.M. Roy, P.H. Licastro, and C.A. Langton. "Effective Diffusion Coefficients for Several Saltstone Waste Forms." Aiken, South Carolina: E.I. du Pont de Nemours and Company, Inc. Savannah River Laboratory. 1985.
Saltstone waste forms, water/cementitious solids = 1.8	Laboratory	Cesium ion	4.1E-07	Highest value measured on potential Saltstone mixture	Kumar, et al. (1985).

Table A3-6. Aqueous Diffusion (continued)

Material Description	Measurement Conditions*	Species	Effective Diffusion Coefficient† (cm <sup>2</sup> /s)‡	Comments	Source
Type 50 sulfate-resistant Portland cement, water/cement = 0.35	Laboratory	Cesium ion	1.1E-08	Determined using Canadian Shield saline water	Johnston, H.M. and D.J. Wilmot. "Sorption and Diffusion Studies in Cementitious Grouts." <i>Waste Management</i> . Vol. 12. pp. 289-297. 1992.
Type 50 sulfate-resistant Portland cement, water/cement = 0.25, 15% silica fume	Laboratory	Cesium ion	2.6E-09	Determined using Canadian Shield saline water	Johnston and Wilmot (1992).
Cement-based grout waste forms	Laboratory	Cesium-137	9E-10 and 5E-09	IAEA proposed leach test on 200-L [53 gal] samples	Seveque, J.L., M.D. de Cayeux, M. Elert, and H. Nougier. "Mathematical Modeling of Radioactive Waste Leaching." <i>Cement and Concrete Research</i> . Vol. 22. pp. 477-488. 1992.
Ordinary Portland cement, fresh sample	Laboratory	Chloride	1.7E-07	Based on internal chloride concentrations, basis of diffusion coefficient calculation not explained, reported value assumed to be effective diffusion coefficient	Jenneson, P.M., A.S. Clough, and R. Hollands. "Profiling Chlorine Diffusion Into Ordinary Portland Cement and Pulverized Fuel Ash Pastes Using Scanning MeV Proton Micro-PIXE." <i>Journal of Materials Science Letters</i> . Vol. 17. pp. 1,173-1,175. 1998.
Ordinary Portland cement with 30% pulverized fuel ash, fresh sample	Laboratory	Chloride	9.3E-09	Based on internal chloride concentrations, basis of diffusion coefficient calculation not explained, reported value assumed to be effective diffusion coefficient	Jenneson, et al. (1998).
Portland cement mortar, no sand, 55% hydration, 0.4 water/cement	Laboratory	Chloride	1.7E-07	Typical values, consult source for full data set	Halamicikova, P., R.J. Detwiler, D.P. Bentz, and E.J. Garboczi. "Water Permeability and Chloride Ion Diffusion in Portland Cement Mortars: Relationship to Sand Content and Critical Pore Diameter." <i>Cement and Concrete Research</i> . Vol. 25. pp. 790-802. 1995.

Table A3-6. Aqueous Diffusion (continued)

Material Description	Measurement Conditions*	Species	Effective Diffusion Coefficient† (cm <sup>2</sup> /s)‡	Comments	Source
Portland cement mortar, no sand, 60% hydration, 0.4 water/cement	Laboratory	Chloride	1.1E-07	Typical values, consult source for full data set	Halamickova, et al. (1995).
Portland cement mortar, 45% sand, 57% hydration, 0.4 water/cement	Laboratory	Chloride	2.3E-07	Typical values, consult source for full data set	Halamickova, et al. (1995).
Portland cement mortar, 55% sand, 72% hydration, 0.4 water/cement	Laboratory	Chloride	8.2E-08	Typical values, consult source for full data set	Halamickova, et al. (1995).
Portland cement mortar, no sand, 48% hydration, 0.5 water/cement	Laboratory	Chloride	7.5E-07	Typical values, consult source for full data set	Halamickova, et al. (1995).
Portland cement mortar, no sand, 56% hydration, 0.5 water/cement	Laboratory	Chloride	3.0E-07	Typical values, consult source for full data set	Halamickova, et al. (1995).
Portland cement mortar, 45% sand, 72% hydration, 0.5 water/cement	Laboratory	Chloride	1.8E-07	Typical values, consult source for full data set	Halamickova, et al. (1995).
Portland cement mortar, 55% sand, 73% hydration, 0.5 water/cement	Laboratory	Chloride	8.4E-08	Typical values, consult source for full data set	Halamickova, et al. (1995).
High performance concrete at 23 °C [73 °F] 180 days	Reported	Chloride	3.3E-09	Value traced to McGrath, P.F. "Development of Test Methods for Predicting Chloride Ingress into High Performance Concrete." Doctor of Philosophy Thesis. Department of Civil Engineering, University of Toronto. Toronto, Canada. 1996.	Boddy, A., E. Bentz, M.D.A. Thomas, and R.D. Hooton. "An Overview and Sensitivity Study of a Multimechanistic Chloride Transport Model." <i>Cement and Concrete Research</i> . Vol. 29. pp. 827-837. 1999.
Typical bridge deck at 23 °C [73 °F], 120 days	Reported	Chloride	2.5E-08	Value traced to McGrath (1996).	Boddy, et al. (1999).
Low cement content concrete (C30)	Laboratory	Chloride	1.1E-08	Using 5-mm-thick concrete disc	Roux, N., C. Andrade, and M.A. Sanjuan. "Experimental Study of Durability of Reactive Powder Concretes." <i>Journal of Materials in Civil Engineering</i> . Vol. 8, No. 1. pp. 1-6. 1996.

Table A3-6. Aqueous Diffusion (continued)

Material Description	Measurement Conditions*	Species	Effective Diffusion Coefficient† (cm <sup>2</sup> /s)‡	Comments	Source
Very high strength concrete (C80)	Laboratory	Chloride	6.0E-09	Using 5-mm-thick concrete disc	Roux, et al. (1996).
Reactive powder concrete (RPC200)	Laboratory	Chloride	2.0E-10	Using 5-mm-thick concrete disc	Roux, et al. (1996).
Laboratory and field concrete samples	Laboratory	Chloride	5.6E-07	Using 50-mm-thick concrete mixture	Samson, E., J. Marchand, and K.A. Snyder. "Calculation of Ionic Diffusion Coefficients on the Basis of Migration Test Results." <i>Materials and Structures</i> . Vol. 36, No. 257. pp. 156-165. 2003.
Concrete, 56% fly ash, water/cement = 0.50	Laboratory	Chloride	5.1E-09	Average for 90 to 1,550 days	Stanish, K. and M. Thomas. "The Use of Bulk Diffusion Tests to Establish Time-Dependent Concrete Chloride Diffusion Coefficients." <i>Cement and Concrete Research</i> . Vol. 33. pp. 55-62. 2003.
Concrete, 25% fly ash, water/cement = 0.50	Laboratory	Chloride	5.8E-09	Average for 90 to 1,550 days	Stanish and Thomas (2003).
Concrete, water/cement = 0.50	Laboratory	Chloride	3.3E-08	Average for 90 to 1,550 days	Stanish and Thomas (2003).
Ordinary Portland cement, water/cement = 0.4	Laboratory	Chloride	4.E-08	Estimated from graph	Castellote, M., C. Alonso, C. Andrade, G.A. Chadbourn, and C.L. Page. "Oxygen and Chloride Diffusion in Cement Pastes as a Validation of Chloride Diffusion Coefficients Obtained by Steady-State Migration Tests." <i>Cement and Concrete Research</i> . Vol. 31. pp. 621-625. 2001.
Ordinary Portland cement, water/cement = 0.4	Laboratory	Chloride	1.6E-08	0.05 molar chloride, nonsteady state	Castellote, M., C. Andrade, and C. Alonso. "Measurement of the Steady and Non-Steady-State Chloride Diffusion Coefficients in a Migration Test by Means of Monitoring the Conductivity in the Anolyte Chamber Comparison With Natural Diffusion Tests." <i>Cement and Concrete Research</i> . Vol. 31. pp. 1,411-1,420. 2001.

Table A3-6. Aqueous Diffusion (continued)

Material Description	Measurement Conditions*	Species	Effective Diffusion Coefficient† (cm <sup>2</sup> /s)‡	Comments	Source
Ordinary Portland cement, water/cement = 0.4	Laboratory	Chloride	2.8E-08	1.0 molar chloride, nonsteady state	Castellote, et al. (2001, pp. 1,411–1,420).
Type 50 sulphate-resistant Portland cement, water/cement = 0.35	Laboratory	Chloride	6.9E-08	Determined using Canadian Shield saline water	Johnston, H.M. and D.J. Wilmot. "Sorption and Diffusion Studies in Cementitious Grouts." <i>Waste Management</i> . Vol. 12. pp. 289–297. 1992.
Type 50 sulphate-resistant Portland cement, water/cement = 0.25, 15% silica fume	Laboratory	Chloride	2.5E-08	Determined using Canadian Shield saline water	Johnston and Wilmot (1992).
Concrete with sand/cement = 1.5	Laboratory	Cobalt-60	6.1E-11	Using 50-mm [2-in]-thick concrete mixture	Plecas, I. and S. Dimovic. "Immobilization of 137Cs and 60Co in Concrete Matrix." <i>Journal of Porous Media</i> . Vol. 9, No. 2. pp. 181–184. 2006.
Concrete with sand/cement = 1.9	Laboratory	Cobalt-60	4.9E-11	Using 50-mm [2-in]-thick concrete mixture	Plecas and Dimovic (2006).
Concrete with sand/cement = 1.3	Laboratory	Cobalt-60	2.5E-11	Using 50-mm [2-in]-thick concrete mixture	Plecas and Dimovic (2006).
Concrete with sand/cement = 1.7	Laboratory	Cobalt-60	1.4E-11	Using 50-mm [2-in]-thick concrete mixture	Plecas and Dimovic (2006).
Simulated cement stabilized metal-bearing sludge	Laboratory	Hydroxide ion	1.8E-06	At pH = 4, results affected by chemical reactions	Islam, M.Z., L.J. Catalan, and E.K. Yanful. "A Two-Front Leach Model for Cement-Stabilized Heavy Metal Waste." <i>Environmental Science and Technology</i> . Vol. 38, No. 5. pp. 1,522–1,528. 2004.
Simulated cement stabilized metal-bearing sludge	Laboratory	Hydroxide ion	9.7E-07	At pH = 7, results affected by chemical reactions	Islam, et al. (2004).

Table A3-6. Aqueous Diffusion (continued)

Material Description	Measurement Conditions*	Species	Effective Diffusion Coefficient† (cm <sup>2</sup> /s)‡	Comments	Source
Concrete for encasing low-level nuclear waste, Type I Portland cement, fly ash, aggregate	Laboratory	Iodide-125	7.8E-11	High reported value from dynamic leach test	Mattigod, S.V., P.F. Martin, G.W. Whyatt, K.E. Schwab, R.J. Serne, and M.I. Wood. "Diffusion and Leaching of Selected Radionuclides (Iodine-129, Technetium-99, and Uranium) Through Category 3 Waste Encasement Concrete and Soil Fill Material." PNNL-13639. Richland, Washington: Pacific Northwest National Laboratory. 2001.
Concrete for encasing low-level nuclear waste, Type I Portland cement, fly ash, aggregate	Laboratory	Iodide-125	3.1E-12	Low reported value from dynamic leach test	Mattigod, et al. (2001).
Concrete for encasing low-level nuclear waste, Type I Portland cement, fly ash, aggregate	Laboratory	Iodide-125	1.3E-10	High reported value from static leach test	Mattigod, et al. (2001).
Concrete for encasing low-level nuclear waste, Type I Portland cement, fly ash, aggregate	Laboratory	Iodide-125	5.4E-12	Low reported value from static leach test	Mattigod, et al. (2001).
Waste encasement concrete; no slag	Laboratory	Iodine-125	4E-11 to 1E-10	ANSI/ANS-16.1 leach procedure; also reported static leach test results, which gave lower diffusion coefficients.	Mattigod, et al. (2001).
Portland cement concrete, water/cement = 0.42	Laboratory	Nitrite	1.5E-08	Leaching test in lime water	Liang, H., L. Li, N.D. Poor, and A.A. Sagues. "Nitrite Diffusivity in Calcium Nitrite-Admixed Hardened Concrete." <i>Cement and Concrete Research</i> . Vol. 33. pp. 139-146. 2003.
Portland cement concrete, water/cement = 0.52, 3.5% fly ash	Laboratory	Nitrite	6.8E-09	Leaching test in lime water	Liang, et al. (2003).

**Table A3-6. Aqueous Diffusion (continued)**

<b>Material Description</b>	<b>Measurement Conditions*</b>	<b>Species</b>	<b>Effective Diffusion Coefficient† (cm<sup>2</sup>/s)‡</b>	<b>Comments</b>	<b>Source</b>
Saltstone, no blast furnace slag	Laboratory	Nitrite	6E-10	Modified IAEA leach procedure	Barnes, M.W., C.A. Langton, and D.M. Roy. "Leaching of Saltstone." Materials Research Society Symposium Proceedings 44. C.M. Jantzen, J.A. Stone, and R.C. Ewing, eds. Pittsburgh, Pennsylvania: Materials Research Society. pp. 865-873. 1985.
Saltstone, no blast furnace slag	Laboratory	Nitrate	4E-10	Modified IAEA leach procedure. Water/cement ratio = 0.45	Barnes, et al. (1985)
Saltstone, no blast furnace slag	Laboratory	Nitrate	2E-09	Modified IAEA leach procedure. Water/cement ratio = 2.8	Barnes, et al. (1985)
Saltstone, with blast furnace slag	Laboratory	Nitrate	5E-09	Modified ANSI/ANS-16.1 leach procedure	Langton, C. "Slag Substituted Concrete for Saltstone Vault Construction." Internal Report DPST-86-830. Aiken, South Carolina: E.L. du Pont de Nemours & Company, Inc., Savannah River Laboratory. 1986.
Saltstone, no blast furnace slag	Laboratory	Nitrate	1.0E-08	Modified ANSI/ANS-16.1 leach procedure	Langton, C.A., S.B. Oblath, D.W. Pepper, and E.L. Wilhite. "Waste Salt Disposal at the Savannah River Plant." <i>Chemical Engineering Communications</i> . Vol. 66. pp. 189-199. 1988.
Saltstone, no blast furnace slag	Laboratory	Nitrate	5E-09	Modified ANSI/ANS-16.1 leach procedure; also studied effect of water saturation	Oblath, S.B. "Leaching From Solidified Waste Forms Under Saturated and Unsaturated Conditions." <i>Environmental Science and Technology</i> . Vol. 23. pp. 1,098-1,102. 1989.

**Table A3-6. Aqueous Diffusion (continued)**

<b>Material Description</b>	<b>Measurement Conditions*</b>	<b>Species</b>	<b>Effective Diffusion Coefficient† (cm<sup>2</sup>/s)‡</b>	<b>Comments</b>	<b>Source</b>
Ordinary Portland cement, water/cement = 0.4	Laboratory	Oxygen	9.E-08	Estimated from graph	Castellote, M., C. Alonso, C. Andrade, G.A. Chadbourn, and C.L. Page. "Oxygen and Chloride Diffusion in Cement Pastes as a Validation of Chloride Diffusion Coefficients Obtained by Steady-State Migration Tests." <i>Cement and Concrete Research</i> . Vol. 31. pp. 621-625. 2001.
Saltstone, with blast furnace slag	Laboratory	Selenium	5E-09	ANSI/ANS-16.1 leach procedure	Harbour, J.R. and A.S. Aloy. "International Program: Summary Report on the Properties of Cementitious Waste Forms." WSRC-STI-2007-00056. Rev. 0. Aiken, South Carolina: Savannah River National Laboratory. 2007.
Hardened sulfate-resistant Portland cement paste	Laboratory	Sodium-22	1.1E-06	Mean value analyzed assuming no sorption	Tits, J., A. Jakob, E. Wieland, and P. Spieler. "Diffusion of Tritiated Water and 22Na+ Through Non-degraded Hardened Cement Pastes." <i>Journal of Contaminant Hydrology</i> . Vol. 61. pp. 45-62. 2003.
Saltstone, no blast furnace slag	Laboratory	Sodium	3E-10	Modified IAEA leach procedure. Water/cement ratio = 0.45	Barnes, et al. (1985).
Type 50 sulphate-resistant Portland cement, water/cement = 0.35	Laboratory	Strontium ion	3.2E-09	Determined using Canadian Shield saline water	Johnston, H.M. and D.J. Wilmot. "Sorption and Diffusion Studies in Cementitious Grouts." <i>Waste Management</i> . Vol. 12. pp. 289-297. 1992.
Type 50 sulphate-resistant Portland cement, water/cement = 0.25, 15% silica fume	Laboratory	Strontium ion	1.7E-09	Determined using Canadian Shield saline water	Johnston and Wilmot (1992).
Concrete with Portland Type 50 cement	Laboratory	Sulfate	2.6E-08	Sample aged 12 months	Turnidajski, P.J., G.W. Chan, and K.E. Philipose. "An Effective Diffusivity for Sulfate Transport into Concrete." <i>Cement and Concrete Research</i> . Vol. 25. pp. 1,159-1,163. 1995.
Concrete with Portland Type 50 cement	Laboratory	Sulfate	1.1E-08	Sample aged 60 months	Turnidajski, et al. (1995).

Table A3-6. Aqueous Diffusion (continued)

Material Description	Measurement Conditions*	Species	Effective Diffusion Coefficient† (cm <sup>2</sup> /s)‡	Comments	Source
Concrete with Portland Type 50 cement	Laboratory	Sulfate	7.5E-08	Sample aged 12 months with saturated CO <sub>2</sub>	Turnidajski, et al. (1995).
Concrete with Portland Type 50 cement	Laboratory	Sulfate	2.2E-08	Sample aged 46 months with saturated CO <sub>2</sub>	Turnidajski, et al. (1995).
Saltstone, no blast furnace slag	Laboratory	Sulfate	9E-11	Modified IAEA leach procedure. Water/cement ratio = 0.45	Barnes, et al. (1985).
Concrete for encasing low-level nuclear waste, Type I Portland cement, fly ash, aggregate	Laboratory	Technetium-99	5.8E-09	High reported value from static leach test	Mattigod, et al. (2001).
Concrete for encasing low-level nuclear waste, Type I Portland cement, fly ash, aggregate	Laboratory	Technetium-99	2.4E-10	Low reported value from dynamic leach test	Mattigod, et al. (2001).
Concrete for encasing low-level nuclear waste, Type I Portland cement, fly ash, aggregate	Laboratory	Technetium-99	7.7E-09	High reported value from static leach test	Mattigod, et al. (2001).
Concrete for encasing low-level nuclear waste, Type I Portland cement, fly ash, aggregate	Laboratory	Technetium-99	4.3E-10	Low reported value from static leach test	Mattigod, et al. (2001).
Saltstone, with blast furnace slag	Laboratory	Technetium-99	<6E-10	Modified ANSI/ANS-16.1 leach procedure	Langton (1986).
Saltstone, with blast furnace slag	Laboratory	Technetium-99	5E-12	ANSI/ANS-16.1 leach procedure	Harbour and Aloy (2007).
Cement-based grout with blast furnace slag	Laboratory	Technetium-99	3E-11	ANSI/ANS-16.1 leach procedure; diffusion coefficient was newly calculated from average leachability index.	Gilliam, T.M., R.D. Spence, W.D. Bostick, and J.L. Shoemaker. "Solidification/Stabilization of Technetium in Cement-Based Grouts." <i>Journal of Hazardous Materials</i> . Vol. 24. pp. 189-197. 1990.
Waste encasement concrete; no slag	Laboratory	Technetium-99	2E-09 to 8E-09	ANSI/ANS-16.1 leach procedure; also reported static leach test results, which gave lower diffusion coefficients.	Mattigod, et al. (2001).

**Table A3-6. Aqueous Diffusion (continued)**

<b>Material Description</b>	<b>Measurement Conditions*</b>	<b>Species</b>	<b>Effective Diffusion Coefficient† (cm<sup>2</sup>/s)‡</b>	<b>Comments</b>	<b>Source</b>
Hardened sulfate-resistant Portland cement paste	Laboratory	Tritiated water (HTO)	2.8E-06	Mean value analyzed assuming no sorption	Tits, J., A. Jakob, E. Wieland, and P. Spieler. "Diffusion of Tritiated Water and <sup>22</sup> Na <sup>+</sup> Through Non-degraded Hardened Cement Pastes." <i>Journal of Contaminant Hydrology</i> . Vol. 61. pp. 45-62. 2003.
Type 50 sulphate-resistant Portland cement, water/cement = 0.35	Laboratory	Tritium	8.2E-08	Determined using Canadian Shield saline water	Johnston, H.M. and D.J. Wilmot. "Sorption and Diffusion Studies in Cementitious Grouts." <i>Waste Management</i> . Vol. 12. pp. 289-297. 1992.
Type 50 sulphate-resistant Portland cement, water/cement = 0.25, 15% silica fume	Laboratory	Tritium	4.8E-08	Determined using Canadian Shield saline water	Johnston and Wilmot (1992).
*Measurement conditions are reported as "laboratory" if measured in a laboratory environment; "field" if an <i>in-situ</i> field measurement; "reported" if the value is derived from an unspecified secondary source. †Effective diffusion coefficient as defined by Eq. (A2-15); includes effects of porosity, tortuosity, and sorption. ‡1 ft <sup>2</sup> /s = 9.3 × 10 <sup>2</sup> cm <sup>2</sup> /s; 25 mm = 1 in.					

**Table A3-7. Summary of Effective Diffusion Coefficient Values for Hanford Grouts (cm<sup>2</sup>/s)\*†**

Species	Grouted Waste Type			
	PSW‡	CRW§	T-106 AN	DSSF¶
B	<10 <sup>-12</sup> to 5 × 10 <sup>-12</sup>	10 <sup>-12</sup> to 5 × 10 <sup>-12</sup>	—	5 × 10 <sup>-10</sup>
C	5 × 10 <sup>-14</sup>	2 × 10 <sup>-13</sup>	< 10 <sup>-11</sup>	—
NO <sub>3</sub>	10 <sup>-10</sup> to 10 <sup>-9</sup>	1.5 ± 0.5 × 10 <sup>-9</sup>	7 ± 0.5 × 10 <sup>-9</sup>	3 ± 3 × 10 <sup>-8</sup>
F	—	10 <sup>-12</sup> to 5 × 10 <sup>-11</sup>	6.5 ± 0.1 × 10 <sup>-9</sup>	1 × 10 <sup>-11</sup>
Na	1 to 3 × 10 <sup>-9</sup>	6 ± 2 × 10 <sup>-9</sup>	6 ± 1 × 10 <sup>-9</sup>	4 ± 2 × 10 <sup>-8</sup>
SO <sub>4</sub>	10 <sup>-12</sup> to 10 <sup>-11</sup>	10 <sup>-9</sup> to 10 <sup>-8</sup>	—	—
Cl	—	—	9 ± 1 × 10 <sup>-9</sup>	—
K	4 to 9 × 10 <sup>-10</sup>	1.3 ± 0.4 × 10 <sup>-9</sup>	—	2 ± 1 × 10 <sup>-8</sup>
Cr	10 <sup>-12</sup> to <10 <sup>-10</sup>	—	—	6 ± 5 × 10 <sup>-11</sup>
Mn	10 <sup>-13</sup> to 10 <sup>-11</sup>	—	—	—
Co	10 <sup>-13</sup> to 10 <sup>-11</sup>	—	<2 × 10 <sup>-11</sup>	—
Ni	—	—	4.3 ± 0.2 × 10 <sup>-10</sup>	—
As	10 <sup>-12</sup> to 10 <sup>-10</sup>	—	—	—
Se	<10 <sup>-12</sup> to 5 × 10 <sup>-10</sup>	—	—	1.5 ± 0.5 × 10 <sup>-10</sup>
Sr	10 <sup>-13</sup> to 10 <sup>-12</sup>	—	2 × 10 <sup>-15</sup>	—
Zr	—	<10 <sup>-12</sup>	—	—
Mo	—	—	9 ± 1 × 10 <sup>-9</sup>	1.4 ± 0.8 × 10 <sup>-8</sup>
Tc	4 × 10 <sup>-11</sup>	—	<7 × 10 <sup>-8</sup> #	5 ± 4 × 10 <sup>-9</sup>
Ag	10 <sup>-13</sup> to 5 × 10 <sup>-11</sup>	—	—	—
Cd	<10 <sup>-12</sup> to 10 <sup>-10</sup>	—	—	—
I	10 <sup>-10</sup> to 5 × 10 <sup>-9</sup>	3.4 to 34 × 10 <sup>-9</sup>	5 to 8 × 10 <sup>-8</sup>	2 ± 2 × 10 <sup>-8</sup>
Cs	10 <sup>-14</sup> to 10 <sup>-12</sup>	1 to 5 × 10 <sup>-15</sup>	3 × 10 <sup>-10</sup>	—
Hg	<10 <sup>-12</sup> to 10 <sup>-8</sup>	—	—	—
Pb	<10 <sup>-11</sup> to <10 <sup>-18</sup>	—	—	—
U	10 <sup>-15</sup> to 10 <sup>-11</sup>	—	—	—
Pu	—	10 <sup>-16</sup> to 10 <sup>-15</sup>	—	—
Am	—	10 <sup>-17</sup> to 10 <sup>-16</sup>	—	—

\*Multiply cm<sup>2</sup>/s by 0.00108 to convert into ft<sup>2</sup>/s  
†Serne, R.J., R.O. Lokken, and L.F. Criscenti. "Characterization of Grouted Low-Level Waste To Support Performance Assessment." *Waste Management*. Vol. 12. pp. 271-287. 1992.  
‡PSW = phosphate-sulfate liquid waste  
§CRW = cladding removal liquid waste  
||T-106 AN = specific tank containing DSSF¶ waste  
¶DSSF = double shell slurry feed waste  
#Value is questionable based on difficulty in measuring original waste inventory

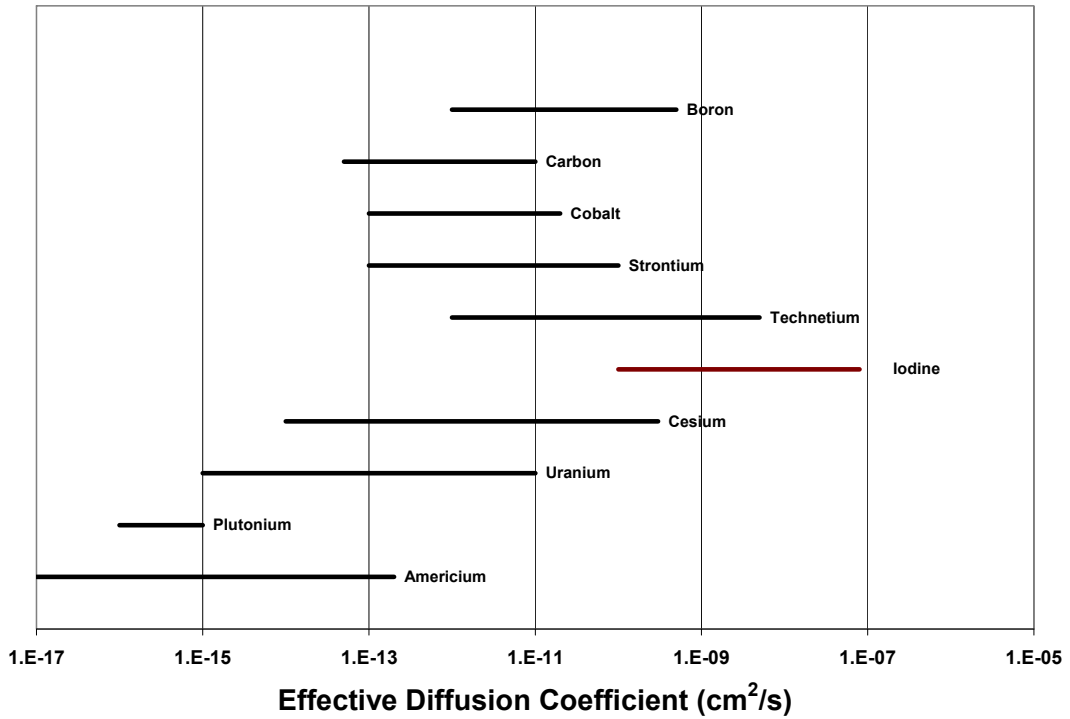


Figure A3-5. Ranges of Effective Diffusion Coefficients Serne, et al. (1992) Reported for Grout Materials

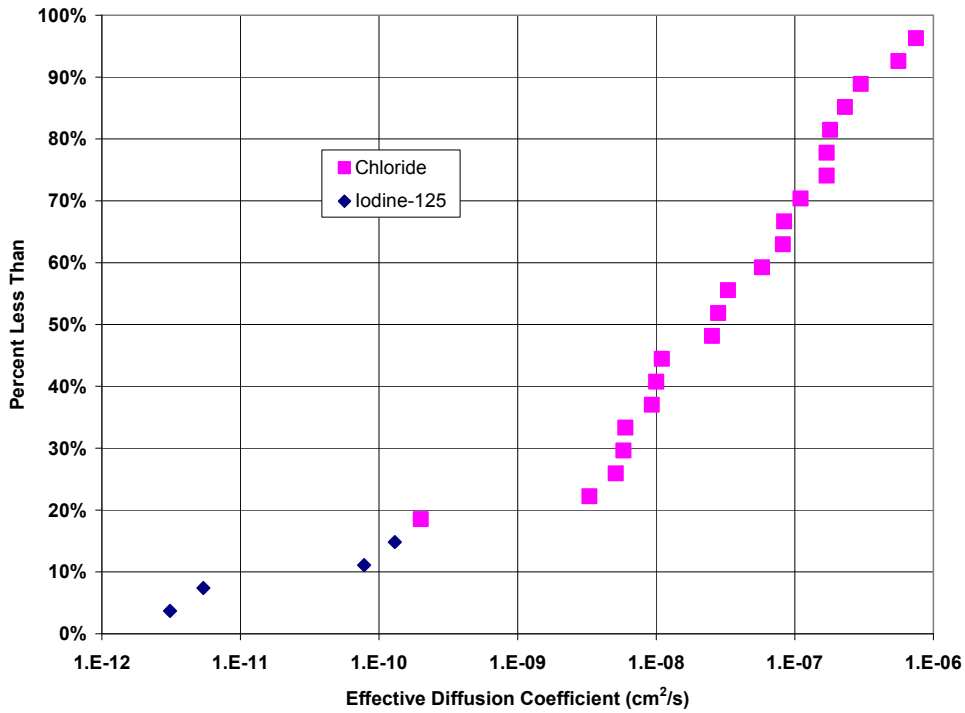


Figure A3-6. Cumulative Distribution Plot of Effective Diffusion Coefficients of Chloride and Iodine-125 Reported for Cementitious Materials Without Macrocracks

bentonite and attributed to anion exclusion effects near the negatively charged surfaces of very small pores. The effective diffusion coefficients for species other than chloride listed in Tables A3–6 and A3–7 are generally less than those for chloride, reflecting chemical interactions with the cementitious material.

### **A3.4 Gas Diffusion Coefficients**

Table A3–8 lists data collected from the technical literature on gas diffusion coefficients in cementitious materials. The only data that could be found related to radon diffusion in building concrete and oxygen diffusion in construction concrete. As Culot, et al. (1976) noted, the literature on gas diffusion of radon contains various definitions of the effective diffusion coefficient. In some cases, the values reported are consistent with the definition of the effective diffusion coefficient in Eq. (A2–15), while in other cases, the values reported appear to not explicitly include the areal effect of air-filled porosity and would represent the effective pore space differing coefficient {Eq. (A2–16)}. In the case of a completely dry concrete, the porosity effect would not significantly affect the reported value of the diffusion coefficient, because including or omitting it would only modify the value by a factor of 0.1 to 0.4 (the total concrete porosity). For partially saturated concrete, the air-filled porosity through which the gas can diffuse will be significantly less than the total porosity and could affect the reported value by one or two orders of magnitude. In most cases, the water saturation of the cementitious materials tested was not reported with the diffusion coefficients, leading to a significant variation in values and ambiguity in applying these values to materials other than those tested. Knudsen diffusion (e.g., Kobayashi and Shuttoh, 1991) can also influence gas diffusion in cementitious materials. Knudsen diffusion occurs in materials with very small pores where the mean free path of the gas molecules is greater than the pore diameter {approximately  $0.1 \mu\text{m}$  [ $4 \times 10^{-6}$  in] at atmospheric pressure}. The Knudsen diffusion coefficient has a value determined by the pore diameter, temperature, and molecular weight of the individual gas molecule, whereas the Fickian diffusion coefficient of a particular gas constituent depends on the overall composition of the gas.

The values reported in Table A3–8 for radon range from approximately  $1 \times 10^{-5}$  to  $1 \times 10^{-3} \text{ cm}^2/\text{s}$  [ $1 \times 10^{-8}$  to  $1 \times 10^{-6} \text{ ft}^2/\text{s}$ ]. For reference, the tracer diffusion coefficient for radon in air is  $1.2 \times 10^{-1} \text{ cm}^2/\text{s}$  [ $1.3 \times 10^{-4} \text{ ft}^2/\text{s}$ ] (Nazaroff, 1992). The data for oxygen diffusion in concrete range from  $1 \times 10^{-4}$  to  $1 \times 10^{-3} \text{ cm}^2/\text{s}$  [ $1 \times 10^{-7}$  to  $1 \times 10^{-6} \text{ ft}^2/\text{s}$ ] and for mortar from  $1 \times 10^{-6}$  to  $1 \times 10^{-4} \text{ cm}^2/\text{s}$  [ $1 \times 10^{-9}$  to  $1 \times 10^{-7} \text{ ft}^2/\text{s}$ ]. The diffusion coefficient of oxygen in air is approximately  $2 \times 10^{-1} \text{ cm}^2/\text{s}$  [ $2 \times 10^{-4} \text{ ft}^2/\text{s}$ ] (Culot, et al., 1976). Applying the values of diffusivity listed in Table A3–8 to transport through a specific cementitious material is not straightforward, because of the influence of water content discussed previously.

## **A4 SUMMARY AND RECOMMENDATIONS**

This appendix summarizes data collected from the technical literature on the water and gas permeability and aqueous and gas diffusivity of cementitious materials. The majority of the research on the transport properties of concrete and mortar relates to concrete and mortar used in civil construction projects, such as roads, bridges, and building foundations.

The saturated hydraulic conductivity of cementitious materials, excluding macrocracks, was found to range over 9 orders of magnitude from approximately  $10^{-14}$  to almost  $10^{-5} \text{ cm/s}$

**Table A3-8. Gas Effective Diffusion Coefficients**

<b>Material Description</b>	<b>Measurement Conditions*</b>	<b>Species</b>	<b>Effective Diffusion Coefficient† (cm<sup>2</sup>/s)‡</b>	<b>Comments</b>	<b>Source</b>
Concrete slabs similar to those used in house construction without reinforcing bars	Laboratory	Radon	4.2E-04	Value may have been divided by gas-filled porosity, which would make the value too high for effective diffusion coefficient	Nielson, K.K., V.C. Rogers, R.B. Holt, T.D. Pugh, W.A. Grondzik, and R.J. de Meijer. "Radon Penetration of Concrete Slab Cracks, Joints, Pipe Penetrations, and Sealants." <i>Health Physics</i> . Vol. 73. pp. 668-678. 1997.
Concrete slabs similar to those used in house construction without reinforcing bars, water/cement = 0.5	Laboratory	Radon	5.0E-04	Value may have been divided by gas-filled porosity, which would make the value too high for effective diffusion coefficient	Renken, K.J. and T. Rosenberg. "Laboratory Measurements of the Transport of Radon Gas Through Concrete Samples." <i>Health Physics</i> . Vol. 68. pp. 800-808. 1995.
Concrete slabs similar to those used in house construction without reinforcing bars, water/cement = 1.0	Laboratory	Radon	1.4E-05	Value may have been divided by gas-filled porosity, which would make the value too high for effective diffusion coefficient	Renken and Rosenberg (1995).
Concrete slabs similar to those used in house construction without reinforcing bars, water/cement = 0.65	Laboratory	Radon	9.1E-04	Value may have been divided by gas-filled porosity, which would make the value too high for effective diffusion coefficient	Renken and Rosenberg (1995).
Fresh concrete used in housing slabs	Laboratory	Radon	1.0E-03	Value corrected to effective diffusion coefficient using porosity of 0.20	Rogers, V.C., K.K. Nielson, R.B. Holt, and R. Snoddy. "Radon Diffusion Coefficients for Residential Concretes." <i>Health Physics</i> . Vol. 67. pp. 261-265. 1994.

Table A3-8. Gas Effective Diffusion Coefficients (continued)					
Material Description	Measurement Conditions*	Species	Effective Diffusion Coefficient† (cm <sup>2</sup> /s)‡	Comments	Source
Fresh concrete used in housing slabs	Laboratory	Radon	3.8E-05	Value corrected to effective diffusion coefficient using porosity of 0.18	Rogers, et al. (1994).
Aged concrete from residential slabs	Laboratory	Radon	1.3E-03	Value corrected to effective diffusion coefficient using porosity of 0.24	Rogers, V.C., K.K. Nielson, R.B. Holt, and R. Snoddy. "Radon Diffusion Coefficients for Aged Residential Concretes." <i>Health Physics</i> . Vol. 68. pp. 832-834. 1995.
Aged concrete from residential slabs	Laboratory	Radon	3.0E-04	Value corrected to effective diffusion coefficient using porosity of 0.20	Rogers, et al. (1995).
Concrete in basement wall	Laboratory	Radon	3.1E-05	Calculated value assumes porosity of 0.25	Culot, M.V., H.G. Olson, and K.J. Schiager. "Effective Diffusion Coefficient of Radon in Concrete, Theory and Method for Field Measurements." <i>Health Physics</i> . Vol. 30. pp. 263-270. 1976.
Concrete and mortar, composition unknown	Laboratory	N <sub>2</sub> -O <sub>2</sub> §	9.0E-05	Value reported in Culot, et al. (1976) from secondary source	Culot, et al. (1976).
Ordinary concrete, air cured, 60% water content	Laboratory	N <sub>2</sub> -O <sub>2</sub>	1.0E-03	Value estimated from bar chart	Kobayashi, K. and K. Shuttoh. "Oxygen Diffusivity of Various Cementitious Materials." <i>Cement and Concrete Research</i> . Vol. 21. pp. 273-284. 1991.
High-early strength, air cured, 60% water content	Laboratory	N <sub>2</sub> -O <sub>2</sub>	4.5E-04	Value estimated from bar chart	Kobayashi and Shuttoh (1991).
Moderate heat, air cured, 60% water content	Laboratory	N <sub>2</sub> -O <sub>2</sub>	1.4E-03	Value estimated from bar chart	Kobayashi and Shuttoh (1991).
Sulfate resistant, air cured, 60% water content	Laboratory	N <sub>2</sub> -O <sub>2</sub>	1.3E-03	Value estimated from bar chart	Kobayashi and Shuttoh (1991).

Table A3-8. Gas Effective Diffusion Coefficients (continued)

Material Description	Measurement Conditions*	Species	Effective Diffusion Coefficient† (cm <sup>2</sup> /s)‡	Comments	Source
30% replacement by blast-furnace slag, air cured, 60% water content	Laboratory	N <sub>2</sub> -O <sub>2</sub>	6.3E-04	Value estimated from bar chart	Kobayashi and Shuttah (1991).
The same as above with 60% replacement, air cured, 60% water content	Laboratory	N <sub>2</sub> -O <sub>2</sub>	9.5E-04	Value estimated from bar chart	Kobayashi and Shuttah (1991).
The same as above with 70% replacement, air cured, 60% water content	Laboratory	N <sub>2</sub> -O <sub>2</sub>	1.0E-03	Value estimated from bar chart	Kobayashi and Shuttah (1991).
20% replacement by fly ash, air cured, 60% water content	Laboratory	N <sub>2</sub> -O <sub>2</sub>	1.2E-03	Value estimated from bar chart	Kobayashi and Shuttah (1991).
Ordinary concrete, water cured for 7 days, 60% water content	Laboratory	N <sub>2</sub> -O <sub>2</sub>	4.5E-04	Value estimated from bar chart	Kobayashi and Shuttah (1991).
High-early strength, water cured for 7 days, 60% water content	Laboratory	N <sub>2</sub> -O <sub>2</sub>	4.6E-04	Value estimated from bar chart	Kobayashi and Shuttah (1991).
Moderate heat, water cured for 7 days, 60% water content	Laboratory	N <sub>2</sub> -O <sub>2</sub>	4.4E-04	Value estimated from bar chart	Kobayashi and Shuttah (1991).
Sulfate resistant, water cured for 7 days, 60% water content	Laboratory	N <sub>2</sub> -O <sub>2</sub>	3.8E-04	Value estimated from bar chart	Kobayashi and Shuttah (1991).
30% replacement by blast-furnace slag, water cured for 7 days, 60% water content	Laboratory	N <sub>2</sub> -O <sub>2</sub>	2.6E-04	Value estimated from bar chart	Kobayashi and Shuttah (1991).
The same as above with 60% replacement, water cured for 7 days, 60% water content	Laboratory	N <sub>2</sub> -O <sub>2</sub>	1.5E-04	Value estimated from bar chart	Kobayashi and Shuttah (1991).
The same as above with 70% replacement, water cured for 7 days, 60% water content	Laboratory	N <sub>2</sub> -O <sub>2</sub>	1.3E-04	Value estimated from bar chart	Kobayashi and Shuttah (1991).
20% replacement by fly ash, water cured for 7 days, 60% water content	Laboratory	N <sub>2</sub> -O <sub>2</sub>	3.3E-04	Value estimated from bar chart	Kobayashi and Shuttah (1991).
Ordinary concrete, water cured for 28 days, 60% water content	Laboratory	N <sub>2</sub> -O <sub>2</sub>	2.4E-04	Value estimated from bar chart	Kobayashi and Shuttah (1991).
High-early strength, water cured for 28 days, 60% water content	Laboratory	N <sub>2</sub> -O <sub>2</sub>	1.8E-04	Value estimated from bar chart	Kobayashi and Shuttah (1991).

**Table A3-8. Gas Effective Diffusion Coefficients (continued)**

<b>Material Description</b>	<b>Measurement Conditions*</b>	<b>Species</b>	<b>Effective Diffusion Coefficient† (cm<sup>2</sup>/s)‡</b>	<b>Comments</b>	<b>Source</b>
Moderate heat, water cured for 28 days, 60% water content	Laboratory	N <sub>2</sub> -O <sub>2</sub>	1.7E-04	Value estimated from bar chart	Kobayashi and Shuttah (1991).
Sulfate resistant, water cured for 28 days, 60% water content	Laboratory	N <sub>2</sub> -O <sub>2</sub>	2.0E-04	Value estimated from bar chart	Kobayashi and Shuttah (1991).
30% replacement by blast-furnace slag, water cured for 28 days, 60% water content	Laboratory	N <sub>2</sub> -O <sub>2</sub>	1.2E-04	Value estimated from bar chart	Kobayashi and Shuttah (1991).
The same as above with 60% replacement, water cured for 28 days, 60% water content	Laboratory	N <sub>2</sub> -O <sub>2</sub>	1.7E-04	Value estimated from bar chart	Kobayashi and Shuttah (1991).
The same as above with 70% replacement, water cured for 28 days, 60% water content	Laboratory	N <sub>2</sub> -O <sub>2</sub>	1.0E-04	Value estimated from bar chart	Kobayashi and Shuttah (1991).
20% replacement by fly ash, water cured for 28 days, 60% water content	Laboratory	N <sub>2</sub> -O <sub>2</sub>	2.0E-04	Value estimated from bar chart	Kobayashi and Shuttah (1991).
Plain cement mortar, W/C = 35%	Laboratory	N <sub>2</sub> -O <sub>2</sub>	5.8E-05	Value estimated from bar chart	Kobayashi and Shuttah (1991).
Plain cement mortar, W/C = 60%	Laboratory	N <sub>2</sub> -O <sub>2</sub>	8.4E-05	Value estimated from bar chart	Kobayashi and Shuttah (1991).
Mortar using cement with replacement slag, W/(C+S) = 35%, S/(C+S) = 30%	Laboratory	N <sub>2</sub> -O <sub>2</sub>	3.4E-05	Value estimated from bar chart	Kobayashi and Shuttah (1991).
Mortar using cement with replacement slag, W/(C+S) = 60%, S/(C+S) = 30%	Laboratory	N <sub>2</sub> -O <sub>2</sub>	3.4E-05	Value estimated from bar chart	Kobayashi and Shuttah (1991).
Mortar using cement with replacement slag, W/(C+S) = 60%, S/(C+S) = 60%	Laboratory	N <sub>2</sub> -O <sub>2</sub>	2.6E-05	Value estimated from bar chart	Kobayashi and Shuttah (1991).
Polymer-modified mortar, Acrylic base W/C = 35%, Ps/(C+Ps) = 7.5%	Laboratory	N <sub>2</sub> -O <sub>2</sub>	1.1E-05	Value estimated from bar chart	Kobayashi and Shuttah (1991).

Table A3-8. Gas Effective Diffusion Coefficients (continued)

Material Description	Measurement Conditions*	Species	Effective Diffusion Coefficient† (cm <sup>2</sup> /s)‡	Comments	Source
Polymer-modified mortar, Acrylic base W/C = 35%, Ps/(C+Ps) = 15%	Laboratory	N <sub>2</sub> -O <sub>2</sub>	4.6E-06	Value estimated from bar chart	Kobayashi and Shuttoh (1991).
Polymer-modified mortar, Acrylic base W/C = 35%, Ps/(C+Ps) = 20%	Laboratory	N <sub>2</sub> -O <sub>2</sub>	4.3E-06	Value estimated from bar chart	Kobayashi and Shuttoh (1991).
Polymer-modified mortar, SBR base W/C = 35%, Ps/(C+Ps) = 7.5%	Laboratory	N <sub>2</sub> -O <sub>2</sub>	2.2E-05	Value estimated from bar chart	Kobayashi and Shuttoh (1991).
Polymer-modified mortar, SBR base W/C = 35%, Ps/(C+Ps) = 15%	Laboratory	N <sub>2</sub> -O <sub>2</sub>	3.4E-06	Value estimated from bar chart	Kobayashi and Shuttoh (1991).
Polymer-modified mortar, SBR base W/C = 35%, Ps/(C+Ps) = 20%	Laboratory	N <sub>2</sub> -O <sub>2</sub>	3.4E-06	Value estimated from bar chart	Kobayashi and Shuttoh (1991).
3 parts pulverized blast-furnace slag/1 part ordinary Portland cement	Laboratory	N <sub>2</sub> -O <sub>2</sub>	1.E-05	20-mm [0.8-in]-thick disc with microcracks, 85% water saturation	Kobayashi and Shuttoh (1991).
<p>*Measurement conditions are reported as "laboratory" if measured in a laboratory environment; "field" if an <i>in-situ</i> field measurement; "reported" if the value is derived from an unspecified secondary source.</p> <p>†Effective diffusion coefficient as defined by Eq. (A2-15); includes effects of porosity, tortuosity, and sorption.</p> <p>‡9.3 × 10<sup>2</sup> cm<sup>2</sup>/s = 1 ft<sup>2</sup>/s; 25 mm = 1 in</p> <p>§Binary diffusion of nitrogen and oxygen.</p>					

[ $10^{-15}$  to  $10^{-8}$  ft/s] (Table A3–1 and Figure A3–1). Although the data suggest a median value for all cementitious materials of  $10^{-9}$  cm/s [ $10^{-11}$  ft/s], the significance of this value is limited because the number of samples in each material type was uneven. The data found on the permeability of grout suggest that the hydraulic conductivity of grout that might be used in tank closures would be in the upper range of that for other cementitious materials. In general, the permeability of cementitious materials without macrocracks is controlled by the capillary porosity, pore size distribution, and aggregate permeability (Neville, 1996). The capillary porosity generally increases with the water/cement ratio. Because grout materials generally have a relatively high water/cement ratio, they might be expected to have a higher permeability than construction concrete, consistent with the data displayed in Figures A3–1 and A3–2. On the other hand, the permeability data specific to grout displayed in Figure A3–3 does not indicate a clear relationship between the water to cement plus pozzolan ratio and permeability. In fact, the data Dixon and Phifer (2007) reported indicate greater variability within specimens of a specific grout formulation than between grout formulations. This suggests that sample preparation and handling may have a strong effect on laboratory-scale permeability measurements and that the transferability of laboratory-scale data to full-scale grout monoliths may be problematic.

The effective water permeability or hydraulic conductivity of cementitious materials also depends on their state of saturation. As with natural porous media, the effective permeability of cementitious materials decreases with water content as fewer water-filled pathways are available for flow. Limited measurements of the hydraulic properties of partially saturated cementitious materials were found in the technical literature. Although the variation of effective water permeability and hydraulic conductivity of cementitious materials with water content can generally be described using relationships developed for natural porous materials such as soils, these relationships may not apply to cementitious materials at very low water content. This is because the water-filled pores will be much smaller than those of most natural materials, except for compacted clay.

Research on cementitious materials containing macrocracks indicates that bulk permeability increases with crack aperture, as would be expected from theory. The data on cracked cementitious materials reported in the literature was entirely from small laboratory specimens. The permeability data reported for these specimens represents the permeability or hydraulic conductivity averaged over the surface area of the specimen as opposed to values intrinsic to the crack. Thus, the data from crack specimens would require additional analysis before being applied to large cementitious structures.

The limited data found on the gas permeability of cementitious materials are listed in Table A3–5. These data all relate to the permeability of concrete without macrocracks. The gas permeabilities of the specimens listed in Table A3–5 fall in the midrange of intrinsic water permeabilities for cementitious materials listed in Table A3–1. The single value for concrete that had been in service (Lampacher and Blight, 1998) is five orders of magnitude higher than that of the laboratory-prepared specimens and falls at the upper end of the range for water permeability data.

With respect to which, if any, of the permeability data listed in Tables A3–1 through A3–4 might be most appropriate for evaluating the performance of cementitious materials used in tank closures, the answer is strongly scale dependent. Most of the data in the technical literature are derived from laboratory-scale specimens with dimensions of a few tens of centimeters [a few inches] and most do not contain macrocracks. The permeability values from these specimens may be appropriate for estimating water flow through the matrix between macrocracks, but not

for estimating flow through a large-scale grout monolith. The data on cracked samples are only useful if the fracture density in the monolith is known or can be estimated, as discussed in Section 6 of the report.

Data collected from the technical literature on the effective aqueous diffusion coefficient for inorganic, ionic species in cementitious materials are provided in Tables A3-6 and A3-7. The effective diffusion coefficients listed in these tables are based on the definition of the effective diffusion coefficient given in Eq. (A2-15) and include the effects of porosity, tortuosity, sorption, and chemical interaction, if any, with the cement. Table A3-6 contains values of the effective diffusion coefficient reported for a variety of cementitious materials under a variety of experimental conditions. The values listed in Tables A3-6 and A3-7 all relate to specimens without macrocracks. Although the values reported in Tables A3-6 and A3-7 span nearly 12 orders of magnitude, the values for most species are likely to be strongly influenced by sorption or chemical reactions. Of the various species for which diffusion coefficients are reported, only a few, such as chloride, iodide, and nitrate, are likely to reflect only the geometric properties of the cementitious materials. The data most relevant to grout that might be used for tank closures are those in Table A3-7 from Serne, et al. (1992). These diffusion coefficients cannot be used to calculate transport through a specific cementitious material without considering the composition of the specific material and its chemical environment.

Table A3-8 lists data collected from the technical literature on gas diffusion coefficients in cementitious materials. The only data that could be found were related to radon diffusion in building concrete and oxygen diffusion in construction concrete. As Culot, et al. (1976) noted, the literature on gas diffusion of radon contains ambiguous definitions of the effective diffusion coefficient. For partially saturated concrete, the air-filled porosity through which the gas can diffuse will be significantly less than the total porosity and could affect the reported value by one or two orders of magnitude. In most cases, the water saturation of the tested cementitious materials was not reported with the diffusion coefficients, leading to a significant variation in values and uncertainty in applying these values to materials other than those tested. Gas diffusion in cementitious materials can also be influenced by Knudsen diffusion as well as Fickian molecular diffusion (e.g., Kobayashi and Shuttoh, 1991). Applying the values of diffusivity listed in Table A3-8 to transport through a specific cementitious material is not straightforward, because of the influence of water content discussed previously. No data were found on gas diffusion coefficients of radon or carbon-14 in grout (radionuclides of possible interest for tank closures).

Only limited research on the properties of cementitious grout that might be directly relevant to waste tank closures was identified. Another limitation of the data presented in this report is that nearly all of the data are from tests on specially prepared small specimens (dimensions of inches) under laboratory conditions, and these results may not be directly applicable to large, aged cementitious structures. Finally, cementitious materials used in construction and those that might be used in tank closures are heterogeneous materials that contain multiple liquid and gas transport pathways. These pathways, ranging from extremely small pore spaces in cement gel and mortar to microcracks in the mortar and around aggregate to macrocracks, all have different transport properties. Thus, the transport properties of a large structure would consist of a combination of the properties of the individual pathways.

## A5 REFERENCES

- Aldea, C.-M., S.P. Shah, and A. Karr. "Permeability of Cracked Concrete." *Materials and Constructions*. Vol. 32. pp. 370–376. 1999a.
- . "Effect of Cracking on Water Chloride Permeability of Concrete." *Journal of Materials in Civil Engineering*. Vol. 11. pp. 181–187. 1999b.
- ASTM International. "ASTM D 5084: Standard Test Methods for Measurement of Hydraulic Conductivity of Saturated Porous Materials Using a Flexible Wall Permeameter." West Conshohocken, Pennsylvania: ASTM International. 2003.
- . "ASTM D 6527: Standard Test Method for Determination of Unsaturated and Saturated Hydraulic Conductivity of Porous Media by Steady-State Centrifugation." West Conshohocken, Pennsylvania: ASTM International. 2001.
- . "ASTM D 3152: Standard Test Method for Capillary-Moisture Relationships for Fine Textured Soils by Pressure-Membrane Apparatus." West Conshohocken, Pennsylvania: ASTM International. 1972.
- Bear, J. *Hydraulics of Groundwater*. New York City, New York: McGraw-Hill Inc. 1979.
- . *Dynamics of Fluids in Porous Media*. New York City, New York: American Elsevier Publishing Company. 1972.
- Bird, R.B., W.E. Stewart, and E.N. Lightfoot. *Transport Phenomena*. New York City, New York: John Wiley & Sons. 1960.
- Boulfiza, M., K. Sakai, N. Banthia, and H. Yoshida. "Prediction of Chloride Ions Ingress in Uncracked and Cracked Concrete." *ACI Materials Journal*. Vol. 100. pp. 38–48. 2003.
- Brooks, R.H. and A.T. Corey. "Properties of Porous Media Affecting Fluid Flow." *Journal of Irrigation and Drainage Division*. Vol. 92, No. IR2. pp. 61–88. 1966.
- Claisse, P.A., H.I. Elsayad, and I.G. Shaaban. "Test Methods for Measuring Fluid Transport in Cover Concrete." *Journal of Materials in Civil Engineering*. Vol. 11. pp. 138–143. 1999.
- . "Absorption and Sorptivity of Cover Concrete." *Journal of Materials in Civil Engineering*. Vol. 19. pp. 105–110. 1997.
- Conca, J. and J. Wright. "Measuring Transport Properties in Grout and Cement." Presentation to Cementitious Materials for Waste Treatment, Disposal, Remediation and Decommissioning Workshop, December 12–14, 2006. Aiken, South Carolina: Westinghouse Savannah River Company. 2006.
- Culot, M.V.J., H.G. Olson, and K.J. Schiager. "Effective Diffusion Coefficient of Radon in Concrete, Theory and Method for Field Measurements." *Health Physics*. Vol. 30. pp. 263–270. 1976.

de Beer, F.C., J.J. le Roux, and E.P. Kearsley. "Testing the Durability of Concrete With Neutron Radiography." *Nuclear Instruments and Methods in Physics Research*. Vol. A, No. 542. pp. 226–231. 2005.

Dixon, K. and M. Phifer. "Hydraulic and Physical Properties of Tank Grouts and Base Mat Surrogate Concrete for FTF Closure." WSRC–STI–2007–00369. Aiken, South Carolina: Westinghouse Savannah River Company. 2007

Garboczi, E.J. and D.P. Bentz. "Multi-Scale Picture of Concrete and Its Transport Properties: Introduction for Non-Cement Researchers." NISTIR 5900. Washington, DC: National Institute of Standards. 1996.

Graham-Bryce, I.J. "Self-Diffusion of Ions in Soil." *Journal of Soil Science*. Vol. 14. pp. 195–200. 1963.

Green, R.T., F.T. Dodge, S.J. Svedeman, R.D. Manteufel, G. Rice, K.A. Meyer, and R.G. Baca. NUREG/CR–6348, "Thermally Driven Moisture Redistribution in Partially Saturated Porous Media." Washington, DC: NRC. December 1995.

Halamickova, P., R.J. Detwiler, D.P. Bentz, and E.J. Garboczi. "Water Permeability and Chloride Ion Diffusion in Portland Cement Mortars: Relationship to Sand Content and Critical Pore Diameter." *Cement and Concrete Research*. Vol. 25. pp. 790–802. 1995.

Hearn, N. "Effect of Shrinkage and Load-Induced Cracking on Water Permeability of Concrete." *ACI Materials Journal*. Vol. 96. pp. 234–241. 1999.

Hillel, D. *Introduction to Soil Physics*. New York City, New York: Academic Press. 1982.

Jenneson, P.M., A.S. Clough, and R. Hollands. "Profiling Chlorine Diffusion Into Ordinary Portland Cement and Pulverized Fuel Ash Pastes Using Scanning MeV Proton Micro-PIXE." *Journal of Materials Science Letters*. Vol. 17. pp. 1,173–1,175. 1998.

Kobayashi, K. and K. Shuttoh. "Oxygen Diffusivity of Various Cementitious Materials." *Cement and Concrete Research*. Vol. 21. pp. 273–284. 1991.

Lampacher, B.J. and G.E. Blight. "Permeability and Sorption Properties of Mature Near-Surface Concrete." *Journal of Materials in Civil Engineering*. Vol. 10. pp. 21–25. 1998.

Marshall, T.J., J.W. Holmes, and C.W. Rose. *Soil Physics*. Third Edition. Cambridge, United Kingdom: Cambridge University Press. 1996.

Martys, N.S. "Survey of Concrete Transport Properties and Their Measurement." NISTIR 5592. Washington, DC: National Institute of Standards. 1995.

Mattigod, S.V., G.A. Whyatt, R.J. Serne, P.F. Martin, K.E. Schwab, and M.I. Wood. "Diffusion and Leaching of Selected Radionuclides (Iodine-129, Technetium-99, and Uranium) Through Category 3 Waste Encasement Concrete and Soil Fill Material." PNNL-13639. Richland, Washington: Pacific Northwest National Laboratory. 2001.

Mattson, E.D., K.L. Dixon, M.A. Phifer, and K.M. Gibbs. "Novel Methods to Characterize Cementitious Material for Performance Assessment Calculations." Poster for Cementitious Materials for Waste Treatment, Disposal, Remediation and Decommissioning Workshop, December 12–14, 2006. Aiken, South Carolina: Westinghouse Savannah River Company. 2006.

Naik, T.R., S.S. Singh, and B.W. Ramne. "Performance and Leaching Assessment of Flowable Slurry." *Journal of Environmental Engineering*. Vol. 127, No. 4. pp. 359–368. 2001.

Nazaroff, W.W. "Radon Transport From Soil to Air." *Reviews of Geophysics*. Vol. 20, No. 2. pp. 137–160. 1992.

Neretnieks, I. "Diffusion in the Rock Matrix: An Important Factor in Radionuclide Retardation?" *Journal of Geophysical Research*. Vol. 85, No. B8. pp. 4,379–4,397. 1980.

Neville, A.M. "Properties of Concrete." London, United Kingdom: John Wiley & Sons. 1996.

Nielson, K.K., V.C. Rogers, R.B. Holt, T.D. Pugh, W.A. Grondzik, and R.J. de Meijer. "Radon Penetration of Concrete Slab Cracks, Joints, Pipe Penetrations, and Sealants." *Health Physics*. Vol. 73. pp. 668–678. 1997.

Rockhold, M.L., M.J. Fyer, and P.R. Heller. "Physical and Hydraulic Properties of Sediments and Engineered Materials Associated With Grouted Double-Shell Tank Waste Disposal at Hanford." PNNL–8813. Richland, Washington: Pacific Northwest National Laboratory. 1993.

Roux, N., C. Andrade, and M.A. Sanjuan. "Experimental Study of Durability of Reactive Powder Concretes." *Journal of Materials in Civil Engineering*. Vol. 8, No. 1. pp. 1–6. 1996.

Sato, H. "Effect of Ionic Charge on Effective Diffusion Coefficient in Compacted Sodium Bentonite." Materials Research Society Symposium Proceedings 608. R.W. Smith and D.W. Shoosmith, eds. Warrendale, Pennsylvania: Materials Research Society. pp. 267–274. 2000.

Savage, B.M. and D.J. Janssen. "Soil Physics Principles Validated for Use in Predicting Unsaturated Moisture Movement in Portland Cement Concrete." *ACI Materials Journal*. Vol. 94. pp. 63–70. 1997.

Schaap, M.G., P.J. Shouse, and P.D. Meyer. "Laboratory Measurements of the Unsaturated Hydraulic Properties at the Vadose Zone Transport Field Study Site." PNNL-14284. Richland, Washington: Pacific Northwest National Laboratory. 2003.

Serne, R.J., R.O. Lokken, and L.F. Criscenti. "Characterization of Grouted Low-Level Waste to Support Performance Assessment." *Waste Management*. Vol. 12. pp. 271–287. 1992.

Scherer, G.W. "New Methods to Measure Permeability." Cementitious Materials for Waste Treatment, Disposal, Remediation and Decommissioning Workshop, December 11, 2006, Aiken County Center for Hydrogen Research. Aiken, South Carolina: Savannah River National Laboratory. 2007.

Thibodeux, L.F. *Environmental Chemodynamics*. New York City, New York: John Wiley & Sons, Inc. 1996.

Tits, J., A. Jakob, E. Wieland, and P. Spieler. "Diffusion of Tritiated Water and  $^{22}\text{Na}^+$  Through Non-degraded Hardened Cement Pastes." *Journal of Contaminant Hydrology*. Vol. 61. pp. 45–62. 2003.

van Brakel, J. and P.M. Heertjes. "Analysis of Diffusion in Macroporous Media in Terms of a Porosity, a Tortuosity and a Constrictivity Factor." *International Journal of Heat and Mass Transfer*. Vol. 17. pp. 1,093–1,103. 1974.

van Genuchten, M.Th. "A Closed-Form Equation for Predicting the Hydraulic Conductivity of Unsaturated Soils." *Soil Science Society of America Journal*. Vol. 44. pp. 892–898. 1980.

Wang, J., D.C. Jansen, S.P. Shah, and A.F. Karr. "Permeability of Cracked Concrete." Report No. 46. Research Triangle Park, North Carolina: National Institute of Statistical Sciences. 1996.

Wong, H.S., N.R. Buenfeld, J. Hill, and A.W. Harris. "Mass Transport Properties of Mature Wasteform Grouts." *Advances in Cement Research*. Vol. 19. pp. 35–46. 2007.

Young, J.F. "A Review of the Pore Structure of Cement Paste and Concrete and Its Influence on Permeability." ACI SP-108. Permeability of Concrete. D. Whiting and A. Walitt, eds. Detroit, Michigan: American Concrete Institute. 1988.

Yu, A.D., C.A. Langton, and M. Serrato. "Physical Properties Measurement Program (U)." WSRC-RP-93-894. Aiken, South Carolina: Westinghouse Savannah River Company. 1993.

## Notation

$g$	—	gravitational acceleration [L/t <sup>2</sup> ]
$k$	—	intrinsic permeability [L <sup>2</sup> ]
$k_R$	—	relative permeability at fluid content $\theta$
$q$	—	volumetric flux [L/t]
$r$	—	characteristic pore radius [L]
$s$	—	macroscopic distance in the direction of flow [L]
$t$	—	time
$C_a$	—	aqueous concentration [M/L <sup>3</sup> ]
$C_s$	—	sorbed concentration [M/M]
$D_0$	—	free aqueous diffusion coefficient [L <sup>2</sup> /t]
$\frac{dC_a}{dx}$	—	macroscopic aqueous concentration gradient [M/L <sup>4</sup> ]
$H$	—	hydraulic head [L]
$K$	—	hydraulic conductivity [L/t]
$K(\theta)$	—	unsaturated hydraulic conductivity at fluid content $\theta$
$K_d$	—	distribution coefficient [L <sup>3</sup> /M]
$P$	—	fluid pressure [M/L-t <sup>2</sup> ]
$P_c$	—	capillary pressure (taken as positive)
$\frac{dP}{ds}$	—	pressure gradient in the direction of flow pressure [M/L <sup>2</sup> -t <sup>2</sup> ]
$S$	—	actual saturation
$S_e$	—	effective saturation
$S_p$	—	sorptivity [L/t <sup>1/2</sup> ]
$S_r$	—	irreducible saturation
$V$	—	cumulative water uptake per unit area [L]
$\alpha$	—	matrix factor accounting for microscopic, tortuous paths and other factors related to pore geometry
$\alpha_p, n$	—	fitting parameters
$\gamma$	—	surface tension [M/t <sup>2</sup> ]
$\theta$	—	fluid (water) content
$\mu$	—	dynamic viscosity [M/L-t]
$\rho$	—	fluid density [M/L <sup>3</sup> ]
$\rho_b$	—	dry bulk density [M/L <sup>3</sup> ]
$\phi$	—	porosity

## **APPENDIX B**

# RADIONUCLIDE SOLUBILITY LIMITS IN CEMENT-BASED MATERIAL PORE FLUIDS

## B1 INTRODUCTION

An important variable in groundwater pathway performance assessments is the contaminant concentration in water at the source. Models for contaminant release vary widely, but typically include a maximum bound on concentration based on a solubility limit. For example, isotopes of a radioelement may be modeled to be released congruently as a nuclear waste form dissolves in water, but the radionuclide concentrations in that water can be capped at an elemental concentration that is controlled by the solubility of a solid phase of that element.

In support of waste determinations for cement-based disposal facilities at the Savannah River Site and Idaho National Laboratory, including both grouted tanks and monolithic waste forms (DOE-ID, 2006; DOE, 2006), the U.S. Department of Energy (DOE) has typically modeled radionuclide release using a partition coefficient or  $K_d$  to constrain radionuclide concentration (Rosenberger, et al., 2005; DOE-ID, 2003). This coefficient, which is also applied in many groundwater transport models, defines the radionuclide concentration by assuming a constant ratio between the mass on the solid waste form and the mass in solution. For the Savannah River Site and Idaho National Laboratory models, the  $K_d$  values are chosen to be appropriate for a cementitious environment (e.g., Bradbury and Sarott, 1995). This approach may not always be the most appropriate for a release calculation, particularly if the waste form is dissolving and the chemical environment is potentially dynamic. Furthermore, if a radionuclide is released at the margin of the cement-based waste form, a release model  $K_d$  that assumes sorption to cement-based material solids may not be appropriate.

It is important, then, to consider other processes that may control, or contribute to the control of, contaminant aqueous concentrations. In this respect, the concept of the solubility limit is useful to consider. If there are reasons that a  $K_d$  model may be inappropriate in a given situation (if, for instance, sorption sites are inaccessible to the solution), a conservative approach may be to define radionuclide concentrations at the source on the basis of solubility (e.g., Denham, 2007). In addition, solubility may add realism to  $K_d$  release models by constraining concentrations.

This appendix reviews available data on solubility limits for selected radioelements in environments expected in Savannah River Site and Idaho National Laboratory cement-based disposal facilities the Ronald W. Reagan National Defense Authorization Act for Fiscal Year 2005 covers. This information will be useful in U.S. Nuclear Regulatory Commission (NRC) staff reviews of disposal facility performance assessments; the reviews are conducted as part of the NRC consultative role established by the Ronald W. Reagan National Defense Authorization Act for Fiscal Year 2005.

### B1.1 Chemical Factors Affecting Solubility

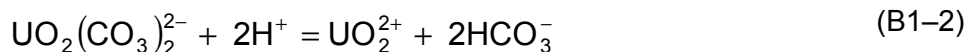
In the context of water–solid interactions affecting contaminant release, solubility is a thermodynamic property of a solid substance in association with water. Solubility is the “total amount of the mineral that has dissolved at equilibrium” (Nordstrom and Munoz, 1994), that is, at saturation, usually expressed as a concentration such as moles of solute per liter of solution. In modeling contaminant release, the solubility *limit* for an element—rather than a solid phase solubility—is typically abstracted into models as a maximum concentration of that element. The solubility limit for an element is the aqueous concentration of the element in equilibrium with the

solid (containing that element as a stoichiometric constituent) that limits the element to its lowest concentration. The solubility limit, therefore, is a property of an element—rather than of a solid phase—for a given set of physiochemical conditions (T, pH, solution composition).

The solubility of a solid is controlled by a reaction such as the following example for schoepite ( $\text{UO}_3 \cdot 2\text{H}_2\text{O}$ ), a uranium (U) mineral typically stable under oxidizing conditions (Murphy and Codell, 1999)



In the presence of schoepite, the reaction in Eq. (B1-1) defines the activity and, thus, the concentration of the dissolved uranyl ion ( $\text{UO}_2^{2+}$ ) at equilibrium in terms of pH. Equilibrium aqueous reactions may also be written for the uranyl ion and other stable dissolved U species; for example



The total mass of dissolved U (i.e., the solubility of schoepite) will include the masses of these other uranyl species in addition to the uranyl ion. Therefore, in the presence of schoepite, the dissolved U concentration is a function not only of the equilibrium reaction in Eq. (B1-1), but also of other equilibria that may be sensitive to geochemical parameters such as pH and bicarbonate ion concentration [e.g., Eq. (B1-2)]. Equilibrium constants for the various reactions are functions of temperature and pressure. The solubility of schoepite, then, is a function of several geochemical and physical variables and must be defined in those terms. Although a complete geochemical description is preferred for thermodynamic calculations, for discussion purposes, defining a few geochemical factors that most strongly influence solubility because of their presence in the solubility reaction or their impact on dissolved ionic species (e.g., pH, Eh, and carbonate species for schoepite in many systems) is often sufficient.

Determination of the solubility limit for an element must also consider which solid phase is controlling the dissolved concentration. If there is another stable U mineral for which the solubility reaction results in lower U concentration than schoepite, that mineral will control the U concentration. This occurs because equilibrium with that other phase will prevent dissolved U from reaching a high enough concentration such that schoepite precipitates. Any additional U added to solution is consumed in precipitating the lower solubility U phase. Thus, thermodynamically defining a solubility limit involves both determining individual phase solubilities and choosing the appropriate solubility-limiting phase.

## **B1.2 Solubility in Release Models**

As mentioned in Section B1, solubility may be used to define aqueous concentrations at the source in release models (e.g., Denham, 2007). This approach may be appropriate if, for example, it cannot be demonstrated that the radionuclide-bearing waste mixes thoroughly with a sorptive matrix such as grout.

Release models do not necessarily assume that a given element will be released at its solubility limit. Other processes, such as coprecipitation and sorption, can limit concentration to a level lower than that constrained by solubility. Consequently, an appropriately chosen solubility limit must be considered a maximum possible concentration; the release model may predict lower,

even much lower, values. A potentially acceptable approach that is commonly employed is to model radionuclide concentrations according to a  $K_d$  model, but to not allow concentrations to exceed a solubility limit.

Another approach may be to calculate a radionuclide effective  $K_d$  for use in release modeling based on the ratio of the known radionuclide concentration in the solid waste form to a solubility-limited concentration in the water. While this approach may appear to be conservative, there is a drawback: as the radionuclide in the waste form is depleted, the effective  $K_d$ -based aqueous concentration will decrease to levels below the solubility limit.

It is possible that the solubility-limiting phase predicted from thermodynamic considerations may not readily form due, for example, to kinetic constraints. Using such a mineral in the model could underpredict the radionuclide concentration. In this case, it may be preferable to select another mineral that, according to experimental studies, forms under the assumed conditions. In general, solubility limits must be evaluated for applicability to specific conditions and for the potential to both underpredict and overpredict concentration limits.

### **B1.3 Predicting Solubility Limits Using Models and Experiments**

Understanding the thermodynamic basis for solubility (Section B1.2) allows the use of models to predict radioelement solubility limits. The most common approach is to employ chemical equilibrium model codes [e.g., EQ3/6 (Wolery, 1992), Geochemist's Workbench<sup>®</sup> (Bethke, 1996), PHREEQC (Parkhurst, 1995), and MINTEQA2 (U.S. Environmental Protection Agency, 1999)] to determine the saturation states of radioelement solid phases over a plausible range of solution chemistries. Once the least soluble solid phase is identified and it is deemed to be stable and likely to form under the conditions of interest, the radioelement aqueous concentration is calculated based on equilibrium with that phase and is established as the solubility limit. The results rely not only on the use of high-quality thermodynamic data, but also on assumptions regarding the attainment of equilibrium and the completeness of the list of solid phases included. Solubility limits may be expressed graphically as functions of important variables such as pH and  $f_{CO_2}$  (which controls dissolved carbon species) so that possible variations in the environment may be understood.

Theoretical solubility models, which rely on assumptions regarding phase stability and equilibrium, must be evaluated in light of data from laboratory experiments designed to measure solubility limits. Apparent mismatches between laboratory and modeling studies of solubility can arise from a number of factors, including experimental procedures that compromise intended conditions (e.g., low oxygen concentration), kinetic suppression of thermodynamically favored phases, and incompleteness of the thermodynamic database supporting the model. To be directly applicable to establishing radioelement solubility limits, laboratory experiments should have the following characteristics:

- They should be designed to avoid interfering chemical reactions. For example, solubility studies of an actinide should exclude other actinides or major metals that may actively precipitate; otherwise, coprecipitation phenomena cannot be excluded.
- The presence or absence of colloids—mobile particles less than 1  $\mu\text{m}$  [ $4 \times 10^{-5}$  in] in size that could stabilize radioelement concentrations in water in excess of solubility limits—should be verified, and any colloids present should be characterized.

- They should not be conducted in the presence of the waste form. Radioelement concentrations from waste form leaching or dissolution studies are useful for understanding radionuclide release, but they do not provide unambiguous solubility information. Because the pure-phase solubility limit is a thermodynamically derived, theoretical maximum concentration of a radioelement, it should not incorporate effects of host waste phases. Therefore, the host phases are relevant to pure-phase solubility only to the degree that they affect aqueous chemistry. For example, sorption processes that can lower aqueous concentration cannot be ruled out in the presence of a waste form substrate. For experiments in the presence of a waste form, concentrations must be considered to be minimum values for solubility limits.
- They should attempt to approach, in a controlled manner, solution–solid equilibrium from both oversaturation (positive saturation index) and undersaturation (negative saturation index). The saturation index is the logarithm of the ratio of the ion activity product to the equilibrium constant for the solid phase dissolution reaction.
- In experiments approaching equilibrium from oversaturation, attempts should be made to identify the pure-phase solids that are precipitating the radioelement from solution.

While not all solubility studies will meet these criteria, they provide useful benchmarks with which to evaluate the data and their applicability to establishing solubility limits. Likewise, solubility models alone should not be applied without proper context. The most useful approach is to evaluate solubility limits in light of a combination of thermodynamic model results, solubility experiments, and waste form experiments. Where uncertainties cannot be reconciled, the conservative approach with respect to modeling radionuclide release is to choose the higher solubility limit. The value of combining thermodynamic models with experimental results is chiefly that the models (i) provide information on the important aqueous and solid species driving solubility limits, (ii) allow extrapolation of experimental results beyond the ranges of chemical variation studied in the laboratory, and (iii) may reveal flaws in experimental approaches or practices.

#### **B1.4 Solubility Limit Modeling Approach in This Report**

As part of the detailed reviews in Section B3, this report documents new thermodynamic equilibrium models for solubility models of selenium (Se), technetium (Tc), U, neptunium (Np), and plutonium (Pu) at 25 °C [77 °F] using the SpecE8 and React components of Geochemist's Workbench Professional 6.0 (Bethke, 1996) with the thermo.com.v8.r6+.dat thermodynamic database. Geochemist's Workbench was chosen for the modeling studies because of its ease of use, graphical interface, and wide acceptance in the geochemical community. SpecE8 calculates an equilibrium aqueous and solid phase assemblage for a single set of chemical conditions, while React allows equilibrium calculations along an evolving chemical pathway or during progressive reaction. The steps taken in the modeling effort are as follows:

- (1) Specific water compositions were defined that represent a range of compositions potentially encountered during aqueous degradation of cement-based materials (Section B2.5).

- (2) A default concentration of the element of interest ( $0.5 \text{ M}^1$  or lower) was input into the water composition, and the “slide” function in the React module was used to simulate element behavior over a range of Eh from a maximum to a minimum value, with constant pH. At each Eh step in React, equilibrium species and solid phase distributions are calculated. The “slide” approach was adopted when initial efforts to perform spot SpecE8 simulations at fixed Eh values for each water led to frequent convergence problems. Initiation of the slides at the high end of the Eh range also helped avoid nonconvergence. Consistency between equivalent SpecE8 and React results was checked for 39 calculations; in only 2 cases were the differences in element concentrations greater than 2 percent. In those 2 cases, in which the SpecE8-calculated Se concentration was 5 and 10 percent lower than the React result, the Se differences were caused by the lack of constant Ca in solution in the React run (see Item 6 in this list). The “slides” from a maximum to a minimum Eh were adopted for convenience and were not intended to simulate the actual progression of conditions during degradation of cement-based materials, which will follow a pH–Eh evolution such as detailed in Section B2. Charge balance was not attempted in the runs, after convergence issues were encountered. Because charge would not have been balanced using ions important to radionuclide speciation, the main effect of this neglect could be on calculation of activity coefficients (which directly affect the calculation of concentrations from thermodynamic equations). The largest imbalances were seen in some of the high-ionic strength Type 1 and 2 waters; spot recalculations indicated that any such effects on radionuclide speciation were negligible (i.e., much less than an order of magnitude). The spot checks were performed by directly adjusting ion concentrations (e.g., Na, K, or Cl) in initial water compositions so as to obtain charge balance. Across the Eh range in a selection of Groups 1 and 2 waters, these adjustments resulted in changes to Se, Tc, Np, U, and Pu concentrations of less than 17 percent. (Se and Tc were checked only over ranges for which they were limited by solubility.)
- (3) The results of the initial run were inspected to identify the solid phase or phases that were saturated and controlled dissolved element concentration over the course of the run.
- (4) In the cases of Tc, U, Np, and Pu, some of the identified solubility-limiting solid(s) were judged to be unlikely to control dissolved concentrations in the systems of interest and were suppressed in subsequent runs (i.e., prevented from precipitating and affecting dissolved element concentration by an input setting in React). This judgment was based on considering (i) whether or not the phase had been identified in relevant experimental studies and (ii) how the predicted element concentrations compared, in a gross sense, with laboratory measured solubility limits. No attempt was made to evaluate the reasons for inappropriate solid phase prediction, but it is suspected that kinetic effects on phase precipitation are one important factor.
- (5) The React slides were run again, with appropriate mineral suppressions, and with the dissolved element either (i) constrained by a defined free mass of the least undersaturated, unsuppressed solid phase from the initial runs or (ii) set to an initial concentration known from iterative analyses to exceed the solubility limit. The latter approach was adopted in cases for which the initially present solid significantly altered

---

<sup>1</sup> Geochemist's Workbench outputs concentrations in molal (m or mole/kg H<sub>2</sub>O). For uniformity in this report, molal values are reported as molar (M or mole/L solution); this is an acceptable approximation because calculated solution densities were always within 2 percent of 1 kg/L.

the initial Eh, which was intended to be constrained by atmospheric oxygen. In this way, the intended water chemistry, including Eh, could be imposed on the system. In the real system, the radioelement will approach the solubility limit from undersaturation, such that solid phase precipitation will be a function of, rather than drive, water chemical characteristics.

- (6) Thermodynamic modeling is an iterative process. Textual and graphical outputs of the React runs were inspected for unexpected results and new runs were conducted as necessary. For example, in some U models with initial concentration set to 0.5 M, the first steps in the React output indicated simultaneous saturation of multiple U minerals. In that case, the input was altered to have dissolved U concentration constrained by the expected solubility-limiting solid for that water chemistry. Another type of spurious result was encountered with multication, soluble solid phases such as calcium selenite (Section B3.1.3). In some cases when Se was set to be constrained by a free mass of this solid phase, the aqueous Ca concentration was drastically altered by dissolution of the highly soluble solid to reach the proper solubility product. Again, this effect is not consistent with the process we were attempting to simulate—approach to saturation of a mineral given an imposed aqueous chemical composition. If Ca were allowed to fluctuate, the results would not reflect a Se solubility limit for the given Ca concentration. This problem was largely remedied by fixing the activity of the dominant  $\text{Ca}^{2+}$  species in the React run.
- (7) React results are typically presented as continuous curves of dissolved element concentration versus Eh, each curve representing a sample water. Some waters were simulated at only one Eh using the SpecE8 module and, thus, are plotted as single points.
- (8) For purposes of plotting and discussion, a concentration value of 0.5 M was used when either there was no solubility control or the calculated value was greater than 0.5 M.

The model results were evaluated in light of published experimental and modeling studies and conclusions were drawn concerning appropriate ranges of solubility limits for given chemical conditions. An explicit approach to evaluating uncertainty was not attempted in this report, but overall model results are typically discussed at the order-of-magnitude scale. A precisely quantified uncertainty estimate would be difficult to support, because not all sources of uncertainty (e.g., choice of solid, neglect of coprecipitation, comparison to experimental results) lend themselves to quantification. Uncertainties in thermodynamic data are typically on the scale of one to two orders of magnitude (Guillaumont, et al., 2003). In predicting solubility limits for Savannah River Site grouted tanks, Denham (2007) estimated a maximum uncertainty of two orders of magnitude for all elements of interest due to thermodynamic data uncertainties. As mentioned in Section B1.3, in assigning solubility limits for performance assessment, uncertainty that is not quantifiable may be addressed by making conservative choices in factors such as solubility-limiting solid phase.

As discussed in this report, different modeling results can arise when different thermodynamic databases are used, adding another layer of uncertainty to solubility predictions. The thermo.com.v8.r6+.dat database, from Lawrence Livermore National Laboratory (based on Delany and Lundeen, 1990), is of high quality but has not been recently updated. The Nuclear Energy Agency has produced a frequently-updated database applicable to nuclear waste disposal systems (e.g., Guillaumont, et al., 2003), but a version compatible with Geochemist's Workbench has not been formally released. A version of the Nuclear Energy Agency database

compatible with Geochemist's Workbench was obtained from the Japan Atomic Energy Agency (2008). For Se, Tc, U, Np, and Pu, we have performed a comparative analysis of solubility model results using this database (renamed NEA.dat).

## **B1.5 Selection of Elements for Review**

The list of radioelements included in this review was adopted from the previous review of natural system sorption coefficient data for Savannah River Site and Idaho National Laboratory, and the basis for inclusion may be found there (Prikryl and Pickett, 2007). The main criterion was potential risk significance in groundwater pathway dose assessments. In the present review, radioelements will be subject to two levels of analysis, depending on consideration of both risk significance and the potential for solubility limits to be exceeded. Five radioelements—Se, Tc, U, Np, and Pu—were selected for more detailed solubility evaluation. All are potentially important in dose assessment models for Savannah River Site and Idaho National Laboratory. In addition, solubility limits for these elements are redox sensitive (i.e., aqueous speciation and solid phase stabilities may differ between oxidizing and reducing environments). Because oxidation-reduction potential is an important variable in understanding the evolution of cement-based waste environments at Savannah River Site and Idaho National Laboratory, these elements warrant closer solubility evaluation. Ten of the elements—carbon, nickel, strontium, niobium, tin, iodine, cesium, lead, americium, and curium—will be briefly discussed in terms of their solubility characteristics. These elements, some of which are redox sensitive, were assigned to this group on the following bases:

- Carbon, strontium, cesium, and lead: Radioisotopes of these elements are expected to be potentially significant to dose, but will exist at very low mass levels in the waste form. Consequently, it is unlikely that solubility limits would be imposed on them in performance assessments or that the radionuclides would reach solubility limits. If a performance assessment were to impose a concentration limit on the combined radioactive and nonradioactive element mass, solubility limits could be more significant for this group. Among this list, strontium most prominently contributes to groundwater dose in Ronald W. Reagan National Defense Authorization Act for Fiscal Year 2005-relevant assessments (e.g., sand pad release at Idaho National Laboratory; DOE-ID, 2006).
- Iodine: Radioactive I-129 is frequently identified as important to dose in Ronald W. Reagan National Defense Authorization Act for Fiscal Year 2005-relevant groundwater dose assessments because of its high solubility limit and high mobility in groundwater as an anionic species. Because iodine is unlikely to reach saturation in solution in cement-based Savannah River Site and Idaho National Laboratory facilities, solubility control of iodine is not invoked in these assessments. Therefore, a detailed solubility evaluation is not necessary.
- Nickel, niobium, tin, americium, and curium: None of these elements are expected to be major dose contributors in Ronald W. Reagan National Defense Authorization Act for Fiscal Year 2005-relevant groundwater pathway assessments, but they are addressed briefly in this report because they may be significant in performance assessments.

## **B1.6 Approach to the Review**

After first establishing the chemical characteristics of the waste form environment, including redox conditions (Section B2), this report will consider the five elements selected for detailed review (Section B3). Published experimental and modeling data will be discussed and new solubility limit models will be developed. Conclusions will be drawn regarding the likely range of solubility limits for the element under the defined range of conditions, considering the quality and applicability of the data and models. Next, the 10 elements chosen for less detailed evaluation will be discussed at a lower level of detail and without consideration of new models (Section B4). The summary and conclusions discussion (Section B5) will include consideration of the important data gaps and how they may be addressed in future studies. Unless specified otherwise, discussions of data and models apply at 25 °C [77 °F].

## **B2 CHEMICAL CONDITIONS RELEVANT FOR RELEASE FROM CEMENT-BASED WASTE FORMS**

The main body of this report discusses the degradation evolution of cement-based materials, including evaluation of the state of knowledge of chemical changes over time. The conclusions of those discussions will be used here to guide evaluation of the possible range in aqueous chemical conditions in contact with radionuclides in Savannah River Site and Idaho National Laboratory cement-based disposal environments.

### **B2.1 Range of Expected Conditions In a Cementitious Environment**

This scenario assumes that cement-based materials are eventually exposed to fluids with some communication with the external environment (see Section 8.5.3 of the main report). Exposure of cements to carbonate-containing water leads to alteration of cement assemblages and eventual loss of the cement pH buffering capacity. The key control on solution pH is evolution of cement phases in response to leaching. At the earliest stages, cement pore water will have pH between 12.5 and 14 (the elevation above 12.5 owing to the presence of soluble sodium and potassium). This stage is likely of short duration compared to succeeding stages because the alkalis will be leached by percolating water. Once alkalis are removed, relatively fresh cement will maintain a pore water pH of about 12.5 as long as portlandite is not exhausted. When portlandite dissolution is complete, leaching of amorphous to poorly crystalline calcium silicate hydrate (C-S-H) continues and the pH begins to decline to about 10.5. Up to this point, aqueous carbonate (of particular interest because it readily forms anionic and neutral actinide complexes that promote actinide mobility) is likely to be relatively low as it is continually consumed by reaction with the alkaline constituents of the cement-based material to form various types of carbonate phases. Once C-S-H is exhausted, those carbonate phases, such as calcite, likely have become abundant and would control pH to around a value of 8. Aqueous carbonate concentration may then rise under the influence of atmospheric CO<sub>2</sub> gas.

At this point in the degradation evolution, it is assumed that, because of the large masses of degraded cement that would have formed in tanks and monoliths at Savannah River Site and Idaho National Laboratory and because calcite is relatively insoluble compared to the cement phases, a pH of around 8 will be maintained in the pore water during the period of interest. This assumption is easily supported at Idaho National Laboratory, where groundwaters have pH values similar to 8 (see summary in Prikryl and Pickett, 2007). Groundwaters at Savannah River Site, however, are considerably more acidic, with typical ambient pH of less than 6 (Prikryl and Pickett, 2007) and low carbonate contents that would promote calcite dissolution. Note,

however, that the waste environment at Savannah River Site is in the unsaturated zone, or in the saturated zone very near the water table and ground surface, such that the degraded material will be persistently exposed to carbon dioxide in air. Therefore, Savannah River Site *saturated* groundwater chemistry—which may not have the higher carbonate and oxygen contents expected in the unsaturated zone—may not provide an appropriate analog for waters contacting degraded cement in Savannah River Site facilities.

The oxidation-reduction potential of the pore water profoundly affects solubilities for the five elements selected for detailed review. Cements alone do not provide for a reducing chemical environment. DOE is expected to add blast furnace slag to its grout mixtures to maintain a low Eh in the pore waters of the cement-based material. Thus, through at least part of their history, cement-based materials in Savannah River Site and Idaho National Laboratory disposal facilities are expected to be exposed to low-Eh conditions. Data are lacking, however, for predicting the long-term durability of those conditions. Radiolysis, for example, may generate oxidizing species, and infiltration of environmental air and water will elevate Eh. We must, therefore, consider scenarios in which oxidizing conditions are present in the waste as a result of introducing atmospheric oxygen.

## **B2.2 Effects of Proposed DOE Formulations**

As discussed elsewhere in this report, the expected DOE grout formulations for tank closure and saltstone disposal will include ordinary Portland cement, fly ash, and blast furnace slag. In the long term, the latter two additives have implications for the Eh and pH evolution of the grout. This is especially true for saltstone, which has a fly ash: blast furnace slag: ordinary Portland cement mass ratio of 8:8:1 (NRC, 2005); in contrast, the stabilizing grout for tank closure at Idaho National Laboratory has a ratio of 0.5:1.5:1 (Table 8-1 of the main report). As discussed in the previous section, slag can contribute to maintaining a reducing chemical environment. The main source of the reducing potential of slag is sulfide sulfur, which originates in the coke and ore used in iron processing and which is concentrated in the blast furnace slag. Thiosulfate, which may form from reaction between the slag sulfide and sulfur(VI) in Portland cement, may also contribute to the reduction capacity of the grout. Many uncertainties remain, however, regarding the long-term performance of slag-derived sulfur in poisoning Eh at low levels. In addition, it may not be possible to predict the initial sulfur content of the grout formulations (Section 8.2.2 of the main report).

Fly ash may contribute to reduction by the action of iron oxides and elemental carbon. Again, exact predictions of these effects are not possible, because of a lack of long-term experimental data and potential variability in fly ash contents of these substances.

With regard to pH evolution, both fly ash and slag will most significantly affect grout by likely shortening the period of high pH buffering. This effect comes about through both dilution of portlandite and reaction between portlandite and the other components (Section 8.2.1).

Section 8.2.8 of the main report discusses potential effects on radionuclide solubility of chemical admixtures (e.g., water reducers and superplasticizers). As explained in that section, Greenfield, et al. (1998) showed that the solubility of Pu, U<sup>IV</sup>, and Am is increased one to two orders of magnitude in cement-equilibrated water containing admixtures compared to water without additives. The result was ascribed to the formation of aqueous complexes of the radionuclides with the admixture and hydroxyl ions. Glaus and van Loon (2004), however, suggested that admixture ions may be strongly adsorbed to cement paste solids, reducing their effectiveness as complexants. In addition, it is uncertain how long admixture complexants may

persist in evolving cementitious system pore waters. There is insufficient information to assess the long-term effects of admixtures on solubility limits.

### **B2.3 Effects of Residual Waste in Tank Heel in Contact With Grout**

Any solubility effects of the residual material containing the radionuclides will depend on its abundance and solid phase chemistry. Very little information is available on the solid phases present in cleaned tank heels at Savannah River Site and Idaho National Laboratory. For Savannah River Site Tank 19, for example, the remaining solids after heel removal are described simply as 99.9 percent “inert chemicals” (DOE, 2005, p. 47) with radionuclides comprising the remaining volume. A similar description applies to Tank 18 (DOE, 2005, p. 60). In the case of Tanks 18 and 19, those solids are likely to be dominated by zeolite, but insoluble metal salts and oxides (chiefly of iron and aluminum) will also be present (Thomas, 2005a,b). Soluble materials appear to have been removed during the tank cleaning process. A survey of relevant Idaho National Laboratory documents did not reveal data on the specific solid phases present on the tank heel after cleaning (DOE-ID, 2006, and references therein). The Idaho National Laboratory tank cleaning process, however, left behind very low masses of residual material. Savannah River Site is also studying more effective cleaning methods that may lead to very low residual masses.

It appears unlikely that, aside from speculative radiolytic effects, the residual materials at the tank base will significantly affect the chemical environment for establishing solubility limits. This conclusion is based on (i) the expected low masses of the residue and (ii) the removal of soluble materials from the residue during cleaning, leaving insoluble salts, oxides, and silicates that will have a lesser impact on solution chemistry than the abundant overlying cement-based materials and their degradation products.

### **B2.4 Summary of Expected Conditions**

The chemical environment for release is controlled primarily by the evolution of the cement-based waste form or entombing grout. Solubility limits should be evaluated over the entire range considered feasible over 10,000 years. The solution pH is expected to range chiefly from approximately 12.5 (early) to 8 (late). To the extent that data are available, this report will also discuss data from the 12.5 to 14 pH range, which may characterize the earliest stages of cement–water interaction. The poisoning capacity afforded by blast furnace slag–cement blends (Section 8.2.2 of the main report) suggests that reducing conditions may dominate early on, with Eh likely poised to the range –200 to –350 mV. (Throughout this appendix, Eh refers to the redox potential relative to the standard hydrogen electrode.) In isolation from air and in the absence of blast furnace slag, ordinary Portland cement would control Eh to around +80 mV (Angus and Glasser, 1985). A later oxidizing environment while portlandite is still present (pH ~12.5), with Eh of around +100 to +200 mV, cannot be ruled out if oxidizing unsaturated zone waters reach the cement. Under degraded conditions, atmospheric conditions may dominate, such that Eh could exceed +750 mV at pH 8 (using the expression of Langmuir, 1997, p. 409). Both reducing and oxidizing conditions, therefore, will be considered with respect to solubility limits. The Eh–pH field that encompasses these proposed conditions is illustrated by the shaded area in Figure B2–1. The timing of this chemical sequence depends on many factors, such as the availability of fast pathways that could cause more rapid degradation and oxidation.

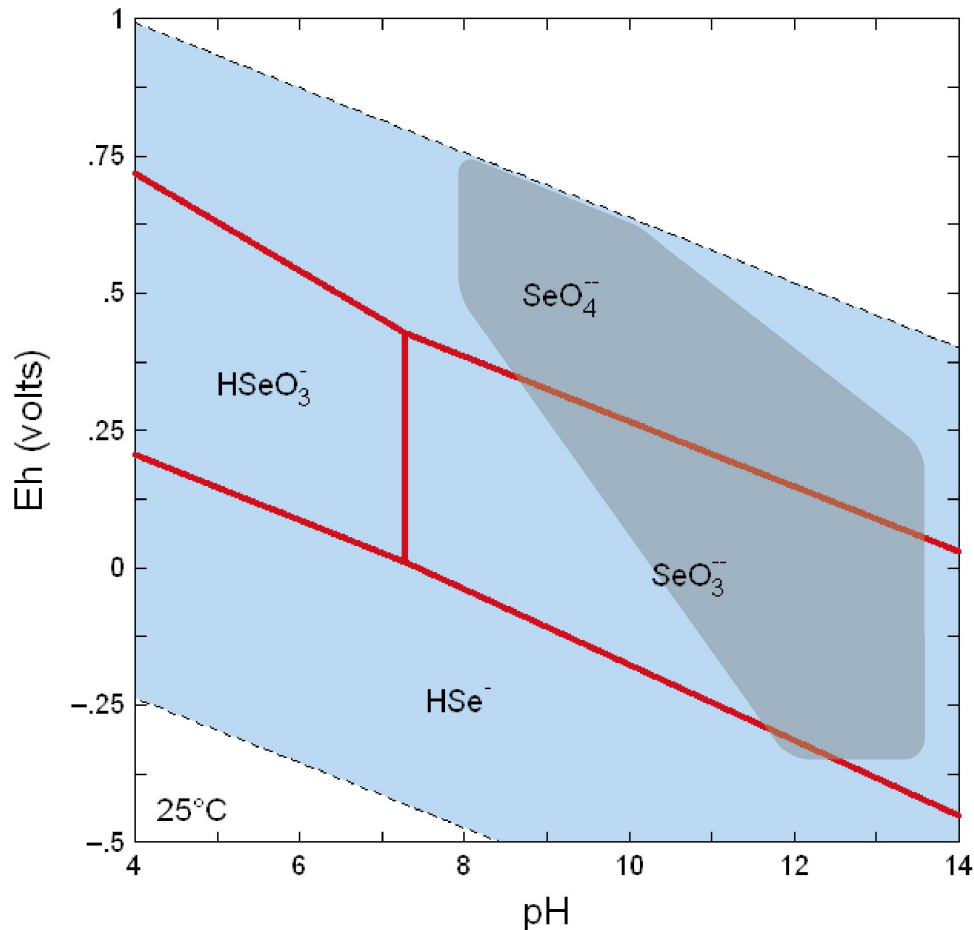


**Figure B2-1. Eh-pH Stability Field for Water With a Shaded Area Representing the Approximate Range of Expected Conditions as Cement-Based Materials Degrade (Section B2.4). Aqueous Species Fields for Se Shown as an Example. Figure Produced Using Geochemist's Workbench Professional Version 6.0 With the thermo.comv8r6+.dat Database.**

## B2.5 Aqueous Conditions for Solubility Models

Water compositions for solubility calculations were selected to span a range of conditions over the lifetime of a cement-based disposal environment (Table B2-1). For most compositions, a range of Eh values was simulated. While not all these solutions can be expected to directly reflect conditions in Savannah River Site or Idaho National Laboratory cement-based waste environments, they represent an inclusively broad range of chemistries. Solutions in contact with relatively fresh ordinary Portland cement (Type 1 waters in Table B2-1) are represented by (i) 1A, a model cement pore solution that has not interacted with groundwater (Berner, 2002, Table 2); (ii) 1B, a calculated solution composition resulting from groundwater reaction with a model cement solid assemblage (Glasser, et al., 1999, Table 6.39); and (iii) 1C, a measured ordinary Portland cement pore water chemistry (Angus and Glasser, 1985, Table III). Because Angus and Glasser (1985) did not report carbonate species, we have performed calculations an inclusively broad range of chemistries. Solutions in contact with relatively fresh ordinary Portland cement (Type 1 waters in Table B2-1) are represented by (i) 1A, a model cement pore

Table B2-1. Water Compositions Selected for Solubility Limit Calculations								
	Type 1—Fresh Ordinary Portland Cement			Type 2—Fresh Blend of Ordinary Portland Cement and Blast Furnace Slag			Type 3—Portlandite and Early C-S-H Evolution	
	Water 1A	Water 1B	Water 1C	Water 2A	Water 2B	Water 2C	Water 3A	Water 3B
pH	13.44	13.4	13.4	12.2	11.88	12.28	12.55	12.5
Na <sup>+</sup> (mol/L)	0.101	0.363	0.058	0.363	4.4e-04		0.169	
K <sup>+</sup> (mol/L)	0.303	0.0039	0.222	0.0039			0.0057	
Mg <sup>++</sup> (mol/L)	1.3e-08	7.43e-11		9e-10		1.42e-08	1e-07	
Ca <sup>++</sup> (mol/L)	8.43e-04	5.62e-04	2.7e-03	8.53e-04	2.2e-03	1.28e-02	0.0201	0.02
Al <sup>+++</sup> (mol/L)	1e-05	1.54e-03		1.74e-04	1.7e-04	1.96e-05	5e-06	
Cl <sup>-</sup> (mol/L)		2.74e-02		2.47e-04			0.16	
F <sup>-</sup> (mol/L)	7.6e-04						1e-04	
CO <sub>3</sub> <sup>--</sup> (mol/L)	2.04e-04	4.42e-02	Zero and 3e-06	3.76e-05	1.1e-04		1e-05	
SO <sub>4</sub> <sup>--</sup> (mol/L)	7.5e-04	2.35e-04		5.56e-04		4.89e-06	1e-04	0.001 and 0.02
H <sub>2</sub> SiO <sub>4</sub> <sup>---</sup> (mol/L)	5e-05	3.23e-04		2.73e-04	1.3e-04	8.4e-06	1.6e-05	1e-04
Eh range	+80 mV to -350 mV	+80 mV to -350 mV	+80 mV to -350 mV	+200 mV to -350 mV	+200 mV to -350 mV	+200 mV to -350 mV	+200 mV to -350 mV	+200 mV to -350 mV
	Berner (2002, Table 2)*	Glasser, et al. (1999, Table 6.39)‡	Angus and Glasser (1985, Table III)** and Allard and Torstenfelt (1985)††	Glasser, et al. (1999, Table 6.41)‡	Berry, et al. (1989, Table 2)¶	Glasser, et al. (1999, Table 6.40)‡	Wieland and Van Loon (2003), Table 3)†	Berner (1992, Figures 1-3)§ and Atkins, et al. (1991)

Table B2-1. Water Compositions Selected for Solubility Limit Calculations (continued)								
	Type 4—C-S-H Evolution and Carbonation						Type 5—Groundwaters	
	Water 3C	Water 4A	Water 4B	Water 4C	Water 4D	Water 4E	Water 5A	Water 5B
pH	12.49	10.5	11.00	10.02	9.16	8.27	5.8	8.1
Na <sup>+</sup> (mol/L)	8.8e-05						8.6e-05	3.57e-04
K <sup>+</sup> (mol/L)	2.2e-05						3.2e-05	4.09e-05
Mg <sup>++</sup> (mol/L)							2.3e-05	5.76e-04
Ca <sup>++</sup> (mol/L)	2.2e-02	0.002	0.001	0.00197	9.3e-04	4.97e-04	1.7e-04	1.10e-03
Al <sup>+++</sup> (mol/L)								
Cl <sup>-</sup> (mol/L)							1.3e-04	2.09e-04
F <sup>-</sup> (mol/L)	7.5e-05						32.e-06	
CO <sub>3</sub> <sup>--</sup> (mol/L)	6.5e-05	Control by calcite, given Ca <sup>++</sup>	Control by calcite	Control by calcite	Control by calcite	9.86e-04	2.6e-04	3.39e-03
SO <sub>4</sub> <sup>--</sup> (mol/L)	5.0e-04	0.001					1.1e-05	2.29e-04
H <sub>2</sub> SiO <sub>4</sub> <sup>--</sup> (mol/L)	1.0e-05	0.001		0.00387	0.00260			3.00e-04
Eh range	+200 mV to -350 mV	From a value constrained by f(O <sub>2</sub> ) equal to 0.2 to 0 mV [Eh at a fixed f(O <sub>2</sub> ) varies with pH]	From a value constrained by f(O <sub>2</sub> ) equal to 0.2 to -100 mV [Eh at a fixed f(O <sub>2</sub> ) varies with pH]	From a value constrained by f(O <sub>2</sub> ) equal to 0.2 to 0 mV [Eh at a fixed f(O <sub>2</sub> ) varies with pH]	From a value constrained by f(O <sub>2</sub> ) equal to 0.2 to +100 mV [Eh at a fixed f(O <sub>2</sub> ) varies with pH]	Constrained by f(O <sub>2</sub> ) = 0.2	Dissolved oxygen = 9 mg/L	+750 mV
	Berner (1999, Table 8)#	Berner (1992, Figures 1-3)§ and Atkins, et al. (1991)	Bradbury and Sarott (1995)##	Greenberg and Chang (1965)§§	Greenberg and Chang (1965)§§	Dissolution of calcite in equilibrium with air, using EQ3/6 Version 7.2b	Prikryl and Pickett (2007, Table 2-1)	Del Debbio and Thomas (1989)¶¶

**Table B2-1. Water Compositions Selected for Solubility Limit Calculations (continued)**

- \*Berner, U. "Project Opalinus Clay: Radionuclide Concentration Limits in the Cementitious Near-Field of an ILW Repository." PSI Bericht 02-26, Nagra NTB 02-22. Villigen, Switzerland: Paul Scherrer Institute. Table 2. 2002.
- †Wieland, E. and L.R. Van Loon. "Cementitious Near-Field Sorption Data Base for Performance Assessment of an ILW Repository in Opalinus Clay." PSI Bericht 03-06. Villigen, Switzerland: Paul Scherrer Institut. Table 3. 2003.
- ‡Glasser, F.P., M. Tyrer, K. Quillin, D. Ross, J. Pedersen, K. Goldthorpe, D.G. Bennett, and M. Atkins. "The Chemistry of Blended Cements and Backfills Intended for Use in Radioactive Waste Disposal." R&D Technical Report P98. Bristol, United Kingdom: U.K. Environment Agency. (Water 3, Table 6.39; Water 4, Table 6.41; Water 8, Table 6.40). 1999.
- §Berner, U.R. "Evolution of Pore Water Chemistry During Degradation of Cement in a Radioactive Waste Repository Environment." *Waste Management*. Vol. 12. pp. 201–219. Figures 1–3. 1992.
- ||Atkins, M., F.P. Glasser, and L.P. Moroni. "The Long-Term Properties of Cement and Concretes." Materials Research Society Symposium Proceedings 212. T. Abrajano, Jr. and L.H. Johnson, eds. Pittsburgh, Pennsylvania: Materials Research Society. pp. 373–386. 1991.
- ¶Berry, J.A., J. Hoble, S.A. Lane, A.K. Littleboy, M.J. Nash, P. Oliver, J.L. Smith-Briggs, and S.J. Williams. "Solubility and Sorption of Protactinium in the Near-Field and Far-Field Environments of a Radioactive Waste Repository." *Analyst*. Vol. 114. pp. 339–347. Table 2. 1989.
- #Berner, U. "Concentration Limits in the Cement Based Swiss Repository for Long-Lived, Intermediate-Level Radioactive Wastes (LMA)." PSI Bericht 99-10. Villigen, Switzerland: Paul Scherrer Institut. Table 8. 1999.
- \*\*Angus, M.J. and F.P. Glasser. "The Chemical Environment in Cement Matrices." Materials Research Society Symposium Proceedings 50. L.O. Werme, ed. Pittsburgh, Pennsylvania: Materials Research Society. pp. 547–556, Table 3. 1985.
- ††Allard, B. and B. Torstenfelt. "Actinide Solubilities and Speciation in a Repository Environment." Technical Report NTB 85-18. Baden, Switzerland: NAGRA. 1985.
- ‡‡Bradbury, M.H. and F.-A. Sarott. "Sorption Databases for the Cementitious Near-Field of a L/ILW Repository for Performance Assessment." PSI Bericht 95-06. Villigen, Switzerland: Paul Scherrer Institut. 1995.
- §§Greenberg, S.A. and T.N. Chang. "Investigation of the Colloidal Hydrated Calcium Silicates II. Solubility Relationships in the Calcium Oxide–Silica–Water System at 25 °C." *Journal of Physical Chemistry*. Vol. 69. pp. 182–188. 1965.
- |||Prikryl, J.D. and D.A. Pickett. "Recommended Site-Specific Sorption Coefficients for Reviewing Non-High-Level Waste Determinations at the Savannah River Site and Idaho National Laboratory." San Antonio, Texas: CNWRA. Table 2-1. 2007.
- ¶¶Del Debbio, J.A. and T.R. Thomas. "Transport Properties of Radionuclides and Hazardous Chemical Species in Soils at the Idaho Chemical Processing Plant." WINCO-1068. Idaho Falls, Idaho: Westinghouse Idaho Nuclear Company, Inc. 1989.

solution that has not interacted with groundwater (Berner, 2002, Table 2); (ii) 1B, a calculated solution composition resulting from groundwater reaction with a model cement solid assemblage (Glasser, et al., 1999, Table 6.39); and (iii) 1C, a measured ordinary Portland cement pore water chemistry (Angus and Glasser, 1985, Table III). Because Angus and Glasser (1985) did both with no dissolved carbon and with a  $\text{CO}_3^{2-}$  concentration based on the upper limit used by Allard and Torstenfelt (1985), a substantial range in dissolved carbonate is therefore reflected in these waters. For each of these waters the model Eh range of  $-350$  to  $+80$  mV was taken from Angus and Glasser (1985).

Solutions in contact with a relatively fresh blend of ordinary Portland cement and blast furnace slag (Type 2 waters) are represented by (i) 2A, a calculated pore water for a 75 percent blast furnace slag blend that has interacted with a saline water (Glasser, et al., 1999, Table 6-41); (ii) 2B, a measured water equilibrated with a blend of blast furnace slag, ordinary Portland cement, and limestone aggregate at a ratio of 7:2:19 (Berry, et al., 1989, Table 2); and (iii) 2C, a calculated pore water resulting from equilibration of pure water with a 75 percent blast furnace slag blend (Glasser, et al., 1999, Table 6.40). These three solutions have lower pH (11.9 to 12.3) than the “initial stage” solutions discussed in the previous paragraph, and a higher upper limit for Eh of  $+200$  mV was assumed.

The next category of pore water simulations (Type 3 waters) represents the stage of cement degradation when portlandite is the chief cement phase, pH is about 12.5, and C-S-H gels have begun to form, corresponding, for example, to Region II of Bradbury and Sarott (1995). These waters are represented by (i) 3A, a “Stage II” model water resulting from groundwater interaction with cement (Wieland and Van Loon, 2003, Table 3); (ii) 3B, a simplified calcium-silica water reflecting the earliest, high-Ca/Si stages of C-S-H evolution (Berner, 1992, Figures 1–3) with a sulfur content based on Atkins, et al. (1991); and (iii) 3C, a model portlandite-saturated solution (Berner, 1999, Table 8). Eh was varied between  $-350$  and  $+200$  mV to simulate a range of redox conditions.

A set of five waters (Type 4) represents progressive carbonation and C-S-H degradation (and decreasing Ca/Si) as the buffering capacity of cement constituents declines. Specific water chemistries used in models are (i) 4A, a simplified calcium–silica water reflecting the latest, low-Ca/Si stages of C-S-H evolution (Berner, 1992, Figures 1–3), with a pH of 10.5, a sulfur content based on Atkins, et al. (1991), and dissolved carbonate controlled by calcite solubility; (ii) 4B, a simplified pH 11, calcite-saturated water based on the Bradbury and Sarott (1995) description of Region III; (iii) 4C, a simplified pH 10, calcite-saturated predominantly Ca-Si water based on measurements by Greenberg and Chang (1965) used in the models of Berner (1992); (iv) 4D, a simplified pH 9, Ca-Si, calcite-saturated water based on experimental measurements by Greenberg and Chang (1965) and used in the models of Berner (1992); and (v) 4E, a model water representing calcite dissolution in pure water in equilibrium with the atmosphere. Eh ranges selected for these waters reflect variation from mildly reducing to equilibrium with atmospheric oxygen.

Finally, as end members, solubility limits were calculated for groundwaters from the Idaho National Laboratory and Savannah River Sites with the implicit assumption that the grout waste form has become essentially unreactive with percolating waters (Type 5). These conditions would be realistic only on very long time scales after the water-accessible grout has fully degraded and a steady-state chemical system established. Constituent values for water 5A represent midpoints of the range presented for the Upper Three Runs aquifer upper zone at Savannah River Site in Prikryl and Pickett (2007, Table 2-1). As mentioned in Section B2.1, there is no particular reason to expect that this specific water will be present in the Savannah

River Site unsaturated zone, but it is an oxidizing water and may reflect geochemical influences of the Savannah River Site subsurface. Composition 5B is a perched water sampled from the Idaho National Laboratory unsaturated zone (Del Debbio and Thomas, 1989).

This chemical characterization includes only elements for which reasonable estimates or measurements exist for evolving cement-based systems. There is insufficient information to indicate an abundance in pore waters of other, potentially important aqueous complexants such as phosphate. Exclusion of elements that may form insoluble solid phases with the radionuclides of interest (e.g., arsenic, which can form uranyl minerals) is conservative.

## B3 DETAILED SOLUBILITY REVIEWS

This section details solubility limits for Se, Tc, U, Np, and Pu under the established range of conditions. Both experimental and modeling results will be addressed, and conclusions will be drawn concerning how consideration of solubility limits affects evaluation of radionuclide release models. New solubility models will be presented using the representative waters of Table B2–1 over a range of Eh values. Kaplan (2006) provides useful context for these discussions through a recent compilation of recommended geochemical parameters for use in modeling radionuclide release and transport at Savannah River Site, including the Saltstone Disposal Facility. Kaplan (2006) did not explicitly address grouted tanks, but the solubility data discussed may also be applicable to the cementitious tank environment. Compared to the present report, the Kaplan (2006) analysis established “apparent solubility concentration limits” that did not necessarily reflect true solubility, but could also incorporate the effects of other processes such as coprecipitation or sorption. While that is a legitimate approach to developing model parameters, the present report is concerned with pure-phase solubility as a control on limiting concentration.

### B3.1 Selenium

The fission product Se-79 is a potentially mobile constituent of cement-based wastes at Savannah River Site and Idaho National Laboratory. Figure B3–1 shows an Eh–pH plot of dissolved Se species. The shaded field on the plot is an approximate representation of the range of expected conditions in the presence of a degrading slag–cement blend. As portlandite and C-S-H degrade and pH decreases, the reducing capacity of the material is also assumed to decrease as contact with oxidizing waters increases and sulfide is oxidized. Therefore, the slag–cement field tends to higher Eh with lower pH as degradation proceeds.

Figure B3–1 shows that, under strongly oxidizing aqueous conditions at pH >8, Se is present in the hexavalent state as the selenate ( $\text{SeO}_4^{2-}$ ) anion (Berner, 1999; Séby, et al., 2001; Berner, 2002; Krupka, et al., 2004). Under moderately oxidizing and reducing conditions, tetravalent Se as the selenite ( $\text{SeO}_3^{2-}$ ) anion predominates. At a given pH, progressively more strongly reducing waters favor the –2 valence state  $\text{HSe}^-$  anion, but Figure B3–1 suggests that these conditions are unlikely in the environment being considered.

At the lowest Eh values considered, it is possible that crystalline elemental  $\text{Se}^0$  solubility may limit dissolved Se to  $10^{-4}$  M or less (Séby, et al., 2001; Kitamura, et al., 2004; Iida, et al., 2001). The  $\text{Se}^0$  stability field, however, is at the margin of the assumed Eh–pH region. Throughout most of the aqueous selenite and selenate stability field (Figure B3–1), Se solubility-limiting phases are more likely to be metal selenates or selenites.

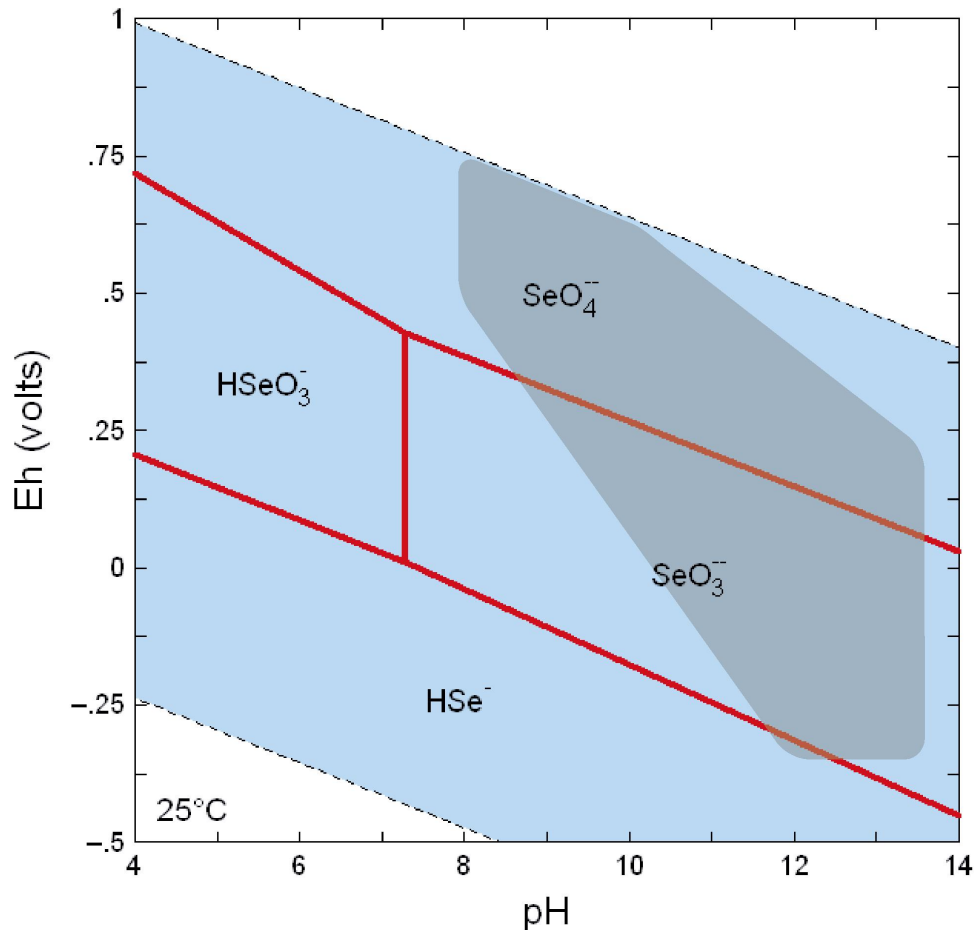


**Figure B3–1. Eh–pH Stability Fields for Aqueous Se ( $1 \times 10^{-8}$  M) in Pure Water at 25 °C [77 °F] (Solids Suppressed) Calculated Using Geochemist’s Workbench Version 6.0 With the thermo.com.v8.r6+.dat Database. The Shaded Area Represents the Approximate Range of Expected Conditions as Cement-Based Materials Degrade (Section B2.4). Addition of Carbon or Sulfur Does Not Alter the Aqueous Species Fields. The Blue Field Defines Water Stability.**

Kaplan (2006) assumed no solubility control of Se under both oxidizing and reducing cementitious conditions.

### B3.1.1 Experimental Data

Few Se phase solubility studies have focused on cementitious conditions. Bayliss, et al. (1992) measured  $\text{FeSe}_2$  solubility in cement-equilibrated water at pH 12.2. For Eh of  $-405$  mV, the aqueous Se concentration, predicted to be  $\text{HSe}^-$ , was  $9 \times 10^{-8}$  to  $5.0 \times 10^{-7}$  M. There were no measurements at higher Eh, which may be more applicable to the assumed conditions (Figure B3–1). Kitamura, et al. (2004) measured crystalline  $\text{Se}^0$  solubilities of up to  $10^{-4}$  M at pH from 11 to 13. Although the expression they derived for  $\text{Se}^0$  solubility predicts a dissolved selenite anion concentration of only  $3 \times 10^{-9}$  M at pH 12 and Eh  $-350$  mV, the predicted solubility quickly increases as pH or Eh increases. Iida, et al. (2001) also measured  $\text{Se}^0$

solubility at high pH and low Eh, but the measurements at pH above 12 were all at Eh below -385 mV. Extrapolated to higher Eh, the dissolved concentrations of their model  $\text{SeO}_4^{2-}$  ion are very low, but are likely to be less than the concentration of selenite in solution. Together these studies show that elemental  $\text{Se}^0$  has low solubility at the boundary of the assumed Eh-pH region, but will not control dissolved Se to low values through most of that region.

Séby, et al. (2001) discuss a broad range of experimental data to elucidate thermodynamic properties of Se substances. These data were not aimed specifically at understanding solubility limits in a cementitious environment. No low-solubility selenate likely to form in a cementitious environment is evident from the data in Séby, et al. (2001). Solubility control of dissolved Se, therefore, is unlikely in the selenate stability field. Calcium selenite ( $\text{CaSeO}_3$ ,  $\text{CaSeO}_3 \cdot \text{H}_2\text{O}$ , or  $\text{CaSeO}_3 \cdot 2\text{H}_2\text{O}$ ), however, may be an important phase in the presence of cement, and the data on this phase from Séby, et al. (2001) will be used in the following section on Se solubility models.

### **B3.1.2 Literature Models**

Chemical models consistently yield high Se solubility limits under oxidizing conditions (e.g., Berner, 2002). However, solubility-limiting phases could be present at lower Eh. When Berner (2002) calculated the Se solubility limit at pH 12.6, Eh -230 mV, and 25 °C [77 °F] using the Nagra/PSI chemical thermodynamic database, he obtained a concentration of about 0.1 M due to  $\text{Se}^0$  [or  $\text{Se}(\text{cr})$ , using his terminology] control. He argued, however, that this result was a function of the presence of  $\text{Se}^0$  as the only Se solid phase in the database. Based on data from Séby, et al. (2001), Berner (2002) proposed  $\text{CaSeO}_3 \cdot \text{H}_2\text{O}$  as the solubility limiting phase, assumed an aqueous  $\text{Ca}^{2+}$  concentration of  $2 \times 10^{-2}$  M, and calculated a solubility of  $1.1 \times 10^{-5}$  M at the given conditions. A higher value of  $7 \times 10^{-4}$  M was obtained at pH 13.4 as a result of a lower assumed  $\text{Ca}^{2+}$  concentration. Berner (2002) used the  $\text{CaSeO}_3 \cdot \text{H}_2\text{O}$  solubility data of Sharmasarkar, et al. (1996), as reported in Séby, et al. (2001), for these calculations. If we take the Sharmasarkar, et al. (1996) solubility product for  $\text{CaSeO}_3 \cdot \text{H}_2\text{O}$  of  $10^{-7.76}$ , assume activity coefficients of one, and use the Angus and Glasser (1985)  $\text{Ca}^{2+}$  cement pore water concentration of  $2.7 \times 10^{-3}$  M, we obtain a dissolved  $\text{SeO}_3^{2-}$  concentration of  $6 \times 10^{-6}$  M.

### **B3.1.3 New Models**

New Se solubility calculations, performed for this report using the representative waters discussed in Section B2.5, are shown in Figure B3-2. The steep drops in Se as Eh decreases at higher pH are due to precipitation of  $\text{Se}^0$ . The lowest solubility-limited Se concentrations ( $10^{-9}$  to  $10^{-8}$  M) correspond to Eh < -290 mV at pH 11.9 to 12.6; in this pH range, calculated solubility limits rise rapidly as Eh rises. At pH 13.4 (Type 1; fresh ordinary Portland cement) and Eh -350 mV, values are much higher—greater than  $3 \times 10^{-3}$  M—and again rise rapidly with Eh. At all pH values, there is no solubility control of Se at highest Eh. (Savannah River Site groundwater 5A, not plotted, also had no Se solubility limit.) Intermediate values between  $1 \times 10^{-3}$  and  $5 \times 10^{-1}$  M are predicted between pH 10 and 12.5, over a portion of the Eh range, on the basis of  $\text{CaSeO}_3 \cdot 2\text{H}_2\text{O}$  precipitation. The calculated Se solubility in these pH 10 to 12.5 waters is strongly dependent on the aqueous calcium concentration, as illustrated in Figure B3-3. Selenium solubility prediction is, therefore, dependent on accurate understanding of calcium behavior in evolving pore waters.

Selenium behavior over the modeled Eh-pH range is shown in Figure B3-4. At all pH values less than 11.9, solubilities are greater than 0.3 M, with lack of solubility control being typical for

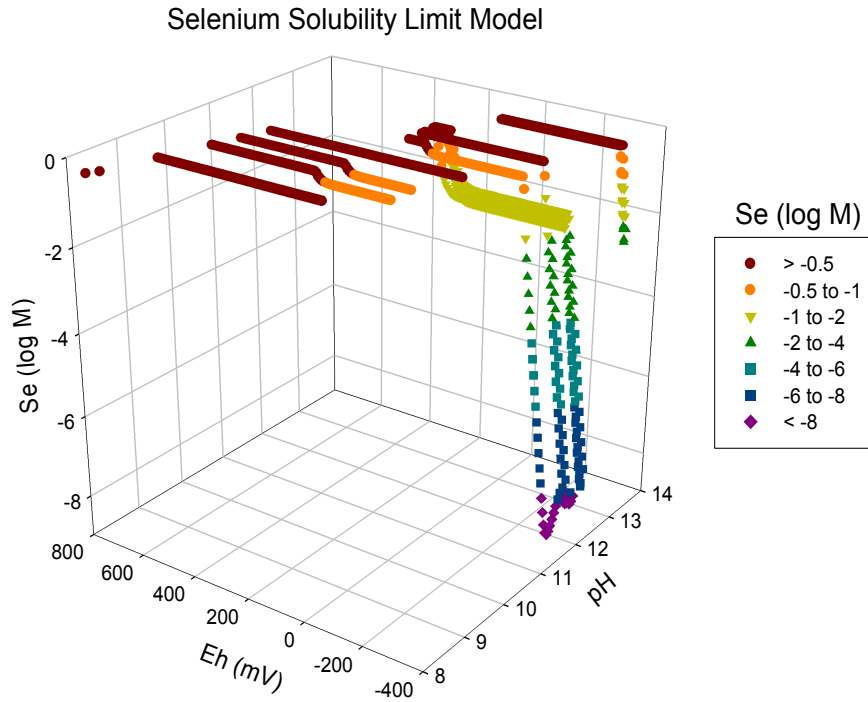


**Figure B3–2. Results of Se Solubility Limit Model Calculated Using Geochemist’s Workbench Version 6.0 (SpecE8 and React Modules) With the thermo.com.v8.r6+.dat Thermodynamic Database. Plotted Se concentrations Are Also Color Coded. Model Values Are for Representative Waters in Table B2–1; Water 5A (pH 5.8) Is Not Shown.**

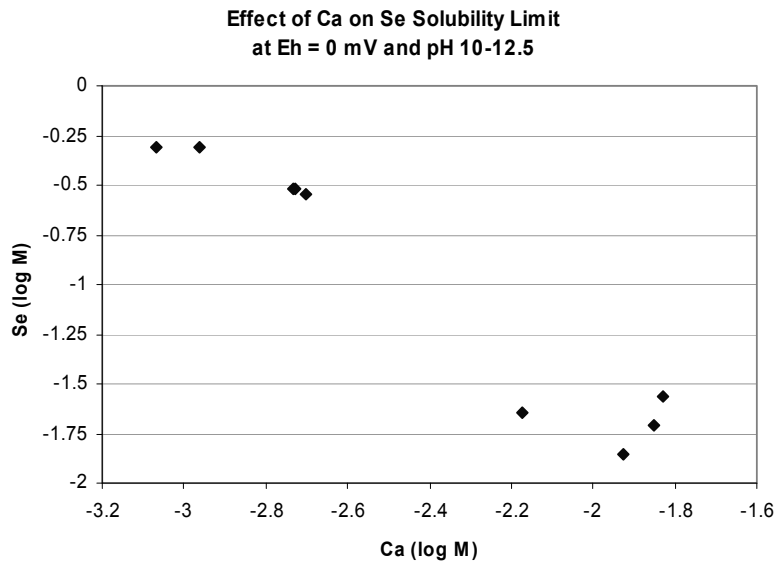


**Figure B3–3. Dissolved Se Concentrations Plotted Against Dissolved Ca for Modeled Waters With pH 10 to 12.5 at Eh = 0 mV. All Simulations Predicted  $\text{CaSeO}_3 \cdot 2\text{H}_2\text{O}$  Precipitation; High-Ca Waters Have Lower Se Concentrations Because the Latter Is Controlled by the  $\text{CaSeO}_3 \cdot 2\text{H}_2\text{O}$  Solubility Product.**

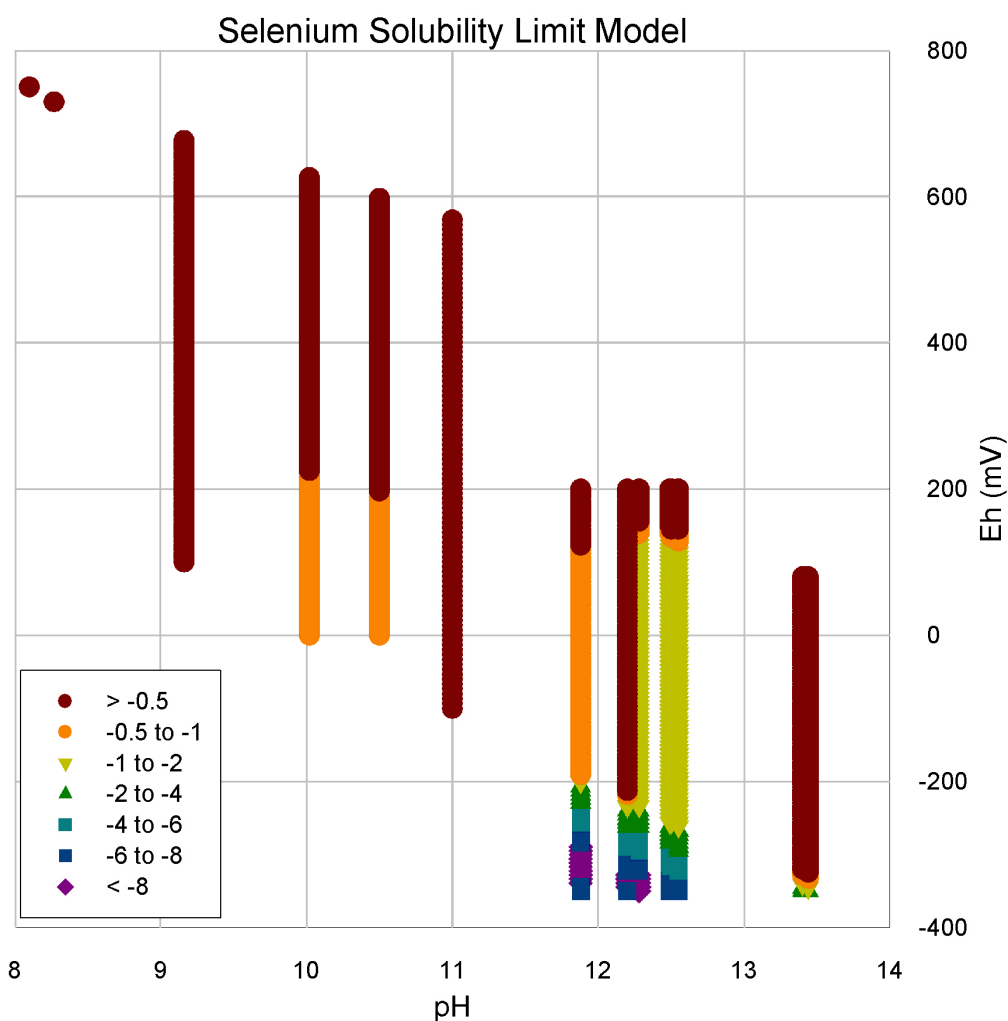


**Figure B3–4. Selenium Solubility Model Results From Figure B3–2, Projected Onto the pH-Eh Plane. Symbols Refer to the Aqueous Se Concentration (log M).**

elevated Eh waters that would result from atmospheric influence. At the highest pH values (Type 1), Se concentration is limited only under the most reducing conditions. For pH 11.9 to 12.6 (Types 2 and 3), Se concentrations below  $10^{-2}$  M are confined to Eh below  $-200$  mV, with concentrations at higher Eh being dependent on Ca content. The new model calculations agree in general with existing models and the experimental data discussed in Section B3.1.1. Metallic  $\text{Se}^0$  is important only at the low-Eh margins of the region of interest, while calcium selenite may exert some limits to Se concentrations above  $10^{-2}$  M as pH evolves from 12.6 to 10.

Table B3–1 identifies and qualitatively ranks the important solution characteristics affecting modeled Se solubility limits.

This set of Se solubility models was also run using the Japan Atomic Energy Agency Nuclear Energy Agency-based database described in Section B1.4. These models differ in their results for Se at lower Eh, as shown by two representative examples in Figure B3–5. The pattern of solubility-limiting solid phases is the same as with the models with thermo.com.v8.r6+.dat: (i) no limit at highest Eh for all pH, (ii) control by  $\text{CaSeO}_3 \cdot \text{H}_2\text{O}$  (note the differing number of waters of

<b>Table B3–1. Qualitative Rating of Effects of Solution Characteristics on Modeled Solubility Limits (L = Low, M = Moderate, H = High)*</b>				
	<b>pH</b>	<b>Eh</b>	<b>Carbonate</b>	<b>Other</b>
Se (Selenium)	L	H ↑	–	Calcium – M (pH 10 to 12.5 only) ↓
Tc (Technetium)	L	H ↑	–	Potassium? (pH 13.4 only)
U (Uranium)	M ↓	H ↑	H (pH < 12 only) ↑	Sodium – H (pH ≥ 11 only) ↓ Silicon – H (pH < 11 only) ↓
Np (Neptunium)	L	H ↑	H ↑	
Pu (Plutonium)	L	M ↓	H (pH < 12 only) ↑	

\*An arrow after the M or H denotes whether the correlation is positive or negative, or shows both positive and negative effects.

hydration in the Nuclear Energy Agency database) at intermediate Eh, and (iii) control by metallic  $\text{Se}^0$  at lowest Eh. The effects of these solids are seen in the water 2B plot in Figure B3–5, with  $\text{CaSeO}_3 \cdot \text{H}_2\text{O}$  saturation at –200 to 150 mV and  $\text{Se}^0$  below –200 mV.

The key differences in the two database results are that  $\text{CaSeO}_3 \cdot \text{xH}_2\text{O}$  is less soluble and  $\text{Se}^0$  is more soluble in the Nuclear Energy Agency database. Taking a conservative approach to reconciling the two results, the higher Se results at intermediate Eh (i.e., greater than  $10^{-2}$  M Se) should be favored and  $\text{Se}^0$  control to less than  $10^{-7}$  M at lowest Eh should not be considered.

### **B3.1.4 Conclusions**

The experimental and modeling data suggest that, through much of the pH–Eh region of interest (Figure B3–1), Se will not be limited to low concentrations by pure solid-phase solubility. At pH of about 12.5 and the lowest Eh of –350 mV (i.e., the lower left of the outlined field in Figure B3–1), it is possible that calcium selenite solubility will limit dissolved Se to below about  $10^{-4}$  M. There is also a possibility of  $\text{Se}^0$  control of low dissolved concentration in this same portion of pH–Eh range. For both phases, however, solubilities rise markedly as conditions deviate from this subregion. Therefore, solubility control should be applied for Se only if pH–Eh conditions can be confidently confined to lowest Eh when pH is around 12.5. As this report's discussions of chemical conditions suggest, there is limited confidence in the durability of these conditions. The conservative approach, therefore, may be to assume no Se solubility control by  $\text{Se}^0$  if the longevity of strongly reducing conditions is uncertain. Attributing solubility control to calcium selenite should be supported by well-constrained aqueous calcium concentrations.

### **B3.2 Technetium**

Like Se, Tc solid phase and aqueous species stabilities are strong functions of pH and Eh due to a range of feasible oxidation states (see discussion in Krupka, et al., 2004). The  $\text{Tc}^{\text{VII}}$  and  $\text{Tc}^{\text{IV}}$  oxidation states dominate aqueous Tc behavior; while data exist on other oxidation states, studies do not support their long-term importance to limiting Tc solubility (e.g., Krupka, et al., 2004; Warwick, et al., 2007). The desire to limit Tc release from cement-based waste forms by reducing mobile  $\text{Tc}^{\text{VII}}$  to  $\text{Tc}^{\text{IV}}$  is a key motivation for using reducing agents such as blast furnace slag (see Section 8.4 of the main report). Under aqueous oxidizing conditions, the pertechnetate anion  $\text{TcO}_4^-$  dominates and solubility-limiting pertechnetate solids are not

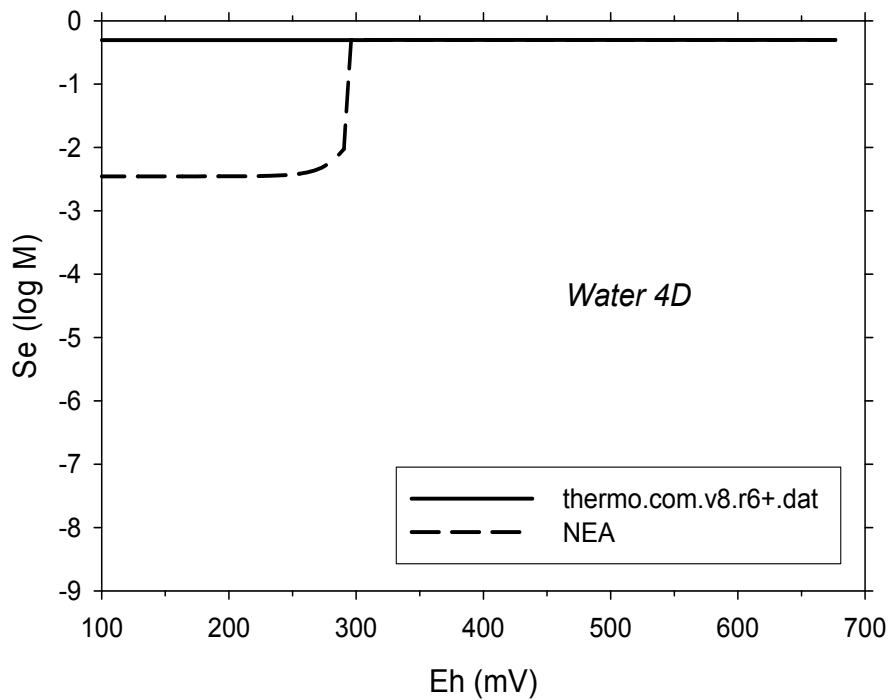
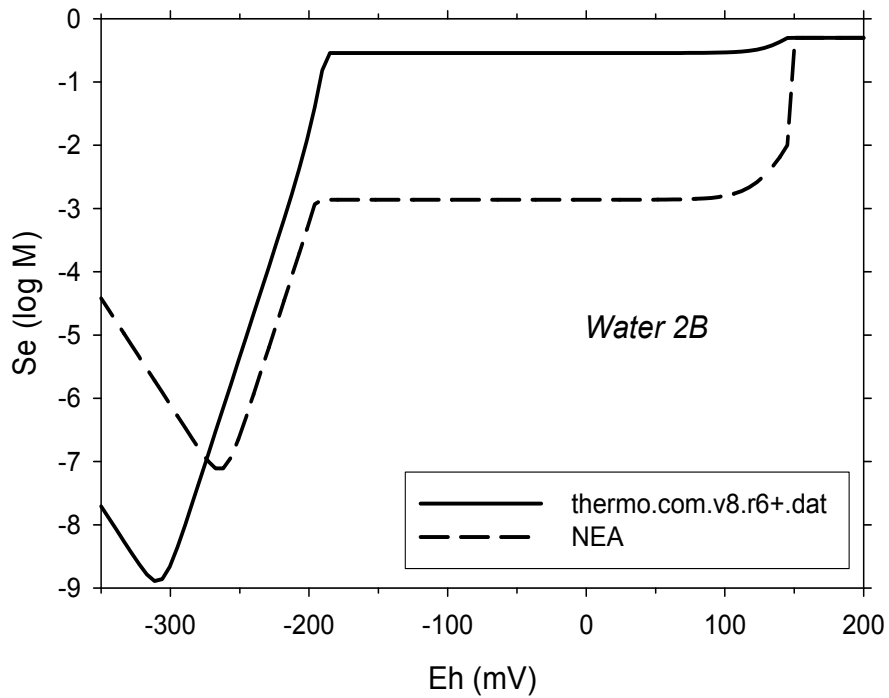


**Figure B3–5. Comparison of Selenium Solubility Limit Models for Waters 2B (pH 11.9) and 4D (pH 9.2) Using Different Thermodynamic Databases. On the Lower Plot, the Two Curves Overlap at Higher Eh.**

expected to form. The Eh–pH stability region for pertechnetate is quite large (Figure B3–6). Under more reducing conditions, the aqueous speciation of  $\text{Tc}^{\text{IV}}$  may be dependent on the abundance of carbonate (Krupka, et al., 2004), but these carbonate species were not present in the database used for the Figure B3–6 calculations or the new solubility models (Section B3.2.3). In the presence of sulfide (a presumed slag ingredient) at low Eh, Tc solubility may be controlled to low levels by formation of  $\text{Tc}^{\text{IV}}$  sulfides such as  $\text{TcS}_2$  and  $\text{Tc}_3\text{S}_{10}$  (Lukens, et al., 2005). (Aqueous Tc sulfur species have not been reported; Krupka, et al., 2004.) Hydrous oxides may also have an impact on solubility. Therefore, the key issue for Tc solubility is whether the conditions under which  $\text{Tc}^{\text{IV}}$  sulfides or other insoluble  $\text{Tc}^{\text{IV}}$  solids will form are attained and maintained in grout.

For the period when initial reducing conditions are maintained in cement-based material, Kaplan (2006) proposed a “reasonably conservative” Tc solubility limit of  $10^{-9}$  M and a “best,” or expected, value of  $10^{-10}$  M. The range Kaplan (2006) considered included highly degraded

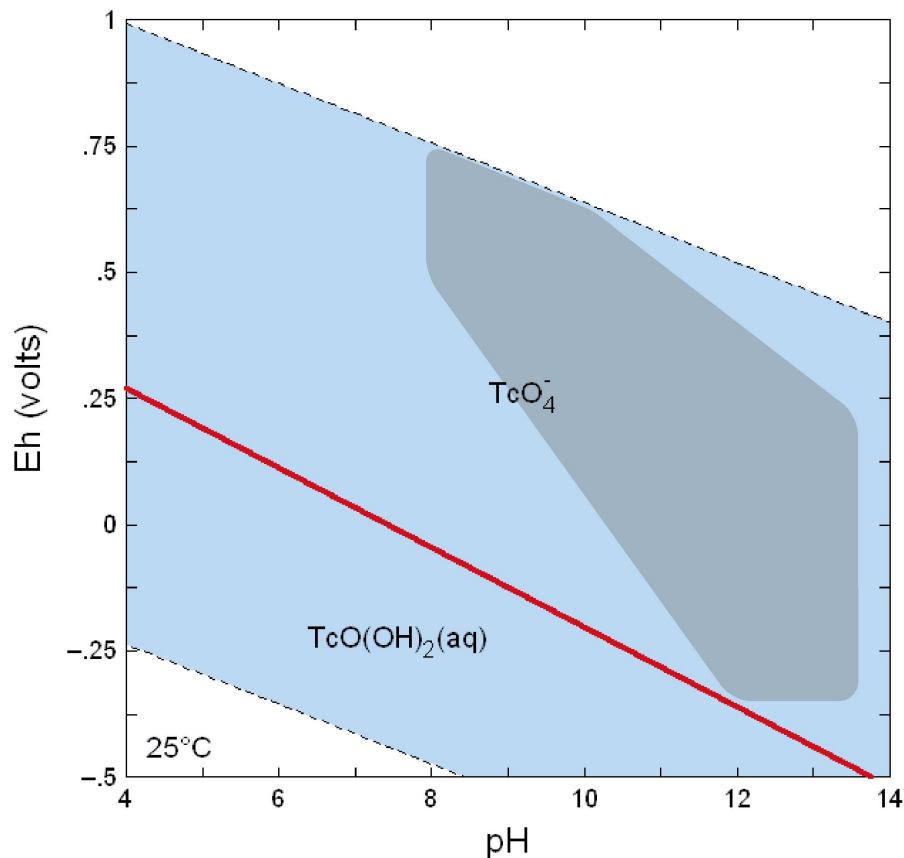


**Figure B3–6. Eh–pH Stability Fields for Aqueous Tc ( $1 \times 10^{-8}$  M) in Pure Water at 25 °C [77 °F] (Solids Suppressed) Calculated Using Geochemist’s Workbench Version 6.0 With the thermo.com.v8.r6+.dat Database. The Shaded Area Represents the Approximate Range of Expected Conditions as Cement-Based Materials Degrade (Section B2). Addition of Carbon or Sulfur Does Not Alter the Aqueous Species Fields. The Blue Field Defines Water Stability.**

conditions when the pH is 5.5—the same as local Savannah River Site groundwater. As our models will confirm, (i) assuming oxidizing conditions is conservative for Tc and (ii) imposition of reducing conditions in determining a Tc solubility limit must be supported in the context of changing conditions during cement degradation in the unsaturated zone.

### B3.2.1 Experimental Data

Krupka, et al. (2004) provided a useful overview of the Tc experimental literature, which will not be detailed here. Pilkington (1990) measured Tc concentrations of around  $10^{-7}$  M in cement-equilibrated solutions at an Eh of  $-450$  mV, but solid phases were not identified. Greenfield, et al. (1998) also measured Tc solubility in cement-equilibrated water at pH 12.3 and low Eh ( $-520$  to  $-510$  mV), obtaining concentrations between  $4 \times 10^{-9}$  and  $1 \times 10^{-8}$  M. These studies assumed that the solubility-limiting phase was  $\text{Tc}^{\text{IV}}$  oxide or its hydrated forms ( $\text{TcO}_2 \cdot x\text{H}_2\text{O}$ ). Lee and Bondietti (1983) identified Tc sulfide solids that formed under reducing conditions in ferrous solutions (not cementitious), and the formula  $\text{Tc}_2\text{S}_7$  was adopted, but never fully verified, for an apparent solubility-limiting  $\text{Tc}^{\text{VII}}$  phase that could form in sulfide-containing cements. Recently, however, Lukens, et al. (2005) identified the Tc solid forming in sulfide-containing cements as a  $\text{Tc}^{\text{IV}}$  phase with the formula  $\text{Tc}_3\text{S}_{10}$  (containing both sulfide and disulfide ions). Lukens, et al. (2005) did not measure the solubility of this phase or define its stability limits in terms of pH and Eh. Much of the Tc experimental literature is concerned with leaching or sorption behavior and is, therefore, not directly applicable to solubility determination.

### B3.2.2 Literature Models

Thermodynamic models have often been employed in attempts to predict Tc release behavior (e.g., Smith and Walton, 1993; Westinghouse Savannah River Company, 1992; Greenfield, et al., 1998; Krupka and Serne, 1998; Berner, 2002; Krupka, et al., 2004). Berner (2002) predicted a solubility limit, controlled by  $\text{TcO}_2 \cdot x\text{H}_2\text{O}$ , of around  $10^{-5}$  M at an Eh of  $-350$  mV for cement pore water; the model solubility limit rose two orders of magnitude at  $-300$  mV. Krupka and Serne (1998) calculated a  $\text{Tc}_3\text{O}_4$  solubility of  $6 \times 10^{-6}$  M at pH 12.5 and Eh  $-267$  mV. Krupka, et al. (2004) showed model results on an Eh–pH plot that suggested solubility control by  $\text{TcO}_2 \cdot 2\text{H}_2\text{O}(\text{am})$  to  $10^{-7}$  M in the ranges pH 12 to 14 and Eh  $-350$  to  $-500$  mV. At higher pH and Eh,  $\text{TcO}_4^-$  anion was stable and solubility was not limited. If  $\text{Tc}^{\text{IV}}$  carbonate complexes were viable (Krupka, et al., 2004), they could stabilize dissolved Tc at low Eh in carbonate-rich waters. Alkaline waters in cementitious systems, however, are not typically carbonate-rich. In an early performance assessment for the Saltstone Disposal Facility, Westinghouse Savannah River Company (1992) calculated a Tc solubility limit of  $10^{-20}$  M for a sulfide-rich cement pore fluid chemistry at pH 14. The solubility-limiting solid was heptavalent  $\text{Tc}_2\text{S}_7$ ; the authors conceded that the result was highly uncertain. Clearly, the experimental and modeling data show the potential for low Tc solubility limits under the assumed conditions. These various results, however, illustrate the difficulty in predicting Tc phase solubilities at high pH and low Eh.

Indeed, thermodynamic data on Tc in this pH/Eh range are highly uncertain and limited in scope (Rard, et al., 1999). Thermodynamic values for hydrated  $\text{Tc}^{\text{IV}}$  oxides are not well constrained, and even the existence of the  $\text{Tc}_2\text{S}_7$  phase has been questioned (Lukens, et al, 2005). In their geochemical review for Hanford disposal facilities, Krupka, et al. (2004, p. 3.24) stated:

Although the thermodynamic stability of  $\text{TcO}_4^-$  is well established, thermodynamic data for other aqueous complexes and solids containing Tc in its various valence states are extremely limited. The absence of such data

precludes the use of thermodynamic calculations to evaluate the environmental behavior of reduced species of dissolved Tc with respect to pH, Eh, and the presence of important dissolved complexing ligands such as dissolved phosphate, sulfate, chloride, and others.

### B3.2.3 New Models

New equilibrium Tc solubility models were performed using the representative waters discussed in Section B2.5. Initial results predicted solubility control at high pH and low Eh by solid phases containing oxidation states other than  $Tc^{VII}$  and  $Tc^{IV}$  (e.g.,  $Tc_3O_4$ , or  $Tc_2^{III}Tc^{II}O_4$ ), or by  $KTcO_4$  in potassium-rich waters. These phases were subsequently suppressed because they have not been identified from experiments (e.g., Warwick, et al., 2007). The results presented here therefore reflect model results when only  $Tc^{VII}$  and  $Tc^{IV}$  solids, aside from  $KTcO_4$ , were allowed to precipitate. The results in Figure B3–7 show a pattern roughly similar to Se. Very low solubilities were calculated only at pH 11.9 to 12.6 (Types 2 and 3), reaching as low as  $7 \times 10^{-8}$  M at  $-350$  mV but increasing rapidly as Eh rises to  $-200$  mV. When Tc solubility was limited (only on the downward sloping portions of the curves in Figure B3–7), the amorphous hydrated

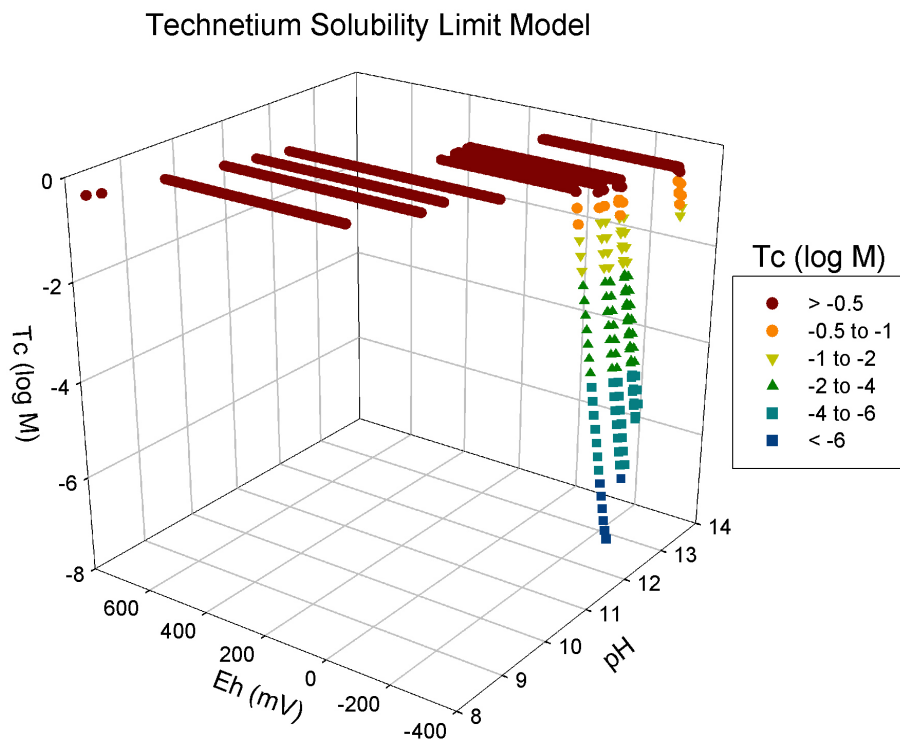


**Figure B3–7. Results of Tc Solubility Limit Model Calculated Using Geochemist’s Workbench Version 6.0 (SpecE8 and React Modules) With the thermo.com.v8.r6+.dat Thermodynamic Database. Plotted Tc Concentrations Are Also Color Coded. Model Values Are for Representative Waters in Table B2–1; Water 5A (pH 5.8) Is Not Shown. Model SolidSuppressions Are Discussed in the Text.**

Tc<sup>IV</sup> oxide TcO<sub>2</sub>•2H<sub>2</sub>O(am) was the responsible precipitate. (Notably, the proposed sulfide Tc<sub>2</sub>S<sub>7</sub> did not approach saturation in any runs that included sulfur.) At pH 13.4 (Type 1), Tc solubilities exceed  $6 \times 10^{-2}$  M. For all pH below 11.9 (Types 4 and 5) and all Eh above -200 mV, Tc concentrations were not limited by solubility. Figure B3–8 best shows Tc concentration behavior over the Eh-pH region of interest.

While suppression of non-Tc<sup>VII</sup> and non-Tc<sup>IV</sup> solids is easily supported, suppression of KTcO<sub>4</sub> is not as clearly justified (although the phase has not been reported in experiments on cement-based systems). This suppression affected model results only for potassium-rich waters 1A and 1C (0.2 and 0.3 M K, respectively). Separate calculations showed that this solid would lower dissolved Tc only to around 0.05 M in these Type 1 waters. This result, if applicable, does not significantly change the overall conclusions of these models that Tc solubility control is important only at very low Eh.

The model results conform to the pattern established in laboratory and previous modeling studies. Technetium solubility appears to be limited only at Eh of -200 mV and lower, particularly for Types 2 and 3 waters. At higher pH (Type 1), solubility is limited only at Eh below -330 mV and, at lower pH (Types 4 and 5), is not limited at all.

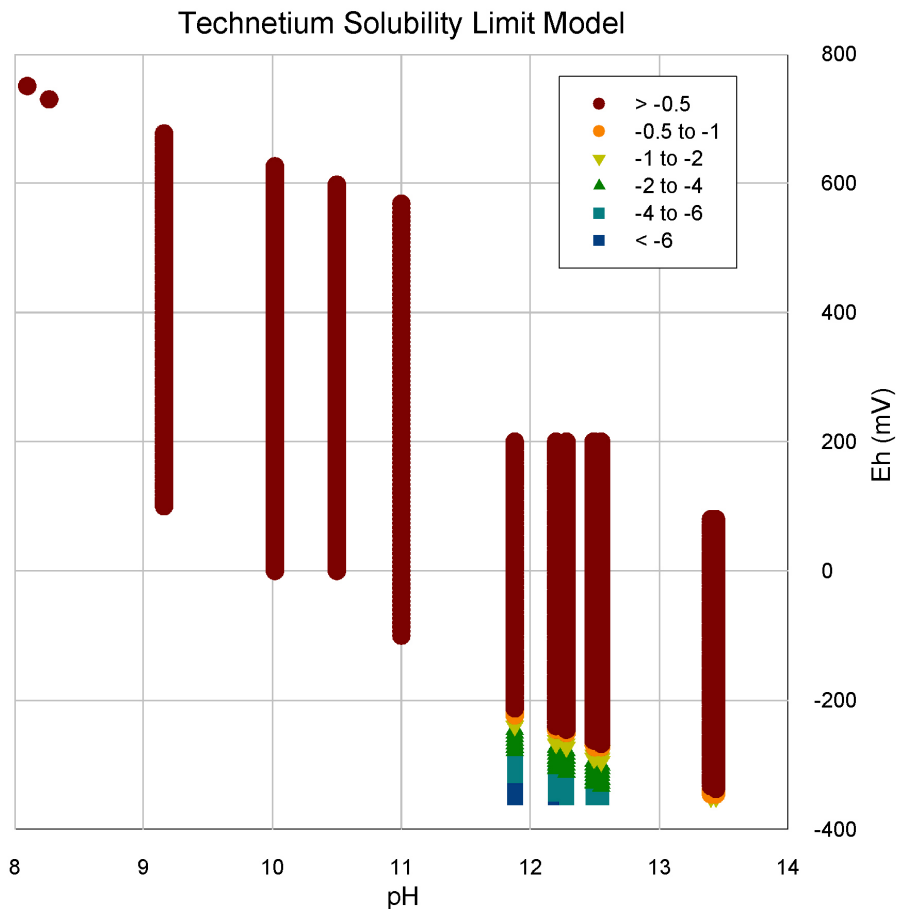


**Figure B3–8. Tc Solubility Model Results From Figure B3–7, Projected Onto the pH–Eh Plane. Symbols Refer to the Aqueous Tc Concentration (log M).**

Table B3–1 identifies and qualitatively ranks the important solution characteristics affecting modeled Tc solubility limits. This set of Tc solubility models, with the same mineral suppressions, was also run using the Japan Atomic Energy Agency Nuclear Energy Agency-based database described in Section B1.4. The key difference in the Nuclear Energy Agency results is that, at lower Eh, Tc concentration is controlled by crystalline  $TcO_2$ , rather than amorphous  $TcO_2 \cdot 2H_2O(am)$ , yielding lower Tc concentrations starting at a higher Eh (Figure B3–9). There is still no solubility control at higher Eh for any waters. Application of the original models using thermo.com.v8.r6+.dat would be more conservative.

### B3.2.4 Conclusions

For the present case, the limitations of solubility modeling and the scarcity of experimental data are compounded by the fact that the lower Eh–pH range of interest lies in the proximate boundary between the stability fields of  $Tc^{VII}$  and  $Tc^{IV}$  (Figure B3–6). In addition, both the reducing capacity of the slag-cement mixture and the formation of potentially solubility-limiting Tc sulfides are dependent on the initial sulfide content and its temporal evolution. In light of these uncertainties and the dominance of  $Tc^{VII}$  species as Eh rises as atmospheric oxygen is introduced, it is prudent to assume that no Tc solubility-limiting phases will form in the cementitious environment unless longevity of strongly reducing conditions can be confidently predicted.

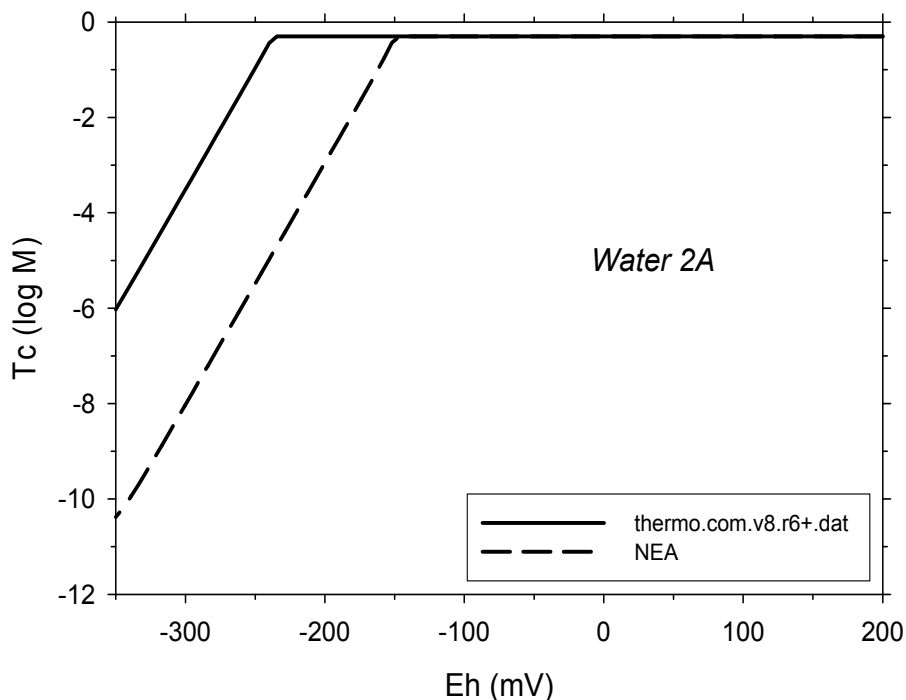


**Figure B3–9. Comparison of Technetium Solubility Limit Models for Water 2B (pH 11.9) Using Different Thermodynamic Databases; the Two Curves Overlap at Higher Eh**

### B3.3 Uranium

A key geochemical feature of U is its redox sensitivity. Under oxidizing conditions, the relatively mobile  $U^{VI}$  oxidation state dominates, whereas  $U^{IV}$  dominates under reducing conditions. In the pH range 8 to 14, U aqueous speciation and, thus, solubility limits are strongly controlled by dissolved carbonate. Figures B3–10 and B3–11 compare calculated U aqueous speciation in a carbonate-free system and in a system in equilibrium with atmospheric  $CO_2$ . Such  $CO_2$  activity is not expected to apply during the high-pH period when  $CO_2$  will be consumed by carbonation reactions with cement phases; the assumed carbon conditions are for comparative purposes only. Because a carbonating cement-based material is a dynamic system, it is difficult to more precisely predict dissolved carbonate concentrations; an attempt to represent the range of expected carbonate concentrations is reflected in the waters chosen for modeling (Table B2-1). For the Eh–pH region of interest (shaded area in Figure B3–11),  $CO_2$  will promote the formation of  $U^{VI}$  anionic carbonate species, which will reduce the  $U^{IV}(OH)_4(aq)$  field and may stabilize higher dissolved U concentrations. It is possible, therefore, that very low-solubility  $U^{IV}$  solid phases may be unstable under most of the conditions of interest.

For young, reducing cement (pH 12.5), Kaplan (2006) recommended conservative and best U solubility limits of  $5 \times 10^{-5}$  M and  $10^{-6}$  M, respectively. For moderately aged (pH 10.5) and aged cements, the corresponding limits were  $5 \times 10^{-6}$  M and  $10^{-7}$  M. For oxidizing conditions, the young and moderately aged cement conservative and best values were  $5 \times 10^{-6}$  M and  $10^{-7}$  M, respectively, while the corresponding values for aged cement were  $5 \times 10^{-5}$  M and  $10^{-6}$  M. (The lower range of values for young cements under oxidizing conditions compared to reducing conditions is unexpected) Kaplan (2006), “aged” conditions assumed a pH of 5.5, corresponding to local groundwaters.

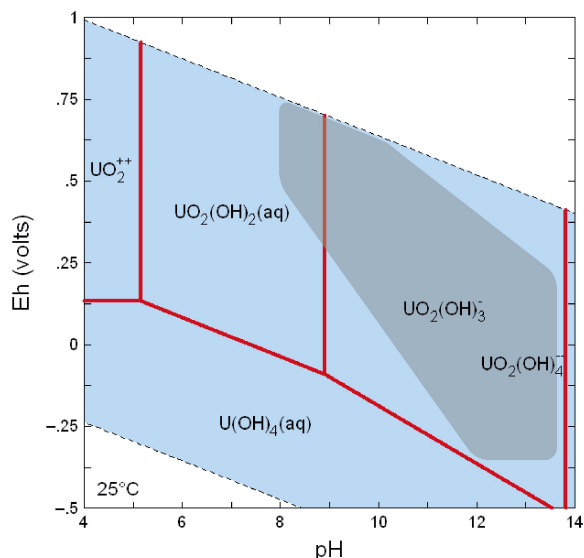


**Figure B3–10. Eh–pH Stability Fields for Aqueous Uranium ( $1 \times 10^{-8}$  M) in Pure Water at 25 °C [77 °F] (Solids Suppressed) Calculated Using Geochemist’s Workbench Version 6.0 With the thermo.com.v8.r6+.dat Database. The Shaded Area Represents the Approximate Range of Expected Conditions as Cement-Based Materials Degrade (Section B2). Addition of Sulfur Does Not Alter the Aqueous Species Fields. The Blue Field Defines Water Stability.**

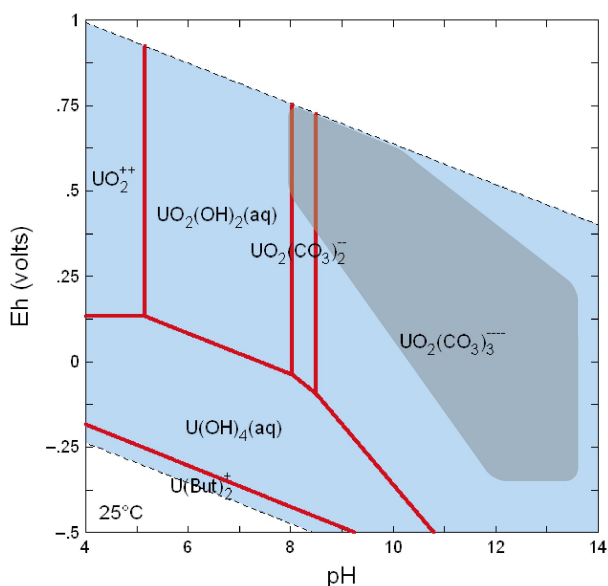


**Figure B3–11. Eh–pH Stability Fields for Aqueous Uranium ( $1 \times 10^{-8}$  M) in Water at Equilibrium With  $\text{CO}_2$  Gas at a Fugacity of  $10^{-3.5}$  atm at  $25^\circ\text{C}$  [ $77^\circ\text{F}$ ] (Solids Suppressed) Calculated Using Geochemist’s Workbench Version 6.0 With the thermo.com.v8.r6+.dat Database. The Shaded Area Represents the Approximate Range of Expected Conditions as Cement-Based Materials Degrade (Section B2). The Blue Field Defines Water Stability.  $\text{U}(\text{But})_2^+$  is a  $\text{U}^{\text{III}}$  Butanoic Acid Complex.**

### B3.3.1 Experimental Data

Numerous studies relevant to U solubility in cementitious waters are available in the literature. Ewart, et al. (1992) measured U solubilities from oversaturation in  $\text{CO}_2$ -free conditions in a water equilibrated with a blend of 90 percent blast furnace slag and 10 percent ordinary Portland cement; pH was adjusted over a range of 5 to 13. Solubility of  $\text{U}^{\text{IV}}$  was measured at about  $2 \times 10^{-7}$  M over the entire pH range. From pH 5 to 10.5, measured  $\text{U}^{\text{VI}}$  solubility decreased from  $10^{-5}$  to  $10^{-7}$  M and then increased again to  $10^{-5}$  at pH 13. Solids were not identified. Pointeau, et al. (2004) obtained quite similar U solubility limits over the pH range 9.3 to 12.2 in waters equilibrated with cement and C-S-H. Maximum U concentrations of 3 to  $5 \times 10^{-6}$  M were obtained at the low and high ends of this pH range and, as in Ewart, et al. (1992), a minimum value ( $2 \times 10^{-7}$  M) was observed at pH 10.5. Krupka and Serne (1998) observed that the high-pH data of Ewart, et al. (1992) were consistent with a thermodynamic model of uranophane  $[\text{Ca}(\text{UO}_2)_2(\text{SiO}_3)_2(\text{OH})_2]$  solubility control.

Moroni and Glasser (1995) performed a systematic experimental study of U solubility in the Ca-U-Si system under nonreducing conditions. Measured U concentrations at lower U loadings at 10 to 13 pH were in the range  $1 \times 10^{-9}$  (or lower) to  $1 \times 10^{-7}$  M; the higher values were associated with solutions compatible with  $\text{Ca}(\text{OH})_2$ . In solutions equilibrated with C-S-H gels, however, concentrations were  $1 \times 10^{-8}$  M and lower. Potential Ca-U mineral phases controlling U solubility were analyzed, but U phases coexisting with  $\text{Ca}(\text{OH})_2$  and C-S-H were not definitively identified. One phase was provisionally identified as hydrated  $\text{CaUO}_4$ , but it was not observed in any mixtures containing silica.

Serne, et al. (1996) obtained U concentrations of  $2 \times 10^{-6}$  to  $2 \times 10^{-8}$  M in cement pore water in air as controlled pH increased from 7.5 to 9.0; these were below a detection limit of about  $10^{-8}$  M at higher pH. Identification of a controlling U mineral was inconclusive, though an amorphous  $\text{CaUO}_4$  phase was hypothesized. Greenfield, et al. (1998) reported U solubility limits in cement-equilibrated water (pH 12, Eh -500 mV) of  $<5 \times 10^{-8}$  M and  $2 \times 10^{-7}$  M. Zhao, et al. (2000), in experiments designed to measure U sorption onto hydrothermally altered cement in the absence of  $\text{CO}_2$ , measured U concentrations varying from  $3 \times 10^{-6}$  M at pH 9.2, decreasing to  $2 \times 10^{-8}$  M at pH 10.7, then increasing to  $3 \times 10^{-7}$  M at pH 11.2. Solubility of no one U mineral could explain the pH trend, but the concentrations exceeded model curves for  $\text{CaUO}_4$ , uranophane, and haiweeite [ $\text{Ca}(\text{UO}_2)_2(\text{Si}_2\text{O}_5)_3 \cdot 5\text{H}_2\text{O}$ ]. Other studies (e.g., Berner, 1999, 1992) have questioned the role of crystalline  $\text{CaUO}_4$  in controlling U concentrations under cementitious conditions, because experimental concentrations typically exceed model  $\text{CaUO}_4$  solubility. Berner (2002) discussed unpublished U solubility studies that yielded a maximum U concentration of  $2 \times 10^{-6}$  M at pH 13.3, projected to  $5 \times 10^{-7}$  at pH 12.22.

The picture that emerges from these studies is that, for cementitious systems over the approximate pH range of 9 to 13, U concentration is limited to maximum values of  $10^{-8}$  to  $10^{-6}$  M. Lower and higher limits are suggested under certain conditions (e.g., Moroni and Glasser, 1995; Ewart, et al., 1992), but these extremes are not consistently observed. In addition, studies do not consistently point to specific U minerals responsible for solubility control.

### B3.3.2 Literature Models

Uranium solubility models for cementitious systems are common in the literature; only relatively few examples are discussed here. Model outcomes have varied considerably over the years as thermodynamic databases have evolved. [For example, Berner (2002) chose not to use his model calculations for U solubility, which implied little solubility control above an Eh of -300 mV, because of the paucity of U phases in his model's database.] Allard and Torstenfelt (1985), noting the low carbonate content of cement pore waters, modeled a  $\text{U}^{\text{IV}}$  solubility limit of  $10^{-6}$  to  $10^{-7}$  M for reducing conditions and a  $\text{U}^{\text{VI}}$  limit under oxidizing conditions of  $10^{-6}$  M. Berner (1992) calculated individual U mineral solubilities as pH evolved during cement degradation at Eh -300mV. With the exception of highly insoluble  $\text{CaUO}_4$ , solubility limits changed from around  $10^{-4}$  M to  $10^{-7}$  M as pH dropped from 13 to 10. Brady and Kozak (1995) calculated U solubilities of  $10^{-8}$  M and lower for cementitious environments; haiweeite was the controlling phase for oxidizing conditions in equilibrium with atmospheric oxygen. Greenfield, et al. (1998) calculated a  $\text{UO}_2(\text{am})$  solubility of  $3 \times 10^{-7}$  M for a pH 12 water at -500 mV.

Krupka and Serne (1998) modeled schoepite and uranophane solubility for a pH range of 4 to 12.5, with Eh varying from +380 to +200 mV over the pH range. Uranophane constrained U to lower concentrations, ranging from  $2 \times 10^{-8}$  to  $1 \times 10^{-5}$  M as pH increased from 8.5 to 12.5. For a model cement pore water at pH 13.4 and Eh -300 mV, Berner (1999) calculated a solubility limit of  $5 \times 10^{-7}$  M, controlled by  $\alpha\text{-Na}_2\text{U}_2\text{O}_7$  and with  $\text{U}^{\text{VI}}$  species dominating dissolved U. As in many U cement models, dissolved carbonate is quite low in this model solution ( $1.4 \times 10^{-4}$  M) such that hydroxide U species dominate over carbonate species. (See Figure B3-11 for the effect on U speciation of carbonate at high pH.)

In an example of the failure of crystalline  $\text{CaUO}_4$  to match solubility data, Serne, et al. (1996) showed that a model solubility curve for that phase gave concentrations approximately three orders of magnitude lower than experimental results.

### B3.3.3 New Models

Clearly, the success of solubility models depends strongly on the comprehensiveness of the supporting thermodynamic database and on selection of the controlling solid phases. In an attempt to refine U predictions, new solubility calculations were performed. In initial runs, very low U solubilities were calculated under many conditions when either  $\text{CaUO}_4$  ( $10^{-14}$  to  $10^{-11}$  M) or haiweeite ( $10^{-13}$ ) was the limiting mineral. (For waters including Si data, haiweeite was always the least soluble U solid.) Because these values differ grossly from experimental data and these two solid phases have not been typically identified in experiments, these solids were suppressed in the models. Example differences in modeled U concentrations between initial runs and those with these two solids suppressed are illustrated in Figure B3–12; the low values in the unsuppressed simulations cannot be justified by experimental data. Apparently erroneous prediction of solubility-limiting phases such as  $\text{CaUO}_4$  and haiweeite may arise from kinetic constraints on their formation, and not necessarily from inaccurate thermodynamic data.

Solubility model results with these mineral suppressions are illustrated in Figure B3–13; water chemical characteristics were discussed in Section B2.5. Calculated solubility limits vary between  $1 \times 10^{-9}$  and  $1 \times 10^{-3}$  M, with no strong overall variations with pH and Eh. For example, values in the high-pH region ( $>11$ ) span the entire range, and the highest values are obtained at Eh as low as  $-200$  mV. Solubility-limiting minerals are  $\text{U}^{\text{VI}}$  phases  $\text{Na}_2\text{U}_2\text{O}_7$ , schoepite, and soddyite;  $\text{U}^{\text{IV}}$  oxide uraninite; and mixed-valent oxides  $\text{U}_4\text{O}_9$ ,  $\text{U}_3\text{O}_7$ , and  $\text{U}_3\text{O}_8$ . Uraninite and the mixed-valent oxides are responsible for the steeply sloping drops in dissolved U with decreasing Eh seen in Figure B3–13. Solubilities of the  $\text{U}^{\text{VI}}$  solids do not show Eh dependence, yielding the flat curves or curve segments in Figure B3–13.

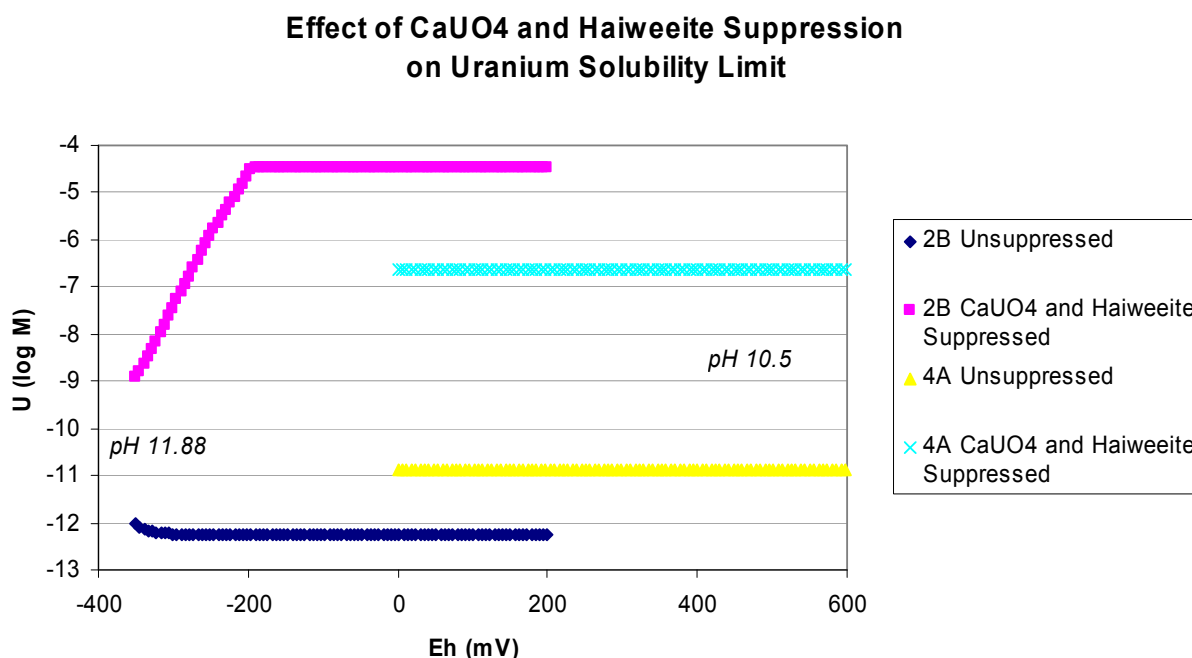


**Figure B3–12. Modeled Uranium Solubility Limit as a Function of Eh, Showing the Effect of Suppressing  $\text{CaUO}_4$  and Haiweeite on Results for Waters 2B and 4A**

### Uranium Solubility Limit Model

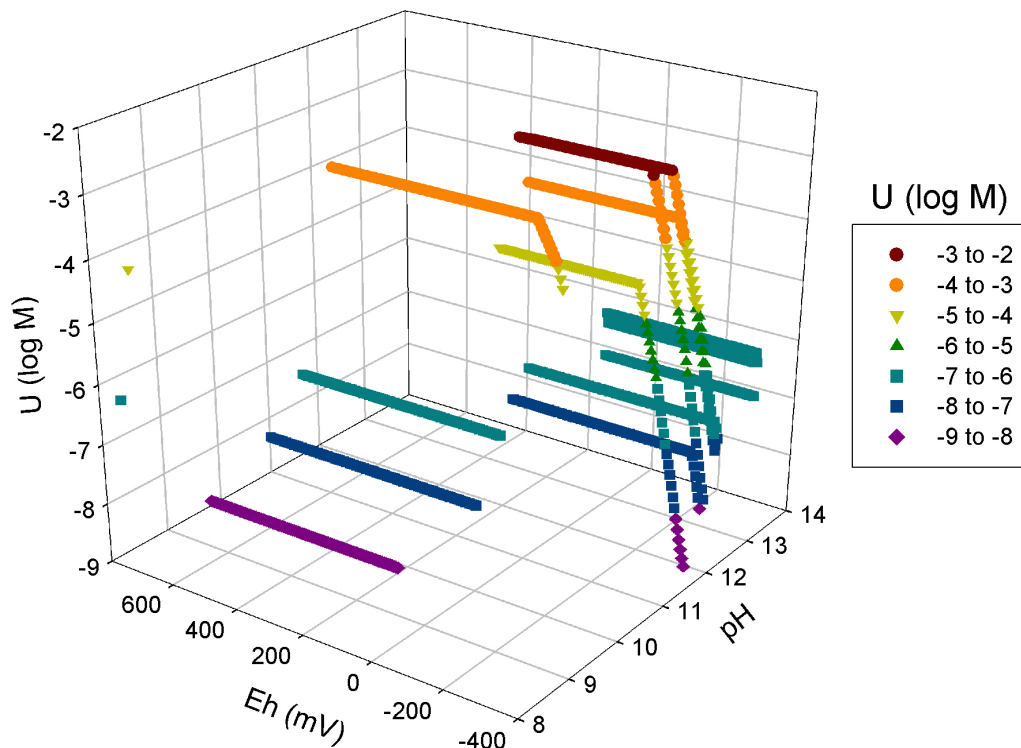


**Figure B3–13. Results of Uranium Solubility Limit Model Calculated Using Geochemist’s Workbench Version 6.0 (SpecE8 and React Modules) With the thermo.com.v8.r6+.dat Thermodynamic Database. Plotted U Concentrations Are Also Color-Coded. Model Values Are for Representative Waters in Table B2–1; Water 5A (pH 5.8) Is Not Shown. Solid Phases  $\text{CaUO}_4$  and Haiweeite Were Suppressed in the Models.**

For all Types 1, 2, and 3 waters (i.e.,  $\text{pH} \geq 11.9$ ) for which Na concentrations were reported (Table B2-1),  $\text{Na}_2\text{U}_2\text{O}_7$  was the modeled solubility-limiting mineral when U oxides were not stable. Those waters with no Na (2C and 3B) are the only ones that reach U concentrations above  $10^{-3}$  M (maroon symbols in Figure B3–13). Dependence of the U solubility limit on Na concentration in this pH range is shown in Figure B3–14. If the model predictions of  $\text{Na}_2\text{U}_2\text{O}_7$  saturation are correct, Na concentrations need to be included in high-pH water chemical compositions. The relatively high sodium concentrations in pore waters of fresh ordinary Portland cement-based tank grouts (similar to Type 1 waters in Table B2–1) and even higher sodium concentrations in fresh saltstone pore waters (DOE, 2006) suggest that, initially, U solubility could be limited to relatively low values by  $\text{Na}_2\text{U}_2\text{O}_7$ .

Aqueous Si concentrations were also important in the models for lower-pH waters, owing to the predicted stability of the uranyl silicate soddyite in some Type 4 waters ( $\text{pH}$  9.2 to 11.0) and the Idaho National Laboratory groundwater ( $\text{pH}$  8.1). The two Type 4 waters that did not have Si in their chemical compositions (4B and 4E) yielded U concentrations more than two orders of magnitude higher than the others. Likewise, Si-absent water 4E had a model U concentration

**Effect of Na on U Solubility**  
**Types 1, 2, and 3 (pH 11.9 - 13.4)**

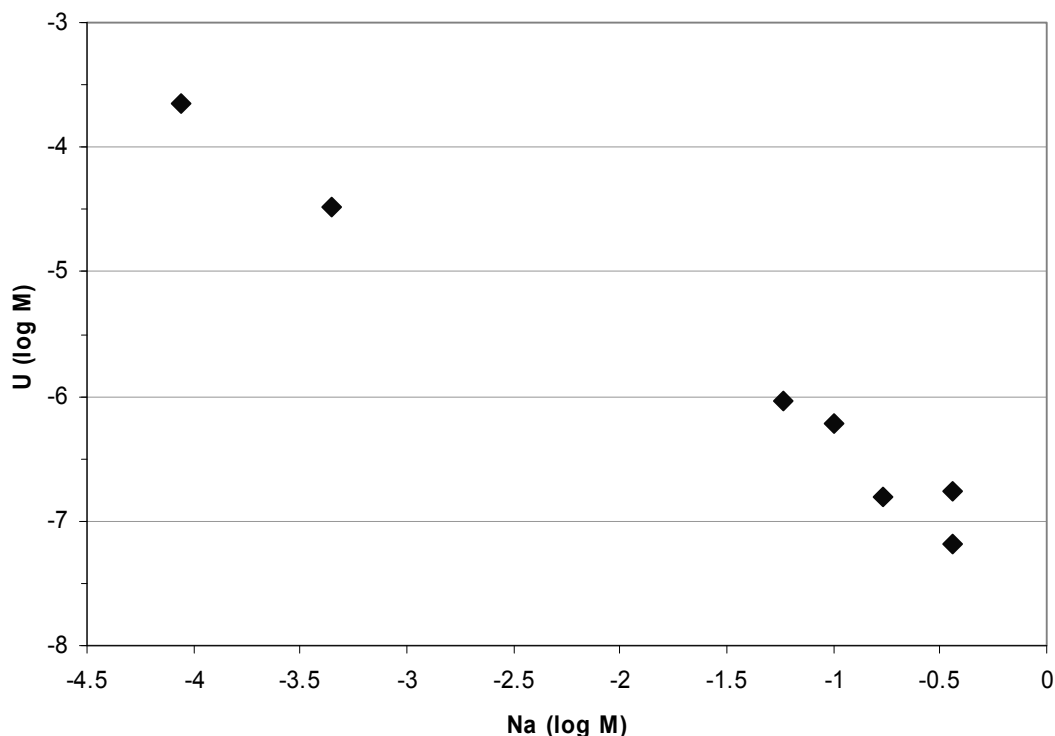


**Figure B3-14. Dependence of Modeled U Solubility Limit on Dissolved Na Concentration in High-pH Waters. Uranium Concentrations Are for Eh > -170 mV, a Range Over Which U Concentrations Are Constant. Waters of These Types That Did Not Include Na in Their Chemical Composition Yielded Even Higher U Concentrations Due to the Lack of Na<sub>2</sub>U<sub>2</sub>O<sub>7</sub> Control.**

100 times higher than Si-containing groundwater 5B at a similar pH. Aside from the low-pH Savannah River Site groundwater (5A; U solubility limit  $9 \times 10^{-6}$  M), schoepite saturation was predicted only for Si-absent water compositions.

The importance of carbonate complexes in enhancing U aqueous concentrations is well established, but carbonate effects on model results were generally subdued owing to relatively low dissolved carbonate concentrations. For example, the addition of  $3 \times 10^{-6}$  M carbon to the carbon-free water 1C composition did not significantly change U behavior. In addition, unusually high U concentrations were obtained for Na-absent waters 2C and 3B (the two curves that exceed  $10^{-3}$  M in Figure B3-13), despite the absence of carbonate in their compositions. Furthermore, the carbonate-rich, pH 13.4 water 1B did not show unusually high U concentrations. In general, carbonate effects could not be distinguished from other chemical effects in this set of models. One model test, however, did demonstrate the importance of carbonate at moderate pH. Water 4D, at pH 9.2, represents a portion of pore water evolution when infiltrating waters are actively carbonating the degraded cement-based material. In an alternative model, dissolved carbon was constrained by atmospheric CO<sub>2</sub> gas (log fugacity = -3.5) and calcium was constrained by calcite saturation. This led to a calculated total inorganic carbon concentration of  $8 \times 10^{-3}$  M (chiefly HCO<sub>3</sub><sup>-</sup>), compared with the calcite-constrained value of  $8 \times 10^{-5}$  M from the nominal 4D model. The resulting

soddyite-controlled U solubility limit was  $3 \times 10^{-5}$  M, compared to  $5 \times 10^{-9}$  M in the nominal model, attributable to the stabilization of the carbonate aqueous species  $\text{UO}_2(\text{CO}_3)_3^{4-}$ . This result shows that if  $\text{CO}_2$  fugacities could rise toward atmospheric levels in carbonating systems, higher aqueous U concentrations could be attained.

The foregoing discussion demonstrated the importance to U solubility models of designating aqueous Na, Si, and carbonate contents. The model results are plotted again in Figure B3–15 with the following exclusions from the original plot in Figure B3–13: (i) waters 2C and 3B, which are high-pH waters that do not include Na (and also lack carbonate) and (ii) waters 4B and 4E, which are lower-pH waters lacking Si. A projection onto the Eh-pH plane is shown in Figure B3–16. The two waters (2B and 3C) that appear to have unusually high modeled U concentrations of  $3 \times 10^{-5}$  and  $2 \times 10^{-4}$  M over most of the Eh range are constrained by  $\text{Na}_2\text{U}_2\text{O}_7$  but have much lower Na contents than other Type 2 and 3 waters (Table B2–1). The low U concentrations at lower pH, in contrast ( $5 \times 10^{-9}$  to  $6 \times 10^{-7}$  M), are controlled by soddyite and are not related to Na content. The increase in aqueous silica with decreasing pH predicted in cement degradation models such as that by Berner (1992) will contribute to soddyite saturation and lower U at pH less than about 11.

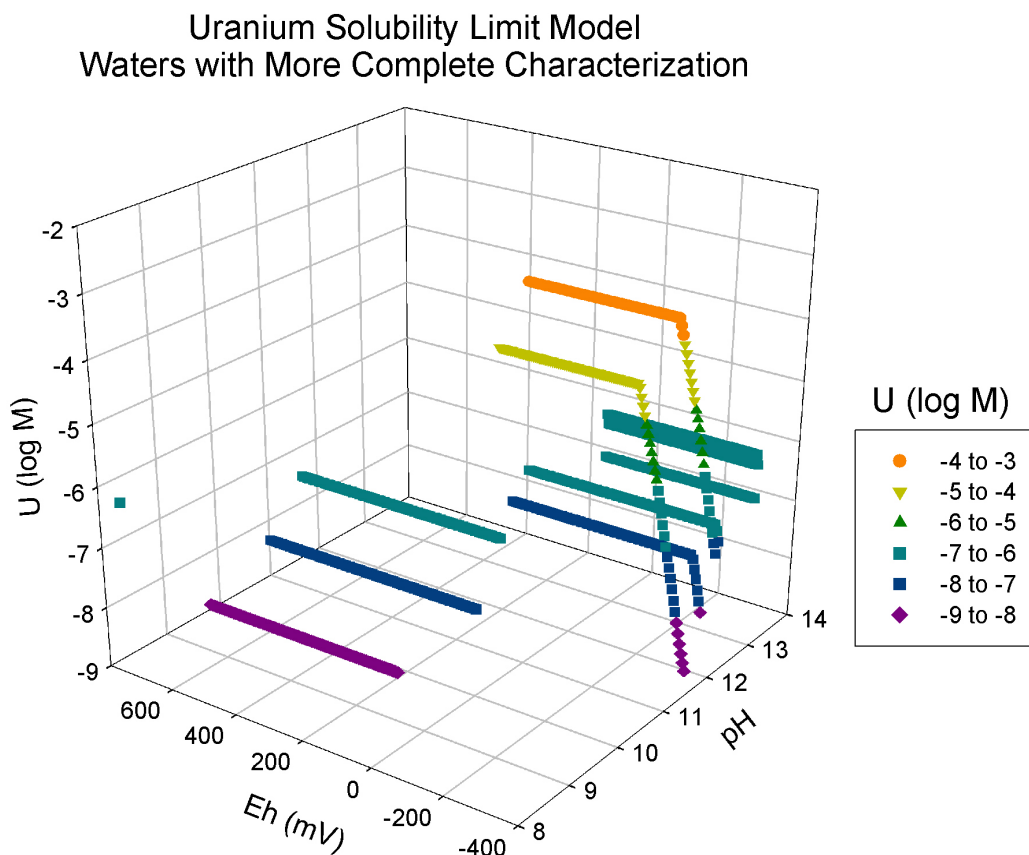


**Figure B3–15. Uranium Solubility Limit Model Results From Figure B3–13, Excluding High-pH Waters Lacking Na Data and Lower-pH Waters Lacking Si Data**

### Uranium Solubility Limit Model Waters with More Complete Characterization

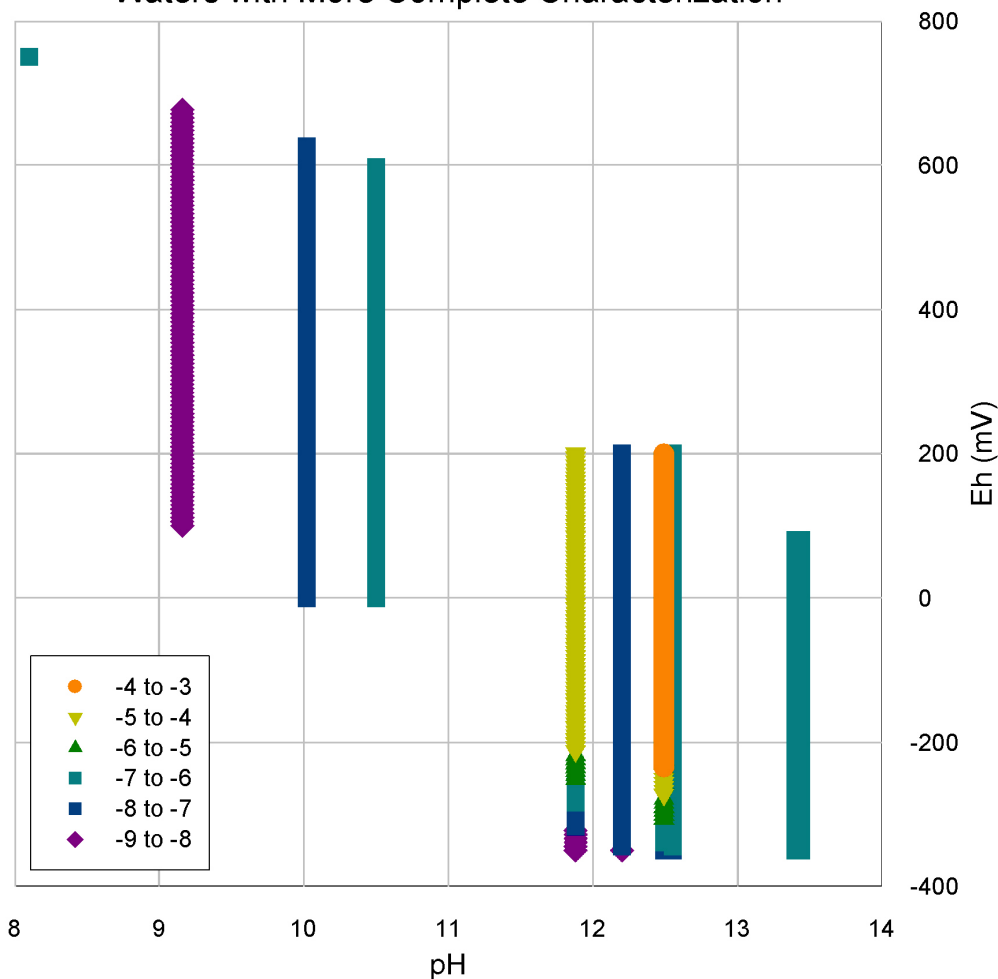


**Figure B3–16. Uranium Solubility Model Results From Figure B3–15 (with some samples excluded as described in the text), Projected onto the pH–Eh Plane. Symbols Refer to the Aqueous U Concentration (log M).**

The overall pattern of modeled U concentrations as pH evolves to lower values (Figures B3–15 and B3–16) shows (i) Type 1 water U concentrations of  $10^{-7}$  to  $10^{-6}$  M, (ii) Type 2 or 3 U concentrations over most of the Eh range of  $10^{-7}$  to  $10^{-6}$  M, with potential excursions to values as high as  $10^{-4}$  M if Na contents are very low, (iii) U concentrations in Types 2 or 3 waters as low as  $10^{-9}$  M at Eh < -200 mV, (iv) a decrease in U toward  $10^{-9}$  M as pH decreases below 11, and (v) a rise in U as pH decreases below about 9. Uranium solubility limits cannot, however, be generalized as simply defined on an Eh–pH plot. More reliable prediction depends on better constraints on evolving water chemistry as degradation proceeds.

Table B3–1 identifies and qualitatively ranks the important solution characteristics affecting modeled U solubility limits.

This set of U solubility models, with the same mineral suppressions, was also run using the Japan Atomic Energy Agency Nuclear Energy Agency-based database described in Section B1.4. For Type 1, 2, and 3 waters (pH 11.9 to 13.4),  $\text{Na}_2\text{U}_2\text{O}_7$  is the controlling solid

over most or all of the Eh range, as in the original models. The resulting dissolved U concentrations are similar and no more than an order of magnitude lower than when using the thermo.com.v8.r6+.dat database. (This summary excludes the waters—2C and 3B—for which Na was not listed. For both these waters, the Nuclear Energy Agency models yielded similar U concentrations to what was calculated using thermo.com.v8.r6+.dat, despite predicting schoepite instead of soddyite control at higher Eh.)

For the lower-pH Type 4 and 5 waters, the main contrast in model results is due to the absence of soddyite in the Nuclear Energy Agency database. For four of the five Type 4 and 5 waters for which Si was listed (excluding 4B and 4E), the original models predicted soddyite control of U solubility. In the Nuclear Energy Agency database models, the saturated solid is schoepite. This contrast yields higher dissolved U concentrations in the Nuclear Energy Agency runs by two to three orders of magnitude, as shown by the representative example in Figure B3–17. Soddyite was possibly omitted from the Japan Atomic Energy Nuclear Energy Agency-based database because the solubility constant for this mineral was merely a "guideline," rather than "recommended" by Guillaumont, et al. (2003). The guideline log K (equilibrium constant) for the soddyite dissolution reaction



in Guillaumont, et al. (2003, p. 255) is 6.2. We have tested the effect of adding this mineral to the Nuclear Energy Agency database. To enter this in NEA.dat, the reaction needs to be

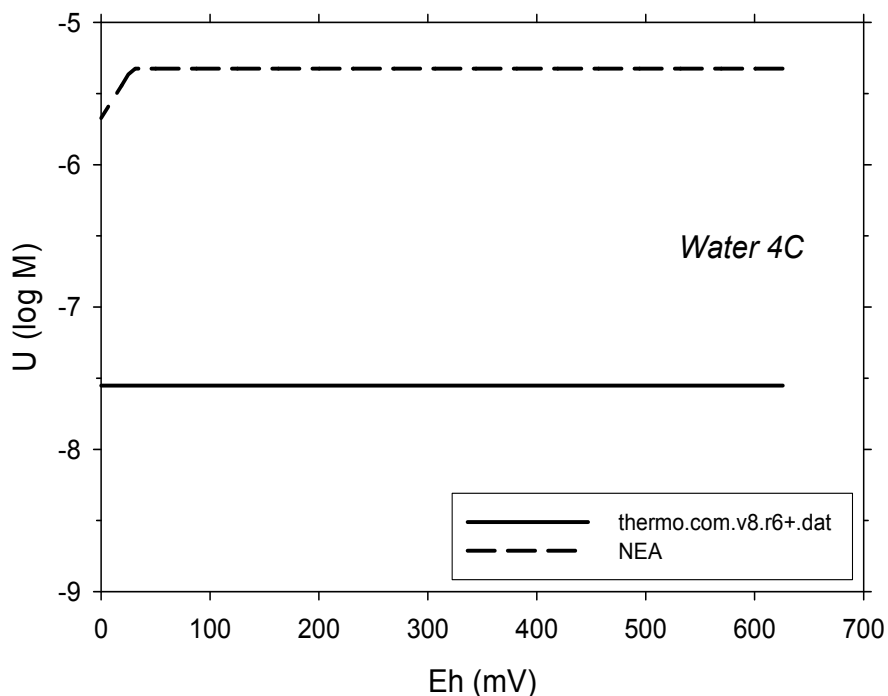
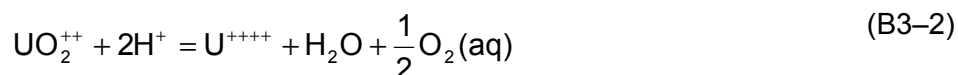
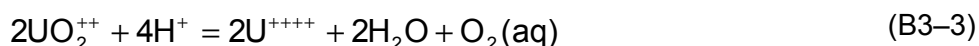


**Figure B3–17. Comparison of Uranium Solubility Limit Models for Water 4C (pH 10.0) Using Different Thermodynamic Databases**

expressed in terms of the aqueous species  $U^{++++}$  and  $H_4SiO_4$ ; the latter species is interchangeable with  $Si(OH)_4(aq)$  (Guillaumont, et al., 2003, pp. 255 and 498). The following reaction from NEA.dat



with a log K of -34.0020, was multiplied by two to get:



with a log K of -68.0040. Equation (B3-3) was added to Eq. (B3-1) to yield:



with a log K of -61.8.

An entry was added to NEA.dat with this reaction [Eq. (B3-4)] and equilibrium constant for the mineral soddyite. The Type 4 and 5 waters for which the original models predicted soddyite saturation (4A, 4C, 4D, and 5B) were run with this modified Nuclear Energy Agency database. In each case, soddyite did not reach saturation and the predicted dissolved U concentration was the same as for the models with the nominal Nuclear Energy Agency database (i.e., much higher than when using thermo.com.v8.r6+.dat; Figure B3-17). Soddyite was not, however, strongly undersaturated, with a saturation index (log Q/K) of -0.6 to -0.1. As a test, the log K for Eq. (B3-4) was changed in the modified NEA.dat file to -62.7 to reflect the use of a log K of 5.35 for Eq. (B3-1) (Giammar and Hering, 2002, after Nguyen, et al., 1992). In this case for waters 4A, 4C, 4D, and 5B, soddyite became the solubility-limiting mineral and dissolved U was lowered by less than 50 percent. This value of 5.35 is within the uncertainty assigned by Guillaumont, et al. (2003). A more recent determination of log K for Eq. (B3-10) is 6.43 (Gorman-Lewis, et al., 2007), which supports the Guillaumont, et al. (2003) guideline value of  $6.2 \pm 1.0$ . The preponderance of recent data on soddyite suggests that the Nuclear Energy Agency results with soddyite added provide reasonable results, with U concentrations as high as approximately  $10^{-5}$  M for pH below 11 (contrast with Figures B3-15 and B3-16). The original models using thermo.com.v8.r6+.dat, in which soddyite was much less soluble, may significantly underpredict U solubility limits in the presence of soddyite.

### B3.3.4 Conclusions

The broad outlines of model results are consistent with the summary of laboratory results as described at the end of Section B3.3.1. Most predicted U solubility limits lie between  $10^{-8}$  and  $10^{-5}$  M, with potential deviations to lower values under the most reducing conditions and to higher values if Na is especially low, such as in Types 2 and 3 waters. Uranium solubility limits are not amenable to generalizations. Clearly, simple assignment of U solubility limits to generic conditions must be carried out with great care, taking into particular consideration aqueous sodium, silica, and carbonate contents, as well as U mineral thermodynamic data.

## B3.4 Neptunium

Like U, Np aqueous behavior is sensitive to redox conditions and dissolved carbonate. Figure B3–18 shows the Eh–pH dependence of Np aqueous speciation in pure water; the two higher Eh species are  $\text{Np}^{\text{V}}$ , while the low-Eh species is  $\text{Np}^{\text{IV}}$ . As seen in Figure B3–19, addition of atmospheric  $\text{CO}_2$  gas replaces the high-pH hydroxide species with a variety of carbonate species. These anionic carbonate species may contribute to aqueous Np stability at high pH (e.g., Neck, 2006); note, however, that the relative sizes of the  $\text{Np}^{\text{V}}$  and  $\text{Np}^{\text{IV}}$  fields do not change dramatically. (Recall, as discussed in Section B3.3, that atmospheric  $\text{CO}_2$  may not apply during earlier stages of cement degradation.)

For young and moderately aged cement under reducing conditions (pH 12.5 and 10.5, respectively), Kaplan (2006) recommended Np solubility limits of  $5 \times 10^{-5}$  M and  $10^{-6}$  M as conservative and best values, respectively. For aged cements, Kaplan (2006) proposed corresponding limits of  $5 \times 10^{-4}$  M and  $10^{-5}$  M. For oxidizing conditions, the young and moderately aged cement conservative and best values were  $5 \times 10^{-7}$  M and  $10^{-8}$  M, respectively, while the corresponding values for aged cement were  $5 \times 10^{-6}$  M and  $10^{-7}$  M.

[Note that for Kaplan (2006), “aged” conditions assumed a pH of 5.5, corresponding to local groundwaters.]

### B3.4.1 Experimental Data

Experimental Np solubility data specific to cementitious conditions are rare. Ewart, et al. (1992, 1986) reported measured Np solubilities for cementitious pore waters in  $\text{CO}_2$ -free conditions.

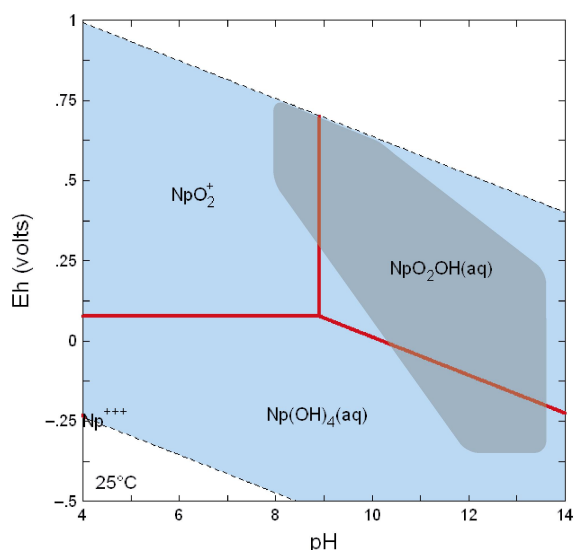


**Figure B3–18. Eh–pH Stability Fields for Aqueous Np ( $1 \times 10^{-8}$  M) in Pure Water at 25 °C [77 °F] (Solids Suppressed) Calculated Using Geochemist’s Workbench Version 6.0 With the thermo.com.v8.r6+.dat Database. The Shaded Area Represents the Approximate Range of Expected Conditions as Cement-Based Materials Degrade (Section B2). Addition of Sulfur Does Not Alter the Aqueous Species Fields. The Blue Field Defines Water Stability.**



match Np concentrations to  $\text{Np}^{\text{V}}$  thermodynamic models despite strong differences in experimental trends. Matches between models and experiments were possible because Ewart, et al. (1986) chose to neglect all Np hydroxyl species, whereas Neck, et al. (1992) were able to match their data using an existing stability constant for the  $\text{NpO}_2(\text{OH})_2^-$  species. Experimental and laboratory results from the latter study were further supported by Neck (2006). Some published models, like Ewart, et al. (1992), show quite low Np solubilities at highest pH. For example, Krupka and Serne (1998) calculated Np solubilities from pH 8 and +400 mV to pH 12.5 and Eh +200 mV; the value decreased monotonically from  $2 \times 10^{-3}$  to  $9 \times 10^{-6}$  M, respectively. The model of Krupka and Serne (1998) did include the  $\text{NpO}_2(\text{OH})_2^-$  species; the authors did not discuss why this species did not cause a Np increase at high pH, but it may be a result of the choice of hydrolysis constants. In all cases cited in this paragraph, the solubility-limiting solid was amorphous  $\text{NpO}_2\text{OH}$ .

For reducing conditions, Berner (2002, 1999) modeled Np solubilities of  $5 \times 10^{-9}$  M at pH 12.6 and 13.4, with Eh of -230 and -300 mV, respectively. The solubility-limiting solid was hydrated  $\text{Np}^{\text{IV}}\text{O}_2$ , and the aqueous species was  $\text{Np}^{\text{IV}}(\text{OH})_4(\text{aq})$ . These results generally agree with the  $\text{Np}^{\text{IV}}$  experimental results of Ewart, et al. (1992). Berner (2002) also calculated a concentration of  $10^{-3}$  M at pH 12.6 and Eh +350 mV, but much of this Np was attributed to a  $\text{Np}^{\text{VI}}$  species whose existence has not been confirmed. Based on models of concrete pore water, Allard and Torstenfelt (1985) selected a solubility limit of  $10^{-7}$  M for reducing conditions and  $10^{-6}$  M for oxidizing conditions.

### B3.4.3 New Models

New models were constructed in this study for the Np solubility limit using the water compositions discussed in Section B2.5. In the initial simulations using the thermo.com.v8.r6+.dat database,  $\text{NpO}_2$  was the solubility-limiting solid phase for all waters at all Eh levels. Excluding the pH 5.8 Savannah River Site groundwater, modeled solubilities varied over the large range from  $4 \times 10^{-18}$  M to  $2 \times 10^{-6}$  M, with strong Eh dependence. In high-pH waters (Types 1, 2, and 3), maximum Np concentrations were  $2 \times 10^{-11}$  M. These initial results clearly did not reproduce existing laboratory data, particularly considering the very low Np concentrations calculated at low Eh. Even the very low concentrations of around  $10^{-9}$  M at high pH from Ewart, et al. (1986) far exceed these values. Furthermore, the models are far below the well-constrained experimental values of Lierse, et al. (1985) and Neck, et al. (1992) and do not account for any increase in Np concentration at high pH due to the  $\text{NpO}_2(\text{OH})_2^-$  species (Neck, et al., 1992; Neck, 2006). The reason for the latter is that the thermodynamic database used for these calculations (thermo.com.v8.r6+.dat) includes only  $\text{NpO}_2\text{OH}(\text{aq})$  and  $\text{NpO}_2\text{OH}^+$  as  $\text{Np}^{\text{V}}$  hydrolysis products. In addition, there is no strong evidence for formation of  $\text{NpO}_2$  in published high-pH solubility experiments; in fact, investigators have concluded that  $\text{Np}^{\text{V}}\text{O}_2\text{OH}$  and  $\text{Np}^{\text{IV}}(\text{OH})_4$  were the solubility controlling phases.

Because  $\text{NpO}_2$  does not appear to be a suitable solubility-limiting solid phase for Np in cement-based systems, the new models were performed with  $\text{NpO}_2$  suppressed. The effect of this suppression on calculated Np concentration was large, particularly at lower Eh (Figure B3–20). In the new simulations, solubility was controlled by  $\text{Np}^{\text{IV}}(\text{OH})_4$  at lower Eh and by  $\text{Np}^{\text{V}}\text{O}_2\text{OH}(\text{am})$  on the flat portions of the curves at high Eh.  $\text{NpO}_2$  suppression was used in all simulations discussed further in this section.

The new model results are summarized on Figures B3–21 and B3–22. The majority of model Np concentrations lie between  $2 \times 10^{-9}$  M and  $4 \times 10^{-5}$  M. There is a strong Eh dependence

**Effect of NpO<sub>2</sub> Suppression on Neptunium Solubility Limit**

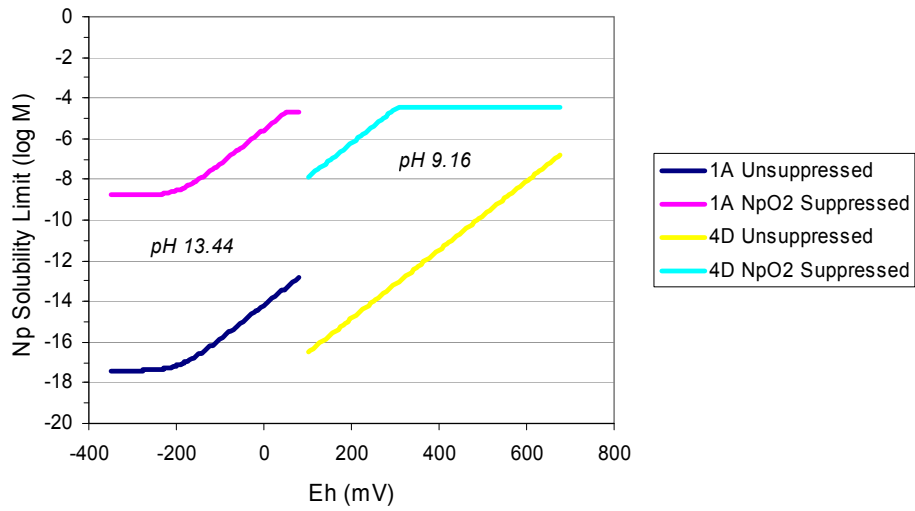


**Figure B3–20. Modeled Np Solubility Limit as a Function of Eh, Showing the Effect of Suppressing NpO<sub>2</sub> Solid on Results for Waters 1A and 4D**

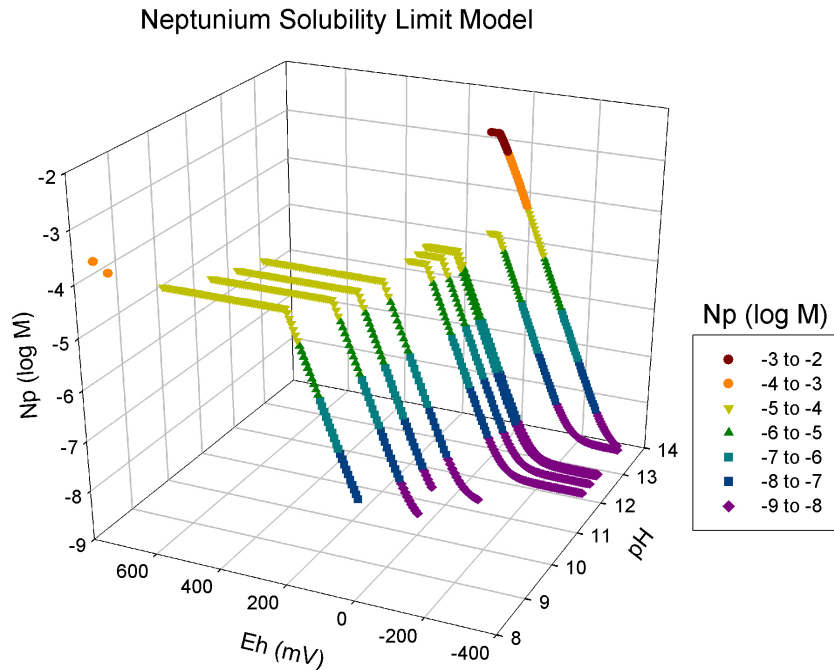


**Figure B3–21. Results of Np Solubility Limit Model Calculated Using Geochemist's Workbench Version 6.0 (SpecE8 and React Modules) With the thermo.com.v8.r6+.dat Thermodynamic Database. Plotted Np Concentrations Are Also Color-Coded. Model Values Are for Representative Waters in Table B2–1; Water 5A (pH 5.8) Is Not Shown. The Solid Phase NpO<sub>2</sub> Was Suppressed in the Models.**

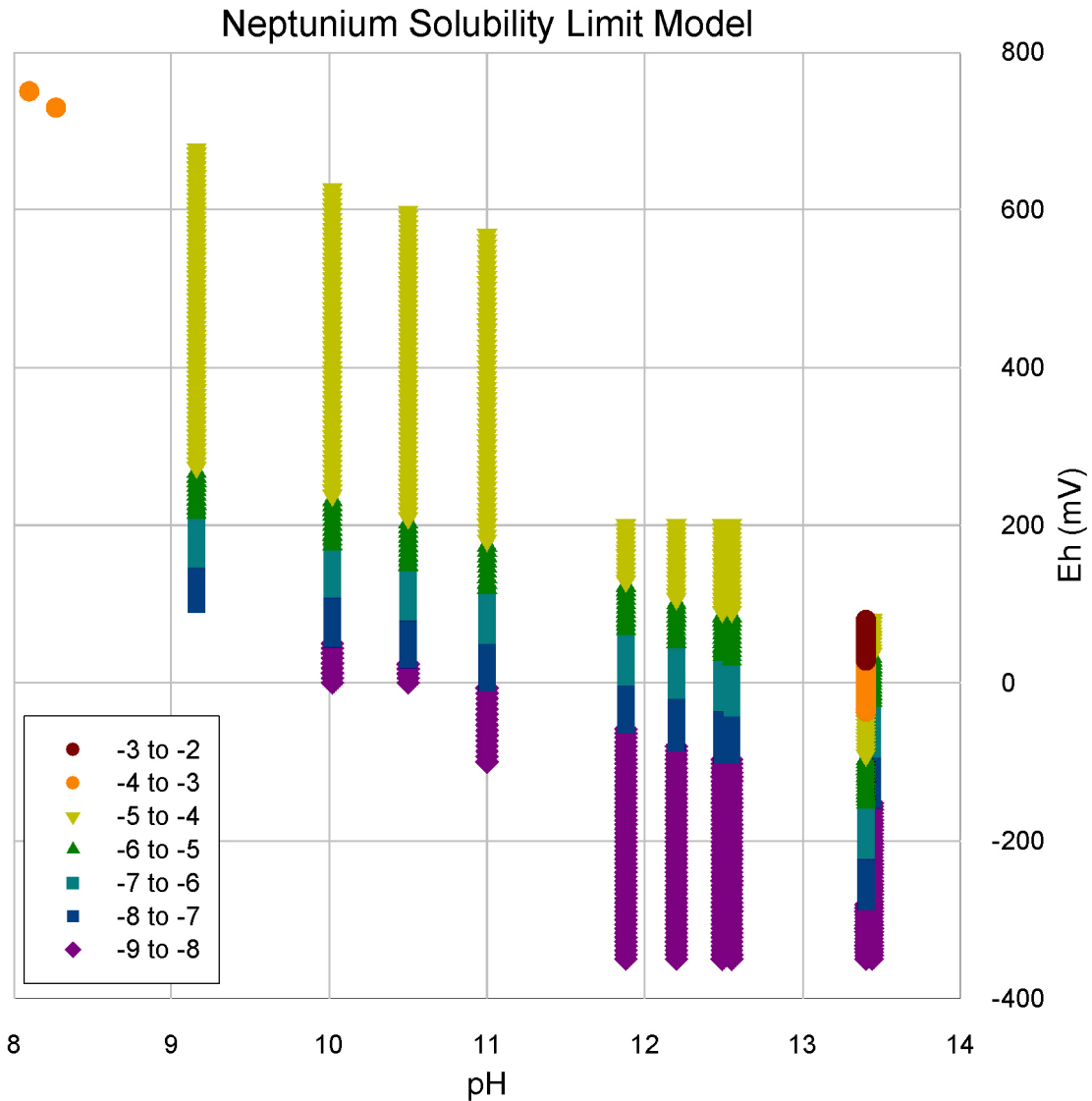


**Figure B3–22. Neptunium Solubility Model Results From Figure B3–21, Projected Onto the pH–Eh Plane. Symbols Refer to the Aqueous Np Concentration (log M).**

that indicates increasing stability of  $\text{Np}^{\text{V}}$  aqueous species—chiefly  $\text{NpO}_2\text{OH}(\text{aq})$ —at the expense of tetravalent  $\text{Np}(\text{OH})_4(\text{aq})$  as the system becomes more oxygenated. The solubility-limiting solid at lower Eh is  $\text{Np}^{\text{IV}}(\text{OH})_4$ , which is the active solid on the downward sloping and lowest portions of the curves in Figure B3–21. The results show that relatively low Np solubility limits are attainable if mildly reducing conditions can be maintained (less than 100 to  $-200$  mV, depending on pH; Figure B3–22). On the high-Eh plateaus (Figure B3–21),  $\text{Np}^{\text{V}}\text{O}_2\text{OH}(\text{am})$  controls solubility to around  $3 \times 10^{-5}$  M while values at about pH 8 are an order of magnitude higher.

An exception to these patterns is water 1B (pH 13.4; Table B2–1), which has unusually high carbonate and modeled Np solubility limits compared to other model cement-based system pore

waters (highest Np curve in Figures B3–21 and B3–22). This high carbonate content stabilizes the  $\text{NpO}_2(\text{CO}_3)_3^{5-}$  complex, enabling very high dissolved Np. It is not clear if such high aqueous carbonate (0.04 M) is achievable in unevolved cement-based systems, so this result must be interpreted with caution.

The lower carbonate contents of the other Type 1, 2, and 3 waters ( $\leq 2 \times 10^{-4}$  M) do not exhibit a significant impact on calculated Np concentrations. The effect of carbonate can also be seen when atmospheric  $\text{CO}_2$  fugacity is assumed to control dissolved carbonate for water 4D (pH 9.2) in place of the nominal carbonate content (see similar analysis for U in Section B3.3.3). A SpecE8 simulation at highest Eh results in a Np concentration of  $1 \times 10^{-3}$  M, compared with  $4 \times 10^{-5}$  M with the nominal composition. Clearly, Np solubility evaluations need to consider the potential for elevated carbonate contents.

Table B3–1 identifies and qualitatively ranks the important solution characteristics affecting modeled Np solubility limits.

This set of Np solubility models, with the same mineral suppressions, was also run using the Japan Atomic Energy Agency Nuclear Energy Agency-based database described in Section B1.4. When using the Nuclear Energy Agency database, modeled Np concentrations at higher Eh are much lower than when using thermo.com.v8.r6+.dat by up to four orders of magnitude (Figure B3–23). At lower Eh, models using both databases predict solubility control by amorphous hydrous Np(IV) oxides, though these are designated with different formulae [ $\text{NpO}_2(\text{am,hyd})$  in Nuclear Energy Agency and  $\text{Np}(\text{OH})_4$  in thermo.com.v8.r6+.dat]. At higher Eh (the plateaus in the representative comparisons of Figure B3–23), Nuclear Energy Agency models predict  $\text{Np}(\text{V})_2\text{O}_5$  solubility control, while  $\text{Np}(\text{V})\text{O}_2\text{OH}(\text{am})$  controlled solubility in the thermo.com.v8.r6+.dat models. Inspection of the database files and the Nuclear Energy Agency report by Guillaumont, et al. (2003) shows that there are two key differences in thermodynamic data accounting for the different model results. First,  $\text{Np}_2\text{O}_5$  is much less soluble in the Nuclear Energy Agency database. Second, the  $\text{NpO}_2\text{OH}(\text{aq})$  aqueous species is much less stable in the Nuclear Energy Agency database; this species is typically dominant in the thermo.com.v8.r6+.dat models, whereas it is replaced by  $\text{NpO}_2^+$ ,  $\text{NpO}_2(\text{OH})_2^-$ , or carbonate species in Nuclear Energy Agency models. Both effects can be seen in the higher Eh portions of Figure B3–23. In the water 2A model, both effects combine to make a difference of four orders of magnitude in modeled Np concentration. In water 4D,  $\text{NpO}_2\text{OH}(\text{aq})$  is not as dominant among Np aqueous species in the thermo.com.v8.r6+.dat model, because of the lower pH, such that the difference between the models is smaller and due mostly to contrasting  $\text{Np}_2\text{O}_5$  solubility. This difference of around two orders of magnitude was also obtained for the other lower pH waters (4E, 5A, and 5B).

These differences in thermodynamic data and modeled solubilities at higher Eh are not easily reconciled. For example, even if the Nuclear Energy Agency data correctly predicted  $\text{Np}_2\text{O}_5$  solubility, it is not clear whether it would be kinetically favored, nor is it clear how long  $\text{NpO}_2(\text{OH})(\text{am})$  would persist and whether it would be replaced by crystalline  $\text{Np}_2\text{O}_5$  in the long term. Experiments on Np solubility at elevated pH typically report  $\text{NpO}_2(\text{OH})(\text{am})$  as the precipitating solid (e.g., Lierse, et al., 1985; Neck, et al., 1992). In the case of aqueous species, the hydrolysis constant for  $\text{NpO}_2(\text{OH})(\text{aq})$  is a matter of some controversy (Neck, 2006; Rao, et al., 2006). In the absence of firm answers to these questions, the higher calculated solubility limits are favored.

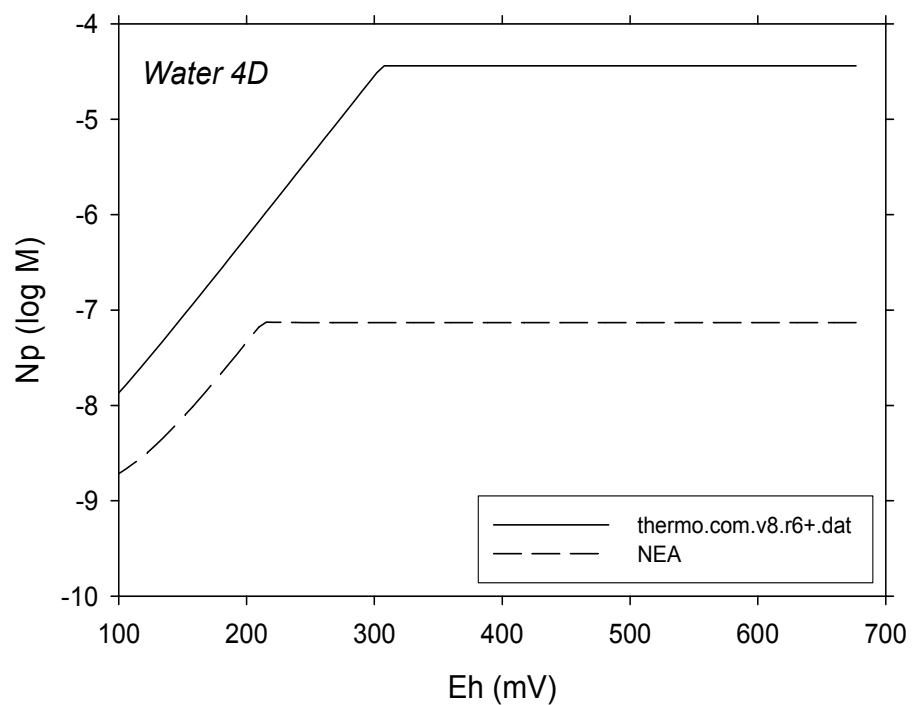
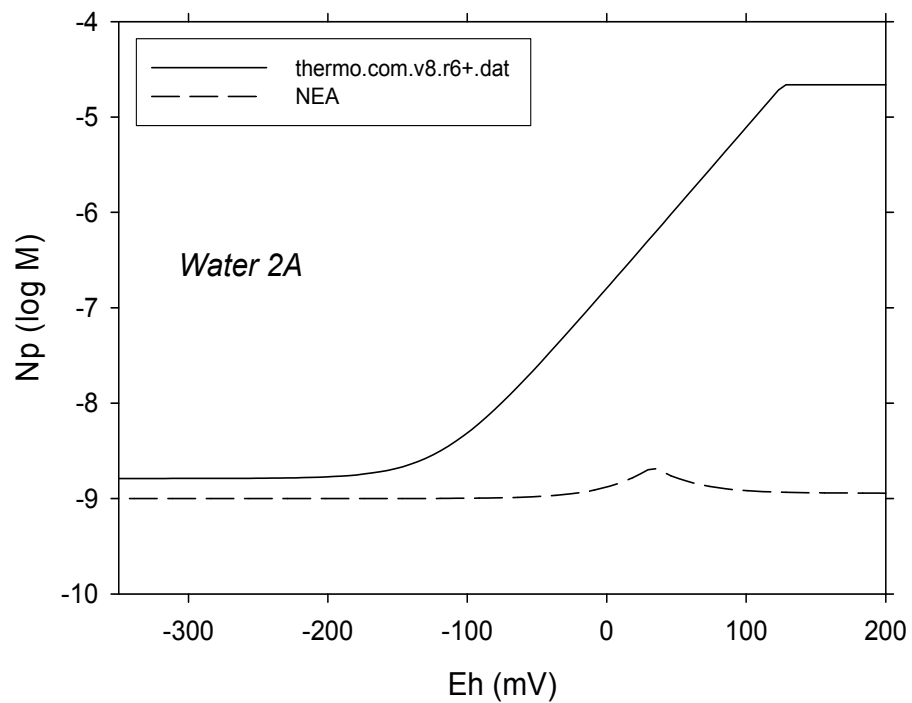


**Figure B3–23. Comparison of Neptunium Solubility Limit Models for Waters 2A (pH 12.2) and 4D (pH 9.2) Using Different Thermodynamic Databases**

### B3.4.4 Conclusions

The new model results agree broadly with experimental data (Section B3.4.1). Taking a conservative approach that favors higher solubility limits in light of uncertainties, the overall picture from surveying laboratory and model results is that in oxidizing systems, Np solubility varies from approximately  $10^{-4}$  M at pH 8 to  $10^{-5}$  M at pH 11–12 under oxidizing conditions. Concentrations may be higher at pH > 13, particularly in the unlikely event carbonate is abundant in solution. In oxidizing systems, dissolved Np will tend to be dominated by  $\text{NpO}_2\text{OH}(\text{aq})$  and  $\text{NpO}_2^+$ . Under reducing conditions, when  $\text{Np}^{\text{IV}}$  dominates in solution as  $\text{Np}(\text{OH})_4(\text{aq})$ ,  $10^{-8}$  M appears to represent a reasonable Np solubility limit, though values as low as  $10^{-9}$  M are possible at lowest Eh (Figures B3–21 and B3–22). These interpretations rely strongly on identifying the solubility-limiting solid phase and correctly modeling dissolved  $\text{Np}^{\text{V}}$  carbonate and hydroxyl species.

### B3.5 Plutonium

Plutonium geochemistry is complicated by the multiple coexisting oxidation states possible under aqueous conditions. Thermodynamically predicted dominant dissolved species are illustrated in Figures B3–24 and B3–25. In a carbonate-free system (Figure B3–24), the two higher Eh stability fields overlapped by the polygon represent  $\text{Pu}^{\text{V}}$  species, while the lower Eh species is  $\text{Pu}^{\text{IV}}$ . (Hexavalent Pu species are also present, but are subordinate in concentration.) When atmospheric  $\text{CO}_2$  is included (Figure B3–25), the  $\text{Pu}^{\text{V}}\text{O}_2\text{OH}(\text{aq})$  field is replaced by an

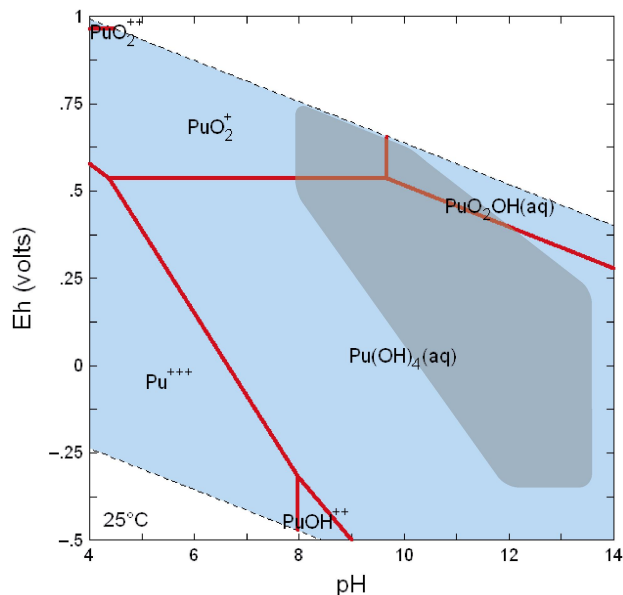


**Figure B3–24. Eh–pH Stability Fields for Aqueous Pu ( $1 \times 10^{-8}$  M) in Pure Water at 25 °C [77 °F] (Solids Suppressed) Calculated Using Geochemist’s Workbench Version 6.0 With the thermo.com.v8.r6+.dat Database. The Shaded Area Represents the Approximate Range of Expected Conditions as Cement-Based Materials Degrade (Section B2). Addition of Sulfur Does Not Alter the Aqueous Species Fields. The Blue Field Defines Water Stability.**

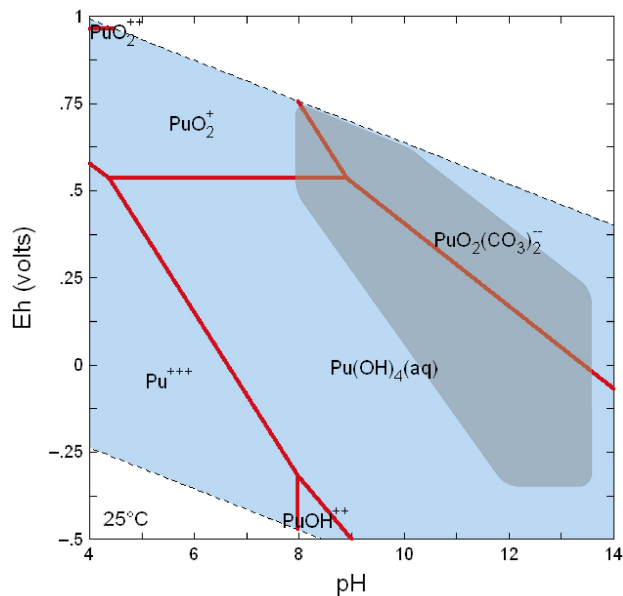


**Figure B3–25. Eh–pH Stability Fields for Aqueous Pu ( $1 \times 10^{-8}$  M) in Water at Equilibrium With CO<sub>2</sub> Gas at a Fugacity of  $10^{-3.5}$  atm at 25 °C [77 °F] (Solids Suppressed) Calculated Using Geochemist’s Workbench Version 6.0 With the thermo.com.r8.r6+.dat Database. The Shaded Area Represents the Approximate Range of Expected Conditions as Cement-Based Materials Degrade (Section B2). The Blue Field Defines Water Stability.**

expanded Pu<sup>VI</sup>O<sub>2</sub>(CO<sub>3</sub>)<sub>2</sub><sup>2-</sup> field, such that three Pu oxidation states are reflected in the dominant species over the range of expected chemistries. Because of the large size of the Pu(OH)<sub>4</sub>(aq) stability field even in carbonate-containing waters (Figure B3–25), Pu solubilities in cementitious waters may, overall, be somewhat less sensitive to carbonate content than U and Np. Nevertheless, Pu carbonate species must be considered (e.g., Yamaguchi, et al., 1994).

For young and moderately aged cement under reducing conditions (pH 12.5 and 10.5, respectively), Kaplan (2006) recommended Pu solubility limits of  $5 \times 10^{-9}$  M and  $10^{-10}$  M as conservative and best values, respectively. For aged cements, Kaplan (2006) proposed corresponding limits of  $5 \times 10^{-8}$  M and  $10^{-9}$  M. For oxidizing conditions, the young and moderately aged cement conservative and best values were  $5 \times 10^{-7}$  M and  $10^{-8}$  M, respectively, while the corresponding values for aged cement were  $5 \times 10^{-6}$  M and  $10^{-7}$  M. [Note that for Kaplan (2006) “aged” conditions assumed a pH of 5.5, corresponding to local groundwaters.]

### B3.5.1 Experimental Data

Ewart, et al. (1992) measured Pu solubility as a function of pH in a concrete-equilibrated water under a nitrogen atmosphere (<100 ppm O<sub>2</sub>). At pH 8, the Pu concentration was  $10^{-8}$  M, dropping to  $10^{-10}$  M at pH 9, then was constant out to pH 13 at around  $7 \times 10^{-11}$  M. The authors modeled this trend in concentration versus pH by assuming solubility control by a Pu(OH)<sub>4</sub> solid, with the dissolved Pu in the flat, high-pH portion dominated by the Pu(OH)<sub>4</sub>(aq) species. Greenfield, et al. (1998) also measured Pu in a concrete-equilibrated water under nitrogen atmosphere at pH 12 and Eh around 190 mV; they obtained a solubility of  $2 \times 10^{-10}$  M. These results suggest a solubility limit of  $10^{-10}$  M for Pu in cement pore water, rising to  $10^{-8}$  M as pH evolves below pH 9.

Studies not focused exclusively on cementitious systems provide further information on Pu solubility through the pH–Eh region of interest. In a series of experiments on Yucca Mountain region groundwaters adjusted to pH 8.5 (Eh ~270 mV), Nitsche, et al. (1994, 1993) obtained Pu concentrations of  $3 \times 10^{-7}$  and  $1 \times 10^{-6}$  M, with the solution dominated by Pu<sup>V</sup>. Another Yucca Mountain study (Efurd, et al., 1998) obtained a value of  $10^{-8}$  M for similar conditions. In interpreting these data and reporting new solids characterization results, Runde, et al. (2002) concluded that Pu concentrations were too high for equilibrium with a solid phase such as amorphous hydrated PuO<sub>2</sub> [sometimes denoted PuO<sub>2</sub>(am, hyd) or Pu(OH)<sub>4</sub>] and proposed that colloidal Pu<sup>IV</sup> species were responsible for the excess. Apparently, ultrafiltration at an estimated 4-nm [ $1.6 \times 10^{-7}$ ] pore size was insufficient to exclude these colloids from the solution.

Neck, et al. (2007) recently summarized data on Pu solubility in carbonate-free solutions, particularly from their studies and from Rai and coworkers (Rai, et al., 1999). For ultracentrifuged Pu solutions maintained in an argon atmosphere (<10 ppm O<sub>2</sub>), results were quite similar to Ewart, et al. (1992). Total dissolved Pu was at about  $10^{-8}$  M at pH 8, decreasing to  $10^{-10}$  M at pH 10, then remaining around  $10^{-10}$  M out to pH 13. The system was not particularly reducing, with Eh varying from about +250 mV to –50 mV as pH increased from 8 to 13. Neck, et al. (2007) modeled the results as resulting from solubility of a hydrous, mixed-valent Pu solid denoted as PuO<sub>2+x</sub>(am, hyd). Unfiltered solutions, however, showed a consistent colloidal Pu<sup>IV</sup> concentration of around  $10^{-8}$  M (log  $-8.3 \pm 1.0$ ) at pH 8 to 13, which the authors attributed to a reproducible equilibrium with dissolved Pu<sup>V</sup>. Neck, et al. (2007) argue that this colloidal component controls aqueous Pu over this pH range and cannot be disregarded. It bears repeating that these experiments do not include solution effects of dissolved carbonate, which is nonetheless relatively low in cementitious waters.

### B3.5.2 Literature Models

A number of researchers have attempted to model Pu solubility in cement pore waters; only a few examples are presented here. The model of Allard and Torstenfelt (1985), applied to both reducing and oxidizing conditions, used PuO<sub>2</sub> as the controlling phase and suggested a limit of less than  $10^{-10}$  M for cementitious waters with Pu(OH)<sub>4</sub>(aq) as the dominant aqueous species. The limit would be three to four orders of magnitude higher at highest pH if the Pu(OH)<sub>5</sub><sup>–</sup> species were stable, but this species has subsequently been shown to have low stability (e.g., Ewart, et al., 1992). Allard and Torstenfelt (1985) also showed that high aqueous carbonate would raise Pu concentrations by one to three orders of magnitude at pH above 8. As discussed in Section B3.5.1, models accompanying experiments by Ewart, et al. (1992) and Greenfield, et al. (1998) confirmed a Pu solubility limit of around  $10^{-10}$  M above pH 9 under conditions that were not strongly reducing. Ewart, et al. (1992) also matched the decrease to  $10^{-8}$  M at pH 8 with their Pu(OH)<sub>4</sub> solubility model.

Brady and Kozak (1995) simulated reactions between a pore water and portlandite and C-S-H under both atmospheric and nonoxygenated, non-CO<sub>2</sub>-exchanging conditions. The Pu concentration limit in the former case was  $2 \times 10^{-7}$  M because of Pu<sup>VI</sup>O<sub>2</sub>(OH)<sub>2</sub> solubility. For the nonatmospheric case, a model solubility limit of  $1 \times 10^{-10}$  M, similar to other published model results for cementitious conditions, was obtained. For pH 8 to 12.5 (with corresponding Eh varying from 400 to 200 mV), Krupka and Serne (1998) modeled a constant Pu solubility limit of  $1 \times 10^{-10}$  M, with Pu<sup>IV</sup>O<sub>2</sub>·H<sub>2</sub>O(am) as the controlling phase. Berner (2002) obtained a somewhat lower limit of  $4 \times 10^{-11}$  M at pH 12.6 and Eh below +300 mV. Clearly, a number of published models, using different codes and databases, have consistently yielded a limit of around  $10^{-10}$  M

for cementitious waters above pH 9. This can be attributed to the apparently low activities of Pu carbonate species and hydrolysis products more hydrolyzed than  $\text{Pu}(\text{OH})_4(\text{aq})$ .

As discussed in Section B3.5.1, the carbonate-free data and models of Neck, et al. (2007) confirm the trend of Ewart, et al. (1992), showing (i) a limit of around  $10^{-10}$  M for waters above pH 9 or 10 and (ii) a rise in solubility to about  $10^{-8}$  M as pH decreases to 8. This Pu mineral solubility trend for ultrafiltered solubility experiments is illustrated schematically in Figure B3–26. Neck, et al. (2007) propose solubility control by  $\text{PuO}_{2+x}(\text{am, hyd})$  for this trend, though in detail their curve rises somewhat at highest pH. The approximately  $10^{-8}$  M colloidal  $\text{Pu}^{\text{IV}}$  trend of Neck, et al. (2007) is also shown in Figure B3–26; the authors argue that this is a thermodynamically controlled concentration curve for unfiltered solutions and thus is more applicable to real systems as a concentration limit. This colloidal concentration is consistent with the data of Runde, et al. (2002).

### B3.5.3 New Models

New equilibrium solubility models were constructed for the water chemistries discussed in Section B2.5. In initial models,  $\text{PuO}_2$  was the solubility-limiting solid for all waters, constraining dissolved Pu to  $10^{-17}$  M at  $\text{pH} \geq 11.9$ , to between  $10^{-17}$  and  $10^{-14}$  M at  $\text{pH}$  9 to 11, and to between  $10^{-13}$  and  $10^{-11}$  M at  $\text{pH} < 9$ . These very low concentrations are inconsistent with experimental studies (Figure B3–26), which also have not identified nonhydrous  $\text{Pu}^{\text{IV}}$  oxide as a viable solid in cement-based systems. The models discussed in this section, therefore, were conducted with  $\text{PuO}_2$  suppressed. Representative effects of  $\text{PuO}_2$  suppression on

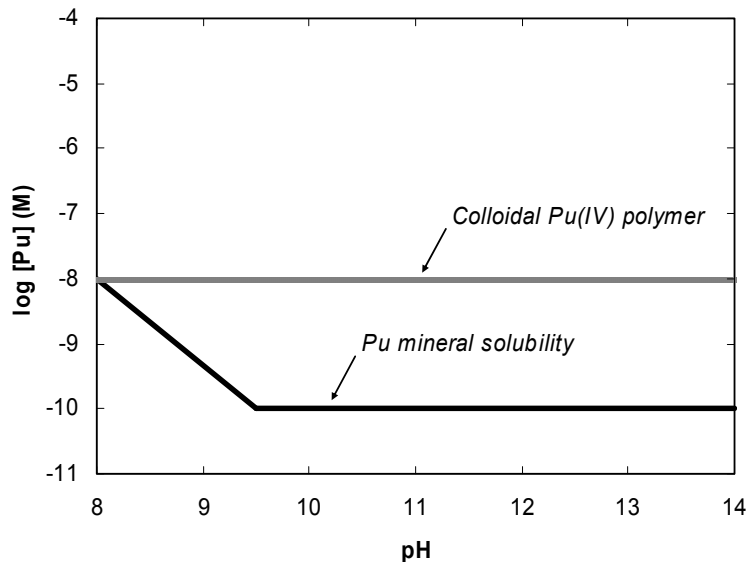


**Figure B3–26. Literature Pu Concentration Limit Trends for Cement-Based Systems. The Colloidal  $\text{Pu}^{\text{IV}}$  Polymer Value at Approximately  $10^{-8}$  M Is From Neck, et al. (2007). The Pu Mineral Solubility Trend Is From Ewart, et al. (1992); Neck, et al. (2007); and Others (See Text).**

Eh-dependent Pu solubility limit patterns are shown in Figure B3–27; modeled Pu concentration is 4 to 8 orders of magnitude higher when PuO<sub>2</sub> is suppressed. In addition, these new thermodynamic models do not account for potential formation of Pu colloids, which could stabilize water concentrations exceeding a theoretical solubility limit.

Model results are illustrated in Figures B3–28 and B3–29. With PuO<sub>2</sub> excluded, the new models predict solubility control by Pu oxyhydroxides, consistent with published experimental and modeling studies. Dissolved Pu is constant at  $2 \times 10^{-9}$  M over most of the Eh-pH space, with Pu(OH)<sub>4</sub> as the solubility-limiting solid and Pu(OH)<sub>4</sub>(aq) as the dominant aqueous species. In Type 4 waters between pH 9 and 11, Pu solubility rises with increasing Eh as the pentavalent species PuO<sub>2</sub><sup>+</sup> and PuO<sub>2</sub>OH(aq) become more stable, but decreases markedly to  $10^{-11}$  to  $10^{-10}$  M at even higher Eh when hexavalent PuO<sub>2</sub>(OH)<sub>2</sub> becomes the stable solid phase. The reason dissolved Pu concentration drops when PuO<sub>2</sub>(OH)<sub>2</sub> is the stable solid is because Pu<sup>IV</sup> and Pu<sup>V</sup> aqueous species become less stable and the PuO<sub>2</sub>(OH)<sub>2</sub> solubility is relatively low (Figure B3–30).

The high carbonate content of water 1B did not result in elevated Pu concentration at pH 13.4; carbonate Pu complexes in the model database are not strong at high pH. High Pu concentration is seen, however, in water 4E (pH 8.27) and Idaho National Laboratory groundwater 5B (pH 8.1), for which the models predicted that dissolved Pu was dominated by the Pu<sup>VI</sup> carbonate species PuO<sub>2</sub>(CO<sub>3</sub>)<sub>2</sub><sup>2-</sup>. That Pu<sup>VI</sup> carbonate species are important at lower pH under oxidizing conditions is also demonstrated by an alternative model applied to water 4D (pH 9.2), in which atmospheric CO<sub>2</sub> gas was set to constrain dissolved carbonate and calcite was used to constrain dissolved Ca. Dissolved carbonate concentration in the alternative

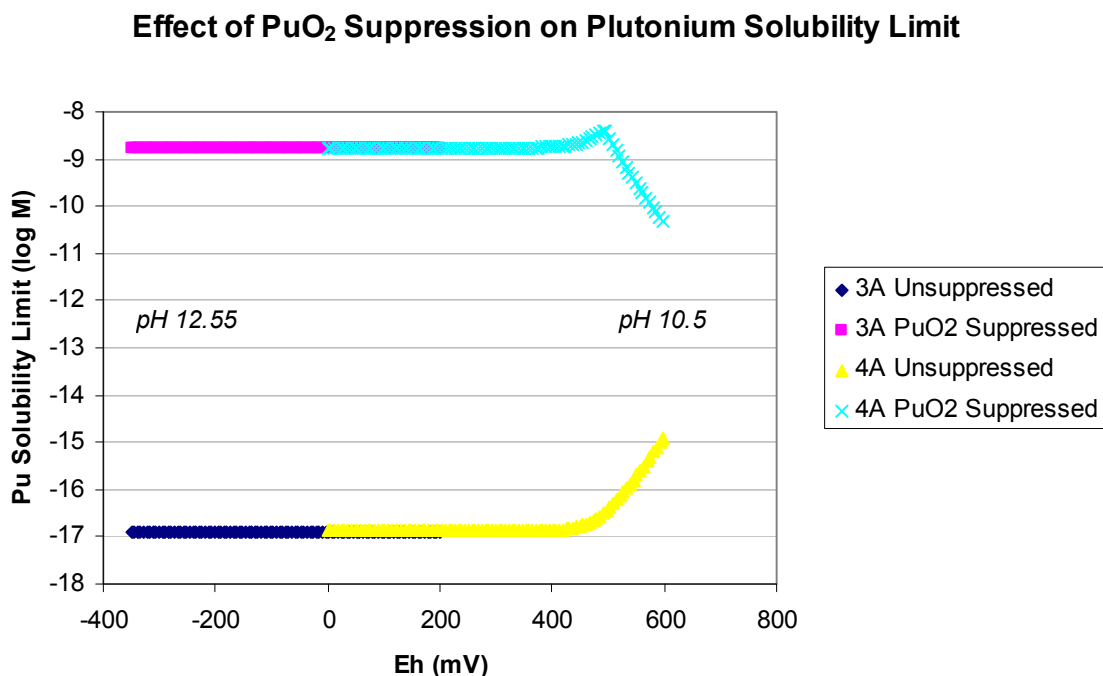


**Figure B3–27. Modeled Pu Solubility Limit As a Function of Eh, Showing the Effect of Suppressing PuO<sub>2</sub> Solid on Results for Waters 3A and 4A**

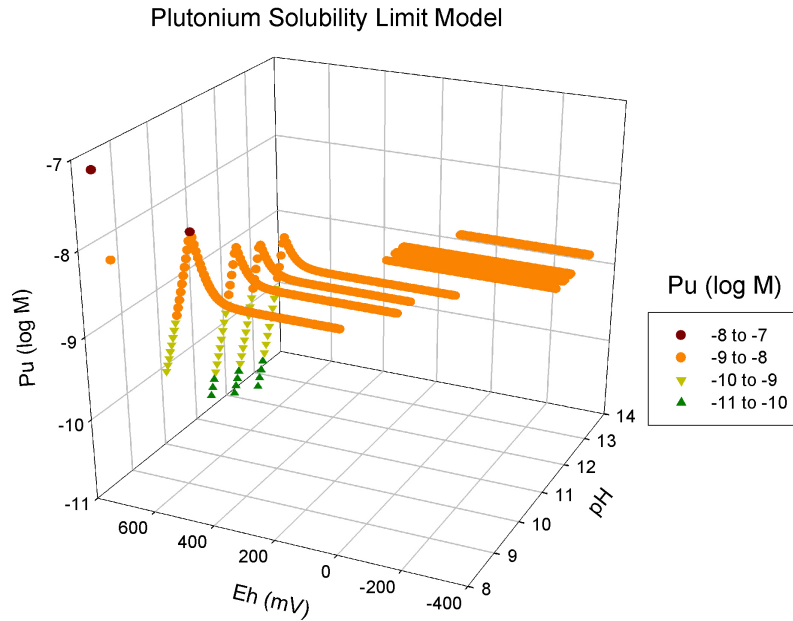


**Figure B3–28. Results of Pu Solubility Limit Model Calculated Using Geochemist’s Workbench Version 6.0 (SpecE8 and React Modules) With the thermo.com.v8.r6+.dat Thermodynamic Database. Plotted Pu Concentrations Are Also Color-Coded. Model Values Are for Representative Waters in Table B2–1; Water 5A (Ph 5.8) Is Not Shown. The Solid Phase PuO<sub>2</sub> Was Suppressed in the Models.**

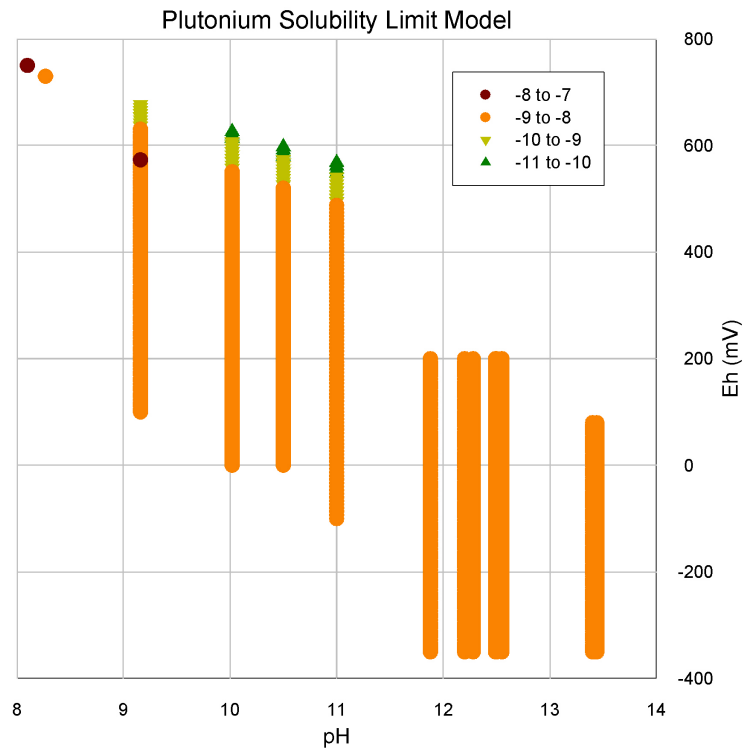


**Figure B3–29. Plutonium Solubility Model Results From Figure B3–28, Projected Onto the pH–Eh Plane. Symbols Refer to the Aqueous Pu Concentration (log M).**

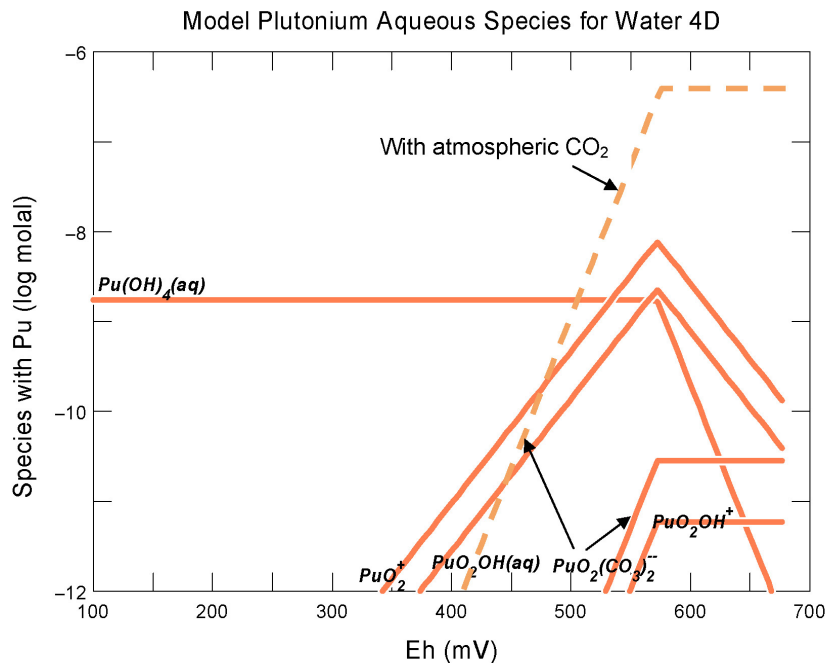


**Figure B3–30. Modeled Aqueous Pu Species Concentrations for Water 4D as Output by the Gtplot Module of Geochemist’s Workbench Version 6.0. The Solid Phase  $\text{PuO}_2$  Was Suppressed in the Model. Two Curves Are Shown for  $\text{PuO}_2(\text{CO}_3)_2^{2-}$ . The Solid Curve Represents the Nominal Model Composition, in Which Total Dissolved Pu Decreases at Eh above 570 mV. The Dashed Curve Shows the Increase in  $\text{PuO}_2(\text{CO}_3)_2^{2-}$  Species Concentration When Dissolved Carbonate Is Constrained by Atmospheric  $\text{CO}_2$ .**

model, at  $8 \times 10^{-3}$  M, is 100 times higher than in the original model. This elevated carbonate stabilizes the  $\text{Pu}^{\text{VI}}$  carbonate species  $\text{PuO}_2(\text{CO}_3)_2^{2-}$ , which dominates dissolved Pu (Figure B3–30). Calculated dissolved Pu as a function of Eh for the original and alternative models is shown in Figure B3–31. At highest Eh, dissolved Pu is over three orders of magnitude higher in the atmospheric  $\text{CO}_2$  model, owing to the higher dissolved carbonate. As was observed also for U and Np, if  $\text{CO}_2$  fugacities could rise toward atmospheric levels in carbonating systems, higher aqueous Pu concentrations could be attained.

The new model results have a similar overall range of Pu concentrations— $10^{-10}$  to  $10^{-8}$  M—as shown by the schematic mineral solubility curve in Figure B3–26 and also yield higher Pu concentrations at lower pH. Over most of the pH and Eh ranges, the model predicts Pu concentrations about one order of magnitude higher than published experiments and models suggested. Experimental studies have not confirmed the drop in dissolved Pu at higher Eh for pH 9 to 11 (Figure B3–29) perhaps due to the influence of atmospheric  $\text{CO}_2$  in laboratory studies, and this drop is not considered a reliable predictor. Our sensitivity study of the effect of dissolved carbonate showed that Pu concentrations exceeding  $10^{-7}$  M may be feasible under atmospheric  $\text{CO}_2$  conditions.

Table B3–1 identifies and qualitatively ranks the important solution characteristics affecting modeled Pu solubility limits.

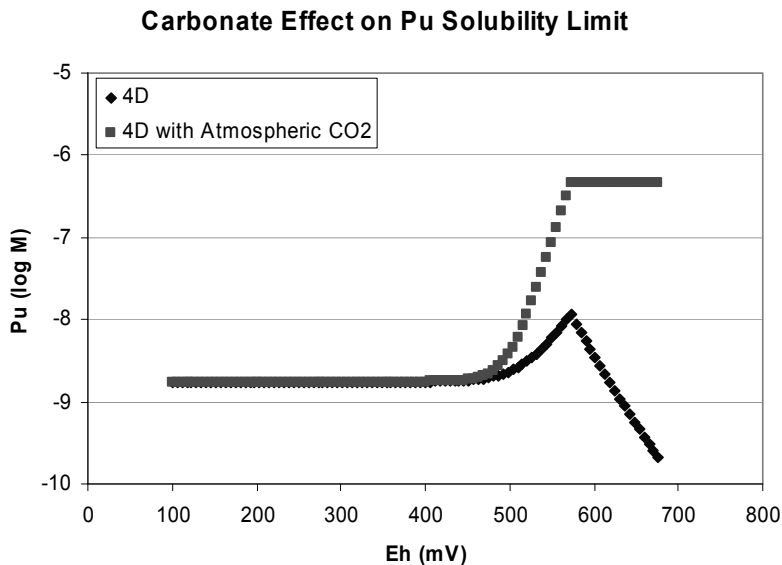


**Figure B3-31. Modeled Pu Solubility Limit in Water 4D With and Without Carbonate Control by Atmospheric CO<sub>2</sub> at a Log Fugacity of -3.5**

This set of Pu solubility models, with the same mineral suppressions, was also run using the Japan Atomic Energy Agency Nuclear Energy Agency-based database described in Section B1.4. Over the majority of the modeled Eh range, the Nuclear Energy Agency models yield Pu concentrations two orders of magnitude lower than the thermo.com.v8.r6+.dat models (Figure B3-32). The two sets of models predict equivalent hydrous Pu(IV) minerals over this range—PuO<sub>2</sub>(am,hyd) for the Nuclear Energy Agency runs and Pu(OH)<sub>4</sub> for thermo.com.v8.r6+.dat—but their solubility constants differ enough to account for the contrasting model results. The flat patterns seen for water 2C in Figure B3-32 are the same for all Type 1, 2, and 3 waters (i.e., pH > 11). The Type 4 waters have the same two-order-of-magnitude contrast at lower Eh, but have markedly different patterns at higher Eh (water 4A in Figure B3-32). While in the original runs, Pu(VI)O<sub>2</sub>(OH)<sub>2</sub> precipitation caused the drop in Pu concentration at high Eh; in the Nuclear Energy Agency runs, an analogous solid—PuO<sub>2</sub>(OH)<sub>2</sub>:H<sub>2</sub>O—is saturated only at the very highest Eh values. The rise in Pu concentration in the Type 4 Nuclear Energy Agency runs is due to increasing stability of the Pu(V)O<sub>2</sub><sup>+</sup>, Pu(V)O<sub>2</sub>OH(aq), and especially Pu(VI)O<sub>2</sub>(OH)<sub>2</sub>(aq) aqueous species in equilibrium with PuO<sub>2</sub>(am,hyd). The fact that the Pu(VI)O<sub>2</sub>(OH)<sub>2</sub>(aq) species is not present in thermo.com.v8.r6+.dat likely accounts for much of the high-Eh contrast in the two sets of model. This higher Pu concentration at high Eh for the Nuclear Energy Agency runs is also seen in water 4E and the Type 5 waters, with significant contributions from Pu carbonate species; the waters near pH 8 (4E and 5B) gave Pu concentrations of 7 × 10<sup>-7</sup> and 6 × 10<sup>-6</sup> M with the Nuclear Energy Agency database.

The lower Eh result from the thermo.com.v8.r6+.dat models of about 2 × 10<sup>-9</sup> M is a more conservative result than the Nuclear Energy Agency models. At highest Eh, the Nuclear Energy Agency model rise due to the Pu(VI)O<sub>2</sub>(OH)<sub>2</sub>(aq) species to over 10<sup>-8</sup> M provides an upper bound for pH 9 to 11, while concentrations may exceed 10<sup>-6</sup> M near pH 8 in the presence of carbonate.

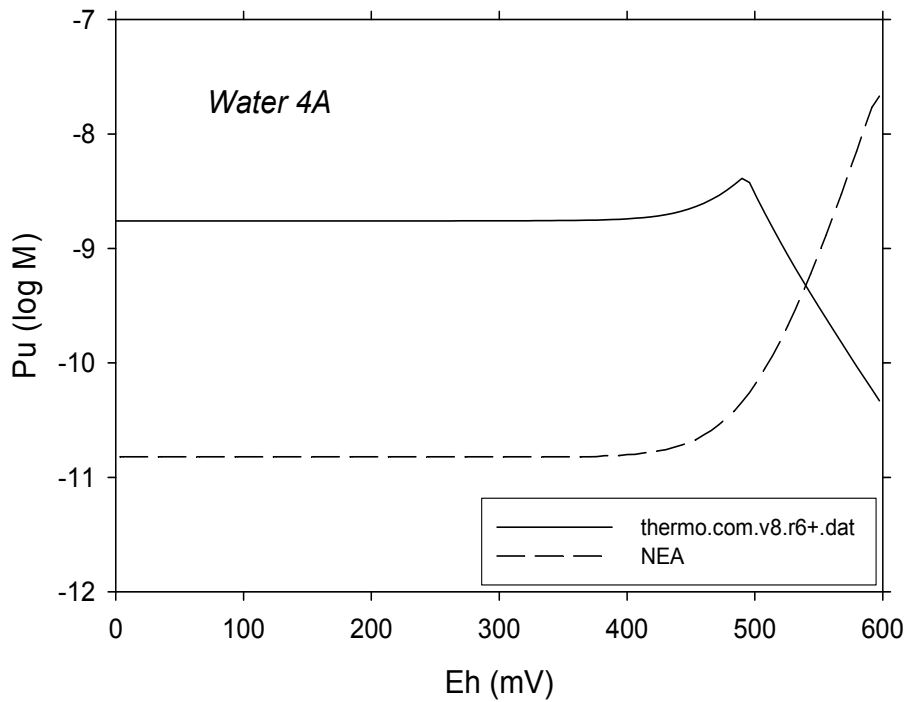
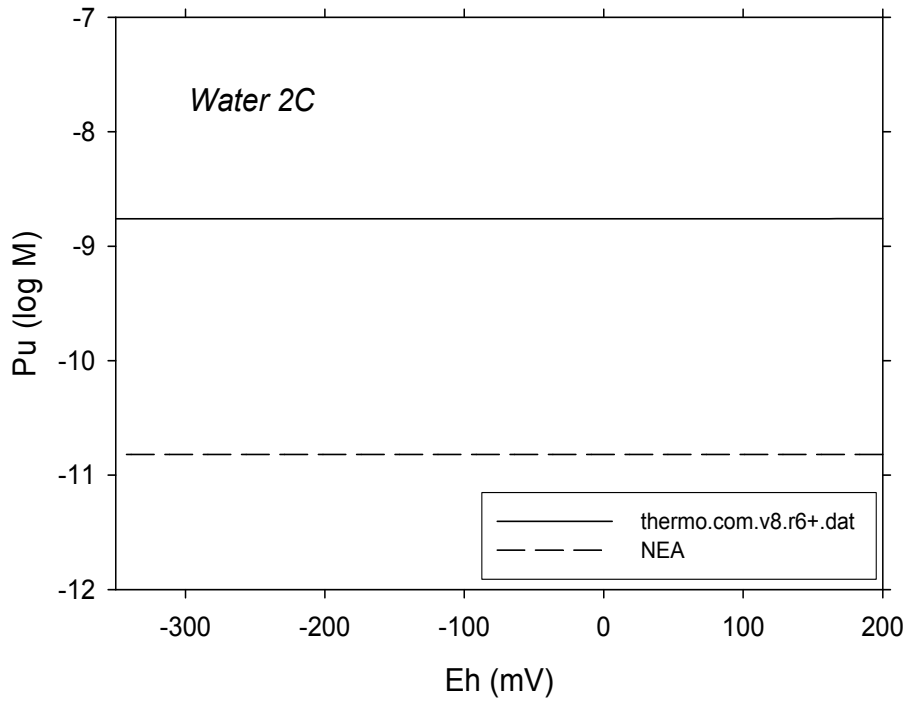


**Figure B3–32. Comparison of Plutonium Solubility Limit Models for Waters 2C (pH 12.3) and 4A (pH 10.5) Using Different Thermodynamic Databases**

### **B3.5.4 Conclusions**

The available data (Figure B3–26) and the new models suggest that, under most conditions in the considered Eh-pH space,  $2 \times 10^{-9}$  M is a reasonably conservative solubility limit for dissolved Pu. As degradation proceeds and pH decreases to a value of 9 and below, the limit on Pu concentrations is more appropriately defined as around  $10^{-8}$  M. Elevation of dissolved carbonate due to atmospheric CO<sub>2</sub> could, however, stabilize Pu concentrations greater than  $10^{-6}$  M. Aqueous carbonate content needs to be well constrained if the Pu solubility limit is to be better defined. The constant, apparently equilibrium  $10^{-8}$  M value for colloidal Pu<sup>IV</sup> polymer over this pH range (Neck, et al., 2007) may more realistically reflect a maximum Pu concentration for most EH values, unless the potential for colloid mobilization can be otherwise excluded.

## **B4 SOLUBILITY SUMMARIES FOR OTHER RELEVANT ELEMENTS**

This section summarizes solubility information for the other elements not detailed in Section B3.

### **B4.1 Carbon**

Carbon-14 may be present in residual waste inventories, and C-14 chemistry is influenced by factors such as carbon dioxide exchange, isotopic exchange, and precipitation. Two recent studies estimate values for solubility of carbon in cementitious waters. Kaplan (2006) recommends a lower solubility at higher pH for both oxidizing and reducing conditions. For young cement at pH 12.5, solubility is approximately  $5 \times 10^{-5}$  M and  $5 \times 10^{-6}$  M for conservative and best values, respectively, and  $5 \times 10^{-3}$  and  $5 \times 10^{-4}$  M for conservative and best values of moderately aged cement at pH 10.5. Krupka, et al. (2004) recommend nearly identical values for both young and moderately aged concrete and appear to be the source of data for Kaplan (2006). Using geochemical reaction path modeling, Brady and Kozak (1995) report carbon solubility at  $6 \times 10^{-4}$  M for oxygenated environments and  $2 \times 10^{-3}$  M for nonoxygenated, CO<sub>2</sub>-free exchange environments. Carbon-14 may be sequestered during carbonation of cement and diluted by ambient nonradioactive carbon in both precipitates and solution. Applying a carbon solubility limit to dissolved C-14 is, therefore, a conservative model approach if the limit is applied only to C-14 and not to bulk carbon.

### **B4.2 Nickel**

Nickel is found in cementitious waters as Ni<sup>2+</sup>. Ochs, et al. (1998) reported experimental solubility of nickel in cementitious waters for fresh cement at pH 13.2 as  $3 \times 10^{-7}$  M. Solubility decreased for portlandite cement at pH 12.5 to less than  $5 \times 10^{-8}$  M. Kaplan (2006) recommends similar conservative and best nickel solubility values of  $5 \times 10^{-6}$  and  $5 \times 10^{-7}$  M, respectively, for both oxidizing and reducing cements at pH 12.5 and 10.5. Krupka, et al. (2004) recommended  $5 \times 10^{-4}$  M and  $5 \times 10^{-7}$  M as conservative and best values, respectively, for young concrete (pH 12.5), with corresponding values of  $5 \times 10^{-4}$  M and  $5 \times 10^{-6}$  M for moderately aged concrete (pH 10.5).

Berner (2002, 1999) calculated nickel solubilities of  $3 \times 10^{-4}$  to  $3 \times 10^{-6}$  M for pH 13.4 and  $3 \times 10^{-7}$  M for pH 12.6. Krupka and Sterne (1998), however, calculated lower values, decreasing with increasing pH from  $6 \times 10^{-6}$  M at pH 9 to  $8 \times 10^{-8}$  at pH 12.5. Brady and Kozak

(1995) modeled nickel solubility at  $4 \times 10^{-4}$  M for oxygenated environments and  $8 \times 10^{-13}$  M for nonoxygenated, CO<sub>2</sub>-free exchange environments.

In summary, most accepted nickel solubility values are close to  $10^{-6}$  M in order of magnitude, but range from as high as  $3 \times 10^{-4}$  M at pH 13.4 (Berner, 1999) to  $1 \times 10^{-8}$  M at pH 11.5 (Krupka and Serne, 1998).

### **B4.3 Strontium**

Strontium is divalent in solution. Reported solubility values for strontium vary by several orders of magnitude among various studies. Serne, et al. (1996) report experimental concentrations in cement leachate as high as  $3 \times 10^{-3}$  M at pH 9 to 13. Berner (2002) recommended strontium solubility of  $3 \times 10^{-3}$  M for pH 12.6 and  $1 \times 10^{-6}$  M for pH 13.4. Ochs, et al. (1998) accepted a literature solubility of  $1 \times 10^{-4}$  M in fresh cementitious water with pH 13.2. Similarly, Brady and Kozak (1995) modeled strontium solubility at  $2 \times 10^{-5}$  M for both oxygenated and nonoxygenated, CO<sub>2</sub>-free exchange environments.

Recommended values by Kaplan (2006) and calculated values by Krupka and Serne (1998) are significantly lower. Both recommend conservative and best values of  $5 \times 10^{-6}$  M and  $5 \times 10^{-7}$  M, respectively, for oxidizing and reducing conditions in pH 12.5 and pH 10.5 waters. Krupka, et al. (2004) suggested conservative and best solubility values of  $2 \times 10^{-5}$  M and  $1 \times 10^{-7}$  M, respectively, for pH 12.5 cementitious waters, increasing to  $2 \times 10^{-4}$  M and  $1 \times 10^{-6}$  M at pH 10.5.

### **B4.4 Niobium**

Kaplan (2006) and Berner (2002) concluded that Niobium (V) has no solubility constraints for cementitious pore waters at pH of 5.5–12.5. Talerico, et al. (2004), however, report a decrease in solubility from  $2 \times 10^{-5}$  to  $2 \times 10^{-9}$  M with an increase in pH from 9 to 12. Krupka, et al. (2004) recommended conservative and best solubility values of  $5 \times 10^{-4}$  M and  $5 \times 10^{-6}$  M, respectively, for young near-field concrete (pH 12.5) but  $1 \times 10^{-3}$  M and  $5 \times 10^{-4}$  M for moderately aged concrete water at pH 10.5.

### **B4.5 Tin**

Tin is typically present as Sn<sup>4+</sup> in cementitious waters. Ochs, et al. (1998) determined experimental tin solubility in cementitious water to be nontemperature-dependent and in the range of  $3 \times 10^{-6}$  M for fresh cement at pH 13.2 and  $4 \times 10^{-8}$  M for a pH 12.5 portlandite solution. Kaplan (2006) recommends similar values of  $5 \times 10^{-7}$  and  $10^{-8}$  M as conservative and best values, respectively, at oxidizing and reducing conditions at both pH 10.5 and 12.5. Experimentally, Aggarwal, et al. (2001) determined solubility of  $3 \times 10^{-8}$  to  $4 \times 10^{-7}$  M with CaSn(OH)<sub>6</sub> as the limiting phase. For near-field water of high pH and young concrete water at 12.5, Krupka, et al. (2004) recommended a slightly higher conservative and best values of  $5 \times 10^{-4}$  and  $5 \times 10^{-6}$  M, increasing to  $1 \times 10^{-3}$  and  $5 \times 10^{-4}$  M at pH 10.5. Berner (2002, 1999) also suggested a best estimate of  $10^{-5}$  M for pH 13.4 and  $10^{-7}$  M at pH 12.6 for cement pore waters.

## **B4.6 Iodine**

Iodine, a halogen, is highly soluble and is typically in solution as iodide. Several studies, including those by Kaplan (2006), Krupka, et al. (2004), Aggarwal, et al. (2001), and Berner (2002), conclude that iodine does not have solubility constraints in cementitious waters, regardless of the pH. Specifically studied pH values cover the range 5.5 to 12.5.

## **B4.7 Cesium**

Cesium is considered to have no solubility constraints in cementitious pore water, regardless of pH. Kaplan (2006), Krupka, et al. (2004), and Berner (1999) each concluded that cesium is not solubility limited.

## **B4.8 Lead**

Lead is among the more soluble of radioelements and is typically present in solution as  $Pb^{2+}$ . Ochs, et al. (1998) demonstrated that lead solubility in cementitious waters of fresh cement (pH 13.2) is  $1 \times 10^{-2}$  M at 22 °C [77 °F] in a  $CO_2$ -free atmosphere. For leached cement (pH 12.5), the solubility was lower ( $4.3 \times 10^{-3}$  M). Sanchez, et al. (2002) reported lower Pb concentrations of about  $2 \times 10^{-5}$  M in noncarbonated solutions in this same pH range, with Pb concentration decreasing as pH decreased to 9. However, unlike the results of Ochs, et al. (1998), these data were from static leaching tests on a Portland cement mixture that could have included the effects of coprecipitation and sorption. The data of Sanchez, et al. (2002), therefore, are not considered applicable as solubility limits.

Kaplan (2006) recommended the same conservative and best solubilities,  $5 \times 10^{-7}$  and  $5 \times 10^{-8}$  M, respectively, for oxidizing cements at pH 12.5 and 10.5 and reducing cements at pH 12.5 and 10.5. These values are taken from those Krupka, et al. (2004) reported for pH 12.5 and 10.5. These results are given as best and conservative values in the context of a near-field environment and on the basis of the presence of lead hydroxy-carbonates, but the supporting information is not traceable from the sources provided in the reference. Kaplan and Myers (2001) calculated very high solubility limits for Pb at pH 12.2 to 12.8.

## **B4.9 Americium**

Americium is typically in solution as a trivalent cation. Ewart, et al. (1992) conducted experiments with americium in cement-equilibrated water with low redox potential that demonstrated a decrease in solubility with increase in pH. Concentrations decreased from  $10^{-7}$  M at pH 8 to  $5 \times 10^{-8}$  M in the range of pH 8.5 to 10.5 and decreased to  $10^{-10}$  M at pH 11 and higher. These experiments were conducted in the presence of calcium carbonate to control the carbonate level in solution and in a nitrogen environment to reduce the atmospheric partial pressure of  $CO_2$  to negligible. They also calculated solubilities the HARPHRQ model predicted, using the HATCHES database (Cross and Ewart, 1990). Calculated results are similar to experimental results.

Krupka and Serne (1998) used MINTEQA2 to calculate values for solubility of trivalent americium in cementitious pore waters, which demonstrated a generally decreasing trend in solubility as pH increases (from  $4 \times 10^{-9}$  M at pH 9.5 to  $2 \times 10^{-12}$  M at pH 12.5). Berner (2002, 1999) reported calculation of a higher solubility limit of  $2 \times 10^{-9}$  M for both pH 13.4 and pH 12.6.

Similarly, Brady and Kozak (1995) reported a calculated americium solubility of  $1 \times 10^{-9}$  M for oxygenated environments and  $4 \times 10^{-9}$  M for nonoxygenated, CO<sub>2</sub>-free exchange environments.

Estimates by Kaplan (2006) of americium solubility vary with pH and type of cement. For young cement at oxidizing conditions and pH close to 12.5, the best estimate solubility is  $5 \times 10^{-10}$  M, similar to the Ewart, et al. (1992) values. Solubility was higher at  $5 \times 10^{-7}$  M for moderately aged, oxidizing cement at pH 10.5. The same estimates are given for reducing conditions at the same pH values and age of cement. Greenfield, et al. (1998) estimate a value of  $5 \times 10^{-11}$  M for experiments using concrete water at pH 12.0 to 12.3, in agreement with a model value.

Other studies show similar results. Krupka, et al. (2004) recommended conservative and best values of  $1 \times 10^{-7}$  and  $1 \times 10^{-9}$  M, respectively, for americium in young concrete at pH 12.5 and  $3 \times 10^{-7}$  and  $3 \times 10^{-8}$  M at the lower pH of 10.5 in moderately aged concrete.

Allard and Torstenfelt (1985) calculated an americium solubility of  $10^{-5}$  to  $10^{-6}$  M in concrete pore waters, assuming stability of the Am(OH)<sub>4</sub><sup>-</sup> aqueous species; the solubility would be much lower at  $10^{-8}$  M if only Am(OH)<sub>3</sub>(aq) were considered. Counter to the Ewart, et al. (1992) findings, Allard and Torstenfelt (1985) concluded that as pH increases, total americium concentration increases. This difference may be due to the inclusion in the Allard and Torstenfelt (1985) model of the highly soluble americium hydroxyl complex Am(OH)<sub>4</sub><sup>-</sup>, which has not been substantiated in subsequent studies.

Overall, Allard and Torstenfelt (1985) give the highest potential solubility as  $10^{-5}$  to  $10^{-6}$  M at pH 13.5, and Krupka and Serne (1998) recommend the lowest solubility as  $2 \times 10^{-12}$  M for pH 12.5. There are several orders of magnitude difference among the various recommendations, and all values at high pH fall in between those values.

## **B4.10 Curium**

Curium solubility behavior is understood by analogy to Am and trivalent lanthanides; its solubility tends to decrease as pH increases. Kaplan (2006) concluded that data for both oxidizing and reducing conditions of young cement (pH 12.5) suggest a solubility of  $5 \times 10^{-10}$  M as a conservative value and  $5 \times 10^{-11}$  M as a best value. For moderately aged cement at pH 10.5, Kaplan (2006) recommended  $5 \times 10^{-7}$  and  $5 \times 10^{-8}$  M as conservative and best values. Calculated values by Krupka and Serne (1998) are similar, but depend only on the pH of the solution in the calculations. They estimate a  $1 \times 10^{-7}$  and  $1 \times 10^{-9}$  M (conservative/best values) for young cement and  $3 \times 10^{-7}$  and  $3 \times 10^{-8}$  M (conservative/best values) for moderately aged cement.

## **B5 CONCLUSIONS**

Sections B3.1.4, B3.2.4, B3.3.4, B3.4.4, and B3.5.4 summarize detailed solubility evaluations for Se, Tc, U, Np, and Pu, while Section B4 summarizes the solubility information for other elements. Important considerations for evaluating solubility limits that are evident in this report are

- The basis for solubility estimations are limited by the investigator's ability to predict geochemical conditions. For example, any solubility limitations on Se and Tc depend

markedly on the ability of the cementitious system to maintain strongly reducing conditions for an extended period of time.

- Degradation experiments and models focused on the longevity of reducing conditions will help reduce uncertainty in solubility behavior, particularly for Tc. Solubility experiments on Tc should be targeted to the relevant conditions.
- Solubility models should not be used to recommend solubility values without considering experimental literature. For example, if the Pu<sup>IV</sup> model of Neck, et al. (2007) is correct, then existing equilibrium modeling codes will predict incorrect Pu concentration limits.
- The quality and comprehensiveness of the supporting thermodynamic database are critical to modeling and evaluating equilibrium solubility limits.
- Identification of the proper solubility-limiting phase is essential to successful modeling. A model cannot be assumed to predict a real system if nonequilibrium effects are important. This observation points once again to the importance of experimental studies, which have often lacked definitive information on solid phases. Combined methods, including advanced spectroscopy, should be used to identify precipitated solid phases in solubility experiments.
- Water chemistry must be completely characterized so that solid phases and aqueous species are accurately predicted. In addition to pH and Eh, important aqueous components that should be well-characterized for degrading cement-based systems include Na, Si, Ca, and carbonate. Performance assessment sensitivity analyses on solubility limits should consider potentially significant uncertainties in these geochemical parameters.
- For U, Np, and Pu, laboratory experiments specifically targeted to water compositions during progressive degradation of cement-based materials would help reduce uncertainties related to effects of compositional parameters such as aqueous carbonate.
- The solubility effects of cement admixtures may be significant and should be addressed in experimental studies.

## B6 REFERENCES

Aggarwal, S., M.J. Angus, R.C. Hibbert, and A. Tyson. "Radionuclide Concentration in Cementitious Pore-Fluids Extracted Under High Pressure." AEAT/R/ENV/0231. Windscale, United Kingdom: AEA Technology. 2001.

Allard, B. and B. Torstenfelt. "Actinide Solubilities and Speciation in a Repository Environment." Technical Report NTB 85-18. Baden, Switzerland: NAGRA. 1985.

Angus, M.J. and F.P. Glasser. "The Chemical Environment in Cement Matrices." Materials Research Society Symposium Proceedings. L.O. Werme, ed. Pittsburgh, Pennsylvania: Materials Research Society. pp. 547–556. 1985.

Atkins, M., F.P. Glasser, and L.P. Moroni. "The Long-Term Properties of Cement and Concretes." *Materials Research Society Symposium Proceedings* Vol. 212. T. Abrajano, Jr. and L.H. Johnson, eds. Pittsburgh, Pennsylvania: Materials Research Society. pp. 373–386. 1991.

Bayliss, S., A. Haworth, R. McCrohon, A.D. Moreton, P. Oliver, N.J. Pilkington, A.J. Smith, and J.L. Smith-Briggs. "Radioelement Behaviour in a Cementitious Environment." *Materials Research Society Symposium Proceedings* 257. C.G. Sombret, ed. Pittsburgh, Pennsylvania: Materials Research Society. pp. 641–648. 1992.

Berner, U. "Project Opalinus Clay: Radionuclide Concentration Limits in the Cementitious Near-Field of an ILW Repository." PSI Bericht 02-26, Nagra NTB 02-22. Villigen, Switzerland: Paul Scherrer Institute. 2002.

———. "Concentration Limits in the Cement Based Swiss Repository for Long-Lived, Intermediate-Level Radioactive Wastes (LMA)." PSI Bericht 99-10. Villigen, Switzerland: Paul Scherrer Institute. 1999.

———. "Evolution of Pore Water Chemistry During Degradation of Cement in a Radioactive Waste Repository Environment." *Waste Management*. Vol. 12. pp. 201–219. 1992.

Berry, J.A., J. Hopley, S.A. Lane, A.K. Littleboy, M.J. Nash, P. Oliver, J.L. Smith-Briggs, and S.J. Williams. "Solubility and Sorption of Protactinium in the Near-Field and Far-Field Environments of a Radioactive Waste Repository." *Analyst*. Vol. 114. pp. 339–347. 1989.

Bethke, C.M. *Geochemical Reaction Modeling, Concepts, and Applications*. New York City, New York: Oxford University Press. 1996.

Bradbury, M.H. and F.-A. Sarott. "Sorption Databases for the Cementitious Near-Field of a L/ILW Repository for Performance Assessment." PSI Bericht 95-06. Villigen, Switzerland: Paul Scherrer Institute. 1995.

Brady, P.V. and M.W. Kozak. "Geochemical Engineering of Low-Level Radioactive Waste in Cementitious Environments." *Waste Management*. Vol. 15. pp. 293–301. 1995.

Cross, J.E. and F.T. Ewart. "HATCHES—A Thermodynamic Database Management System." Nirex Report NSS/R212. United Kingdom: Nirex Ltd., Harwell Laboratory. 1990.

Del Debbio, J.A. and T.R. Thomas. "Transport Properties of Radionuclides and Hazardous Chemical Species in Soils at the Idaho Chemical Processing Plant." WINCO-1068. Idaho Falls, Idaho: Westinghouse Idaho Nuclear Company, Inc. 1989.

Delany, J.M., and S.R. Lundeen. "The LLNL Thermochemical Database." Report UCRL-21658. Livermore, California: Lawrence Livermore National Laboratory. 1990.

Denham, M.E. "Conceptual Model of Waste Release from the Contaminated Zone of Closed Radioactive Waste Tanks." WSRC-STI-2007-00544. Aiken, South Carolina: Savannah River National Laboratory. 2007.

DOE. DOE-WD-2005-001, "Basis for Section 3116 Determination for Salt Waste Disposal at the Savannah River Site." Washington, DC: DOE. 2006.

———. DOE-WD-2005-002, "Draft Section 3116 Determination for Closure of Tank 19 and Tank 18 at the Savannah River Site." Rev. 0. Washington, DC: DOE. 2005.

DOE-ID. DOE/NE-ID-11226, "Basis for Section 3116 Determination for the Idaho Nuclear Technology and Engineering Center Tank Farm Facility." Rev. 0. Idaho Falls, Idaho: DOE-ID. 2006.

———. DOE-ID-10966, "Performance Assessment for the Tank Farm Facility at the Idaho National Engineering and Environmental Laboratory." Rev. 1. Errata December 2, 2003. Idaho Falls, Idaho: DOE-ID. 2003.

Efurd, D.W., W. Runde, J.C. Banar, D.R. Janecky, J.P. Kaszuba, P.D. Palmer, F.R. Roensch, and C.D. Tait. "Neptunium and Plutonium Solubilities in a Yucca Mountain Groundwater." *Environmental Science and Technology*. Vol. 32. pp. 3,893–3,900. 1998.

Ewart, F.T., J.L. Smith-Briggs, H.P. Thomason, and S.J. Williams. "The Solubility of Actinides in a Cementitious Near-Field Environment." *Waste Management*. Vol. 12. pp. 241–252. 1992.

Ewart, F.T., R.M. Howse, H.P. Thomason, S.J. Williams, and J.E. Cross. "The Solubility of Actinides in the Near-Field." *Materials Research Society Symposium Proceedings 50*. L.O. Werme, ed. Pittsburgh, Pennsylvania: Materials Research Society. pp. 701–708. 1986.

Giammar, D.E. and J.G. Hering. "Equilibrium and Kinetic Aspects of Sodyyite Dissolution and Secondary Phase Precipitation in Aqueous Suspension." *Geochimica et Cosmochimica Acta*. Vol. 66. pp. 3,235–3,245. 2002

Glasser, F.P., M. Tyrer, K. Quillin, D. Ross, J. Pedersen, K. Goldthorpe, D.G. Bennett, and M. Atkins. "The Chemistry of Blended Cements and Backfills Intended for Use in Radioactive Waste Disposal." R&D Technical Report P98. Bristol, United Kingdom: U.K. Environment Agency. 1999.

Glaus, M.A. and L.R. Van Loon. "A Generic Procedure for the Assessment of the Effect of Concrete Admixtures on the Retention Behaviour of Cement for Radionuclides: Concept and Case Studies." PSI Bericht NR. 04-02, Nagra NTB 03-09. Villigen, Switzerland: Paul Scherrer Institute. 2004.

Gorman-Lewis, D., L. Mazeina, J.B. Fein, J.E.S. Szymanowski, P.C. Burns, and A. Navrotsky. "Thermodynamic Properties of Sodyyite From Solubility and Calorimetry Measurements." *The Journal of Chemical Thermodynamics*. Vol. 39. pp. 568–575. 2007.

Greenberg, S.A. and T.N. Chang. "Investigation of the Colloidal Hydrated Calcium Silicates II: Solubility Relationships in the Calcium Oxide–Silica–Water System at 25°C." *Journal of Physical Chemistry*. Vol. 69. pp. 182–188. 1965.

Greenfield, B.F., D.J. Ilett, M. Ito, R. McCrohon, T.G. Heath, C.J. Tweed, S.J. Williams, and M. Yui. "The Effect of Cement Additives on Radionuclide Solubilities." *Radiochimica Acta*. Vol. 82. pp. 27–32. 1998.

Guillaumont, R., T. Fanghänel, J. Fuger, I. Grenthe, V. Neck, D.A. Palmer, and M.H. Rand. *Chemical Thermodynamics, Volume 5: Update on the Chemical Thermodynamics of Uranium, Neptunium, Plutonium, Americium and Technetium*. New York City, New York: Elsevier Science Publishing Company. 2003.

Iida, Y., T. Yamaguchi, S. Nakayama, T. Nakajima, and Y. Sakamoto. "The Solubility of Metallic Selenium Under Anoxic Conditions." *Materials Research Society Symposium Proceedings* 663. K.P. Hart and G.R. Lumpkin, eds. Warrendale, Pennsylvania: Materials Research Society. pp. 1,143–1149. 2001.

Itagaki, H., S. Nakayama, S. Tanaka, and M. Yamawaki. "Effect of Ionic Strength on the Solubility of Neptunium(V) Hydroxide." *Radiochimica Acta*. Vols. 58 and 59. pp. 61–66. 1992.

Japan Atomic Energy Agency. "Thermodynamic Database." File 050000g0.tdb. 2008. <<http://migrationdb.jaea.go.jp/english.html>> (28 March 2008).

Kaplan, D. "Geochemical Data Package for Performance Assessment Calculations Related to the Savannah River Site (U)." WSRC–TR–2006–00004. Rev. 0. Aiken, South Carolina: Washington Savannah River Company. 2006.

Kaplan, D.I. and J.L. Myers. "Long-Term Dynamics of Lead Solubility in a Cementitious Groundwater Environment." WSRC–TR–2000–00416. Aiken, South Carolina: Westinghouse Savannah River Company. 2001.

Kitamura, A., M. Shibata, and H. Kitao. "Solubility Measurement of Iron-Selenium Compounds Under Reducing Conditions." *Materials Research Society Symposium Proceedings* 807. V.M. Oversby and L.O. Werme, eds. Warrendale, Pennsylvania: Materials Research Society. pp. 609–614. 2004.

Krupka, K.M. and R.J. Serne. NUREG/CR–6377, PNNL–11408, "Effects on Radionuclide Concentrations by Cement/Groundwater Interactions in Support of Performance Assessment of Low-Level Radioactive Waste Disposal Facilities." Richland, Washington: Pacific Northwest National Laboratory. 1998.

Krupka, K.M., R.J. Serne, and D.I. Kaplan. "Geochemical Data Package for the 2005 Hanford Integrated Disposal Facility Performance Assessment." PNNL–13037. Rev. 2. Richland, Washington: Pacific Northwest National Laboratory. 2004.

Langmuir, D. *Aqueous Environmental Geochemistry*. Upper Saddle River, New Jersey: Prentice Hall. 1997.

Lee, S.Y. and E.A. Bondietti. "Technetium Behavior in Sulfide and Ferrous Iron Solutions." *Materials Research Society Symposium Proceedings* 15. D.G. Brookins, ed. Pittsburgh, Pennsylvania: Materials Research Society. pp. 315–322. 1983.

Lierse, C., W. Treiber, and J.I. Kim. "Hydrolysis Reactions of Neptunium(V)." *Radiochimica Acta*. Vol. 38. pp. 27–28. 1985.

Lukens, W.W., J.J. Bucher, D.K. Shuh, and N.M. Edelstein. "Evolution of Technetium Speciation in Reducing Grout." *Environmental Science and Technology*. Vol. 39. pp. 8,064–8,070. 2005.

Moroni, L.P. and F.P. Glasser. "Reactions Between Cement Components and U(VI) Oxide." *Waste Management*. Vol. 15. pp. 243–254. 1995.

Murphy, W.M. and R.C. Codell. "Alternate Source Term Models for Yucca Mountain Performance Assessment Based on Natural Analog Data and Secondary Mineral Solubility." *Materials Research Society Symposium Proceedings* 556. D.J. Wronkiewicz and J.H. Lee, eds. Warrendale, Pennsylvania: Materials Research Society. pp. 551–558. 1999.

Neck, V. "Comment on Hydrolysis of Neptunium(V) at Variable Temperatures (10–85°C) by L. Rao, T.G. Srinivasan, A. Yu. Garnov, P. Zanonato, P. Di Bernardo, and A. Bismondo." *Geochimica et Cosmochimica Acta*. Vol. 70. pp. 4,551–4,555. 2006.

Neck, V., M. Altmaier, A. Seibert, J.I. Yun, C.M. Marquardt, and T. Fanghänel. "Solubility and Redox Reactions of Pu(IV) Hydrous Oxide: Evidence for the Formation of PuO<sub>2+x</sub>(s, hyd)." *Radiochimica Acta*. Vol. 95. pp. 193–207. 2007.

Neck, V., J.I. Kim, and B. Kanellakopulos. "Solubility and Hydrolysis Behaviour of Neptunium(V)." *Radiochimica Acta*. Vol. 56. pp. 25–30. 1992.

Nguyen S. N., R.J. Silva, C.H. Weed, and J.E. Andrews Jr. "Standard Gibbs Free Energies of Formation at the Temperature 303.15K of Four Uranyl Silicates: Soddyite, Uranophane, Sodium Boltwoodite, and Sodium Weeksite." *Journal of Chemical Thermodynamics*. Vol. 24. pp. 359–376. 1992.

Nitsche, H., K. Roberts, T. Prussin, A. Muller, K. Becraft, D. Keeney, S.A. Carpenter, and R.C. Gatti. "Measured Solubilities and Speciations From Oversaturation Experiments of Neptunium, Plutonium, and Americium in UE-25P #1 Well Water From the Yucca Mountain Region." LA-12563-MS. Los Alamos, New Mexico: Los Alamos National Laboratory. 1994.

Nitsche, H., R.C. Gatti, E.M. Standifer, S.C. Lee, A. Müller, T. Prussin, R.S. Deinhammer, H. Maurer, K. Becraft, S. Leung, and S.A. Carpenter. "Measured Solubilities and Speciations of Neptunium, Plutonium, and Americium in a Typical Groundwater (J-13) From the Yucca Mountain Region." LA-12562-MS. Los Alamos, New Mexico: Los Alamos National Laboratory. 1993.

Nordstrom, D.K. and J.L. Munoz. *Geochemical Thermodynamics*. Second Edition. Boston, Massachusetts: Blackwell Scientific Publications. 1994.

NRC. "U.S. Nuclear Regulatory Commission Technical Evaluation Report For the U.S. Department Of Energy Savannah River Site Draft Section 3116 Waste Determination for Salt Waste Disposal." Washington, DC: NRC. 2005.

Ochs, M., D. Hager, S. Helfer, and B. Lothenbach. "Solubility of Radionuclides in Fresh and Leached Cementitious Systems at 22 °C and 50 °C." *Materials Research Society Symposium Proceedings* 506. I.G. McKinley and C. McCombie, eds. Warrendale, Pennsylvania: Materials Research Society. pp. 773–780. 1998.

Parkhurst, D.L. "User's Guide to PHREEQC—A Computer Program for Speciation, Reaction-Path, Advective-Transport, and Inverse Geochemical Calculations." U.S. Geological Survey Water-Resources Investigations Report 95-4227. 1995.

- Pilkington, N.J. "The Solubility of Technetium in the Near-Field Environment of a Radioactive Waste Repository." *Journal of Less-Common Metals*. Vol. 161. pp. 203–212. 1990.
- Pointeau, I., C. Landesman, E. Giffaut, and P. Reiller. "Reproducibility of the Uptake of U(VI) Onto Degraded Cement Pastes and Calcium Silicate Hydrate Phases." *Radiochimica Acta*. Vol. 92. pp. 645–650. 2004.
- Prikryl, J.D. and D.A. Pickett. "Recommended Site-Specific Sorption Coefficients for Reviewing Non-High-Level Waste Determinations at the Savannah River Site and Idaho National Laboratory." San Antonio, Texas: CNWRA. 2007.
- Rai, D., N.J. Hess, A.R. Felmy, D.A. Moore, M. Yui, and P. Vitorge. "A Thermodynamic Model for the Solubility of  $\text{PuO}_2(\text{am})$  in the Aqueous  $\text{K}^+\text{-HCO}_3^-\text{-CO}_3^{2-}\text{-OH}^-\text{-H}_2\text{O}$  System." *Radiochimica Acta*. Vol. 86. pp. 89–99. 1999.
- Rao, L., T.G. Srinivasan, A.Y. Garnov, P. Zanonato, P. Di Bernardo, and A. Bismondo. "Response to the Comment by V. Neck on "Hydrolysis of Neptunium(V) at Variable Temperatures (10–85 °C), *Geochimica et Cosmochimica Acta* 68, 4821–4830." *Geochimica et Cosmochimica Acta*. Vol. 70. pp. 4,556–4,562. 2006.
- Rard, J.A., M.H. Rand, G. Anderegg, and H. Wanner. *Chemical Thermodynamics, Volume 3: Chemical Thermodynamics of Technetium*. New York City, New York: Elsevier Science Publishing Company. 1999.
- Rosenberger, K.H., B.C. Rogers, and R.K. Cauthen. "Saltstone Performance Objective Demonstration Document (U)." CBU–PIT–2005–00146. Rev. 0. Aiken, South Carolina: Westinghouse Savannah River Company. 2005.
- Runde, W., S.D. Conradson, D.W. Efurud, N. Lu, C.E. VanPelt, and C.D. Tait. "Solubility and Sorption of Redox-Sensitive Radionuclides (Np, Pu) in J–13 Water From the Yucca Mountain Site: Comparison Between Experiment and Theory." *Applied Geochemistry*. Vol. 17. pp. 837–853. 2002.
- Sanchez, F., C. Gervais, A.C. Garrabrants, R. Barna, and D.S. Kosson. "Leaching of Inorganic Contaminants From Cement-Based Waste Materials as a Result of Carbonation During Intermittent Wetting." *Waste Management*. Vol. 22. pp. 249–260. 2002.
- Séby, F., M. Potin-Gautier, E. Giffaut, G. Borge, and O.F.X. Donard. "A Critical Review of Thermodynamic Data for Selenium Species at 25°C." *Chemical Geology*. Vol. 171. pp. 173–194. 2001.
- Serne, R.J., D. Rai, P.F. Martin, A.R. Felmy, L. Rao, and S. Ueta. "Leachability of Nd, U, Th, and Sr, From Cements in a  $\text{CO}_2$  Free Atmosphere." Materials Research Society Symposium Proceedings 412. W.M. Murphy and D.A. Knecht, eds. Pittsburgh, Pennsylvania: Materials Research Society. pp. 459–467. 1996.
- Sharmasarkar, S., K.J. Reddy, and G.F. Vance. "Preliminary Quantification of Metal Selenite Solubility in Aqueous Solutions." *Chemical Geology*. Vol. 132. pp. 165–170. 1996.

Smith, R.W. and J.C. Walton. "The Role of Oxygen Diffusion in the Release of Technetium from Reducing Cementitious Waste Forms." Materials Research Society Symposium Proceedings 294. C.G. Interrante and R.T. Pabalan, eds. Pittsburgh, Pennsylvania: Materials Research Society. pp. 247–253. 1993.

Talerico, C., M. Ochs, and E. Giffaut. "Solubility of Niobium(V) Under Cementitious Conditions: Importance of Ca-Niobate." Materials Research Society Symposium Proceedings 824. J.M. Hanchar, S. Stroes-Gascoyne, and L. Browning, eds. Warrendale, Pennsylvania: Materials Research Society. pp. 443–448. 2004.

Thomas, J.L. "Characterization of Tank 19 Residual Waste." WSRC–TR–2002–00052. Rev. 3. Aiken, South Carolina: Westinghouse Savannah River Company. 2005a.

———. "Characterization of Tank 18 Residual Waste." U–TR–F–00005. Rev. 2. Aiken, South Carolina: Westinghouse Savannah River Company. 2005b.

U.S. Environmental Protection Agency. "MINTEQA2/PRODEFA2, A Geochemical Assessment Model for Environmental Systems: User Manual Supplement for Version 4.0." Athens, Georgia: U.S. Environmental Protection Agency, National Exposure Research Laboratory, Ecosystems Research Division. 1999.

Warwick, P., S. Aldridge, N. Evans, and S. Vines. "The Solubility of Technetium (IV) at High pH." *Radiochimica Acta*. Vol. 95. pp. 709–716. 2007.

Westinghouse Savannah River Company. "Radiological Performance Assessment for the Z-Area Saltstone Disposal Facility (U)." WSRC–RP–92–1360. Rev. 0. Aiken, South Carolina: Westinghouse Savannah River Company. 1992.

Wieland, E. and L.R. Van Loon. "Cementitious Near-Field Sorption Data Base for Performance Assessment of an ILW Repository in Opalinus Clay." PSI Bericht 03-06. Villigen, Switzerland: Paul Scherrer Institute. 2003.

Wolery, T.J. "EQ3/6, A Software Package for Geochemical Modeling of Aqueous Systems: Package Overview and Installation Guide (Version 7.0)." UCRL–MA–110662 PT1. Livermore, California: Lawrence Livermore National Laboratory. 1992.

Yamaguchi, T., Y. Sakamoto, and T. Ohnuki. "Effect of the Complexation on Solubility of Pu(IV) in Aqueous Carbonate System." *Radiochimica Acta*. Vol. 66/67. pp. 9–14. 1994.

Zhao, P., P.G. Allen, E.R. Sylwester, and B.E. Viani. "The Partitioning of Uranium and Neptunium Onto Hydrothermally Altered Concrete." *Radiochimica Acta*. Vol. 88. pp. 729–736. 2000.